TACTICAL WEAPON
GACIAC
GUIDANCE & CONTROL
INFORMATION ANALYSIS CENTER

GACIAC PR-89-02

1

PROCEEDINGS OF THE WORKSHOP ON HIGH TEMPERATURE SUPERCONDUCTIVITY

23-25 May 1989

Conducted at Tom Bevill Conference Center
University of Alabama
Huntsville, Alabama

SPONSORED BY:

This DoD scientific and technical workshop is jointly sponsored by the U.S. Army Missile Command (MICOM), the U.S. Army Strategic Defense Command (USADC), and the U.S. Army Research Office (ARO) Huntsville, Alabama

APPROVED FOR PUBLIC RELEASE:
DISTRIBUTION UNLIMITED

Published by GACIAC
IIT Research Institute
10 West 35th Street

NOTICES

PROCEEDINGS. This proceedings has been published by the Tactical Weapon Guidance and Control Information Analysis Center (GACIAC) as a service to the defense community. GACIAC is a DoD Information Analysis Center, administered by the Defense Technical Information Center, operated by IIT Research Institute under Contract No. DLA900-86-C-0022. GACIAC is funded by DTIC, DARPA, and U.S. Army, U.S. Navy, and U.S. Air Force Laboratories/Controlling Activities having an interest in tactical weapon guidance and control. The Director of GACIAC is Dr. Robert J. Heaston. The Contracting Officer is Mrs. S. Williams, DESC, Dayton, Ohio. The Contracting Officer's Technical Representative is Mr. Chalmer D. George, and the alternate is Mr. Howard C. Race, AMC Smart Weapons Management Office, ATTN: AMSMI-SW, Redstone Arsenal, Alabama 35898-5222.

UNCLASSIFIED

SECURITY CLASSIFICATION OF THIS PAGE

REPORT DOCUMENTATION PAGE

Form Approved OMB No. 0704-0188

1a. REPORT SECURITY CLASSIFICATION UNCLASSIFIED	1b. RESTRICTIVE MARKINGS Unclassified/Unlimited
2a. SECURITY CLASSIFICATION AUTHORITY	3. DISTRIBUTION/AVAILABILITY OF REPORT Unclassified/Unlimited Approved and Cleared for Public Release
2b. DECLASSIFICATION/DOWNGRADING SCHEDULE	
4. PERFORMING ORGANIZATION REPORT NUMBER(S) GACIAC PR-89-02	5. MONITORING ORGANIZATION REPORT NUMBER(S)
6a. NAME OF PERFORMING ORGANIZATION IIT Research Institute GACIAC 6b. OFFICE SYMBOL (If applicable)	7a. NAME OF MONITORING ORGANIZATION AMC Smart Weapons Management Office AMSMI-SW/Chalmer D. George
6c. ADDRESS (City, State, and ZIP Code) 10 West 35th Street Chicago, Illinois 60616-3799	7b. ADDRESS (City, State, and ZIP Code) Redstone Arsenal, Alabama 35898-5222
8a. NAME OF FUNDING/SPONSORING ORGANIZATION MICOM/U.S. Army Missile Command (See Reverse) 8b. OFFICE SYMBOL (If applicable)	9. PROCUREMENT INSTRUMENT IDENTIFICATION NUMBER DLA900-86-C-0022
8c. ADDRESS (City, State, and ZIP Code) Huntsville, Alabama 35898-5222	10. SOURCE OF FUNDING NUMBERS PROGRAM ELEMENT NO. 62802 S; PROJECT NO. 1.0; TASK NO.; WORK UNIT ACCESSION NO.

11. TITLE (Include Security Classification)
Proceedings of the Workshop on High Temperature Superconductivity. (u)

12. PERSONAL AUTHOR(S)
Various; Dr. Frank Madarasz, Technical Program Chairman

13a. TYPE OF REPORT	13b. TIME COVERED	14. DATE OF REPORT (Year, Month, Day)	15. PAGE COUNT
Proceedings	FROM May 89 TO Nov 89	November 1, 1989	361

16. SUPPLEMENTARY NOTATION This report is available only from GACIAC. Reproduction is not authorized except by specific permission. (410948) $75.00

17. COSATI CODES		
FIELD	GROUP	SUB-GROUP
20	03	
09	01	

18. SUBJECT TERMS (Continue on reverse if necessary and identify by block number)
Superconductors, High Temperature, Research, Theories, Concepts, Experimentation, Materials, Properties, Electrical Properties, Optical Properties, (See Reverse)

19. ABSTRACT (Continue on reverse if necessary and identify by block number)
This Proceedings contains the papers for the Workshop on High Temperature Superconductivity presented at the workshop. The workshop was conducted at the University of Alabama at Huntsville on 23-25 May 1989. For a long time it has been recognized that superconductivity offers a whole new realm of device performance in such applications as microwave components, radiating elements, detectors, and high speed electronics. However, the cost and complexity of liquid helium cooling systems represented an unyielding impediment to the development of practical systems. High temperature superconductivity, having less stringent cryogenic requirements, provides the impetus to the development of truly practical systems. The topics to be covered during the workshop include basic high temperature superconductivity research, theory, and experimentation; the electrical, optical, thermal, magnetic, and mechanical properties of materials; the fabrication and characterization of thin films; small scale applications such as computer electronics, SQUIDS, and IR detectors; large scale applications such as energy storage, magnets, magnetic shields and switches; (SEE REVERSE)

20. DISTRIBUTION/AVAILABILITY OF ABSTRACT ☐ UNCLASSIFIED/UNLIMITED ☒ SAME AS RPT. ☐ DTIC USERS	21. ABSTRACT SECURITY CLASSIFICATION UNCLASSIFIED
22a. NAME OF RESPONSIBLE INDIVIDUAL Chalmers D. George	22b. TELEPHONE (Include Area Code) (205) 876-3666 22c. OFFICE SYMBOL AMSMI-SW

DD Form 1473, JUN 86 *Previous editions are obsolete.*

SECURITY CLASSIFICATION OF THIS PAGE
UNCLASSIFIED

8.a NAME OF FUNDING/SPONSORING ORGANIZATION (cont)

U.S. Army Strategic Defense Command (USADC), and the U.S. Army Research Office (ARO).

18. SUBJECT TERMS (cont)

Thermal Properties, Mechanical Properties, Magnetic Fields, Thin Films, Infrared Detectors, Energy, Storage, Devices, Sensors, Papers, Abstracts.

19. ABSTRACTS (cont)

and superconducting/semiconducting hybrid devices. Thirty-six papers were presented. This DoD scientific and technical workshop was jointly sponsored by the U.S. Army Missile Command (MICOM), the U.S. Army Strategic Defense Command (USASDC), and the U.S. Army Research Office (ARO) for the purpose of exchanging and disseminating information on current advancements in the science and technology of high temperature superconductors, with emphasis on strategic and tactical military applications.

GACIAC PR-89-02 NOVEMBER 1989

PROCEEDINGS OF THE WORKSHOP ON HIGH TEMPERATURE SUPERCONDUCTIVITY

23-25 MAY 1989

CONDUCTED AT THE
TOM BEVILL CONFERENCE CENTER
UNIVERSITY OF ALABAMA
HUNTSVILLE, ALABAMA 35805

JOINTLY SPONSORED BY

U.S. ARMY MISSILE COMMAND
U.S. ARMY STRATEGIC DEFENSE COMMAND
U.S. ARMY RESEARCH OFFICE

Distribution: Unclassified/Unlimited
and Cleared for Public Release

Published by GACIAC
IIT Research Institute
10 West 35th Street
Chicago, Illinois 60616-3799

GACIAC -- A DoD Information Analysis Center
Operated by IIT Research Institute, 10 West 35th Street, Chicago, IL 60616-3799
DoD Technical Sponsor - Joint Service Guidance and Control Committee
Members from OSD, Army, Navy, Air Force, and DARPA

THIS PAGE IS INTENTIONALLY BLANK

Workshop On High Temperature Superconductivity
23-25 May 1989
Huntsville, Alabama

FOREWORD

Planning for this workshop began with the recognition that the Army strategic and tactical communities share some common goals on the technology level for high temperature superconductivity. The workshop was also viewed as being consistent with the cautious investment strategy adopted by the Army for high temperature superconductor technology in recognition that the technology base budget is limited, and there are many institutions active in this technology in industry, academia, and Government. Federal agencies with active programs in superconductivity include the Department of Defense, Department of Energy, Department of Commerce, the National Aeronautics and Space Administration, and the National Science Foundation. One objective of the meeting was therefore to provide a forum for the exchange of information between Army scientists and engineers and their colleagues in other institutions, and the opportunity to assess the potential for technology insertion in current Army and DoD programs.

In order to be in a position to exploit the potential of high temperature superconductivity quickly for Army applications, a task force was formed in 1987 by the U.S. Army Laboratory Command (LABCOM) with Dr. Gerald J. Iafrate as chairman, and members from the Materials Technology Laboratory (MTL), Harry Diamond Laboratories (HDL), and the Army Research Office (ARO). Other Army centers and laboratories that participated as observers in this effort included the U.S. Army Missile Command and the U.S. Army Strategic Defense Command. The task force identified the following potential capabilities as offering the Army combat advantages: ultra-stable, low noise, frequency control cavities for secure communication; magnetic confinement and shielding for lightweight radars, sensors, and detectors for millimeter wave and infrared electronics; ultra high-energy pulse power conditioning for electromagnetic hyperkinetic weapons; hybrid semiconductor-superconductor devices; and interconnects and striplines for MIMIC and VHSIC technologies.

The in-house cooperative involving LABCOM, Center for Night Vision and Electro-Optics (CNVEO), and Armaments Research, Development, and Engineering Center (ARDEC) grew out of the task force. This cooperative works closely with the Strategic Defense Initiative, the Defense Research Projects Agency, and the Army Strategic Defense Command in developing external contractual programs. The Strategic Defense Command is pursuing the application of thin film coating of high temperature superconductivity to large surface area devices such as radio frequency cavities and stripline oscillators for application in free electron lasers and neutral particle beam systems. It is clear that progress toward strategic goals will have a benefit for tactical systems and vice versa; for this reason close cooperation is essential. The workshop was viewed as a timely step toward coordination within the Army community.

FOREWORD (cont'd)

High temperature superconductivity is expected to have an impact on several of the 13 emerging technologies identified in the Army TECHNOLOGY BASE MASTER PLAN. Superconductivity is also one of the 22 critical technologies in the Department of Defense CRITICAL TECHNOLOGY PLAN submitted to the Congress on 15 March 1989 in response to Public Law 100-456, the National Defense Authorization Act for Fiscal Year 1989. This DoD critical technology includes both large-scale low temperature superconductivity which is relatively mature but with only limited applications in military systems, and the high temperature superconductivity for which approximately 80 percent of the FY 89 DoD budget is allocated. The DoD tactical and strategic defense programs are divided into three categories: large surface area materials for applications to microwave cavities, waveguides and magnetic shields; small surface area materials for applications in infrared detectors and signal processors; and high current, high power applications. The original objective of the meeting was to focus the theme on the first two categories.

Joint sponsorship of the workshop was provided by the U.S. Army Strategic Defense Command, the U.S. Army Research Office, and the U.S. Army Missile Command. Members of the steering committee were Dr. Larry Atha, Dr. Jefferson Bennett, Dr. Bobby Guenther, Dr. George Tanton, Mr. Richard Rogers, Mr. Douglas Ennis, Dr. Palmer Peters, Dr. Jan Bijvoet, Dr. Frank Madarasz, Ms. Noreen Schlaack, and Mr. William C. Pittman.

The steering committee acknowledges the dedicated effort of Dr. Frank Madarasz, Technical Program Chairman, for arranging the outstanding program. Thanks are also due all the speakers and session chairmen for their participation. The usual skillful administration for the meeting was provided by Ms. Jeri McAllister and Ms. Mindy Tumarkin.

For the Steering Committee
William C. Pittman

WORKSHOP ON HIGH TEMPERATURE SUPERCONDUCTIVITY

23-25 MAY 1989

Tom Bevill Conference Center
University of Alabama
Huntsville, Alabama

Technical Program Chairman:	Dr. Frank Madarasz University of Alabama in Huntsville
General Chairmen:	Dr. George Tanton U.S. Army RD&E Center Redstone Arsenal, Alabama
	Dr. Larry Atha U.S. Army Strategic Defense Command
Program Committee:	Dr. Frank Madarasz University of Alabama in Huntsville
	Dr. George Tanton U.S. Army RD&E Center Redstone Arsenal, Alabama
	Dr. Jay Farrell Science Applications International Corporation
Sponsor Committee:	Mr. William Pittman U.S. Army Missile Command
	Messrs. Richard Rodger and Douglas Ennis U.S. Army Strategic Defense Command
	Dr. Jefferson Bennett U.S. Army Missile Command
	Dr. Bobby Guenther U.S. Army Research Office
	Mr. Jan A. Bijvoet Consortium for Superconducting Materials and Applications
	Ms. Noreen Schlaack Teledyne Brown Engineering
Administration:	Ms. Jeri McAllister IIT Research Institute/GACIAC Huntsville, Alabama

WORKSHOP ON HIGH TEMPERATURE SUPERCONDUCTIVITY

23-25 May 1989

AGENDA

TUESDAY 23 MAY 1989

SESSION I:	**Chairman:** Dr. Frank L. Madarasz University of Alabama in Huntsville
7:50-8:00	Introduction
8:00-8:55	"High Temperature Superconductivity: Concepts, and Phenomenology Dr. Gerald Iafrate, U.S. Army LABCOM, Ft. Monmouth
9:00-9:45	"Overview of Materials Properties" J.L. Smith, W.L. Hults, A.P. Clarke and K.A. Johnson, Los Alamos National Laboratories
9:50-10:35	"Structure and Properties Correlation in High T_c Superconductors" Dr. M.K. Wu, Columbia University
10:35-10:50	**BREAK**
SESSION II:	**Chairman:** Dr. George Tanton U.S. Army RD&E Center, Redstone Arsenal, Alabama
10:50-11:35	"Superconductivity in High Magnetic Fields: New Problems and Issues" Dr. Lance Delong, National Science Foundation and University of Kentucky
11:40-12:25	"Thermal Properties of High T_c Materials" D.T. Morelli and Joseph Heremans, General Motors Research Laboratory
12:25-1:45	**LUNCH**
SESSION III:	**Chairman:** Dr. Larry Ahta U.S. Army Strategic Defense Command
1:45-2:30	"The Photoresponse of Superconductors" Dr. Ulrich Strom, Naval Research Laboratory

AGENDA (Cont.)

2:35-3:20 "SQUIDs and Fluxon Devices"
Dr. Orest Symko, University of Utah

3:20-3:30 **BREAK**

SESSION IV: **Chairman:** Dr. John Miller
University of North Carolina

3:30-4:15 "High Frequency Superconducting Electronics"
J. Zmuidzinas and J.R. Tucker, University of Illinois

4:20-5:05 "High-Frequency Cavity Applications and Measurements of High-Temperature Superconductors"
D. Wayne Cooke and E.R. Gray, Los Alamos National Laboratories

WEDNESDAY 24 May 1989

SESSION V: **Chairman:** Dr. Daniel Rogovin
Rockwell International Science Center

8:00-8:45 "The Chemistry of High Temperature Superconductors"
Dr. Edward Teller, Hoover Institute and Lawrence Livermore Laboratory

8:45-9:20 "Transient Microwave Response of Superconducting Devices to Laser Radiation"
Daniel Rogovin and Nathanial Glass, Rockwell International Science Center

9:20-9:45 Improved $YBa_2Cu_3O_{7-x}$/Noble Metal Thick Films
J.H. Miller, Jr. S.L. Holder and J.D. Hunn, University of North Carolina

9:45-10:00 **BREAK**

SESSION VI: **Chairman:** Dr. John Miller
University of North Carolina

10:00-10:25 "Flux Creep in Polycrystalline Oxide Superconductors"
M.E. McHenry, M.P. Maley, J.O Willis, J.D. Thompson, K.C. Ott, G.H. Kwei, J.R. Cost, D.E. Peterson, J.L. Smith and W.L. Hults, Los Alamos National Laboratories

AGENDA (Cont.)

10:25-10:50 "RF Measurements on High T_c Superconductors"
C.L. Bohn, J.R. Delayen, and M.T. Lanagan, Argonne National Laboratory

10:50-:11-15 "Superconducting Stripline Resonators and High T_c Materials"
D.E. Oates, M.i.T. Lincoln Laboratory

11:15-11:40 "High Transport Current and Increased Critical Temperature in Bi-Sr-Ca-Cu-O Oxide System"
Kumiko Imai and Hironori Matsuba, The Furukawa Electric Co., Ltd.

11:40-12:05 "Preparation and Characterization of Single-Phase ($Bi_{2-x}Pb_xSr_2Ca_2Cu_3O_y$) Ceramic Superconductors"
H.L. Luo and S.M. Green, Y. Mei and A.E. Manzi, University of California, San Diego

12:05-1:30 **LUNCH**

SESSION VII: **Chairman:** Dr. M.K. Wu
Columbia University

1:30-1:55 "Sequentially Evaporated Thin Y-Ba-Cu-O Superconductiong Films on Microwave Substrates"
G.J. Valco and N.J. Rohrer, Ohio State University; J.D. Warner and K.B. Bhasin, NASA Lewis

1:55-2:20 "Focused Ion Beam Patterning of High T_c Superconducting Thin Films"
P.A. Polakos and L.R. Harriott, AT&T Bell Laboratories

2:20-2:45 "Low Surface Resistance Thin Films of $Tl_2Ca_2Cu_3O_{10}$ Produced by Chemical Deposition and Laser Ablation"
W.L. Olson, M. Eddy, T.W. James, McD. Robinson, D.D.P. Casavant, E.J. Smith, A. Cardona and R.B. Hammond, Superconductor Technologies Inc.

2:45-3:10 "Triode Magnetron Sputtered Superconducting Y-Ba-Cu-O Thin Films"
George F. McLane and Robert L. Pfeffer, U.S. Army LABCOM, Ft. Monmouth; W. Savin, New Jersey Institute of Technology, Newark; and C. Wrenn, Vitronics, Inc., Eatontown, NJ

3:10-3:25 **BREAK**

AGENDA (Cont.)

SESSION VIII: **Chairman:** Dr. Palmer Peters
NASA, Marshall Space Flight Center

3:25-3:50 "Light Dection Using Superconducting Films"
Ulrich Strom, J.C. Culbertson, and S.A. Wolf, Naval Research Laboratory

3:50-4:15 "High Temperature Superconducting Detector Response Model"
J.N. Farrell, Science Application International Corporation

4:15-4:40 "Y-Ba-Cu-O Thin Films as High Speed Infrared Detectors"
Hoi S. Kwok, J.P. Zheng, and Q.Y. Ying, University of New York at Buffalo

THURSDAY 25 May 1989

SESSION IX: **Chairman:** Dr. John H. Miller
University of North Carolina

8:00-8:25 "Electrical Response of High T_c Superconducting Films to Laser Radiation"
M.G. Forrester, J. Talvacchio and A.I. Braginski, Westinghouse R&D Center

8:25-8:50 "Electronic Device Research at Los Alamos in High T_c Superconducting Thin Films"
Ross A. Lemons, Los Alamos National Laboratories

8:50-9:15 "Infrared Study of (Bi, Pb)-Sr-Ca-Cu-Oxide High-T_c Superconductors"
H.L. Luo, University of California, San Diego and B.H. Loo, University of Alabama in Huntsville

9:15-9:30 "In-Situ Diagnostics of Laser Ablated Firms of YBaCuO"
P.W. Morrison, Jr., D.G. Hamblen, and P.R. Solomon, Advanced Fuel Research, Inc.; L. Lynds, B.R. Weinberger, and T.W. Grudkowski, United Technologies Research Center

9:30-9:55 "Fabrication and Characterization of High Temperature Superconducting SQUID Sensors"
I.S. Gergis, J.A. Titus, P.H. Kobrin, and A.B. Harker, Rockwell International Science Center

9:55-10:10 **BREAK**

AGENDA (Cont.)

SESSION X: **Chairman:** Dr. Orest Symko
University of Utah

10:10-10:35 "Magnetic Shielding with High T_c Superconductors"
O.G. Symko, W.J. Yeh, and D.J. Zheng, University of Utah; S. Kulkarni, Ceramatec, Inc.

10:35-11:00 "The Electrical Field Induced by a Gravitational Wave in a Superconductor: A Principle for a New Gravitational Wave Antenna"
Huei Peng, University of Alabama in Huntsville

11:00-11:15 "Theory of Superconductivity Theories"
A.J. Fennelly, Teledyne Brown Engineering and J.A. Fennelly, University of Alabama in Huntsville

11:15-11:40 "Superconducting Stripline Resonator Performance"
B.R. McAvoy, G.R. Wagner, J.D. Adam, and J. Tavacchio, Westinghouse R&D Center

11:40-12:05 "Production of Wires and Coils from High-Temperature Superconducting Materials"
M.T. Lanagan, U. Balachandran, M.T. Cao, S.E. Dorris, J.T. Dusek, K.C. Goretta, R.B. Poeppel, J.P. Singh, and C.A. Youngdahl, Argonne National Laboratory

12:05-12:30 "Processing of High Temperature Superconductors via Hot Isostatic Pressing"
K.T. Richards and R.H. Benfer, U.S. Army Materials Technology Laboratory

12:30-12:55 "Superconducting Antennas"
R.C. Hansen, Consulting Engineer

12:55-1:00 **CLOSING REMARKS**

Workshop on High Temperature Superconductivity
23-25 May 1989
Huntsville, Alabama

TABLE OF CONTENTS

TABLE OF CONTENTS (Cont.)

TABLE OF CONTENTS (Cont.)

THIS PAGE IS INTENTIONALLY BLANK

Presented at the Workshop on High Temperature Superconductivity
23-25 May 1989 GACIAC PR 89-02

High Temperature Superconductivity: Concepts, Issues, and Phenomenology

Gerald J. Iafrate

U.S. Army Electronics Technology and Devices Laboratory (LABCOM)
Fort Monmouth, New Jersey 07703-5000

ABSTRACT

A review of the basic technical issues relevant to the effective utilization of high temperature superconductivity in electronic device and component applications is presented. Many of the key issues pertain to material science; in this discourse, however, other more fundamental consequences of high temperature superconductivity are addressed, which inherently influence, and in fact, may limit the role of high temperature superconductivity in many conventional technology applications. BCS theory is used to estimate the characteristics of high temperature superconductivity and to provide insight into the use as well as the potential limitations of high temperature superconductivity in high-impact technology areas.

INTRODUCTION

The recent discovery of high temperature superconductivity rivals the invention of the transistor, both as a scientific novelty and in terms of potential technological impact. In the scientific community, this discovery is viewed as a remarkable manifestation of nature; much excitement and speculation has been generated concerning the impact of high temperature superconductivity on a wide variety of commercial and military applications. Although there is ample cause for enthusiasm, there are two major issues yet to be resolved before viable applications can be realized. The first, the materials issue, concerns the synthesis of stable, reproducible materials with useable electromagnetic properties and current densities. The second, the concepts issue, involves the elucidation of fundamental physical limitations inherent in the phenomena of high temperature superconductivity.

In this paper, a synopsis of the discovery is presented, and an elucidation of the fundamental technical issues embodying high temperature superconductivity is given. Some of the key issues are concerned with material science; in this article, however, other more fundamental consequences of high temperature superconductivity are addressed, which inherently influence, and in fact, may limit the role of superconductivity in technological applications.

The basic microscopic theory of Bardeen, Cooper and Schrieffer (BCS) is used to estimate the characteristics of high temperature superconductors - - - the critical distances over which the superconductivity occurs, the coherence length, are quite small (~15 angstroms), and the critical magnetic fields needed to destroy the superconductivity have extreme type-II values, with lower critical fields of less than 1 kG and upper critical fields of well over 150 kG. The magnitude of the estimated characteristics has led us to identify the possible use as well as the potential limitations of high-temperature superconductors in high-impact technology areas. In addition, the magnitude of the coherence lengths are comparable to the size of a unit cell thereby suggesting that the high temperature superconductivity is localized to within lattice dimensions; this microscopic localization could have a profound influence on the superconductive transport and magnetic properties. The importance of including a temperature dependence in the electron-electron coupling strength is also highlighted.

PRESENT MATERIAL STATUS AND ISSUES

High temperature superconductivity is observed in the class of rare-earth compounds (RE)$Ba_2Cu_3O_{9-x}$ (RE refers to rare-earth) at temperatures of ~90K, well above the temperature of liquid nitrogen. The discoverers of this observation, K. A. Muller and J. G. Bednorz of IBM (Zurich), were recently awarded the 1987 Nobel Prize in physics for their efforts. To date, this material has been synthesized in polycrystalline bulk and oriented thin film forms; the high temperature superconductivity has been observed in these materials only when the oxygen content is seven oxygen atoms per molecule (x=2). The major material problem, commonly referred to as the oxygen problem, is to control chemically and maintain this specific oxygen content under a variety of different environmental and temperature cycling conditions.

To prepare these materials as superconductors, in both thin film or bulk forms, with the appropriate oxygen content, it is necessary to heat the materials at a temperature as high as 900°C in oxygen. When the materials are subsequently heated in vacuum, or in gasses, the materials are observed to lose oxygen. With loss of oxygen, these materials not only lose their superconductivity but they become semiconducting. The oxygen content, and therefore the superconductivity, can be restored by heating the materials to 550°C in oxygen. Thus the oxygen content must be maintained during all processing steps or must be restored as a

final step. This experimental fact has serious implications for surface and junction technologies. It is also noted that materials displaying good superconducting properties also degrade after several days of exposure to room ambients, especially humidity.

The need to expose the materials to 900°C annealing cycles in oxygen is very detrimental to useful application in microelectronics; 900°C is a very high temperature compared to those used to process silicon and gallium arsenide circuits, which can tolerate temperatures of only 450°C and 350°C respectively after final processing. It therefore remains to determine the thermal and chemical stability, radiation damage sensitivity, and reaction kinetics with substrates and passivating overlayers of these materials as well as their compatability with manufacturing processing techniques.

Thin films of high temperature superconducting materials have been synthesized by painting, plasma spraying, evaporation, sputtering, and chemical vapor deposition onto various substrates. To date, the only process which has produced useful critical current densities of thin film material has been its evaporation on the substrate strontium titanate. All other methods have produced material with subcritical current density values. It is also noted that these ceramic materials have limited formability and therefore require special production techniques to prepare the materials in wire and sheet forms.

CHARACTERISTICS OF HIGH TEMPERATURE SUPERCONDUCTIVITY

The microscopic theory of Bardeen, Cooper and Schrieffer (BCS) is used to estimate the characteristics of high temperature superconductors. Within the BCS theory, the critical temperature, T_c, and the zero temperature energy gap, Δ_0, are given by

$$\frac{1}{g} = \int_0^{\beta_c \hbar\omega_0/2} \frac{\tanh y}{y}\, dy \tag{1}$$

and

$$\frac{1}{g} = \int_0^{\hbar\omega_0/\Delta_0} \frac{1}{(y^2+1)^{\frac{1}{2}}}\, dy \tag{2}$$

where $g=D(E_F)V$ and $\beta_c=1/kT_c$. As observed from equations (1,2), the critical temperature and the energy gap depend on two basic model dependent parameters: $g=D(E_F)V$ where $D(E_F)$ is the single particle density of states at the Fermi surface and V is the electron-phonon coupling constant, and $\hbar\omega_o$, the cut-off energy for the electron-electron attractive interaction. Other relevant parameters that characterize the superconducting state are the coherence length $\xi=\hbar V_F/\pi\Delta_o$ (V_F is the Fermi velocity), the thermodynamic critical magnetic field $H_c=(4\pi D(E_F)\Delta_o 2)^{\frac{1}{2}}$ and the London penetration depth $\lambda_L=(mc^2/4ne^2)^{\frac{1}{2}}$ (m is twice the electron mass and n is one-half the conduction electron density).

BCS theory was developed originally to explain the occurence of low temperature superconductivity through phonon mediated electron-electron interactions. As such, V was identified as the electron-phonon coupling constant and, consequently, it has been shown that[1] $g\leq\frac{1}{2}$; in addition, $\hbar\omega_o$ was approximately equal to the phonon cut-off energy, the Debye energy, so that $T_c\leq 35K$ in accordance with Eq.(1).

In this analysis, BCS theory is utilized as a generic superconductive electron-electron pairing theory, where V is considered to be a generalized electron-charge deformation coupling constant, and $\hbar\omega_o$ is assumed to be a cut-off energy for high frequency electron collective excitations.

For arbitrary values of "g" and $\hbar\omega_o$, the zero temperature energy gap is found by direct integration of Eq.(2) to be

$$\Delta_o=\hbar\omega_o/\sinh(1/g) \tag{3}$$

Solving for $\hbar\omega_o$ in Eq.(3) and substituting this result into the upper limit of Eq.(1), we get

$$\frac{1}{g}=\int_o^{[R(g)/4]\sinh(1/g)}\frac{\tanh y}{y}dy \tag{4}$$

where R(g) is given by

$$R(g)=2\Delta_o/kT_c \tag{5}$$

Although $2\Delta_o$ and kT_c depend on both "g" and $\hbar\omega_o$, it is clear that $R(g)=2\Delta_o/kT_c$ depends only on "g". A straightforward analysis of Eq(4) shows that R is bounded,

with a range $3.51<R<4$ as $o<g<\infty$. A numerical integration of Eq(4) shows the explicit dependence of R upon "g"; the resulting numerical integration is displayed in Fig. I.

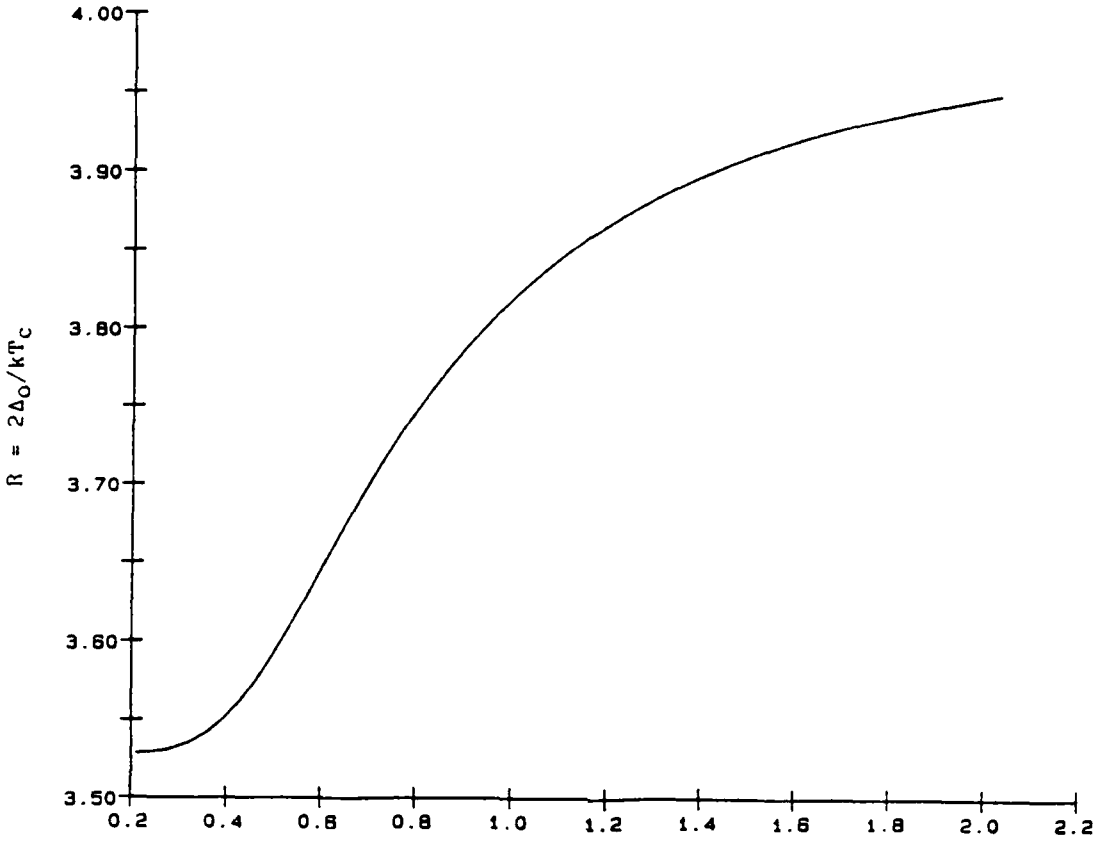

FIG. I Numerical Integration of Eq.(4) to obtain $R(g) = 2\Delta_o/kT_c$

Interestingly, there have been many reported experimental observations[2] of $R > 4$ in high temperature superconducting materials. Actually, values of $R > 4$ can be achieved within BCS theory if the generalized electron-charge deformation coupling constant V used in "g" is assumed to be temperature dependent. Letting $g_c=D(E_F)$ $V(T_c)$ and $g_o=D(E_F)$ $V(T=0)$, it can be shown from the BCS theory that (assuming that the cut-off energy for the interaction is independent of temperature)

$$R = 4\frac{g_o}{g_c} \tag{6}$$

in the strong coupling limit ($g_c>>1$) and

$$R = 3.51\, e^{-\frac{1}{g_o}\left(1-\frac{g_o}{g_c}\right)} \tag{7}$$

in the weak coupling limit ($g_c, g_o < \frac{1}{2}$). For values[3] of

$$\frac{g_o}{g_c} > 1$$

it is clear from Eq.(6) that R can be greater than four in the strong coupling limit, and less than "3.51" (as seen from Eq. (7) in the weak coupling limit.

It then follows from this analysis that the coherence length can be written explicitly as

$$\xi = 2\hbar V_F / \pi R(g) k T_c \tag{8}$$

where R(g) is bounded as shown in Fig. I. The inverse dependence of coherence length on critical temperature raises a major point concerning the spatial extent of the high temperature superconductive pairing interaction. The coherence lengths are quite small at $T_c \simeq 95K$, approaching the size of a unit cell. For example, using values of $2\Delta_o/kT_c = 3.9$ and $\Delta_o \simeq 20$ mev from recently reported[2] results on single crystal thin films of $YBa_2Cu_3O_7$, we find that $g \simeq 1.42$ from Fig. I and $\hbar\omega_o \simeq 11.48$ mev from Eq.(3). Using these parameters and rough estimators for V_F and $D(E_F)$, the coherence length, the distance over which two electrons attract in the superconductive pairing interaction, is quite small, about 15 angstroms, and the London penetration depth, the penetration distance of a magnetic field into the superconductor, is quite large, about 1400 angstroms. For these magnitudes of coherence length and penetration depth, the superconductor is categorized as an extreme type-II superconductor with an extremely small lower critical magnetic field and huge upper critical magnetic field (the lower critical magnetic field is the field below which the superconductor is perfectly diamagnetic; the upper critical magnetic field is the field above which the superconductivity is totally quenched); lower critical fields are very low giving rise to limited effectiveness in shielding large magnetic fields (see Table I).

TABLE I. COMPARISON OF LOW/HIGH TEMPERATURE SUPERCONDUCTOR PROPERTIES

	CONVENTIONAL LOW T_c	NEW HIGH T_c
CRITICAL TEMPERATURE	~1-25½K (HELIUM TEMP)	~95½K (LIQ N TEMP)
CURRENT DENSITY	~10^6 Amp/cm^2	~10^3 Amp/cm^2 ~10^5 Amp/cm^2 on $SrTiO_3$
CRITICAL MAGNETIC FIELDS		
H_c	~0.6 kGauss	~10 kGauss
H_{c1}	~0.4 kGauss	~0.7 kGauss
H_{c2}	~ 3 kGauss	≳ 150 kGauss
PENETRATION LENGTH	~400 Å	~1400 Å
CRITICAL LENGTH	~1000 Å	~15 Å
ENERGY GAP	~0.1 mev	~50. mev
MECHANISM	-LATTICE DEFORMATION	-ELECTRONIC

It is interesting to note that in high temperature superconductors, the coherence lengths are about the size of a molecular unit cell so that the superconductivity is confined to a very small microscopic region of the sample. In contrast (see Table I), in a low temperature superconductor such as niobium, the coherence lengths are many hundred times larger than a unit cell thereby rendering the superconductivity truly macroscopic. The localized nature of the superconductivity makes the high temperature superconductors more sensitive to radiation and very unattractive for technologies that require ultrathin, laterally homogeneous, spatial tolerances such as Josephson junctions.

Because high temperature superconductivity is confined to an atomically microscopic region, there will be many limitations to conventional applications of this material even if it were fabricated in a perfect form. The atomic confinement gives rise to very anisotropic superconducting properties and suggests the need for a transport theory based on electron pair hopping; the anisotropy may in fact be helpful in exploiting many unconventional applications not thought

possible with relatively isotropic, low temperature superconductors - this conjecture remains as a challenge and opportunity to explore novel applications of high temperature superconductivity heretofore not possible with low temperature superconductivity.

The atomic nature of high temperature superconductivity inferred by such small coherence lengths suggests that the macroscopic electromagnetic and transport properties may well be described by electron-pair dynamics and dispersion through a large array of identical superconducting cells or weak links. The author is currently pursuing a high temperature phenomenological theory based on such a model; detailed results of the theoretical analysis as well as comparison with available experimental parameters will be forthcoming shortly.

Current experimental evidence indicates that the superconductivity arises from the interaction of electrons from neighboring atomically thin sheets of dense electric charge through interconnected electron channels; these channels are believed to arise from bridged oxygen atoms present in the $(RE)Ba_2Cu_3O_7$ configuration. While the presence of oxygen is vital to the occurrence of high temperature superconductivity, its volatility in the perovskite system makes the material somewhat unstable to environmental and external chemical activity. As an alternative it might be possible to develop man-made structures that provide an interaction similar to the one described above thereby yielding controllable, high temperature superconductivity under more desirable environmental and device processing conditions.

In summary, the fundamental technological issues described herein must be addressed and resolved if high temperature superconductivity is to be realized in many commercial and military applications. The primary challenge is to identify opportunities for possible near term technology insertion, while looking for new applications heretofore not possible with low temperature superconductors, and exploring alternatives to ceramics, perhaps artifically created structures, to exploit this remarkable phenomenon for future technology applications.

ACKNOWLEDGEMENTS

The author acknowledges assistance from E. Potenziani for the numerical integration of Eq.(4), and from C.S. Kavina for the preparation of the manuscript.

REFERENCES

1. J. M. Blatt, Theory of Superconductivity, p.206, Academic Press, New York (1964).
2. J. Kirtley, R.T. Collins, Z. Schlesinger, W. Gallagher, R. Sandstrom, T. Dinger, and D. Chance, Phys Rev B., V35, 8846 (1987).
3. A. Rothwarf, Phys. Lett., V26A, 43 (1967).

THIS PAGE IS INTENTIONALLY BLANK

Presented at the Workshop on High Temperature Superconductivity
23-25 May 1989 GACIAC PR-89-02

OVERVIEW OF MATERIALS PROPERTIES

J. L. Smith, W. L. Hults, A. P. Clarke, and K. A. Johnson
Exploratory Research and Development Center
Los Alamos National Laboratory
Los Alamos, New Mexico 87545

Some of the history of superconductivity is reviewed from a materials point of view. It is suggested that dielectric properties are important to high T_c superconductivity. Details for the production and use of high quality $YBa_2Cu_3O_{7-\delta}$ are presented.

Recently the history of superconductivity has become: the discovery in 1911 by Kamerlingh Onnes; the Meissner effect and Bardeen-Copper-Schrieffer (BCS) theory came along; and then finally Bednorz and Müller discovered high T_c superconductivity in 1986, after a long spell of no progress. There are even people who believed that the BCS theory was so comprehensive that there was nothing left to do from 1957 until high T_c's showed up. This view ignores a great deal of materials work on superconductivity, which seems to have become respectable science only in recent years. For example, NbN was found to be superconducting at about 15 K in 1941, which moved T_c's from the liquid helium range into the pumped liquid hydrogen range.[1] This is the first paper ever to advertise high T_c's. This caused a flurry of interest in NbN as an infrared detector by both Germany and the U.S. during World War II, but no use of this discovery was made by the time the war ended. It was not until 1960 that the first application for superconductors was found. The story of how Rudi Kompfner challenged Bernd Matthias to make something useful out of superconductors is chronicled in Physics Today.[2] This challenge led to the first high field superconducting magnet by the end of 1960. Quantum interference devices based on Josephson junctions of niobium were developed within ten years. However, it is the materials of superconductivity that is the topic here, and Bernd T. Matthias deserves the most credit for making a science of their quest. He was a student of Paul Scherrer at the ETH in Zurich. For his thesis, he grew single crystals of barium titanate from a barium chloride flux and discovered the ferroelectric properties of this Perovskite. This is a now familiar theme of searching for new physics in unexplored materials. W. H. Zachariasen and Enrico Fermi in 1950 encouraged Matthias and John K. Hulm to switch their successful and structural-chemical approach from super dielectrics to superconductors because superconductivity had no theoretical model. Their switch and subsequent success led to an enormous number of new materials that, by the measure of high T_c, culminated in 1973 with John Gavaler's 23 K for Nb_3Ge.[3] By the early 1980's it had also become clear that the so-called heavy-electron materials contained a new class of superconductors. Although all of their transition temperatures were below 1 K, their very unusual properties awakened sleeping theoretical interest in superconductivity.[4]

Matthias, from the time he first heard of the BCS theory, believed that the theory only applied to the p-electron metals, those on the right side of the periodic table of the elements. Clearly, the transition metals are more complex.[5] For example, their superconducting isotope effects on T_c do not follow the BCS theory. Superconductivity and magnetism fight each other for the ground state in these d- and f-electron elements.[6] However it is compounds, not the pure elements, that hold the applications of interest in superconductivity. Figure 1 shows the resistivities of: Nb_3Sn, an A-15 compound in the family of niobium-based, formerly high T_c compounds; several uranium-based heavy-electron superconductors; and $YBa_2Cu_3O_{7-\delta}$, a recent high T_c material.[7] As the Nb_3Sn is cooled from room temperature, its resistivity does not drop linearly as for a typical metal. It drops more slowly leading to a characteristic shape containing a "bulge" above linearity. This bulge remains the only known precursor of superconductivity, something that signals that superconductivity may occur at a lower temperature. It arises because an enhanced electron-phonon scattering maintains the resistivity at a rather high value as the material cools. It is the electron-phonon interaction that is at the heart of the BCS theory, and their enhanced interaction makes these A-15 compounds such good superconductors.[8] One can then take the point of view that the electron-phonon superconductors are *bad* metals because this bulge is so different from the behavior of a typical metal.

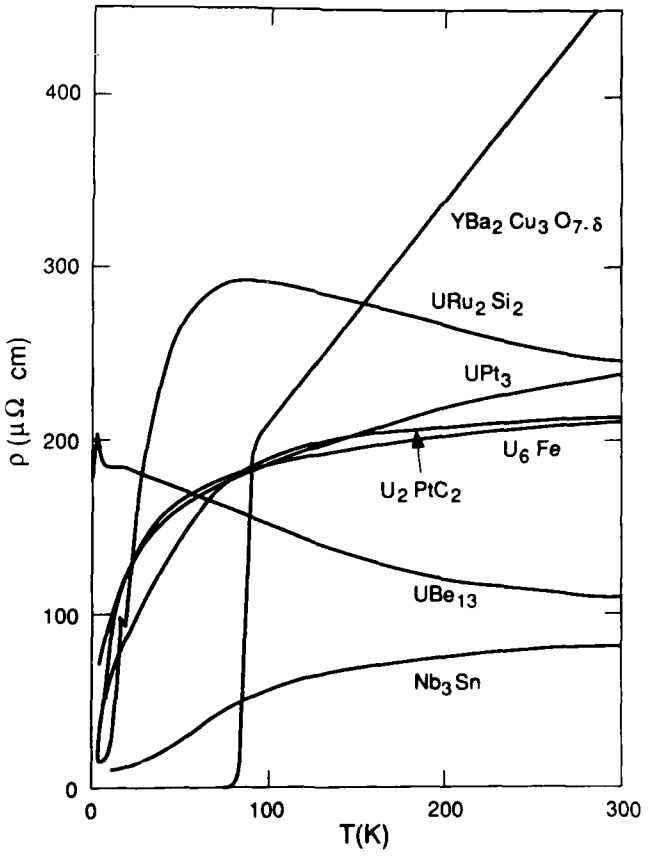

Figure 1. The resistivity of several superconductors.

The heavy-electron superconductors in Fig. 1 show properties near room temperature that suggest they would order antiferromagnetically at low temperatures. Their magnetic susceptibilities indicate local moments and an antiferromagnetic interaction. This is seen in a plot of inverse susceptibility that extrapolates to zero at a negative temperature. However, near 1 Kelvin these materials superconduct. Their large entropy, which seems to be about the right magnitude for an electron spin system, goes into a huge superconducting anomaly in the heat capacity proving that the entropy must be associated with the conduction electrons. This can be viewed as conduction electrons with a large (100-1000 enhancement) effective mass compared to bare electrons. This is the source of the appellation heavy-electron superconductor. It is now generally believed that some sort of magnetic interaction is the cause of the unexpected superconductivity, and as its characteristic energy is tens of Kelvins, the huge scattering in Fig. 1 (much greater than a bulge) is magnetic in its origin. We think we know what a superconductor looks like when magnetic interactions are the source of the superconductivity; it looks like the heavy-electron types. These superconductors could be called *bad* antiferromagnets, because above 100 K they look magnetic. But something goes wrong as they are cooled, and they superconduct near 1 K.

Figure 1 also shows the high T_c superconductor $YBa_2Cu_3O_{7-\delta}$. Its resistivity is quite high, but one ascribes that property to so few charge carriers. The resistivities of all *quality* high T_c materials are linear (not semiconducting), and hence, look very metallic.[9] So what is going on? If we know what electron-phonon and magnetic superconductors look like, what are these? Let us consider the genealogy of the scientists. K. Alex Müller, like Matthias, was a student of Scherrer who had them both cut their teeth on ferroelectrics. C. W. Chu was a Matthias student; M. K. Wu was a Chu student. Thus, their $YBa_2Cu_3O_{7-\delta}$,[10] in Fig. 1 has in some sense, its origins in ferroelectrics and Perovskites. High dielectric constants have been found in related materials.[11] W. A. Little, long ago considered that a dielectric and some nearby electrons could lead to high T_c superconductivity.[12] The point is quite simple: if one is studying Perovskites, where large dielectric constants and ferroelectricity show up, perhaps the presence of carriers that go superconducting can do so from the point of view that the material is a *bad* ferroelectric. After all, linear resistance is not the sign of a *bad* metal and weakly temperature-dependent susceptibility near room temperature is not the sign of a *bad* antiferromagnet.

This sort of reasoning is not what gave respectability to looking for new superconductors, but it is how the superconductors were found. However, in order to justify so many measurements on the new materials, where the goal is to understand the source of the high T_c superconductivity, logic demands high quality samples. This field has seen many bad samples studied with very precise experiments. At Los Alamos many small groups of people are working to produce various materials and in various forms, all of very high quality. It seems appropriate to describe the findings of one of these efforts for bulk $YBa_2Cu_3O_{7-\delta}$ (Y123). Each of the findings is very important.

The goal was to push the most generally useful synthesis technique to its limits, rather than try various techniques. The starting materials were Y_2O_3, $BaCO_3$, and CuO. In high purity form and after at least 24 hours of drying, reproducible stoichiometry was achieved including slight adjustments of starting weights made as indicated

by chemical analysis of the final product. Stoichiometry much better than 1 % is needed if second phases at grain boundaries are to be avoided. The poorly mixed powder is put into agate vials with agate balls and shaken very vigorously for 24-48 hours. The amount of powder in the vial must be adjusted so that it remains loose and attains an almost normal distribution of submicron particle size. This material is compressed in a die to a modest ≈ 1/2 kbar pressure and placed on a finished disk of Y123 in a platinum crucible. It is capped with an inverted platinum crucible (loose fitting) as a radiation shield, and put into an air furnace at 940°C. Up to 100 grams of starting powder can be processed in a single batch. Larger quantities have not been tried. Liquid phase sintering must be avoided as it leads to macroscopic separation of phases, which this recipe avoids. This submicron starting powder, heated in a differential scanning calorimeter, shows only a small endothermic peak from 790 to 820°C (from a phase change in the $BaCO_3$ or reaction of the $BaCO_3$ with CuO) up to formation of a liquid phase immediately above 940°C. It should be noted that air pressure in Los Alamos is usually below 600 mm Hg.

In this air furnace, the temperature is dropped to 890°C and immediately reheated to 940°C every four hours as fast as the furnace will cycle, which is about 15 minutes. After about one week of this thermal cycling, the weight change of the sample shows that the CO_2 is gone. At the temperatures of cycling, no feature appears in a differential scanning calorimeter check of the final product. Also, it does not serve to assist in venting CO_2 from the furnace. It clearly enhances grain growth, and over a period of weeks, can bring back homogeneity to a sample that has suffered from liquid phase sintering. Thus, it seems that the 50°C cycle puts in some strain or possibly microcracks in this highly anisotropic material that promotes grain growth and concomitant homogenization. The best material is very porous (less than 70% dense), fine grained, and homogeneous. This porosity makes possible the full oxygenation of the material at the end of the process.

This material is then pulled from the hot furnace; ball-milled for 8-12 hours; repressed; and put back into the furnace for cycling for about 48 hours. More of these steps can be used which seems to not change the superconducting properties. They may offer a slight reduction of second phases (already well below the 1% level). The material is pulled again and upon a final 8-12 hours of ball milling, the pressed pellets (again resting on an old Y123 sample with two platinum crucibles) are put into an oxygen (1 bar) furnace at 430°C. It is heated to 920-960°C (the precise temperature is not critical) in 4-6 hours, sintered for 24 hours, cooled to 430°C in 4-6 hours, heated back to 920-960°C in 4-6 hours, sintered for 2-12 hours, cooled to 430°C in 12-36 hours, left to oxygenate at 430°C for 1-7 days, and pulled from the furnace. This extra cycling is useful, probably because of enhanced cracking to keep the porosity high. A slight improvement in the superconducting transition width occurs if the oxygen is switched to nitrogen or helium during the final sinter and switched back to oxygen after the furnace is at 430°C. We are still investigating this observation.

These pellets show the sharpest transitions (around 93K) that have been observed here. The critical currents (measured with dc current) are around 300 A/cm^2. The pellets are quite stable in air, showing no change in superconducting properties over months. However scanning electron microscopy shows some deterioration after a

few days. These disks show impurity phase levels that are possibly as low as 100 ppm in the 1 μm surface layer.[13] The rf surface resistance of these disks is lower than any we know of for any polycrystalline high T_c material. It is well below copper, and is inferior only to single crystals of Y123.[14] Furthermore, the superconducting shielding fraction of this material is unchanged by grinding (until particle size is of the order of the superconducting penetration depth), a property that we have seen in no other Y123 material. We emphasize that this material is remarkably free of second phases and homogeneous by all of our measurements. A differential scanning calorimeter measurement on the final product shows *nothing* until the sample melts ca. 1000°C.

We are presently investigating how this material can be used to further our work on applications. It is obviously desirable to take this material to greater than 90% of theoretical density to lock in the oxygen. We have been using shock waves to achieve this. In the past year, as we have learned how to improve our material, we have moved the critical current from zero to 200 A/cm^2. Analysis of the amount of cracking shows that the 200 A/cm^2 material is carrying 10^6 A/cm^2 between cracks, in agreement with critical current measurements on the material deduced from hysterisis measurements in a squid magnetometer at 75 K. In these 200 A/cm^2 materials the oxygen concentration is unaltered by heat treatment, and we are now studying how to further heal the cracks. Clearly, the production and study of these high quality materials are critical to the development of applications of high temperature superconductors.

We thank B. I. Bennett, D. W. Cooke, M. P. Maley, W. J. Medina, F. M. Mueller, E. J. Peterson, J. A. O'Rourke, R. B. Schwarz, J. D. Thompson, and J. O. Willis for their assistance and enthusiasm. APC's present address is : Sputtered Films Inc., 314 Edison Avenue, Santa Barbara, CA 93103. Work performed under the auspices of the U.S. Department of Energy, Office of Basic Energy Sciences, Division of Materials Sciences and the U.S. Department of Defense, Defense Advanced Research Projects Agency.

REFERENCES

1. G. Aschermann, E. Friederich, E. Justi, and J. Kramer, Physik. Zeitschr. *42*, 349 (1941).
2. J. K. Hulm, J. E. Kunzler, and B. T. Matthias, Physics Today, January 1981, p.34.
3. See e.g. *Superconductivity in d- and f- Band Metals*, D. H. Douglass ed. (Plenum, New York, 1976).
4. See e.g. Z. Fisk, D. W. Hess, C. J. Pethick, D. Pines, J. L. Smith, J. D. Thompson, and J. O. Willis, Science *239*, 33 (1988).
5. B. T. Matthias, *Superconductivity*, F. Chilton, ed. (North-Holland, Amsterdam, 1971) p.69.
6. J. L. Smith and E. A. Kmetko, J. Less-Common Metals *90*, 83 (1983).
7. Z. Fisk, H. Borges, M. McElfresh, J. L. Smith, J. D. Thompson, H. R. Ott, G. Aeppli, E. Bucher, S. E. Lambert, M. B. Maple, C. Broholm, and J. K. Kjems, Physica C *153-155*, 1728 (1988).
8. Z. Fisk and A. C. Lawson, Solid State Comm. *13*, 277 (1973); Z. Fisk and G. W. Webb, Phys. Rev. Lett. *36*, 1084 (1976).
9. Z. Fisk, private communication.
10. M. K. Wu, J. R. Ashburn, C. J. Torng, P. H. Hor, R. L. Meng, L. Gao, Z. J. Huang, Y. Q. Wang, and C. W. Chu, Phys. Rev. Lett. *58*, 908 (1987).
11. D. Reagor, E. Ahrens, S-W. Cheong, A. Migliori, and Z. Fisk, Phys. Rev. Lett. *62*, 2048 (1989).
12. See e.g. W. A. Little, ref. 5, p.50.
13. D. W. Cooke, M. S. Jahan, J. L. Smith, M. A. Maez, W. L. Hults, I. D. Raistrick, D. E. Peterson, J. A. O'Rourke, S. A. Richardson, J. D. Doss, E. R. Gray, B. Rusnak, G. P. Lawrence, and C. Fortgang, Appl. Phys. Lett. *54*, 960 (1989).
14. D. W. Cooke, E. R. Gray, R. J. Houlton, B. Rusnak, E. Meyer, G. P. Lawrence, M. A. Maez, B. Bennett, J. D. Doss, A. Mayer, W. L. Hults, and J. L. Smith, submitted to Phys. Rev. B.

Abstract of Paper Presented at the
Workshop on High Temperature Superconductivity
23-25 May 1989 GACIAC PR 89-02

Structure and Properties Correlation in High T_c Superconductors

Dr. M.K. Wu
Department of Materials Science
Henry Krumb School of Mines
School of Engineering and Applied Sciences
Columbia University

ABSTRACT

Two years ago, an empirical correlation on the formation of oxide compounds with proper perovskite structure was developed. By assuming an optimum condition in the framework of this primitive correlation in conjunction with the crystal structure of the superconducting La-M-Cu-O (214) system, we determined the nominal composition and subsequently discovered the first 90 K oxide superconductor Y-Ba-Cu-O (123). Based on a similar argument we also predicted the substitution of bismuth to yttrium. Another oxide Y-Sr-Cu-O with T_c at 85 K was also discovered under the same empirical protocol. Recently, by carefully examining all the existing high T_c oxide superconductors, an improved correlation between the superconducting transition temperature and the interplanar (CuO planes) distance was found. Detailed structure and properties correlation of the high T_c superconducting oxides will be discussed.

THIS PAGE IS INTENTIONALLY BLANK

Presented at the Workshop on High Temperature Superconductivity
23-25 May 1989 GACIAC PR 89-02

SUPERCONDUCTIVITY IN HIGH MAGNETIC FIELDS: NEW PROBLEMS AND ISSUES

L. E. De Long
Department of Physics and Astronomy
University of Kentucky
Lexington, KY 40506-0055

ABSTRACT

An overview is given of the present understanding of the upper critical magnetic field H_{c2} of high temperature and other exotic superconductors. Traditional models of H_{c2} and their failures are summarized. Topics for further research are surveyed, including flux creep, anisotropic pairing, Fermi surface instabilities, field- and temperature-dependent normal state properties, heavy Fermi liquid and strong coupling effects, superconducting glass phases, and their potential influence on H_{c2} are discussed. Particular emphasis is given to the unexplained phenomenon of positive curvature of the phase boundary at low fields.

I. Anomalous Critical Field of High Temperature Superconductors

Although high temperature oxide superconductors (HTO) have been known since late 1986 [1], accurate determinations of many of their fundamental superconducting and normal state properties are still lacking. Early measurements [2-4] of the upper critical magnetic field H_{c2} on sintered samples yielded immeasurably high values at finite temperatures and pronounced positive curvature of the phase boundary (see Fig. 1). However, substantial broadening of the resistive transition curves in applied magnetic fields was also continually observed, and impeded clear interpretation of data.

This behavior persisted in subsequent measurements on higher quality sintered samples and single

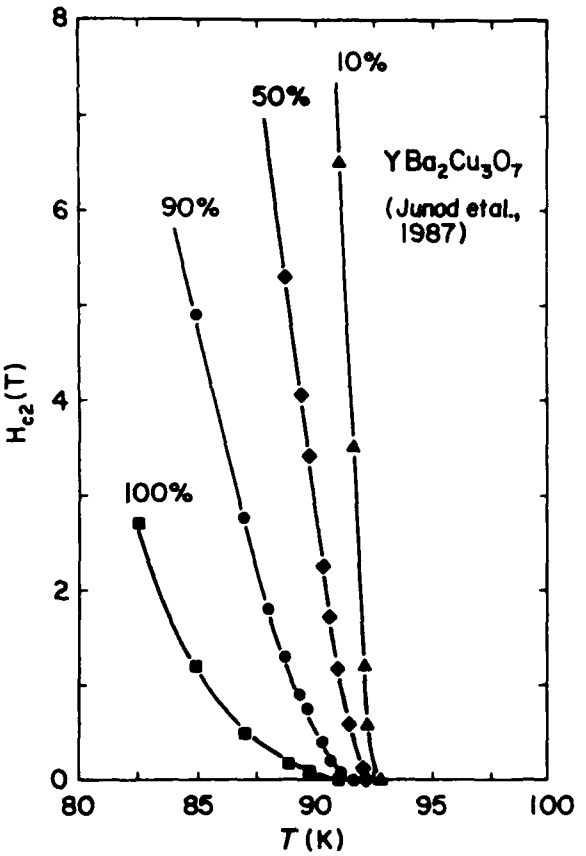

Fig. 1. Upper critical field H_{c2} vs. temperature T for polycrystalline $YBa_2Cu_3O_7$. The successively lower-temperature curves correspond to resistive transitions that are 10, 50, 90, and just 100 % complete, respectively. After Ref. 4.

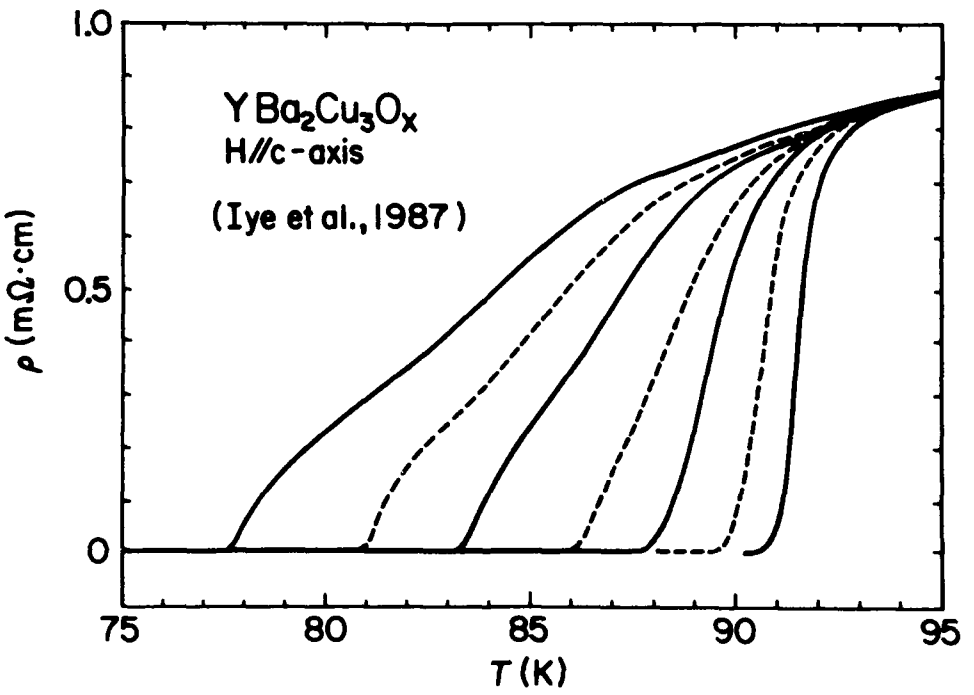

Fig. 2. Resistivity ρ vs. temperature T for a single crystal of $YBa_2Cu_3O_x$ with magnetic field H applied parallel to the tetragonal c-axis. The successively lower-temperature curves correspond to H = 0, 3, 10, 20, 40, 60, and 90 kOe, respectively. After Ref. 6.

crystals [5,6] (see Fig. 2). Inhomogeneities in cation doping and oxygen stoichiometry or twinning were widely suspected to be responsible for poorly defined transition anomalies. In addition, rapid decreases of the critical current density J(T,H) with increasing field H and temperature T [7,8], and finite resistivity $\rho(T,H)$ below the onset temperature T_o [5,6] continually appeared, even in the most carefully prepared samples.

More recent work [9-11] suggests that the extremely short coherence length at T=0, ξ_o, and the high anisotropy and weak c-axis coupling of CuO layers leads to a very weakly pinned flux lattice. It now seems likely that a substantial part of the observed smearing of transition anomalies and degradation of superconducting properties is a result of strong, thermally activated flux creep--a situation that threatens the development of many proposed applications of existing materials.

However, similar anomalies have also been observed in other materials where it is probable that different mechanisms are at play. Field and temperature dependences of the normal state properties [12-18], as well as competing groundstates such as charge- and spin-density waves (CDW and SDW), can also cause positive curvature and low temperature enhancement of $H_{c2}(T)$ [19,20].

Additional research will be necessary to determine the microscopic interactions that give rise to the anomalous behavior of H_{c2} for HTO. Important information concerning the microscopic mechanism of superconductivity can be derived from measurements of the upper critical field.

II. Origin of the Upper Critical Magnetic Field

Shortly after the discovery of superconductivity, H. K. Onnes and W. Tuyn [21,22] discovered that magnetic fields had an adverse effect on T_c. Several decades passed before microscopic arguments could be given to explain the antagonism between magnetism and superconductivity. Essentially all of our current understanding is based on the BCS model for electron-phonon-induced superconductivity [23], although a variety of interactions or many-body effects can theoretically lead to a superconducting instability [24].

All known superconductors, including the HTO, exhibit behavior (e.g., the Josephson effect and flux quantization) consistent with correlated motion of paired electrons, as originally hypothesized by Cooper [25]. The BCS theory assumes that correlations between paired electrons and the positive ions of the crystal lattice reduce the Coulomb energy of the crystal and lead to a phase transition at T_c. The net reduction in electronic energy is represented by the superconducting gap energy $\Delta(T)$, as shown in Fig. 3. The simplest example of such a state is a pair of single-electron Bloch functions with crystal momenta $\mathbf{k}$ and $-\mathbf{k}$, and spins σ and $-\sigma$, respectively, moving in an "isotropic" environment (e.g., a s-band in a simple cubic crystal).

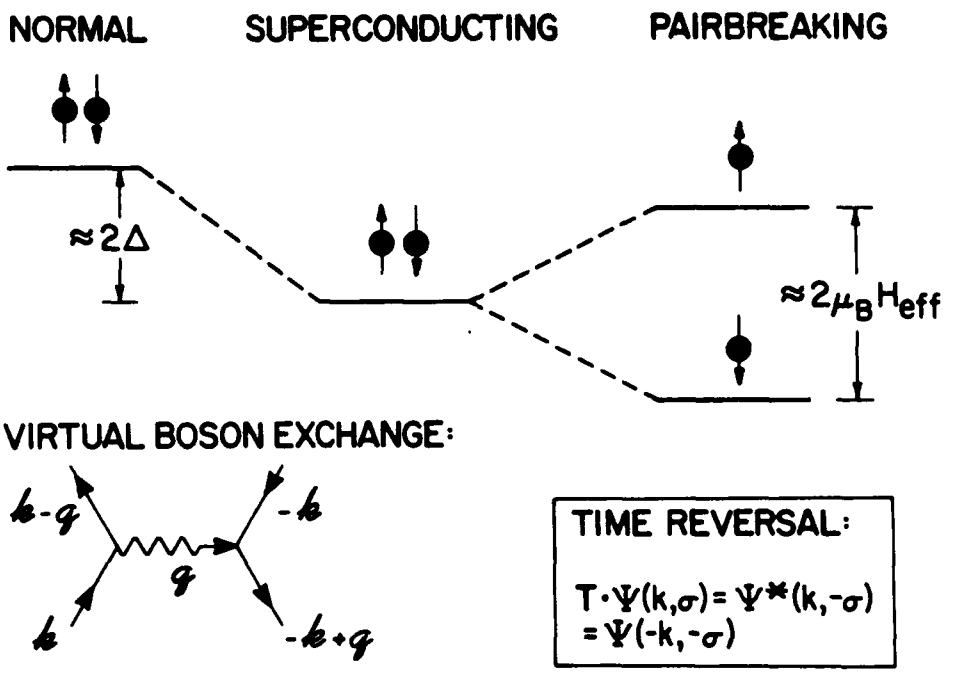

Fig. 3. Cooper pairing of electrons results in the lowering of the energy of an electron pair by 2Δ, twice the gap energy. This energy advantage is optimized via exchange of a virtual phonon of wavevector **q** between electron states Ψ whose wavevectors **k** and spins σ are conjugates under time reverse (**T**). Magnetic perturbations break time reverse symmetry and destroy the equivalence of the electrons of a pair; and this is schematically shown as a splitting ("breaking") of the Cooper pair by an effective field H_{eff}. However, such pairbreaking interactions are best thought of as drastically reducing the Coulomb correlation energy gained by the Cooper pairing process.

Moving electrical charges such as Bloch electrons are strongly affected by the application of a magnetic induction **B**, which leads to energy shifts of their quantum states via orbital and spin susceptibilities. Semiclassically, these shifts in energy can be viewed as a consequence of the Lorentz force $\mathbf{F} = (-eh/2\pi m)\mathbf{k} \times \mathbf{B}$ acting on the orbital motion, and the magnetic torque $\tau = -\mu_B \sigma \times \mathbf{B}$ exerted on the spin magnetic moment (Zeeman effect). Note that these interactions change sign between the two members of a Cooper pair.

The Lorentz force acts to reduce the gap by exciting Meissner currents that screen out the applied induction and add kinetic energy to the electronic system; these effects are accompanied by a further loss of gap energy (increase in Coulomb energy) due to the interference of the magnetic forces with the correlated motion of Cooper pairs wherever **B** is nonzero. The Zeeman effect stablizes the spin-down electrons in the normal state at higher field strengths. These hostile effects on the superconducting state are known as "magnetic pairbreaking", since they remove the symmetry between the two states of a Cooper pair, as illustrated in Fig. 3. The Lorentz force is associated with "orbital pairbreaking" coupled

to **k**, and the Zeeman interaction is denoted as "Pauli pairbreaking", since the coupling between **B** and σ in the normal state is via the Pauli paramagnetic susceptibility.

Anderson pointed out [26] that the fact that the quantum mechanical wavefunction $\Psi(\mathbf{k},\sigma)$ of one electron of a Cooper pair transforms into that of the other under time reversal (note that $\mathbf{T}\,\Psi(\mathbf{k},\sigma) = \Psi^*(\mathbf{k},-\sigma) = \Psi(-\mathbf{k},-\sigma)$ for a Bloch function) was a crucial aspect of Cooper pairing. De Gennes [27] has given a simple and elegant explanation of how magnetic interactions lead to the breaking of time-reverse pairs and a reduction in the transition temperature, and the reader is referred to this discussion for further details. Werthamer, Helfand, Hohenberg and Maki [28] calculated $H_{c2}(T)$ via a gauge-invariant solution of the Gor'kov equations for finite T and H, and arbitrary electronic mean free path l_{tr}, including spin-orbit scattering and Pauli pairbreaking. The underlying physics of the WHHM model is quite basic and fundamental, although there are a number of simplifying assumptions that should be noted:

1) Isotropic, weak-coupled BCS superconductor with an instantaneous, short-ranged pairing interaction.
2) Semiclassical electron dynamics in the normal state (i.e., no Landau quantization effects).
3) Microscopic parameters such as the Fermi velocity v_F, transport scattering rate τ_{tr}^{-1} and Pauli spin susceptibility χ_p are not T- or H-dependent.

Effective mass (v_F) anisotropy, Fermi liquid renormalizations and multiple band effects can also be included in a variety of approximate extensions of this model [29-31].

An important question is to what extent these assumptions are valid in the case of high-T_c materials. In fact, there is already a substantial body of evidence that these assumptions are not strictly applicable to more conventional superconductors, as will be discussed below.

III. The Intrinsic Pairbreaking Scale $H_{c2}^*(0)$

WHHM provided a general and widely used expression for the upper critical field phase boundary, based on a microscopic theory of electron-phonon pairing in "conventional superconductors":

$$\ln t = U(t,h) \qquad (1)$$

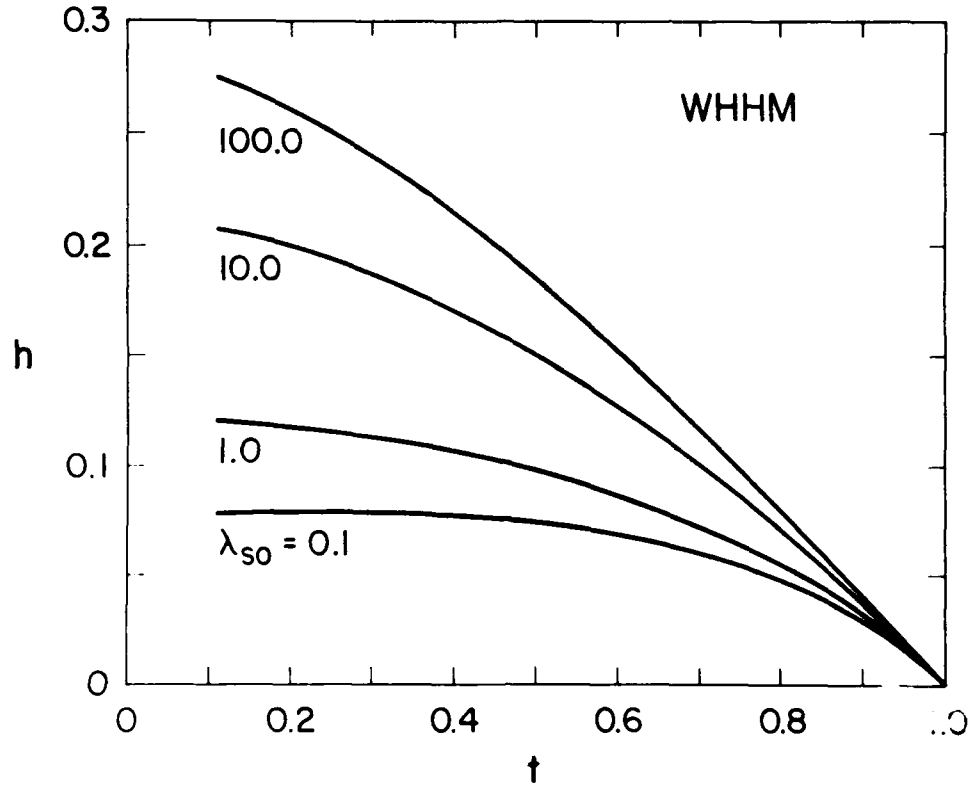

Fig. 4. Reduced upper critical field h vs. reduced temperature t, as predicted by the WHHM model. The different curves correspond to the values of the spin-orbit scattering parameter λ_{so} shown. Note that h cannot exceed the value corresponding to $H_{c2}(T) = H_{c2}^*(T)$.

where $t = T/T_{co}$ and $h \propto H/H_{c2}^*(0)$ are reduced variables for the "universal pairbreaking function" u [30,32]. T_{co} is the zero-field transition temperature. $H_{c2}^*(0)$ is the maximum possible value of H_{c2}, attained only at t=0 in the absence of Pauli pairbreaking [29,30]; in this case, upper critical field data for all superconductors would fall on the same universal curve given in Eq. 1.

Pauli pairbreaking causes only negative deviations from the universal curve of Eq. 1, as shown in Fig. 4. At higher fields [33], the degree of deviation from the universal curve depends on the strength of spin-orbit scattering, parameterized by $\lambda_{so} = h/6\pi^2 k_B T_c \tau_{so}$, where τ_{so} is the spin-orbit scattering time:

$$H_{c2}(T) = H_{c2}^*(T) - \frac{H_{c2}^*(0)}{(1.781)\,\lambda_{so}} \left[\frac{H_{c2}(T)}{H_p(0)}\right]^2 \leq H_{c2}^*(0) \qquad (2)$$

Although it is not widely appreciated, many conventional superconductors have been found to exhibit marked deviations from the predictions of the WHHM model, such as positive curvature of H_{c2}, and the

so-called "spin-orbit catastrophe", whereby the measured $H_{c2}(T \rightarrow 0) > H_{c2}^{*}(0)$, the maximum critical field allowed by the theory [28]. These effects were discussed by Orlando and coworkers [29,31] for A15 materials such as Nb_3Sn, and Decroux and Fischer [30] for certain Chevrel phases such as Mo_6Se_8.

Important clues to these puzzles have been gained in experiments with HF superconductors, whose H_{c2} data deviate markedly from the WHHM predictions [13,14,18]. Moreover, these systems exhibit [34-36] strongly T- and H- dependent heat capacities, magnetic susceptibilities and electrical resistivities just above T_c. Unfortunately, underlying microscopic parameters such as the Fermi velocity v_F (and therefore γ), τ_{tr}^{-1} (and therefore ρ) and χ_p, are assumed not to be T- or H-dependent in the WHHM model [12-14]. *Present-day high purity samples of both HTO and HF superconductors certainly do not satisfy these assumptions*. These complications will be discussed further below.

III. Questions for Further Research

There are a number of mechanisms besides weak flux pinning that could lead to positive curvature of

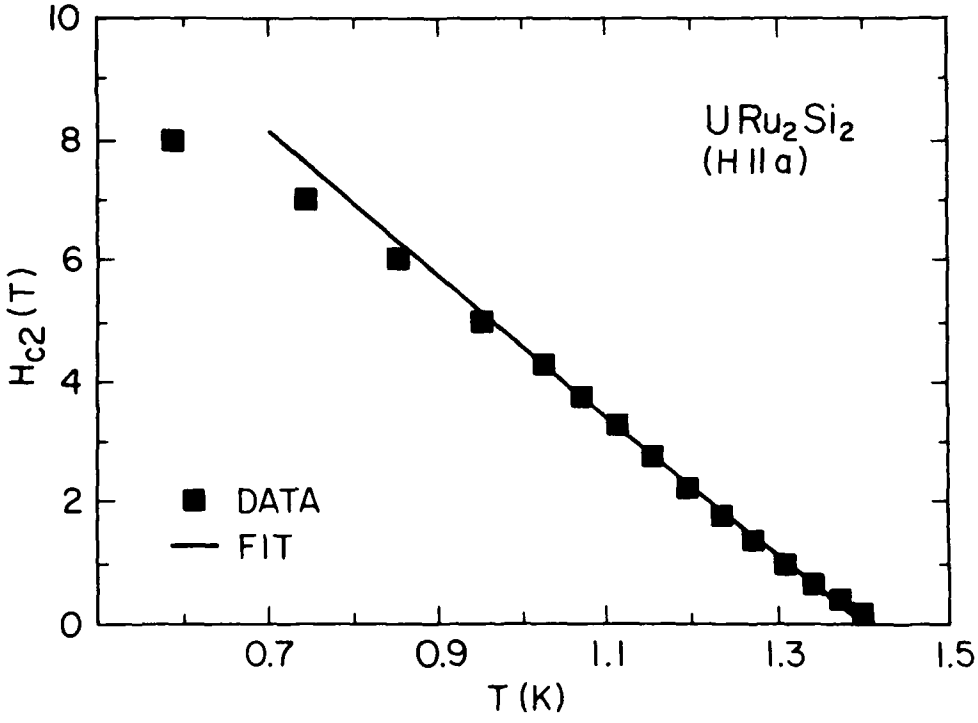

Fig. 5. Upper critical field H_{c2} vs. temperature T for single- crystal URu_2Si_2 with the tetragonal **a**-axis parallel to the applied field **H**. Note that the simple Ginzburg-Landau theory (solid line) is not expected to agree with higher field data. After Ref. 42.

$H_{c2}(T)$. Moreover, the flux creep model cannot explain the enhancement of H_{c2} (i.e., $>H_{c2}^*(0)$) that is already observed in transition metal and heavy fermion materials, or treat the influence of field- or temperature-dependent normal state properties on H_{c2}. We summarize below several of the mechanisms for positive curvature that are most germane to high-T_c materials.

1) **Anisotropic pairing states--** These are "exotic" pairing states (e.g., "d-wave") with order parameters that have lower symmetry than the crystal lattice [37,38]. These states are thought to be responsible for superconductivity in nearly or weakly magnetic heavy fermion compounds. Anisotropic pairing can lead to remarkable effects in finite fields or under stress [39], causing strong positive curvature or kinks in $H_{c2}(T)$, or first order phase transitions far below the H_{c2} phase boundary [40,41]. The more recent H_{c2} results of Kwok et al. [42] show that the positive curvature found for URu_2Si_2 can be interpreted in terms of a theoretical [40] crossover from one component of an anisotropic superconducting order parameter to another due to a coupling with a SDW onset temperature T_m = 17.5 K, as shown in Fig. 5.

However, care must be exercised in interpreting H_{c2} data of even the highest quality. For example, the empirical method of Ref. 12 can be used [43] to produce excellent fits of the entire phase boundaries of UPt_3 and URu_2Si_2, as shown in Figs. 8 and 9, below. On the other hand, more recent H_{c2} data [44] for exceptionally good samples of UPt_3 show evidence of a sharp kink in the phase boundary that cannot be reproduced by any model except for an anisotropic pairing theory [41]. Additional evidence [45] for anisotropic pairing states has been found in the heat capacity data for UPt_3; a double saw-tooth transition anomaly whose field dependence correlates with the existence of the kink in H_{c2} is observed [46].

Similar evidence for anisotropic pairing states has been found for $YBa_2Cu_3O_7$, where a double-saw-tooth anomaly has been seen in the heat capacity in both polycrystalline [47] and single-crystal [48] materials (see Fig. 6); and a kink has been observed in some data for H_{c2} [49] (see Fig. 7). Volovik [50] has offered an analysis of $YBa_2Cu_3O_7$ in terms of anisotropic pairing states perturbed by the orthorhombic distortion of the high-temperature tetragonal crystal lattice. Additional theoretical analyses [51] of the fluctuations near T_c has also provided support for anisotropic pairing in $YBa_2Cu_3O_7$. However, the uncertainties in sample metallurgy due to oxygen defect distribution and symmetry have complicated the identification of the pairing state and its exact relationship to the observed anomalies [52]. Further investigations will be necessary to clarify the phase stability and symmetry of the order parameter of the 1-2-3 and other HTO.

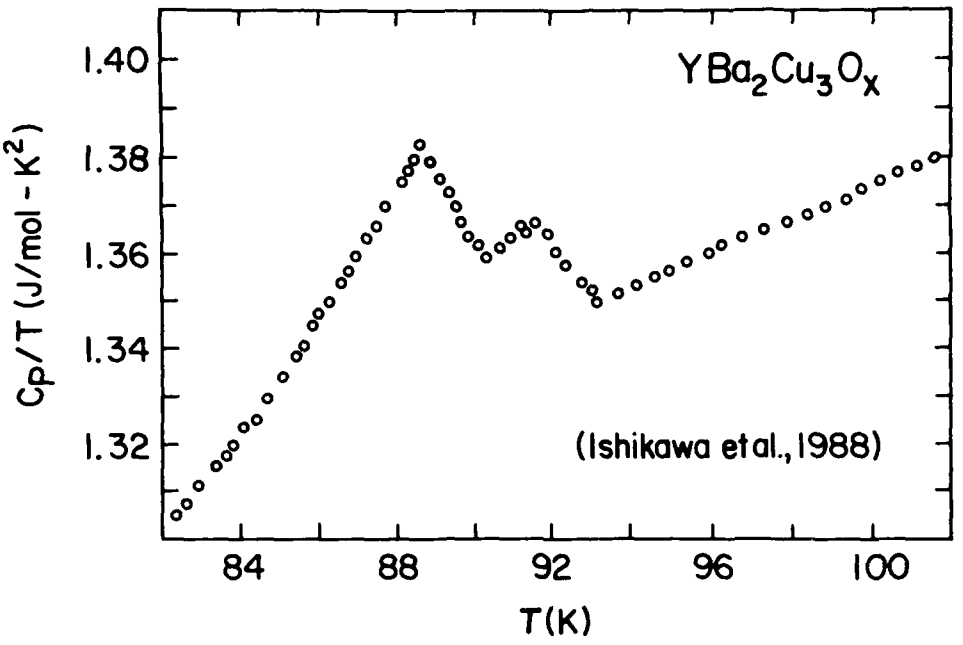

Fig. 6. Heat capacity C_p divided by temperature T versus T for a polycrystalline sample of $YBa_2Cu_3O_x$. After Ref. 47.

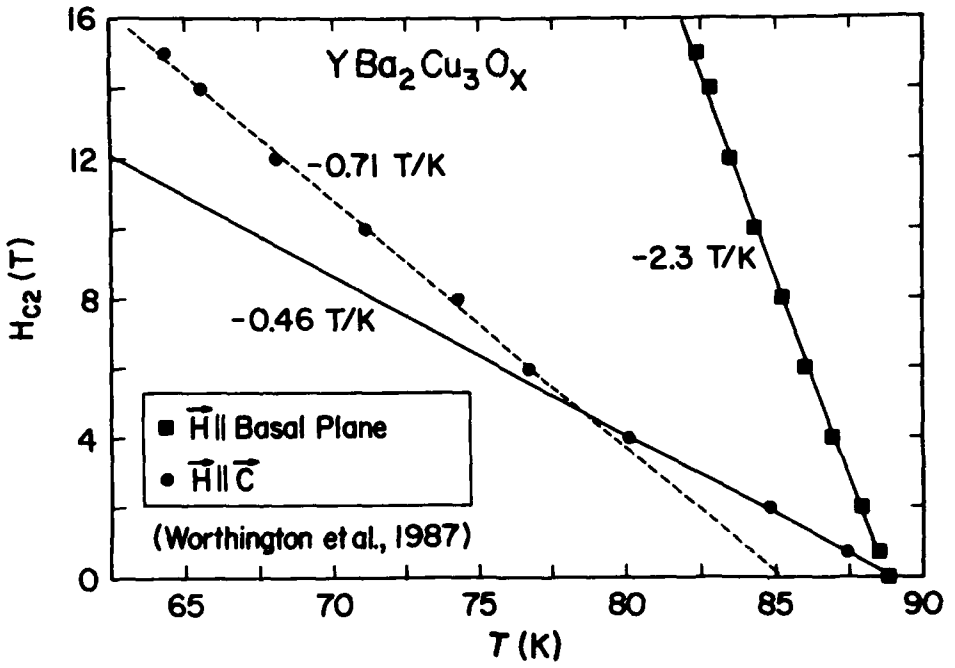

Fig. 7. Upper critical field H_{c2} versus temperature T for a single crystal of $YBa_2Cu_3O_x$. The values of straight-line initial slopes (estimated with solid lines) for two orientations of the applied field H are shown. A lower temperature estimate (estimated with the dashed line) illustrates the interesting possibility of an abrupt change ("kink") in slope due to a change in anisotropic order parameter symmetry. After Ref. 49.

2) **Fermi surface instabilities--** CDW or SDW instabilities are favored in low-dimensional systems such as HTO or layered transition metal dichalcogenides with nesting features or nearly half-filled bands at the Fermi energy. Theoretical arguments [19,20,53] predict the occurrence of positive curvature and the absence of Pauli limiting for superconductors with either CDW or SDW gapping. We may also anticipate the phenomenon of reentrant superconductivity, occuring when two competing order parameters (e.g., superconducting and spin-density wave) are present [54], similar to the case of ferromagnetic superconductors [55].

A number of magnetic measurements [56-59] have demonstrated that long-range magnetic order and superconductivity are mutually exclusive in HTO materials; however, the two phenomena are closely linked in the sense that planar Cu^{+2} moments and strong magnetic fluctuations persist (both above and below T_c) in samples with sufficient carrier doping to be superconducting [60,61]. The onset of superconductivity is evidently connected with the loss of three-dimensional magnetic correlations, possibly resulting in short-range magnetic order of the Cu^{+2} moments or weak spin-density wave order among the conduction holes. These latter phenomena could be difficult to observe, making a correlation between them and upper critical field behavior difficult.

Incommensurate magnetic scattering has been observed in the $(La,Sr)_2CuO_4$ system [61-63], and evidence has been presented for structural modulations or CDW instabilities [64,65], as well as theoretical arguments for Fermi surface nesting [66,67], in a number of HTO materials. However, it is not at all clear what the exact relationship is between these incommensurate structures and T_c. For example, superlattice modulations have been observed [68-70] in the $Bi_2Sr_2Ca_xCu_yO_z$ system, but it appears that the oxygen stoichiometry dominates T_c, independent of the structural modulations [71].

3) **Heavy Fermi liquid renormalizations and field-dependent normal state properties--** Normal state properties such as the electrical resistivity, the Pauli susceptibility, and the electronic heat capacity, may be strongly renormalized by manybody effects in nearly magnetic and/or narrow-band metals, or systems close to a metal-insulator transition [72-75]. The electronic self-energy can become strongly energy dependent under these circumstances, leading to unusual temperature dependences of various physical properties associated with the fermion mass [72].

An early attempt to supplement the WHHM model for manybody renormalizations of normal state parameters was undertaken by Orlando and Beasley [31], although they did not take into account any temperature-dependent effects. In the presence of Pauli limiting, the scale of pairbreaking, and therefore the size of the measured $H_{c2}(T)$, is still set by $H_{c2}^*(0)$, which can be expressed in several different parameterizations (SI units):

$$H_{c2}^*(0) = \eta_1(\lambda_{tr}) \{ (1.661 \times 10^{29}) (\gamma T_{co}/k_F^2)^2 + \gamma T_{co} \rho \} \quad (3a)$$

$$= \eta_2(\lambda_{tr}) \{ (8.226 \times 10^{11}) (T_{co}/v_F)^2 + (T_{co}/v_F) l_{tr}^{-1} \} \quad (3b)$$

$$= \eta_3(\lambda_{tr}) \Phi_o \xi_o^{-2} \{ 1 + (0.882) \xi_o l_{tr}^{-1} \} \quad (3c)$$

k_F is the Fermi wavevector, λ_{tr} is a parameter proportional to $\xi_o l_{tr}^{-1}$, Φ_o is the flux quantum, and the $\eta_i(\lambda_{tr})$ are slowly varying functions that extend the WHHM model to strong coupling. Equations 3a-3c explicitly show the dependence of the pairbreaking scale on normal state parameters. Therefore, the field-

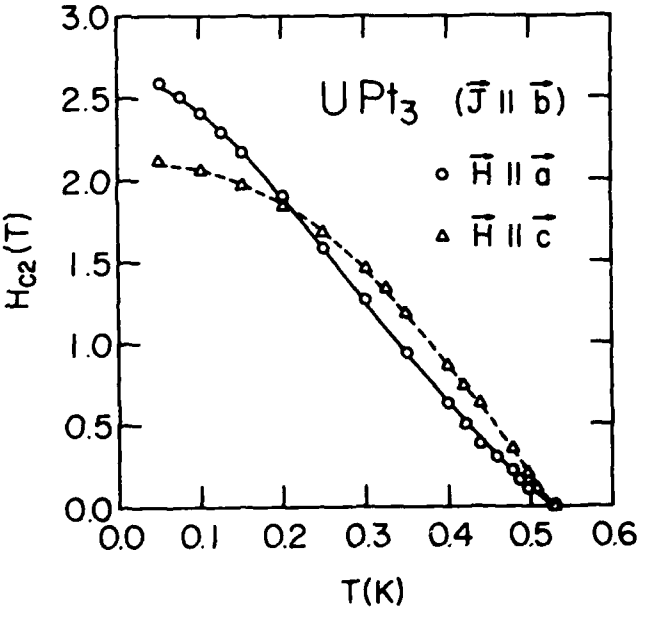

Fig. 8. Upper critical field H_{c2} vs. temperature T for a single crystal of UPt_3, with external field **H** parallel to either the hexagonal **a** or **c** axes, and the measuring current held in the **b** direction. The solid and dashed lines represent model fits of the data obtained by enhancing the intrinsic pairbreaking scale $H_{c2}^*(0)$. After Ref. 12.

and temperature-dependences of these parameters are expected to be evidenced by anomalies in the curvature and magnitude of H_{c2} [12,15,18].

De Long et al. [12] obtained the first quantitative fits of the unexplained and anomalous H_{c2} data for the heavy fermion materials U_6Fe, U_6Co, and UPt_3, using a simple, yet powerful modification of the WHHM model that will be described in more detail below (see Figs. 8 and 9). A key to this success was noting that the anomalous curvatures (positive or negative) of H_{c2} were perfectly correlated with the sign of the magnetoresistance near T_{co} for all of the known HF and narrow-band superconductors, including UBe_{13} and $CeCu_2Si_2$. The physical basis of this fitting technique is still not clear, but it has been

tentatively attributed to a variety of mechanisms such as magnetoresistance, strong coupling or anisotropic pairing.

At present, there is no agreement concerning the influence of strong manybody renormalizations on the properties of HTO, but the proximity of magnetic order and metal-insulator transitions to the superconducting phases of these materials demands that their potential effects be considered in analyses of the upper critical field and other data.

4) **Hyperstrong coupling--** Upper critical field [12] and neutron scattering [76] data for HF superconductors suggest that the presence of magnetic fluctuations may lead to the replacement of the Debye temperature (as the pairing cutoff scale) by a magnetic excitation energy ω_c *that is comparable to* T_c, implying that the anomalous magnitude and curvature of H_{c2} is due to "hyperstrong coupling" [12]. Observations of extremely large magnetic energy scales and clearly defined magnetic excitations at energies expected for pairbreaking processes in HTO materials could be evidence of a similar situation [57,60-63].

We, in collaboration with colleagues at Argonne National Laboratory, obtained [12] the first quantitative fits of the anomalous H_{c2} data for the HF superconductors U_6Fe, U_6Co, and UPt_3, using a modification of an ad hoc scaling of the WHHM model due to Decroux and Fischer (DF) [30]. DF were able to account for the *high values of* $H_{c2}(0)$ *found for* Mo_6Se_8 *single crystals* and alloys only by assuming an empirical model in which the orbital pairbreaking scale was renormalized according to $H_{c2}^*(T) \rightarrow \beta_{DF}(T)\, H_{c2}^*(T)$, where ($\beta_o \geq 1$):

$$\beta_{DF}(T) = \beta_o / \{ 1 + (\beta_o - 1) t^2 \} \qquad (4)$$

DF did not consider T- and H-dependent normal state parameters, nor did they consider the positive curvature of $H_{c2}(T)$ frequently observed at lower fields to be an *intrinsic* property of their materials. However, by reconsidering the widespread occurrence of positive curvature of H_{c2} as intrinsic and fundamental, De Long and coworkers have shown that not only can the DF scaling be accurately applied to a wide range of materials as an analytic tool (in the spirit of the McMillan or Allen-Dynes equations [77] for $T_c(\lambda, \mu^*)$), but that the method also appears to have more fundamental implications.

After consideration of the effects of magnetoresistance, it was found that the entire enhancement (e.g., $\beta_{DF}(T)$) of H_{c2}^* could be quantitatively modeled as a strong coupling correction, provided the

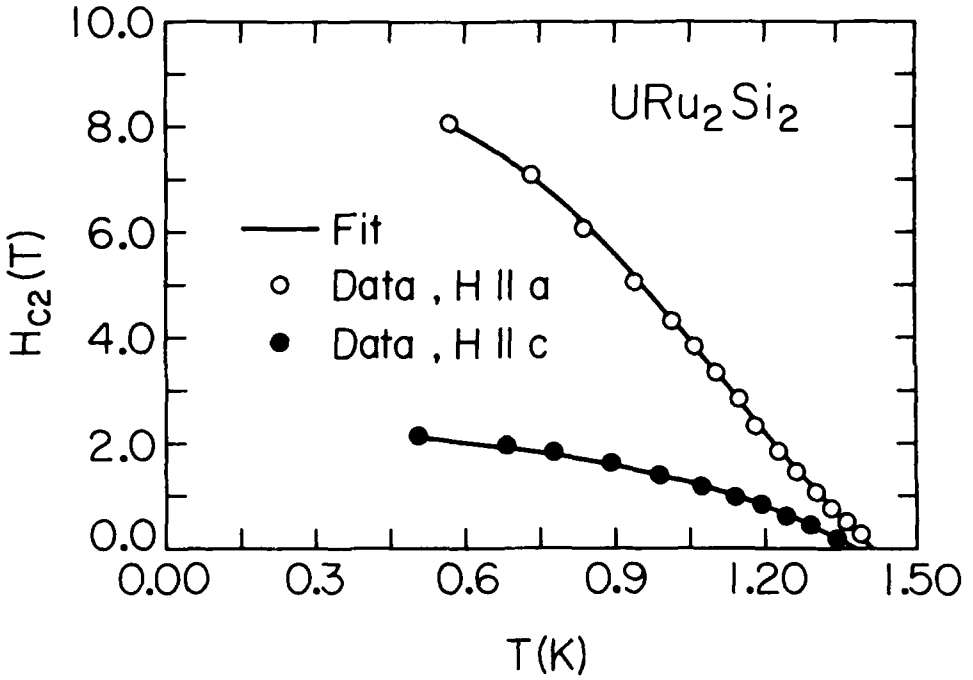

Fig. 9. Upper critical field H_{c2} vs. temperature T for single- crystal URu_2Si_2 with either the tetragonal **a**- or **c**-axis parallel to the applied field **H**. Experimental data are the same as shown in Fig. 5. The curves represent fits of the data over the entire experimental range using a phenomenological extension of the WHHM model presented in Ref. 12 (compare to the Ginzburg-Landau fit of Fig. 5). After Ref. 43.

associated pairing cutoff energy ω_c was comparable to T_{co}! Theoretical calculations [78] by Schossmann and Schachinger have quantitatively verified both the strong coupling interpretation and anomalously low value of $\omega_c \approx 6$ K in the case of U_6Fe, implying that it is highly unlikely that this effect is related to a traditional electron-phonon interaction.

The "hyperstrong coupling" suggested by this analysis can be interpreted as evidence of a low-lying branch of magnetic excitations with a characteristic "Debye" temperature $\propto \omega_c$ that acts as the cutoff for superconducting pairing [12-14]. Subsequent to this work, Aeppli et al. [76] directly observed such magnetic excitations in neutron scattering studies of UPt_3 and measured a corresponding Debye energy $\omega_c \approx 2$ K, in excellent agreement with the H_{c2} analysis [12] of UPt_3. Norman [79] has used experimental data to calculate the heat capacity, magnetic susceptibility and anisotropic pair potential for UPt_3. He has found that low frequency spin fluctuations, such as directly measured by Aeppli and coworkers, and inferred by De Long et al. from H_{c2} data, are crucial to a proper description of the

normal and superconducting state data.

Recent experimental results [80] for $H_{c2}(T)$ (see Fig.9) and the magnetoresistance $\Delta\rho(T,H) = \rho(T,H) - \rho(T,0)$ for a single crystal sample of URu_2Si_2 have been obtained. The anomalously high magnitude and positive curvature of the **H** || **a** data are precisely fit by the rescaled WHHM model. The pairing cutoff energy ω_c is being deduced at the time of this writing, and will be compared to the results of inelastic neutron scattering data [81].

Further work is needed to apply the above approach to a wider variety of materials, including HTO.

5) **Flux creep and superconducting glass effects--** Flux creep has been implicated as a mechanism for *fictitious* positive curvature of H_{c2}, as mentioned in the begining of this article. A review of certain flux creep phenomena has been given by Tinkham and Lobb [82]. However, positive curvature of $H_{c2}(T)$ due to flux creep is difficult to distinguish from "superconducting glass" effects, usually assumed to occur in collections of superconducting granules (present in polycrystalline or ceramic samples) weakly linked through nonsuperconducting surface barriers [83-85]. However, Malozemoff et al. [84] have described a method of measuring field-cooled (FC), zero-field-cooled (ZFC) and remanent (RM) dc magnetization of samples to distinguish flux pinning from glass phenomena.

The main effect of flux creep and glass effects is to obscure the true equilibrium phase boundary as opposed to creating intrinsic new mechanisms for positive curvature of H_{c2}. Malozemoff et al. [86] pointed out that the phase boundary determined via dynamic transport measurements was really the "irreversibility line" $H_{irr}(T,\omega)$, which was shown to approach H_{c2} in the limit of infinite measuring frequency ω. They also suggested that reversible dc diamagnetic onsets occurred at H_{c2}. Welp et al. [87] have recently demonstrated that a wide enough temperature interval of reversibility exists just below $T_c(H)$ to allow a meaningful determination of H_{c2} via dc measurements of the magnetization for $YBa_2Cu_3O_7$. Although recent work gives hope that the effects of flux creep may be sorted out of data, the situation is still far from resolved [88], and the techniques used to determine H_{c2} will have to be carefully applied and refined in future experiments.

6) **Novel "intrinsic superconducting glass" phase--** We believe that a novel, "intrinsic superconducting glass" ("ISG") state can be realized in *single crystal* samples that support coexistance of either a CDW or SDW state with superconductivity. Any sort of disorder (twins, chemical dopants, strain, etc.) that could act either as a pinning center or as a local mechanism for modulating or reorienting

the CDW or SDW order parameter, would necessarily affect the superconducting order parameter via interaction terms in the free energy. Short-range magnetic order may also give rise to similar effects.

The essential point is that a *density wave order parameter and the superconducting order parameter compete for Fermi surface.* Regions of the crystal may either: 1) segregate into normal-density-wave and superconducting volumes; 2) support interpenetrating superconducting and normal-density-wave (possibly "gapless") states almost everywhere. We also would expect to see an ISG due to a spatial phase mixture in materials close to a thermodynamic phase boundary (between a normal lattice-distorted phase and a superconducting phase) in situations where strong first order transitions are involved.

Interference effects could create "weak links" or phase modulations of relevant order parameters analogous to the "extrinsic" or granular superconducting glass state ("ESG"). However, it is highly likely that various magnetic and elastic properties will exhibit effects that could identify the ISG state as distinct from the ESG or normal type II (flux creep) phase, where pinning sites *are not associated with a competing order parameter.*

To our knowledge, no one else has advanced a glass state due to competing order parameters. Additional evidence in support of this idea includes recent observations of magnetization memory effects [88], "intrinsic pinning" [89], and vortex mobility and tunnelling effects in vibrating reed [90] and ultrasonic [91] experiments. M. P. A. Fisher [92] has given theoretical arguments that a similar phase ("vortex glass") should exist in HTO, but did not identify the potential of a competing density wave order parameter to nucleate it.

IV. Conclusion

There is clearly a need to pursue further research into the behavior of the upper critical field of a number of materials. We have not discussed a number of additional subjects in this brief overview. For example, the high T_c, quasi-two-dimensionality and short coherence length of HTO should lead to significant fluctuation effects [93-95] near T_c, and these can complicate the gathering of H_{c2} data and the associated identification of flux creep effects [96-98]. The influence of low-dimensionality and the temperature dependence of the coherence length must also be kept in mind in analyzing H_{c2} data for HTO [99,100]. Flux *flow* (not identical to flux *creep*) effects can also be important in broadening the superconducting transition, and have not as yet received a great deal of attention.

The myriad effects that can be considered in analyses of H_{c2} data require one to maintain a broad perspective and a cautious attention to previous work on a variety of superconducting materials. It is often suggested that the HTO and heavy fermion (HF) superconductors have many common characteristics [101] such as a competition between magnetic order (SDW or spin fluctuations) and superconductivity, a proximity of electron localization (CDW or metal-insulator transition), short

coherence length, anisotropic pairing states, strong coupling, large effective mass, etc. However, there is yet no clear identification of a mechanism that would explain the similarities between the HTO and HF materials.

It would also be a grave mistake to ignore more conventional types of superconductors as our understanding of the HF and HTO materials grows. The layered transition metal dichalcogenides such as $NbSe_2$, TaS_2 and $NbSe_3$ have anisotropic coherence lengths, high magnitudes of H_{c2}, large magnetoresistance, and an intriguing competition between superconductivity and CDW states [100,102,103]. Their appreciable positive curvature of H_{c2} [104] is particularly interesting. The observation of structural modulations or CDW instabilities [64,65], and proposed Fermi surface nesting [66,67] in a number of HTO materials makes a comparison of them with the layered dichalcogenides very attractive. Future theories of HTO materials must be consistent with the behavior of conventional superconductors.

V. Acknowledgements

The author would like to thank Dr. G. W. Crabtree, Dr. B. Dobrowski, Dr. D. G. Hinks, Prof. R. Joynt, Dr. W-K. Kwok, Prof. J. W. Lynn, Dr. M. R. Norman, Dr. B. C. Sales, Prof. J. Sauls and Prof. T. Tsuneto for stimulating discussions and preprints. The author is particularly grateful to Dr. V. Volovik for pointing out some of the references relating to evidence for anisotropic order parameters in HTO and stimulating conversations. The support of experimental research at the University of Kentucky by a grant from Research Corporation is gratefully acknowledged.

VI. References

1. J. G. Bednorz and K. A. Mueller, Z. Phys. B **64**, 189 (1986).
2. W. K. Kwok, G. W. Crabtree, D. G. Hinks, D. W. Capone, J. D. Jorgensen and K. Zhang, Phys. Rev. B **35**, 5343 (1987).
3. J. Z. Sun et al., Phys. Rev. Lett. **58**,1574 (1987).
4. A. Junod, A. Bezinge, T. Graf, J. L. Jorda, J. Muller, L. Antognazza, D. Cattani, J. Cors, M. Decroux, O. Fischer, M. Banovski, P. Genoud, L. Hoffmann, A. A. Manuel, M. Petter, E. Walker, M. Francois and K. Yvon, Europhys. Lett. **4**, 247 (1987).
5. J. S. Moodera, R. Meservey, J. E. Tkaczyk, C. X. Hao, G. A. Gibson and P. M. Tedrow, Phys. Rev. B **37**, 619 (1988).
6. Y. Iye, T. Tamegai, H. Takeya and H. Takei, Jap. J. Appl. Phys. **26**, L1057 (1987).
7. T. R. Dinger, T. K. Worthington, W. J. Gallagher and R. L. Sandstrom, Phys. Rev. Lett. **58**, 2687 (1987).
8. O. Laborde, J. L. Tholence, P. Lejay, A. Sulpice, R. Tournier, J. J. Capponi, C. Michel and J. Provost, Solid State Commun. **63**, 877 (1987).
9. Y. Yeshurun and A. P. Malozemoff, Phys. Rev. Lett. **60**, 2202 (1988).
10. M. Tinkham, Phys. Rev. Lett. **61**, 1658 (1988).
11. T. T. M. Palstra, B. Batlogg, L. F. Schneemeyer and J. V. Waszczak, Phys. Rev. Lett. **61**, 1662 (1988).

12. L. E. De Long, G. W. Crabtree, L. N. Hall, D. G. Hinks, W. K. Kwok and S. K. Malik, Phys. Rev. B **36**, 7155 (1987).
13. L. E. De Long, in: L. C. Gupta and S. K. Malik, eds., "Theoretical and Experimental Aspects of Valence Fluctuations and Heavy Fermions" (Plenum, New York, 1987), pp. 65-76 (1987).
14. L. E. De Long, in: S. A. Wolf and V. Z. Kresin, eds., "Novel Superconductivity" (Plenum, New York, 1987), pp. 253-264.
15. M. Tachiki, S. Maekawa and S. Takahashi, Phys. Rev. B **31**, 228 (1985).
16. E. W. Fenton and G. C. Aers, Solid State Commun. **56**, 337 (1985).
17. M. B. Maple, J. W. Chen, S. E. Lambert, Z. Fisk, J. L. Smith, H. R. Ott, J. S. Brooks and M. J. Naughton, Phys. Rev. Lett. **54**, 477 (1985).
18. U. Rauchschwalbe, U. Ahlheim, F. Steglich, D. Rainer and J. J. M. Franse, Z. Phys. B **60**, 379 (1985).
19. L. N. Bulaevskii, A. A. Guseinov and A. I. Rusinov, Sov. Phys. JETP **44**, 1243 (1976).
20. K. Machida, T. Koyama and T. Matsubara, Phys. Rev. B **23**, 99 (1981); K. Machida, J. Phys. Soc. Japan **53**, 712 (1983).
21. H. K. Onnes, Commun. Phys. Lab. Univ. Leiden, **Nos. 140b, 141b** (1914).
22. W. Tuyn and H. K. Onnes, Commun. Phys. Lab. Univ. Leiden, **No. 174a** (1926).
23. J. Bardeen, L. N. Cooper and J. R. Schrieffer, Phys. Rev. **106**, 162 (1957).
24. See various papers in: S. A. Wolf and V. Z. Kresin, "Novel Superconductivity" (Plenum, New York, 1987)
25. L. N. Cooper, Phys. Rev. **104**, 1189 (1956).
26. P. W. Anderson, J. Phys. Chem. Solids **11**, 26 (1959).
27. P. G. de Gennes, "Superconductivity of Metals and Alloys" (Benjamin, New York, 1966), Chapt. 8.
28. N. R. Werthamer, E. Helfand and P. C, Hohenberg, Phys. Rev. **147**, 295 (1966); K. Maki, Phys. Rev. **148**, 362 (1966).
29. T. P. Orlando, E. J. McNiff, Jr., S. Foner and M. R. Beasley, Phys. Rev. B **19**, 4545 (1979).
30. M. Decroux and O. Fischer, in: M. B. Maple and O. Fischer, eds., "Superconductivity in Ternary Compounds II" (Springer-Verlag, Berlin, 1982), Chapt. 3; M. Decroux, Ph.D. thesis, U. Geneva (1980, unpub.).
31. T. P. Orlando and M. R. Beasley, Phys. Rev. Lett. **46**, 1598 (1981).
32. M. B. Maple, L. E. De Long and B. C. Sales, in: K. A. Gschneidner, Jr. and L. Eyring, "Handbook on the Physics and Chemistry of Rare Earths" (North Holland, Amsterdam, 1978), Chapt. 11.
33. P. Fulde and K. Maki, Phys. Rev. **141**, 275 (1966).
34. H. M. Mayer, U. Rauchschwalbe, C. D. Bredl, F. Steglich, H. Rietschel, H. Schmidt, H. Wuehl and J. Beuers, Phys. Rev. B **33**, 3168 (1986).
35. J. J. M. Franse, A. de Visser, A. Menovsky and P. H. Frings, J. Magn. Magn. Mater. **52**, 61 (1985).
36. L. E. De Long, G. W. Crabtree, L. N. Hall, D. G. Hinks, W. K. Kwok and R. B. Mattingly, Jap. J. Appl. Phys. **26**, Supp. 26-3, 565 (1987).
37. G. E. Volovik and L. P. Gor'kov, Sov. Phys. JETP **61**, 843 (1985).
38. M. Sigrist and T. M. Rice, Z. Phys. B **68**, 9 (1987).
39. M. Sigrist, R. Joynt and T. M. Rice, Europhys. Lett. **3**, 629 (1987).
40. R. Joynt and T. M. Rice, Phys. Rev. B **38**, 2345 (1988); R. Joynt, Supercond. Sci. Tech. **1**, 210 (1988).
41. D. W. Hess, Bull. Am. Phys. Soc. **34**, 848 (1989); D. W. Hess, T. A. Tokuyasu and J. A. Sauls, to be published.
42. W. K. Kwok, L. E. De Long, G. W. Crabtree, D. G. Hinks and R. Joynt, to be published.
43. L. E. De Long, D. Togliatti, G. W. Lehman, W-K. Kwok, G. W. Crabtree, K. G. Vandervoort, D. G. Hinks and R. Joynt, to be presented at the Int. Conf. on the Physics of Highly Correlated Electron Systems, Santa Fe, NM, Sept., 1989.
44. L. Taillefer, F. Piquemal and J. Flouquet, Physica C **153-155**, 451 (1988).
45. R. A. Fisher, S. Kim, B. F. Woodfield, N. E. Phillips, L. Taillefer, K. Hasselbach, J.

Flouquet, A. L. Giorgi and J. L. Smith, Phys. Rev. Lett. **62**, 1411 (1989).
46. K. Hasselbach, L. Taillefer and J. Flouquet, to be published.
47. M. Ishikawa, Y. Nakazawa, T. Takabatake, A. Kishi, R. Kato and A. Maesono, Physica C **153-155**, 1089 (1988).
48. S. E. Inderhees, M. B. Salamon, N. Goldenfeld, J. P. Rice, B. G. Pazol, D. M. Ginzberg, J. Z. Liu and G. W. Crabtree, Phys. Rev. Lett. **60**, 1178 (1988).
49. T. K. Worthington, W. J. Gallagher and T. R. Dinger, Phys. Rev. Lett. **59**, 1160 (1987).
50. G. E. Volovik, Physica Scripta **38**, 502 (1988).
51. J. F. Annett, M. Randeria and S. R. Renn, Phys. Rev. B **38**, 4660 (1988).
52. H. Duan, L. Lu and D. Zhang, Solid State Commun. **67**, 809 (1988); D. Zhang, H. Duan, B. Ma, L. Lu and S. Lin, Physica C **156**, 761 (1988).
53. A. M. Gabovich and A. S. Shpigel, Phys. Rev. B **38**, 297 (1988).
54. V. E. Yurkevich, B. N. Rolov and H. E. Stanley, Czech. J. Phys. **B28**, 241 (1978).
55. W. A. Fertig, D. C. Johnston, L. E. De Long, R. W. McCallum, M. B. Maple and B. T. Matthias, Phys. Rev. Lett. **38**, 987 (1977).
56. D. C. Johnston, A. J. Jacobson, J. M. Newsam, J. T. Lewandowski, D. P. Goshorn, D. Xie and W. B. Yelon, in: D. L. Nelson, M. S. Whittingham and T. F. George, eds., "Chemistry of High Temperature Superconductors" (Amer. Chem. Soc. Symp. Ser., Vol. 351, ACS, Washington, DC, 1987), p. 136.
57. J. M. Tranquada, J. Appl. Phys. **64**, 6071 (1988); J. M. Tranquada, J. Less-Common Metals **153** (1989).
58. J. W. Lynn and W-H. Li, J. Appl. Phys. **64**, 6065 (1988).
59. Y. J. Uemura, J. Appl. Phys. **64**, 6087 (1988).
60. K. B. Lyons and P. A. Fleury, J. Appl. Phys. **64**, 6075 (1988).
61. R. J. Birgeneau, Y. Endoh, K. Kakurai, Y. Hidaka, T. Murakami, M. A. Kastner, T. R. Thurston, G. Shirane and K. Yamada, Phys. Rev. B **39**, 2868 (1989).
62. G. Aeppli, S. M. Hayden, H. A. Mook, Z. Fisk, S-W. Cheong, D. Rytz, J. P. Remeika, G. P. Espinosa and A. S. Cooper, Phys. Rev. Lett. **39**, 2868 (1989).
63. H. Yoshizawa, S. Mitsuda, H. Kitazawa and K. Katsumata, J. Phys. Soc. Japan **57**, 3686 (1988).
64. S. Pei, N. J. Zaluzec, J. D. Jorgensen, B. Dabrowski, D. G. Hinks, A. W. Mitchell and D. R. Richards, to appear in Phys. Rev. B; J. D. Jorgensen, H. B. Schuettler, D. G. Hinks, D. W. Capone II, K. Zhang, M. B. Brodsky and D. J. Scalapino, Phys. Rev. Lett. **58**, 1024 (1987).
65. E. A. Hewat, C. Chaillout, M. Godinho, M. F. Gorius and M. Marezio, Physica C **157**, 228 (1989); S. Pei, N. J. Zaluzec, J. D. Jorgensen, B. Dobrowski, D. G. Hinks, A. W. Mitchell and D. R. Richards, to appear in Phys. Rev. B, Rapid Commun.
66. L. F. Mattheiss and D. R. Hamann, Phys. Rev. Lett. **60**, 2681 (1988); L. F. Mattheiss, Phys. Rev. Lett. **58**, 1028 (1987).
67. J. Yu, A. J. Freeman and J. H. Xu, Phys. Rev. Lett. **58**, 1035 (1987).
68. J. B. Torrance, Y. Tokura, S. J. LaPlaca, T. C. Huang, R. J. Savoy and A. I. Nazzal, Solid State Commun. **66**, 703 (1988); C. C. Torardi et al., Phys. Rev. B **38**, 225 (1988).
69. S. A. Sunshine et al., Phys. Rev. B **38**, 893 (1988).
70. O. Eibl, Solid State Commun. **67**, 703 (1988).
71. B. C. Chakoumakos, J. D. Budai, B. C. Sales and E. Sonder, to appear in the Proceedings of the Mat. Res. Soc. Spring Meeting, 1989; E. Sonder, B. C. Chakoumakos and B. C. Sales, to appear in Phys. Rev. B (1989).
72. P. A. Lee, T. M. Rice, J. W. Serene, L. J. Sham and J. W. Wilkins, Comments Condens. Mat. Phys. **12**, 99 (1986).
73. L. E. De Long, Phys. Rev. B **33**, 3556 (1986).
74. Z. Fisk, D. W. Hess, C. J. Pethick, D. Pines, J. L. Smith, J. D. Thompson and J. O. Willis, Science **239**, 33 (1988).
75. T. Penny et al., J. Magn. Magn. Mater. **54-57**, 370 (1986).
76. G. Aeppli, E. Bucher, C. Broholm, J. K. Kjems, J. Baumann and J. Hufnagl, Phys. Rev. Lett. **60**, 615 (1988).

77. W. A. McMillan, Phys. Rev.**167**, 331 (1968); P. B. Allen and R. C. Dynes, Phys. Rev. B **12**, 905 (1975).
78. M. Schossmann and E. Schachinger, Phys. Rev. B **33**, 6123 (1986); and private communication of unpublished results.
79. M. R. Norman, Phys. Rev. Lett. **59**, 232 (1987); M. R. Norman, Phys. Rev. B **37**, 4987 (1988); M. R. Norman, Phys. Rev. B **39**, 7305 (1989); M. R. Norman, preprint submitted to Phys. Rev. B.
80. L. E. De Long, R. B. Mattingly, S. Ren, W. K. Kwok, D. G. Hinks and G. W. Crabtree, Bull. Am. Phys. Soc. **34**, 850 (1989); and to be published.
81. C. Broholm, Ph.D. thesis, Riso National Laboratory, Denmark, 1988 (unpublished).
82. M. Tinkham and C. J. Lobb, in: H. Ehrenreich and D. Turnbull, eds., "Solid State Physics" (Academic Press, New York, 1989), Vol. 42, pp. 91-134.
83. K. A. Muller et al., Phys. Rev. Lett. **58**, 1143 (1987).
84. A. P. Malozemoff, L. Krusin-Elbaum, D. C. Cronemeyer, Y. Yeshurun and F. Holtzberg, Phys. Rev. B **38**, 6490 (1988).
85. Y. Yeshurun, A. P. Malozemoff, F. Holtzberg and T. R. Dinger, Phys. Rev. B **38**, 11828 (1988).
86. A. P. Malozemoff, T. K. Worthington, Y. Yeshurun, F. Holtzberg and P. H. Kes, Phys. Rev. B **38**, 7203 (1988).
87. U. Welp, W. K. Kwok, G. W. Crabtree, K. G. Vandervoort and J. Z. Liu, Phys. Rev. Lett. **62**, 1908 (1989).
88. C. Rossel, Y. Maeno, and I. Morgenstern, Phys. Rev. Lett. **62**, 681 (1989).
89. G. J. Dolan, G. V. Chandrashekhar, T. R. Dinger, C. Feild and F. Holtzberg, Phys. Rev. Lett. **62**, 827 (1989).
90. S. Gregory, C. T. Rogers, T. Venkatesan, X. D. Wu, A. Inam and B. Dutta, Phys. Rev. Lett. **62**, 1548 (1989).
91. M. J. Mc Kenna, A. Hikata, J. Takeuchi, C. Elbaum, R. Kershaw and A. Wold, Phys. Rev. Lett. **62** 1556 (1989).
92. M. P. A. Fisher, Phys. Rev. Lett. **62**, 1415 (1989).
93. C. J. Lobb, Phys. Rev. B **36**, 3930 (1987).
94. A. Kapitulnik, M. R. Beasley, C. Castellani and C. Di Castro, Phys. Rev. B **37**, 537 (1988).
95. V. L. Ginzburg, Physica C **153-155**, 1617 (1988).
96. B. Ya. Shapiro, JETP Lett. **46**, 569 (1988).
97. R. Ikeda, T. Ohmi and T. Tsuneto, to appear in J. Phys. Soc. Japan (1989); R. Ikeda, to appear in J. Phys. Soc. Japan (1989).
98. M. Hikita and M. Suzuki, Phys. Rev. B **39**, 4756 (1989); T. A. Friedmann, J. P. Rice, J. Giapintzakis and D. M. Ginsberg, Phys. Rev. **39**, 4258 (1989).
99. N-C. Yeh and C. C. Tsuei, Phys. Rev. B **39**, 9708 (1989).
100. L. N. Bulaevskii, Adv. Phys. **37**, 443 (1988).
101. C. J. Pethick and D. Pines, in: S. A. Wolf and V. Z. Kresin, "Novel Superconductivity" (Plenum, New York, 1987), pp. 201-214.
102. R. H. Friend and D. Jerome, J. Phys. C: Solid State Phys. **12**, 1441 (1979).
103. M. Naito and S. Tanaka, J. Phys. Soc. Japan **51**, 228 (1981).
104. B. W. Pfalzgraf and H. Spreckels, J. Phys. C: Solid State Phys. **27**, 4359 (1987).

THIS PAGE IS INTENTIONALLY BLANK

Presented at the Workshop on High Temperature Superconductivity
23-25 May 1989 GACIAC PR-89-02

THERMAL PROPERTIES OF HIGH-T_c MATERIALS

May 23, 1989

D.T. Morelli and J. Heremans
General Motors Research Laboratories
Warren, Michigan 48090-9055

ABSTRACT

We describe results of a set of experiments on the thermal conductivity of various high-T_c superconductors and related compounds. It is shown that in the normal state, nearly all of the heat is carried by lattice vibrations, or phonons, rather than charge carriers, as is the normal situation in a superconductor. The dominance of lattice conduction over charge carrier conduction is a direct consequence of the small density of free carriers in this system. In superconducting samples of the $RBa_2Cu_3O_{7-\delta}$ composition (where R is yttrium or a rare earth element), the thermal conductivity is constant in the normal state and increases as the samples become superconducting. This behavior implies strong scattering of heat carrying phonons by free electrons, which become fewer in number at temperatures below T_c, due to Cooper pairing. Thus the nature of the thermal conductivity of the 1-2-3 phase is not inconsistent with a strong electron-phonon coupling. Measurements on a single crystal of semiconducting La_2CuO_4 reveal anomalous dips in the heat conductivity in temperature ranges in which magnetic transitions occur in the lattice. The size and temperature dependence of the phonon mean free path in this case point to scattering of lattice vibrations by spins. It is stressed that more measurements are required on high quality single crystals of all phases, both superconducting and nonsuperconducting, in order to provide definite conclusions with regard to pairing mechanisms in these systems.

INTRODUCTION

Although more than two years have passed since the first discoveries of superconductivity in ceramic oxides, a question yet to be answered is whether the electron pairing which results in superconductivity is due to "standard" phonon mediation or another, more exotic, mechanism, such as coupling via plasmons (Ihara, et. al., 1987) or magnetic interactions [Anderson, 1987, Anderson, et. al., 1987).

In the Bardeen-Cooper-Schrieffer (BCS) theory of conductivity, electrons are paired together via an effective attraction mediated by the electron-phonon interaction. It is of significance to ask whether the electron-phonon interaction in these materials, or indeed, in any material, is large enough to produce critical temperatures of 90 K and above. In this respect, thermal conductivity measurements are an indispensible tool. Since both phonons and charge carriers are capable of carrying heat, thermal conductivity data can yield important information not only about the electron and phonon spectra, but also about interactions between them. On the other hand, the thermal conductivity should also be sensitive to heat conduction and scattering by magnetic spins. As we shall see below, the results of such measurements do indeed shed some very important light on the properties of these materials, and also pose more questions about their behavior which must be answered.

THERMAL CONDUCTIVITY OF 1-2-3 PHASE

Figure 1 shows the thermal conductivity of a sintered sample of $YBa_2Cu_3O_{7-\delta}$ from 2-140 K. Details of the sample preparation and measurement technique are given elsewhere (Morelli, et. al., 1987). Similar results are

---

Ihara, H., Hirabayaschi, M., Terada, N., Kimura, Y., Senzaki, K., Akimoto, M., Bushida, K., Kawashima, F., and Uzaka, R., 1987 Jpn. Jour. Appl. Phys. 26, 908.

Anderson, P.W. 1987 Science 235, 1196.

Anderson, P.W., Baskaran, G., Zou, Z., and Hsu, T. 1987 Phys. Rev. Lett. 58, 2790.

Morelli, D.T., Heremans, J., and Swets, D.E., 1987 Phys. Rev. B 36, 3917.

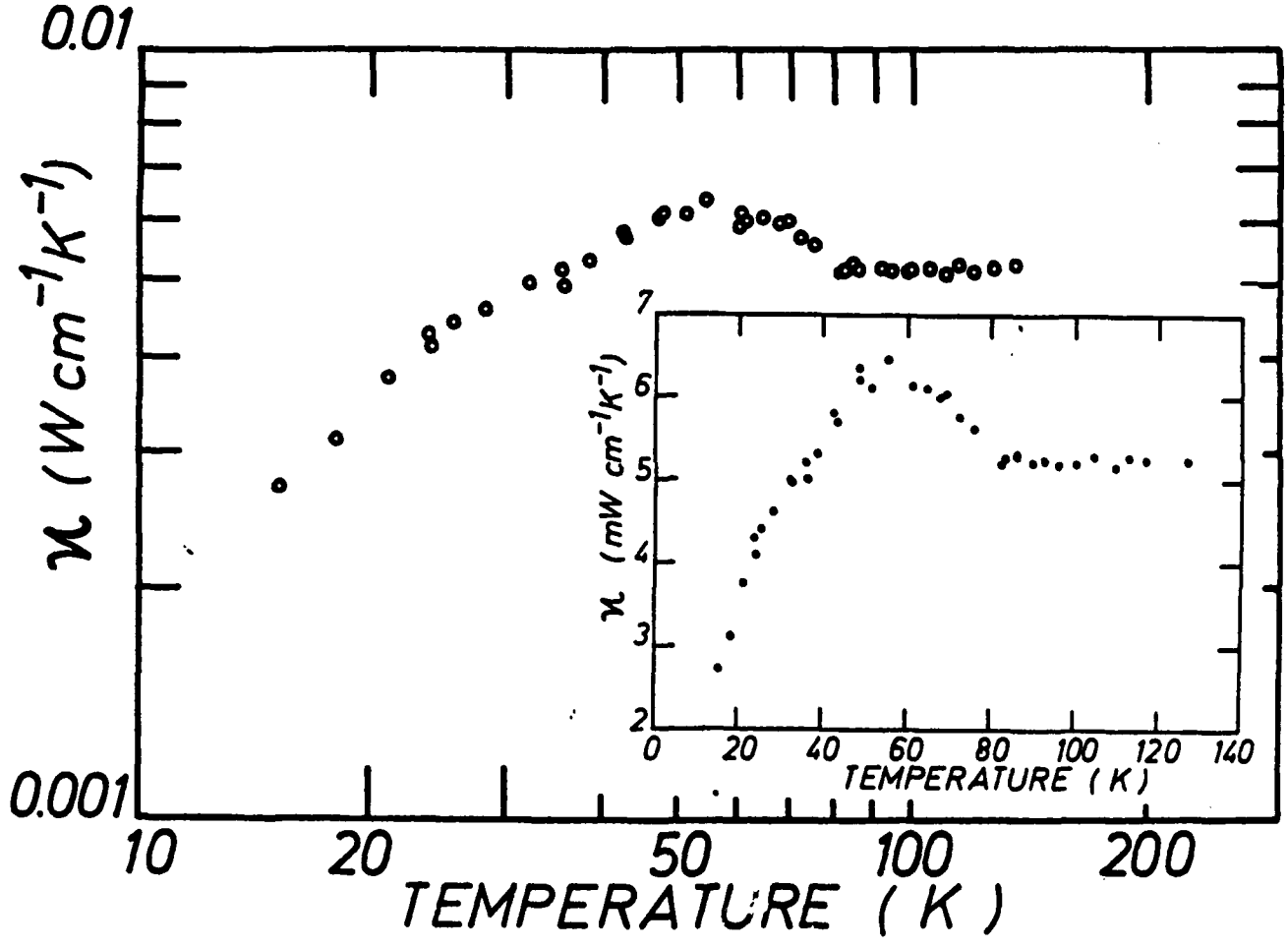

Figure 1. Thermal conductivity of $YBa_2Cu_3O_7$.

obtained when a rare earth element is substituted for Y in the lattice (Heremans, et. al., 1988). The inset shows the same data on a linear plot. Two outstanding features of these results are: 1) above about 100 K, the thermal conductivity is nearly constant, and 2) upon cooling below $T_c \sim 83$ K, the thermal conductivity rises sharply. These results have since been verified by other workers [Bayot, et. al., 1987, Uher and Kaiser, 1987, Jezowski, et. al., 1987]. Figure 2 summarizes some measurements on 1-2-3 superconductors. As stated above, the thermal conductivity is the sum of carrier and phonon contributions:

$$\kappa = \kappa_c + \kappa_p$$

One can make an estimate of the carrier contribution by using the Wiedemann-Franz law in conjunction with electrical resistivity data. This law states that, if carriers are being scattered elastically, then

$$\kappa_c \rho = L_o T$$

where ρ is the electrical resistivity and $L_o = 2.45 \times 10^{-8}$ W Ω K^{-1}. If there is significant inelastic scattering of carriers, then this law gives an upper limit to κ_c. At 100 K, $\rho = 12$ mΩ cm for the sample in Figure 1. This yields $\kappa_c = 2 \times 10^{-4}$ W cm^{-1} K^{-1}, more than an order of magnitude smaller than the observed value. Thus we conclude that nearly all of the heat is being transported by phonons in this material. The lattice thermal conductivity will be affected upon cooling into the superconducting state if phonons are being scattered to some extent by electrons. As the electrons coalesce into Cooper pairs, they no longer exchange energy with the phonons, and κ_p will

---

Heremans, J., Morelli, D.T., Smith, G.W., and Strite, S.C., 1988 Phys. Rev. B 37, 1604.

Bayot, V., Delannay, F., DeWitte, C., Erauw, J.-P., Gonze, X., Issi, J.-P., Jonas, A., Kinany-Alaoui, M., Lambricht, M., Michenaud, J.-P., Minet, J.-P., and Piraux, L. 1987 Solid State Comm 63, 983.

Uher, C., and Kaiser, A.B., 1987 Phys. Rev. B 36, 5680.

Jezowski, A., Mucha, J., Rogacki, K., Horyn, R., Bukowski, Z., Horobiowski, M., Rafalowicz, J., Stepien-Damm, J., Sulkowski, C., Rojnar, E., Zaleski, A.J., and Klamut, J. 1987 Phys. Lett. A 122, 431.

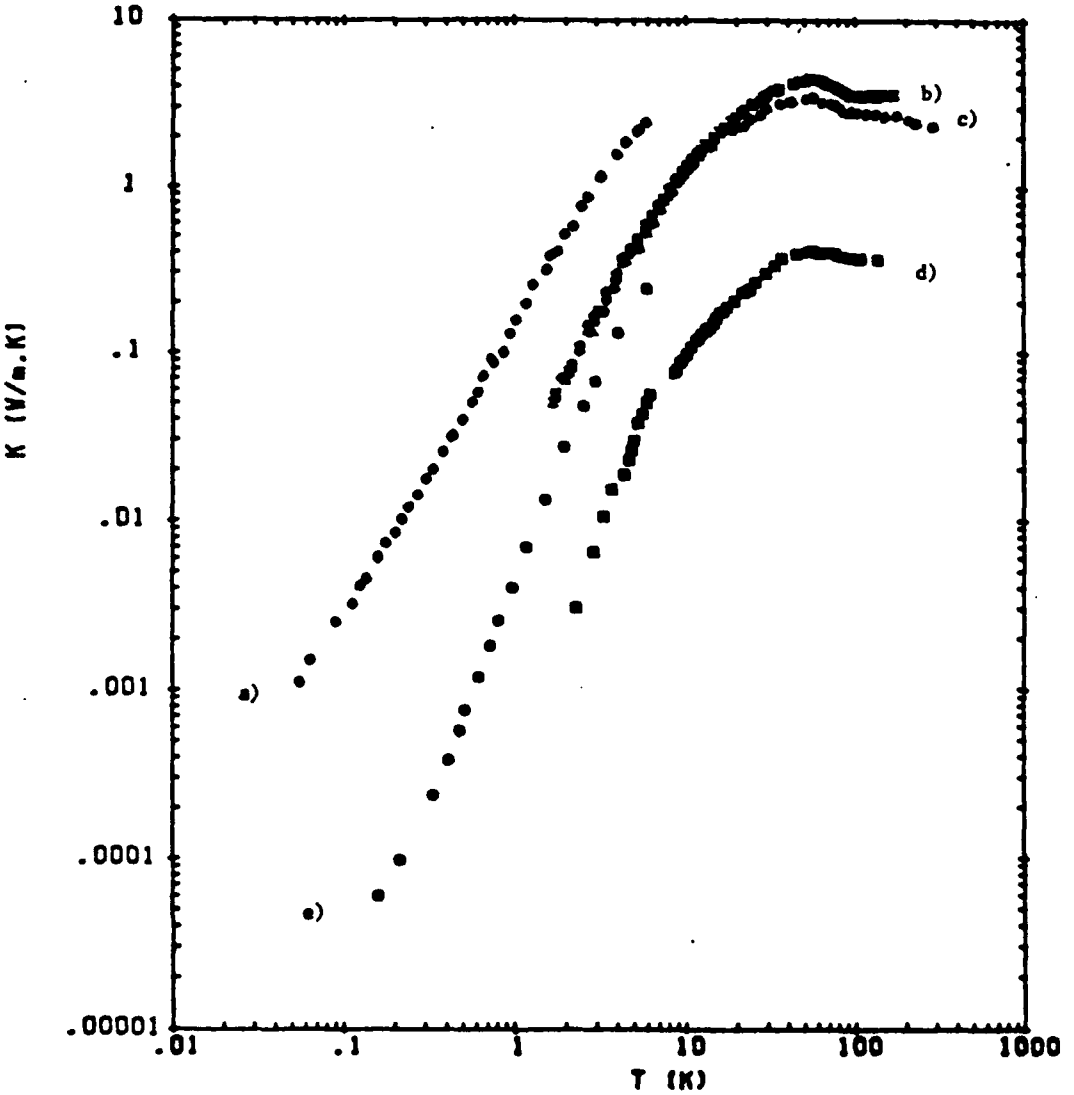

Figure 2. Summary of thermal conductivity measurements on 1-2-3 superconductors: a) Graebner, et. al, single crystal; b) Uher and Kaiser, sintered material; c) Bayot, et. al, sintered material; d) Morelli, et. al., sintered material; e) Freeman, et. al., sintered material.

Graebner, J.E., Schneemayer, L.F., Cava, R.J., Wasaczak, J.V., and Rietman, E.A., 1988 Mater. Res. Soc. Symp. Proc. 99, 745.

Uher, C. and Kaiser, A.B., 1987 Phys. Rev. B 36, 5680.

Bayot, V., Delannay, F., DeWitte, C., Brauw, J.-P., Gonse, X., Issi, J.-P., Jonas, A., Kinany-Alaoui, M., Lambricht, M., Michenaud, J.-P., Minet, J.-P., and Piraux, L. 1987 Solid State Comm 63, 983.

Morelli, D.T., Heremans, J., and Swets, D.E., 1987 Phys. Rev. B 36, 3917.

Freeman, J.J., Friedmann, T.A., Ginsberg, D.M., Chen, J., and Zangvil, A., 1987 Phys. Rev. B 36, 8786.

increase. This is precisely what we observe in Figure 1. Furthermore, when electrons are the dominant scatterers of phonons it has been shown (Ziman, 1960) that

$$\rho_p \kappa_p = k_B^2 T/(n_a^2 e),$$

where ρ_p is the phonon-limited electrical resistivity and n_a is the number of carriers per atom. Experimentally, the electrical resistivity above T_c is linear in temperature (Heremans, et. al., 1988). If this behavior is ascribed to phonon scattering, then the above equation implies that κ_p is temperature independent above T_c, also in accord with our observations. From equation {3} we find $n_a = 0.13$ for our sample. Thus the constancy of the normal state lattice conduction as well as the increase in κ_p below T_c are both consistent with a strong electron-phonon coupling in the normal state of the 1-2-3-superconductors.

THERMAL CONDUCTIVITY OF SINGLE CRYSTAL La_2CuO_4

While experiments on sintered samples of high temperature superconductors have yielded valuable information about the electron-phonon coupling in these materials, the poor crystalline quality of the pressed materials has made systematic comparisons of data from different crystals very difficult. it would be much more preferable to obtain thermal conductivity data on good, high quality single crystals, where the role of defects and impurities is greatly reduced. Such measurements require large crystals (many millimeters on a side), which unfortunately are not yet available. One system which is related to the high temperature superconductor lanthanum barium copper oxide is the parent material, La_2CuO_4, which is a semiconductor. We have measured the thermal conductivity of this material in single crystal form, both perpendicular and parallel to the Cu-O planes [Morelli, et. al., 1989]. This

---

Ziman, J. 1960 Electrons and Phonons, Clarendon Press, Oxford, p. 321.

Heremans, J., Morelli, D.T., Smith, G.W., and Strite, S.C. 1988 Phys. Rev. B 37, 1604.

Morelli, D.T., Heremans, J., Doll, G., Picone, P.J., Jenssen, H.P., and Dresselhaus, M.S. 1989 Phys. Rev. B 39 804.

material is known to undergo a transition from 2D to 3D antiferromagnetic order below 300 K (Shirane, et. al., 1987). In figure 2, we show the thermal conductivity in the [001] and [110] directions, i.e., perpendicular and parallel to the Cu-O planes, respectively, as well as an intermediate direction designated [221]. As in the 1-2-3 case, all of the heat in La_2CuO_4 single crystals is carried by phonons. Below 100 K this crystal behaves as a typical dielectric, with a peak in the thermal conductivity around 40 K. At higher temperature, however, there occur anomalous dips in the thermal conductivity, specifically at 250 K in the [001] and near 130 K in the [110] direction. Our susceptibility results show that χ exhibits a sharp maximum at 250 K for magnetic field in the [001] direction, and a much broader maximum, extending from 120 K to 250 K, for field in the [110] direction. Thus the sharpness and broadness of the dips in the thermal conductivity reflect the magnetic order-disorder transition occuring in the lattice. A qualitative explanation of this behavior is the following: above the Neel temperature, the system exhibits no staggered moment, and the disordered spins scatter phonons at a temperature-independent rate. Since the specific heat is a monotonically increasing function of temperature, this means that the thermal conductivity above T_N will rise as the temperature increases. Below T_N, on the other hand, the spins begin to order, and the phonon-spin scattering time will scale with the magnetic order parameter, which increases with decreasing temperature. Thus cooling below T_N also causes the thermal conductivity to increase. In this picture, therefore, the minimum in the thermal conductivity is correlated with the magnetic transition in the lattice. Thus for La_2CuO_4, the thermal conductivity results suggest a strong coupling between phonons and magnetic excitations in the crystal.

CONCLUSIONS

Like many other measurements on high-T_c materials, the thermal conductivity provides answers and poses new questions. The results show the predominance of phonons in carrying heat in these materials, and also highlight the role played by electrons as scatterers in the conduction

---

Shirane, G., Endoh, Y., Birgeneau, R.J., Kastner, M.A., Hidaka, Y., Oda, M., Suzuki, M., and Murakami, T. 1987 Phys. Rev. Lett. 59, 1613.

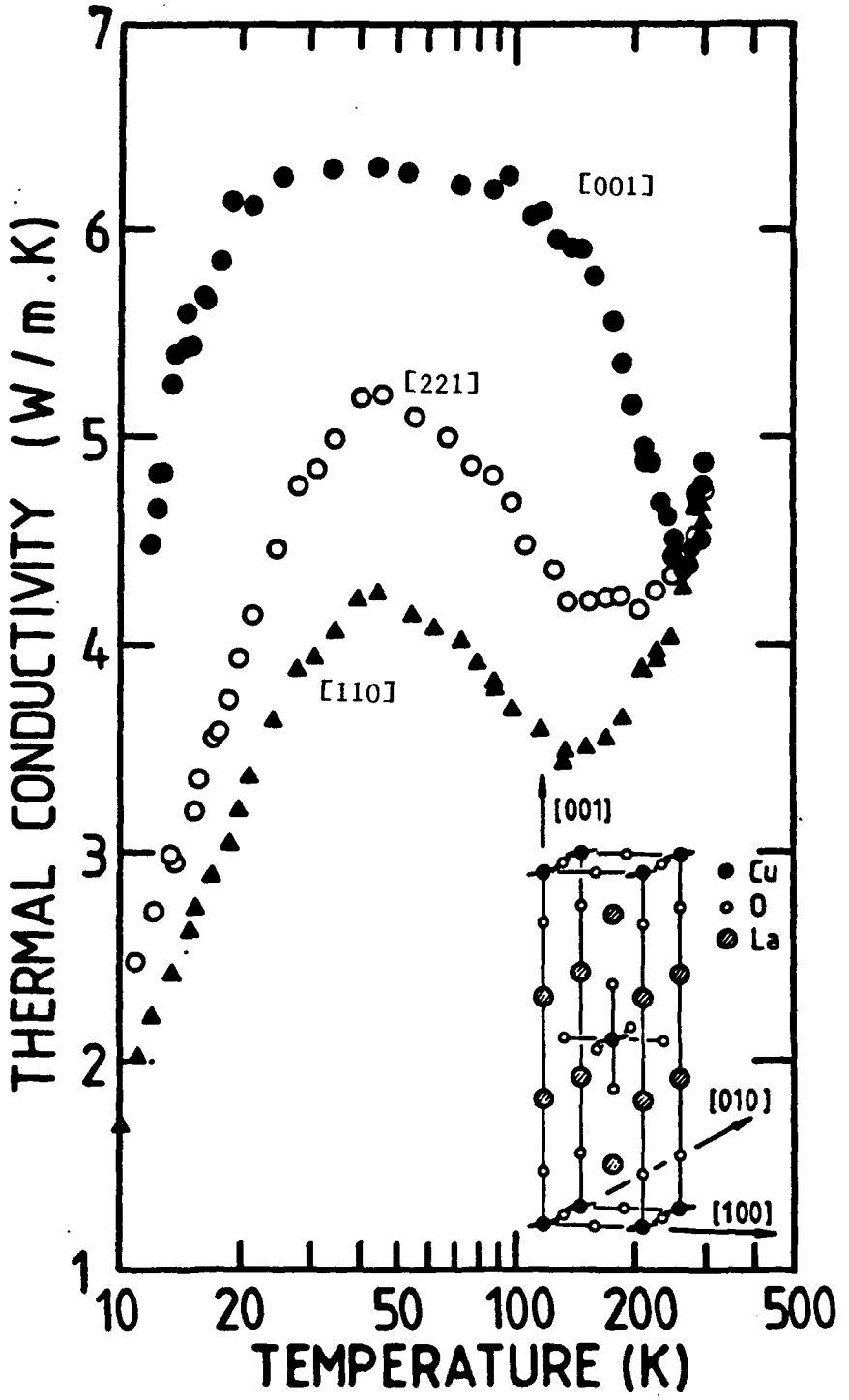

Figure3 . Thermal conductivity of single crystal La_2CuO_4.

process, at least in the 1-2-3 superconductors. On the other hand, the results on single crystal 2-1-4 parent material indicate that magnetic effects also have a profound effect on the lattice heat conduction. Thus while the experimental results on the thermal conductivity are not inconsistent with a strong phonon-electron coupling, magnetic effects also play a role and may have an important bearing on superconductivity in these systems. Clearly, more systematic investigations on a wider variety of both superconducting and nonsuperconducting materials are required. It must be stressed that it is imperative that these studies be performed on high quality single crystalline material in order to minimize the effects of extrinsic and spurious effects on the thermal conductivity.

THIS PAGE IS INTENTIONALLY BLANK

Abstract of Paper Presented at the
Workshop on High Temperature Superconductivity
23-25 May 1989 GACIAC PR 89-02

The Photoresponse of Superconductors

Dr. Ulrich Strom
Naval Research Laboratory
Washington, DC 20375

ABSTRACT

Various optical detection mechanisms for superconducting films will be reviewed. The discussion will be divided into the response to radiation with energy substantially below and substantially above the superconducting gap energy, respectively. Special emphasis will be placed on the transport and infrared optical properties of granular superconductors and the relationship of these properties to the photoresponse. Finally, a brief review will be given of investigations of nonequilibrium superconductivity phenomena using optical techniques.

THIS PAGE IS INTENTIONALLY BLANK

Presented at the Workshop on High Temperature Superconductivity
23-25 May 1989 GACIAC PR-89-02

SQUID AND FLUXON DEVICES

Orest G. Symko, Department of Physics, University of Utah
Salt Lake City, Utah 84112

ABSTRACT

Principles involved in SQUID and fluxon devices are presented. An outline of the applications is made showing the advantages as well as the limitations.

1. INTRODUCTION

Superconductivity has led to the development of devices and electronics which offer extremely high sensitivity and very high speeds. Important building blocks in this area have been SQUID devices. Because of improvements in superconducting circuit fabrication in recent years, relatively new devices based on fluxons have also been developed and they present a variety of new applications. Since the operation of both types of devices, SQUID and fluxon, relies extensively on some of the basic properties of superconductors[1] their essential features will first be briefly outlined, followed by a description of the devices and their applications. The important features are:

(a) zero resistance
(b) Meissner effect
(c) magnetic flux quantization
(d) Josephson effects

At a critical temperature T_c, the resistance of a superconductor drops rapidly to zero, implying that a large number of electrons are involved in this transition. It is a second order phase transition in zero magnetic field. According to the BCS theory, current in a superconductor is carried by

pairs of electrons, Cooper pairs; their motion can be described by a single wavefunction. Because there is no resistance, these electron pairs maintain phase coherence over indefinitely large distances. Indeed this can be observed by setting up a persistent current in a ring or in a coil. The electron pairs can then be simply represented by a wavefunction

$$\psi\ (r,t) = |\psi_o(r,t)|e^{i\theta(r,t)} \qquad (1)$$

where the square of the modulus gives the pair density and θ is the phase of the waves describing the electron pairs. Since phase coherence is maintained, the question arises as to whether it is possible to observe interference and diffraction phenomena in this system and to use such effects for devices.

The magnetic behavior of a superconductor is equally interesting; it has led to the fundamental understanding of the superconducting state. While in a perfect conductor, the magnetic induction inside the material would remain at B = constant, in a bulk superconductor the induction B satisfies the condition that B = 0. This is known as the Meissner effect. Hence, a superconductor is a perfect diamagnetic material which excludes the inside field by maintaining surface currents. The surface current density varies with distance from the surface according to:

$$J(x) = J_o \exp. - x/\lambda_L \qquad (2)$$

where λ_L is known as the London penetration depth. This characteristic dimension depends inversely on the density of superconducting charge carriers. In type II superconductors above a critical field H_{c_1}, flux starts to enter the material producing quantized vortices, fluxons. These fluxons, known as Abrikosov vortices, can move when a current is passed through the material because of the Lorentz force acting on them.

When a current flows in a superconductor, the phase difference between 2 points depends on the wavelength of the superconducting electron pairs. It is determined by the current density and the external magnetic field. By taking the phase difference around a closed loop, it must be an integral multiple of 2π; this leads to the quantization of magnetic flux inside the

ring in units of h/2e, the flux quantum ϕ_o. Its value is 2.07×10^{-7} Gauss cm^2 and it sets the scale for devices whose operation is based on flux quantization. When a superconducting ring is cooled below T_c, the total flux through it will be an integral multiple of flux quanta and it will remain in that state, since the flux through a resistanceless circuit must be constant. To change the state of the ring it must be driven normal, either with a field larger than the critical field or by raising its temperature above T_c. However, there is another method of changing the state of the ring and that is by tunneling when a barrier is placed in series with the ring.

The Josephson effects deal with the phenomenon of tunneling by superconducting electrons through a barrier. Indeed, if an insulating barrier is placed between 2 superconducting electrodes, the Cooper pairs can tunnel through the barrier without resistance and hence with no voltage across it. Such a current flow depends on the phase difference $\Delta\theta$ across the barrier and is usually presented as

$$i = i_o \sin\Delta\theta \qquad (4)$$

where i_o is the critical current of the barrier and it is a strong function of the barrier thickness. When a magnetic field is applied to the junction, it will affect the phase of the superconducting electrons and thus cause the junction to exhibit a diffraction pattern in its critical current. This is shown in Fig. 1. Consequently an external magnetic flux will reduce the junction current to zero when the flux through the barrier is equal to an integral multiple of 2π, i.e. a small external magnetic field can switch a junction off.

When a voltage V is maintained across the junction, the phase of the Cooper pairs will vary in time at a frequency of 2 eV/h leading to an ac current, according to equation 4. The frequency of this current is 483.6 MHz per microvolt across the junction.

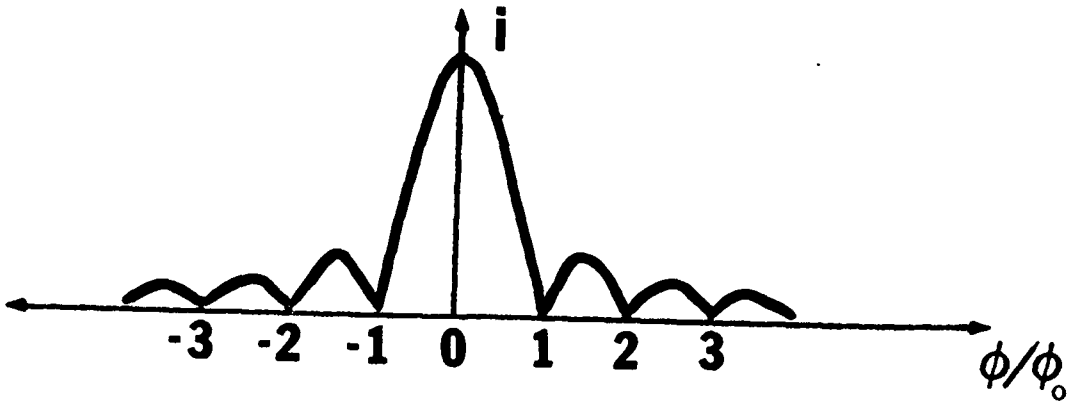

Fig. 1. Diffraction pattern of a Josephson junction; critical current as a function of external flux normalized to ϕ_0.

2. SQUID DEVICES

In order to obtain high resolution in magnetic field, a large area has to be used, since the flux ϕ depends on the field and the area. Since the junction is usually small this is achieved by using an interferometer which consists of a relatively large area loop or ring coupled to the junction; the junction area could also be increased but this would raise the capacitance and hence reduce its speed. The fabrication of the interferometer can be achieved by using a single junction connected to a ring as shown in Fig. 2a; a measurement of its impedance would determine the state of the junction. The interferometer could also be a ring interrupted by 2 junctions (or more) as in Fig. 2b and a measurement of the dc current through it would also determine the state of the junction. In the first case we have a r.f.-biased SQUID (Superconducting Quantum Interference Device) while in the second case it is a dc-biased SQUID. For both the response is periodic in units of ϕ_0 to the flux passing through the loop[2].

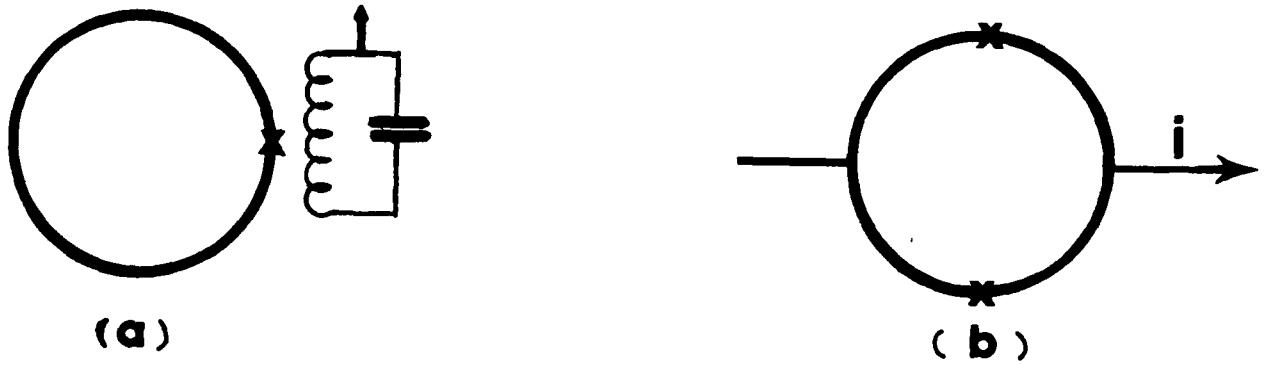

Fig. 2. SQUID sensors. (a) rf-biased (b) dc-biased.

The large enhancement of the sensitivity to magnetic fields achieved by increasing the area of the loop has an upper limit. This limit is dictated by the thermal noise of the device. For a SQUID of inductance L at the temperature T, the flux noise ϕ_n is set by the Equipartition Theorem, ϕ^2_n = LkT. The size of the SQUID must not be large or else the noise level will smear the quantum effect.

In the single-junction device, the rf-biased SQUID, its impedance is measured by a tank circuit coupled to it, the bias current being usually at about 20 MHz. The magnitude of the voltage across the tank circuit is an oscillatory function with period ϕ_0, of the external flux coupled to the device. In order to linearize its response, negative feedback is used by sending back into the tank circuit coil the output current, thus using the device as a self-balancing null-detector[3]. Sensitivities of $10\text{-}^4\phi_0/\sqrt{Hz}$ are usually achieved. For the dc-biased SQUID its critical current is an oscillatory function of the external magnetic flux applied to it[2], the period being ϕ_o. Here as well the voltage across the junction is an oscillatory function of magnetic flux coupled to it. The magnetic flux resolution is typically $10\text{-}^4\phi_0/\sqrt{Hz}$. Recently a dc SQUID was developed[4] such that the flux noise level was $\phi_n = 8.4\text{x}10\text{-}^8\phi_0/\sqrt{Hz}$. This was possible by making the loop inductance very small (the loop was 17.5 μm across) and by reducing the temperature down to 290 mK.

Since the SQUID is a device sensitive to magnetic flux, it is important to consider how to couple to it efficiently flux from a sample. This is particularly important when the sample conditions have to be changed, the temperature or magnetic field for example, without interfering with the SQUID. Usually a flux transformer is used for that purpose. This is shown in Fig. 3. Since in a circuit with zero resistance, the total flux through it must be constant, any flux change from a sample coupled to a pick-up coil of the transformer will be transported to the SQUID coil in that circuit by the induced current. Such a flux transformer can also act as a spatial filter[5] with the pick-up coil being in a gradiometer configuration; by a suitable choice of gradiometer dimensions and characteristics, unwanted signals can be

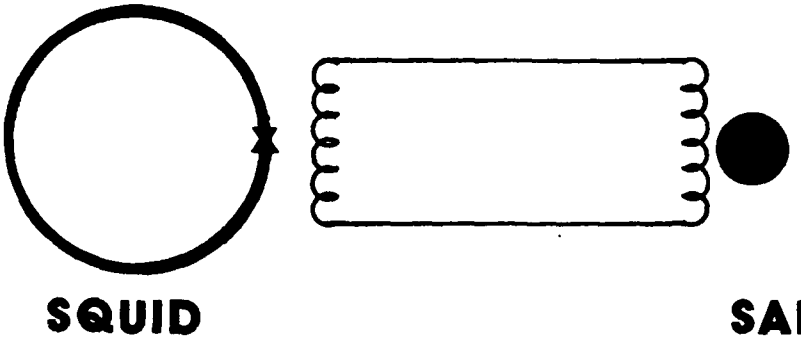

Fig. 3. Coupling a signal from sample to rf-biased SQUID using flux transformer .

effectively eliminated. This allows the full sensitivity to be used for measuring sample signals. Although the transformer is usually a 3-dimensional device planar transformers have recently been developed with high performance characteristics.

The applications of SQUID devices can be divided essentially into 2 groups: those at low frequencies and the ones for high speed operations. Magnetometers usually fall in the first group. Although there is a variety of configurations, the basic idea is to couple by means of a flux transformer the magnetic flux from a sample to the SQUID which is d.c.-biased or r.f.-biased. By using the flux transformer as a gradiometer, the gradient order being dictacted by the application, extremely high sensitivity has been achieved. The SQUID magnetometer has been used to detect the bulk dc magnetization of nuclear spins[6], the detection of magnetic resonance[7], and the behavior of many magnetic systems. Sensitivities[4] of $\approx 10^3$ spins/$\sqrt{Hz}$ at T=300mK have been demonstrated. The applications of SQUID magnetometers to biomagnetism[8] have made major advances in that field, especially in the detection of the magnetic fields due to the heart activity, the brain, and neurons[9]. An extremely important factor has been the very low noise achieved by the SQUI magnetometer. There is an advantage, especially at low frequencies, in measuring a magnetic signal as opposed to an electrical one in biomagnetism where there are problems in detector drift and contact potentials. Consequently the SQUID has become the ideal device for many biomagnetic studies. A SQUID can also be used to measure very small voltages[10]; this can be achieved by making it a null current sensor in a potentiometer circuit. In such a configuration it is possible to detect the rms Johnson noise in a 10^{-8} ohm resistor at 1K, which is 8×10^{-16} V/$\sqrt{Hz}$.

The applications presented above have used the SQUID at low frequencies, covering the range from dc to tens of kiloHertz, and they have been analog applications. Should the need arise, the SQUID can be adapted to higher frequency ranges. For example it was used to make a radio-frequency amplifier of very high sensitivity for the detection[11] of NMR and NQR; its performance was demonstrated up to 200 MHz.

In the field of digital electronics, the very high speed of SQUIDS offers many interesting applications. The basic building block is a very fast switch and the SQUID can perform this task very well. Fig. 4 shows how it can be adapted for this role by having a control line over it. The magnetic field of the control line will cause destructive or constructive interference of the electron-pair waves in the junctions. This leads to two states: superconductive or resistive, and hence switching action can be produced. The advantages of this circuit are in the very high sensitivity, switching speed in the picosecond range, and in the very low power dissipation, being orders of magnitude less than semiconductor devices. A variety of logic circuits have been developed and used for signal processing[12]. These include OR gates and AND gates. The SQUID is also the building block in a variety of Analog-to-Digital converters where it has been used as a quantizer[13], or else as the elements of the comparator.[14]

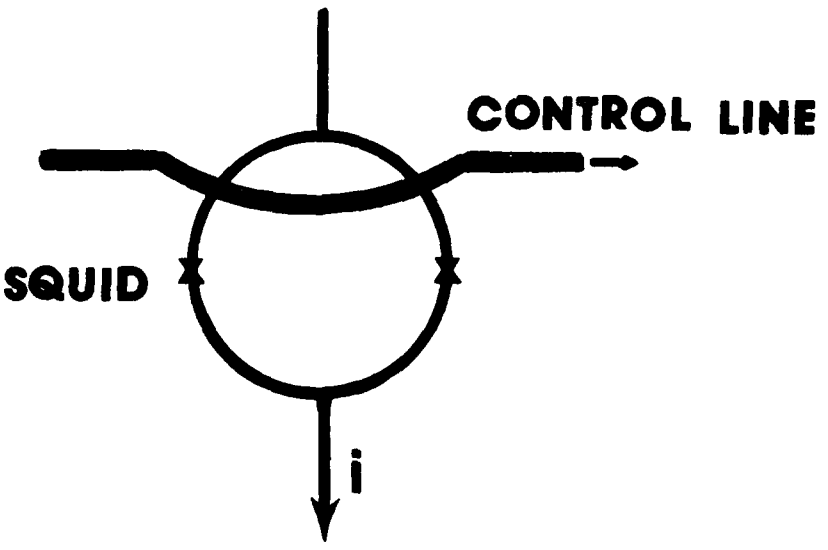

Fig. 4. SQUID as a switch.

3. FLUXON DEVICES

A bulk superconductor will screen exponentially a magnetic field from its interior, whether it is an external magnetic field or the self-field due to transport currents (equation 2), the characteristic dimension being the penetration depth λ_L. A similar situation can arise in certain Josephson junctions. Induced or transport currents are confined to the edges within a characteristic length λ_J, the Josephson penetration depth. It depends inversely on the density of charge carriers, i.e. the critical current density; it performs a role similar to the London penetration depth λ_L in bulk superconductors. It is given by

$$\lambda_J = \left| \phi_0 / 2\pi \, \mu_0 (2\lambda_L + t) \, J_c \right|^{1/2} \qquad (5)$$

where t is the barrier thickness and μ_0 the free space permeability. Screening will exist if one of the dimensions of the junction, L, is larger than λ_J. Similarly to a type II superconductor, quantized flux will start to enter the junction above a critical field H_{c_1}. These quanta are referred to as fluxons and they can behave as particles and waves. When there is a bias current through the junction, there will be a Lorentz force on the fluxons which can cause them to move inside the barrier. This is illustrated in Fig. 5. The behavior of fluxons in long Josephson junctions leads to a variety of interesting non-linear effects[15] as well as all sorts of applications. For a long uniform junction fluxon penetration starts to occur at a magnetic field H_{c_1} given by

$$H_{c_1} = (4/\pi) J_c \lambda_J \qquad (6)$$

By placing a control line over a long Josephson junction fluxons can be generated in the junction; the current in the control line can produce magnetic fields above H_{c_1}. A bias current passing through the junction will

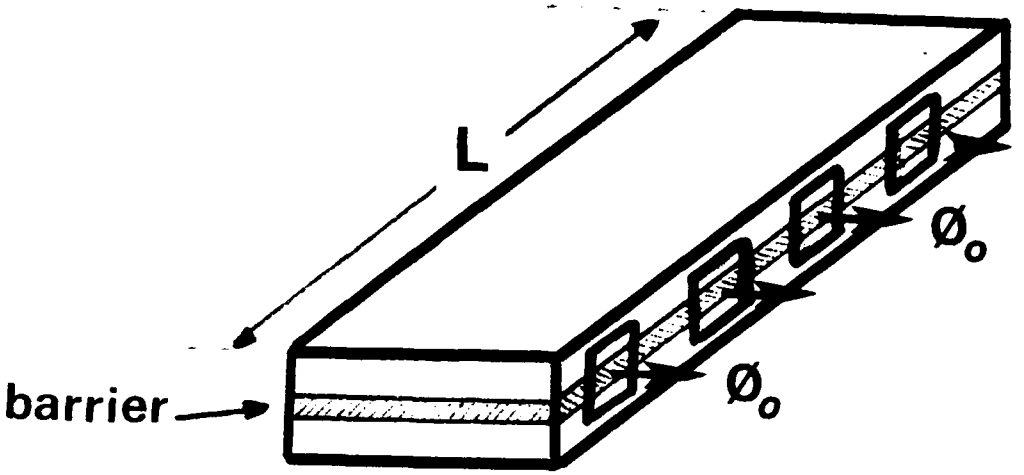

Fig. 5. Fluxons in long Josephson junction.

exert a Lorentz force on the fluxons causing them to move. Because of this motion a voltage will be generated across the junction and it will be proportional to the control current. Hence we have a device which acts as a current-controlled voltage source. The forces acting on the fluxons are due to the bias current and the frictional effects in the barrier and the electrodes, leading to motion which can be best described by a perturbed sine-Gordon equation, in normalized units, for the electron-pair phase ϕ,

$$\phi_{xx} - \phi_{tt} + \alpha\phi_t - \beta\phi_{xxt} + \sin\phi = \nu \qquad (7)$$

Here α is the damping parameter related to quasiparticles in the junction and β is the surface resistance parameter due to losses in the penetration depth of the top and bottom electrodes. The drive term ν can be dc or/and ac and it is normalized to the critical current of the junction. Subscripts indicate partial derivatives with respect to position x or time t.

The long Josephson junction with a control line is an interesting device for studies of the dynamics of fluxons and also for applications to electronics. Actually this device has similarities with the semiconductor FET. Here fluxons play the same role as holes or electrons in the semiconductor devices. The control current determines how many fluxons are generated in the junction and consequently it determines the voltage across the junction. In the SQUID devices there was flux quantization in the loop, in the long junction there is flux quantization in the barrier leading to

Josephson fluxons; the motion of fluxons however is dissipative.

Two questions arise about this device: what is its speed and does it have gain? The speed of the fluxons is determined by the bias current and it saturates at the value of the speed $\bar{c}$ of electromagnetic waves in the junction. This speed is given by $\bar{c} = c/\sqrt{t/d}$ where c is the speed of light in vacuum, t the junction thickness and d the magnetic thickness of the junction. The intrinsic response of this device will essentially be the transit time for a fluxon along the barrier. This can be of the order of picoseconds for a junction with L being a few microns long. The gain characteristics can be obtained by considering the flux-flow phenomenon in the junction. When fluxons are generated by the control line, they can be packed together and they then behave like electromagnetic waves rather than particles. The induced voltage is then given[16] by $V = n\phi_0 v/L$, i.e.

$$V = r_m I_S \tag{8}$$

where I_S is the control current and r_m the transresistance of the device. The equivalent circuit for this device is given in Fig. 6 with R_L being the load resistor and R_D the dynamic resistance due to fluxon motion. This leads to a current gain given by:

$$I_o/I_S = r_m/(R_D + R_L) \tag{9}$$

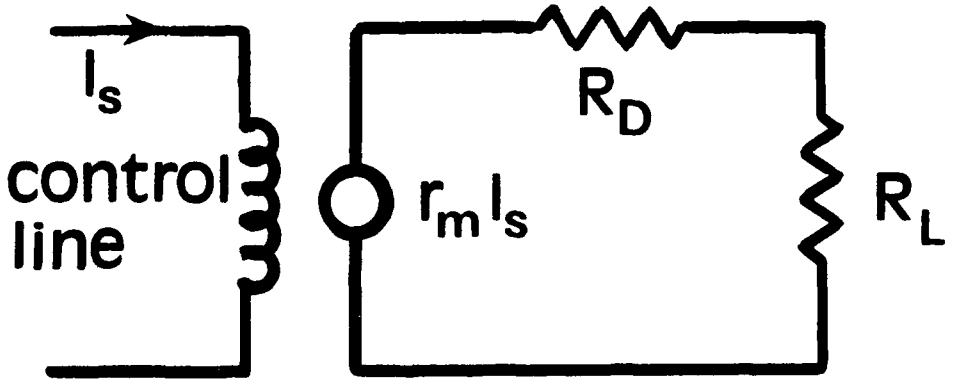

Fig. 6. Equivalent circuit for long Josephson junction.

and the transresistance r_m is given by

$$r_m = \mu_0 d\bar{c}/W_s \tag{10}$$

with W_s being the width of the control line. Materials like NbN with a large λ_L will have a large magnetic penetration distance d and hence a large transresistance. Since r_m has a wide linear range this device can be used in a practical flux-flow amplifier. Indeed current gains larger than ten have been quoted[16]. It is interesting to note that this device is the dual of a FET which is a voltage controlled current source. It has gain, it is inverting, and it is non-latching in the voltage state. Also it has a wide dynamic range, increasing with the energy gap of the material.

In the above analysis a uniform current distribution in the junction has been assumed. Although $L > \lambda_J$, a uniform current distrubution [17] can be achieved by using fingers for injecting the current at appropriate parts along the junction. In fact the gain of the device is strongly dependent on the current distribution[18]. Since so far the devices have been physically quite long, their full potential has not been explored; however improvements in fabricating high current density junctions will lead to smaller λ_J and hence smaller devices.

It is difficult to observe directly fluxon motion in long Josephson junctions[19]. However because of the dynamics of the fluxons, the I-V curves provide evidence for their motion. This is seen, in the voltage state, as a series of current steps on the I-V curves. Two types of steps are seen. First, fluxons are reflected from the junction ends becoming anti-fluxons at each reflection; this leads to standing waves in the junction. Such a mode is seen as current steps at voltages $V = n\phi_0\bar{c}/L$ and it is referred to as zero-field steps (ZFS). The second mode occurs in a magnetic field when the fluxon array behaves like an electromagnetic wave which can excite resonant modes of the junction; the long junction is essentially a cavity with its own

resonances. The excitation of these modes leads to current steps at voltages $V = n\phi_0\bar{c}/2L$ and the steps are known as Fiske steps. In both cases the step structure indicate resonances inside the junction. The existance of fluxons in the junction has been confirmed by laser[20] and electron beam scans[21].

When fluxons are reflected in a long junction or absorbed at the junction edges electromagnetic radiation is emitted and these mechanisms can lead to oscillators in the millimeter and submillimeter wavelength regions. One type of oscillator is based on the resonant fluxon oscillations[22]. The emitted frequencies have discrete values given by

$$f = n\bar{c}/2L \tag{11}$$

where n is an integer corresponding to different harmonics. A major difficulty with this oscillator is the relatively small tuneability and the low power output ($\sim 10^{-12}$W). The linewidth of the oscillations is determined mainly by the thermal noise[23], typical values being a few kiloHertz at a frequency of 10 GHz., The second type of oscillator uses the fluxon flow mode[24] where fluxons are generated at one edge, accelerated by the bias current, and absorbed by a load at the other edge. The oscillator frequency is determined by an external magnetic field H_e according to

$$f = \mu_0 \, d\bar{c} H_e/\phi_0 \tag{12}$$

The upper limit of this oscillator is expected to be the energy gap Δ of the electrodes of the junction since $f = \Delta/e\phi_0$. For a gap of 2.5 meV as in NbN, the upper frequency should be approximately 1THz. The continuous tuneability of this oscillator and its relatively higher power output, $\sim 10^{-6}$ watt, make this device suitable for circuits such as the local oscillator for a receiver, and for spectroscopy. The emitted radiation can be coupled capacitively or inductively to a small detector Josephson junction whose I-V curve displays Shapiro steps due to the radiation. Since a narrow linewidth is desirable, the steepness of the current step is very important here.

Digital applications of fluxon devices show much promise at to speed and sensitivity. A fluxon in a junction can be used as an information bit.

It can be stored in a potential well created by magnetic fields of control lines and it can be moved by suitable magnetic fields. This principle[25] has been used in a fluxon shift register[26]. Fig. 7 shows the basic arrangement, the control lines being used to trap and to move the fluxons. A proposal has been made for using fluxons in logic networks[27].

Fluxon devices have not yet achieved the popularity of SQUID devices; this is due, in part, to the difficulty in fabricating a device which is long and yet free of defects and pinholes in the barrier. With improvements in fabrication techniques, the potentials of long junctions have been recognized and already explored for a few applications.

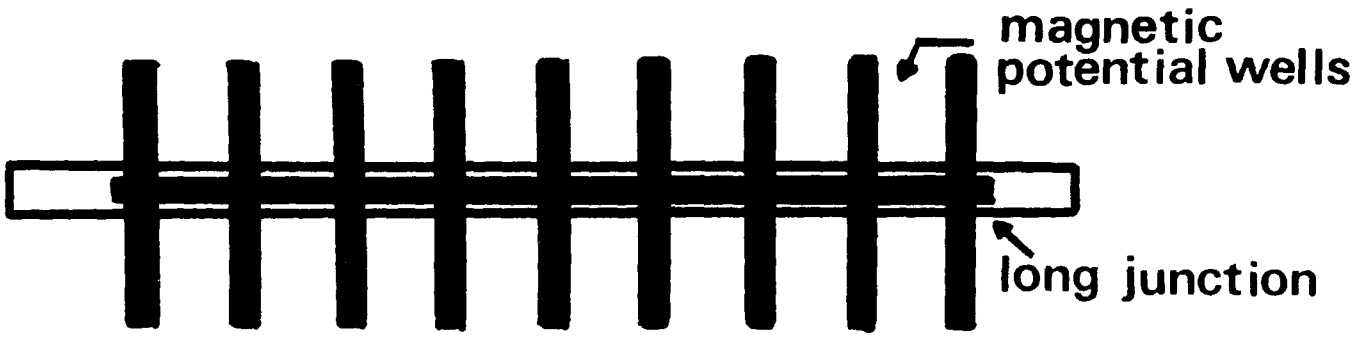

Fig. 7. Basic shift register.

4. HIGH T_c DEVICES

The recent discoveries of high temperature superconductors have opened the possibility of developing superconducting electronics which can operate at 77K or even higher temperatures, thus reducing the cost of refrigeration. The achievements are very encouraging. SQUIDS, both rf[28] and dc biased[29], have been developed with impressive characteristics. Since the operating temperature will be higher than 4.2K, higher noise levels are expected than with conventional superconducting devices; the performance however is expected to be better than with regular semiconductor devices. Thin-film TlBaCaCuO dc SQUIDS have been developed[30] for 77K operation with noise levels of ~ 10^{-5} - 10^{-6} $\phi_0/\sqrt{Hz}$ at 1kHz. This is comparable to commercially available devices operating at 4.2K. RF-biased SQUIDS have also been developed with quite good

characteristics. The magnetic resolution is quoted to be ~ 4 x $10^{-4}\phi_0/\sqrt{Hz}$ at 75K. These junctions consist of weak links which were fabricated using the "break junction" technique at helium temperatures or at room temperature. As the fabrication techniques improve and the devices become better, it is important that they be well shielded. Superconducting shields, in the shape of tubes, have been developed[31] for shielding SQUIDS and devices at relatively low magnetic field disturbances (maximum of ~ 50 Gauss). The new ceramic superconductors are granular in nature with many defects in the material. These defects (there is a variety of them) tend to form weak links and arrays of Josephson junctions in bulk and thin film samples. Some of these junctions have the characteristics of long Josephson junctions with Josephson fluxons moving inside them. These fluxons have been responsible for some of the microwave losses at low magnetic fields.

Although Josephson junctions have not been fabricated yet, in part due to the very short coherence lengths in the high T_c materials, the naturally occuring junctions have made it possible to develop[32] already a few devices. These new materials offer interesting challenges.

REFERENCES

1. M. Tinkham, Introduction to Superconductivity, McGraw Hill Book Company, 1975.
2. J. Clarke, Proc. of the IEEE, 61 (1973) 8.
3. R. A. Webb, R. P. Giffard, and J. C. Wheatley, J. Low Temp. Phys. 13 (1973) 383.
4. D. D. Awschalom, J. R. Rozen, M. B. Ketchen, W. J. Gallagher, A. W. Kleinsasser, R. L. Sandstrom, and B. Bumble, Appl. Phys. Lett. 53 (1988) 2108.
5. P. Costa Ribeiro, A. C. Bruno, C. C. Paulsen, and O. G. Symko, Rev. Sc. Instr. 58 (1987) 1510.
6. E. C. Hirschkoff, O. G. Symko, L. L. Vant-Hull, and J. C. Wheatley, J. of Low Temp. Phys. 2 (1970) 653.
7. R. V. Chamberlin, L. A. Moberly, and O. G. Symko, J. of Low Temp. Phys. 35 (1979) 337.
8. S.J. Williamson and L Kaufman, J. of Magn. and Magnetic Materials 22 (1981) 129.
9. J. P. Wikswo, Jr., Rev. Sc. Instr. 53, (1982), 1846.
10. J. E. Lukens, R. J. Warburton, and W. W. Webb, J. Appl. Phys. 42 (1971) 27.
11. N. Q. Fan, M. B. Heaney, J. Clarke, D. Newitt, L. L. Wald, E. Hahn, A. Bielecki, and A. Pines, IEFE Trans. on Magn., MAG - 25 (1989) 1193.
12. T. Van Duzer, NATO Advanced Study Institute, Superc. Electr. Il Ciocco, Italy 1988, Springer - Verlag 1989.

13. J. P. Hurrell, D. C. Pridmore - Brown, and A. H. Silver, IEEE Trans. Electron Device, ED-27 (1980), 1887.
14. C. A. Hamilton, F. L. Lloyd, R. L. Kautz, IEEE Trans. on Magn. MAG-21 (1985) 197.
15. K. K. Likharev, Dynamics of Josephson Junctions and Circuits, Gordon and Breach Science Publishers, 1986.
16. T. Hashimoto,T. Nagatsuma, K. Enpuku, and K. Yoshida, IEEE Trans. on Magn. MAG-23 (1987) 723.
J. Jan and J. E. Nordman, IEEE Trans. on Magn. MAG-23 (1987) 163.
B. J. Van Zeghbroeck, IEEE Trans. on Magn. MAG-21 (1985) 916.
17. K. K. Likharev, V. K. Semenov, O. V. Snigirev, and B. N. Todorov, IEEE Trans. on Magn. MAG - 15 (1979) 420.
18. B. Lee, O. G. Symko and D. J. Zheng, 1987 Intern. Superc-Electronics Conf., Tokyo, Japan, p.204.
19. A. Matsuda and T. Kawakami, Phys. Rev. Lett. 51, (1983) 694.
20. J. R. Lhota, M. Scheuermann, P. K. Kuo, and J. T. Chen, IEEE Trans. on Magn. MAG-19 (1983) 1024.
21. J. Bosch, R. Gross, M. Koyanagi, and R. P. Huebener, Phys. Rev. Lett. 54 (1985) 1448.
22. M. Cirillo, I. Modena, P. Carelli and V. Foglietti, Phys. Lett. A 132 (1988) 20.
23. E. Joergensen, V. P. Koshelets, R. Monaco, J. Mygind, M. R. Samuelson, and M. Salerno, Phys. Rev. Lett. 49 (1982) 1093.
24. T. Nagatsuma, K. Enpuku, K. Sneoka, K. Yoshida, and F. Irie, J. Appl. Phys. 54 (1983) 3302.
25. T. A. Fulton, R. C. Dynes, and P. W. Anderson, Proc. of the IEEE 61 (1973) 28.
26. T. A. Fulton and L. N. Dunkleberger, Appl. Phys. Lett. 22 (1973) 232.
27. K. Nakajima, Y. Onodera, and Y. Ogawa, J. Appl. Phys. 47 (1976) 1620.
28. J. E. Zimmerman, J. A. Beall, N. W. Cromar, and R. H. Ono, Appl. Phys. Lett. 51 (1987) 617.
29. R. H. Koch, C. P. Umbach, G. J. Clark, P. Chaudhari, and R. B. Laibowitz, Appl. Phys. Lett. 51 (1987) 200.
30. R. H. Koch, W. J. Gallagher, B. Bumble, and W. Y. Lee, Appl. Phys. Lett.54 (1989) 951.
31. O. G. Symko, W. J. Yeh, D. J. Zheng, and S. Kulkarni, J. Appl. Phys. 65 (1989) 2142.
32. J. Clarke, Nature 333 (1988) May 5, p 29.

THIS PAGE IS INTENTIONALLY BLANK

Presented at the Workshop on High Temperature Superconductivity
23-25 May 1989 GACIAC PR-89-02

High-Frequency Superconducting Electronics

J. Zmuidzinas and J. R. Tucker
University of Illinois
Urbana, IL 61801

ABSTRACT

The discovery of the new high-T_c materials raises the possibility of much more extensive development and practical utilization of superconductors in electronic devices and circuits. The primary advantages over existing semiconductor technology are the high-frequency response and ultra-low noise that could potentially be realized in high-T_c integrated circuits, which would at the same time require far less cooling power than conventional low-T_c superconductors. Here we briefly survey the principle high-frequency electronic applications of present-day superconductors, and offer our opinion on a stategy for capitalizing on the use of high-T_c materials in the future.

1. INTRODUCTION

Considerable progress has been made in recent years in the field of high-frequency analog superconducting electronics. Components such as mixers, oscillators, amplifiers, phase-shifters, low-loss transmission lines, and antennas can now be fabricated using thin-film technology and microlithography. Refractory metal superconductors such as Niobium (Nb) and Niobium Nitride (NbN) are increasingly used, having transition temperatures of 9K and 16K, respectively. These materials yield more reliable and stable electronic properties than comparable lead-alloy devices. In many cases, the performance of the individual superconducting components greatly exceeds that of their semiconductor counterparts, both in speed and sensitivity.

An important example is the SIS quasiparticle mixer[1], which is now the most sensitive detector of millimeter wave radiation. It utilizes single-electron tunneling in a superconductor-insulator-superconductor (SIS) junction as the nonlinear mixing element, in place of a semiconductor Schottky diode. Photon-assisted tunneling at dc biases below the gap voltage is then exploited to approach the quantum limit for mixer noise temperature, $T_M \approx h\nu/k$, set by the Heisenberg uncertainty principle. An additional quantum effect, known as conversion gain, is also used to amplify the incoming signal in the process of frequency down-conversion. This phenomenon is forbidden in all "classical" resistive mixers such as Schottky diodes; and it is this gain effect that allows practical SIS receivers to approach the quantum limit for sensitivity today in the millimeter wave region 30 GHz<ν<300 GHz.

Josephson effect oscillators have been operated at frequencies as high as 1000 GHz[2], and it now appears feasible to engineer these devices with sufficient power and spectral purity to serve as local oscillators in SIS receivers[3,4]. Active devices such as mixers and oscillators can be integrated through the use of planar superconducting transmission lines. Low-loss propogation at submillimeter wavelengths has already been demonstrated[5]. In contrast, severe attenuation produced by ohmic dissipation in normal metal transmission lines generally limits their practical use to frequencies below 100 GHz. High-performance passive components such as couplers, filters, resonators, and impedance matching networks can also be fabricated using superconducting transmission lines.

2. SO WHY AREN'T SUPERCONDUCTING DEVICES USED MORE TODAY?

According to the foregoing considerations, it seems that the potential now exists to develop the advantages of integrated superconducting electronics, using conventional low-T_c Nb-based superconductors. This is indeed the case, but progress is relatively slow. The major driving force at the present time is the desire of the astronomy community for more sensitive receivers at millimeter, and especially at submillimeter, wavelengths. Such instruments are crucial to future explorations of the interstallar medium, the cosmic background, and a host of other issues central to our view of the universe. The problem here is that the total resources available for this activity are extremely meager. On the other hand, enormous resources are now being committed to research on GaAs semiconductor electronics with the goal of increased speed. Some electronic functions that are now performed by semiconductors could eventually be performed faster and better by superconductors, but the cryogenic requirements and lack of an integrated technology preclude their use today.

The high-T_c materials may greatly reduce, or even eliminate, the need for elaborate cryogenics. Furthermore, the high-frequency limit for superconducting electronics is determined by the superconductor energy gap, which is ≈700 GHz for Nb and ≈1400 GHz for NbN. High-T_c materials have much larger energy gaps, and should therefore allow operating frequencies to be extended well into the submillimeter wave region. At the present time, however, the high current density films and tunnel junctions that are required for high-frequency electronic applications remain to be developed. These fundamental materials problems are readily apparent, and they must receive appropriate research funding. On the other hand, it should be recognized that the development of an advanced integrated circuit technology based upon superconducting materials faces basic engineering problems as well. At frequencies beyond about 300 GHz, the problem of providing efficient antenna structures for detectors and arrays, for example, is extremely challenging. If we expect to utilize this submillimeter wave spectral region effectively, some thought should be given now to the development of an integrated superconductor electronics capability based upon the presently-available Nb technology, which could then be replaced by high-T_c materials as they become available. While the advent of suitible high-T_c films may seem a long way off today, their revolutionary

potential would seem to justify a modest effort in this direction. Some low-T_c circuit applications would be of direct relevance to the DOD. Integrated receiver circuits would be useful for communications, imaging systems, and radar, for example. Research applications of high-speed superconductor electronics include fundamental device physics, submillimeter astronomy, submillimeter and far-infrared spectroscopy of molecules and materials, plasma diagnostics, remote sensing, and ultrahigh-speed circuit testing.

3. FUTURE DEVELOPMENT OF SUBMILLIMETER WAVE MIXERS

As an example of work now in progress on high-frequency superconducting electronics, we shall briefly describe the current effort at the University of Illinois to extend SIS mixer operation into the submillimeter wave region at 800GHz. Submillimeter wave SIS receivers require junctions with small RC products. The RC product is independent of area, and can only be reduced by decreasing the thickness of the insulating oxide tunnel barrier. This is generally accompanied, however, by an increased subgap leakage current which adversely effects mixer performance. Thus, it is advantageous to choose a junction fabrication technology which produces high-quality tunnel barriers with very small leakage currents. Junctions fabricated using Nb/Al-oxide/Nb trilayers are particularly suitable in this regard[6,7], and have already demonstrated good performance in millimeter wave mixers[8,9]. The junction areas must be reduced to $\leq 1\mu m^2$ in order to meet impedance matching requirements at submillimeter wavelengths, however.

Small-area ($\approx 1\mu m^2$) Nb/Al-oxide/Nb junctions have only recently been fabricated[10,11]. Working in collaboration with F. Sharifi, D. J. Van Harlingen, and K. Y. Lo [12], we have followed a similar process in fabricating junctions with areas as small as $0.5\mu m^2$. Very briefly, a Nb/Al-oxide/Nb trilayer sandwich is deposited over a relatively large area $\approx 10\mu m \times 10\mu m$. Next a small portion of this trilayer ($\approx 1\mu m^2$) is masked with photoresist, and the top Nb layer surrounding this area is removed using reactive ion etching. An SiO_2 insulating film is then evaporated around the remaining $1\mu m^2$ of the top Nb film. Finally, Nb contacts are deposited onto the two junction electrodes.

This process produces the high-quality junctions required for SIS mixers. We have fabricated junctions with an area $3\mu m^2$ having subgap to normal resistance ratios $R_{sg}/R_N \approx 35$. For these junctions, $\omega R_N C \approx 3$ at 230 GHz. Junctions with areas of $1\mu m^2$ and $\omega R_N C \approx 3$ at 800 GHz have been fabricated with somewhat degraded characteristics $Rsg/R_N \approx 7$. Although the latter junctions are quite adequate for use at 800 GHz, we are confident that the subgap leakage can be significantly reduced (without affecting the $R_N C$ product) by optimization of the trilayer deposition parameters.

Low-noise SIS mixers require efficient coupling of the incident radiation into the tunnel junction. This coupling is maximized by: 1) matching the antenna pattern of the mixer to the incident radiation, and 2) matching the junction impedance to that of the mixer mount. At millimeter wavelengths, these conditions are met by employing properly designed feedhorns and single-mode waveguide mounts. At submillimeter wavelengths, it becomes increasingly difficult to achieve the mechanical tolerances needed to

fabricate the required horns and mounting structures. For this reason, quasi-optical mixers in which an integrated planar feed antenna and an SIS junction are fabricated onto a single substrate using photolithographic techniques become attractive. However, the antenna must be carefully designed to insure that it produces a beam pattern which couples efficiently to the telescope, and that the antenna and junction impedances are well matched. These issues have not been adequately addressed in previous work at submillimeter wavelengths. Our approach here will be to trade the extremely broad bandwidth possible with frequency-independent designs such as bowtie, spiral, and log-periodic antennas in return for optimized performance over a narrower bandwidth.

Our 800 GHz mixer design consists of a twin-slot planar feed antenna, a single $1\mu m^2$ Nb/Al-oxide/Nb SIS junction, and a tapered transmission line joining the junction to the two slot antennas. A hyperhemispherical lens is used to focus the incident radiation onto the twin-slot antenna. A somewhat similar configuration for a quasi-optical Schottky diode mixer was previously described by Kerr, et al.[13]. The pricipal differences are that the Schottky design omitted the hyperhemispherical lens, used a quarter-wave section of transmission line for matching instead of a taper, and fed the two slots in series instead of in parallel.

The propogation of 800 GHz signals with negligible loss requires the use of superconductors in place of normal metals in the microstrip transmission lines. It is also necessary here to use NbN instead of Nb, since 800 GHz is above the gap frequency for Nb. We have developed a program which calculates the characteristic impedance and attenuation of superconducting microstrip lines taking into account the surface impedance of the superconducting films. This program is based on the work of Whitaker, et al.[5]. We have also made detailed calculations of the antenna pattern for our twin-slot design. The overall efficiency of coupling radiation into the junction is estimated to be in the range 0.4-0.65. This should provide extremely good mixer performance, when combined with the high-quality junctions we have fabricated. Furthermore, this sensitivity will be usable, since the mixer will be well coupled to a telescope. The saturation power of the mixer should be fairly high, because a relatively large (for 800 GHz), low-impedance junction will be used. Also, the $1\mu m^2$ junction size will allow the Josephson current to be easily suppressed by a magnetic field.

This basic mixer design is also likely to be useful at millimeter wavelengths. By including a shunt inductor to compensate for the junction capacitance and by using an anti-reflection coating on the hyperhemisphere, the coupling efficiency should improve to ≈ 0.7 (the antenna efficiency), which would then be comparable to that of standard waveguide mounts. Eliminating the necessity for waveguide mounts would greatly simplify the construction of millimeter wave SIS mixers, and would significantly enhance the prospects for 2-dimensional imaging arrays.

REFERENCES

[1] J. R. Tucker and M. J. Feldman, "Quantum detection at millimeter wavelegths", Reviews of Modern Physics, vol. 57, 1055, 1985.

[2] R. P. Robertazzi and R. A. Buhrman, "NbN Josephson tunnel junctions for terahertz local oscillators", preprint.

[3] A. K. Jain, K. K. Likharev, J. E. Lukens, and J. E. Savageau, "Mutual phase locking in Josephson junction arrays", Physics Reports, vol.109, 309, 1984.

[4] T. Nagatsuma, K. Enpuku, F. Irie, and K. Yoshida, "Flux-flow type Josephson oscillator for millimeter and submillimeter region", J. Appl. Phys., vol. 54, 3302, 1983.

[5] J. F. Whitaker, R. Sobolewski, D. R. Dykaar, T. Y. Hsiang, and G. A. Mourou, "Propogation model for ultrafast signals on superconducting dispersive striplines", IEEE Trans. Microwave Theory Tech., vol, MTT-36, 277, 1988.

[6] M. Gurvich, M. A. Washington, and H. A. Huggins, Appl. Phys. Lett., vol. 42, 472, 1983.

[7] A. W.Lichtenberger, C. P. McClay, R. J. Mattauch, M. J. Feldman, S.-K. Pan, and A. R. Kerr, IEEE Trans. Magn., preprint.

[8] J. Inatani, T. Kasuga, A. Sakamoto, H. Iwashita, and S. Kodaira, IEEE Trans. Magn., vol. MAG-23, 1263, 1987.

[9] S.-K. Pan, A. R. Kerr, J. W. Lamb, and M. J. Feldman, National Radio Astronomy Observatory, Electronics Division Internal Report No. 268, 1987.

[10] M. Yuda, K. Kuroda, and J. Nakano, Japn. J. Appl. Phys., vol. 26, L166, 1987.

[11] T. Imamura and S. Hasuo, J. Appl. Phys., vol. 64, 1586, 1988.

[12] J. Zmuidzinas, F. Sharifi, D. J. Van Harlingen, and K. Y. Lo, in Proc. International Symposium on Submillimeter and Millimeter Astronomy, Kona, Hawaii, October 3-6, 1988.

[13] A. R. Kerr, P. H. Siegel, and R. J. Mattauch, 1977 IEEE MTT-S Int. Microwave Symp. Digest, p. 96, 1977.

THIS PAGE IS INTENTIONALLY BLANK

Presented at the Workshop on High Temperature Superconductivity
23-25 May 1989 GACIAC PR-89-02

HIGH-FREQUENCY CAVITY APPLICATIONS AND MEASUREMENTS OF HIGH-TEMPERATURE SUPERCONDUCTORS

D. W. Cooke and E. R. Gray
Los Alamos National Laboratory
Los Alamos, New Mexico 87545

ABSTRACT

A potentially important application of high-temperature superconductors will be high-frequency accelerating cavities. Currently these materials are not competitive with Nb at liquid helium temperature or with Cu at room temperature. However, available data on high-quality single crystals suggest that the relatively poor rf properties (high surface resistance and low surface magnetic field) of bulk and film specimens are due to materials properties that can be eliminated by improved processing techniques. Recent progress in the fabrication of thin films, for example, demonstrates that this is indeed the case.

1.0 INTRODUCTION

A potentially important application of high-temperature superconductors (HTS) is radiofrequency (rf) accelerating cavities. The present industry standard is niobium, which, because of its relatively low transition temperature ($T_c \approx 9.3$ K), must operate at or below liquid helium temperature to achieve the desired high Q values. From a cryogenics viewpoint alone it is thus obvious that HTS ($T_c \sim 90$ K) offers a potential advantage over conventional superconductors. However, for HTS to effectively compete with Nb it must exhibit similar properties at higher temperature--namely, low values of surface resistance (R_s) at relatively high rf power levels. These two requirements have not been simultaneously met with HTS; however, no experimental or theoretical evidence exists which would imply that they are unattainable.

Research results to date suggest that the poor high-frequency performance is attributable in part to the granular nature of these materials. That is, they are comprised of superconducting regions separated by non-superconducting grain boundaries, which may contain insulating or metallic impurities. Elimination of the grain boundaries, and, consequently, of the impurities, will certainly lower R_s, as evidenced by recent single-crystal results.[1] Of course there are many other materials-related properties, such as poor stoichiometry, inclusions, grain size, etc., that may be deleterious to high-frequency performance. Nevertheless, the essential point is that poor

[1] D. L. Rubin, K. Green, J. Gruschus, J. Kirchgessner, D. Moffat, H. Padamsee, J. Sears, Q. S. Shu, L. F. Schneemeyer, and J. V. Waszczak, Phys. Rev. B **38**, 6538 (1988).

performance is strongly correlated with materials processing, and not with any inherent physical property. Consequently, with improved materials fabrication techniques, one can realistically expect to achieve high-frequency cavity performance of HTS in the very near future.

2.0 HIGH-FREQUENCY SUPERCONDUCTIVITY: FUNDAMENTALS

The primary advantage of superconducting cavities over non-superconducting ones is that a much smaller fraction of the input power is dissipated in the cavity walls (Joule heating). Because the power dissipation increases as the square of the accelerating voltage, it is clear that Cu cavities become very inefficient and expensive at higher particle kinetic energies. Alternatively, superconducting cavities have surface resistances that are 5 - 6 orders of magnitude lower than Cu. After factoring in the increased refrigeration costs required to maintain the requisite low temperatures (typical operating temperatures are 1.5 - 2 K for Nb), there is still a net gain of a factor of several hundred in overall operating cost of the accelerator.[2] A further improvement in accelerator technology could be realized if materials with low R_S existed at relatively high temperatures. This would eliminate the need for costly liquid helium refrigeration. High-temperature superconductors (T_C ~ 90 K) meet this latter requirement, and, with improved processing techniques, are expected also to satisfy the first one.

For a superconducting sample in a high-frequency cavity, the surface resistance, R_S, is defined by

$$P_s = \frac{1}{2} R_s H_s^2 \qquad (1)$$

where P_S represents the Joule losses per unit surface area of the sample, and H_S is the surface magnetic field. In the normal conducting regime ($T>T_C$) R_S is given by the usual skin-depth formula

$$R_s = \sqrt{\frac{\mu\omega}{2\sigma}} \qquad (2)$$

where μ is the permeability, ω is the measuring frequency and σ is the conductivity. At $T<T_C$ (superconducting regime) the charge carriers condense into Cooper pairs. In the presence of a dc field these pairs carry all the current, thereby shielding the normal electrons, and resulting in zero dc electrical resistance. In the presence of a high-frequency field the situation is more complicated and is most easily understood in terms of a "two-fluid model", one fluid associated with the normal conducting electrons and the other with the superconducting ones. When a high-frequency field is applied, the Cooper pairs move frictionlessly. They do, however, have inertial mass;

---

2 H. Padamsee, Cornell Univ., CLNS 88/844, Presented to MIT DOE/EPRI Workshop, Salem, Massachusetts, June 22-24, 1988.

therefore, forces must be applied to cause the reversal of their motion. These forces are related to electric fields which must exist in the skin layer of the superconductor. Thus normal electrons are continually accelerated and decelerated which leads to dissipation (Joule losses). The analytic expression which describes the surface resistance for a classical superconductor is[3]

$$R_S(\omega, T) = A\frac{\omega^2}{T}\exp[-\frac{\Delta(T)}{k_B T}] + R_{res} \qquad (3)$$

where $\Delta(T) = \alpha k_B T_C$ and $\alpha = 1.7 - 2.3$. R_{res} is a temperature-independent resistance which depends upon the quality of the material surface. Figure 1 depicts $R_S(T)$ for Nb_3Sn ($T_C = 18$ K) taken at a frequency $\omega = 8$ GHz, and clearly illustrates the behavior described by Eq. (3). Formally, BCS theory yields a result for R_S that is similar to Eq. (3), but includes other material parameters such as London penetration depth, coherence length, and electron mean free path.

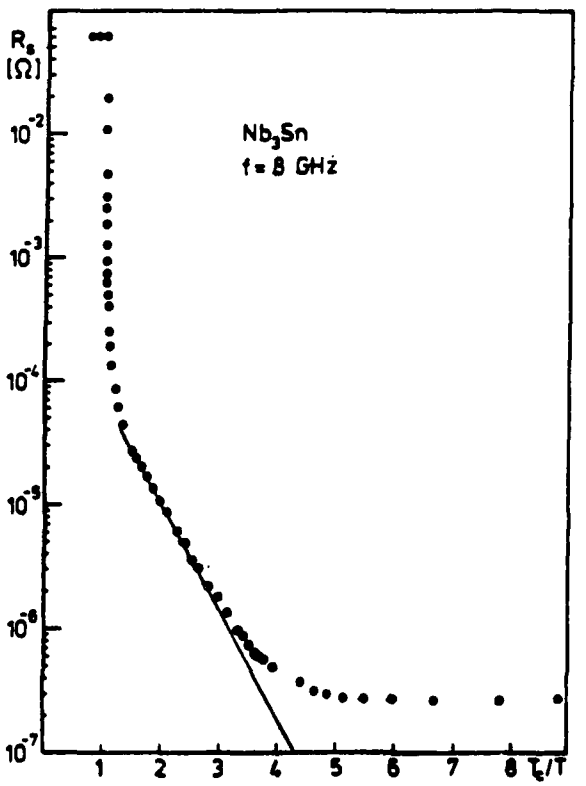

Figure 1. Surface resistance of Nb_3Sn (T_C=18 K) taken at 8 GHz. The straight line is proportional to $\exp[-\frac{\Delta(T)}{K_B T}]$. Taken from Ref. 3.

3 H. Piel, M. Hein, N. Klein, A. Michalke, G. Müller, and L. Ponto, Physica C **153-155**, 1604 (1988).

Of equal importance in the application of HTS to accelerators is the critical surface magnetic field H_S. This parameter determines the maximum accelerating voltage attainable before breakdown of superconductivity occurs. The numerical value of H_S is not equal to H_{C1} (lower critical magnetic field) as might be expected. For high frequencies it is possible for the Meissner state to exist in magnetic fields higher than H_{C1}, a field referred to as the superheating magnetic field, H_{Sh}. This results from the fact that a finite amount of time is required for a vortex to nucleate.[4] For Type II superconductors near H_{C1} the time is ~ 10^{-6} sec, whereas the high-frequency period is ~ 10^{-8} sec. For extreme Type-II superconductors, theory predicts that $H_{Sh} \sim 0.75\ H_C >> H_{C1}$, where H_C is the thermodynamic critical field. In Nb and Nb_3Sn critical fields greater than H_{C1} have indeed been measured.[4] In the case of Nb, H_C is 2000 Oe, which corresponds to an accelerating field of ~ 50 MV/m.[5] H_C for $YBa_2Cu_3O_7$ (YBCO) has been estimated to be as high as 27,000 Oe,[6] corresponding to a maximum accelerating field of 400 MV/m! Unfortunately, thermal breakdown is not the only impediment to attaining high electric fields in superconducting cavities. Generally, field emission loading and multipacting limit the maximum accelerating field to values much lower than those determined by H_{Sh}.[7] Preliminary measurements of electric-field breakdown and secondary electron emission in HTS materials have been made.[8]

3.0 CHARACTERIZATION TECHNIQUES

Surface resistance is the HTS high-frequency parameter most frequently measured; its value determines the potential of these materials for use in accelerating cavities. There are, however, many more research groups producing HTS samples than are measuring R_S, and a backlog of samples usually exists. It is important to determine which available specimens are likely to yield low values of R_S. The more conventional solid-state techniques do not necessarily provide this answer. For example, dc resistance determines the minimum percolative path of the bulk material but does not provide much information about the surface properties--a sharp resistive transition does not imply a low value of R_S. Thus, it is necessary to screen HTS material, be it bulk, film, or single crystal, so that time is not wasted on measurements of poor quality specimens. Ideally, these screening

---

4 T. Yogi, G. J. Dick, and J. E. Mercereau, Phys. Rev. Lett. **39**, 826 (1977).

5 H. Padamsee, Cornell Univ., CLNS 88/864, Presented to 1988 LINAC Conference, October, 1988.

6 T. K. Worthington, W. J. Gallagher, and T. R. Dinger, Phys. Rev. Lett. **59**, 1160 (1987).

7 G. Müller, M. Hein, N. Klein, H. Piel, L. Ponto, U. Klein, and M. Peiniger, Presented to European Particle Accelerator Conference, Rome, June 7-11, 1988.

8 Varian Corp., private communication.

techniques will be quick, simple, and inexpensive. Two measurement methods have emerged that satisfy the above-stated criteria, eddy current[9] and thermally stimulated luminescence.[10]

The eddy-current apparatus, shown schematically in Fig. 2, consists of a split coil connected to a resonant (~ 20 MHz) tank circuit of fixed capacitance. When an HTS sample (bulk, film, or crystal) is introduced between the coils, eddy currents are induced in it which modify the mutual inductance of the resonant circuit. The magnitude of the induced eddy currents depends on the conductivity of the sample, which, in turn, depends on the temperature.

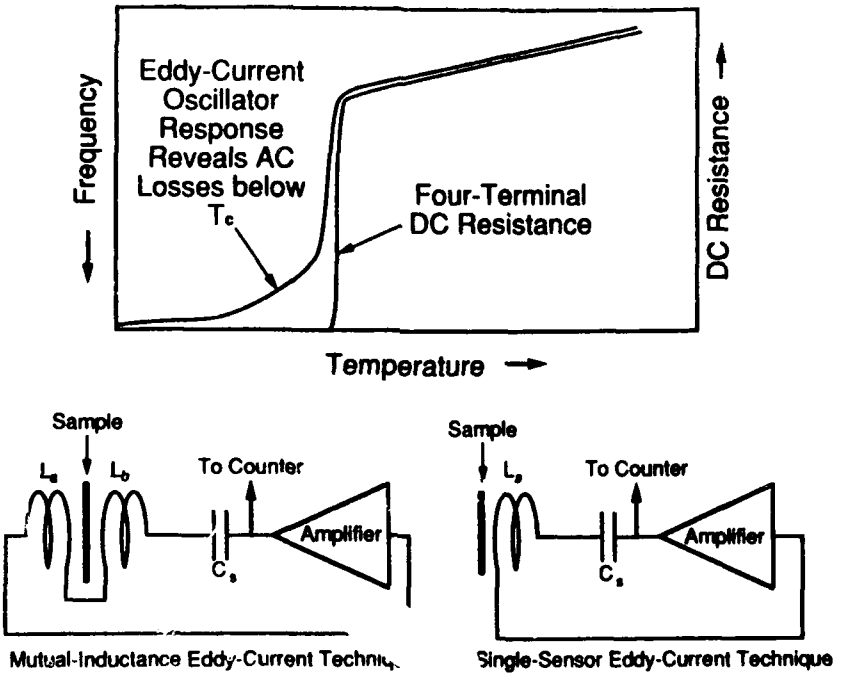

Figure 2. Schematic of eddy-current apparatus showing both the split-coil and single-coil configurations. Upper portion shows comparison between typical eddy-current and dc resistance data.

A plot of the resonant frequency vs. temperature produces a curve similar to the one shown in Fig. 2. The data are acquired in ~1 hr by the computer-controlled system. A principal advantage of the technique is that no electrical contacts are required for the measurement, this is especially important for thin films. Above T_C the technique probes a sample volume comprised of the surface area, A_S, and depth, δ, given by the normal skin-depth equation

---

9 J. D. Doss, D. W. Cooke, C. W. McCabe, and M. A. Maez, Rev. Sci. Instrum. 59, 659 (1988); J. D. Doss, D. W. Cooke, P. N. Arendt, M. Nastasi, R. E. Muenchausen, and J. R. Tesmer, Superconductor Sci. and Tech. To be published.

10 D. W. Cooke, M. S. Jahan, J. L. Smith, M. A. Maez, W. L. Hults, I. D. Raistrick, D. E. Peterson, J. A. O'Rourke, S. A. Richardson, J. D. Doss, E. R. Gray, B. Rusnak, G. P. Lawrence, and C. Fortgang, Appl. Phys. Lett. **54**, 960 (1989).

$$\delta = \sqrt{\frac{2}{\mu\omega\sigma}} \qquad (4)$$

where μ is the magnetic permeability, ω is the measuring frequency, and σ is the electrical conductivity. In the superconducting state ($T<T_C$), the volume consists of A_S and the magnetic field penetration depth, $\lambda(T)$, given by the empirical formula

$$\lambda(T) = \frac{\lambda(0)}{\sqrt{1-\left(\frac{T}{T_C}\right)^4}} \qquad (5)$$

where $\lambda(0)$ is the penetration depth at T=0, taken to be 1500 - 1900 Å.[11] The essential feature is that the technique is probing the surface region, which is also the region of interest in the high-frequency measurement.

A second useful screening technique is thermally stimulated luminescence (TSL). The basic utility of the method lies in the fact that only insulators, and not metals, luminesce. Therefore, if insulating impurities such as metal carbonates and oxides exist within ~ 1μm of the superconducting surface, they will, upon excitation, exhibit TSL. These impurities, which result from improper processing of the material, contribute to high values of R_S, and, consequently, must be removed from the HTS surface. Because HTS materials are opaque with relatively large absorption coefficients (10^4 - 10^6 cm^{-1}), the TSL photons emanate from with ~ 1μm of the surface, which is precisely the region that determines R_S.

Experimental equipment for TSL measurements consists of a heater and photomultiplier tube enclosed in a light-tight box. A high-voltage power supply and amplifier control the signal, which can be plotted on an x-y recorder. Excitation can be done with x- or γ-radiation without any harm to the superconducting properties. A typical readout time is ~ 85 sec. Interpretation of the results is straightforward, if any TSL signal is observed it must be coming from insulating impurities residing near the surface, and these must be removed if low values of R_S are to be achieved. We have used this method to screen bulk, single-crystal, and in some cases, films of HTS material to estimate R_S. A quantitative correlation of R_S with TSL for bulk specimens is given in Fig. 3.[12]

---

11 D. W. Cooke, R. L. Hutson, R. S. Kwok, M. Maez, H. Rempp, M. E. Schillaci, J. L. Smith, J. O. Willis, R. L. Lichti, K.-C. B. Chan, C. Boekema, S. P. Weathersby, J. A. Flint, and J. Oostens, Phys. Rev. B **37**, 9401 (1988); D. W. Ccoke, R. L. Hutson, R. S. Kwok, M. Maez, H. Rempp, M. E. Schillaci, J. L. Smith, J. O. Willis, R. L. Lichti, K.-C. B. Chan, C. Boekema, S. P. Weathersby, and J. Oostens, Phys. Rev. B **39**, 2748 (1989).

12 D. W. Cooke, B. Bennett, E. R. Gray, R. J. Houlton, W. L. Hults, M. A. Maez, A. Mayer, J. L. Smith, and M. S. Jahan, Appl. Phys. Lett., submitted.

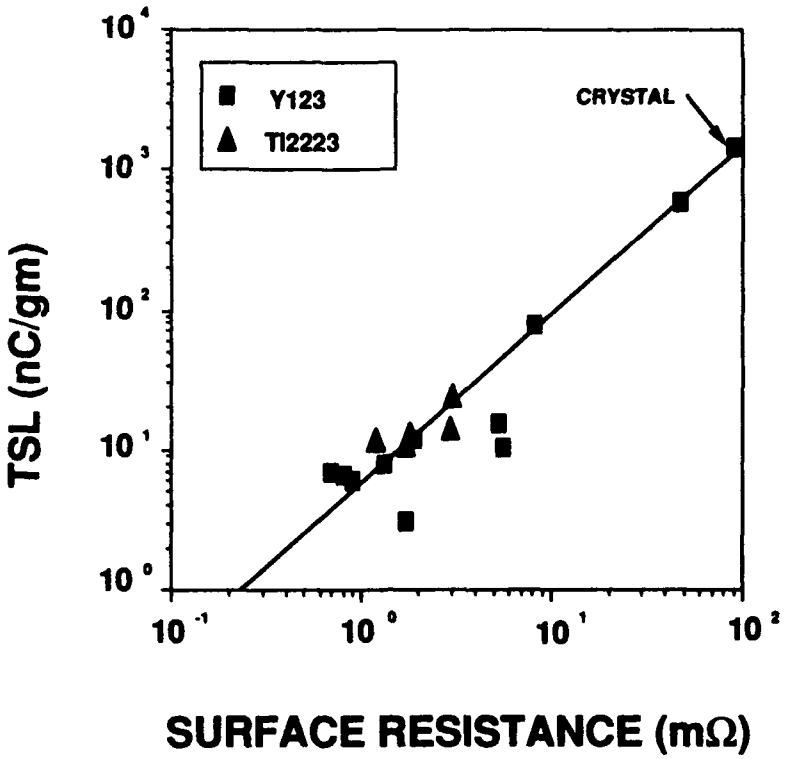

Figure 3. Correlation of TSL with R_S. Data were taken at 3 GHz and 4K on bulk specimens (except as noted).

These two screening techniques, eddy current and TSL, have proved useful in assesssing the quality of HTS for high-frequency measurements. Obviously, a great deal of time (and money for liquid helium) can be saved by screening out those samples that, for one or more reasons, are characterized by high values of R_S. Figure 4 illustrates an experimental scheme for methodically evaluating a large number of HTS samples.

4.0 SURFACE RESISTANCE AND CRITICAL FIELDS

Several techniques for measuring R_S are presently in use. These include cavity perturbation,[1,13,14,15] replacement of the end wall of a cylindrical cavity with a superconducting sample,[16,17,18] half-wave resonant

---

13 M. Hagen, M. Hein, N. Klein, A. Michalke, F. M. Mueller, G. Müller, H. Piel, R. W. Röth, H. Sheinberg, and J. L. Smith, J. Magn. Magn. Mat. **68**, L1 (1987).

14 D. W. Cooke, E. R. Gray, R. J. Houlton, B. Rusnak, E. Meyer, G. P. Lawrence, M. A. Maez, B. Bennett, J. D. Doss, A. Mayer, W. L. Hults, and J. L. Smith, J. Appl. Phys., submitted.

15 S. Sridhar and W. L. Kennedy, Rev. Sci. Instrum. **59**, 531 (1988).

16 N. Klein, G. Müller, H. Piel, B. Roas, L. Schultz, U. Klein, and M. Peiniger, Appl. Phys. Lett. **54**, 757 (1989).

coaxial line,[19] stripline resonator,[20] and disk resonator.[21] Each of these techniques has particular advantages and disadvantages. For example, bulk specimens are conveniently measured in a cavity by the perturbation technique (see Fig. 5), where the electromagnetic field probes all sides of the sample. This is not the most suitable method for measuring R_S of film specimens, however, because the electromagnetic field probes not only the superconducting film, but also the substrate and interface. Assuming that the electrodynamic losses in the substrate are much smaller than those in the film, and that no unusual losses occur at the film/substrate interface, R_S values can be extracted from this measurement.

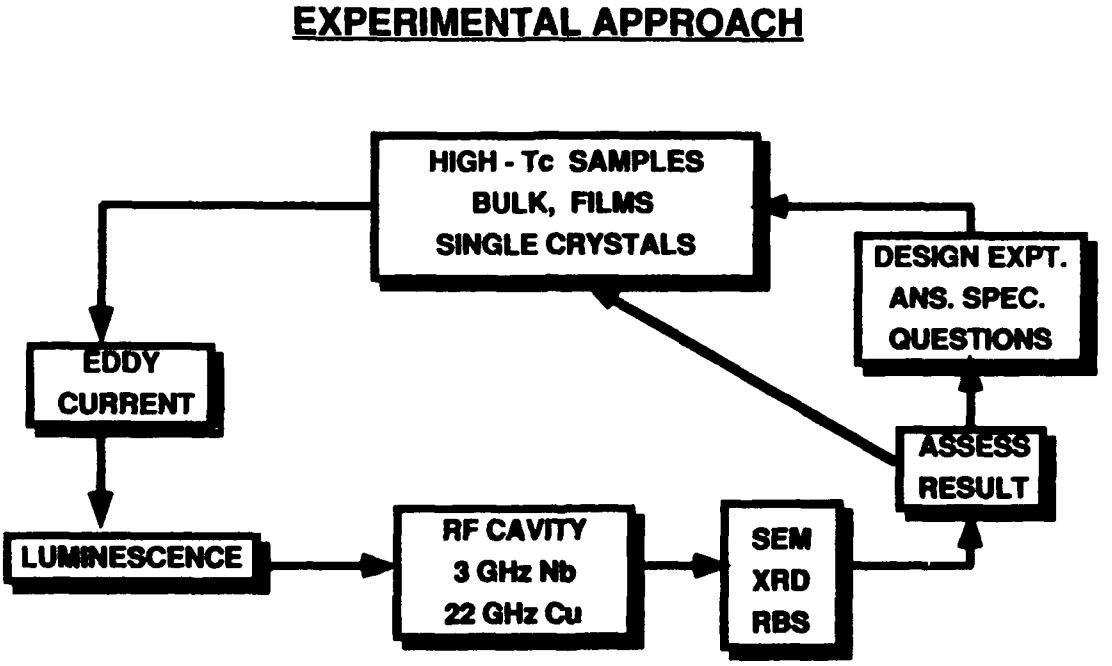

Figure 4. Experimental scheme for evaluating the quality of HTS samples.

---

17 D. W. Cooke, E. R. Gray, R. J. Houlton, B. Rusnak, E. A. Meyer, J. G. Beery, D. R. Brown, F. H. Garzon, I. D. Raistrick, A. D. Rollett, and R. Bolmaro, Appl. Phys. Lett., submitted.

18 J. P. Carini, A. N. Awasthi, W. Beyermann, G. Grüner, T. Hylton, K. Char, M. R. Beasley, and A. Kapiltunik, Phys. Rev. B **37**, 9726 (1988).

19 J. R. Delayen, K. C. Goretta, R. B. Poeppel, and K. W. Shepard, Appl. Phys. Lett. **52**, 930 (1988).

20 M. S. Dilorio, A. C. Anderson, and B.-Y. Tsaur, Phys. Rev. B **38**, 7019 (1988).

21 A. Fathy, D. Kalokitis, E. Belohoubek, H. G. K. Sundar, and A. Safari, Phys. Rev. B **38**, 7023 (1988).

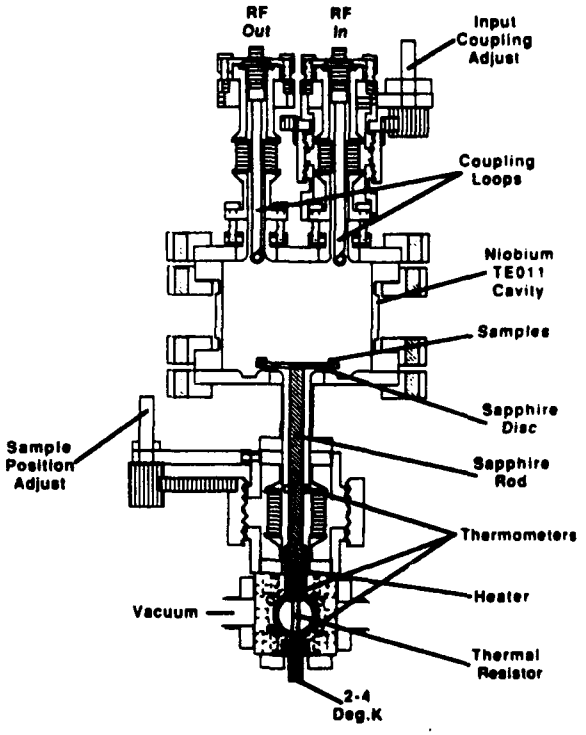

Figure 5. Schematic diagram of a 6-GHz cavity used to measure surface resistance of HTS samples. (From Ref. 1).

A more appropriate technique for measuring films is the end-wall replacement technique shown in Fig. 6. In this configuration the end wall of a cylindrical TE_{011} fundamental mode cavity is replaced by the superconducting film. For this geometry there are no microwave losses at the junction between the end wall and cylindrical body of the cavity. Moreover, the electromagnetic field distribution is easily calculated for this mode. By solving Maxwell's equations with the appropriate boundary conditions it is found that 26% of the cavity losses occur at the end wall. Thus, the reciprocal Q of the sample, $1/Q_S$, is obtained by subtracting the reciprocal Q of the empty cavity, $1/Q_C$, from that of the cavity with the sample, $1/Q_{C+S}$, i.e.,

$$\frac{1}{Q_s} = \frac{1}{Q_{c+s}} - \frac{1}{\eta Q_c} \qquad (6)$$

where η is an enhancement factor (1.26) that artificially increases the bare cavity Q to a value consistent with no losses in the end wall. The surface resistance is computed from the measured Q values of the sample and a known material, stainless steel for the system described,

$$R_s = \frac{Q'R'_s}{Q_s} \qquad (7)$$

where the primes stand for the appropriate values of the standard material (R_S' = 239 mΩ at 22 GHz).

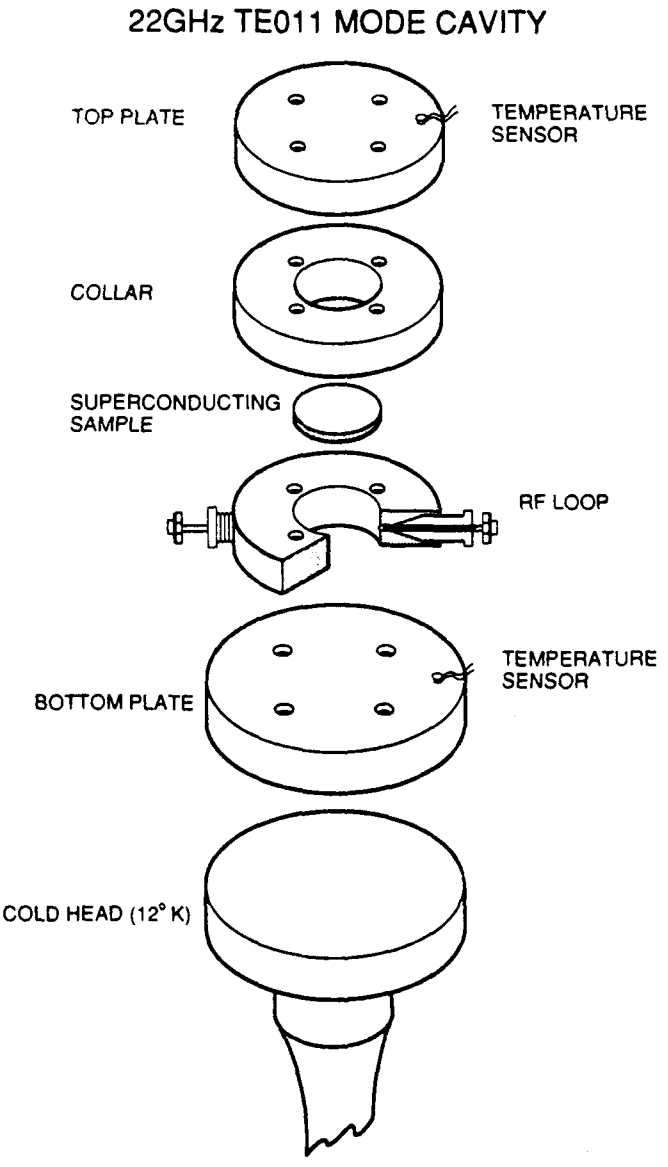

Figure 6. Schematic of a typical cavity used for measuring R_S of films. Note that the film forms the end wall of the cavity.

The temperature dependence of R_S is obtained by cooling the Cu cavity to 15 K with a closed-cycle refrigerator and slowly warming it to RT while measuring the corresponding Q values. A computer-controlled network analyzer automatically determines the resonance peak and half-power points from which the Q is calculated. The sensitivity of this Cu cavity is limited by its intrinsic Q (~ 65,000) to R_S values of approximately 2 mΩ. Lower R_S values can be obtained with the use of a superconducting Nb cavity, which has a much higher Q (~ 2 X 10^6) at 4 K.

Shown in Fig. 7 are typical surface-resistance curves for films of YBCO e-beam deposited onto $SrTiO_3$ and $LaGaO_3$ substrates, and measured in the Cu cavity shown in Fig. 6. For comparison with Eq. (3) and Fig. 1, we have plotted the data as log R_S vs. T_C/T (T_C = 90 K). Notice that there does not exist a distinct linear region in the curve of Fig. 7; For $T<T_C/2$, R_S is dominated by R_{res}, which, as discussed below, may be attributed in part to the interaction of the microwave field with the substrate. The sharp peaks observed in the $SrTiO_3$ curve are caused by the strong temperature dependence of the permittivity ε of this substrate (ε rises from near 1000 at 100 K to 25,000 at 4 K).[18] In contrast, ε for $LaGaO_3$ is ~ 25 at RT and is relatively temperature-independent.[22] Therefore, no oscillations in R_S occur in films grown on this substrate.

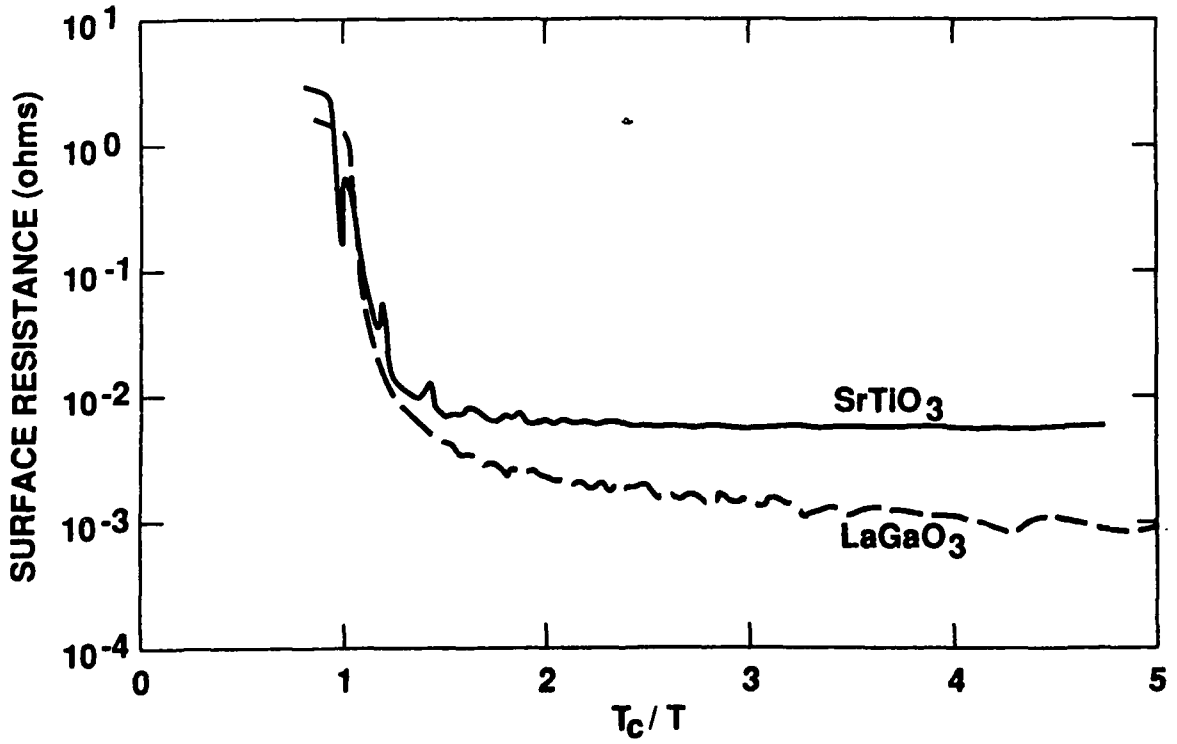

Figure 7. Surface resistance curves for YBCO films (0.8 μm) electron-beam deposited onto $SrTiO_3$ and $LaGaO_3$ substrates. Measurements were made in the 22-GHz cavity shown in Fig. 6. (T_C=90 K).

22 R. L. Sandstrom, E. A. Giess, W. J. Gallagher, A. Segmüller, E. I. Cooper, M. F. Chisholm, A. Gupta, S. Shinde, and R. B. Laibowitz, Appl. Phys. Lett. **53**, 1874 (1988).

The low-temperature value of YBCO on $SrTiO_3$ is 6 ± 2 mΩ, regardless of the thickness of the film.[17] However, similar films deposited onto $LaGaO_3$ show low-temperature values near 1 ± 2 mΩ (see Fig. 7). That is, they exceed the sensitivity of the Cu cavity and must be measured with a Nb cavity. The result of this measurement shows that the true value of R_S for the $LaGaO_3$-based film is 0.2 ± 0.1 mΩ at 4 K and 22 GHz, about a factor of two above Nb. A summary of representative R_S vs. ω data will be given later.

A primary advantage of the stripline resonator method for measuring R_S is that it can operate at different frequencies. It thus has the capability to determine R_S vs. frequency ω for the same specimen. A typical stripline resonator used at Lincoln Laboratories is shown in Fig. 8.[23] A sine wave is applied at the input, and the output is synchronously monitored with a spectrum analyzer. Resonances are observed at frequencies for which the line length l is an integer multiple of half wavelengths, i.e., $l = n\lambda/2$. A frequency range of ~ 0.5 - 20 GHz can be covered. Additionally, if the upper ground plane is comprised of the film and substrate, it is possible to obtain information on the substrate. Power measurements are also easily made with the stripline technique. A disadvantage of the technique is that it is not as sensitive as a Nb cavity unless it is an all HTS stripline resonator.

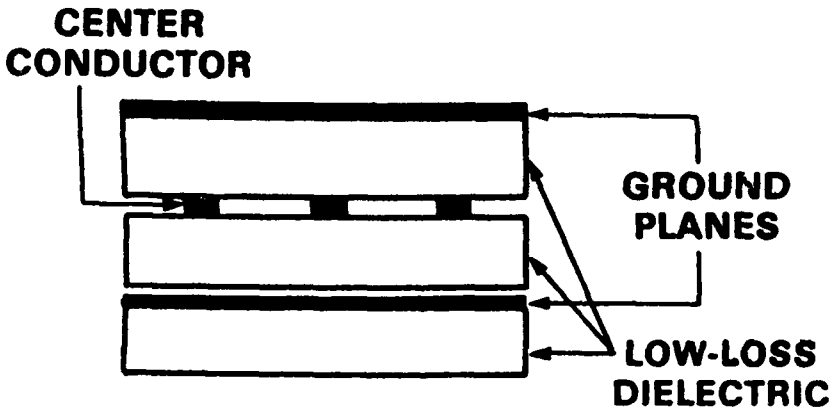

Figure 8. Typical stripline resonator for measuring R_S of HTS samples. (From Ref. 23).

Stripline measurements on the same $LaGaO_3$-based YBCO film that was measured in the 22 GHz Cu and Nb cavities, and described above, show that R_S is, within experimental error, similar to Nb. The particular configuration used in this experiment had the YBCO film as the upper ground plane, Nb as the center conductor and lower ground plane, and sapphire as the low-loss dielectric. $LaGaO_3$ separated the upper ground plane from

23 D. E. Oates, these proceedings.

the Nb center conductor. Although this is not the optimum arrangement for maximum sensitivity, the R_S data do agree with the cavity measurement.

Low-frequency (150 - 450 MHz) R_S measurements on bulk superconductors are readily made in a half-wave resonant coaxial line such as the one shown in Fig. 9.[24] The outer conductor is made of Cu and the HTS sample comprises the half-wave resonant line. The entire apparatus is filled either with liquid nitrogen or helium. An advantage of this technique is that in high-power (critical field) measurements the heat generated within the sample can be easily dissipated because of its direct contact with the cryogen bath.

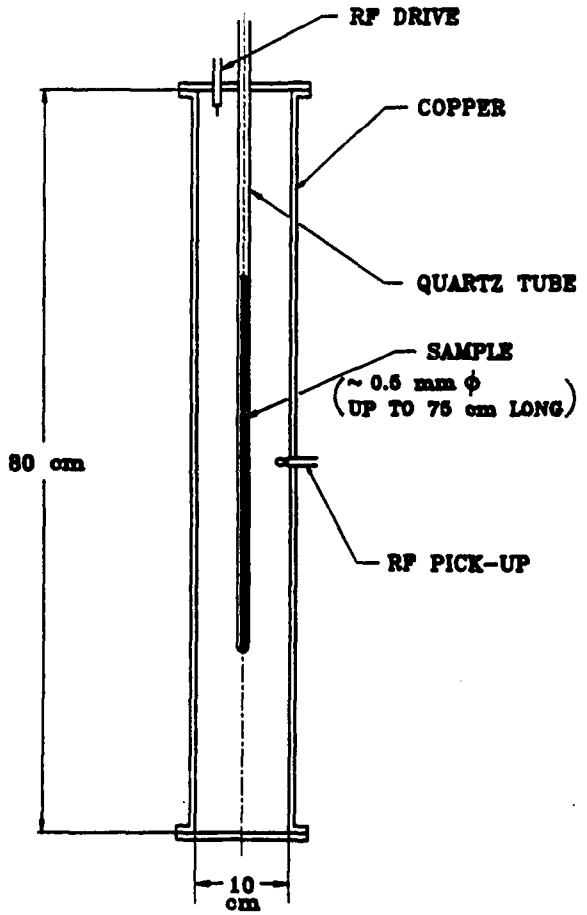

Figure 9. Half-wave coaxial resonant line used to measure R_S of HTS samples. (From Ref. 24).

During the approximately two and one-half years since the discovery of HTS, numerous laboratories have investigated the high-frequency properties of these materials. A representative collection of the laboratories

---

[24] C. L. Bohn, J. R. Delayen, and M. T. Lanagan, these proceedings.

engaged in this research, the samples measured, and best R_S results to date are given in Table 1. For comparison with Cu, Au, and Nb, selected R_S values are plotted as a function of frequency in Fig. 10.

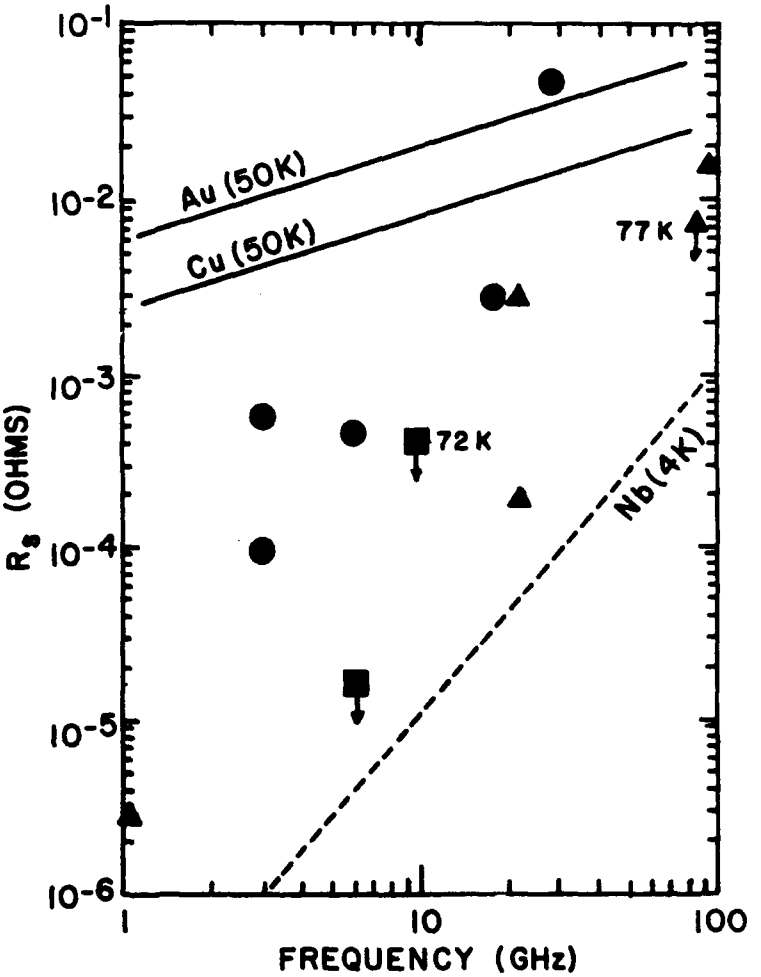

Figure 10. Surface resistance of bulk (●), film (▲), and crystal (■) HTS samples. The arrows indicate that plotted values are upper limits. Data are taken from Table 1.

The best R_S value for a bulk specimen of YBCO is ~ 0.1 mΩ (3 GHz and 4 K). This value, obtained only after repeated grinding and sintering of the material and after prolonged heat treatment, is still two orders of magnitude higher than Nb. Initial speculation was that some intrinsic property of HTS, such as zeroes of the superconducting gap on the Fermi surface, might prevent attainment of low R_S values. Single-crystal and film data clearly demonstrate that intrinsic properties are not responsible for the high values of R_S observed in bulk material. A more reasonable conclusion is that the superconducting grains are coupled by weak-link Josephson junctions, which are more prevalent in bulk than in high-quality single-crystal or film material. We reiterate the central theme: Lower values of R_S can be attained in HTS material by improved fabrication techniques.

TABLE 1
Summary of High Frequency Data

Laboratory	Frequency (GHz)	Technique	HTS Material	Lowest R_S (mΩ)	R_S(μΩ) Scaled to1 GHz
Argonne	0.15-1.5	TEM Cu Coax	YBCO rod	$\tilde{<}$ 0.0011 (4.2K, 175 MHz)	$\tilde{<}$ 35.9
	1.5-40	TE Cu Cavity	YBCO on Ag(80 μm)	22 (4.2K, 2.65 GHz)	3130
			BSCCO on Ag (80 μm)	6.5 (4.2K, 2.65 GHz)	930
			Pb-doped BSCCO (bulk)	45 (4.2K, 29.2 GHz)	53
Cornell	5.95	TE Nb Cavity	YBCO Crystal	< 0.015 (2K, 5.95 GHz)	< 0.4
				< 0.5 (77K, 5.95 GHz)	<14.1
			YBCO (grain aligned)		
			H ∥ C	8.1 (3K, 5.95 GHz)	229
			H ⊥ C	0.45 (3K, 5.95 GHz)	13
David Sarnoff Res.	10	Disk Resonator	YBCO (bulk)	3.8 (10K, 10 GHz)	38
Japan Atomic Energy Res. Inst.	7	Monolithic TM Cavity	YBCO	$Q_u \sim 10^6$ (25K, 7 GHz)	-
Los Alamos	3	TM Nb Cavity	YBCO (bulk)	0.1 (4K, 3 GHz)	11
			BSCCO	3.3 (4K, 3 GHz)	367
			TBCCO	0.6 (4K, 3 GHz)	66
	22	TE Cu Cavity	TBCCO on MgO (5 μm)	6.5 (15K, 22 GHz)	13.4
			YBCO on $SrTiO_3$ (0.5 and 1.5 μm)	6.0 (15K, 22 GHz)	12.4
		TE Nb Cavity	YBCO on $LaGaO_3$ (0.8 μm)	0.2 (4K, 22 GHz)	0.4
Lincoln Lab	0.5-20	Micro-Stripline	YBCO on $LaGaO_3$ (0.8 μm)	< 0.003 (4.2K, 1.0 GHz)	< 3
			YBCO on YSZ	0.39 (4.2K, 0.6 GHz)	1080
NRL	18	TE Cu Cavity	TBCCO (bulk)	3 (6K, 18 GHz)	9.3
Northeastern	8	Monolithic TE Cavity	YBCO	$Q_u \sim 10^5$ (4.2K, 8 GHz)	-
	9.6	TE Pb Cavity	YBCO (bulk)	4.9 (4.2K, 9.6 GHz)	53
			LSCO (bulk)	11.3 (4.2K, 9.6 GHz)	123
	10	TE Nb Cavity	YBCO (crystal)	< 0.4 (72K, 10 GHz)	< 4
UCLA	102	TE Cu Cavity	YBCO on $SrTiO_3$ (a-axis)	300 (4.2K, 102 GHz)	29
	102		YBCO on $SrTiO_3$ (c-axis)	15 (4.2K, 102 GHz)	1.45
	148		YBCO on $LaGaO_3$ (0.5 μm)	100 (4.2K, 148 GHz)	4.6
	148		TBCCO on MgO	200 (77K, 148 GHz)	9.1
Westinghouse	10	Nb Stripline	YBCO on $SrTiO_3$ (0.5 μm) (a-axis)	4 (4.2K, 10 GHz)	40
Wisconsin	7.0-16.7	TE Cu Cavity	YBCO on $SrTiO_3$	~ 1.0 (4.2K, 8.3 GHz)	~ 14.5
Wuppertal	3-87	TM Nb Cavity	YBCO (bulk)	0.1 (4.2K, 3 GHz)	11
		TE Cu Cavity	YBCO on $SrTiO_3$ (0.6 μm)	< 8 (77K, 86.7 GHz)	< 1.1
			YBCO on $LaGaO_3$ (0.5 μm)	18 (20K, 86.5 GHz)	2.4
			YBCO on Ag (10-30 μm)	18 (77K, 21.5 GHz)	39
				< 3 (4.2K, 21.5 GHz)	< 6.5
				Copper (4K)	1200
				Niobium (4K)	0.2

Many high-frequency electronic applications of HTS require only that R_S be lower than Cu. For an accelerating cavity, however, low R_S at high power levels is required. In general, the field dependence of R_S for bulk and film specimens is strong, the superconducting state does not exist above ~ 5 Oe. In contrast, single crystal results show that the superconducting state persists for surface fields up to 93 Oe at 20 K (5.95 GHz).[1] This value is, however, far inferior to the best value achieved in Nb (1600 Oe). These results suggest that weak-link behavior may be responsible both for high R_S values and poor surface-field performance. These measurements were done in cavities where the superconducting samples were in vacuum. Owing to the poor thermal conductivity of HTS, it has been suggested that the breakdown of superconductivity, as observed in these measurements, occurs because the heat being deposited in the sample cannot be readily dissipated.[25]

Alternatively, measurements of the field dependence of R_S on bulk $YBa_2Cu_3O_7$ done in a coaxial resonator, where the sample was bathed in liquid cryogen, show that the superconducting state does not break down for fields as high as ~ 640 Oe (77 K and 190 MHz).[25] The corresponding R_S value for this surface magnetic field is 5% of the normal value. These results are encouraging and emphasize the importance of thermal conductivity in any cavity design utilizing HTS.

5.0 FUTURE PERSPECTIVES

Tremendous progress has been made in reducing R_S of HTS materials. In the approximately two years since the first R_S value of HTS was reported (YBCO bulk),[13] improved processing and fabrication techniques have led to films of 1-inch diameter that are competitive with Nb at 4 K.[17] Moreover, recent results on the power dependence of R_S suggest that, in principle, surface magnetic fields greater than 600 Oe can be attained. Thus, values of the two most important parameters that determine the suitability of HTS for cavity applications, R_S and H_S, indeed suggest that no fundamental limitation exists, which should discourage further developmental work on these materials. This does not imply that these are the only problems requiring solution before an HTS accelerating cavity can be constructed. Other considerations are film thickness (determined by London penetration depth), thermal conductivity, substrate, substrate backing material, film degradation with time, radiation sensitivity, and field emission. Nevertheless, recognizing that the current status of Nb cavities has evolved over a period ~ 20 years, it is not unreasonable to expect that some research and development time will be required to make HTS cavities that are competitive with Nb.

Future improvements in HTS high-frequency properties will likely come from improved processing techniques. For example, *in situ* annealed films, as opposed to post-deposition films, yield lower values of R_S.[16] These improvements may result from better oxygenation, and/or elimination of non-reacted metals in the material. Certainly the lower annealing temperature (~ 500°C) of *in situ* processing will help to reduce the problem of

---

[25] J. R. Delayen and C. L. Bohn, Phys. Rev. B, submitted.

substrate interaction with the superconductor, which commonly occurs at elevated temperatures (for example, ~ 860°C encountered in post-deposition processing).

Finally, it is noteworthy that progress to date on high-frequency HTS materials has evolved from experimental work with minimal guidance from theory.[26,27] As a better theoretical picture emerges, however, it is expected that new ideas will be infused into the experimental work leading to further improvements in high-frequency properties.

The cooperation of and stimulating interactions with many researchers in this field are appreciated. In particular, we acknowledge our collaborators at Los Alamos, P. Arendt, B. Bennett, J. G. Beery, D. Brown, J. D. Doss, H. Frost, F. H. Garzon, R. G. Houlton, W. L. Hults, M. S. Jahan, H. H. S. Javadi, G. P. Lawrence, M. A. Maez, A. Mayer, E. Meyer, I. D. Raistrick, A. D. Rollett, B. Rusnak, J. L. Smith, and T. P. Starke. Also, H. Piel and his collaborators at Wuppertal, G. Müller, N. Klein, M. Hein, R. Röth, and S. Orbach, have provided invaluable assistance to our program. We have also benefited from fruitful collaborations with H. Padamsee, S. Sridhar, A. Portis, D. E. Oates, J. Josefowicz, and G. Grüner.

---

26 T. L. Hylton, A. Kapitulnik, M. R. Beasley, J. P. Carini, L. Drabeck, and G. Grüner, Appl. Phys. Lett. **53**, 1343 (1988); T. L. Hylton, and M. R. Beasley, Phys. Rev. B, submitted.

27 J. I. Gittleman and J. R. Matey, J. Appl. Phys. **65**, 688 (1988).

THIS PAGE IS INTENTIONALLY BLANK

Presented at the Workshop on High Temperature Superconductivity
23-25 May 1989 GACIAC PR-89-02

Comparison of New and Old Theories of Superconductivity

Dr. Edward Teller

Hoover Institution, Stanford, CA 94305-6010

Lawrence Livermore National Laboratory, Livermore CA 94550

The first thing I want to say is that I believe we are talking about something that is both very important and very refreshing. I understand that yesterday one of my daring colleagues from Los Alamos made a statement that what we are talking about is a little more real than cold fusion--and I think it is. Between us--and this is a strict secret, which nobody must repeat to more than two people--what we are talking about may also be more real than the superconducting supercollider. There is no doubt that that great machine can be constructed. There is also no doubt that it will succeed. There is also no doubt that what they will find will be more interesting. But, I predict they will not find a single thing that they predict. That is why it will be really interesting.

I think the same criticism holds to some extent for our work. We cannot predict either. The best prediction that I can offer today about a far more limited field is more than a little vague and nebulous. But it is remarkable how everybody--in pure science, applied science, military science--got interested in this field. Their instincts are healthy, and I hope and plead that similar instincts exist in the people who make the budget, so that almost as much money will be spent on high-temperature

superconductivity as on the SSC. Now I will stop making outrageous propaganda and start talking about facts.

Superconductivity in general has been explained in a beautiful and satisfactory way, but not in detail. The one thing that the rightly famous BCS theory does not do is to predict what substances will become superconducting and at what temperatures that will occur. In that regard, its failures are really spectacular. For instance, the theory correctly predicts that the heavier isotope should always have the lower transition temperature (T_c). Yet, in that recently famous substance palladium hydride, there is a strong isotope effect in the opposite direction, and I have not found anybody who can explain it.

I think there are things that we must understand, and furthermore I claim that there are very clear indications of where to look for the explanations. If you take simple substances like elements, you find superconductivity only at low temperatures. If you look for other characteristics, like heavy fermions, you find superconductivity at low temperatures. If you look for organic superconductors, you find superconductivity at low temperatures. We have found superconductivity at higher temperatures in two cases, and those substances share one characteristic: they both have a special crystallographic feature, a different one in the two cases.

The first case of high-temperature superconductivity was, of course the A15 crystals which have superconductivity around 20° K. I just read a beautiful paper about it, written in 1975. I found

A15 described in that paper as high-temperature superconductivity. But that was in 1975. The A15 substances are modifications of the remarkable perovskite lattice with particles in a simple cubic lattice, additional particles that are body-centered, and finally particles that are face-centered. That in itself is the perovskite lattice, not A15. In A15, the atoms that should be in the face centers are replaced by two atoms and moved apart by one-quarter of a lattice distance so that in that direction there are twice as many lattice points, which are half the lattice distance apart.

For instance, in the Nb_3Sn compound, there are Sn atoms in the simple cubic lattice positions and in the body center positions. But the two atoms of niobium in the face centers constitute three chains, one in the x-, one in the y-, and one in the z-direction. Almost all such superconductors contain niobium. Some of them contain vanadium for the element which is three-fold. There is very little doubt that it is the third electrons (the d-electrons) of vanadium or niobium that somehow are involved along those three straight lines. The niobiums are crowded.

Furthermore, as my reading of the 1975 paper clearly shows, those materials tend to function even though, or perhaps because. stoichiometry is violated. They are sensitive to lattice vibrations. The crystals are cubic, but at low temperatures, they go tetragonal. Their becoming tetragonal competes and is clearly connected with superconductivity. That is the story of the old high-temperature superconductivity.

Now, the new high-temperature superconductivity. We all know

we have a perovskite plane, although the whole crystal is not a perovskite. The whole crystal is composed of cation oxides with the formula of cation-O_x, where x is the number of oxygens per cation. The number of oxygens per cation can be 0, 1, or 2. In the yttrium plane, there is no oxygen. In the barium, bismuth, or thallium plane, there is one oxygen. But in the characteristic copper plane, which never is absent, there are always two oxygens; that is the perovskite plane, CuO_2. That plane is always present, just as the niobium or vanadium chains are always there in the A15 superconductors. Under proper conditions, you get the same transition temperature: in the old case at about 20° K, in the new cases at about 100° K.

Now I will anticipate my prediction: There will be room temperature superconductivity. It will not be the famous 1-2-3 compound, and it will not be in a substance with a perovskite plane. It will have some other chemical structure as different from the 1-2-3compound as the 1-2-3 compound is different from the A15 compounds. I am trying to look for what is common in those examples.

In trying to do that, I have studied, to an incomplete extent, the Bardeen-Cooper-Schieffer effort, and I came away with boundless admiration and with strictly bounded understanding. The applications and the theory have become beautifully complex, and the basic ideas are simple. You start out with borrowing some energy and emitting a photon. Then the photon is emitted, and an electron is transferred from one orbit to another.

In a metal, where you imagine you have a fermi distribution

(which, of course, I will assume), the electron will be transferred from an energy just below the fermi surface to an energy just above the fermi surface. We can say that we have created a hole in the fermi distribution and an electron outside the fermi distribution. Furthermore, it is found that big momentum changes associated with the emission of short wave phonons are the most important.

As a second step, you pay back your dues, not completely but almost completely, in that the phonon is reabsorbed. But the electron does not go back in the hole where it belongs. Instead, you excite a second electron and thereby produce a second electron and a second hole. Those form the famous Cooper pairs. Cooper pairs in superposition can form what looks like valence orbitals. (This is not the usual way to describe them.) We saturate the spins and form standing orbits occupied twice.

The foregoing is a crude description of the starting point for the explanation of low-temperature superconductivity in simple metals. My claim is that, if you start from simple assumptions in the explanation of high-temperature superconductivity, then the BCS mathematics follows. Then we have a good chance of getting a superconducting transition. We have a good chance for that transition to be a second order transition lacking latent heat. And we have a good chance of having a situation where the number of pairs to be found above T_c is zero, while just below T_c, the number of pairs is small. And then the number increases and saturates at absolute zero. Those are the characteristics that I will stick with.

In BCS, you start from a fermi surface, take practically any lattice vibration, and go from a state of an electron just below the fermi surface to just above the fermi surface. In the 1-2-3 compounds and related compounds, you start from an insulator or, perhaps a little more accurately, from an intrinsic semiconductor with a very small gap, and the transition is from the top of a filled electron band to the bottom of an unfilled electron band. All that comes, I believe, as no surprise.

I now want to go on a step and name the transition. Where does the electron come from. There is little doubt about it. In agreement with Müller from the Rüslikon Laboratory in Switzerland, with Jim Smith from Los Alamos, and with others, I assume that an electron is taken from the top of the O^{2-} band of the perovskite layer.

I want to give a reason why that is a natural assumption. I told you that the crystal has layers: cation-no oxygen, cation-one oxygen, cation-two oxygens, barring some deviations from stoichiometry. One layer, the perovskite layer, has twice as many oxygens as the next best. The oxygen ions are big ones, and you have considerable crowding. I observed one of my theoretical colleagues trying to make calculations about that layer, and his groans were to be heard on the next floor. The problem is how to accommodate so many huge O^{2-} ions in the little space available. So in those crystals, there must be tension. The perovskite layers would like to expand; the other layers would like to contract. It is only a moderately good fit.

Now the tendency to expand is, of course, due to the Van der

Waals repulsion. And the Van der Waals repulsion is due to the outermost electrons. Among the outermost electrons, it is particularly due to the topmost electrons in the O^{2-} band. If you remove one of those topmost electrons, I can hear the perovskite layer utter a sigh of relief and contract slightly. Here is the coupling with lattice vibrations, that is, a contraction of the perovskite lattice and the transfer of the topmost electrons.

But the question is: where are those electrons going? I have fought a battle with myself, and that battle is undecided. I do not know where the electrons go. I will tell you what I believed up to a couple of months ago, and I am rapidly changing my mind. I used to believe that the whole matter is primarily an internal affair in the perovskite layer. I assumed a transfer of electrons from the top of the O^{2-} band to the tenth orbit of the 3 d-orbits on copper. The coppers are supposed to have nine d-electrons, and that circumstance gives rise to a magnetic moment. A natural assumption is that the electrons would remain in the perovskite layer. It is possible. I now suspect that something else is going on.

I will concentrate on this second hypothesis. First, I want to tell you a little more about the electrons that are being transferred. They are near the top of the O^{2-} band. At the top of the band, the electron orbits have nodes between every neighboring pair of oxygens. That produces a system of nodes where two nodes cross on every cation of the lattice. That holds for the copper ions in the perovskite layer. But it holds equally for the barium, the yttrium, or the copper plane, or for the

thallium, or bismuth, or lanthanum. In all those locations, you have two nodes crossing. Therefore, you have an electron state with an angular momentum component parallel to the z-axis with m = 2.

Therefore, if I establish a strong overlap, a strong interaction with an electron orbit on a cation, that electron orbit better be a d-electron or an f-electron that can have an m = 2 component parallel to the z-axis. I found that there is no example in the experimental material where an unfilled d- or f-orbit would be very far away. If those orbits are close in energy, the crystal field can change the effective energy by a few volts. So I say the electron comes from the perovskite plane, from the top of the O_2 band, and that is where the strong interaction with the lattice resides. It comes from the top of this electron band. It goes into the bottom of a d-electron band or an f-electron band.

Now the theory can proceed as usual. Those transitions induce a crystal contraction in the x - y plane wherever an electron transition occurs. If you let it be duplicated by a second electron, then the contraction will be doubled and the energy of distortion quadrupled. In that sense then, the two electrons strongly attract each other and make a pair.

The effective mass of the electron and hole depend on the direction. In the z-direction, it is probably very big. The electrons and holes adhere to one plane in first approximation, and little depends on the momentum of the hole in the z-direction. In the x - y direction, it is an entirely different matter. The

hole energy depends very sharply on those components of the momentum. That is due to the strong overlap of the oxygen wave functions.

The d- or f-wave functions into which the electrons are supposedly transferred have a smaller overlap. The ions are not pressed against each other as badly as the oxygens are. For the electrons in their new orbit, we will have a band of normal width. So we have a filled band that has a sharp top, and an open band with a not particularly shallow bottom. The gap between the two is quite small, perhaps a fraction of a volt. Furthermore, the gap may be sensitive to density, sensitive to pressure, particularly in the x - y direction.

Notice that the transition requires little energy only if the electron is near the top of the oxygen band and near the bottom of the d- or f-band of the cations. The two bands get close to each other only when the momentum values are near to zero. Therefore, we get coupling with phonons only for low phonon momenta.

What is the result then, if I pursue this picture? In the BCS theory, I could have the interaction of all phonon wavelengths, which can result in a representation of the motion of a single ion in the lattice or the motion of a pair of ions even if their relative position is sharply defined. For example, when two mercury atoms get closer together, a virtual bond may be formed between them, associated with a mixing of s- and p-wave functions. Even though the s- and p-bands are separated, they are in different Brillouin zones. For mercury, we know that two Brillouin zones overlap. When the fermi surface crosses the

boundaries between the Brilloiun zones, there will be some mixing of the s- and p-bands. In our case, when you transfer an electron away from the O^{2-}, maybe onto a two valence copper (but, in my opinion, more likely unto a neighboring plane), then there is a strong interaction. That is, to my mind, essentially the explanation. From this point onward, the details may be copied from the BSC theory with one exception. That one exception I want to emphasize: only low momenta, very particularly low phonon momenta, will occur.

If I increase the momentum of the phonon, the energy gap between the oxygen layer and the cation layers will widen, and the contribution will be less. Furthermore, the wave function of the oxygen band electrons may no longer have a node between each pair of oxygens. At the bottom of the oxygen band, there is a zero derivative rather than a zero value in the middle between two neighboring oxygens. The wave function now has no node on the positive ions and no longer resembles a d-electron. So the energy difference between the electron states increases, and the matrix element connecting them decreases.

Therefore, high wave numbers will not participate in the transition. If only low wave numbers participate, then, according to the uncertainty principle, you cannot make a wave packet of small extensions. You cannot localize the interaction except on a few lattice cells, let us say five or ten lattice cells, and in two dimensions that would include 25 to 100 lattice cells. One Cooper-like pair will relieve those 25 or 100 oxygens from some of their mutual repulsion. That may lead to a change in lattice

density by probably one percent, more or less.

The hole wants to be localized because that will give a strong effect on making the density greater. The electron wave functions also will be localized because of their attraction to the holes, but that is a weaker effect. So I imagine that the crystal will break down into dense regions and less dense regions. The holes will be concentrated in the dense regions. The electrons will also be concentrated in the dense regions but to a lesser extent. They will extend into the outer regions, and there will be an average charge difference with the dense regions in general being positive, and the expanded regions being negative. Each of those regions will have an excess of a fractions, probably a small fraction, of two electron charges. The interaction of all those will determine the lattice configuration.

What I have described so far is the state of the superconductor without a current. I have not even described that sufficiently because I have talked about those dense and expanded regions as though they were standing still. They are not. What I described is part of the wave function.

To get the complete wave function, take the configuration just described, shift it by one lattice cell, and add that with the same phase; then shift it again and again and add with the same phase. I can now quite obviously construct the current-carrying states by superposing the same wave functions but with appropriate phase shifts. As the whole structure moves, the holes, which are more strongly tied to the dense regions, will have practically the same velocity as the dense regions, but the

electrons will lag behind. Therefore, the whole structure carries a current corresponding to less than two holes. That, being a structure extending over the whole crystal, will be practically unstoppable.

Whenever I get to this point, the question always arises: What is your prediction? What is new? I want to predict, sharply and dangerously (if I am wrong, I am wrong) that there should be an incommensurable lattice of a lattice distance of may 50 or 100 Angstroms. I would like to call it a superlattice that spontaneously establishes itself at T_c and below. The lattice may be observed due to density changes, which will be very weak near T_c. Even at absolute zero, the changes will be weak. The amplitudes of the new Bragg peaks will be proportional to the density change, and their intensity, to the squares of the density change. That could well be as low as 10^{-6} of the normal Bragg peaks.

We are looking at peaks in the reciprocal lattice that have very low spacing, occur near the Bragg peaks and are probably covered up by the natural broadening of the Bragg peaks. So I have talked myself out of a possible check; but not quite so. You might try to find the new peaks using soft x-rays. I want to use soft x-rays of a wavelength of may 10 to 20 Angstroms. That would be approximately a kilovolt x-ray. If you use that, you will not see the regular Bragg peaks because the wavelength is now too long. The soft x-rays are strongly absorbed. One may use thin films on a foundation. (You do not want to see that foundation.)

So there is an experiment that could be performed. I am

expecting dense regions occupying columns in the z-directions. When I look at them in the x - y plane, I may find a hexagonal superlattice that is incommensurate with the normal lattice. Indeed, it cannot bear a rational relation. The one is tetrahedral, and the other is hexagonal.

I would like to come to the first and most uncertain point. How about the A15 superconductors? I expect that in the niobium or vanadium atoms or ions, there is a competition between the d- and s-states. The electron donors are tin, germanium, or whatever else, which are present in a 1:3 ratio. The transfer of electrons may be reinforced by some distortion along the chains.

That is a vague enough description that I can be neither proud of nor frightened by it.

For novel superconductors, I would look at insulators, or rather semiconductors, among organic compounds or among the infinity of other chemical compounds. I would look for pairs of electrons for which a displacement of ions can produce a big energy change. In that way, in due time, maybe 100 years, maybe next year, we will quite possibly find room temperature superconductivity among organic compounds.

Very fortunately, we have a new technique, a technique to deposit two-dimensional crystals layer by layer. We need not rely on pouring together a few compounds and cooking and waiting. Having found A15, having found 1-2-3, I think that it would be a true miracle if we could not get further.

I do not know what is the composition of this audience. I will assume that we are all good physicists here. We have to make

a big sacrifice to make progress. We have to put up with the chemists. They really play a very important role and will continue to do so.

Presented at the Workshop on High Temperature Superconductivity
23-25 May 1989 GACIAC PR 89-02

TRANSIENT MICROWAVE RESPONSE OF SUPERCONDUCTING DEVICES TO LASER RADIATION

11 April 1989

D. Rogovin and N.E. Glass
Rockwell International Science Center
Thousand Oaks, CA 91360

ABSTRACT

Recent experiments on high T_c superconductors have indicated that the conventional models of superconducting electrodynamics, developed within the framework of BCS theory, may adequately treat the new materials. We employ such a convential scheme to examine the transient electrodynamics of thin film superconductors that are driven far from equilibrium by both CW and pulsed laser radiation. We formulate the problem using the rate equations of Rothwarf and Taylor(RT), in conjunction with Parker's T* model of nonequilibrium superconductivity. This model utilizes the Mattis-Bardeen equations to determine how the microwave and far-infrared electrodynamics are changed as the system evolves towards steady-state or as it responds to pulsed radiation.

The RT equations present the problem in terms of the interacting system of quasi-particles and phonons. We have shown that a third particle, the unknown boson responsible for the pairing interaction in the new materials, can be introduced into the rate equations, in such a way that its presence serves only to renormalize the time and length scales of the conventional problem.

We have applied this model to examine the optically driven transient behavior of microwave transmission through thin film superconductors and microwave propagation in superconducting waveguides. For conventional superconductors, we find that low laser powers can dramatically alter the propagation characteristics of wave guiding devices operating at centimeter through submillimeter wavelengths. At low temperatures, the attenuation of a superconducting stripline can be enhanced by orders of magnitude near the pair-splitting frequency. The phase velocity of the microwaves well below this frequency can also be dramatically changed. For Nb, these changes are predicted to be achievable on nanosecond time scales and should be even faster with the new high T_c superconductors. Such behavior offers device applications as optically controlled microwave intensity modulators and phase shifters.

1.0 INTRODUCTION

Optical control of microwave devices is an area of current interest to device physics. Due to their unique physical characteristics lasers are particularly attractive as the control mechanism for microwave modulators, phase shifters, switches and generators.[1]

Superconductors, particularly the new high transition temperature ceramic oxide superconductors, may offer special advantages for accomplishing these tasks at low laser powers and high speeds over a broad range of spectral wavelengths. In this paper we examine a number of device concepts, specifically modulators and phase shifters, based on optical control of superconducting striplines in conventional superconductors and comment on the possibilities for the new high T_c materials.

In Section (2), we examine the kinetics of superconductors driven out of equilibrium by either visible or infrared laser radiation, within the context of the RT equations,[2] for situations in which the quasi-particle response time is the slowest relaxation time in the problem. For conventional superconductors, this is almost always the case,especially at low temperatures. For example, in Nb the phonon relaxation time is on the order of 4 picoseconds, whereas the quasi-particle(qp) recombination time is on the order of hundreds of picoseconds for temperatures on the order of $T_c/2$. Following this, we apply the same basic approach, but suitably altered , and examine the case of the new materials. For these superconductors, pairing probably arises from the interaction of the conduction electrons with a boson, other than phonons. Phonons, however, should still enter into the kinetics, if only through the interaction of the superconducting thin film with the substrate and temperature bath. At the present time it is not possible to state with any degree of assurity the response times for the new ceramic oxide superconductors. However, the fact that their transition temperature is higher implies that their basic interactions strengths are stronger and therefore their response should be faster.

In Section(3), we examine the electrodynamics of laser irradiated superconducting thin films within the context of the Mattis-Bardeen theory[3] and Parker's T* theory.[4] In Section(4), we extend these discussions to superconducting waveguides and examine the propagation characteristics for such devices in the presence of laser light. Both CW and pulsed cases are examined. Finally, in Section (5), we summarize our results.

2.0 KINETICS

We address the following physical situation: a superconducting thin film or stripline, deposited on a substrate such as sapphire,is immersed in a low temperature reservoir and irradiated by a visible or infrared laser,as depicted in Figure 1.

If a conventional superconductor is used, then the laser radiation will split Cooper pairs which will appear as quasi-particles high up in the conduction band. These qp will, in turn, relax to the bottom of the conduction band emitting high energy phonons which are sufficently energetic that the also split Cooper pairs; thereby creating more quasi-particles. In particular, these high-energy phonons are responsible for most of the additional qp that are created by the laser light. Ultimately, the qp fall to the bottom of the conduction band, remaining in equilibrium with the high energy phonons. Finally, the qp will recombine to form Cooper pairs and the superconductor eventually returns to equilibrium. This state of affairs can be adequately modelled with the RT equations and Parker's T* model. Consider the situation for the new ceramic oxide superconductors. Here, pairing probably does not arise from the electron-phonon interaction, but most likely involves some other type of boson-electron coupling. Accordingly, following the spirit of the RT equations it is reasonable to introduce an additional species in the kinetic equations; namely, the one resposible for superconductivity. Since the thin film is still coupled to the substrate as well as the thermal bath, it is essential to retain the phonons as well as the quasi-particles.

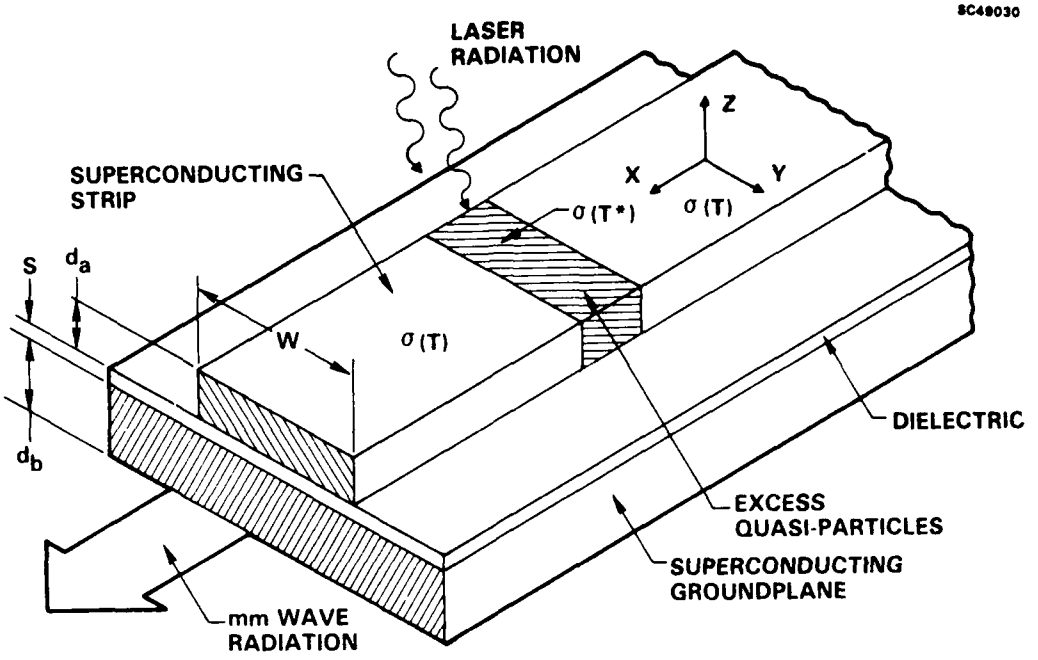

Figure 1. Thin film superconducting stripline irradiated by laser light.

In Section (2.1), we outline our approach to the kinetics of conventional superconductor and in (2.2) we discuss a possible phenomological scheme for the new materials.

2.1 Rate Equations for Conventional Superconductors

Our starting point is the RT equations for the density of quasi-particles, N_{qp} and phonons N_{ph} driven out of equilibrium by qp (I_{qp}) currents which are induced by the external laser fields. For simplicity, we shall assume that the system is spatially homogenous. Accordingly, the RT equations are

$$\frac{\partial N_{pq}}{\partial t} = I_{qp} - 2RN_{qp}^2 + \frac{2}{\tau_B} N_{ph} \tag{2.1a}$$

$$\frac{\partial N_{ph}}{\partial t} = RN_{qp}^2 - \frac{1}{\tau_B} N_{ph} - \left(\frac{N_{ph} - N_{ph}^o}{\tau_{es}}\right) \tag{2.1b}$$

In Eqs. (2.1), τ_B is the time for a phonon to break a pair, τ_{es} is the time it takes for a high-energy phonon to leave the device, R is the qp recombination coefficient and N_{ph}^o is the equilibrium phonon density of the reservoir. In the absence of external drive fields, $I_{qp} = 0$, the system is in steady-state so that all time derivatives are zero and the solution to Eqs. (2.1) is

$$N_{ph} = N_{ph}^o \tag{2.2a}$$

$$\frac{N_{qp}^o}{\tau_R^o} = \frac{N_{ph}^o}{\tau_B} \; . \tag{2.2b}$$

The quantity, τ_R^o is the equilibrium qp recombination time and is given by the inverse of twice the qp recombination coefficient times the equilibrium qp density. Equation (2.2b) arises from detailed balance between the high energy phonons and the thermally excited qp.

Next, we estimate the time scales that govern changes in the qp and phonon densities and adiabatically eliminate the phonon density from the RT equations. This can be accomplished by scaling the densities and the time coordinate as dimensionless quantities. With N_{qp}^{ss} defined as the steady-state qp density, we introduce u as

$$u = \frac{N_{qp}}{N_{qp}^{ss}} \tag{2.3a}$$

or

$$u = \frac{N_{qp}}{N_{qp}^{o}} \quad , \tag{2.3b}$$

depending on whether the final state is or is not the equilibrium state. For the phonons we normalize to the reservoir density, N_{ph}^{o}

$$v = \frac{N_{ph}}{N_{ph}^{o}} \quad . \tag{2.4}$$

The natural time scale to use is

$$\tau_R = \frac{1}{(2RN_{qp}^{ss})} \tag{2.5a}$$

or

$$\tau_R^o = \frac{1}{(2RN_{qp}^{o})} \tag{2.5b}$$

depending again on the final state of the system. With respect to the steady-state values we introduce the dimensionless time as

$$s = \frac{t}{\tau_R} \quad . \tag{2.6}$$

When the final state is the equilibrium state, we replace τ_R by τ_R^o in Eq. (2.6). Using these definations, with the steady-state values for u and τ_R, we find that the RT equations become

$$\frac{\partial u}{\partial s} = \frac{\tau_R}{N_{qp}^{ss}} I_{qp} - u^2 + \frac{2\tau_R N_{ph}^{o}}{\tau_B N_{qp}^{ss}} v \tag{2.7a}$$

$$\frac{\tau_{ph}}{\tau_R}\frac{\partial v}{\partial s} = \left[\frac{I_{qp}}{N^o_{ph}} + \frac{1}{\tau_{es}}\right]\tau_{ph} + \frac{\tau_{ph}}{2\tau_R}\frac{N^{ss}_{qp}}{N^o_{ph}}u^2 - v \quad . \tag{2.7b}$$

Here, we have introduced the phonon lifetime,

$$\tau_{ph} = \frac{\tau_B\tau_{es}}{\tau_B + \tau_{es}} \quad . \tag{2.8}$$

If the phonon density is to adiabatically follow the qp density, we require that $\tau_{ph} << \tau_R$. We can estimate the time scales as follows. Conventional theory asserts that $\tau_{ph} >> \tau_B$ for $T << T_c$, which implies that $\tau_R >> \tau_{ph}$ which follows from Eq. (2.8). Thus, even if there is only weak coupling to the reservoir, the phonon lifetime is short compared to the qp lifetime and the phonon density will adiabatically follow the qp density, so that

$$N_{ph} = \frac{N^o_{ph}}{\left(1 + \frac{\tau_{es}}{\tau_B}\right)} + R\tau_{ph}N^2_{qp} \quad . \tag{2.9a}$$

The qp density obeys

$$\frac{\partial N_{qp}}{\partial t} = I_{qp}\frac{2R}{\left(1 + \frac{\tau_{es}}{\tau_B}\right)}\left(N^2_{qp}\right) - \left(N^o_{qp}\right)^2 \quad . \tag{2.9b}$$

If the pair-breaking time is short compared to the phonon escape time, so that the qp and phonons are in equilibrium with each other (but not with the bath), then Eq. (2.9a) reduces to the a nonequilibriun generalization of detailed balance

$$\frac{N_{ph}}{\tau_{ph}} = \frac{N_{qp}}{2\tau_R} \quad . \tag{2.10}$$

2.2 Rate Equations for the New Superconductors

At the present time, it is not clear what mechanism is responsible for the high transition temperatures exhibited by the ceramic oxide superconductors. Under these circumstances it might seem somewhat hasty to initiate kinetic studies of these materials. Our purpose here is, however, far more modest. We wish only to demonstrate that one can show that equations similar to Eqs. (2.9) may also apply to the new superconductors without making very drastic assumptions. We shall assume that the pairing hypothesis is valid and that pairing arises by means of the virtual exchange of a boson excitation. If one of these excitations is absorbed by a pair it will split and decay into two excited qp. Similarly, two qp can recombine to form a Cooper pair and emit a boson. Such processes should (at least close to equilibrium) be adequately described by equations similiar to the RT equations, except that the phonon is replaced by the boson responsible for superconductivity. However, this description does not include any mechanism for the superconductor

to dissipate energy into the thermal bath. To remedy this, we shall include the phonons as well. Specifically, we shall assume that the phonons are directly coupled to the boson that is responsible for pairing. One can also assume that the phonons are coupled to the quasi-particles as well; however, this should not materially effect the relaxation process and will be ignored for simplicity. We shall also assume that the only current generated by the laser beam is a qp current as occurs in the case of conventional superconductors. Thus, the generalization of the RT equations we use consists of the following system of three coupled equations for the qp(N_{qp}),the boson (N_B) and the phonon (N_{ph}) densities

$$\frac{\partial N_{qp}}{\partial t} = I_{qp} - 2RN_{qp}^2 + \frac{2}{\tau_B} N_B \tag{2.11a}$$

$$\frac{\partial N_B}{\partial t} = RN_{qp}^2 - \frac{N_B}{\tau_B} + g(N_{ph} - N_B) \tag{2.11b}$$

$$\frac{\partial N_{ph}}{\partial t} = g(N_B - N_{ph}) - (N_{ph} - N_{ph}^o)/\tau_{es} \quad . \tag{2.11c}$$

In Eqs. (2.11), R is the qp recombination coefficient, τ_B is the pair-breaking time, g is phonon-boson interaction parameter, I_{qp} is the laser-induced qp current, τ_{es} is the phonon escape time and N_{ph}^o is the reservoir phonon density. At sufficently low temperatures, the qp recombination time will be the slowest time in the system and both the phonon and boson density will adiabatically follow the quasi-particles. Thus, adiabatically eliminating N_{ph} and N_{qp} we have for the time-evolution of the qp density

$$\frac{\partial N_{qp}}{\partial t} = I_{qp} + \frac{2gN_{ph}^o}{1 + g(\tau_B + \tau_{es})} - 2RN_{qp}^2 \frac{g\tau_B}{(1 + g(\tau_{es} + \tau_B))} \quad . \tag{2.12}$$

The boson and phonon densities which adiabaticaaly follow the qp, are given by

$$N_B = \frac{(1 + g\tau_{es})RN_{qp}^2 + gN_{ph}^o}{(1 + g\tau_B)(1 + \tau_{es}) - g\tau_B\tau_{es}} \tau_B \tag{2.13a}$$

$$N_{ph} = RN_{qp}^2/g + (1 + \frac{1}{g\tau_B}) N_B \quad . \tag{2.13b}$$

An examination of Eq. (2.12) reveals that it has the same form as appears with the conventional superconductors, except that the various time scales and interaction strengths are renormalized from the convential form. If Eq. (2.13b) is inserted into (2.13a) and the appropriate limits taken, a nonequilibrium generalization of detailed balance is obtained.

2.3 Quasi-Particle Response to Laser Radiation

We consider two cases:

1. Approach to Steady-State with CW Laser Light
2. Response to Pulsed Laser Light

These are discussed separately below.

2.3.1 Approach to Steady-State

For this case we assume that the laser is turned on suddenly at the time t = 0, and examine the time evolution of the qp density as it approaches equilibrium. The laser-induced qp current is given by $I_{qp} = I\theta(t)$ and the qp density is

$$\frac{N_{qp}(t)}{N^o_{qp}} = \sqrt{1+Q}\left(\frac{\cosh(t/\tau_R) + \sqrt{1+Q}\sinh(t/\tau_R)}{\sinh(t/\tilde{\tau}_R) + \cosh(t/\tilde{\tau}_R)}\right) \tag{2.14}$$

where Q and τ_R are defined as

$$Q = \left(1 + \frac{\tau_{es}}{\tau_B}\right)\tau^o_{qp}\frac{I_{qp}}{N^o_{qp}} \quad . \tag{2.15a}$$

$$\tilde{\tau}_R = \tau_R\left(1 + \frac{\tau_{es}}{\tau_B}\right) \tag{2.15b}$$

Figure 2 depicts the approach to steady-state of the qp density after the laser has been switched on for the case in which Q = 73.

2.3.2 Response to a Pulsed Laser

If the laser is switched on at t = 0 and off at $t = t_o$, the qp current is $I_{qp}(t) = I\theta(t)\theta(t_o - t)$. The time evolution of the qp density during the interval $0 < t < t_o$ is given by Eqs. (2.14) and (2.15). After the pulse is switched off, qp recombination processes gradually bring the system back to equilibrium with the bath. In particular, for $t > t_o$

$$\frac{N_{qp}(t)}{N^o_{qp}} = \frac{N_o\cosh((t - t_o)/\tilde{\tau}^o_R) + \sinh((t - t_o)/\tilde{\tau}^o_R)}{N\ \text{sihn}((t - t\ )/\tilde{\tau}^o_R) + \cosh((t - t)/\tilde{\tau}^o_R)} \tag{2.16}$$

where N_o is the value of the qp density at the time the pulse ends. Figure 2 depicts the transient behavior of the qp density.

2.4 Magnitude of the Laser Drive Current and QP Response Time

The proceeding calculations show that the departure from equilibrium,as well as the response time τ_R depend upon Q. Here, we use Parker's T* theory to obtain numerical values for Q in terms of laser power for conventional superconductors.[4]

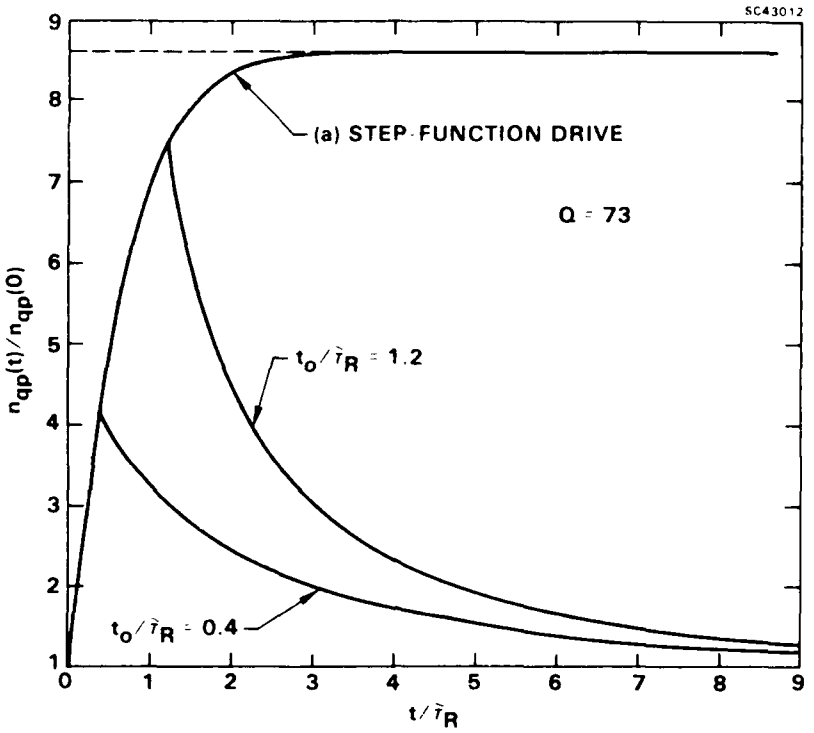

Figure 2. Evolution of the nonequilibrium quasiparticle density (with respect to its equilibrium value) as a function of time [normalized to the rise-time-constant (to steady state), $\tilde{\tau}_R$]. Curve (a): Approach to steady state, for sudden-switching-on at t = 0 of drive current to a constant value (Q). Lower two curves: Response to a time-pulse -- on at t = 0, off at t = t_o, and constant Q at) < t < t_o.

For the purposes of comparison, it is convenient to isolate the temperature-dependent factors that appear in the current. Before doing so we note that Q depends on the phonon lifetime which in turn depends on the ratio of the the phonon escape time to the pair-breaking time. Following convention, we shall take the ratio τ_B/τ_{es} as an adjustable parameter, which is independent of temperature. For low temperatures this is an excellent approximation. Thus, we define a new dimensionless current Q' which is independent of temperature

$$Q = Q'/\gamma(T) \tag{2.17a}$$

where

$$\gamma(T) = \frac{[R\tau^o]}{N(0)\Delta(0)} N_{qp}^2 \tag{2.17b}$$

The T-dependence is therefore stored in the equilibrium qp density as the quantity τ^o, defined in Ref. 5, is independent of temperature.

For an optically driven superconductor we express Q' as a function of the light intensity S, following Parker's analysis

$$Q'(S) = \left[\frac{F\tau^o(1 + \tau_{es}/\tau_B)}{2N(0)\Delta^2(0)}\right] \frac{A}{\partial} S \tag{2.18}$$

where A is the film's absorptance, F is the fraction of energy resulting in qp creation and $\tilde{d}$ is the depth in which qp are created uniformly by the laser beam. This is the lesser of the film thickness d, or the penetration depth. If we take F ≈ 1 and use low temperature optical data for A and $\tilde{d}$ at Nd:Yag wavelengths for radiation incident on a 1 μm film, we arrive at the following estimates:

$$S = 45\ \text{mW/cm}^2(1 + \tau_{es}/\tau_B)^{-1}Q \simeq (0.45 \rightarrow 23\ \text{mW/cm}^2)Q' \text{ for Al}$$

$$S = 2\ \text{KW/cm}^2(1 + \tau_{es}/\tau_B)^{-1}Q \simeq (1 \rightarrow 100\ \text{W/cm}^2)\ Q' \text{ for Nb}$$

where we have taken $\tau_{es}/\tau_B = (4d/\eta v_{ph})/\tau_B$ as approximately $1/\eta$ for Al and $20/\eta$ for Nb, with $1/\eta = 1 \rightarrow 100$. Thus, for values of Q' on the order of unity, as will occur in ther examples we discuss later, correspond to laser powers on the order of mW/cm^2 for Al and a few W/cm^2 for Nb.

We note that in the large Q limit, the rise time to steady-state is independent of temperature as one would expect on physical grounds. However, the time it takes to return to the original equilibrium state, after the laser pulse has been shut off, depends on temperature.

If the dynamics of the ceramic oxide superconductors are similar to convential materials, then higher laser intensities will be required to achieve a particular value of Q'. In particular, within BCS theory, Q'(S) scales as T_c^{-4} so that a factor of ten increase in the transition temperature will greatly enhance the laser power requirements. This can be offset by increasing τ_{es}/τ_B by a corresponding value, so that resonable laser powers are required. Note, that τ_B should be much shorter for the new T_c materials because the interaction strength is greater.

3.0 STATISTICAL MECHANICS IN THE T* - APPROACH

In Section (2), we calculated the total qp density $n_{qp}(\vec{r},t)$ for various external driving fields. What is required, however, in order to determine the electrodynamic response of the system, is knowledge of the energy distribution of the qp density. For the case in which a superconductor is driven from equilibrium by a strong electromagnetic field at optical frequencies, and then probed by a weak microwave field, the well-known T* model of Parker has been shown to be effective.[4]

It is assumed in this model that the optically excited qp come into equilibrium with the phonons of energy > 2Δ, at an effective temperature T*. The value of T* is determined by BCS theory to correspond to the value of n_{qp}. We briefly outline the equations that we employ in implementing the Parker model, since these equations will serve in the later discussion.

We wish to look at systems driven far from equilibrium, when many qp are created, for the purpose of exploring departures from the linear response to the driving fields. Thus, at this point, we avoid using any linearized equations, and we employ the exact relation between n_{qp} and Δ,

$$n_{qp} = 4N(0) \int_{\Delta}^{\infty} \frac{EdE}{(E^2 - \Delta^2)^{1/2}(e^{E/kT} + 1)} \quad . \tag{3.1}$$

In Eq. (3.1), if n_{qp} is the equilibrium density, n_{qp}^{o} , then T is the ambient temperature and Δ is the equilibrium gap $\Delta(T)$; but if n_{qp} is the nonequilibrium density, then T is replaced by the effective temeprature T* and Δ is the nonequilibrium gap $\Delta(T^*)$. Using the weak coupling result $\Delta(0) = 1.764kT_c$, the integral in Eq. (3.1) can be transformed into

$$n_{qp}^{o} = 4N(0)\Delta(0)I(\beta,\mathscr{T}) \tag{3.2a}$$

$$n_{qp} = 4N(0)\Delta(0)I(\beta^*,\mathscr{T}^*) \quad , \tag{3.2b}$$

where

$$\beta = \frac{\Delta(T)}{kT} \qquad \text{and} \qquad \beta^* = \frac{\Delta(T^*)}{kT^*} \tag{3.3}$$

$$\mathscr{T} = \frac{T}{T_c} \qquad \text{and} \qquad \mathscr{T}^* = \frac{T^*}{T_c} \tag{3.4}$$

with

$$I(\beta,\mathscr{T}) = \int_0^\infty dy\left(1 + \exp\left[\beta^2 + (1.764/\mathscr{T})^2 y^2\right]^{1/2}\right)^{-1} \quad . \tag{3.5}$$

One of the two variables β and $\mathscr{T}$, which are arguments of I, can be eliminated by use of the BCS gap equation, from which we find, in the case of weak coupling,

$$\mathscr{T} = \mathscr{T}(\beta) = \frac{1.764}{\beta}\, e^{F(\beta)} \quad , \tag{3.6}$$

or for T* and $\Delta(T^*)$, $\mathscr{T}^* = \mathscr{T}(\beta^*)$, where

$$F(\beta) = \frac{-\beta}{2} \int_0^\infty \frac{x \sinh^{-1} x \operatorname{sech}^2\left(\left[1 + x^2\right]^{1/2} \beta/2\right)}{(1 + x^2)^{1/2}}\, dx \quad . \tag{3.7}$$

The RT equations give us a normalized qp density n_{qp}/n_{qp}^{o} , which the two equations (3.2a) and (3.2b) allow us to express as

$$\frac{n_{qp}}{n_{qp}^{o}} = \frac{I(\beta^*, \mathscr{T}(\beta^*))}{I(\beta,\mathscr{T})} \quad . \tag{3.8}$$

We know the left-hand side of Eq. (3.8) and also the denominator on the right-hand side. Therefore, β^* is the only unknown, and is found numerically. After we haved found β^*, we substitute it back into Eq. (3.6) to find T^*/T_c, and substitute it into the gap equation to find the nonequilibrium gap Δ:

$$\frac{\Delta}{\Delta(0)} = \frac{\Delta(T^*)}{\Delta(0)} = e^{F(\beta^*)} \quad . \tag{3.9}$$

Finally, the distribution function for the nonequilibrium case, $f^*(E)$, is found by evaluating the Fermi function $f_0(E,T)$ at T^*: $f^*(E) = f_0(E,T^*)$. When the physical quantities pertaining to the nonequilibrium superconducting state are properly normalized [e.g., $\delta\Delta/\Delta(T)$ and $f^*(\bar{E})$ where $\bar{E} = E/\Delta(T)$] , they are all material-independent.

When n_{qp} on the left-hand side of Eq. (3.1) or (3.8) is a function of "t", we can solve for β^* (as well as Δ and f) as a function "t". This time-dependent T^* approach is legitimate when the time-scale for the changing drive current (for example, the pulse-width of the square-wave drive due to a pulsed laser) is long compared to the time for the qp to relax to the bottom of the conduction band and Eq. (2.10) is satisfied. This statement follows fromt he fact that detailed balance imples that the qp and the phonons are in equilibrium with one another. We shall use the time-dependent RT kinetics to obtain the time-dependent conductance and thin-film transmittance.

4.0 ELECTRODYNAMICS

We treat the electrodynamical response of a superconducting thin film by use of the Mattis-Bardeen (hereafter MB) equations.[3] The MB equations give the AC conductivity of the superconductor, with respect to its normal-state conductivity: $\sigma/\sigma_n = (\sigma_1 - \sigma_2)/\sigma_n$. These equations, valid in the extreme local (dirty) limit and in the extreme anomalous limit, have long been applied successfully to treat thin films.

The MB expression for the conductivity employs the qp distribution function f and the energy gap Δ. Again following Parker's model, we can obtain the nonequilibrium value for σ/σ_n by using the T^* values: $f_0(E,T^*)$ and $\Delta(T^*)$. The MB equations for σ_1/σ_n and σ_2/σ_n can be cast as explicit functions of β, as defined in Eqs. (3.3), and of $\epsilon \equiv \hbar\omega/\Delta(T)$. With the definition that $\epsilon^* = \hbar\omega/\Delta(T^*)$, the change in conductivity, i.e., the difference between the nonequilibrium and equilibrium values, is expressed as:

$$\delta\sigma_i/\sigma_n = \sigma_i(\epsilon^*,\beta^*)/\sigma_n - \sigma_i(\epsilon,\beta)/\sigma_n, \text{ for } i = 1 \text{ or } 2 \; . \tag{4.1}$$

When we plot $\delta\sigma/\sigma_n$ (or an electrodynamic function thereof) versus Q, and repeat this for different temperatures, the results are material independent, but a given value of Q on the different T-curves does not correspond to a given driving power. When we plot the electrodynamics versus Q', however, the results are material-dependent (via γ), but a given value of Q' on a different T-curves corresponds to a given power. The same is true for the superconducting parameters ($\delta\Delta/\Delta(T)$, δf, $\delta T/T$) themselves, from which the electrodynamic results follow.

Our steady-state results for $\delta\sigma_1/\sigma_1$ and $\delta\sigma_2/\sigma_2$ are shown in Figure 3. The fractional change in the real part of σ is seen to be much greater than in the imaginary part. The real part is determined by n_{qp}, and there is a large fractional change in this quantity due to the pair breaking by the optical drive. The imaginary part, on the other hand, is mostly determined by the pair density, which undergoes only small fractional changes. The largest changes are seen for frequencies just below the gap, reflecting the reduction in the gap $\delta\Delta$.

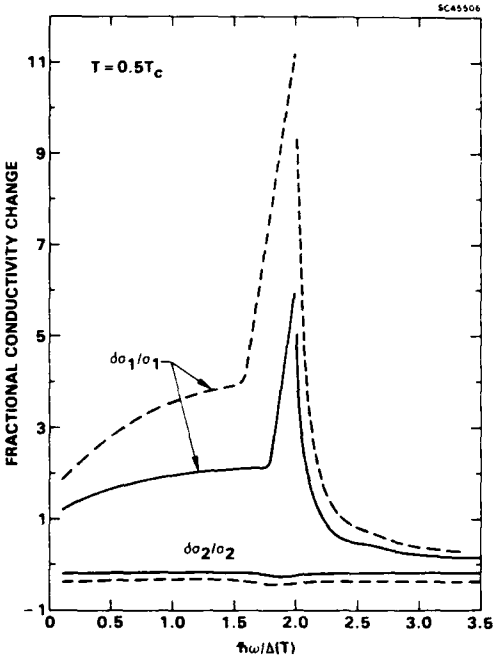

Figure 3. The fractional change in the (complex-) conductivity, between equilibrium and steady state, for a superconducting thin film. Versus the probe frequency, expressed as the photon energy divided by the equilibrium gap-energy, $\epsilon = \hbar\omega/\Delta(T)$. The upper two curves show the real part, $\delta\sigma_1/\sigma_1$, and the lower two curves the imaginary part, $\delta\alpha_2/\sigma_2$. At ambient temperature, $T = 0.5T_c$. Dashed curves: for an external effective drive-current of $Q = 30$ ($Q' = 1.597$ for Al). Solid curves: for $Q = 10$ ($Q' = 0.532$).

The transient response to pulsed laser radiation can be obtained from the solutions of the RT equations, given by Eqs. (2.14) and (2.16). Figure 4 depicts the time evolution of the fractional change in the real part of the conductivity for a pulse of duration $t_o = 1.2\tau_R$ for $Q = 1.6 \times 10^5$ at $t = 0.25T_c$ (for Nb, this means $Q' = 3$). The curves correspond, in the case of Nb, to the three frequencies 17, 60 and 240 GHz. The fractional change in σ_1 is greatest at the shortest wavelengths, reflecting the role of the qp density in σ_1. A comparison of $\delta\sigma_1/\sigma_1$ to $\delta n_{qp}/n^o_{qp}$ shows that the transient behavior of these quantities is quite similar.

To describe the transmittance t_s of a superconducting thin film on a dielectric substrate, we use the simplified analysis of Glover and Tinkham,[6] in which we neglect edge effects and multiple reflections in the substrate. In the normal state, the transmittance is $t_N = [1 + Z_o/(\eta + 1)R_N]^{-2}$, where $R_n = (1/\sigma_n d)$ is the DC resistance per square of the film, Z_o is the impedance of free space, d the film thickness, and η the index of refraction for the substrate. Evaluating the σ_1 in the expression for t_s at ϵ^*, T^* and then again at ϵ, T and subtracting the results, we find

$$\frac{\delta t_s}{t_s} = \frac{[(t_N^{-1/2} - 1)^{-1} + \sigma_1/\sigma_n]^2 + (\sigma_2/\sigma_n)^{1/2}}{[(t_N^{-1/2} - 1)^{-1} + \sigma_1^*/\sigma_n]^2 + (\sigma_2^*/\sigma_n)^2} - 1 \qquad (4.2)$$

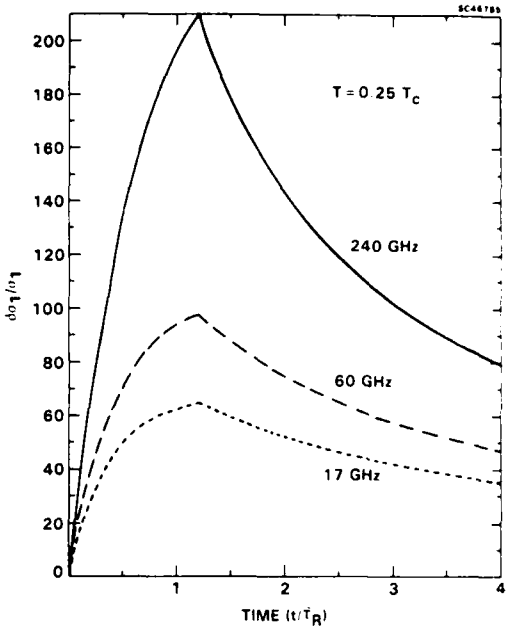

Figure 4. Fractional change in the real part of the conductivity vs time, for a light pulse of duration $t_o = 1.2\tilde{\tau}_R$ and strength $Q = 1.6 \times 10^5$ at $T = 0.25T_c$ ($Q' = 3$ for Nb) For frequencies which in Nb correspond to 240 GHz, 60 GHz (long dash) and 17 GHz (short dash).

where $\sigma_i = \sigma_i(\epsilon,\beta)$ and $\sigma_i^* = \sigma_i(\epsilon^*,\beta^*)$. Similarly, $\delta t_s/t_N$ is found by evaluating the σ_i in the following equation:

$$\frac{t_s}{t_N} = [[t_N^{1/2} + (1 - t_N^{1/2})(\sigma_1/\sigma_n)]^2 + [(1 - t_N^{1/2})(\sigma_2/\sigma_n)]2]^{-1} \qquad (4.3)$$

first at ϵ^*, T^* and then at ϵ, T and subtracting the two. These results demonstrate that the quantities $\delta t_s/t_N$ and $\delta t_s/t_s$ both depend on the film thickness and material properties only through the t_N, and this quantity is a function of only the resistance R_N and substrate index n.

Figure 5 demonstrates the results for $\delta t_s/t_N$ versus the normalized frequency ϵ^*, for the case of a steady-state driving field with $Q = 10$, 30, and 50 when the ambient temperature is $T/T_c = 0.5$ ($Q' = 0.532$, 1.597, 2.662 for Al), and with $R_N = 170\ \Omega$ and $n = 2.07$. The solid lines in Figure 6 show $\delta t_s/t_N$ versus Q' for two fixed frequencies, for the same system as in Figure 5. The solid lines in Figure 7 are also $\delta t_s/t_N$ versus Q', but for the ambient temperture given by $\beta = 7$ ($T/T_c = 0.2518$).

For the same optical pulse as in Figure 4, the time evolution of the thin-film transmission is depicted in Figure 8. For Nb, the curves correspond to the frequencies 17, 60, and 135 GHz. The values of R_N and n (170 Ω and 2.07) are the same as in Figure 5. The transient behavior of $\delta t_s/t_s$ follows $\delta n_{qp}/n_{qp}^o$, reflecting the fact that for these frequencies far below the pair splitting frequency, the excess qp govern the fractional change in transmission. Figure 8(b) demonstrates the although the lowest frequencies exhibit the largest fractional change, it is the higher frequencies that experience the greatest absolute change. Within the pulse time t_o, at 135 GHz, the transmittance increases from 0.033 to 0.08, whereas at 60 GHz, it increases from 0.006 to 0.02.

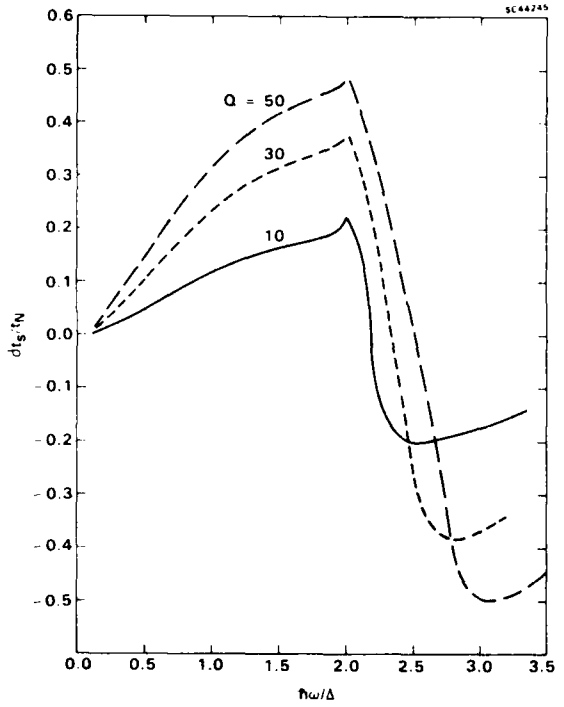

Figure 5. The change in the transmittance δt_S of a superconducting thin film, between its equilibrium and externally driven steady-state, with respect to the normal state transmittance ($t_N = 0.337$). Versus the probe frequency, expressed as the photon energy divided by the equilibrium gap energy, $\hbar\omega/\Delta$. At an ambient temperature of $T = 0.5T_c$. For three different effective drive currents: Q = 10, 30 and 50 (Q' = 0.532, 1.597, 2.662 for Al).

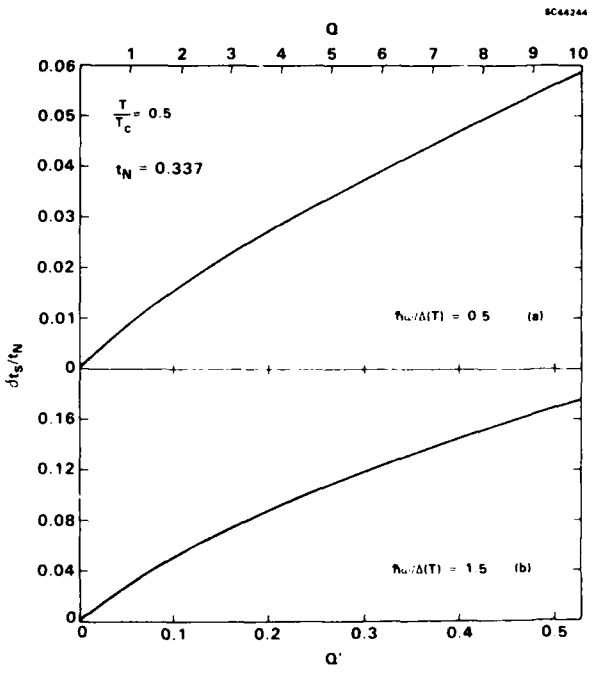

Figure 6. The change in the transmittance δt_S of a superconducting thin film, between its equilibrium and externally driven steady-state, with respect to the normal state transmittance ($t_N = 0.337$ at low frequency). Versus the effective external drive current: Q on the upper axis and temperature-independent Q' (for Al) on the lower axis. At ambient temperature, $T = 0.5T_c$. For two-probe frequencies: $\hbar\omega/\Delta(T) = 0.5$ and 1.5. Solid curves: the exact T*-model plus Mattis-Bardeen electrodynamics. Dashed curves: perturbative electrodynamics to first order in $\delta\Delta/\Delta$.

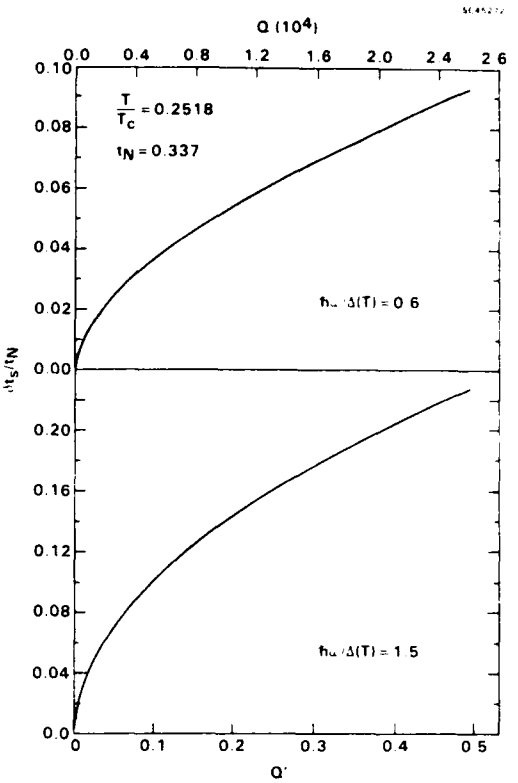

Figure 7. Same as Fig. 6, except that the ambient temperature corresponds to $\beta = 7$, or $T \simeq 0.2518T_c$; and the two probe frequencies are given by $\hbar\omega/\Delta(T) = 0.6$ and 1.5. Q on the upper axis in unites of 10^4.

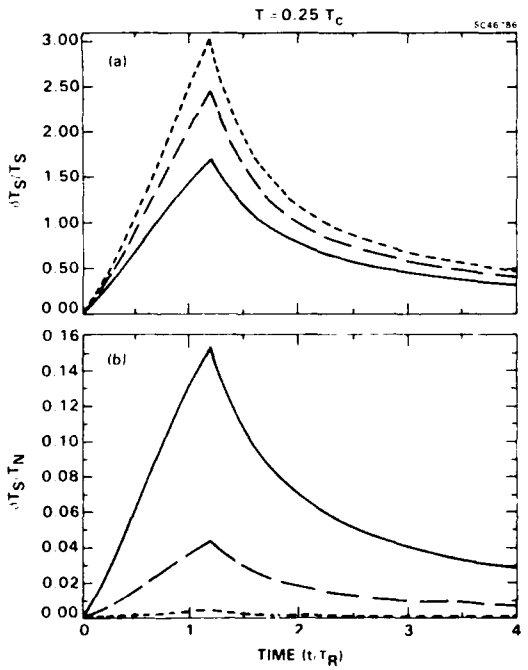

Figure 8. Time evolution of change in microwave transmittance induced by light pulse of duration $t_Q = 1.2\tilde{\tau}_R$ and strength $Q = 1.6 \times 10^5$ at $T = 0.25T_c$ ($Q' = 3$ for Nb). Normalized in (a) to its equilibrium superconducting value and in (b) to its normal state value ($t_N = 0.337$). For three frequencies, which in Nb correspond to 135 GHz (solid), 60 GHz (long dash) and 17 GHz (short dash).

Laser radiation provides a convenient means to achieve optical control of microwave propagation in superconducting waveguides and striplines. The attenuation and phase velocity in a superconducting waveguide are known functions of the conductivity.[7] We have used these functions together with the present theory of the laser-driven nonequilibrium state.[8] Figure 9 depicts the resulting frequency dependence of the equilibrium (solid curve) and laser-driven (dashed) steady-state attenuation and phase velocity of microwaves propagating in a $Nb/Nb_2O_5/Nb$ waveguide. The Nb_2O_5 is 0.1 μm thick and the Nb films, which are equally illuminated, are several micrometers thick (thick-film limit). The laser power, given by Eq. (2.18) with $Q' = 3$, is $3 \rightarrow 300$ W/cm^2, depending on η. Figure 10(a) reveals that laser radiation significantly enhances microwave attentuation below the pair splitting frequency.[9] For example, at the interesting frequencies of 240, 135 and 94 GHz, the attenuation is increased from 34 to 2×10^4 dB/m, from 22 to 10^4 dB/m, and 15 to 6×10^3 dB/m, respectively. Thus, if a 2 mm strip is irradiated, it will, neglecting qp diffusion, decrease the intensity of a 240 GHz wave by 40 dB, a 135 GHz wave by 20 dB, and a 94 GHz wave by 12 dB.

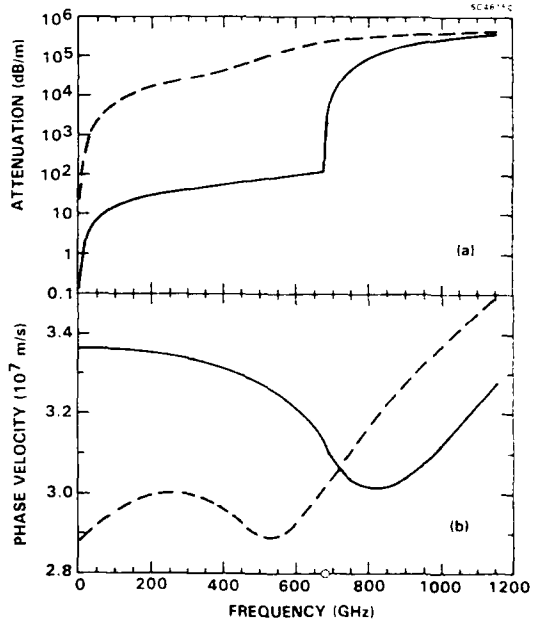

Figure 9. Frequency dependence of the attenuation and phase velocity in a $Nb/Nb_2O_5/Nb$ waveguide at $T = 0.25T_c$: (a) attenuation in equilibrium (solid) and in laser driven steady-state (dotted) with $Q = 1.6 \times 10^5$. (b) Phase velocity in equilibrium (solid) and in laser driven steady state with $Q = 1.6 \times 10^5$ ($Q' = 3$).

Figure 10(b) contrasts the phase velocity, V in equilibrium with that under irradiation and reveals that below 710 GHz, the equilibrium velocity exceeds the laser driven one, whereas, above 710 GHz, the reverse is true. Below 100 GHz, the fractional change in phase velocity is about 10%, a useful feature for phase-shifting microwave radiation. Specifically, at 60 GHz, the laser will decrease V from 3.62×10^7 m/s tp 2.929×10^7 m/s, a change of nearly 15%. Accordingly, in the absence of qp diffusion, the difference in phase of a 60 GHz wave propagating over a pathlength of 1 mm in the presence vs the absence of laser radiation is 94°. Since the attenuation over 1 mm is 3 dB, such a system might be useful as a phase shifter. At 17 GHz, there is virtually no attenuation and the phase shift is about 30° over the same pathlength.

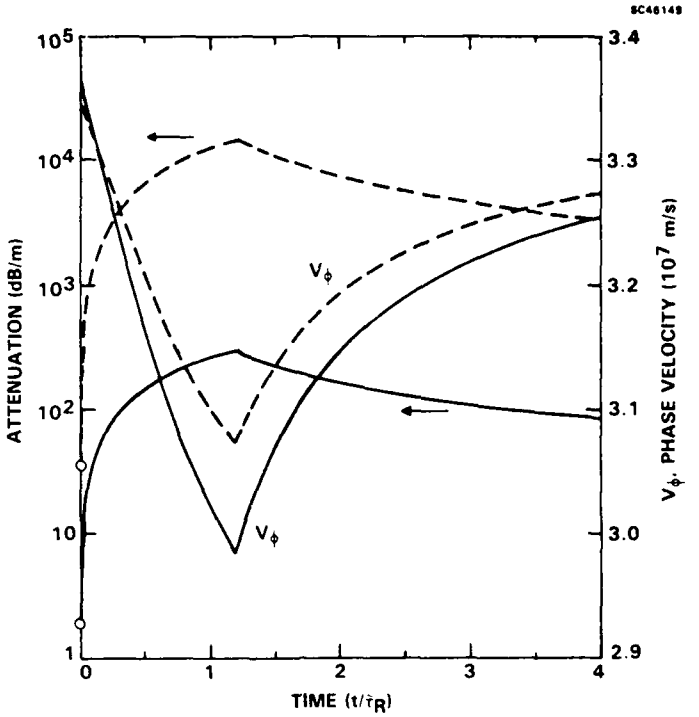

Figure 10. Transient response of the attenuation and phase velocity of a $Nb/Nb_2O_5/Nb$ waveguide at $T = 0.25T_c$. The response of 17 GHz (solid) and 240 GHz (dashed) guided waves to a laser pulse of duration $1.2\tilde{\tau}_R$ with $Q = 1.6 \times 10^5$ ($Q' = 3$).

We have also studied the transient behavior of microwave propagation in this same $Nb/Nb_2O_5/Nb$ waveguide when it is irradiated by $1.2\tilde{\tau}_R$ laser pulse. Figure 11 depicts the time evolution of the attenuation and phase velocity for 17 GHz and 240 GHz waves. The attenuation curve at 240 GHz is especially interesting for its applicability to millimeter-wave modulation. Duiring the time $t_o = 1.2\tilde{\tau}_R$ (e.g., 1.2 ns for $\eta = 0.73$) that the laser is on, the attenuation rises from 34 to 1.46×10^4 dB/m -- the peak attenuation across a 1 mm strip being 15 dB. Recovery of the equilibrium value of the attenuation is longer than the rise time; nevertheless, in just $12\tilde{\tau}_R$, the attenuation falls to 1 dB over the 1 mm strip. Faster recovery times can be achieved by going to higher operating temperatures: raising T/T_c from 0.25 to 0.5 will cut the recovery time by a factor of 40 (i.e., to $\tilde{\tau}_R/4$). The time evolution of the attenuation tracks that of the qp. On the other hand, the phase velocity recovers its equilibrium value much faster: after dropping from 3.35×10^7 m/s to a minimum of 3.07×10^7 m/s during the pulse time, the phase velocity recover 85% of its lost velocity in the next $4t_o$ (e.g., 4.7 ns for $\eta = 0.73$).

Finally, for the new ceramic oxide superconductors, we expect faster response times, greater laser power requirements with phase shifting possible at shorter wavelengths, without serious enhanced attenuation.

5.0 DISCUSSION AND CONCLUSION

In this paper, we have examined a formalism for treating superconductors that are driven from equilibrium by external fields -- specifically optical laser fields -- whose amplitudes may vary in time. This formalism is based on the framework of Parker's T* model, incorporating the RT and MB equations. To solve the RT equations with time dependence, we have introduced an adiabatic

elimination of the phonons from the kinetics. We have shown now that elimination of the phonons from the RT equations leads to a single equation for the qp.

In applying this formalism, our interest focused specifically on the qp response to a pulsed optical laser field, and on the resulting, transient, microwave electrodynamics of superconducting thin films and thin-film waveguides. We presented analytic solutions for the qp response to both CW and pulsed laser fields of arbitrary strength. Our numerical implementation of the theory was performed for the case of superconducting Al and Nb films illuminated by a uniform pulsed laser.

The laser pulses considered here were of length $1.2\tilde{\tau}_R$ = 22 ps × $(1 + \tau_{es}/\tau_s)$, which for a resonable value of around 50 for τ_{es}/τ_B means nanosecond time scales. Recovery times were seen to be around 10 times the rise time at $0.25T_c$ and 40 times faster at $0.5T_c$. Within this time scale, at $0.25T_c$, a 60 to 200 fold increase in the real part of the conductivity was calculated for frequencies of 17 to 240 GHz. An accompanying 4 to 2.5 fold increase in the thin film transmittance was found, suggesting the possibility of an optically-controlled switch for microwave radiation. Required power levels are from mW/cm^2 (al) to a few W/cm^2 (Nb).

On the same time scale, the laser pulse was calculated to enhance the attenuation of $Nb/Nb_2O_5/Nb$ waveguide from 20 to 1 × 10^4 dB/m, suggesting the possibilities of a microwave intensity modulator using pairs of appropriately timed laser pulses. Faster times might be achieved by using superconductors with faster recombination times -- either by raising the reservoir temperature (thereby increasing the small microwave losses of the device) or by utilizing materials with a higher T_c, such as NbN or possibly the new ceramic oxides. Lower laser powers can be achieved with (1) a light source that optimizes the ratio of absorptance to penetration depth, (2) a substrate that increases the value of τ_{es}/τ_B [though at the sacrifice of slower speeds -- see Eq. (2.53)], or (3) thinner films.

Still on the same time scales, but for the longer wavelengths (≤ 60 GHz), the calculations here showed that an optically-driven $Nb/Nb_2O_5/Nb$ waveguide can significantly depress the phase velocity without serious attenuation: almost a 90° phase shift was calculated for a 60 GHz wave over a propagation distance of 1 mm. Since it is usually sufficient to operate on a microsecond scale for phase shifting applications, larger values of τ_{es}/t_B could be used, to permit very low laser intensities to achieve large phase shifts.

REFERENCES

1. See C.H. Lee, ed., Picosecond Optoelectronic Devices (Academic Press, NY (1984).
2. A. Rothwarf and B. Taylor, Phys. Rev. Lett. 19, 27 (1967).
3. D. Mattis and J. Bardeen, Phys. Rev. 11, 412 (1958).
4. W. Parker, Phys. Rev. B12, 3667 (1975).
5. J. Chang and D.J. Scalapino, J. Low Temp. Phys. 31, 1 (1978).
6. R. Glover and M. Tinkham, Phys. Rev. 108, 3 (1957).
7. R.L. Kautz, J. Appl. Phys. 49, 308 (1978).
8. N. Glass and D. Rogovin, Appl. Phys. Lett. 54, 182 (1989).
9. The pair-splitting frequency in Figure 9 is 8% below the measured value because we used the ideal BCS weak-coupling approximation $\Delta(0) = 1.764\ kT_c$ with the experimental value of T_c.

Presented at the Workshop on High Temperature Superconductivity
23-25 May 1989 GACIAC PR-89-02

IMPROVED $YBa_2Cu_3O_{7-x}$/NOBLE METAL THICK FILMS

24 May 1989

J. H. Miller, Jr., S. L. Holder, and J. D. Hunn
Department of Physics and Astronomy
University of North Carolina
Chapel Hill, North Carolina 27599-3255

ABSTRACT

Composite thick films of $YBa_2Cu_3O_{7-x}$ and noble metals have been prepared on alumina substrates using paint-on and spin-coating methods. It is found that thick films containing greater than about 10% silver or gold by weight have greatly reduced normal resistivities for $T > T_c(onset)$ and significantly enhanced $T_c(R=0)$ as compared with undoped and palladium-doped films processed under identical conditions. These results are interpreted in terms of enhanced grain growth induced by melting and improved coupling between grain boundaries caused by proximity-induced electron pairing in the noble metal regions.

INTRODUCTION

Since the discovery of superconductors with $T_c > 77$ K,[1] considerable progress has been made in the deposition of high quality HTS thin films using a variety of techniques, and low surface impedances have been measured at high frequencies on epitaxially grown $YBa_2Cu_3O_{7-x}$ films.[2] However, epitaxial thin film deposition techniques suffer from some important drawbacks, including high cost and limitations on substrate materials and geometries, which may limit the development of applications. Thick films offer a number of significant advantages over thin films, including low cost, ease of deposition and patterning, rapid prototyping capability, and the possibility of patterning films onto a wide range of substrate materials

and geometries over arbitrarily large areas. The primary disadvantage of thin films has been that their transport properties, such as critical current density and microwave surface impedance, has been dominated by their microstructure.[3-18] In particular, weak coupling between grain boundaries, surface roughness, and interdiffusion between film and substrate act to degrade performance. According to the weakly coupled grain model proposed by Hylton *et al*,[19] as either the grain dimensions or grain boundary critical current densities become small, the surface impedance becomes dominated by the grain boundaries. Thus, any improvement in grain size, grain allignment, or coupling between grains is likely to be important for applications.

DISCUSSION OF RESULTS

Experiments conducted in our laboratory[20] demonstrate that the addition of silver to $YBa_2Cu_3O_7$ thick films patterned onto alumina substrates significantly improves their temperature-dependent resistivities. More recently, we have also found that the addition of gold also improves thick film quality. $YBa_2Cu_3O_7$ powder was mixed with various quantities of noble metal powder and the resulting composite powders were mixed with suitable organic vehicles to make inks. Films of the resulting inks were painted or spin coated onto alumina substrates, and then processed following the procedure of Budhani *et al*.[5] Propylene carbonate has been found to be a suitable vehicle for direct painting, while poly (ethylene glycol methyl ether), which is more viscous, yields reasonable quality spin coated films of uniform thickness. The undoped and silver-doped films were sintered at 750°C for 4 hr., quickly ramped up to 1000°C, held at 1000°C for 30 min., and then furnace cooled. For the gold-doped films it was found necessary to heat up to ~1070°C, slightly above the melting point of gold, for about 15 min. during the final sintering step in order to obtain signifant improvement as compared with undoped films. All samples were annealed at 450°C in flowing O_2 for 2-4 hr. The resistance measurements were done using the conventional four point probe method with silver paint contacts.

Figures 1(a) and 1(b) show plots of resistivity as a function of

temperature for representative painted-on $YBa_2Cu_3O_7$ thick films with no silver added and 10% silver added by weight, respectively. The film with no silver added has a resistivity of about 60 mΩ-cm just above the transition onset, and zero resistance is attained for T < 50K. By contrast the film with 10% silver added exhibits metallic behavior above T_c, with a resistivity of only 1.5 mΩ-cm just above $T_c(onset)$, and zero resistance is attained at $T_c(R=0)$ = 82K. The cross-sectional areas of films were determined using a Dektak surface profilometer and the critical current was measured using a pulsed technique to minimize heating at the contacts. The critical current density of the film corresponding to Fig. 1(b) was found to be J_c = 80A/cm^2, which compares favorably with values reported in the literature for thick films patterned onto alumina. Figure 2 shows a family of temperature-dependent resistivity curves for $YBa_2Cu_3O_{7-x}$/silver composite thick films which were processed as described above, except for an additional two hour oxygen annealing step. The T_c is observed to increase by about 40K and the normal resistivity is found to decrease by over two orders of magnitude for the film with 30% silver as compared with the undoped film. A slight increase in $T_c(onset)$ in $YBa_2Cu_{3-x}Ag_xO_7$ bulk samples has been reported by Michael and Mukhlif.[21] For silver concentrations significantly greater than 30% we continue to observe an improvement in the normal resistivity, but the film morphology and the width of the superconducting transition are found to be extremely sensitive to starting material grain size, vehicle, and processing conditions. A detailed study of $YBa_2Cu_3O_{7-x}$ thick films with greater than 30% noble metal concentrations is thus an ongoing subject for investigation.

We have found that the addition of up to 30% palladium by weight yields essentially no improvement of thick films that are processed under identical conditions to those described above, and show characteristics similar to the 5% palladium-doped sample whose temperature-dependent resistivity characteristics are exhibited in Fig. 1(a). This indicates that an enhanced coupling between superconducting grains partially results from melting of the noble metal during the sintering step, since the melting point of silver is 962°C, as compared with 1552°C for palladium.[22] Figures 3(a) and 3(b)

show scanning electron micrographs comparing undoped and 10% silver doped $YBa_2Cu_3O_{7-x}$ thick films, respectively, indicating that considerable melting has taken place in the $YBa_2Cu_3O_{7-x}$/Ag composite film, as well as enhanced grain growth. Energy dispersive X-ray (EDX) analysis indicates that the noble metals tend to concentrate between, rather than within, the superconducting grains.

INTERPRETATION OF RESULTS AND CONCLUSION

Silver and gold are both known to be fairly nonreactive with $YBa_2Cu_3O_{7-x}$. We believe that these metals enhance the coupling between superconducting grains by means of proximity-induced electron pairing in the noble metal regions, and contribute to enhanced grain growth when the film is heated above the melting point of the noble metal. It has been found that silver and gold form excellent contacts to high T_c superconductors,[23-28] and studies of the magnetic field-dependence of contact critical currents provide evidence for proximity-induced pairing in gold contacts on $YBa_2Cu_3O_{7-x}$.[29] In addition, Mankiewich *et al*[30] have recently observed a proximity-induced supercurrent in an $YBa_2Cu_3O_7$/Au/$YBa_2Cu_3O_7$ S-N-S weak link, where the width of the normal region was 1 μm. Using expressions given by Likharev,[31] they estimated the proximity-induced coherence length in the normal (gold) region to be $\xi_N \sim 700$Å at 4.2K, approximately two orders of magnitude greater than the longitudinal and transverse Ginzburg-Landau coherence lengths of $YBa_2Cu_3O_7$. It has also been demonstrated that the addition of silver[32-34] or silver-oxide[35] improves the strength, ductility, and critical current density of bulk high T_c superconductors, which is important for the development of useful wires and tapes. The use of noble metals thus appears to hold considerable promise for accelerating the development of both film and bulk applications of high T_c superconductors.

ACKNOWLEDGMENTS

The authors are grateful to G. N. Holder, Mark Kellam, Nalin Parikh, and Charles Childs for their valuable assistance. This work was partially supported by grants from the University of North Carolina at Chapel Hill and

the North Carolina Board of Science and Technology. One of the authors (JHM) acknowledges receipt of an A. P. Sloan Research Fellowship, while another (JDH) is a recipient of a Dupont Fellowship.

REFERENCES

1. M. K. Wu, J. R. Ashburn, C. J. Torng, P. H. Hor, R. L. Meng, L. Gao, Z. J. Huang, Y. Q. Wang, and C. W. Chu, *Phys. Rev. Lett.* **58**, 908 (1987).
2. N. Klein, G. Müller, H. Piel, B. Roas, L. Schultz, U. Klein, and M. Peiniger, *Appl. Phys. Lett.* **54**, 757 (1989).
3. H. Koinuma, T. Hashimoto, M. Kawasaki, and K. Fueki, *Jpn. J. Appl. Phys.* **26**, L399 (1987).
4. H. Koinuma, T. Hashimoto, T. Nakamura, K. Kishio, K. Kitazawa, and K. Fueki, *Jpn. J. Appl. Phys.* **26**, L761 (1987).
5. R. C. Budhani, Sing-Mo H. Tzeng, H. J. Doerr, and R. F. Bunshah, *Appl. Phys. Lett.* **51**, 1277 (1987).
6. K. Takahashi, S. Shimomura, A. Nagasawa, M. Ohta, and K. Kakegawa, *Jpn. J. Appl. Phys.* **26**, L1991 (1987).
7. A. K. Gupta, V. S. Tomar, M. Johri, N. D. Kataria, S. K. Agarwal, B. Jayaram, and A. V. Narlikar, *Thin Solid Films* **158**, L45 (1988).
8. I. Shih and C. X. Qiu, *Appl. Phys. Lett.* **52**, 748 (1988).
9. Y. Tzeng, in *High Temperature Superconducting Materials: Preparations, Proerties, and Processing,* William E. Hatfield and John H. Miller, Jr., editors (Marcel-Dekker, 1988) pp. 159-166.
10. M. Itoh and H. Ishigaki, *Jpn. J. Appl. Phys.* **27**, L420 (1988).
11. J. Tabuchi, A. Ochi, K. Utsumi, and M. Yonezawa, *J. Ceram. Soc. Jpn.* **96**, 450 (1988).
12. N. W. Cody, U. Sudarsan, and R. Solanki, *Appl. Phys. Lett.* **52**, 1531 (1988).
13. K. Hoshino, H. Takahara, and M. Fukutomi, *Jpn. J. of Appl. Phys.* **27**, L1297 (1988).
14. K. Yoshiara, K. Kagata, S. Yokoyama, T. Hiroki, H. Higuma, T. Yamazaki, and K. Nakahigashi, *Jpn. J. Appl. Phys.* **27**, L1492 (1988).
15. N. P. Bansal, R. N. Simons, and D. E. Farrell, *Appl. Phys. Lett.* **53**, 603 (1988).
16. J. Tabuchi and K. Utsumi, *Appl. Phys. Lett.* **53**, 606 (1988).
17. M. Sacchi, F. Siratti, B. Morten, and M. Prudenziati, *Appl. Phys. Lett.* **53**, 1110 (1988).
18. A. Z. Lin, H. Q. Li, F. W. Liu, and L. Tang, *Jpn. J. Appl. Phys.* **27**, L1204 (1988).
19. T. L. Hylton, A. Kapitulnik, M. R. Beasley, John P. Carini, L. Drabeck, and George Grüner, *Appl. Phys. Lett.* **53**, 1343 (1988).
20. J. H. Miller, Jr., S. L. Holder, J. D. Hunn, and G. N. Holder, *Appl. Phys. Lett.* **54**, 2256 (1989).
21. S. S. Michael and N. A. Mukhlif, *Mat. Res. Bull.* **23**, 1797 (1988).
22. R. C. Weast and M. J. Astle, editors, *Handbook of Chemistry and Physics, 60th Edition* (CRC Press, Boca Raton, Florida, 1980), pp. B-122 and B-104.

23. Y. Tzeng, A. Holt, and R. Ely, *Appl. Phys. Lett.* **52**, 155 (1988).
24. J. W. Ekin, A. J. Panson, and B. A. Blankenship, *Appl. Phys. Lett.* **52**, 331 (1988).
25. R. Caton, R. Selim, A.M. Buoncristiani, and C. E. Byvik, *Appl. Phys. Lett.* **52**, 1014 (1988).
26. A. D. Wieck, *Appl. Phys. Lett.* **52**, 1017 (1988).
27. K. Mizushima, M. Sagoi, T. Miura, and J. Yoshida, *Appl. Phys. Lett.* **52**, 1101 (1988).
28. J. W. Ekin, T. M. Larson, N. F. Bergren, A. J. Nelson, A. B. Swartzlander, L. L. Kazmerski, A. J. Panson, and B. A. Blankenship, *Appl. Phys. Lett.* **52**, 1819 (1988).
29. A. D. Wieck, *Appl. Phys. Lett.* **53**, 1216 (1988).
30. P. M. Mankiewich, D. B. Schwartz, R. E. Howard, L. D. Jackel, B. L. Straughn, E. G. Burkhardt, and A. H. Dayem, Proc. SPIE- Int. Soc. Opt. Eng., **948**, 37 (1988).
31. K. K. Likharev, *Rev. Mod. Phys.* **51**, 101 (1979).
32. E. A. Early, C. L. Seaman, M. B. Maple, and M. T. Simnod, *Physica C***153-155**, 1161 (1988).
33. R. Prasad, N. C. Soni, A. Mohan, S. K. Khera, K. U. Nair, C. K. Gupta, C. V. Tomy, and S. K. Malik, *Mat. Lett.* **7**, 9 (1988).
34. W. J. Nellis and L. D. Woolf, *MRS Bulletin*, January 1989, pp. 63-66.
35. P. N. Peters, R. C. Sisk, E. W. Urban, C. Y. Huang, and M. K. Wu, *Appl. Phys. Lett.* **52**, 2066 (1988).

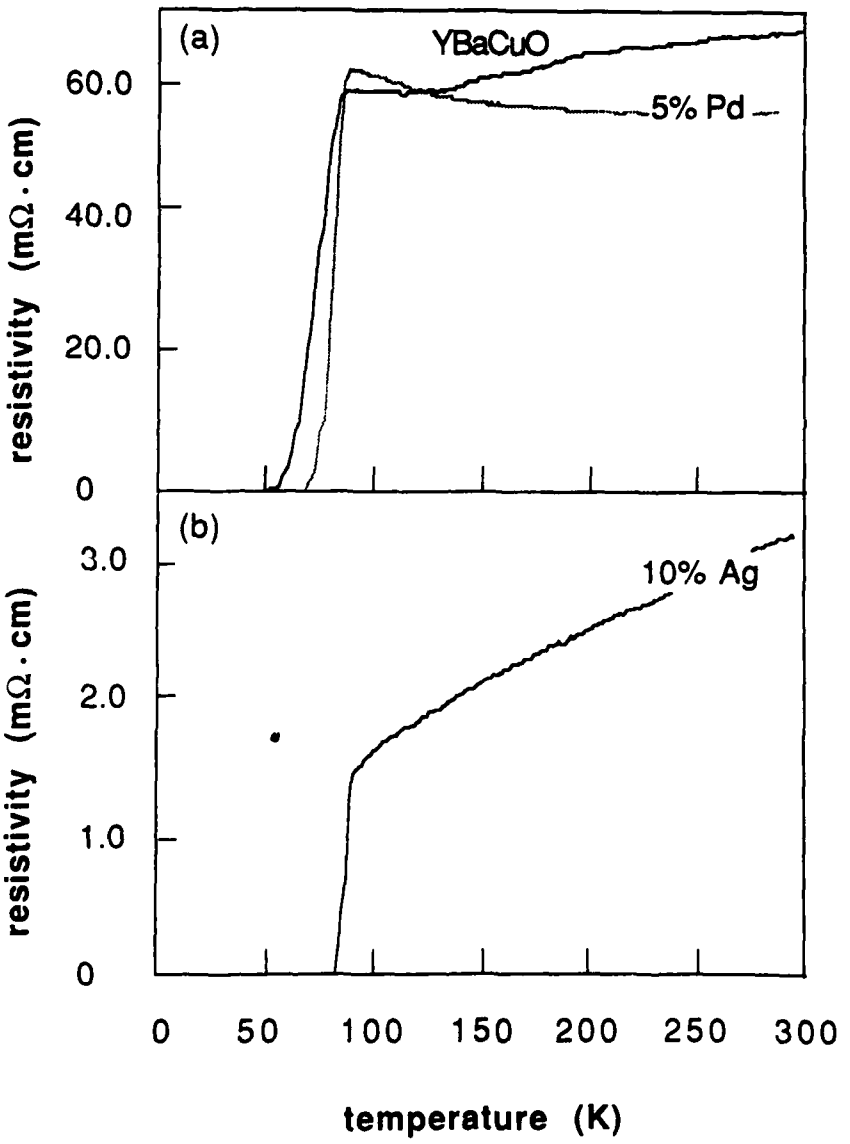

Figure 1. Temperature-dependent resistivities of $YBa_2Cu_3O_{7-x}$ thick films on alumina substrates which are processed under identical conditions, as described in the text. (a) "Control" film with no silver added (dark curve) and film with 5% palladium added by weight (light curve). (b) Film with 10% silver added.

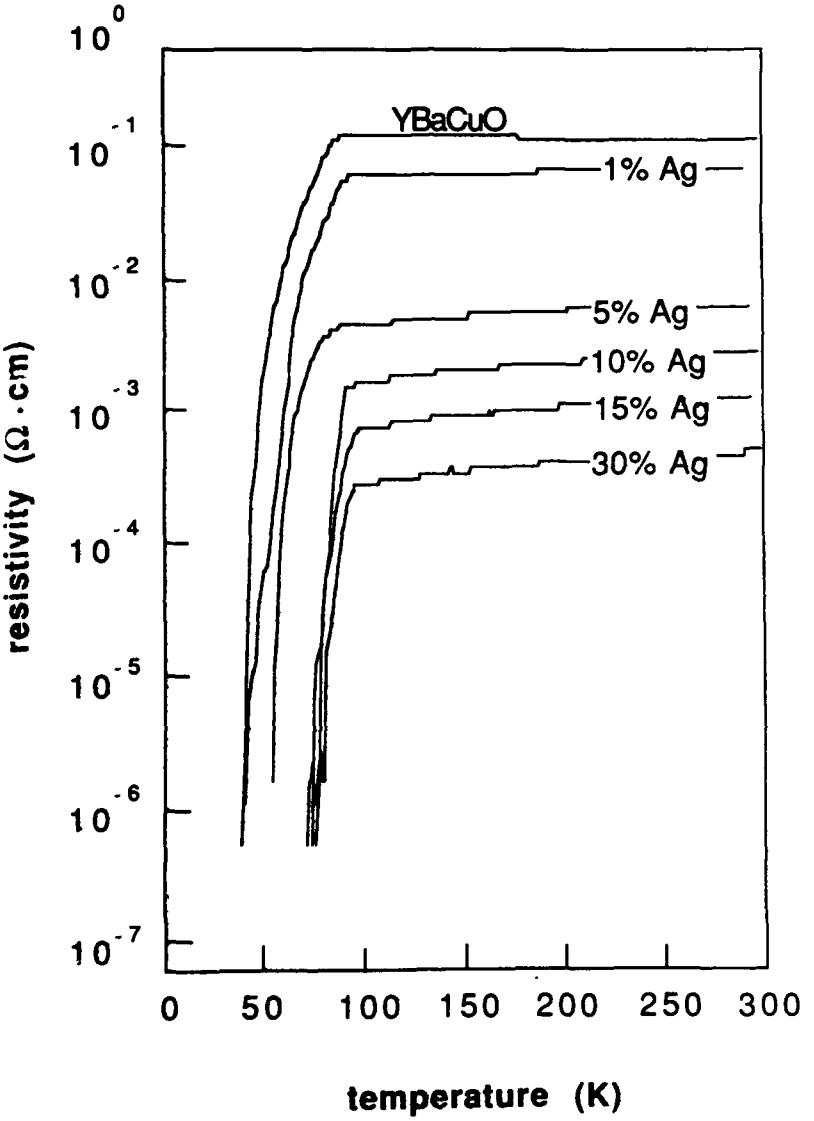

Figure 2. Temperature-dependent resistivities of $YBa_2Cu_3O_{7-x}$/Ag composite thick films plotted on a semilogarithmic scale, with silver concentration as a parameter.

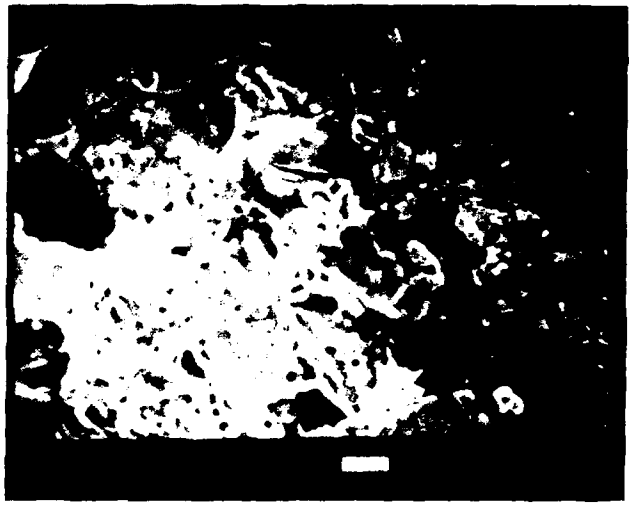

(a)

(b)

Figure 3. Scanning electron micrographs showing undoped (**a**) and 10% Ag doped (**b**) $YBa_2Cu_3O_{7-x}$ thick films. The dark area in the upper right of (**a**) is the edge of a silver paint contact. Each white bar represents 5 μm.

THIS PAGE IS INTENTIONALLY BLANK

Presented at the Workshop on High Temperature Superconductivity
23-25 May 1989 GACIAC PR-89-02

Flux Creep in Polycrystalline Oxide Superconductors. (U)

15 May 1989

M. E. McHenry, M. P. Maley, J. O. Willis, J. D. Thompson, K. C. Ott,
G. H. Kwei, J. R. Cost, D. E. Peterson, J. L. Smith and W. L. Hults
Los Alamos National Laboratory
Los Alamos, New Mexico 87544

(U) Abstract

(U) Measurement of the time dependence of the magnetization carries information as to the number and energy distribution of pinning sites in the material. This in turn gives important information as to the determinants of the critical current density in hard superconductors . High field relaxation measurements probe the nature of the intrinsic flux pinning within the grains of the superconducting material. Flux creep and the consequent decay of the critical current density remains one of the major technological stumbling blocks in the application of oxide superconductors. The time dependence of the magnetization as a function of applied field and temperature has been studied in a variety of materials including the Y-123, Tl-2223 and $Ba_{0.6}K_{0.4}BiO_3$ superconductors. The results of these measurements are discussed in terms of a thermally activated flux creep model from which the volume pinning energies may be inferred for each of these materials. Further, results of studies of the influence of chemical and irradiation effects on the volume pinning energy will be reviewed.

1.0 (U) Introduction

(U) Decay of magnetization with a logarithmic time dependence has been observed in conventional superconductors[1] and explained in terms of thermally activated motion of vortices[2]. This form of relaxation is of current interest in that it has been observed to be a prominent feature in the recently discovered high T_c oxide superconductors, $La(Ba)_2CuO_4$[3,4], $YBa_2Cu_3O_{7-\delta}$[5-8], $Bi_4Sr_3Ca_3Cu_4O_y$[9-10], $Ba_{0.6}K_{0.4}BiO_3$[11] and $Tl_2Ca_2Ba_2Cu_3O_x$[12-14]. The study of magnetic relaxation in these oxide materials offers considerable insight in that large thermal energies are accessible because of their high T_c's[8]. Characterization of the temperature dependence of the relaxation allows for a description of the distribution of pinning energies in the material f(E) as well as the average pinning energy U_0. In this paper we review pertinent models of relaxation and describe and summarize our measurements in a variety of oxide materials. These results reveal the highest pinning energies to occur in Tl-2223 superconductors while the Ba-K-Bi-O superconductors show the most constricted hysteresis loops, the shallowest irreversibility lines and

not surprisingly the lowest pinning energies. Further, experiments designed to influence the numbers and energies of pinning barriers through neutron irradiation and chemical means will also be discussed. Specifically, results of comparative studies on the kinetics of flux motion in neutron irradiated vs. unirradiated Y123 materials will be shown for the first time.

2.0 (U) Intragranular Flux Creep Model

(U) In the flux creep model[15] the thermally activated hopping rate for fluxons is expressed in terms of an Arrhenius Law:

$$R = R_0 \exp(\frac{-U_0}{kT}) \sinh(\frac{-\Delta W}{kT}) \qquad [1]$$

where U_0 represents the average pinning energy in the material and R_0 is an attempt frequency. ΔW is the driving force due to the flux gradient which is proportional of the critical current density of the material. The change in the magnetic flux density with respect to time can be expressed as:

$$\frac{dB}{dt} = RB = R_0 B \exp(\frac{-U_0}{kT}) \sinh(\frac{-\Delta W}{kT}) \qquad [2]$$

In the case of a substantial driving force term ($\Delta W >> kT$) then $\sinh(\Delta W/kT) \sim \exp(\Delta W/kT)$. In this limit, by virtue of the dependence of ΔW on J_C and B, a logarithmic time dependence to the magnetic flux density and consequently the magnetization can be derived. In the weak pinning limit ($\Delta W << kT$), which occurs at high temperatures and fields, $\sinh(\Delta W/kT) \sim \Delta W/kT$ and non-logarithmic time dependence (~exponential) is deduced. Phenomenological models[2] which relate the pinning energy and driving force terms to the specific pinning sites and the nature of the pinning (single fluxon or collective pinning) express the driving force in terms of the pinning force density ($J_C B$), an activated volume for flux motion (V) and a hop distance (a) for fluxons:

$$\Delta W = J_C B V a \qquad [3]$$

Using the fact that in the absence of thermal excitations $J = J_{C0}$ (the critical current density in the absence of thermal activation) and $U_0 - \Delta W = 0$, then the average (volume) pinning energy may be expressed:

$$U_0 = J_{C0} B V a \qquad [4]$$

(U) The flux creep model has been much heralded in the study of the new high T_C superconductors. Equation [2], when equated with a thermally activated EMF, and the dependence

of ΔW on J_c is included, predicts the shape of the I-V characteristic observed in many of these materials[16]. Logarithmic decay in the magnetization, as will be discussed further here, is also a hallmark of the model. With the use of a minimum voltage criterion the model predicts a specific frequency dependence to the critical current density[17]. In the weak pinning regime novel dissipation effects have also been observed and explained in terms of thermally activated flux motion[18].

(U) The utility of the flux creep model has been further extended by development of scaling law arguments for the field and temperature dependence of the pinning energy at high fields and temperatures where collective pinning is operative. In this case the activation volume is limited in two dimensions by the flux lattice spacing $a_0 = (\phi_0/B)^{1/2}$ Tinkham[19] has recently parameterized U_0 using Ginzburg-Landau theory parameters to yield a scaling expression for the dimensionless parameter $\gamma_0 = U_0/kT$ and where $t = T/T_c$:

$$\gamma_0 = \frac{U_0}{kT} \sim \frac{(1-t)^{\frac{3}{2}}}{B} \qquad [5]$$

This scaling has been used to explain the $B^{2/3}$ dependence of the irreversibility temperature, the temperature above which the field cooled (FC) and zero-field cooled susceptibilities are indistinguishable, and of the width of resistive transitions, ΔT, in a field.

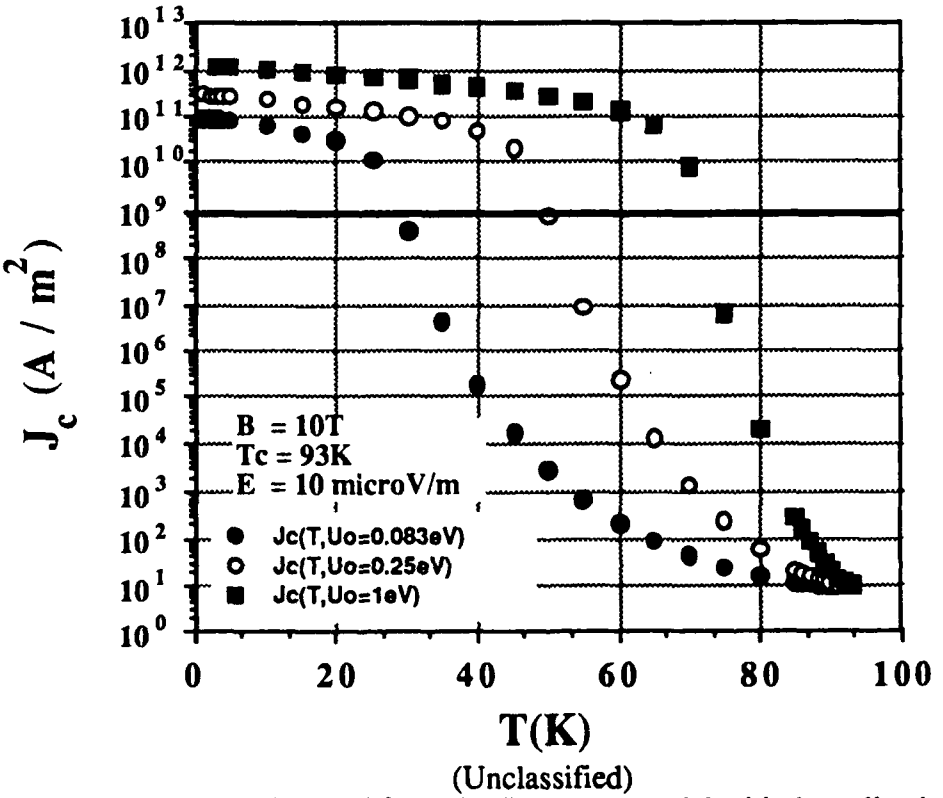

(Unclassified)

Figure One: (U) $J_c(T)$ as calculated from the flux creep model with the collective pinning parameterization of the average pinning energy

(U) To illustrate the importance of thermally activated flux creep to materials performance, a flux creep limited critical current density has been parameterized using expressions [2], [3] and [4] and the scaling law of [5]. Figure One shows the dependence of J_c on T for various choices of U_0, for a field of 10 T, a minimum voltage criterion of 10^{-6} V/cm and a material with Tc = 93K. Notable is the extraordinary temperature dependence of J_c in this model. It can be seen that only for $U_0 > 1$eV that J_c exceeds 10^9 A/m^2, a typical magnet criterion, at 75K.

3.0 (U) Experimental Techniques

(U) Sample preparation details for sintered $YBa_2Cu_3O_{7-\delta}$ and $Tl_2Ca_2Ba_2Cu_3O_x$ superconductors are described in reference 14 and those for $Ba_{0.6}K_{0.4}BiO_3$ in reference 11. Preparation of the irradiated $YBa_2Cu_3O_{7-\delta}$ and the unirradiated control sample is discussed in reference 20. The irradiated Y123 was examined after a total fast neutron (E > 0.1 MeV) fluence of 3×10^{18} n/cm^2 and with T_c depressed to 82 K, as compared to 92 K observed for the unirradiated material.

(U) Magnetic relaxation measurements were made using a Quantum Design magnetometer. The procedure for acquiring the magnetic relaxation data consisted of cooling in zero field (ZFC) and, after waiting to attain a stable temperature, application of the field. The first magnetization point was taken after the ~2 minutes required to latch the field. Subsequent magnetization points were taken every 2 minutes for the duration of the experiment which was typically 1 hour. Between runs the field was removed and the sample heated to above its transition. Equilibrium magnetization values (M_{eq}) were approximated as the magnetization of a slowly field-cooled (FC) sample at the temperature in question. It was ascertained that negligible relaxation occurred from this field-cooled state.

4.0 (U) Results and Discussion

(U) Figure Two illustrates typical magnetization vs. time data for a polycrystalline Tl-2223 sample in an applied field of 1 kG, and as a function of temperature. For low temperatures and fields this magnetic relaxation data is accurately described by the empirical relationship:

$$M = M_0 + A \ln(t) \qquad [6]$$

which is a hallmark of the flux creep model. This expression is not particularly accurate for high fields and high temperatures (i.e. for very small driving force). In the flux creep model this temperature dependence is a manifestation of the temperature dependence of the volume pinning

energy U_0 and the temperature dependent critical current density as given in the following expression:

$$A = \frac{d(M(t)-M_{eq})}{d\ln(t)} = \left(\frac{kT}{U_0}\right)\frac{J_{c0}r}{4c} = \left(\frac{kT}{U_0}\right)(M_0-M_{eq}) \qquad [7]$$

The first expression is that derived by Yeshurun et al.[8] with r denoting the grain size, the second comes out of a phenomenological relaxation model[21] or alternatively from the first in conjunction with the Bean[22] model expression for the critical current density. Notable in this time dependence is an almost 20% decay of the magnetization from its initial value at 70 K over the experimental duration of ~1 hour. This behavior underscores the use of the terminology "giant flux creep" and points to its dramatic effect on magnetic properties. In Ba-K-Bi-O superconductors flux creep is an equally important problem though a giant flux creep is not observed[11]. This is because critical current densities are so dramatically low in these materials that there is a very small metastable flux

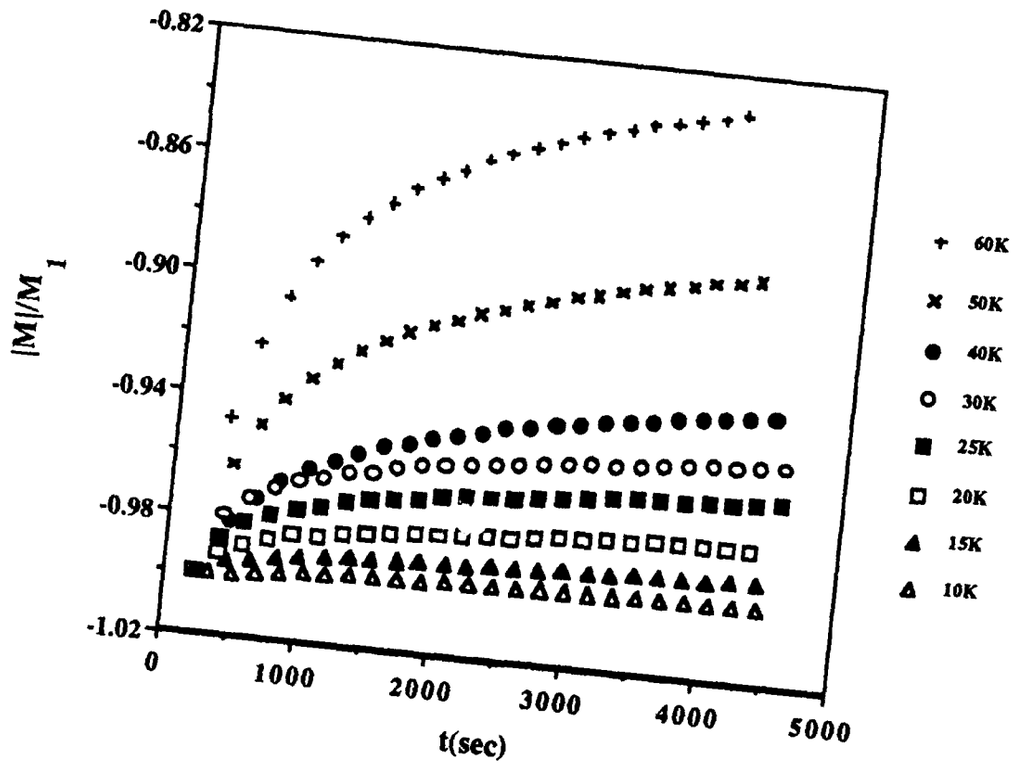

(Unclassified)

Figure Two: (U) Absolute value of the magnetization, |M|(t), for H = 1 kG, normalized by its initial value, as a function of time and temperature for a sintered Tl-2223 sample.

concentration present at the beginning of these experiments. This points to the importance, as expressed in [7], of the ratio of the excess magnetization (M_0 - M_{eq}) in determining the creep rate. It can be further seen from [7] that the slopes of the quantity (M_0 - M_{eq})/A vs. 1/T yields the volume pinning energy which is the pertinent quantity to be derived from these experiments.

(U) The volume pinning energies have now been measured for many oxide superconductors by extracting from data, like that shown in Figure Two, the temperature dependence of the magnetic relaxation rates and of the field cooled magnetization ($M_{FC} \sim M_{eq}$). The details of such analysis for various materials are discussed in references 8,10,11, and 13. Table One summarizes results derived for the volume pinning energy for several polycrystalline oxide superconductors. Also shown is the value of the pinning energy for a single crystal of the Bi-Sr-Ca-Cu-O material which represents the smallest pinning energy reported to date. It can be seen that Ba-K-Bi-O also has a relatively small pinning energy as well. The disappointing pinning energies observed in the bismuthate superconductors have been attributed to the absence of twin boundaries which have been postulated to enhance the pinning observed in the Y123 materials.[9] Also notable is the fact that the Tl-2223 material exhibits the highest pinning energy observed to date in the oxide materials. Certainly, some part of the enhancement can be explained in terms of the higher T_c (~115 K) in this material. It is clear that, since the Tl-2223 material is untwinned, the enhanced pinning must be related to other defects in these materials.

Tl-2233	0.33 eV
Y123 (Sample One)	0.17 eV
$Ba_{0.6}K_{0.4}BiO_3$	0.08 eV
Bi-Sr-Ca-Cu-O (Ref 9)	0.01 eV
Y123 (Unirradiated)	0.18 eV
Y123 (Irradiated 3 x 10^{18} n/cm^2)	0.13 eV

(Unclassified)

Table I: (U) Comparison of pinning energies for several oxide superconductors and comparison of unirradiated and neutron irradiated Y123.

(U) One of the most important open questions in the study of flux creep and pinning energies in oxide superconductors is the extent to which this behavior can be modified by controlling microstructural features of the superconductor. The energy saved by the normal core of a fluxon being located in a region of depressed order parameter, i.e., a region of normal material or a defect, represents the barrier to be overcome by thermal activation. Conventional wisdom suggests that the most effective pinning occurs when the defect or impurity size is well matched to

the size of the normal core. The fact that coherence lengths are very small in the oxide superconductors, on the order of 10-20 Å, or sizes approaching unit cell sizes, makes such matching conditions difficult to attain.

(U) We have initiated a program to study the influence of chemical impurities and the introduction of defects in controlled ways on the pinning properties of these superconductors. It has been documented that substitution of Zn for Cu in the Y123 superconductors results in depression of the order parameter and consequent degradation of T_c. Recently, we have examined samples with 0.2% and 0.7% substitution of Zn for Cu in the Y123 superconductor. Preliminary results indicate a slight enhancement in J_c but with little influence on the volume pinning energies.

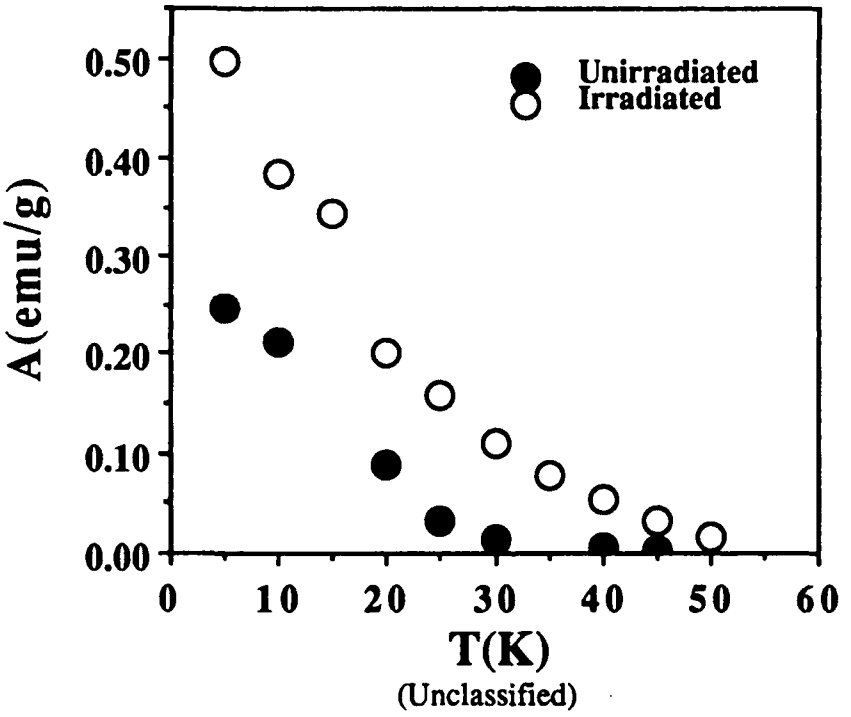

Figure Three: (U) Comparison of the flux creep rate for unirradiated and neutron irradiated Y123 in an applied field of 1 T.

(U) The second method employed to change the microstructural features of Y123 materials has been through fast neutron irradiation. In a previous study[20], it was shown that for sequential fast neutron irradiation, with the total neutron fluence ranging from 0.0 to 3.0 x 10^{18} n/cm^2, the critical current density (in zero field and at 7 K) was enhanced by a factor of 2-3 with the maximum enhancement occurring at a fluence of ~1 x 10^{18} n/cm^2. After experiencing the full dose of radiation, magnetic relaxation measurements were performed on both the irradiated sample (total fluence of 3.0 x 10^{18} n/cm^2) and on a control sample of the unirradiated material. At all fields

examined (0.1, 0.3, 1, and 2 T) dramatic differences were discernible between the irradiated and the unirradiated sample. The most dramatic manifestation was at high fields (1 and 2 T) where the largest enhancements in J_C were observed. Figure Three illustrates this difference showing the temperature dependence of the magnetic relaxation rate A, as described by [6], for both the irradiated and unirradiated samples in an applied field of 1 T. Apparent from this data is the fact that the relaxation rate is substantially enhanced for the irradiated sample. This enhancement is, however, compensated for by the enhancement in the critical current density (and the excess magnetization) so that the overall effect on the pinning energy can be inferred to be small.

(U) Table One summarizes the results of fits to the previously described Arrhenius law, for the irradiated and unirradiated samples, in the reference field of 1kG. It can be seen that the average pinning energy in the irradiated sample is somewhat smaller than in the unirradiated sample. This is perhaps not too surprising given that T_C is depressed to 82 K in the irradiated material as compared to the 92 K value for the unirradiated sample. Given the more than two-fold increase in the critical current density, then expression [5] implies that the quantity Va has been reduced by a factor of ~3. It is certainly reasonable that the jump distance should be reduced because of the increased defect density of the irradiated material. Further, the critical current density increase is apparently due to the increased number density of pinning sites in the material and not due to any marked increase in the volume pinning energy, which has actually decreased slightly. It should be noted that relaxation measurements on the irradiated sample were studied at a fluence well above that which yielded the largest enhancement in J_C. It is conceivable that the pinning energy for a sample with the optimum fluence, in terms of the enhancement in J_C, would be much different especially in light of a smaller depression of T_C at lower levels of neutron fluence. These preliminary results on the influence of neutron irradiation on pinning properties suggest that important new information will be derived from contemplated future studies of the pinning energy and its dependence on fluence.

5.0 (U) Conclusions

(U) Magnetic relaxation measurements on oxide superconductors have been used to probe the volume average pinning energies in these materials. Pinning energies are highest in the Tl-2223 materials with anomalously small values observed in the bismuthate superconductors. Critical current densities have been modified through chemical means with little change in the volume pinning energy. Both critical current densities and volume pinning energies were altered through the introduction of defects by neutron irradiation. Only fractional changes in the pinning energy were observed in contrast to the nearly order of magnitude increases required for applications of these materials at liquid nitrogen temperature. The dramatic changes in the critical

current density for irradiated Y123 do not produce comparably large changes in the pinning energy, which was observed actually to decrease slightly. Instead, the improved critical current densities appear to be related to an increase in the number density of pinning sites.

6.0 (U) References

1. Y. B. Kim, Rev. Mod. Phys.**36**, 39 (1964).
2. P. W. Anderson, Phys. Rev. Lett. **9**, 309 (1962).
3. K. A. Muller, M. Takashige and J. G. Bednorz, Phys. Rev. Lett. **58**, 1143 (1987).
4. A. C. Mota, A. Pollini, P. Visani, K. A. Muller, J. G. Bednorz, Phys. Rev. B **36**, 401 (1987).
5. M. Touminen, A. M. Goldman, M. L. McCartney, Phys. Rev. B **37**, 548 (1988).
6. U. Atzmony, R. D. Schull, C. K. Chiang, L. J. Swartzendruber, L. H. Bennett, J. Appl. Phys. **63**, 4179, (1988).
7. M. E. McHenry, M. Foldeaki, J. McKittrick, R. C. O'Handley and G. Kalonji, Physica B **153-55**, 310, (1988).
8. Y. Yeshurun and A. P. Malozemoff, Phys. Rev. Lett.. **60**, 2202, (1988).
9. Y. Yeshurun, A. P. Malozemoff, T. K. Worthington, R. M. Yandrofski, L. Krusin-Elbaum, F. H. Holtzberg, T. R. Dinger, and G. V. Chandrashekhar, Cryogenics **29**, 258, (1989).
10. B. D. Biggs, M. N. Kunchur, J. J. Lin, S. J. Poon, T. R. Askew, R. B. Flippen, M. A. Subramanian, J. Gopal, A. Krishnan, and A. W. Sleight; Phys. Rev. B **39**,7309, (1989).
11. M. E. McHenry, M. P. Maley, G. H. Kwei, and J. D. Thompson, Phys. Rev. B **39**, (1989).
12. M. Fang, D. K. Finnemore, D. E. Farrell, N. R. Bansal, Cryogenics **29**, 347, (1989).
13. M. E. McHenry, M. P. Maley, E. L. Venturini and D. L. Ginley, Phys. Rev. B **39**, 4784, (1989).
14. J. R. Thompson, J. Brynestad, D. M. Kroeger, Y. C. Kim, S. T. Sekula, D. K. Christen, E. D. Specht, Phys. Rev. B **39**, 6652, (1989).
15. Y. B. Kim, C. F. Hempstead, and A. R. Strnad, Phys. Rev. Lett. **9**, 306, (1962).
16. J. Z. Sun, K. Char, M. R. Hahn, T. G. Geballe, and A.Kapitulnik, Appl. Phys. Lett. **54**, 663, (1989).
17. T. K. Worthington, Y. Yeshurun, A. P. Malezemoff, R. M. Yandrofsky, F. H. Holtzberg, and T. R. Dinger, *Proceedings of the International Conference on Magnetism, Paris* 25-29 July 1988, to be published in J. Physique (Paris).
18. T. M. Palstra, B. Batlogg, L. F. Schneemeyer, and J. V. Waszczak, Phys. Rev. Lett. **61**, 1662 (1988).
19. M. Tinkham, Phys. Rev. Lett. **61**, 1658, (1988).
20. J. O. Willis, J. R. Cost, R. D. Brown, J. D. Thompson, and D. E. Peterson, Mat. Res. Soc. Symp. Proc. **99**, 391, (1988).
21. M. Foldeaki, M. E. McHenry, R. C. O'Handley, Phys. Rev. B.**39**, (1989).
22. C. P. Bean, Phys. Rev. Lett. **8**, 250 (1962).

THIS PAGE IS INTENTIONALLY BLANK

Presented at the Workshop on High Temperature Superconductivity.
23-25 May 1989 GACIAC PR-89-02

RF MEASUREMENTS ON HIGH-T_c SUPERCONDUCTORS

C. L. Bohn, J. R. Delayen, and M. T. Lanagan
Argonne National Laboratory
Argonne, Illinois 60439

ABSTRACT

We have fabricated bulk and thick-film samples of Y-based and Bi-based high-T_c superconductors and measured their rf properties as functions of temperature, frequency, and rf field amplitude. Our motivation was to determine whether these materials and fabrication processes would be useful in resonant cavities for particle accelerators. The rf surface resistance of the samples typically depended strongly on field amplitude, but the samples remained superconducting up to the highest fields we could apply (~640 gauss). For example, at 220 MHz, the surface resistance of a bulk polycrystalline $YBa_2Cu_3O_{7-x}$ sample ranged from $\lesssim$2 μΩ at $\lesssim$0.05 gauss and 4.2 K to 6.3 mΩ at 640 gauss and 77 K. Our measurements on Bi-based samples indicated that the rf surface resistance of highly textured bulk Pb-doped $Bi_2Sr_2Ca_2Cu_3O_y$ was substantially better than the undoped $Bi_2Sr_2CaCu_2O_y$ thick films at cryogenic temperatures, i.e., $T \leq 77$ K.

1. INTRODUCTION

In many high-power rf applications it is desirable to store large energy densities for long times with the aid of resonant cavities. Examples include resonant structures for particle acceleration[1] and for the generation of high-power microwaves.[2,3] In turn, the most useful cavities will have the largest intrinsic quality factors ($Q = 2\pi f_o U/P$, where f_o is the resonant frequency, U is the stored energy, and P is the power dissipated in the cavity walls). The low rf surface resistance of superconductors make these materials desirable for the construction of high-Q cavities. With critical temperatures (T_c) higher than the temperature of liquid nitrogen, and with the potential for sustaining surface fields as high as 27,000 gauss while remaining superconducting,[4] the ceramic-oxide superconductors are candidates for use in these applications.

Unlike the dc resistance, the rf surface resistance of a material in the superconducting state is not zero, nor is it necessarily low. In the framework of a two-fluid model, most, but not all, of the electrons are bound in Cooper pairs; the remainder are normal-conducting.[5] The inertia of the Cooper pairs keeps them from responding quickly enough to high-frequency radiation to prevent penetration of the radiation into the superconductor. The rf field which leaks into the superconductor drives the normal-conducting electrons, which in turn collide with the lattice and deposit thermal

---

1. J.R. Delayen, "Superconducting Accelerating Structures for High-Current Ion Beams," Nucl. Instru. and Meth. A (in press).

2. R.A. Alvarez, D. Birx, D. Byrne, M. Mendonca, and R.M. Johnson, IEEE Trans. Magnetics, 17, 935 (1981).

3. G.J. Dick, IEEE Trans. Magnetics, 11, 441 (1975).

4. T.K. Worthington, W.J. Gallagher, and T.R. Dinger, Phys. Rev. Lett., 59, 1160 (1987).

5. I.M. Khalatnikov and A.A. Abrikosov, Adv. in Physics, 29, 45 (1959).

energy. According to Bardeen-Cooper-Schrieffer (BCS) s-wave theory, for temperatures $T \lesssim 0.5\ T_c$ the rf surface resistance is approximately:[6]

$$R_s \approx \frac{A}{T} f^2 \exp\left(-\frac{\Delta}{T}\right)$$

where A is a constant, f is the rf frequency, and Δ is the binding energy of a Cooper pair. In general, a constant term R_o called the residual surface resistance needs to be added. It is caused by irregularities in the material and is therefore unpredictable theoretically. The rf surface resistance of most low-T_c superconductors, such as lead and niobium, follow this prediction. On the other hand, that of the high-T_c ceramics appears to deviate from the theory, particularly with regard to temperature dependence.[7,8]

The high-T_c ceramics are characteristically poor thermal conductors;[9] therefore, the use of high-conductivity substrates will probably be required to keep the ceramics cold while they are exposed to high rf fields. From a materials-processing standpoint, silver has been found to be compatible.[10] We have fabricated a variety of bulk samples, and thick films on silver substrates, of $YBa_2Cu_3O_{7-x}$ (YBCO) and Bi-Sr-Ca-Cu-O (BSCCO), and have measured their rf surface resistances versus temperature and rf field amplitude at frequencies

---

6. A. Abrikosov, L. Gorkov, and I. Khalatnikov, Sov. Phys. JETP, 8, 182 (1959).

7. W.L. Kennedy and S. Sridhar, Sol. State Comm., 68, 71 (1988).

8. T.L. Hylton, A. Kapitulnik, M.R. Beasley, J.P. Carini, L. Drabeck, and G. Gruner, Appl. Phys. Lett., 53, 1343 (1988).

9. J. Heremans, D.T. Morelli, G.W. Smith, and S.C. Strite III, Phys. Rev. B, 37, 1604 (1988).

10. M.T. Lanagan, K.C. Goretta, J.P. Singh, G.T. Goudey, J.T. Dusek, D.I. Dos Santos, and R.B. Poeppel, "Ceramic Fabrication Technology for High-T_c Materials," in Proc. of the 2nd Annual Conf. on Superconductivity and Applications, Buffalo, NY, 18-20 April 1988.

from 150 MHz to 40 GHz. In this paper, we describe our measurement techniques and notable results, and we comment on future initiatives for research and development of high-T_c superconductors for high-power rf applications in light of the results.

2. MEASUREMENT APPARATUSES

A standard technique for determining the rf surface resistance (R_s) of a sample involves the use of resonant cavities. The sample is inserted in the cavity and modifies the quality factor of the cavity. Measurement of the quality factor before and after sample insertion enables the calculation of R_s.[11,12]

We employ two types of cavities in our measurements. In the transverse electromagnetic (TEM) cavity (Figure 1), a rod-shaped sample is supported on-axis inside a long, cylindrical outer conductor using a quartz tube. The sample behaves as a resonant coaxial line such that its length corresponds to one half-wavelength of the rf field. In the transverse electric (TE) cavity (Figure 2), the sample forms the bottom plate of a cylindrical cavity which we made to resonate in the TE_{012} and/or TE_{011} modes. We have constructed 8 cavities, 6 TE and 2 TEM, for the measurement of samples ranging from small size up to 15-cm-diameter plates. The capabilities and frequencies of these cavities are given in Table 1.

In a typical experiment to measure R_s versus temperature, the temperature of the cavity was monitored with sensors mounted at the top and bottom outer surfaces of the cavity. The cavity and sample were cooled to 4.2 K with liquid helium and a measurement was taken. The helium was subsequently boiled away using a small heater, and the cavity was allowed to warm slowly enough that the two sensors recorded

---

11. S. Sridhar and W.L. Kennedy, Rev. Sci. Instru., 59, 531 (1988).

12. J.R. Delayen, K.C. Goretta, R.B. Poeppel, and K.W. Shepard, Appl. Phys. Lett., 52, 930 (1988).

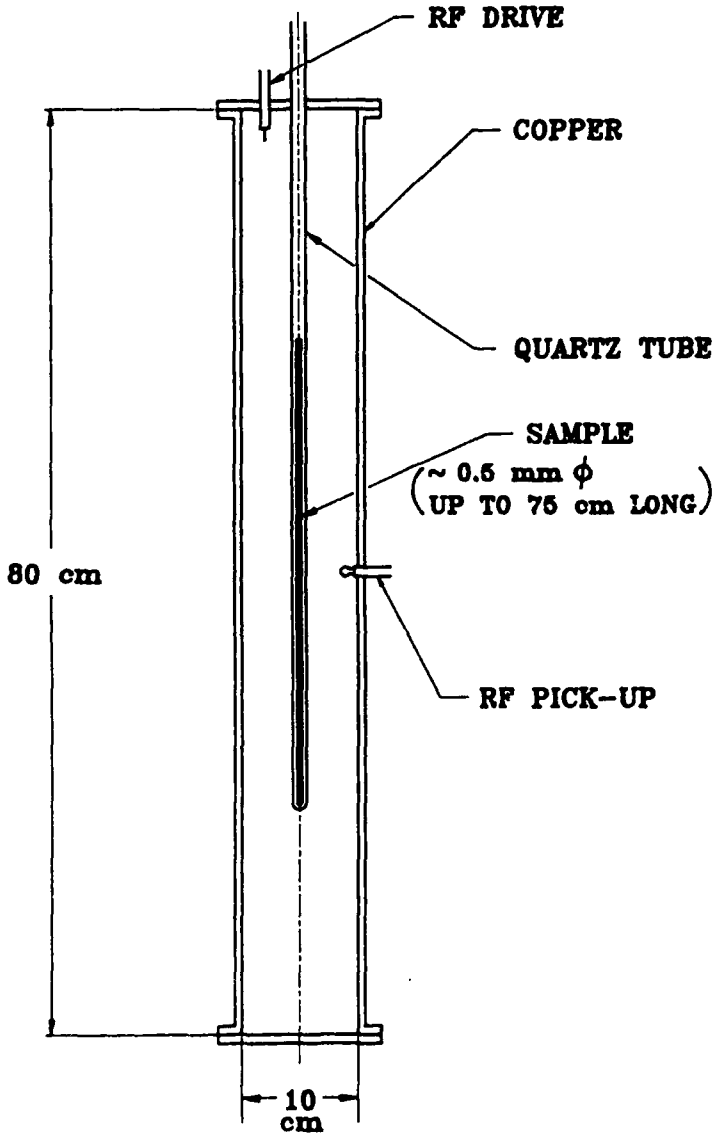

Figure 1. Generic TEM cavity. The sample is a rod which acts as a resonant coaxial line.

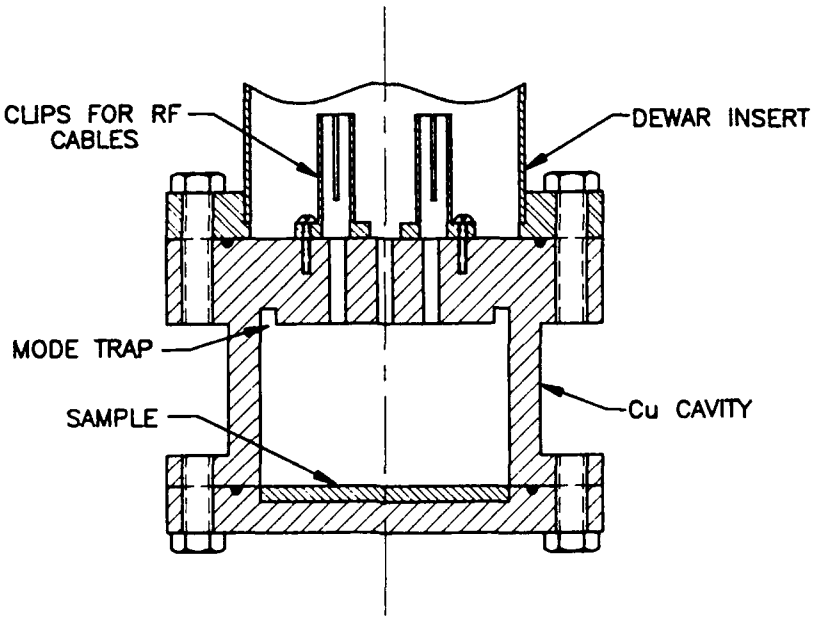

Figure 2. Generic TE cavity. The sample is the bottom surface of the cavity. This drawing is for the 8.0-12.4 GHz cavity of Table 1.

Table 1. Apparatuses for RF Measurements

Cavity	Frequencies	Capabilities
TEM Cu	150-600 MHz	Large Samples (rods) RF Breakdown
TEM Cu	600-1500 MHz	Large Samples (rods) RF Breakdown
$TE_{011,012}$, TEM Cu,Nb	1.5-4 GHz	Large Samples (rods and plates to 200 cm^2) Small Samples (disks, single crystals) RF Breakdown
$TE_{011,012}$ Cu	8.0-12.4 GHz	Large Samples (disks and plates to 20 cm^2)
$TE_{011,012}$ Cu	12.4-18 GHz	Medium Samples (disks and plates to 7 cm^2)
$TE_{011,012}$ Cu, Nb	26.5-40 GHz	Small Samples (disks and plates to 1.7 cm^2, single crystals)

the same temperature to within 0.5 K. This assured a condition of approximate thermal equilibrium in the cavity.

For isothermal measurements of R_s as a function of rf field amplitude, a TEM cavity was used. The cavity and quartz tube were flooded with either liquid helium or liquid nitrogen so that, at all times, the temperature of the sample was known unambiguously. The peak rf magnetic field at the surface of the sample was determined from the voltage reading of a calibrated pickup probe located halfway between the end-plates of the cavity, as shown in Figure 1.

Additional details on these cavities and the measurement techniques can be found elsewhere.[13-15]

3. RESULTS

3.1 BULK POLYCRYSTALLINE YBCO ROD

We fabricated several bulk ceramic YBCO rods from phase-pure YBCO powder which was combined with several organics to form a plastic mass and then extruded.[16] After firing, one such rod had a diameter of 0.44 mm and a length of 80 cm. To do measurements at different frequencies, we broke the rod to obtain the desired length. Initial measurements at low rf field amplitude (B_{rf}) were taken at 4.2 K and 77 K after fabrication, and the rod was then stored in air for ten months. Both low-field and high-field measurements were then made. The low-field measurements from the two time periods agreed, indicating that the rf properties of the sample were stable over the

---

13. C.L. Bohn, J.R. Delayen, D.I. Dos Santos, M.T. Lanagan, and K.W. Shepard, IEEE Trans. Magnetics, 25, 2406 (1989).

14. J.R. Delayen and C.L. Bohn, Phys. Rev. B (submitted).

15. C.L. Bohn, J.R. Delayen, U. Balachandran, and M.T. Lanagan, Appl. Phys. Lett. (submitted).

16. M.T. Lanagan, R.B. Poeppel, J.P. Singh, D.I. Dos Santos, J.K. Lumpp, U. Balachandran, J.T. Dusek, and K.C. Goretta, J. Less-Com. Met. (in press).

ten-month interval. The lowest R_s measured was $\lesssim$1.1 μΩ at 4.2 K and 175 MHz.

The low-field behavior of R_s is plotted in Figure 3. It is characterized by a sharp transition between the superconducting state and the normal state. The frequency dependence of R_s was approximately quadratic at all temperatures below $T_c \approx 91$ K and was approximately square-root just above T_c. The temperature dependences of Figure 3 did not follow either BCS theory or a single power law over a wide temperature range.

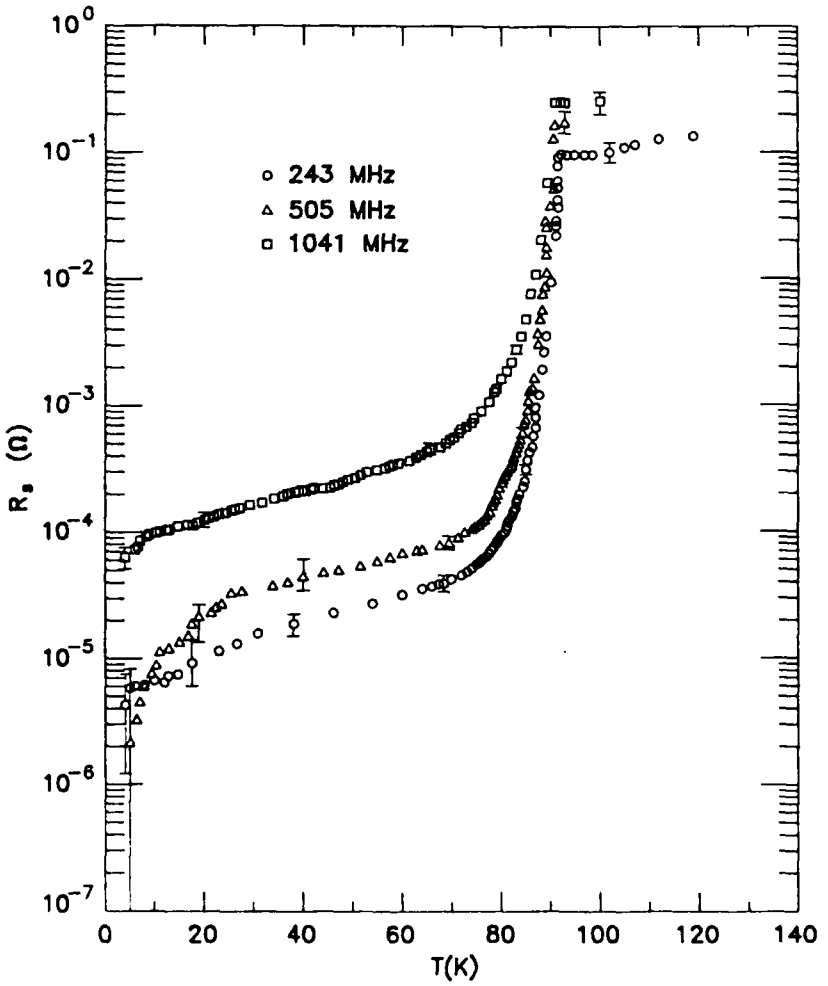

Figure 3. Surface resistance of bulk YBCO versus temperature at three frequencies and at low field ($B_{rf} \lesssim 0.05$ G).

The dependence of R_s on the rf field amplitude at the center of the sample for T = 4.2 K and 77 K is illustrated in Figure 4. The surface resistance increased monotonically as B_{rf} was raised, passing through a transition region characterized by a strong B_{rf}-dependence, and saturating at a value roughly 5 percent of the normal-state surface resistance just above T_c. The sample remained superconducting out to the highest field achieved, $B_{rf} \cong 640$ G (at 77 K and 190 MHz). In the transition regions, R_s was strongly dependent on temperature and exhibited a frequency dependence which was approximately quadratic. In the high-field region, on the other hand, R_s showed a weak dependence on both temperature and frequency.

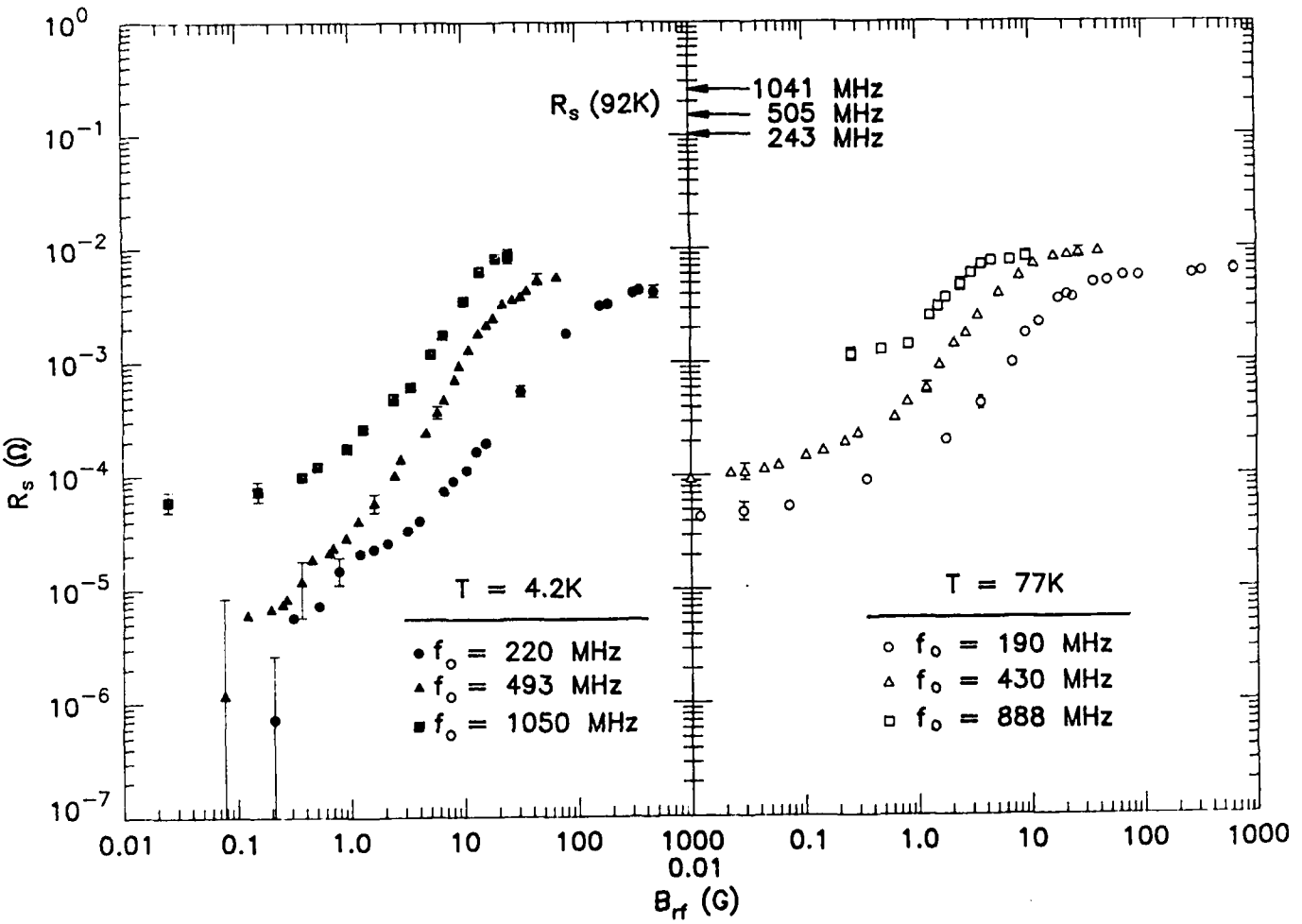

Figure 4. Surface resistance of bulk YBCO versus rf field amplitude at T = 4.2 K and T = 77 K.

3.2 THICK POLYCRYSTALLINE FILMS ON SILVER SUBSTRATES

In earlier efforts, thick films of YBCO were fabricated by applying slurries to silver substrates, and several of these films had rf surface resistances comparable to bulk specimens.[17,18] It is possible to lower the surface resistance of bulk YBCO by introducing regrinding steps during calcination and by increasing the sintering time.[19] In fabricating and testing an 80-μm-thick, 15-cm-diameter film of YBCO on silver, we found that increasing oxygen annealing time also aids in lowering R_s. Figure 5 indicates the effect of a 3-day

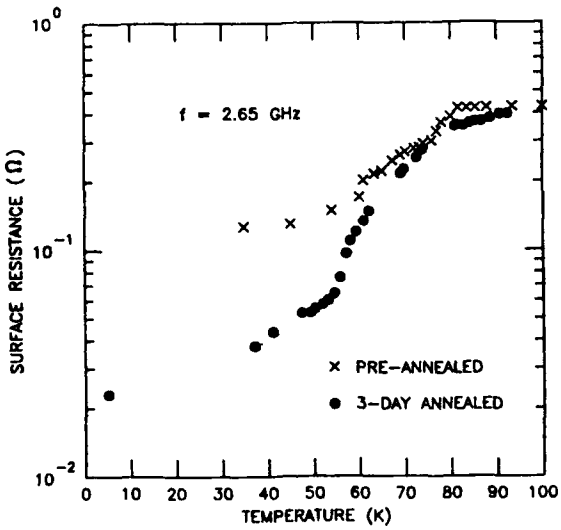

Figure 5. Effect of annealing time on the surface resistance at 2.65 GHz of a thick YBCO film of surface area 182 cm^2 on silver.

---

17. J.R. Delayen and M.T. Lanagan, "High-Power RF Applications of High-T_c Superconductors," in Proc. of the 2nd Annual Conf. on Superconductivity and Applications, Buffalo, NY, 18-20 April 1988.

18. C.L. Bohn, J.R. Delayen, D.I. Dos Santos, M.T. Lanagan, and K.W. Shepard, op. cit.

19. H. Piel, N. Hein, N. Klein, U. Klein, A. Michalke, G. Mueller, and L. Ponto, Physica C, 152, 1604 (1988).

anneal on this sample; the low-temperature surface resistance was reduced by a factor 3-5. The otherwise high values of R_s and the broad transition to the superconducting state of this particular early sample are attributed to inhomogeneities caused by difficulties in maintaining a uniform temperature while firing the sample due to its large surface area.

We have recently fabricated thick films of BSCCO on silver, again by applying high-viscosity slurries.[20] Two different processing techniques were used; "4336" samples were produced using powders derived from the compound $Bi_4Sr_3Ca_3Cu_6O_x$, and a "2212" sample was produced using powders derived from $Bi_2Sr_2CaCu_2O_x$. All of the films were approximately 80-μm thick; the 4336 samples had diameters of 1.3 cm and 15 cm, and the 2212 sample had a 5.1 cm diameter. None of the samples was entirely phase-pure as judged by x-ray diffraction.

The rf surface resistance of these samples was measured as a function of temperature at low rf field amplitude ($\lesssim$0.1 gauss) using three of the copper TE cavities described in Table 1. The data is shown in Figure 6. The 4336 samples had $T_c \approx 81$ K, and the 2212 sample had $T_c \approx 83$ K. The surface resistances measured at low temperatures were approximately consistent with a quadratic frequency dependence, indicating that the rf performance of the 4336 and 2212 films were comparable despite their very different processing procedures. At low temperatures, the 2212 sample behaved like room-temperature copper at the X-band frequencies of the rf fields to which it was exposed. The performance of these films was also similar to that achieved recently in bulk BSCCO. For a 2212 pellet of surface area 0.013 cm^2, a surface resistance of 3.0 mΩ at 3 GHz, 4.2 K, and low field has been reported,[21] which is comparable in magnitude to R_s of the 15-cm-diameter 2212 film with larger surface area (182 cm^2).

---

20. C.L. Bohn, J.R. Delayen, U. Balachandran, and M.T. Lanagan, op. cit.

21. D.W. Cooke, E.R. Gray, R.J. Houlton, B. Rusnak, E. Meyer, G.P. Lawrence, M.A. Maez, B. Bennett, J.D. Doss, A. Mayer, W.L. Hults, and J.L. Smith, Phys. Rev. B (submitted).

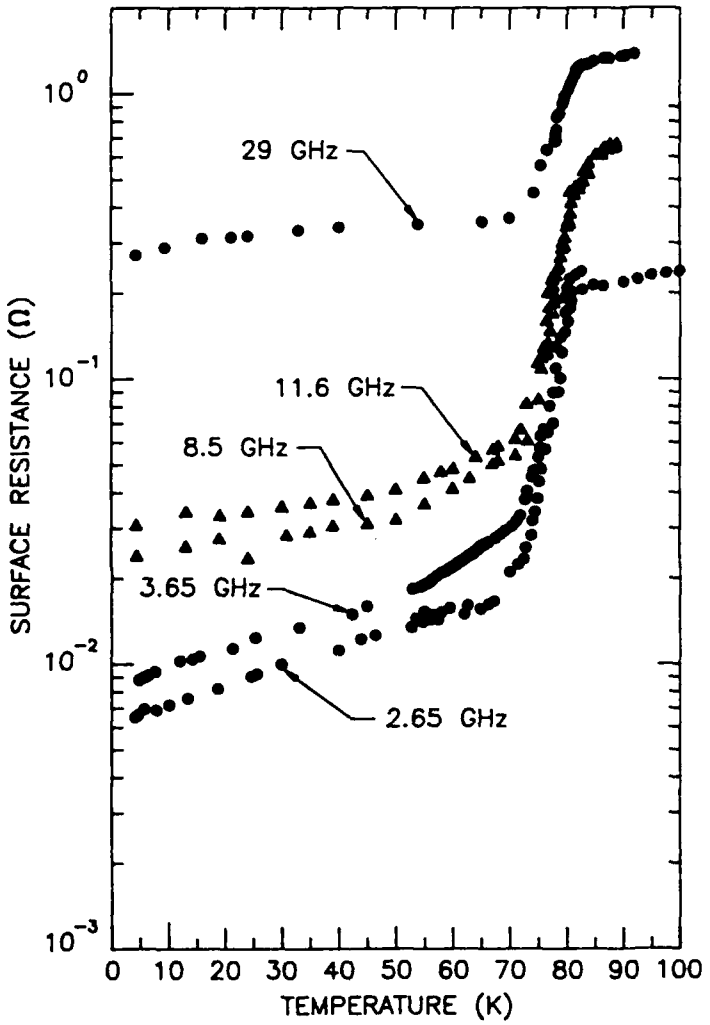

Figure 6. RF surface resistance versus temperature of BSCCO thick films on silver at low field ($B_{rf} \lesssim 0.1$ G). Circles correspond to the 4336 samples; triangles correspond to the 2212 sample.

As a first step toward identifying ways to improve the rf properties of polycrystalline BSCCO, we acquired a highly textured bulk sample of $Bi_{1.6}Pb_{0.4}Sr_2Ca_2Cu_3O_y$ of dimensions 2 cm in diameter by 0.5 mm in thickness. The introduction of Pb into the BSCCO lattice results in zero dc resistance at temperatures near 110 K.[22] We measured the surface resistance of the sample as a function of temperature at 29.2 GHz in a TE cavity at low field. As is seen in

22. H.L. Luo and S.M. Green, this Proceedings.

Figure 7, the transition from the normal state to the superconducting state started at $T_c \approx 110$ K; it was broad by comparison with the transition of the thick film on silver. At temperatures $T \lesssim 77$ K, the surface resistance of the Pb-doped sample was lower than that of the undoped sample by a factor ~5.

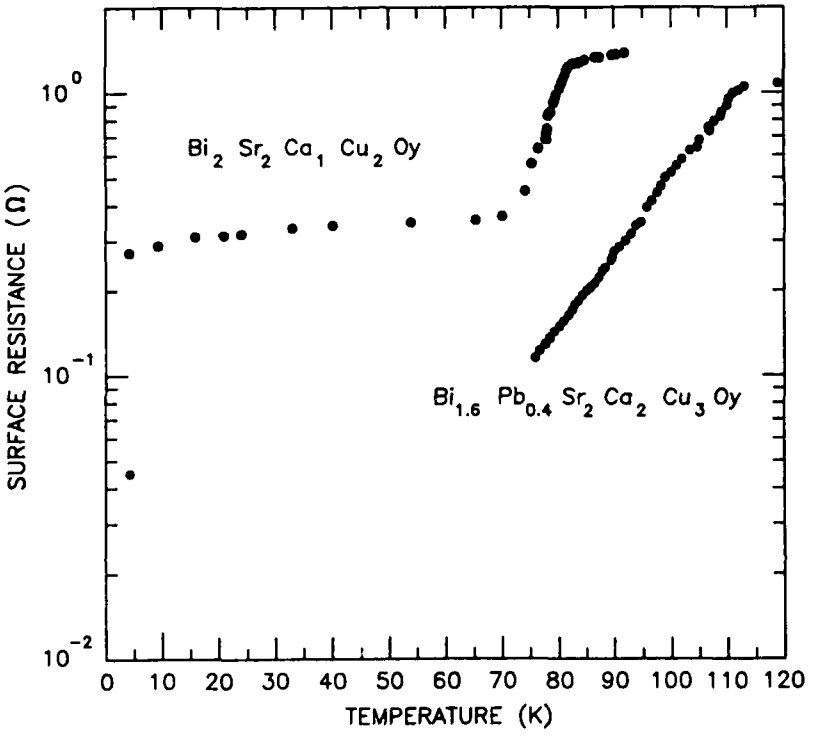

Figure 7. Comparison of rf surface resistance versus temperature at low field of bulk Pb-doped BSCCO versus BSCCO thick film on silver at 29.2 GHz.

4. DISCUSSION

Resonant superconducting cavities for high-power rf applications need to have low surface resistances while sustaining high peak fields on the cavity walls. For example, a resonant structure for accelerating charged particles will require surface resistances no higher than a few tens of micro-ohms at surface fields as high as a few hundred gauss and at frequencies in the range 200-1800 MHz. Our data on bulk YBCO (Figure 4) indicate that at low fields, sufficiently

low surface resistances are achieved, but at high fields (e.g., $\gtrsim$100 gauss) the surface resistance is too large by a factor of ~100. Our observation that the sample remains superconducting at high rf field is favorable, however.

The BSCCO thick films may also have surface resistances of interest at low fields. If they have a quadratic frequency dependence over a sufficiently wide range of frequencies, then, for example, their low-field, low-temperature surface resistance at 200 MHz would be ~40 μΩ. If the highly textured bulk sample of Pb-doped BSCCO also exhibits a quadratic frequency dependence, its projected surface resistance at low field and low temperature is ~2 μΩ at 200 MHz, a value comparable to that observed in the bulk YBCO sample.

Other investigators have also seen a pronounced rf-field dependence of R_s in polycrystalline high-T_c superconductors,[23] though it is uncertain whether single crystals exhibit this property. An attempt to find field-dependence in YBCO single crystals gave results which were nearly independent of field.[24] However, it seems that this data refers to upper bounds. Thus, although it is clear that the surface resistance of single crystals can be lower than polycrystals, the field dependence of the surface resistance of single crystals is still an open question.

The poor thermal conductivity of the ceramic oxides motivates the development of thin films on high-conductivity substrates. The minimum film thickness must be of the order of 1 μm, corresponding to a few rf penetration depths, in order to shield the substrate from the rf field. To coat complicated geometries, for example structures used

---

23. H. Padamsee, K. Green, J. Gruschus, J. Kirchgessner, D. Moffat, D.L. Rubin, J. Sears, Q.S. Shu, R. Buhrman, D. Lathrop, T.W. Noh, S. Russek, and A. Sievers, "Microwave Superconductivity for Particle Accelerators - How the High-T_c Superconductors Measure Up," in Proc. of the 2nd Annual Conf. on Superconductivity and Applications, Buffalo, NY, 18-20 April 1988.

24. D.L. Rubin, K. Green, J. Gruschus, J. Kirchgessner, D. Moffat, H. Padamsee, J. Sears, Q.S. Shu, L.F. Schneemeyer, and J.V. Waszczak, Phys. Rev. B, 38, 6538 (1988).

in ion accelerators,[25] a method that does not involve line-of-sight deposition may be needed, such as chemical vapor deposition. Accordingly, the next step toward practical high-power rf applications of these materials is the production of suitable thin films, first on large surface areas, and second on complicated shapes.

In view of the high-field properties of polycrystalline ceramics described here, it is necessary to measure the surface resistance versus field of thin films. Information from these measurements will aid those who fabricate the films in an iterative process to reduce the high-field surface resistance to useful levels. To initiate this process, we are now building a niobium cavity for high-field measurements at 850 MHz of flat samples with surface areas nominally 6.5 cm^2. In the meantime, until a method for producing films with adequate rf properties is found, niobium will continue to be the material of choice for the construction of high-power resonators.

We are grateful to Dr. Huey-Lin Luo of the University of California at San Diego for providing the Pb-doped BSCCO sample. This work was supported by the U.S. Department of Energy under contract W-31-109-ENG-38 and by the U.S. Army Strategic Defense Command.

25. J.R. Delayen, "Heavy-Ion Superconducting Linacs," in Proc. of the 1989 Particle Accelerator Conf., Chicago, Ill., 20-24 March, 1989.

THIS PAGE IS INTENTIONALLY BLANK

Presented at the Workshop on High Temperature Superconductivity
23-25 May 1989 GACIAC PR-89-02

SUPERCONDUCTING STRIPLINE RESONATORS AND HIGH-T_c MATERIALS*

D. E. Oates

Lincoln Laboratory, Massachusetts Institute of Technology
Lexington, Massachusetts 02173

ABSTRACT

The use of high-transition-temperature (T_c) superconducting resonators to stabilize oscillators operating between 1 and 10 GHz is discussed. Measurements of surface resistance are presented and related to resonator quality factor (Q). Projections of resonator Q and oscillator phase noise are discussed. Improved materials should offer greater than 20 dB reduction in noise over competing technology. The implications of flicker noise in reaching this level of performance are discussed, and preliminary measurements of flicker noise in the high-T_c materials are reported.

I. INTRODUCTION

The discovery of the high-T_c superconducting materials has stimulated interest in many applications, one of which is resonators for the stabilization of low-phase-noise oscillators which could be operated at liquid nitrogen temperatures (77 K). The ability of present day Doppler radar systems to detect small-cross-section targets in the presence of clutter is limited by the phase noise in the local oscillator. A reduction of 10 to 20 dB would increase the sensitivity a corresponding amount. Superconducting resonators hold the promise of providing such improvement because they are known to have high Q and high power-handling capability, both of which lead directly to lower phase noise. Qs of 10^6 for thin-film stripline resonators operating at 1 GHz and 10^5 at 10 GHz with a power handling capacity of nearly 1 W are achievable with niobium at liquid helium temperatures. Better performance than niobium is expected for the high-T_c materials at liquid nitrogen temperatures. Cavity resonators have demonstrated Qs higher than the stripline values, but because of the difficulties in fabricating the three-dimensional cavity structure, especially in the high-T_c oxide materials, the stripline structure is preferable for most applications. Stripline eliminates the radiation losses of microstrip and it has the advantage of planar fabrication techniques; the coupling and resonant frequency are determined photolithographically and the structure can be made compact and environmentally rugged.

*This work was supported by the Department of the Air Force and Army.

The resonator Q is determined by the radio-frequency (rf) surface resistance R_s of the superconducting material which, although low, is not identically zero as it is at dc.[1] At any ac frequency and finite temperature, resistive losses are present because the kinetic inductance of the superconducting electrons causes a coupling of the field to the normal electrons with their associated dissipation. Thus a superconducting material is characterized by a surface resistance that typically increases as frequency squared. This loss can become appreciable at microwave and millimeterwave frequencies and can severely limit the Q of a resonator. The measurements of the rf surface resistance which have been made to date show that R_s is very dependent on film fabrication. As discussed below, our estimates of resonator Q presently rely upon measured surface resistance. The best reported values of R_s are more than ten times better than copper at 1-10 GHz and 77 K and projections based on a simple two-fluid model indicate that there is still considerable room for improvement in R_s.

High input power is also required which translates into high critical current (J_c) values. Presently, in the high-T_c materials, both surface resistance and critical current are orders of magnitude better in thin films than in bulk ceramic materials, dictating the use of thin films to meet the low-phase-noise requirements. We thus concentrate on the properties of deposited thin film materials.

In the following we summarize the measurements of surface resistance and then show how R_s is used to calculate resonator Q. Detailed calculations of oscillator phase noise will be presented, including such factors as amplifier flicker noise and power-handling capability of the superconductor.

II. MEASUREMENTS OF R_s

The surface resistance of the oxide superconductors has been measured by our group at Lincoln Laboratory in $YBa_2Cu_3O_x$ (YBCO)[2] and more recently in $Bi_2Sr_2CaCu_2O_x$ (BSCCO). The measurements are made using the stripline resonator structure shown in Fig 1. The resonator comprises a length of transmission line one-half wavelength long at the fundamental frequency and two ground planes above and below the line. Overtone resonances occur at all multiples of the fundamental frequency. The resonator is capacitively coupled to the external circuit by gaps in the stripline. The structure is made from niobium deposited on sapphire substrates, but to evaluate R_s of a new film the niobium bottom ground plane is replaced with a film of the material to be tested. The dielectric properties of the substrate of the test film do not affect the resonator properties. When the R_s of the test film is large compared to that of the niobium, we can ignore the contribution of the niobium to the Q. The resonator Q is measured as a function of frequency between 0.5 and 18 GHz, and R_s versus frequency is extracted from the Q measurements as described in Section IV.

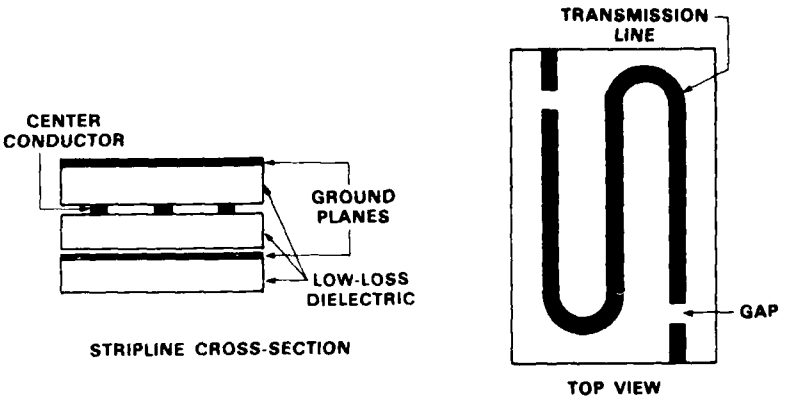

Fig. 1. Schematic view of the stripline resonator. On the left is a cross-section showing dielectrics and conductors. On the right is a top view of the center section showing the center conductor which has been patterned photolithographicaly. The gap shown determines the coupling to the resonant section of line.

Other measurements of R_s have been done, notably by groups at UCLA,[3] the University of Wuppertal,[4] and Rockwell.[5] Figure 2 shows a collection of measurements of R_s at various frequencies. The Lincoln Laboratory measurements on YBCO show a T_c of about 85 K but surface resistance a few orders of magnitude larger than that of the best reported films. The lowest values of surface resistance have been obtained by the Wuppertal group for oriented thin films of YBCuO deposited on $SrTiO_3$ by laser ablation. The reported R_s values measured at 77 K and 86 GHz are more than an order of magnitude lower than that of copper. Extrapolation to frequencies lower than 10 GHz implies an R_s more than 100 times better than copper. These best-yet values of R_s are used later in Section IV to estimate potential resonator Qs.

The use of the stripline resonator to measure R_s has several advantages over the more traditional cavity methods.[4] To measure the R_s of a test film in a cavity it is usual to replace one end face of a cylindrical cavity with the film under test. The Q is limited to that produced by the material which makes up the body of the cavity, usually copper or niobium. Thus it is difficult to measure R_s lower than that of the starting material of the cavity. In the stripline resonator method, however, it is possible to make the entire structure, ground planes and signal plane, from the high-T_c material under test so that the Q of the device is not limited by some other conductor. R_s values even lower than that of niobium, as are eventally expected for the high-T_c films, can thereby be measured.

materials as a function of ac magnetic field has not yet been measured, so stripline techniques can provide unique information. Thus stripline resonator measurements yield R_s with high sensitivity and can be used to give R_s as a function of frequency, temperature, and ac magnetic field.

III. DIELECTRIC MATERIAL CONSIDERATIONS

In addition to low-rf-loss thin films, low-dielectric-loss substrates compatible with the thin-film-deposition process must also be employed. The Q of a resonator results from several contributions. Thus,

$$Q_L^{-1} = Q_{ex}^{-1} + Q_C^{-1} + Q_D^{-1} \tag{1}$$

where Q_L is the loaded Q, Q_{ex} represents the loading of the resonator and can be adjusted by varying the coupling to the external circuit, Q_C reflects the conductor loss and is inversely proportional to the rf surface resistance of the conductors, andQ_D results from losses in the dielectric and is related to the loss tangent (tan δ) by

$$Q_D = 1/\tan\delta. \tag{2}$$

As can be seen from expressions (1) and (2), tan δ lower than 2×10^{-6} is necessary to achieve Qs larger than 500,000.

The stripline resonator structure shown in Fig. 1 can also be used to measure loss tangents at 4.2 K by replacing the sapphire top ground plane with one of the materials to be tested on which a niobium film has been deposited. Measurements of the dielectric loss at 4.2 K of single crystals of MgO have been performed in our laboratory and imply a tan δ of better than 1.2×10^{-6} at 500 MHz and 4.2 K. Also, our preliminary measurements on $LaGaO_3$ show a tan δ of 2×10^{-6} at 500 MHz and 4.2 K. These values are adequate for high-Q resonators at 4.2 K and we are investigating tan δ at higher temperatures.

IV. PREDICTIONS OF PHASE NOISE

In this section we analyze an oscillator stabilized by a stripline resonator. To calculate the phase noise of such an oscillator, we must estimate the Q expected for the stripline structure and the maximum oscillator power which the resonator can support. As will be shown, high values of both are desired for low phase noise. The

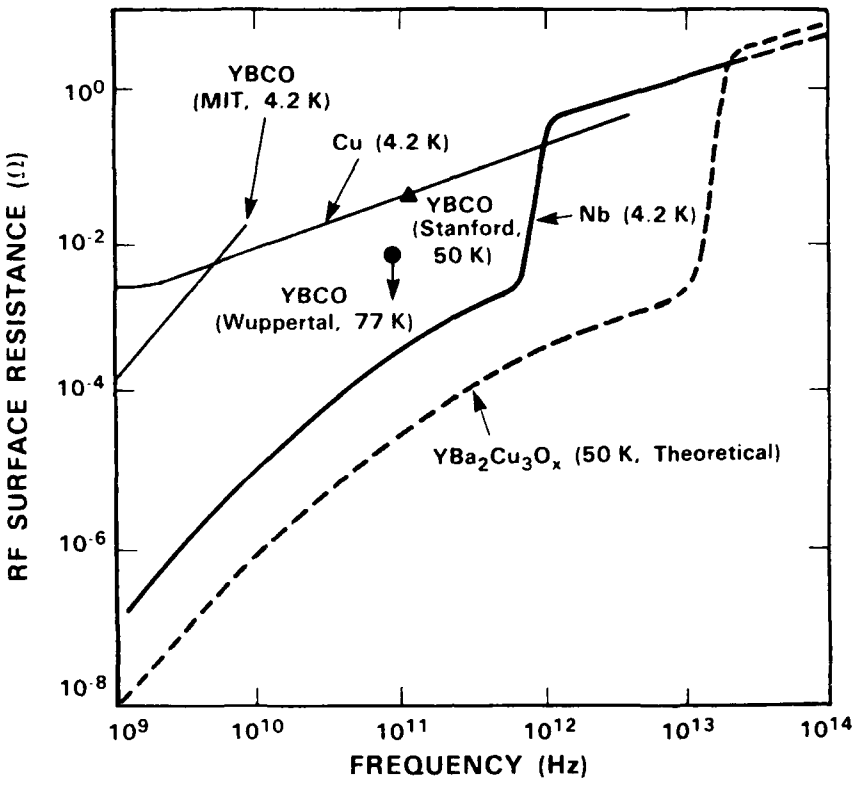

Fig. 2. Measurements of RF surface resistance R_s vs frequency. Various measurements are shown. Also shown are calculations for copper, and for niobium at 4.2 K and the result of two-fluid-model estimate for $YBa_2Cu_3O_{7-X}$ at 50 K.

Although measuring the frequency dependence of R_s using a stripline resonator is simple, obtaining the frequency dependence using a cavity is very difficult and time-consuming because a separate cavity is needed for each frequency. Measurement of R_s as a function of temperature is also possible with a stripline resonator made entirely of high-T_c material. These temperature-dependent measurements can be done at the maximum sensitivity. Temperature dependence using the cavity technique can only be done with a copper cavity which lowers the sensitivity.

Because the power density in a stripline resonator is high, measurements of R_s as a function of ac magnetic field at high fields are possible. As we discuss in Sec. IV, the current in the center conductor can easily exceed the critical current density for modest input powers. For example an input power of only -20 dBm will produce a current density of 10^7 A/cm^2 in a 50 -Ω characteristic impedance stripline center conductor on a 0.5-mm-thick dielectric of $\varepsilon = 10$ when the $Q = 10^6$. This current density produces a magnetic field of 1000 gauss at the surface of the superconductor, a field large enough to be practical interest yet difficult to produce in a cavity. R_s in the high-T_c

detailed method for calculation of Q and maximum power will be published elsewhere[6] and we just quote the results here. The attenuation constant α_c for our stripline geometry is given by

$$\alpha_c = 6.87\ R_s.$$

We have chosen the width of the stripline as 6 mm, the dielectric thickness as 2 mm, and the dielectric constant as 9.65.

We can then relate Q_c to α by

$$Q_c = \frac{\pi}{\alpha_c \lambda} \tag{3}$$

where λ is the wavelength in the resonator.

The high Qs and high input power necessary for low phase noise in the oscillators translate into very high current densities for the conductors. The maximum power is that power for which the critical current density J_c is not exceeded. To calculate the maximum allowable power incident on the resonator, we consider the currents flowing at resonance and derive the result,

$$P_c = \frac{n\pi Z_o I_{max}^2}{8 r_v (1 - r_v) Q}$$

where Z_o is the characteristic impedance of the stripline, I_{max} is the critical current, r_v is the voltage insertion ratio, and Q is the unloaded Q. (The insertion loss IL is given by IL = -20 log r_v.)

To calculate the Q, we assume $R_s = 2.7 \times 10^{-5}\ \Omega$ at 5 GHz and 77 K. This value of R_s is obtained by extrapolating the results from the Wuppertal measurements of oriented YBCO deposited on $SrTiO_3$, done at 87 GHz, to lower frequencies by assuming that R_s is proportional to f^2, which is expected on theoretical grounds and has been observed for most measurements of the high-T_c films. To calculate P, we assume a critical current density of 5×10^6 A/cm^2 at 77 K. Values of critical current density of approximately this magnitude have been reported by several groups. For these values, and assuming an insertion loss of 15 dB, we obtain an unloaded Q of 7.3×10^5 at 5 GHz and a maximum input power of 0.83 W.

From the standard Leeson model of the phase noise of a feedback oscillator,[7] the single-sideband noise is given by

$$L(f) = 10\log\left[N^2\left(1+\frac{f_o^2}{4Q^2f^2}\right)\bullet\left(\frac{\alpha_f}{2\pi f}+\frac{GFkT}{P_c}\right)\right]$$

where L(f) is in dBc/Hz, P_c is the oscillator power, G the loop gain, F the amplifier noise figure, f the offset frequency in Hz, Q the resonator quality factor, f_o the oscillator frequency, α_f the flicker-noise constant which must be empirically determined from the 1/f measurements, T the absolute temperature, k is Boltzmann's constant and N the frequency-multiplication factor.

The flicker (1/f) noise can originate in either the amplifier or the resonator or both. Since the flicker noise is not well understood theoretically, it must be empirically determined. We can make reasonable estimates for the amplifier, but for the resonator we must rely on experimentally determined values. Our projections of phase noise that follow assume that the contribution of the resonator to the flicker noise is small compared to the amplifier contribution, but the total phase noise at offsets of less than about 5 kHz is dominated by the flicker noise. If the flicker noise contribution of the superconducting resonator is larger than that of the amplifier, then the actual phase noise will be greater than the following predictions. The importance of the resonator flicker noise has led us to undertake the measurements described in Sec. V.

Figure 3 shows the projected phase noise at 10 GHz for a superconducting-resonator-stabilized oscillator operating at 5 GHz, frequency-doubled to obtain 10 GHz. The parameters are Q of 7.3×10^5, G of 18 dB, F of 3 dB, P_c of +27 dBm (0.5 W), and α_f of 4×10^{-12}. This value of α_f is that normally assumed for a GaAs FET amplifier. The parameter values chosen for these curves are the best currently available but should not be considered final because improvements in R_s would result in higher Qs. We have, for instance, assumed room-temperature operation for the amplifier, but when the amplifier is operated at the cryogenic temperatures, noise performance would be improved. Also shown in Fig. 4 are the phase-noise curves for SAW oscillators[8] and for quartz crystal oscillators.[9] Clearly the superconducting oscillator provides better performance than other technologies.

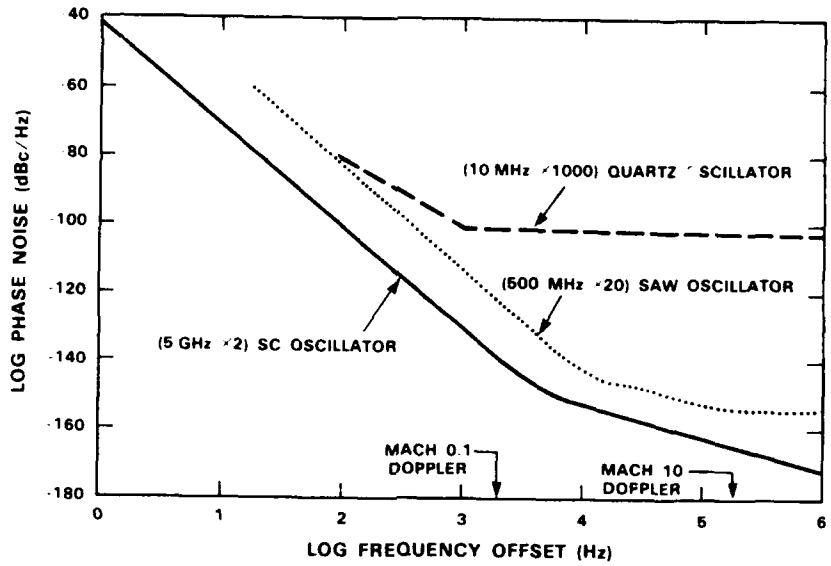

Fig. 3. Projected value of the single-sideband phase noise at 10 GHz for an oscillator stabilized with a superconducting resonator. See text for the detailed parameters of the oscillator. Also shown are the phase noise for the best SAW oscillator and a production quartz crystal oscillator.

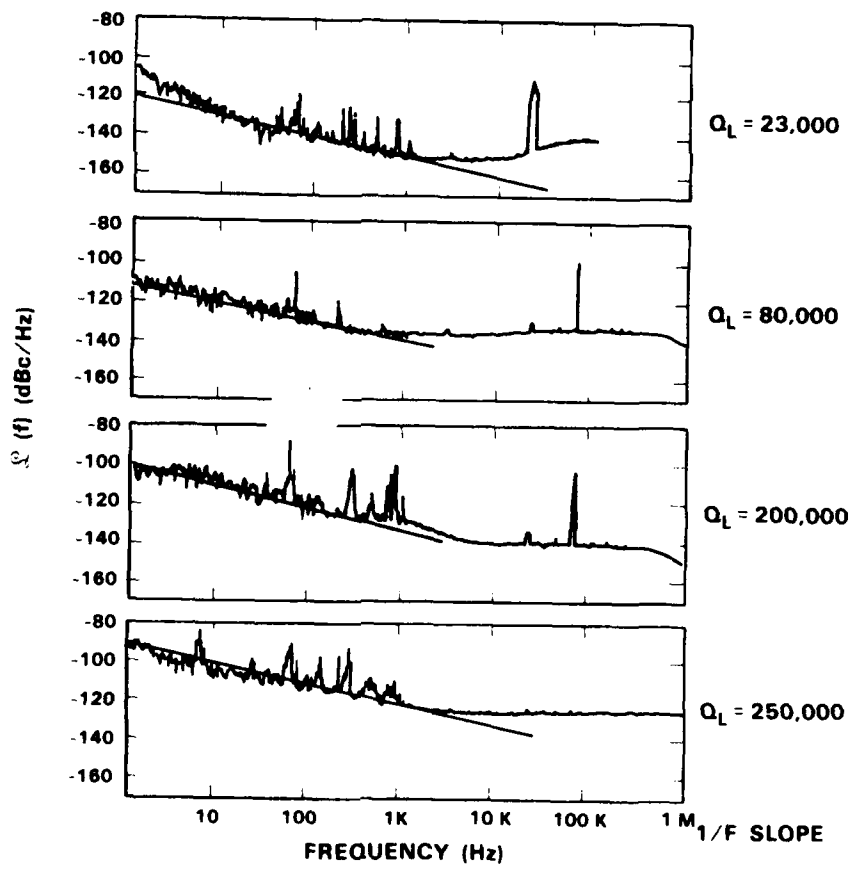

Fig. 4. Set of four residual-noise measurements in Nb resonators with the indicated values of Q_L, the loaded Q. Plotted is L(f), the single sideband phase noise, versus offset frequency from the carrier. The noise follows the expected 1/f frequency dependence. The straight lines indicate a 1/f dependence.

V. RESIDUAL NOISE MEASUREMENTS

Because of the importance of 1/f noise and because no measurements are known to us, we have made a series of measurements using the stripline structure shown in Fig. 1. The substrates for these devices are silicon (p-type, 30 Ω-cm) and the conductors are deposited niobium. The gap in the stripline determines the coupling of the resonator to the external circuit and thus affects Q_L, the loaded Q, which can be varied by changing the size of the gap in the line. The fundamental resonant frequency of these devices is 1.1 GHz. The gap size has been varied from 150 μm to 500 μm. This range of gap sizes gives a Q_L which varies from 23,000 to 300,000. The largest Q_L is very close to the intrinsic Q for the niobium-on-silicon resonators. Table 1 summarizes the devices used in the measurements.

Table 1

Gap μm	Q_L	L(f=Hz) dBc/Hz
150	23,000	-120
300	80,000	-110
400	200,000	-100
500	250,000	- 95

Measurements of the residual noise are shown in Fig. 4. Plotted is the single-sideband phase noise L(f) in dBc/Hz as a function of the offset frequency from the carrier for each of the devices measured. The data exhibits the expected behavior for a resonator, namely, a flat region dominated by the system noise floor at large offset frequencies joined to region of 1/f slope at small offset frequencies extending to less than 1 Hz. As can be seen from the data, the noise increases with increasing Q_L. The 1/f noise is often characterized by the value of the noise at 1-Hz offset from the carrier. This parameter, L(f = 1 Hz), is shown in Table 1.

A useful model of 1/f noise in acoustic resonators has been developed[10] which assumes that the source of the 1/f noise is fluctuations of the center frequency of the resonator which have a 1/f frequency distribution. Since the slope of $\phi(f)$, the transmitted phase, is proportional to Q_L, the same amplitude center-frequency fluctuation should produce higher phase noise as Q_L is increased. Since L(f) is a measure of the power in the fluctuation, the 1/f noise should increase as the square of Q_L according to this model. The result agrees well with our data. The measured 1/f noise of these niobium resonators at 1-Hz offset from the carrier is larger than the measured values for good quality surface-acoustic-wave resonators which have a value of -130 dBc/Hz at 1-Hz offset.[11] The measured

values are large enough to limit the performance of oscillators stabilized with these resonators. Sources of the 1/f noise, such as temperature fluctuations, vibration sensitivity, and conduction processes in the film, are being investigated.

We have also measured the 1/f noise of the resonators containing a high-T_c film as the lower ground plane. Figure 5 shows a typical example of the results obtained with a BSCCO film fabricated at Lincoln Laboratory[12] by means of sequential e-beam evaporation of the constituents on a MgO substrate. The film was annealed at 870° C in O_2 following evaporation. The BSCCO served as the lower ground plane in an otherwise all-niobium resonator. The resonator had a $Q_L = 10^4$ and was measured at the fundamental frequency of 550 MHz. The 1-Hz intercept, L(f=1 Hz) is -90 dBc. These are typical results for the high-T_c ground planes that we have measured. All films show a 1/f noise which is significantly higher than that of niobium. The origin of the 1/f noise is not well understood and may be related to the quality of the films which we have tested. We will soon measure the 1/f noise in films deposited in a manner which is known to produce lower values of R_s and we expect that the noise properties will improve.

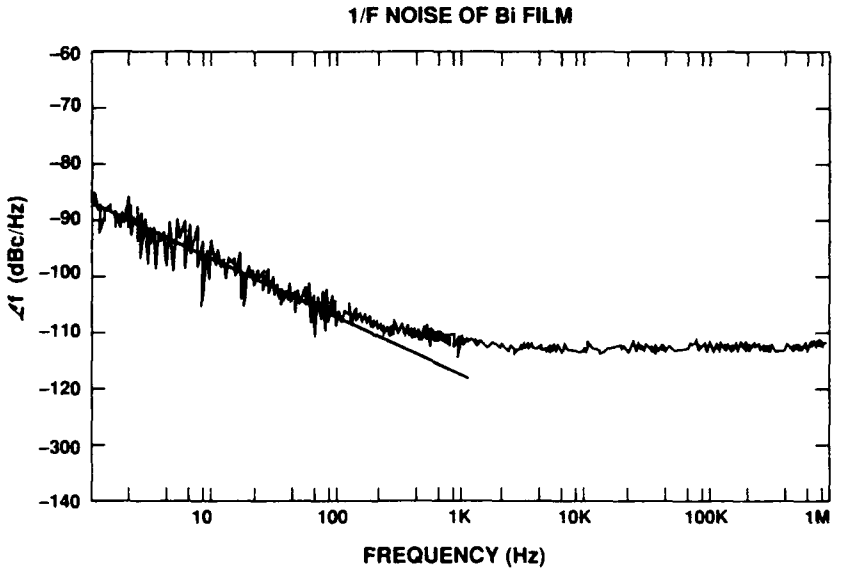

Fig. 5. Typical results of 1/f noise measurements using a resonator with one ground plane of the high-T_c material.

VI. CONCLUSIONS

High-T_c materials have now advanced sufficiently that the best reported T_c, R_s and J_c indicate that high-Q microwave frequency resonators operating at 77 K can be envisioned. Projected phase-noise performance is very

good, bettering the competing technologies by a significant amount. However, the currently measured values of flicker noise are too high to reach the level of performance consistent with the other parameters. We believe that as the high-T_c superconducting film quality increases, the 1/f noise will decrease, but this parameter remains a major obstacle to application of these materials as resonators for oscillator stabilization. Additionally, further progress must be made in producing films reliably with low R_s over large areas on substrates with low tan δ.

ACKNOWLEDGMENTS

We thank B. T. Chai of Allied Signal for samples of $LaGaO_3$ for us to evaluate, and J. Steinbeck of RADC for discussions and films of BSCCO to evaluate. We thank R. P. Konieczka for assembling the resonators and A. J. Kelley for photolithography. We also thank R. W. Ralston and R. S. Withers for support and technical guidance.

REFERENCES

(1) T. Van Duzer and C. W. Turner, Principles of Superconductive Devices and Circuits, New York: Elsevier North Holland, 1981.

(2) M. S. DiIorio, Alfredo C. Anderson and B.-Y. Tsaur, "RF Surface Resistance of YBaCuO Thin Films," Phys. Rev. B, vol. 38, pp. 7019-7022, 1988.

(3) J. P. Carini, A. M. Awasthi, W. Beyermann, G. Gruener, T.Hylon, K. Char, M. R. Beasley and A. Kapitulnik, "Millimeter-Wave Surface Resistance Measurements in Highly Oriented $YBa_2Cu_3O_{7-X}$ Thin Films," Phys, Rev. B, vol. 37, pp. 9726-9729, 1988.

(4) N. Klein, G. Mueller, H. Piel, B. Roas, L. Schultz,U. Klein and M. Peiniger, "Millimeterwave Surface Resistance of Epitaxially Grown $YBa_2Cu_3O_{7-X}$ Thin Films," Appl. Phys. Lett., vol. 54, pp. 757-759.

(5) W. Ho, P. J. Hood, W. F. Hall, P. Kobrin, A. B. Harker, and R. E. DeWames, "Millimeter-Wave ComplexConductivity Measurements of Bi-Ca-Sr-Cu-O Superconducting Thin Films," Phys. Rev. B, vol. 38, pp. 7029-7032, 1988.

(6) D. E. Oates and A. C. Anderson, "Superconducting Stripline Resonators and High-T_c Materials," IEEE Transactions on MTT, to be published.

(7) D. B. Leeson, "A Simple Model of Feedback Oscillator Noise Spectrum," Proc. IEEE, vol. 54, pp. 329-330, 1966.

(8) G. K. Montress, T. E. Parker and M. J. Loboda, "Extremely Low Phase Noise SAW Resonator Oscillator Design and Performance," 1987 Ultrasonics Symposium Proceedings, pp. 47-52, 1987.

(9) E. A. Gerber, T. Lukaszek and A. Ballato, "Advances in Microwave Acoustic Frequency Sources," IEEE Trans. Microwave Theory Tech., vol. MTT-34, pp. 1002-1016, 1986.

(10) T. E. Parker, "Characteristics and Sources of Phase Noise in Stable Oscillators," Proceedings of the 41stAnnual Symposium on Frequency Control, pp. 99-110, 1987.

(11) M. J. Laboda, T. E. Parker, J. A. Greer and G. K. Montress, "Reduction of Close-to-Carrier Phase Noise in Surface Acoustic Wave Resonators," 1987 Ultrasonics Symposium Proceedings, pp. 43-46, 1987.

(12) J. Steinbeck, B-Y. Tsaur, A. C. Anderson, andA. J. Strauss, "Preparation of Superconducting Bi-Sr-Ca-Cu-O Thin Films by Sequential Electron Beam Evaporation and Oxygen Annealing," Appl. Phys. Lett., vol. 54, pp. 466-468, 1989.

Presented at the Workshop on High Temperature Superconductivity
23-25 May 1989 GACIAC PR-89-02

High Transport Current and Increased Critical Temperature in Bi-Sr-Ca-Cu-O Oxide System

Kumiko Imai and Hironori Matsuba
Yokohama R&D Laboratories The Furukawa Electric Co.,Ltd.
2-4-3,Okano,Nishi-ku,Yokohama,Japan-220

1. Introduction

The various superconducting phase in the Bi-Sr-Ca-Cu-O oxide system have been reported.[1] Much research has been conducted to obtain high critical temperature,Tc, single phase with a transition temperature of 110K, of which the nominal composition is $Bi_2Sr_2Ca_2Cu_3O_{10+y}$ (referred to as the 2223 phase).
It has been reported that the most of the high Tc single phase has been obtained by substituting of Pb, though more than hundreds of hours and a physical process are necessary.[2-4] The low Tc $Bi_2Sr_2CaCu_2O_x$ phase (referred to as the 2212 phase) with a transition temperature of 85k can be obtained with a shorter sintering time and with a simple process compared to the high Tc phase. It has been reported that Tc of the 2212 phase is changed sensibly by the processing conditions, and the maximum 'zero' resistivity critical temperature of the 2212 phase reached 85K.[5-6]

We found a method to obtain superconductors composed mostly of the 2212 phase with a higher Tc of 95K and with excellent critical current Jc, and consequently, found that the critical temperature varies with annealing conditions. In this report, the dependence of Tc on annealing conditions and the electric behaviors of these samples are described.

2. Control of Critical Temperature

Preparation of Samples

Bulk samples were prepared by sintering for 15 hours. The molecular ratio of material powder was Bi:Sr:Ca:Cu=2:2:1:2. which is the same proportion as that of the low Tc phase.[7-9] The size of samples was about 3mm X 1mm X 20mm, and the average of the specific gravity was 6.[illegible]g/cm^3. The X-ray powder diffraction measurement revealed that the samples were mainly structured with the low Tc phase,[10] and some other impurities were included. These samples were structured with thin layered grains as shown in Fig.1. The samples showed 'zero' resistivity at 95K with an 1 mA current.

Experiments and the Results

The samples were annealed in an oxygen atmosphere at various temperatures for about fifteen hours. Then the transition temperatures of the magnetic susceptability were measurerd. The transitions are shown in Fig. 2. Table 1 shows the annealing conditions of the samples and the corresponding transition temperatures of magnetic susceptibility. The shorter the anealing time was, or, the lower the anealing temperature, the more broad the transition became. Annealing at 400° C gave the lowest critical temperature of 80K. X-ray powder diffraction measurements of these treated samples showed the same 2212 structure pattern as that of the untreated (original) sample, implying that no significant structural change occured by the treatment. Oxygen contents of the annealed samples were determined being extrapolated by charge valences measured by chemical titration[11]. Oxygen ratio of nominal composition $Bi_2Sr_2CaCu_2O_x$ versus the transition temperature are shown in Fig.3. The increase in oxygen was very small, and even by treatment at 400° C, it amounts to only about 0.03 molecular ratio in the formula of $Bi_2Sr_2Ca_1Cu_2O_{8+x}$. When the samples were annealed in an nitrogen atomsphere at 400° C, critical temperature Tc remained unchanged, implying that small excess contents of oxygen in the samples exert a great influence on Tc. Furthermore, when the samples were annealed sequentially for a longer time or at a different temperature, the transition temperature of magnetic susceptability was only decided by the final annealing condition. The fact demonstrates that any other atoms, such as bismuth, except oxygen are not lost through the annealing process.

Discussion

It was confirmed from our experimental results that Tc decreases with the increase in oxygen contents. This result agrees with the results in other research that Tc of bismuth oxide superconductors are sensitive to heat treatment.[12,13] It has been reported that Bi-O binding energy or oxidation state in bismuth depends on oxygen content, and that no detectable change of the oxidation state in copper was observed due to oxygen contents.[8,12] The excess oxygen atoms have been thought to intercalate in Bi-O layers. Hole contents in the Bi-O layer are changed either by the deficiency at the bismuth site or by the contents of oxygen. We would suggest that the critical temperature in the bismuth oxide system depends on the contents of oxygen rather than on a deficiency at the bismuth site.

3. Current-voltage (I-V) curve mesurements

Method of measurement

Samples of BSCCO having different critical temperatures were prepared and

the dimensions of the samples were about 0.1 x 0.2 x 2 cm^3. I-V properties were measured by the four probe method. Because of a big measuring current reaching 100A, pulsive current was used to avoid errors due to the heat generation at the current terminals. The system diagram of the measurement is shown in Fig.4. An example of the pulse wave and the resultant voltage curve are shown in Fig.5. The generated peak voltage between the two current electrodes was from 0.2 to 0.3 volt when the peak current was 100A. This implies that the resulting temperature rise in the superconductor close to the current electrodes is estimated at 20K, however, the measuring time is so short that the measurement is terminated before the temperature rise propagates to the voltage electrodes. In these measurements, the temperature rise due to the resistivity of the superconductors is negligible, because it is, at a maximum estimate, 0.01K. To ascertain the estimates, durations of the pulse currents, whose pulse heights were 100A, were varied from 30msec to 160ms. The same I-V curves were given when measuring the different pulse durations. It was also confirmed that the voltage curves during the period of current increase were just the same as those during the succeeding period of decrease.

Results and discussion

Fig.6 (a)-(d) shows the current-voltage curves. The I-V curves fit power-laws at all temperatures and in all the different samples. This suggests that the power-law is intrinsic property of these superconductors. By a relaxation measurement of the permanent current around a superconducting ring[14], we showed that the power-law can be extended to lower voltages of less than 1 micro volt. Therefore, we imagine that these superconductors do not have 'zero' resistivity at any small current. The dissipation behavior of single cristals in high-temperature superconductors is described by a thermally activated flux motion.[15,16] Palstra et al[15] obtained a universal function which describes the resistivity of $Bi_{2.2}Sr_2Ca_{0.8}Cu_2O_{8+X}$ as a function of temperature T and of magnetic field H:

$$\rho(T,H,\phi) = \rho_0 \exp[-U_0(H,\phi)/T],$$

where activation energy U_0 is between 300k and 3000K for the magnetic field between 0.1T and 12T in two orientation. The resistivity behavior of our polycrystalline $Bi_2Sr_2Ca_1Cu_2O_{8+X}$ is shown in Fig.7 for which data are extracted from Fig.6 (c), where BSCCO has the same critical temperature as that of the single crystal described above. We have an experimental result showing that the resistivity of BSCCO at 0.01T behaved in the same way as that at 0T. Then, the polycristalline BSCCO has less resistivity than that of a single crystal in a magnetic field of 0.01T oriented perpendicularly to the basal plane. Activation energy,U_0 of the polycrystalline BSCCO is 7110K and this activation energy is larger than that of the single crystal. The differences suggest

that the dissipation behavior of the polycrystalline BSCCO is controlled by grain boundaries and this implies that the grain boundary gives a stronger pinning site.

The I-V characteristics of an array of Josephson junctions exibit power-law behavior.[17-19] Power-law behaviors were found in polycrystalline YBCO and ErBCO superconductors[20,21]. Dubson[21] et al ascribe the behavior to the disorder in the intergrain coupling because the behavior was observed at temperatures very close to the critical temperature. England[20] et al found $V \propto (I-I_C)^x$ in the scaling behavior and describes the behavior as a coherence transition in which isolated grains 3-dimensionally couple to form a bulk superconductor.

We obtained a simple power-law $V \propto I^x$ as shown in Fig.6. The dependence of current-voltage exponent x on temperature is shown in Fig.8. The dependence well resembles the experimental results of the Josephson junction square array made by the ion beam sputtering technique[18]. We think that the resemblance implies that the polycrystalline BSCCO couples 2-dimensionally. The explanation is strengthened by the fact that the polycrystalline BSCCO is structured with thin layered grains, as shown in Fig.1.

The dependence of the critical current of high temperature superconductors on temperature has been investigated theoretically[22-23] and experimentally[24-28]. Extracting data from Fig.6, the temperature dependence of the critical current density of the polycrystalline BSCCO is plotted in Fig.9. The dependence fits a power-law $Jc \propto (1-T/Tc)^b$ with $b \approx 2$ at temperatures near Tc. Setsune et al[26] obtained a power-law with $b \approx 2$ in BSCCO thin films and they attribute the behavior to the presence of layered structures in their film. Deutscher et al[22] predict that near Tc, $Jc \propto (1-T/Tc)^2$ which is induced by supposing the existence of a Josephson junction. Even though experiments over a wider range of temperatures are required to clearly describe the temperature dependence, this result again strengthens the description that dissipation behavior of the polycrystalline bulk BSCCO superconductors is controlled by a 2-dimensionally coupled Josephson junction existing between the layers.

4. Conclusion

We have found a sintering method to increase the critical temperature of bulk BSCCO superconductors up to 95K and to give excellent critical current density above 1000 A/cm^2 at 77K. The critical temperature strongly depended on the oxygen contents in the superconductors.

We have found that I-V characteristics of the bulk BSCCO superconductors follows a power-law over a wide range of temperature, implying that the dissipation behavior of the bulk BSCCO is determined by Josephson junctions existing between layered grain baundaries.

References

[1] H.Maeda, Y.Tanaka, M.Fukutomi and T.Asano, Jpn.J.Appl.Phys.27 L209 (1988)

[2] M.Takano, J.Takada, K.Oda, H.Kitaguchi, Y.miura, Y.Ikeda, Y.Tomii and H.Mazaki, Jpn.J.Appl.Phys. 27 L1041 (1988)

[3] N.Murayama, E.Sudo, M.Awano, K.kani and Y.Torii, Jpn.J.Appl.Phys. 27 L1856 (1988)

[4] T.Ishida, H.Mazaki and T.Sakuma, Jpn.J.Appl.Phys. 27 L1626 (1988)

[5] M.Kawasaki, S.Nagata, K.Takeuchi, H.Koinuma, Jpn.J.Appl.Phys. 27 L2227 (1988)

[6] M.S. Hybertsen and L.F.Mattheiiss, Phys.Rev.Lett. 60 1661 (1988)

[7] F.Herman, R.V.Kasowaski, W.Y.Hsu, Phys.Rev. B 38 204 (1988)

[8] J.M.Tarascon, W.R.McKinnon, P.Barboux, B.G.Bagley, L.H.Greene, G.W.Hull, Y.LePage, N.Stoffiel and M.Giroud, Phys.Rev. B 38 8885 (1988)

[9] S.A.Sunshine, T.Siegist, L.F.Schneemeyer et al. Phys. Rev. B 38 893 (1988)

[10] M.Onoda, A.Yamamoto, E.Takayama-Muromachi and S.Takekawa, Jpn.J.Appl.Phys. 27 L833 (1988)

[11] K.Kurusu and H.Takami submitted The Analyst

[12] P.A.P.Lindberg, P.Soukiassian, Z.-X.Shen, S.I.Shah, C.B.Eom, I.Lindau, W.e.Spicer and T.H.Geballe, Apple.Phys.Lett. 53 1970 (1989)

[13] D.E.Morris, C.T.Hultgren, A.M. Markelz, J.Y.T.Wei, N.G. Asmar and J.H.Nickel, distributed in SC gloval'89

[14] H.Matsuba,A.Yahara,and K.Imai Electrochemical Soc. HTTcST2 704 HTS, 1989

[15] T.T.M.Palstra,B.Batlogg,L.F.Schneemeyer, and J.V.Waszczak, Phys. Rev. Lett. 61 1662 (1988)

[16] Y.Yeshurun and A.P.Malozemoff, Phys. Rev. Lett. 60,2202 (1988)

[17] B.J.van Wees, H.S.J.van der Zant and J.E.Mooij, Phys.Rev.B 35 7291 (1987)

[18] J.P.Carini, Phys. Rev. B 38 63 (1988)

[19] K.K.Mon and S.Teitel, Phys. Rev. Lett. 62 673 (1989)

[20] P.England, T.Venkatesan, X.D.Wu, and A.Inam, Phys.Rev.Lett. 38 7125 (1988)

[21] M.A.Dubson,S.T.Herbert,J.J.Calabrese,D.C.Harris,B.R.Patto,and J.C.Garland, Phys. Rev. Lett. 60 1061 (1988)

[22] G.Deutscher and K.A.Mueller, Phys. Rev. Lett. 59,1745 (1987)

[23] J.R.Clem,B.Bumble,S.I.Raider,W.J.Gallagher, and Y.C.Shih, Phys. Rev. B 35 6637 (1987)

[24] J.W.C.de Vries, M.A.M.Gijs, G.M.Stollman,T.S.Baller,and G.N.van Veen, J.Appl.Phys.64,426 (1988)

[25] L.H.Allen,P.R.Broussard,J.H.Claassen,and S.A.Wolf, Appl.Phys.Lett. 53,1338 (1988)

[26] J.Aponte,H.C.Abache,A.Sa-Neto,and M.Octavio, Phys. Rev. B 39, 2233 (1989)

[27] K.Setsune,K.Hirochi,H.Adachi,Y.Ichikawa,and K.Wasa, Appl.Phys. Lett. 53, 600 (1988)

[28] S.B.Ogale,D.Dijkkamp,and T.Venkatesan, Phys. Rev. B 36, 7210 (1987)

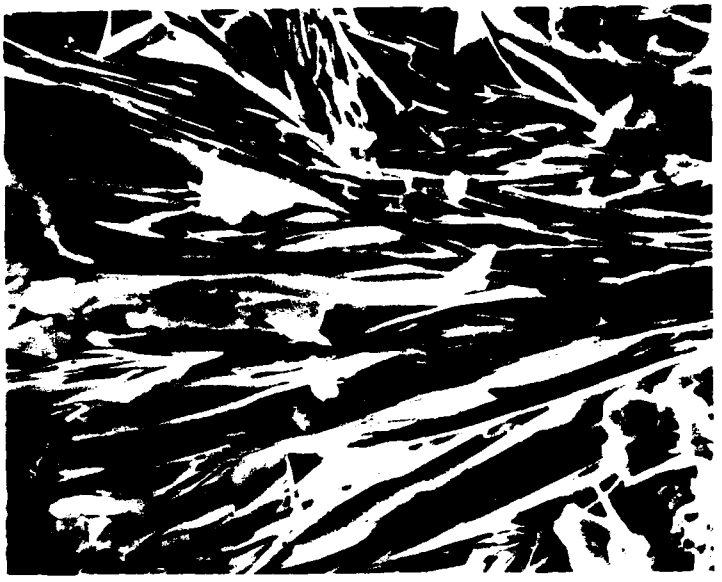

Fig.1 SEM photograph of the fractured surface of the sintered $Bi_2Sr_2Ca_1Cu_2O_{8+x}$ sample with A critical temperature of 95K and with a critical current of 1000 A/cm^2

Table 1 Annealing conditions of the original samples and the resultant critical temperatures, Tcm. The critical temperatures were determined by the midpoints of transitions of magnetic susceptability

Tcm (K)	Annealing condition
94	880°C x 15 hours
89	600°C x 15 hours
85	500°C x 15 hours
80	500°C x 15 hours + 400°C x 15 hours

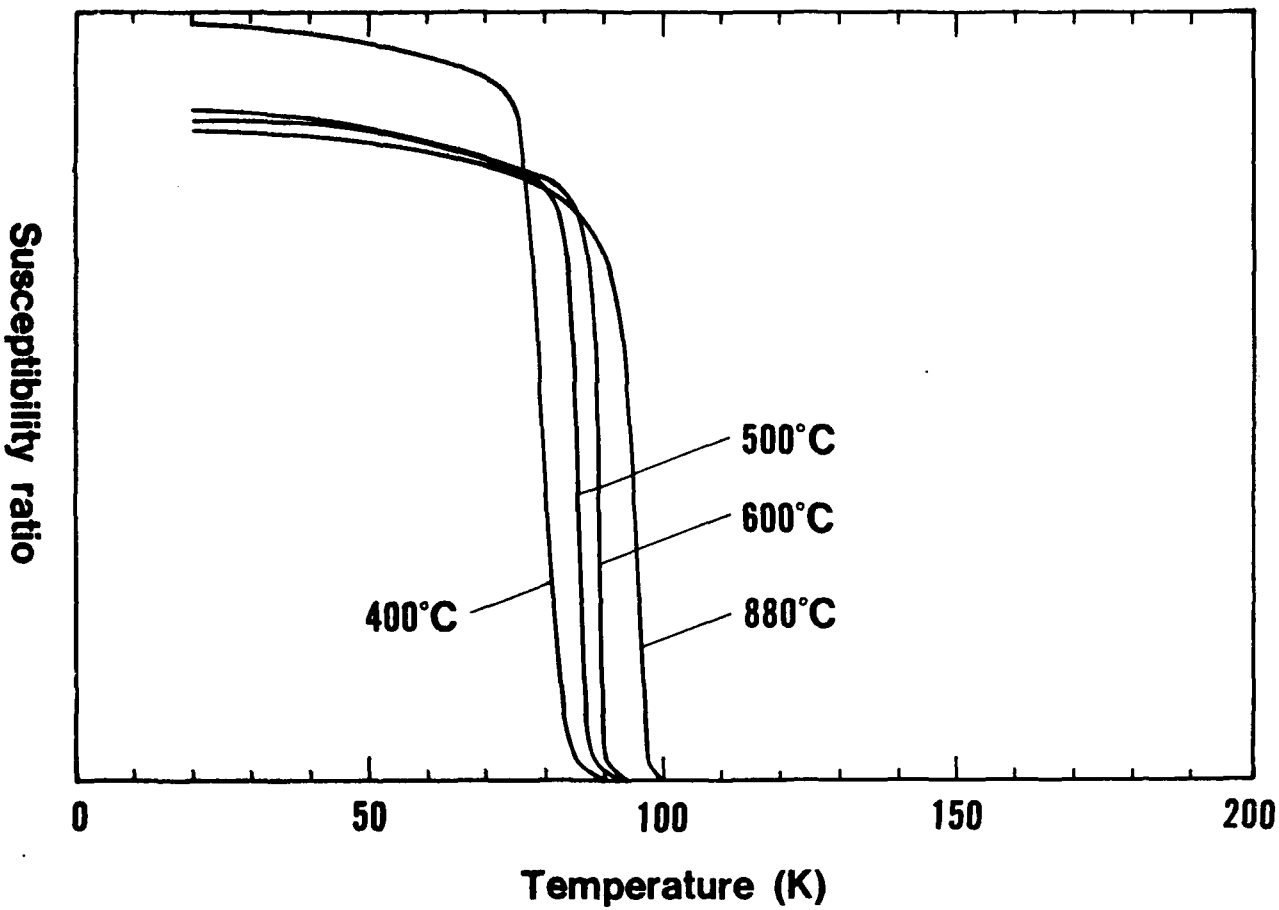

Fig.2 Temperature dependence of susceptibilities of the polycrystalline $Bi_2Sr_2Ca_1Cu_2O_{8+x}$ samples annealed with various temperatures. Numbers pointing curves indicate the annealing temperatures of the samples.

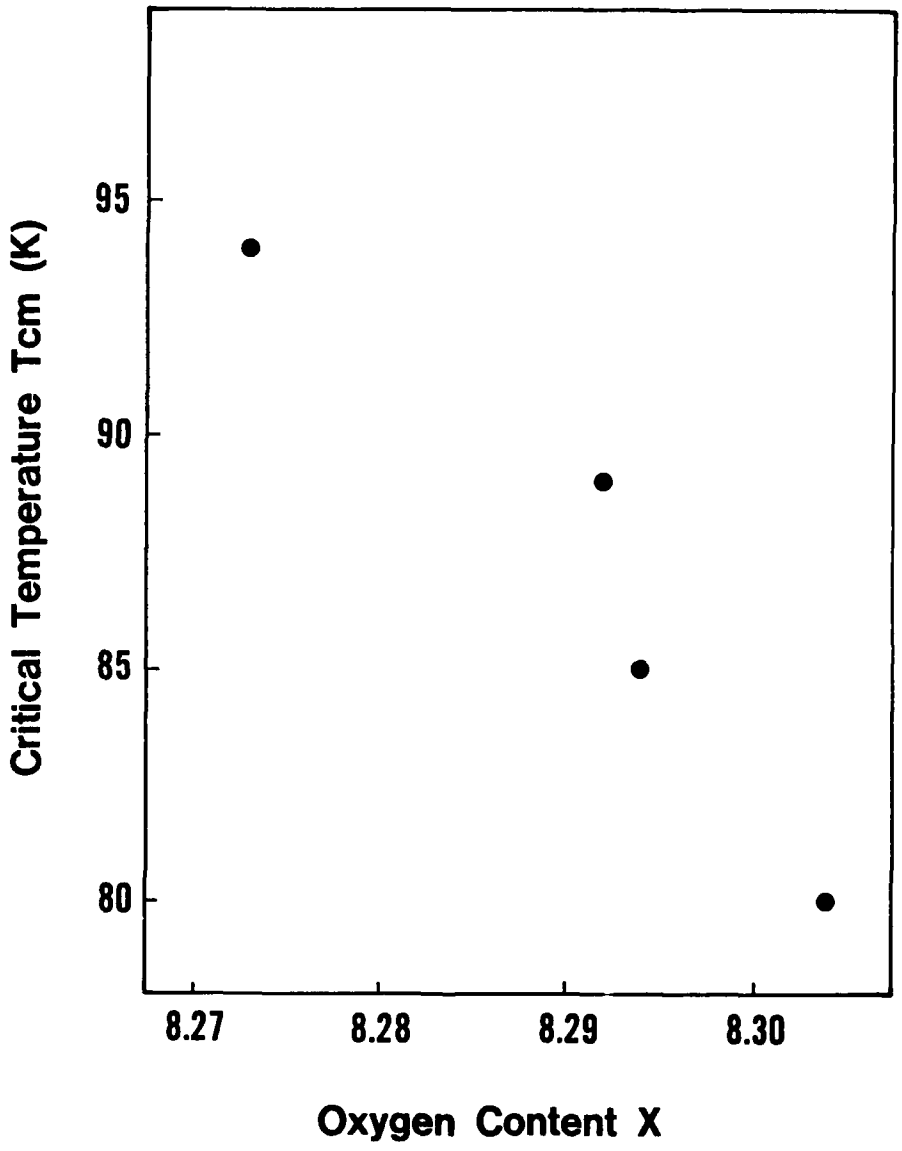

Fig.3 Oxygen contents versus the critical temperature of the polycrystalline $Bi_2Sr_2Ca_1Cu_2O_{8+x}$ samples. The oxygen contents were changed by annealing the samples having Tc of 94K in an oxygen atmosphere with various temperatures.

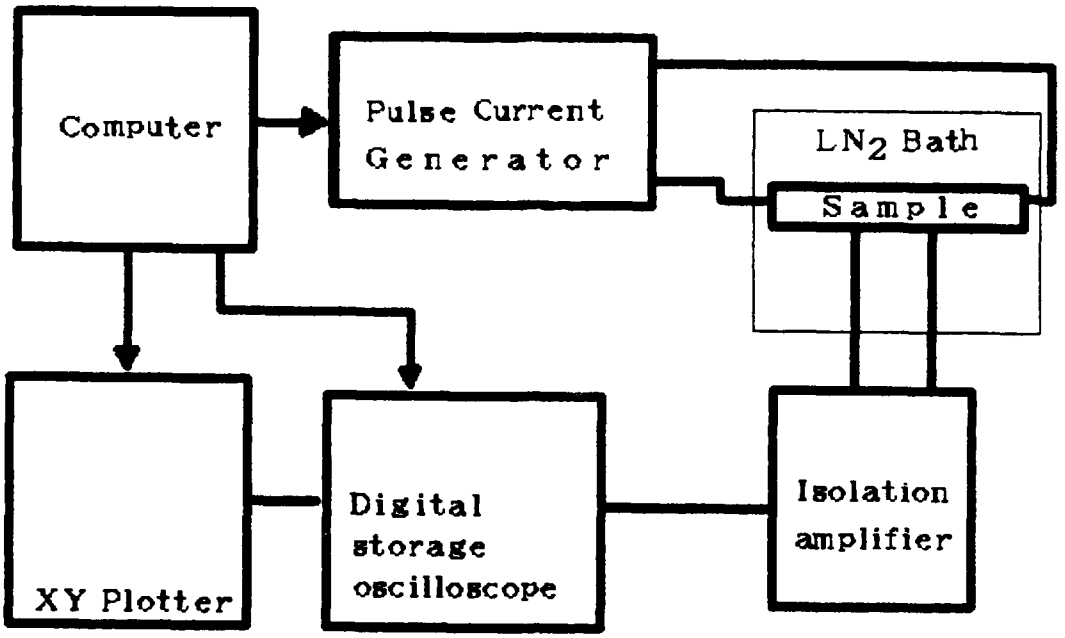

Fig.4 System diagrams for the measurement of I-V properties of bulk superconductors. Samples are cooled in liquid nitrogen, of which the temperature rangeis from 65K to 78K being changed by external pressure control.

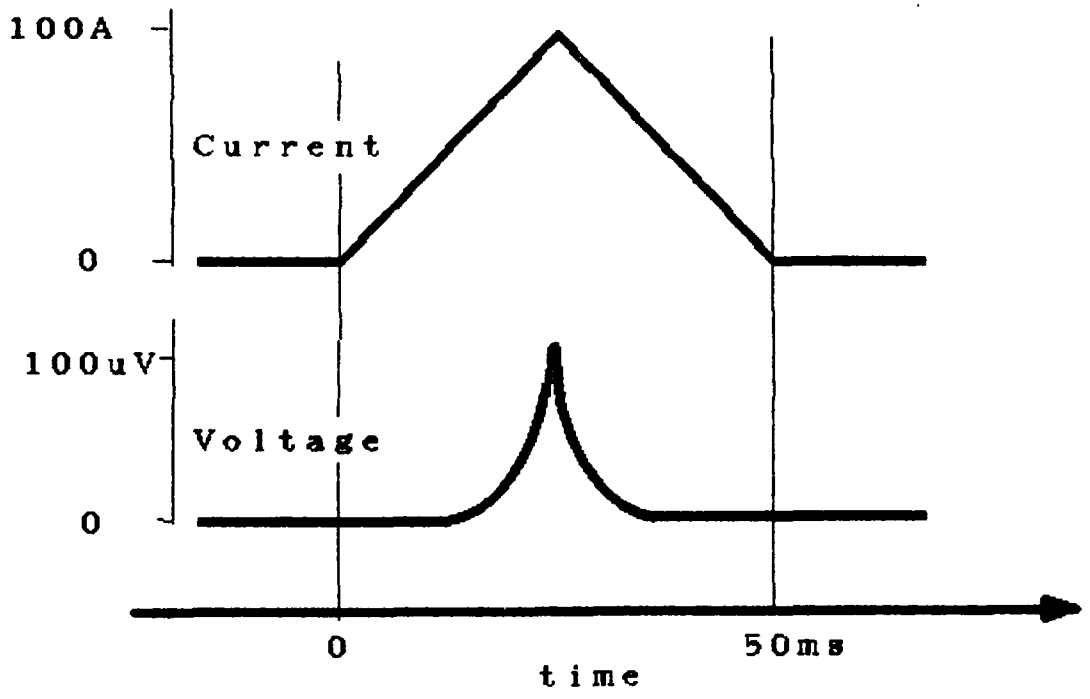

Fig.5 Current pulse wave shape and the corresponding generated voltage across the voltage electrodes. The current and the voltage are stored in a digital storage oscilloscope and are analyzed after the current pulse is terminated.

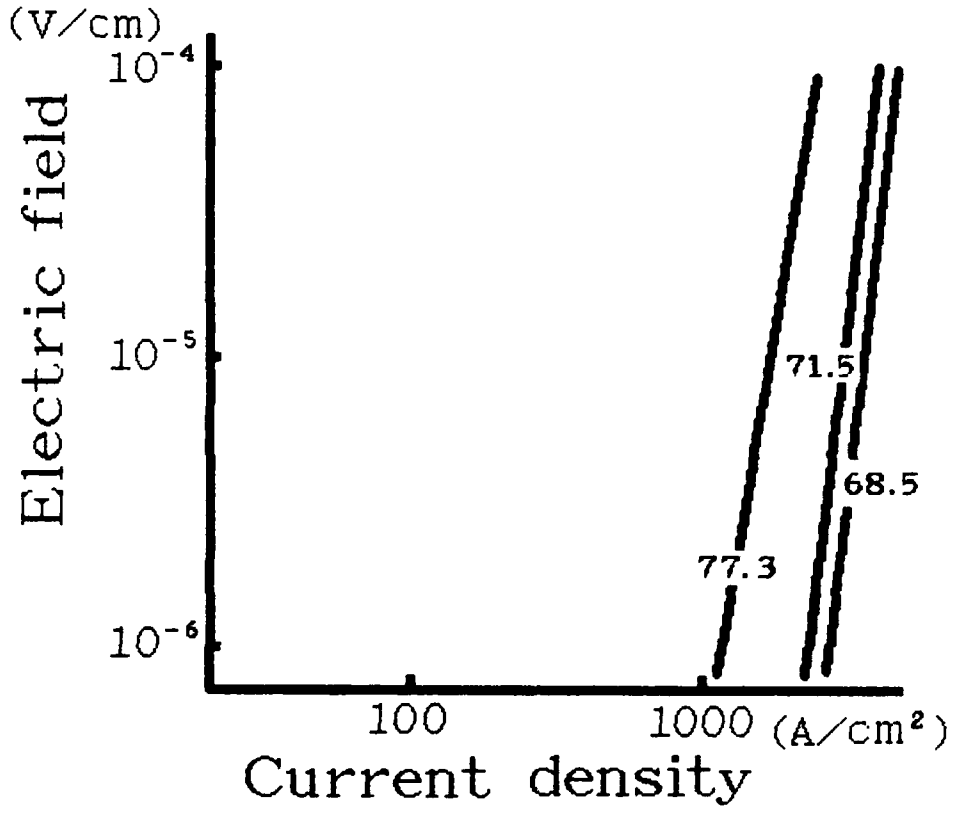

Fig.6 (a) A sample with the critical temperature of 94K

A set of I-V curves of the polycrystalline $Bi_2Sr_2Ca_1Cu_2O_{8+x}$ samples with various critical temperatures , measured at various temperatures. Numbers pointing at each lines indicate the measured temperatures.

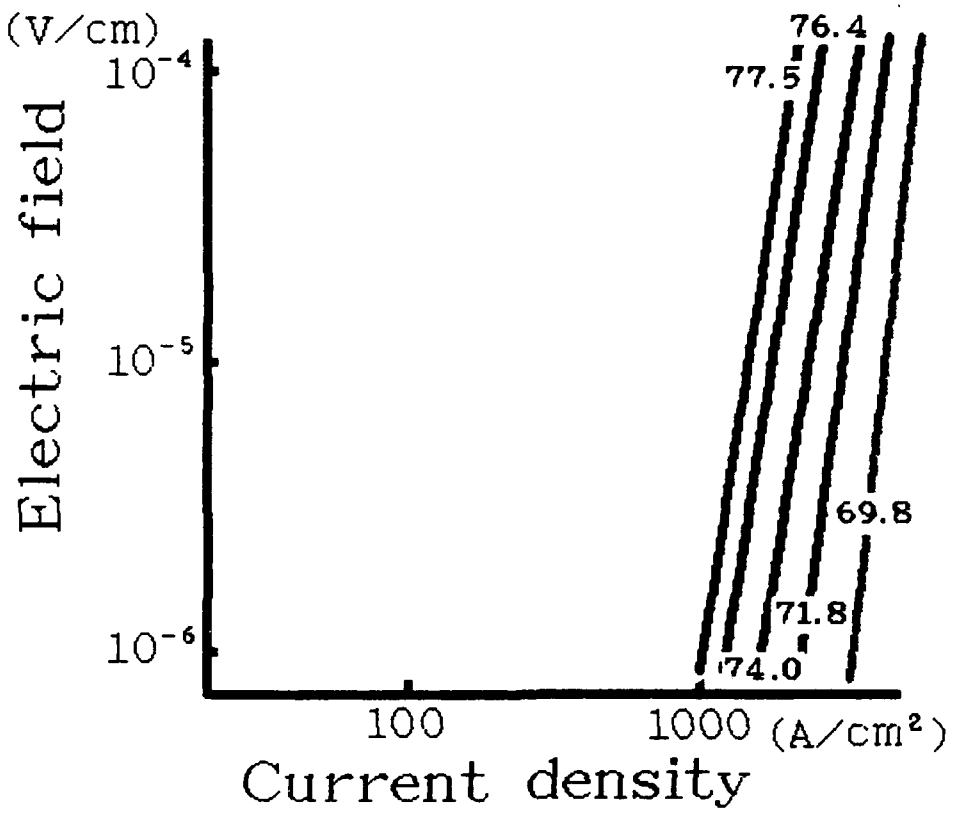

Fig.6 (b) A sample with the critical temperature of 89K

A set of I-V curves of the polycrystalline $Bi_2Sr_2Ca_1Cu_2O_{8+x}$ samples with various critical temperatures , measured at various temperatures. Numbers pointing at each lines indicate the measured temperatures.

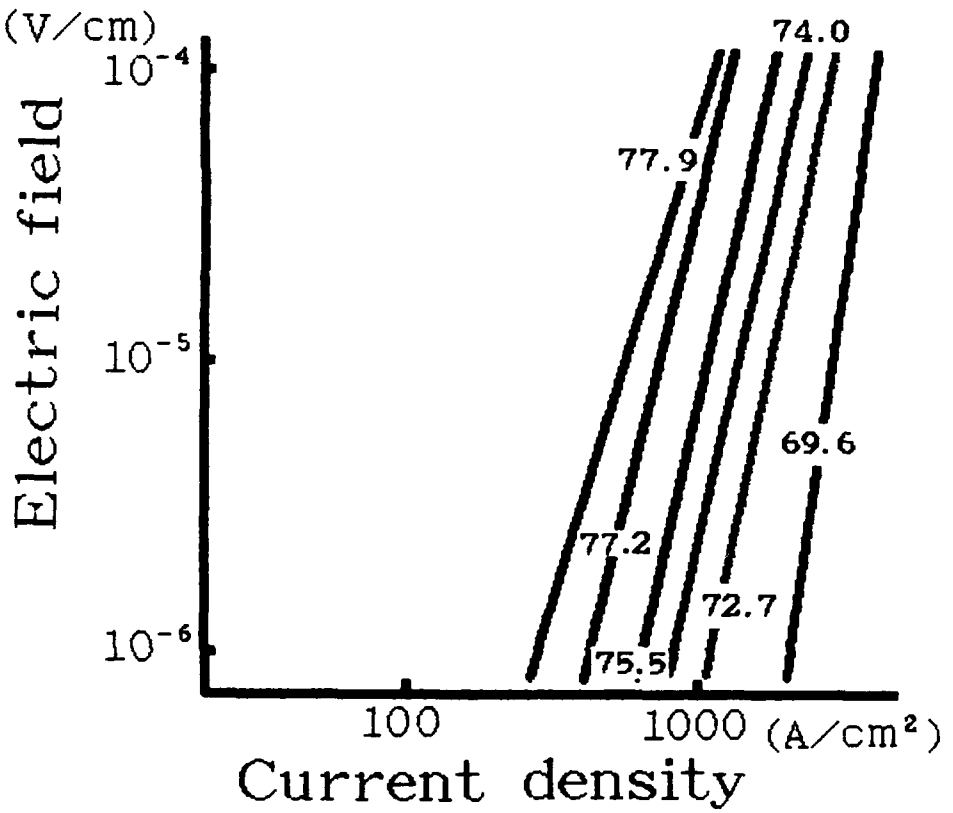

Fig.6 (c) A sample with the critical temperature of 85K

A set of I-V curves of the polycrystalline $Bi_2Sr_2Ca_1Cu_2O_{8+x}$ samples with various critical temperatures , measured at various temperatures. Numbers pointing at each lines indicate the measured temperatures.

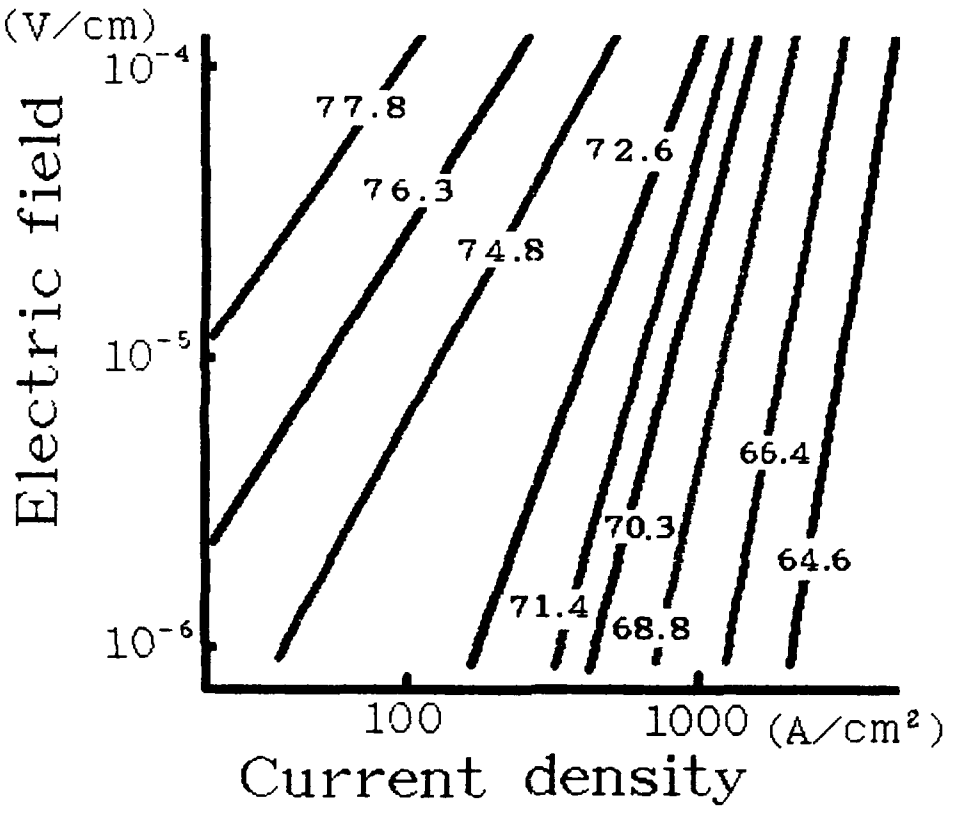

Fig.6 (d) A sample with the critical temperature of 80K

A set of I-V curves of the polycrystalline $Bi_2Sr_2Ca_1Cu_2O_{8+x}$ samples with various critical temperatures , measured at various temperatures. Numbers pointing at each lines indicate the measured temperatures.

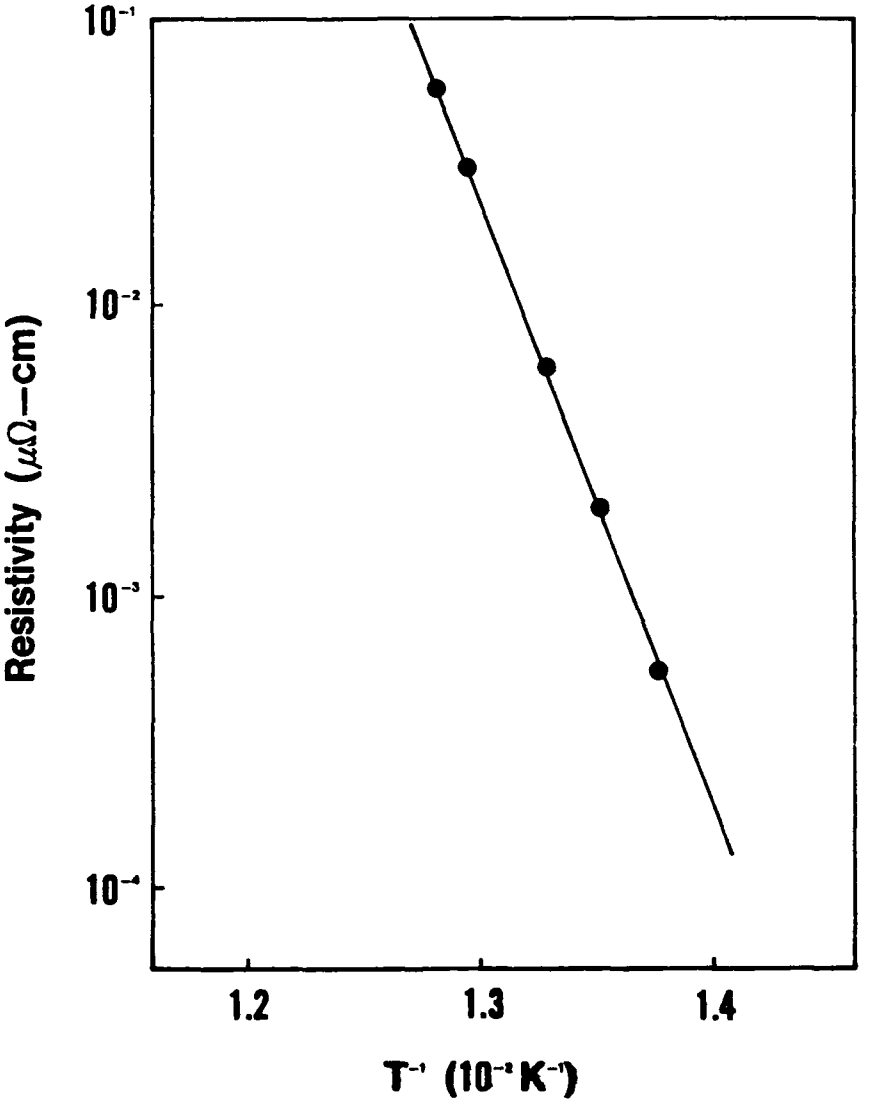

Fig.7 Arrhenius plot of the electrical resistivity of the polycrystalline $Bi_2Sr_2Ca_1Cu_2O_{8+x}$. Activation energy U_0 is given by the slope.

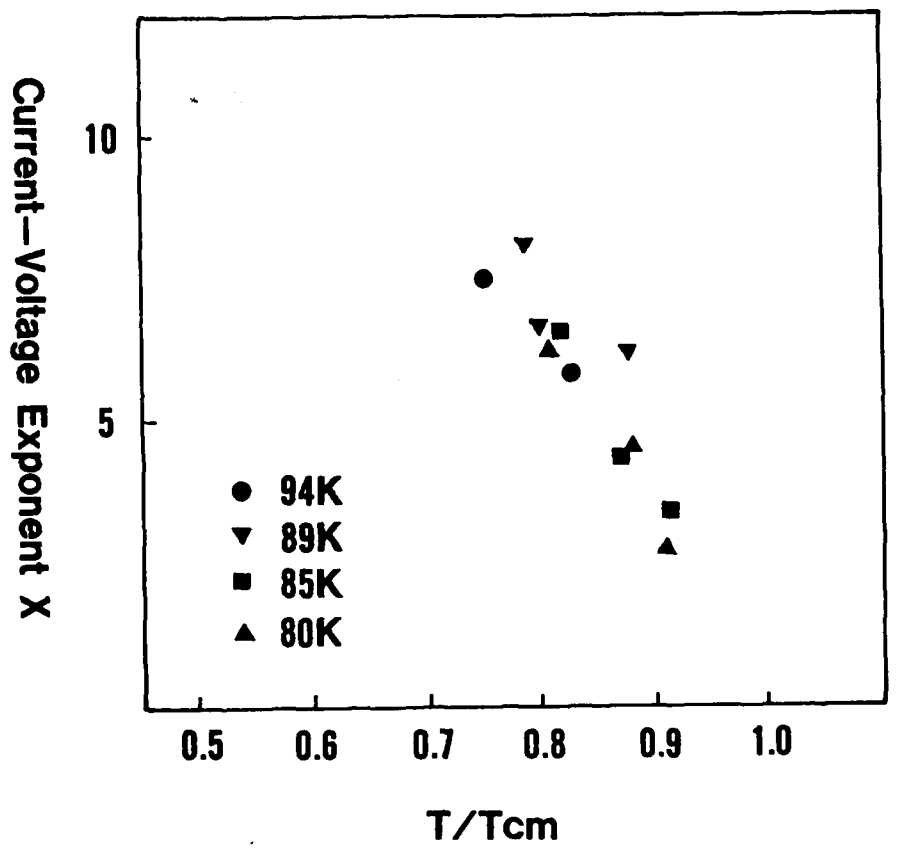

Fig.8 The dependence of current-voltage exponent x on temperature The plots are extracted from Fig.6 and the temperatures are divided by the corresponding critical temperature to normalize the temperature dependence.

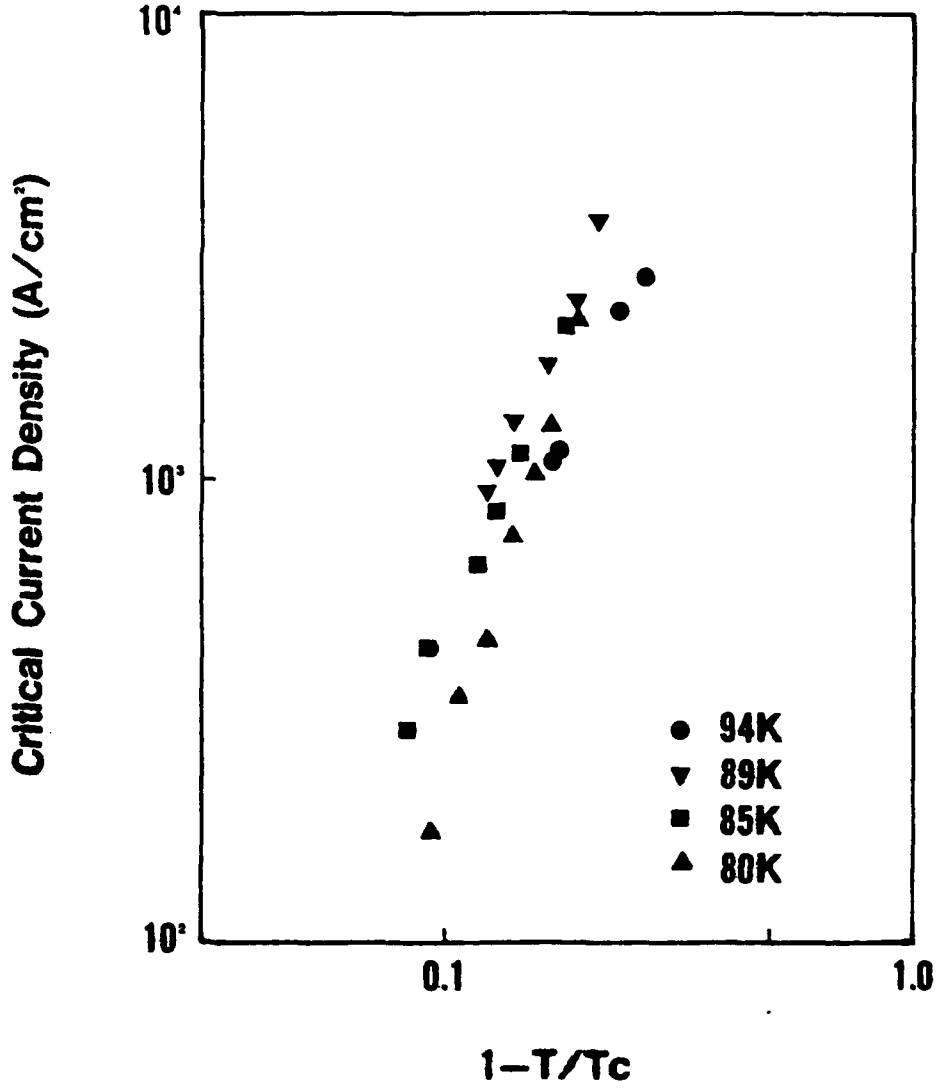

Fig.9 The temperature dependence of critical current density of the polycrystalline $Bi_2Sr_2Ca_1Cu_2O_{8+x}$.
The plots of critical current are extracted from I-V curves in Fig.6 on the criterion of 1 micro volt/cm.

Presented at the Workshop on High Temperature Superconductivity
23-25 May 1989 GACIAC PR-89-02

Preparation and Characterization of Single-Phase $Bi_{2-x}Pb_xSr_2Ca_2Cu_3O_y$ Ceramics Superconductors

May 23-25, 1989

H. L. Luo, S. M. Green, Yu Mei and A. E. Manzi
Departament of Electrical and Computer Engineering, R-007
University of California, San Diego
La Jolla, CA 92093-0407

ABSTRACT

Through repeated homogenizing processes at precisely controlled temperature and ambient, single-phase Pb-doped $Bi_2Sr_2Ca_2Cu_3O_y$ with $T_c \approx 111$ K has been synthesized. Powder x-ray diffraction patterns are employed to verify that repetitive grinding and sintering leads to the virtual disappearance of peaks corresponding to the other related superconducting phases of this complex system. The dimensions of the face-centered pseudo-tetragonal unit cell are determined to be 5.4×5.4×37.1 Å^3. The Meissner and shielding current effects shown by dc magnetic susceptibility measurements of the as-sintered and pulverized specimens at various stages of processing demonstrate that the proper high T_c superconductor can be synthesized in single-phase form.

Introduction

The newly discovered superconducting Bi-Sr-Cu-oxide system[1] has been expanded to a family of compounds by incorporating Ca and additional Cu into the pseudo-tetragonal lattice. The three known members of the family can be described with the general formula $Bi_2Sr_2Ca_{n-1}Cu_nO_y$ (n = 1, 2, 3 which are referred according to the number ratio of metallic ions, as 2201, 2212, 2223). When properly prepared, all three phases are superconductive, having transition temperatures (T_c) increasing with n, in the range 10-20, 75-85, 105-115 K[2,3] respectively. Because the structures are intimately related there is usually substantial intergrowth of the three phases within a given sample. Consequently, electrical resistivity measurements on such multiphase samples usually exhibit a superconducting onset at ~ 110 K, but the point of zero resistance is not reached until ~ 70 K or even much below[2-7]. Therefore, in the study of this superconducting oxide system, to purify the n = 3 phase (2223, T_c ~ 110 K) remains a top priority.

This report describes a preparation process which yields ceramic material of single 2223 phase with T_c ~ 113 K. The essence of the process lies in the partial substitution of Bi by Pb. Repetitive mixing, grinding and annealing under carefully selected oxygen ambient and at precisely controled temperature, are also very important.

Experimental Procedures

Two groups of samples were studied. Group A comprised compositions of $Bi_2Sr_2CuO_y$, $BiSrCaCu_2O_y$ and $Bi_2Sr_2CaCu_2O_y$ which were prepared solely for the purpose of reference and comparison. Major effort was directed towards group B which consisted of the sequence $Bi_{2-x}Pb_xSr_2Ca_2Cu_3O_y$, x = 0 ~ 0.35.

Appropriate amounts of starting material (Bi_2O_3, PbO, $CaCO_3$, $SrCO_3$ and CuO, all in powder form, 99.9% pure or better) were thoroughly mixed in an agate mortar. The mixture was prefired in an alumina combustion boat at 750 C for 10 ~ 12 hours in air. This calcining step promoted the initial reaction of Bi_2O_3 as well as the decomposition of carbonates. The reacted powders were reground, mixed and fired just below the liquidus (850 ~ 880 C) for 48 hours in air. This homogenizing process was repeated at least twice more and the total processing time was usually about 1 week. Part of the

powders were pressed into discs (1 ~ 2 cm diameter and 1 ~ 2 mm thick) for bulk measurements. It is important that samples be cooled to room temperature slowly (2 ~ 3 degrees per min.) after the very last heat treatment.

In the controled oxygen ambient experiments, a post annealing step at 740-750 C for 12-14 hours in 10 ~ 100 mtorr of partial oxygen pressure was added. Again the samples were cooled slowly to room temperature.

Powder x-ray diffraction patterns were obtained using Ni-filtered CuKα radiation (λ = 1.5418 Å) over the interval 2θ = 20 ~ 50° in which most of the strong peaks appeared. Lattice parameters were computed using a least-squares fit. Bar-shaped samples with dimensions 10×3×2 mm^3 were cut from the pressed disks for resistivity (ρ) and dc susceptibility (χ) measurements. ρ(T) was measured over the range 6 ~ 295 K using the standard four-probe technique with 1 mA (dc or rms ac at 40 Hz). For the ac measurement the detection limit for ρ was ~ 0.5 $\mu\Omega$ cm below which the sample resistance was considered to be zero.

χ(T) measurements were conducted using a SQUID magnetometer (Quantum Design MPMS) over the temperature interval 5 ~ 295 K. The shielding-current and Meissner effects were obtained by cooling the sample in zero-field and at 10 or 20 Oe respectively.

Results and Discussion

X-ray diffraction patterns of the 2201, 2212 and 2223 phases are clearly identified as shown in Tables 1-3. The pseudo-tetragonal crystal structures of the superconducting Bi-Sr-Ca-Cu-oxides (BSCCO) are highly anisotropic. For all three phases, the lattice constants a and b remain virtually unchanged in the range of 5.37 ~ 5.41 Å. When n increases from 1 to 2 and from 2 to 3, with the incorporation of added Ca and Cu-O layers, the c-parameter increases by nearly a constant stack of 6.2 Å.

Table 1. Powder x-ray diffraction data for $Bi_2Sr_2CuO_y$

hkl	2θ	I_{obs}/I_o	d_{obs} (Å)	d_{calc} (Å)
006	21.75	19	4.086	4.092
113	25.85	61	3.447	3.445
008	29.20	56	3.058	3.069
115	29.85	100	2.993	3.004
200	33.40	69	2.683	2.685
208	44.85	28	2.021	2.021
11 11	47.20	14	1.926	1.924
220	47.90	23	1.899	1.899

Lattice parameters: a = 5.368 Å, b = 5.373 Å, , c = 24.55 Å,

Table 2. Powder x-ray diffraction data for $Bi_2Sr_2CaCu_2O_y$

hkl	2θ	I_{obs}/I_o	d_{obs} (Å)	d_{calc} (Å)
008	23.15	7	3.842	3.838
113	24.85	9	3.583	3.585
115	27.65	36	3.236	3.248
00 10	29.13	7	3.065	3.070
117	31.15	19	2.871	2.884
200	33.20	100	2.698	2.707
202	33.71	7	2.659	2.664
00 12	35.10	25	2.557	2.558
20 10	44.65	36	2.029	2.030
220	47.55	57	1.912	1.914
20 12 224	48.95	9	1.861	1.859 1.857

Lattice parameters: a = 5.409 Å, b = 5.418 Å, c = 30.70 Å

Table 3. Powder x-ray diffraction data for $Bi_{1.7}Pb_{0.3}Sr_2Ca_2Cu_3O_y$

hkl	2θ	I_{obs}/I_o	d_{obs} (Å)	d_{calc} (Å)
008	19.17	6	4.630	4.637
111	23.43	10	3.797	3.799
00 10	23.98	29	3.711	3.710
113	24.40	19	3.648	3.649
115	26.25	57	3.395	3.395
117 00 12	28.83	88	3.097	3.098 3.092
119	31.94	53	2.802	2.801
200	33.17	100	2.701	2.700
00 14	33.77	28	2.654	2.650
11 11	35.52	25	2.527	2.528
206	36.25	8	2.478	2.474
20 10	41.33	7	2.184	2.183
20 12	44.60	23	2.032	2.034
220	47.61	40	1.910	1.909
11 17 20 14	48.06	19	1.893	1.895 1.892

Lattice parameters a = 5.400 Å, b = 5.401 Å, c = 37.101 Å

Among the three closely related superconducting phases in the BSCCO system, the 2223 phase appears to be the most difficult to prepare. The likely reason is that, at the optimum temperature of preparation, interdiffusion of metallic ions is too sluggish to achieve the proper stacking sequence of the ions. Consequently, considerable intergrowth leads to the multiphase formation. The coexistence of all three phases is illustrated by the ρ(T) and χ(T) data shown in Figure 1. When a small amount of Pb is introduced in place of Bi, the 2223 phase becomes more readily formed.[8-10] Transmission electron micrographs reveal that,[11] without Pb addition, the specimen consisted primarily of grains with 2212 phase in the exterior and 2223 in the interior. Such configuration accounts for the two-stage resistive transition of the BSCCO system reported earlier. When Pb is added, grains comprised only of single 2223 phase have grown in sufficient number to form complete conducting paths which yield a sharp and clean superconducting transition as displayed in Figure 2. However, the χ(T) curve shown in Figure 2 suggest appreciable amount of the 2212 phase is present.

For polycrystalline samples, the χ(T) data, in particular the field-cooled Meissner curve, is very useful for the identification of superconducting phases. Figure 2 clearly indicates the presence of two phases (2223 with T_c = 107 K and 2212 with T_c = 75 K). After repetitive regrinding, mixing and homogenizing heat treatment, material consisting of single 2223 phase is obtained as shown in Figure 3. This claim is based on the exceptionally sharp and clean transition at 111 K demonstrated by the Meissner curve. The small kink (new 100 K) in the shielding current curve is due actually to the coupling among grains. A typical x-ray diffraction pattern of the refined 2223 phase is shown in Figure 4, which provides cleaner and more definitive details of the structure than that reported in the literature.[10,12-15]

The interesting question to be raised is what is the role played by Pb replacing Bi. A direct observation of such substitution is the slight lowering of the melting point of the material (from 880 C to 850 C). When Pb ions enter into the lattice sites, they are in a different valence state than that of Bi. This alteration of valence can change the local/global defect or ordering arrangements of oxygen ions which tend to promote diffusion. Any enhancement in the interdiffusion of metallic ions would facilitate the proper stacking sequence of the ions.

The exact oxygen contents of the BSCCO system have not been determined. Comparing with the $YBa_2Cu_3O_{7-\delta}$ (YBCO) and related compounds, the BSCCO phases are distinctive in two accounts: (1) The intercalation of oxygen occurs at ~ 750°C as compared to ~ 400 C for YBCO. (2) The net change of oxygen in YBCO can reach one atom per formula unit while the corresponding numbers for 2201, 2212 and 2223 phases are much smaller. The range of oxygen content of the high-T_c superconducting oxides is directly related to the stability of the compounds. Unlike YBCO which exhibits its highest T_c after being annealed in pure oxygen, the 2223 phase actually reaches the best T_c only after annealing in an environment of very low oxygen partial pressure. (Figure 5).

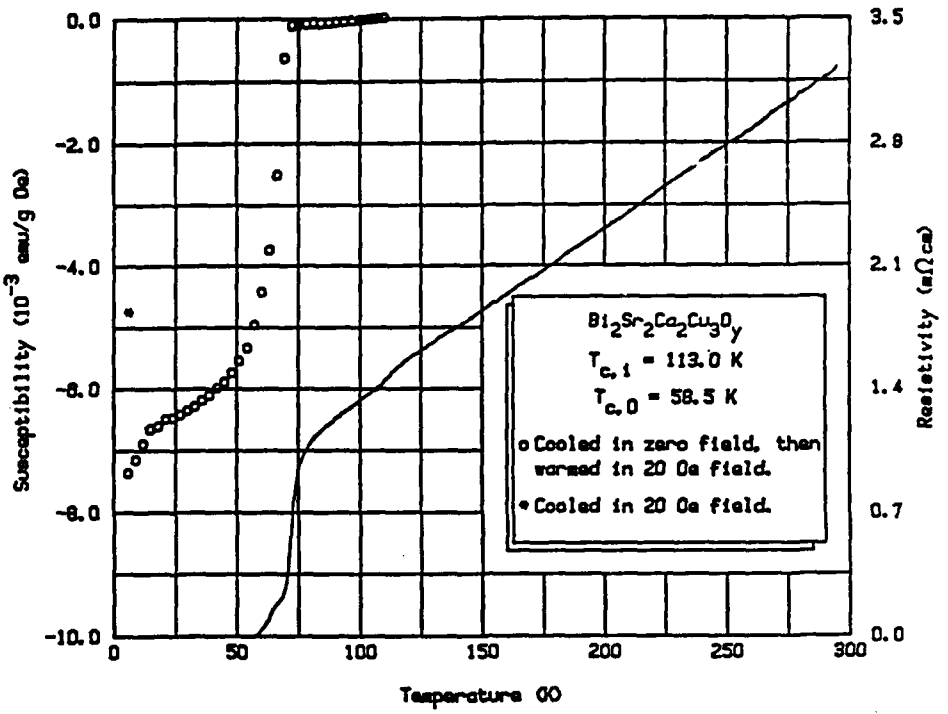

Figure (1) Susceptibility and resistivity vs temperature of a Pb-free sample containing 2201, 2212 and 2223 phases.

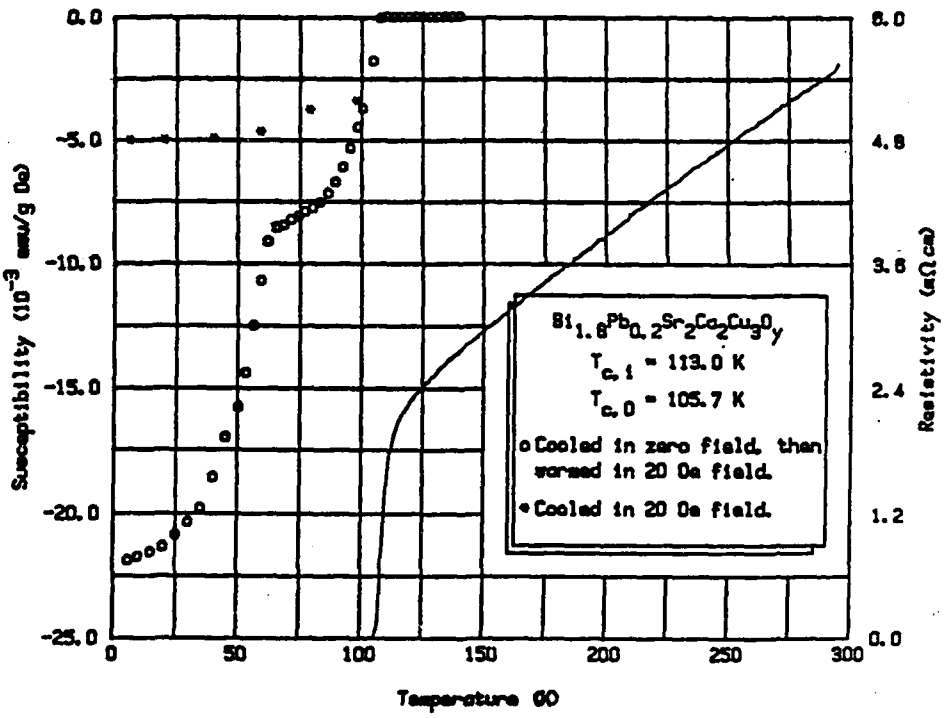

Figure (2) Susceptibility and resistivity vs temperature of a Pb-doped sample containing 2212 and 2223 phases.

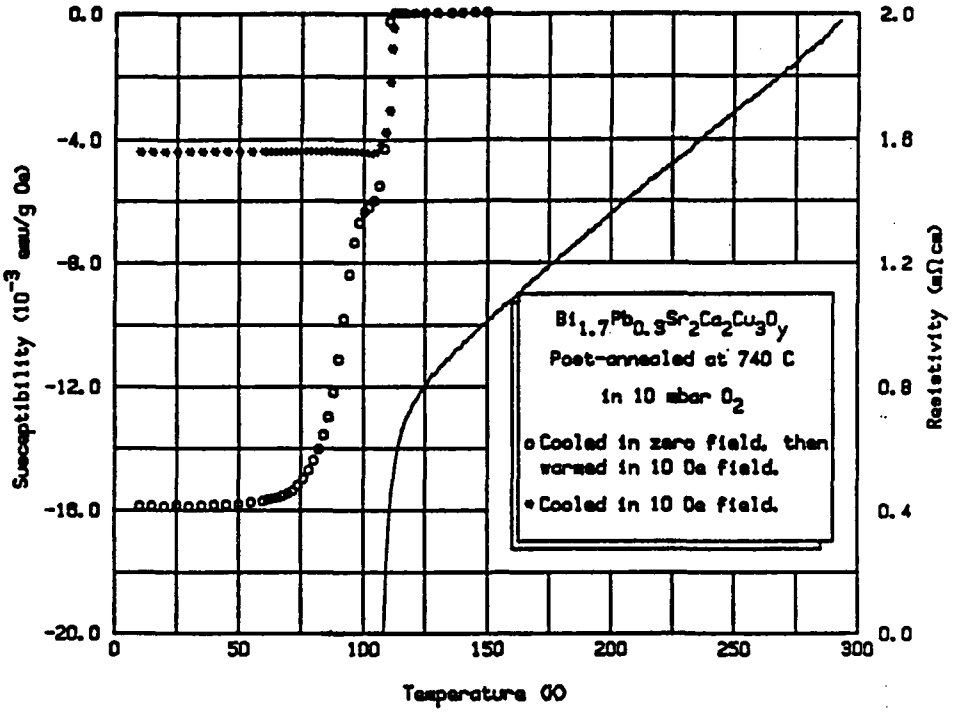

Figure (3) Susceptibility and resistivity vs temperature of a Pb-doped single 2223-phase material.

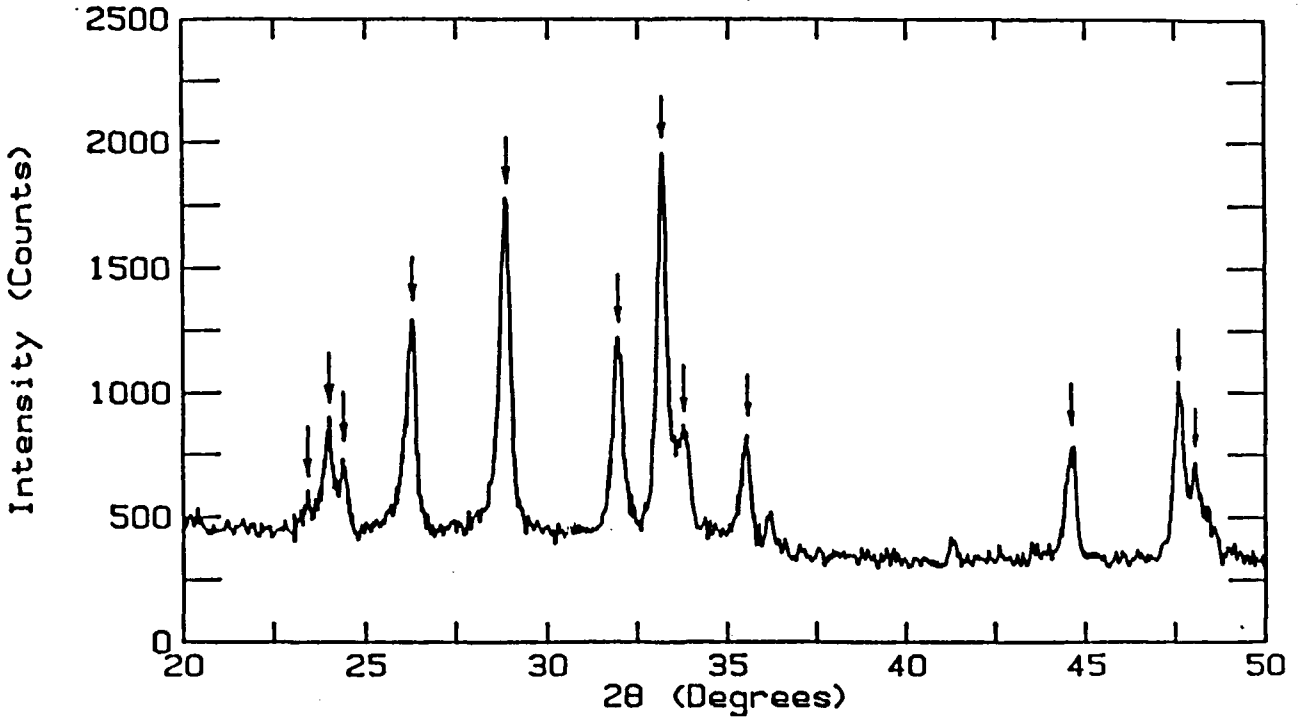

Figure (4) Powder x-ray diffraction pattern of the 2223 phase, using Cu K_α radiation. The arrows indicate the peaks used to compute the lattice parameters.

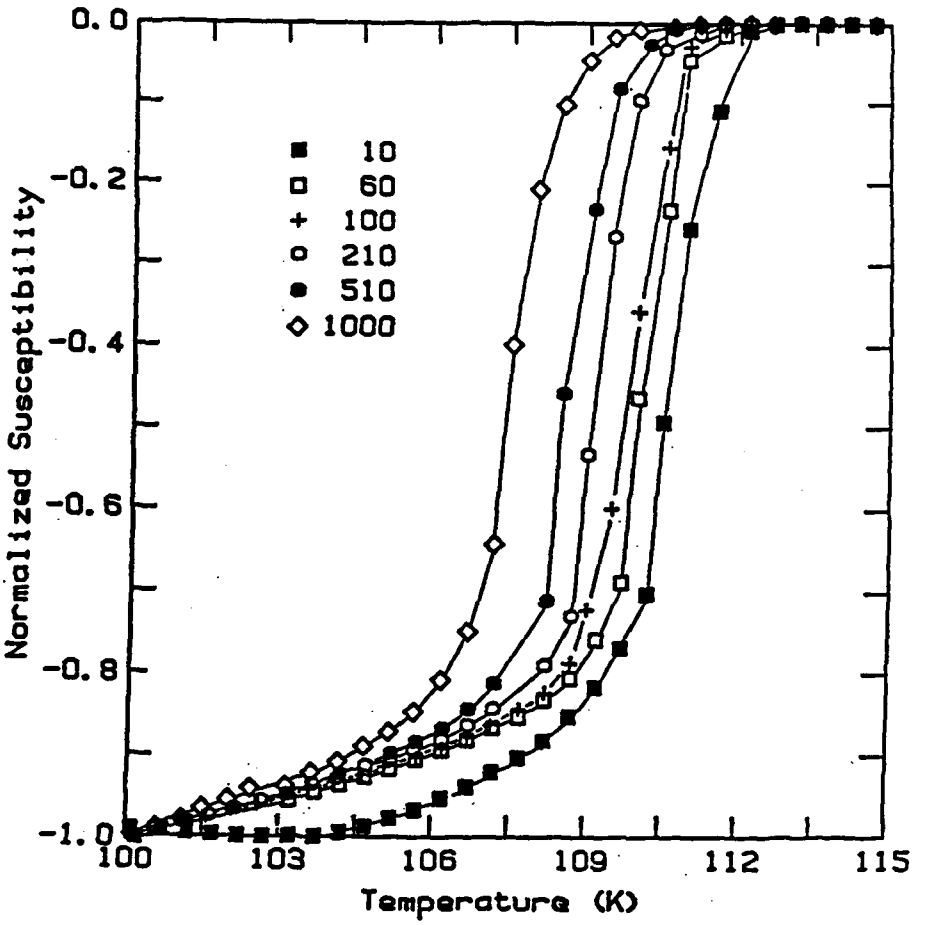

Figure (5) The effect of partial oxygen pressure on the T_c of a single 2223-phase sample.

Conclusion

By partially substituting Pb for Bi and by repeated grinding, mixing and homogenizing heat treatments, single phase material of $(Bi, Pb)_2Sr_2Ca_2Cu_3O_y$ with T_c = 110 K can be synthesized. The Meissner effect exhibited in the susceptibility experiments is a good measure for phase identification.

Acknowledgement

This research is supported by the California MICRO Program and Hughes Aircraft Co.

References

[1] C. Michel, M. Hervieu, M. M. Borel, A. Grandin, F. Deslandes, J. Provost and B. Raveau, *Z. Phys. B* **68,** 421 (1987).

[2] M. Maeda, Y. Tanaka, M. Fukutomi and T. Asano, *Jpn. J. Appl. Phys. Lett.* **27,** L209 (1988).

[3] R. M. Hazen, C. T. Prewitt, R. J. Angel, N. L. Ross, L. W. Finger, C. G. Hadidiacos, D. R. Veblen, P. J. Heaney, P. H. Hor, R. L. Meng, Y. Y. Sun, Y. Q. Wang, Y. Y. Xue, Z. J. Huang, L. Gao, J. Bechtold and C. W. Chu, *Phys. Rev. Lett.* **60,** 1174 (1988).

[4] M. A. Subramanian, C. C. Torardi, J. C. Calabrese, J. Gopalakrishnan, K. J. Morrissey, T. R. Askew, R. B. Flippen, U. Chowdhry and A. W. Sleight, *Science* **239,** 1015 (1988).

[5] S. M. Green, Yu Mei, C. Jiang, H. L. Luo and C. Politis, *Mod. Phys. Lett* **B2,** 915 (1988).

[6] J. M. Tarascon, Y. Le Page, P. Barboux, B. G. Bagley, L. H. Greene, W. R. McKinnon, G. W. Hull, M. Giroud and D. M. Hwang, *Phys. Rev.* **B37,** 9382 (1988).

[7] Yu Mei, S. M. Green, C. Jiang and H. L. Luo, *J. Appl. Phys.* **64,** 6795 (1988).

[8] S. M. Green, C. Jiang, Yu Mei, H. L. Luo and C. Politis, *Phys. Rev.* **B38,** 5016 (1988).

[9] R. J. Cava, B. Batlogg, S. A. Sunshine, T. Siegrist, R. M. Fleming, R. Rabe, L. F. Schneemeyer, D. W. Murphy, R. B. van Dover, P. K. Gallagher, S. H. Glarum, S. Nakahara, R. C. Farrow, J. J. Krajewski, S. M. Zahurak, J. V. Waszcak, J. H. Marshall, P. Marsh, L. W. Rupp Jr., W. F. Peck and E. A. Rietman, *Physica C* **153-155,** 560 (1988).

[10] B. W. Statt, Z. Wang, M. J. G. Lee, J. V. Yakhmi, P. C. De Camargo, J. F. Major and J. W. Rutter, *Physica C* **156,** 251 (1988).

[11] R. Ramesh, G. Thomas, S. M. Green, C. Jiang, Yu Mei, M. L. Rudee and H. L. Luo, *Phys. Rev.* **B38,** 7070 (1988).

[12] J. M. Tarascon, W. R. McKinnon, P. Barboux, D. M. Hwang, B. G. Bagley, L. H. Greene, G. W. Hull, Y. LePage, N. Stoffel and M. Giroud, *Phys. Rev. B* **B38,** 8885 (1988).

[13] S. M. Green, Yu Mei, A. E. Manzi and H. L. Luo, *J. Appl. Phys.* (in press 1989).

[14] N. Murayama, E. Sudo, M. Awano, K. Kani and Y. Torii, *Jpn. J. Appl. Phys. Lett.* **27,** L1629 (1988).

[15] U. Balachandran, D. Shi, D. I Dos Santos, S. W. Graham, M. A. Patel, B. Tani, K. Vandervoort, H. Claus and R. B. Poeppel, *Physica C* **156,** 649 (1988).

THIS PAGE IS INTENTIONALLY BLANK

Presented at the Workshop on High Temperature Superconductivity
23-25 May 1989 GACIAC PR-89-02

SEQUENTIALLY EVAPORATED THIN Y-Ba-Cu-O SUPERCONDUCTING FILMS ON MICROWAVE SUBSTRATES

21 April, 1989

G.J. Valco and N.J. Rohrer
Department of Electrical Engineering
Ohio State University
Columbus, Ohio 43210

J.D. Warner and K.B. Bhasin
National Aeronautics and Space Administration
Lewis Research Center
21000 Brookpark Rd.Cleveland, Ohio 44135

ABSTRACT

The development of high T_c superconducting thin films on various microwave substrates is of major interest to evaluate their applications in space electronic systems. Thin films of $YBa_2Cu_3O_{7-\delta}$ have been formed on $SrTiO_3$, MgO, ZrO_2 coated Al_2O_3 and $LaAlO_3$ substrates by multi-layer sequential evaporation and subsequent annealing in oxygen. The technique allows controlled deposition of Cu, BaF_2 and Y layers, as well as the ZrO buffer layers, to achieve reproducibility for microwave circuit fabrication. The three layer structure of $Cu/BaF_2/Y$ is repeated a minimum of four times. The films have been annealed in an ambient of oxygen bubbled through water at temperatures between 850 °C and 900 °C followed by slow cooling (-2 °C/minute) to 450 °C, a low temperature anneal, and slow cooling to room temperature. Annealing times have ranged from 15 minutes to 5 hrs at high temperature and 0 to 6 hr at 450 °C. Silver contacts for four probe electrical measurements have been formed by evaporation followed with an anneal at 500 °C. The films have been characterized by resistance-temperature measurements, energy dispersive x-ray spectroscopy, x-ray diffraction and scanning electron microscopy. Critical transition temperatures have ranged from 30 K to 87 K as a function of the substrate, composition of the film, thicknesses of the layers and annealing conditions. Microwave ring resonator circuits are also patterned on these MgO and $LaAlO_3$ substrates.

1.0 INTRODUCTION

The development of thin films of the high critical temperature (T_c) superconducting oxides on various microwave substrates is of major interest as it allows evaluation of the superconductors for application in space electronic systems. A large amount of work has been reported on these films on substrates such as strontium titanate ($SrTiO_3$) and yttrium stabilized zirconia (YSZ), however these substrates are not suitable for microwave applications due to large dielectric constants or microwave losses. Substrates which are more suitable for microwave applications include magnesium oxide (MgO), sapphire, alumina (Al_2O_3) and lanthanum aluminate ($LaAlO_3$). These substrates have dielectric constants of approximately 10, 9.4 or 11.6, 9.8 and 15.3[1] respectively, although the dielectric constant of $LaAlO_3$ may be somewhat higher[2]. $LaAlO_3$ substrates are of particular interest since they have a comparable crystal structure to $SrTiO_3$ but significantly better microwave properties.

---

[1] R. W. Simon, C. E. Platt, A. E. Lee, G. S. Lee, K. P. Daly, M. S. Wire, J. A. Levine and M. Urbanik, "Low-loss Substrate for Epitaxial Growth of High-Temperature Superconductor Thin Films," Appl. Phys. Lett., 53(26), 2677 (1988).

[2] F. A. Miranda, N. L. Gordon, V. O. Heinen, B. T. Ebihara and K. B. Bhasin, "Measurement of Complex Permitivity of Microwave Substrates in the 20 to 300 K Temperature Range From 26.5 to 40.0 GHz," Accepted for presentation at the Cryogenic Engineering Conference, July 24-28, 1989, Los Angeles, CA.

A large variety of techniques have been used to form high temperature superconducting thin films. One such technique consists of the sequential evaporation of a multi-layer stack containing the constituents of the superconductor followed by annealing in an oxygen ambient[3,4,5,6,7,8]. When performed by electron beam evaporation from a multi-hearth gun, this technique allows deposition of films with little spatial variation of stoichiometry across the substrate as all components of the film are evaporated from the same point in space. The stoichiometry of the films is also easily adjusted by controlling the thickness of the individually deposited layers. This technique has been employed with a variety of starting materials; Y, Ba and Cu metals themselves, oxides and BaF_2.

We have performed sequential evaporation of Cu, Y and BaF_2 to study the formation of superconducting films on $SrTiO_3$, MgO, sapphire, alumina and $LaAlO_3$ substrates. For the sapphire and alumina substrates, we have used a thin film of ZrO_2 as a buffer layer. We have varied the stoichiometry of the films by adjusting the thicknesses of the individual layers. Films of fixed composition have also been differently annealed to assess the influence of annealing conditions. The resistivity of the films has been measured with a standard four point probe technique between the temperatures of 10 K and 300 K.

2.0 EXPERIMENTAL PROCEDURE

Deposition of the films was performed in a CHA Industries electron beam evaporator. The system is equipped with a four hearth gun, allowing deposition of the multi-layer stack without breaking vacuum. Thickness of the layers was controlled via an Inficon XTC thickness monitor and rate controller. The depositions were calibrated by measurements of step heights using a surface profilometer. The ZrO_2 buffer layers for the sapphire and alumina substrates were also deposited in this evaporator.

A cross sectional drawing of the structure of a typical as deposited film is shown in Figure 1. Copper was deposited on the substrate first. This was followed by a layer of yttrium which was followed by barium fluoride. For most of our depositions, this multi-layered sequence was repeated four times for a total of twelve layers. For substrates on which a buffer layer was employed, the ZrO_2 layer was deposited prior to deposition of the first copper layer. The thicknesses of the individual layers are varied to alter the composition of the film. We reference the composition of the films through the barium/yttrium and copper/yttrium atomic ratios. We have investigated the properties of films with barium/yttrium ratios ranging from 1.9 to 4.0 and copper/yttrium ratios ranging from 2.8 to 3.5. We have used barium fluoride rather than elemental barium since barium fluoride is less reactive.

The deposited films were annealed in a hot wall, programable, quartz tube furnace. The furnace was purged with oxygen prior to inserting the samples. In some cases, the furnace was heated to the annealing temperature prior to insertion of the samples. The samples were pushed into the preheated furnace using a fast push of approximately 30 sec duration or a slow push with a 5 minute duration. Otherwise the samples were pushed into the center of the cool furnace and the

---

3 A. Mogro-Campero and L. G. Turner, "Thin Films of Y-Ba-Cu-O on Silicon and Silicon Dioxide," Appl. Phys. Lett., 52, 1185 (1988).

4 C. X. Qiu and I. Shih, "Y-Ba-Cu-O Thin Films Prepared by a Multi-Layer Vacuum Method," Appl. Phys. Lett., 52, 587 (1988).

5 C-A. Chang, C. C. Tsuei, C. C. Chi and T. R. McGuire, "Thin Film YBaCuO Superconductors Formed by Cu/BaO/Y_2O_3 Layer Structures, Appl. Phys. Lett. 52, 72 (1988).

6 Z. L. Bao, F. R. Wang, Q. D. Jiang, S. Z. Wang, Z. Y. Ye, K. Wu, C. Y. Li, and D. L. Yin, "YBaCuO Superconducting Thin Films With Zero Resistance at 84 K by Multilayer Deposition," Appl. Phys. Lett. 51, 946 (1987).

7 N. Hess, L. R. Tessler, U. Dai and G. Deutscher, "Preparation and Patterning of YBaCuO Thin Films Obtained by Sequential Deposition of $CuO_x/Y_2O_3/BaF_2$, Appl. Phys. Lett. 53, 698 (1988).

8 G. J. Valco, N. J. Rohrer, J. D. Warner and K. B. Bhasin, "Sequentially Evaporated Thin Y-Ba-Cu-O Superconductor Films: Composition and Processing Effects," American Institute of Physics Conference Proceedings, to be published.

temperature was ramped to the annealing temperature at rates from 20 °C/minute to 80 °C/minute. Annealing temperatures ranged from 850 °C to 900 °C. The duration of the anneals ranged from 15 minutes to 3 hr. The temperature was then ramped to 450 °C at a rate of -2 °C/minute. The samples were held at 450 °C for 6 hr and then the temperature was ramped to room temperature at -2 °C/minute. During the high temperature portion of the anneal the ambient consisted of ultra high purity oxygen bubbled through room temperature water to assist in removal of fluorine from the films. Dry oxygen was used during all other portions of the annealing process.

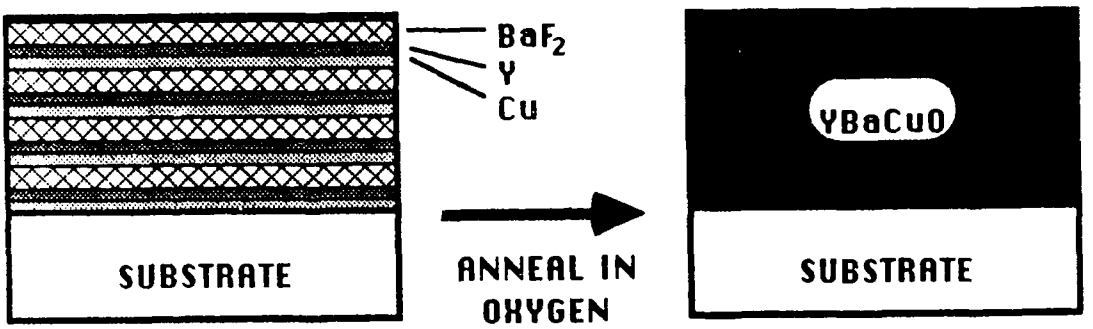

Figure 1: Schematic representation of the as deposited multi-layer structure of the film on the left and the superconducting film after annealing on the right.

Ohmic contacts were formed on the films to allow measurement of the resistance as a function of temperature. Most of the samples were rectangular in shape with widths of approximately 5 mm and lengths of approximately 1 cm. The contacts for these samples were deposited by evaporation of 1 μm of silver through shadow masks to produce four stripes across the width of the samples. The contacts were annealed in dry oxygen at 500 °C for 1 hr. They were placed in the tube furnace at room temperature and the temperature was ramped up at 20 °C/minute. At the end of the anneal the temperature was ramped to 250 °C at a rate of -2 °C/minute and then to room temperature at -1 °C/minute.

To allow measurement of the resistance of the films as a function of temperature, the samples were cooled in a closed cycle helium refrigerator. They were mounted onto a sample holder and gold ribbon bonds were made between the silver contacts and bonding posts. A four probe DC measurement was employed to determine the resistance as the sample temperature was lowered. A few samples were measured both while cooling or while heating, with the same results in both directions. The criteria for determination of T_c was the resistivity decreasing to the noise level of approximately 10^{-9} Ω-cm. Measurements were continued to well below the transition temperature for superconducting films or to approximately 10 K for non-superconducting films.

Scanning electron microscopy (SEM) was employed to observe the morphology of several of the films. In addition, some films on $SrTiO_3$ substrates were analyzed by x-ray diffraction spectroscopy (XDS) to check orientation and the presence of other phases. Auger electron spectroscopy (AES) was employed to study the film/buffer/substrate interfaces of several samples with ZrO_2 buffer layers.

3.0 RESULTS

The annealing cycle and composition of the film have a major influence on the properties of the resulting film. Figure 2 shows the normalized resistance as a function of temperature for four samples deposited at the same time onto $SrTiO_3$ but annealed with different procedures. The composition of the as deposited films was Cu/Y=3.11 and Ba/Y=2.20. They were annealed for 45 minutes at either 850 °C, 875 °C or 900 °C and with either a fast push (30 sec) or a slow push (5 minutes) into the center zone of the furnace. There is a marked improvement in the critical temperature, transition width and normal state resistance characteristic of the films as the annealing temperature was increased from 850 °C to 900 °C. The difference between the two samples annealed at 850 °C with different push rates demonstrates the influence of the heating rate during the anneal. The film annealed at 900 °C and given the slow push was the best.

Figure 3 shows the effect of heating rate for films with the optimal as deposited composition (Cu/Y=3.00, Ba/Y=2.25) on $SrTiO_3$. All of these films were annealed for 45 minutes at 900 °C with heating rates of either a slow push (5 minutes), 50 °C/minute ramp or 20 °C/minute ramp. The intermediate heating rate, 50 °C/minute, resulted in the film with the sharpest resistive transition and a critical temperature of 85 K.

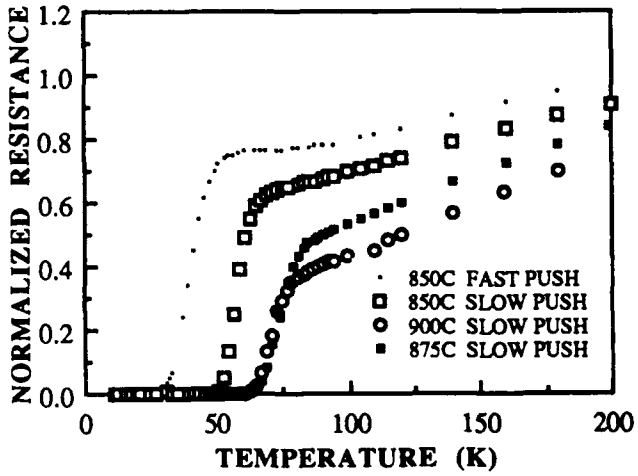

Figure 2: Resistance normalized to 300 K as a function of temperature for four samples on $SrTiO_3$ substrates with different annealing cycles. Cu/Y=3.11, Ba/Y=2.20. Annealed 45 minutes.

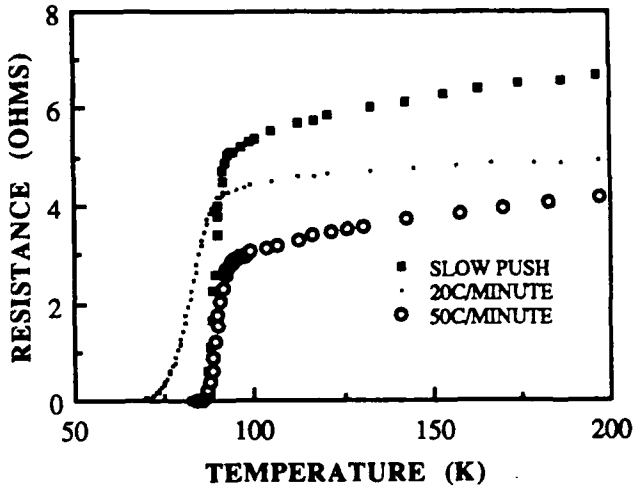

Figure 3: Resistance as a function of temperature for three samples on $SrTiO_3$ substrates with different annealing cycles. Cu/Y=3.00, Ba/Y=2.25. Annealed 45 minutes at 900 °C.

Figure 4 shows the distribution of transition temperature for films with various ratios of Cu/Y and Ba/Y. Each film was made with a 12 layer deposition and had a thickness between 1.0 and 1.2 μm before annealing. All of the samples were annealed for 45 minutes at 900 °C using a slow push. A detailed discussion of the variation of the resistive transition with composition is given in a previous paper by the authors[8]. Those films deposited with a Ba/Y ratio of greater than approximately 2.2 have a metallic normal state resistance-temperature characteristic. This was also true of two films with larger Ba/Y ratios (3.0 and 4.0) which did not completely achieve zero resistance although they had a sharp onset and narrow transition width.

The morphology of the films is dependent on the initial rate of heating during the anneal. For the films of Figure 3, discussed above, the film with the 50 °C/minute heating rate has a dense "basketweave" morphology. SEM micrographs typical of this morphology were presented in an earlier paper by the authors[9]. X-ray diffraction spectroscopy showed that this film has primarily the a-axis oriented perpendicular to the substrate but does show some c-axis orientation. The basketweave morphology was also present

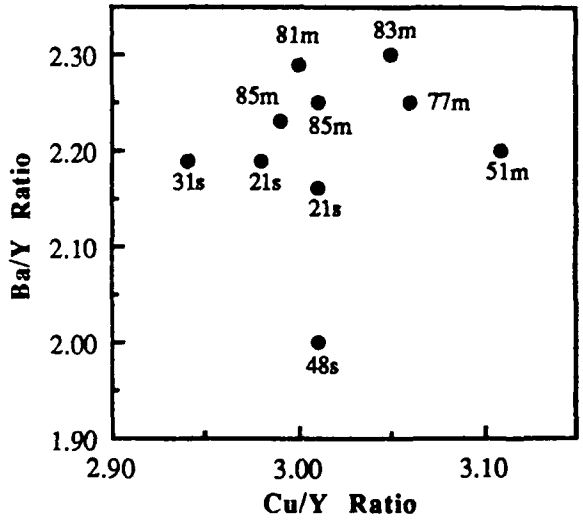

Figure 4: Distribution of T_c for films of various composition on $SrTiO_3$ annealed at 950 °C for 45 minutes with a slow push. The number with each point indicates the critical temperature while the letter indicates the behavior in the normal state: metallic or semiconducting.

9 G. J. Valco, N. J. Rohrer, J. J. Pouch, J. D. Warner, K. B. Bhasin, "Characterization of ZrO2 Buffer Layers for Sequentially Evaporated Y-Ba-Cu-O On Si and Al_2O_3 Substrates," Proceedings of the Conference on the Technology of Thin Film Superconductors, submitted for publication.

in the film annealed with the 5 minute push, although it was not as dense. The film on the sample heated at a rate of 20 °C/minute did not exhibit the basketweave structure, but had shorter, randomly oriented grains that appeared to lie parallel to the surface of the substrate. The critical current density was an order of magnitude larger for the sample with the 50 °C/minute heating rate than for the film heated at 20 °C/min. The presence of the oriented basketweave morphology is also enhanced with thinner films[9].

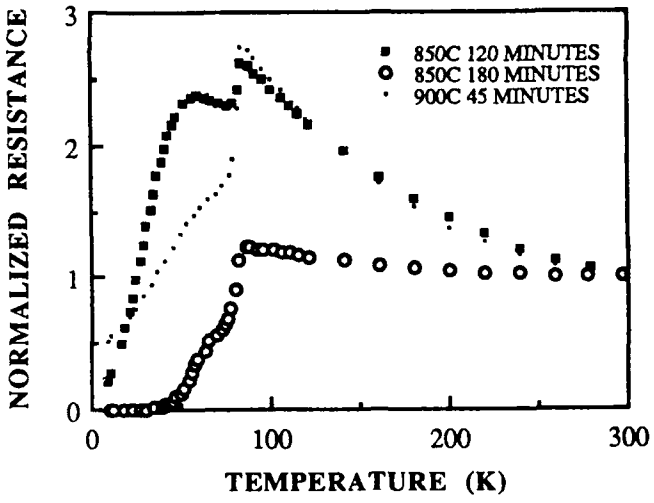

Figure 5: Resistance normalized to 300K as a function of temperature for three samples on MgO substrates with different annealing cycles. Cu/Y=3.02, Ba/Y=2.26.

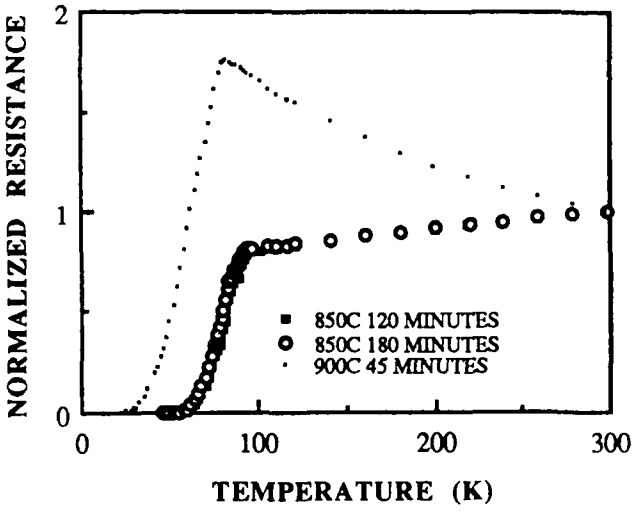

Figure 6: Resistance normalized to 300K as a function of temperature for three samples on MgO substrates with different annealing cycles. Cu/Y=3.01, Ba/Y=2.00.

In contrast with the films on $SrTiO_3$ substrates, films on MgO require lower annealing temperatures but longer durations. Figures 5 and 6 show the normalized resistance-temperature characteristics for films of two different composition on MgO substrates which were annealed under different conditions. The samples indicated by the squares have been annealed at 900 °C for 45 minutes in a procedure identical to that used for $SrTiO_3$. The samples indicated by the crosses and circles had been annealed at 850 °C for 120 and 180 minutes respectively. In Figure 5, the films had an as deposited composition of Cu/Y=3.02 and Ba/Y=2.26, which is near the optimum composition used on $SrTiO_3$ substrates. Although none of the samples became superconducting, they all showed an onset of superconductivity and there is a clear improvement for the lower temperature, long duration anneal. The data presented in Figure 6 are for samples with an as deposited composition of Cu/Y=3.01 and Ba/Y=2.00. The sample anncaled at 900 °C had a semiconducting behavior in the normal state, a very broad transition with a long tail, and never achieved zero resistance while the samples annealed at 850 °C displayed a metallic behavior in the normal state and achieved zero resistance at approximately 51 K.

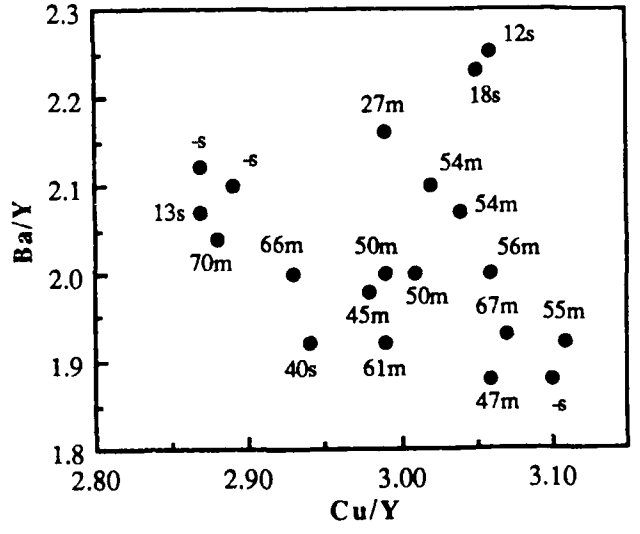

Figure 7: Distribution of T_c for films of various composition on MgO annealed at 850 °C for 3 hr. The number with each point indicates T_c while the letter indicates the behavior in the normal state : metallic or semiconducting.

Figure 7 shows the distribution of T_c for several films on MgO as a function of Cu/Y and Ba/Y ratio. All of these samples were annealed at 850 °C for 3 hrs with a slow push into the furnace. It is apparent that the as deposited composition to produce good films on MgO is different than for $SrTiO_3$, with the major difference being a lower Ba/Y ratio. Films with compositions toward the center of the plot have metallic normal state behavior, while those with extreme compositions exhibit a semiconducting behavior. Many of these films have broad resistive transitions with a shoulder as in Figure 5 and long low resistance tails. The film with the best T_c had an as deposited composition of Cu/Y=2.88 and Ba/Y=2.04, and its resistance-temperature characteristic is shown in Figure 8.

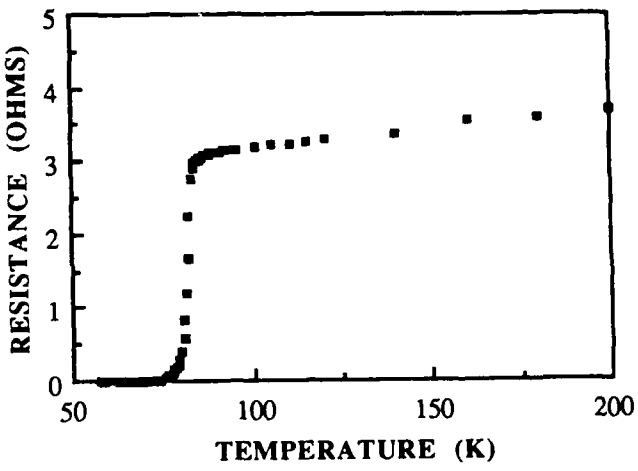

Figure 8: Resistance as a function of temperature for a film on MgO. Cu/Y=2.88, Ba/Y=2.04. Annealed at 850 °C for 3 hr.

ZrO_2 buffer layers were used for films on Si, sapphire and Al_2O_3 substrates as described above. Detailed Auger analysis of the performance of the buffer layers on silicon and sapphire substrates has been previously reported[9]. The key features of the performance of these buffer layers determined by the Auger analysis was that ZrO_2 appears to form a stable buffer layer for $YBa_2Cu_3O_{7-\delta}$ films on sapphire. In contrast with the films on silicon, the films on sapphire with 0.2 μm buffer layers exhibited zero resistance for a variety of compositions and there was an improvement in the resistive transition with increased annealing duration similar to that observed for MgO substrates. Superconducting films were achieved on silicon when thicker 0.5 μm and 0.9 μm buffer layers were deposited.

We have extended the use of ZrO_2 buffer layers to form superconducting $YBa_2Cu_3O_{7-\delta}$ films on Al_2O_3 substrates. The resistance-temperature characteristic of a film with an as deposited composition of Cu/Y=3.10 and Ba/Y=1.88 is shown in Figure 9. The sample was annealed for 180 minutes at 850 °C. It had a metallic normal state characteristic and reasonably sharp transition. Its critical temperature was 72 K due to a low resistance tail on the transition. The distribution of critical temperature for films of several compositions on alumina substrates is shown in Figure 10. The dependence of the properties of these films on composition more closely resembles that of films on MgO than on SrTiO3.

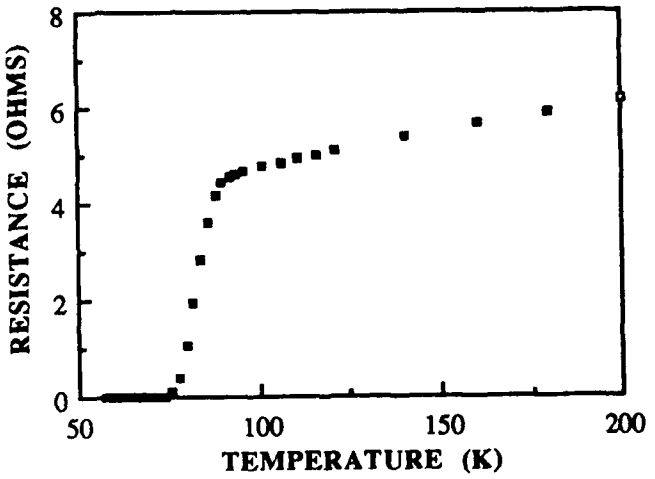

Figure 9: Resistance as a function of temperature for a film on alumina with a ZrO_2 buffer layer. Cu/Y=3.10, Ba/Y=1.88. Annealed 3 hr at 850 °C.

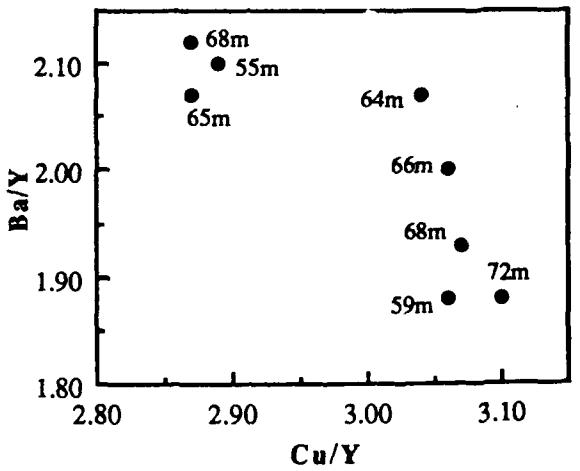

Figure 10: Distribution of T_c for films of various composition on alumina with a ZrO_2 buffer. Annealed at 850 °C for 3 hr. The number with each point is T_c while the letter shows the normal state behavior: metallic or semiconducting.

Figure 11 shows the normalized resistance as a function of temperature for three films formed on $LaAlO_3$. The films were deposited at the same time with a composition of Cu/Y=3.00 and Ba/Y=2.25 and a twelve layer sequence, but a total thickness of only 0.5 μm before annealing. The films was annealed at 950 °C for 45 minutes with heating rates of 50 °C/minute or 100 °C/minute or a slow push. All of the films had a metallic characteristic above the transition temperature. The film which received the slow push into the furnace had the highest critical temperature, approximately 80 K.

Microstrip ring resonators have been designed for measurement at 30 GHz on $LaAlO_3$ and MgO substrates. Films on these substrates are being patterned into ring resonators via lift-off lithography.

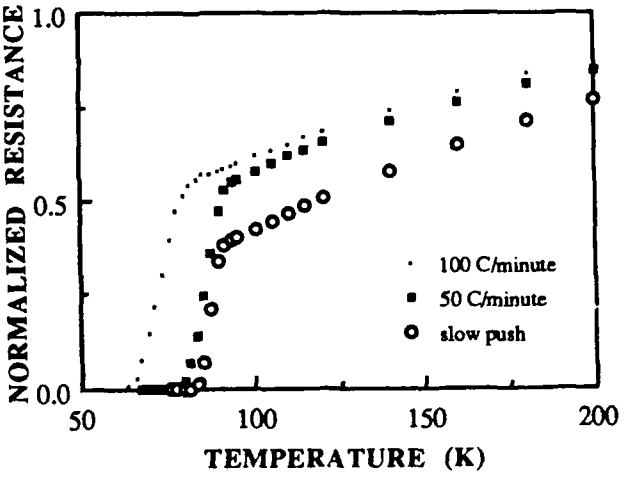

Figure 11: Normalized resistance as a function of temperature for three films $LaAlO_3$ with different annealing procedures. Cu/Y=3.00, Ba/Y=2.25. Annealed 45 minutes at 900 °C.

4.0 SUMMARY AND CONCLUSIONS

We have employed multi-layer sequential electron beam evaporation to form superconducting films on several different substrates. The best films have been formed of $SrTiO_3$ where we have achieved a critical temperature of 87 K. Superconducting films have also been achieved on MgO, sapphire, alumina and recently on $LaAlO_3$ substrates for which a critical temperature of 80 K was obtained. The superconducting films on $LaAlO_3$ and MgO are being used in the fabrication of microstrip ring resonators to allow testing of the microwave properties of the films at 30 GHz.

5.0 ACKNOWLEDGEMENTS

The authors would like to acknowledge the assistance on H. Y. To for many of the depositions on MgO and alumina substrates, J. J. Pouch for Auger measurements, and M. Stan for critical current density measurements. This research is supported by The National Aeronautics and Space Administration, Lewis Research Center under cooperative research agreement NCC 3-105.

THIS PAGE IS INTENTIONALLY BLANK

Abstract of Paper Presented at the
Workshop on High Temperature Superconductivity
23-25 May 1989 GACIAC PR 89-02

Focused Ion Beam Patterning of High T_c Superconducting Thin Films

P.A. Polakos and L.R. Harriott
AT&T Bell Laboratories
600 Mountain Avenue
Room 1E-234
Murray Hill, NJ 07974

ABSTRACT

A 20 KeV Ga ion beam was used to pattern features of sub-micron size in epitaxial films of superconductor material by physical sputtering. The films were prepared by coevaporation of BaF_2, Y, Cu on $SrTiO_3$ substrates and subsequently annealed in an wet oxygen ambient. The resulting films were nominally 2000 A thick with T_c > 90 K and j_c (77° > $10^6 A/cm^2$. Coarse patterning was done with photolithographic techniques. Bridge structures were then milled with the focused ion beam to have final dimensions which were small than 0.3μ in width and 0.5μ in length. The milling process and its end point were monitored with secondary ion mass spectroscopy. Bridges with dimensions as small as 0.5μ showed no change in T_c or j_c.

We have demonstrated that focused ion beam micromachining is capable of producing sub-micron superconducting structures and is a suitable technique for fabricating devices such as SQUIDs and the study of grain boundary effects in the films.

THIS PAGE IS INTENTIONALLY BLANK

Abstract of Paper Presented at the
Workshop on High Temperature Superconductivity
23-25 May 1989 GACIAC PR 89-02

Low Surface Resistance Thin Films of $Tl_2Ca_2Ba_2Cu_3O_{10}$ Produced by Chemical Deposition and Laser Ablation*

W.L. Olson, M. Eddy, T.W. James, McD. Robinson,
D.D.P. Casavant, E.J. Smith, A. Cardona, and R.B. Hammond
Superconductor Technologies Inc.
460 Ward Drive, Suite F
Santa Barbara, CA 93111

ABSTRACT

We report the synthesis and characterization of thin films of $Tl_2Ca_2Ba_2Cu_3O_{10}$ produced by both chemical deposition and laser ablation on a variety of substrates including single crystal magnesia and sapphire. The best films show single-phase x-ray diffraction spectra with rocking curves as narrow as 0.28°, zero resistance transitions of 111 K, normal-state resistivities of 300 microohm-cm, and magnetic susceptibility transitions as narrow as 5 K. We have studied the millimeter-wave surface resistance of several films at 148 GHz, and measured surface resistances as low as 250 mohms at 77 K. This is the lowest measured surface resistance for any superconductor at this temperature and frequency. It scales (as the frequency squared) to nine times better than oxygen-free high-purity copper (OFHC) at 77 K.

We are currently developing these films for applications in passive microwave and millimeter-wave electronics. We are investigating applications as low noise, low loss delay lines; high Q, low loss resonators; low loss phase shifters; etc. We shall report progress in the development of the thin film materials as well as the development of practical superconducting microwave devices.

*Partially supported by US DARPA under Contract No. N00014-88-C-0713.

THIS PAGE IS INTENTIONALLY BLANK

Presented at the Workshop on High Temperature Superconductivity
23-25 May 1989 GACIAC PR-89-02

Triode Magnetron Sputtered Superconducting Y-Ba-Cu-O Thin Films

George F. McLane and Robert L. Pfeffer
U.S. Army Electronics Technology and Devices Laboratory
Fort Monmouth, New Jersey 07703-5000

William Savin
New Jersey Institute of Technology
Newark, New Jersey 07102

Christopher Wrenn
Vitronics, Incorporated
Eatontown, New Jersey 07724

Abstract

Triode magnetron sputtering has been used to deposit Y-Ba-Cu-O thin films from a $YBa_2Cu_3O_x$ target. To circumvent the resputtering effect observed in the area directly above the target, substrates were placed outside this re-sputtering region. Films deposited onto unheated MgO substrates were amorphous and insulating, with copper-rich compositions as determined by RBS measurements. Post-deposition annealing in oxygen at temperatures in the range 850-900°C produced films with semiconductor-like properties. Rapid heat-up of films to around 900°C in a He environment followed by slow cooling in oxygen produced films which exhibited a linear metal-like decrease in resistance when cooled from room temperature with superconducting onset temperatures around 90K and a broad transition to zero resistance.

1.0 Introduction

Since the discovery of high temperature superconducting $YBa_2Cu_3O_x$, many techniques have been used to deposit this material in thin film form, including electron beam deposition,[1] laser ablation,[2] and sputtering.[3] Single-target sputtering offers a potentially simple technique for thin film deposition, but establishment of the correct film composition can be difficult. Among the parameters which have been found to affect film composition are substrate temperature, gas pressure, and target-substrate distance and orientation. Films deposited onto unheated substrates require a post-deposition annealing process to establish the proper crystallinity and oxygen content. This paper describes results obtained through use of a triode magnetron dc sputtering technique to deposit Y-Ba-Cu-O films from a $YBa_2Cu_3O_x$ target onto unheated MgO substrates, followed by high temperature annealing. Film characteristics are determined by Rutherford backscattering spectrometry (RBS), x-ray diffraction (XRD), scanning electron microscope (SEM), energy dispersive x-ray analysis (EDAX), and four-point probe electrical resistance measurements.

2.0 Experiment

Triode magnetron dc sputtering was used to deposit Y-Ba-Cu-O thin films from a 2.25 inch diameter $YBa_2Cu_3O_x$ target (Lambertville Ceramics) in 10^{-3} torr argon atmosphere with a power level of 120 watts. Films were deposited onto unheated MgO (100) substrates, and the composition of these as-deposited films was determined by RBS measurements. Post-deposition annealing was performed to establish the proper film crystallinity and oxygen content. This was done by heating the films to the 850-900^{o}C range in a furnace with flowing oxygen followed by slow cooling in oxygen, and also by rapidly heating the films in a He atmosphere to around 900^{o}C followed by slow cooling in oxygen.

1. R.B. Laibowitz, R.H. Koch, P. Chaudhari, and R.J. Gambino, Phys. Rev. B35, 8821 (1987).

2. S. Venkatesan, X.D. Wu, B. Dutta, A. Inam, M.S. Hegde, D.M. Hwang, C.C. Chang, L. Nazar, and B. Wilkens, Appl. Phys. Lett. 54, 581 (1989).

3. R.E. Somekh, M.G. Blamire, Z.H. Barber, K. Butler, J.H. James, G.W. Morris, E.J. Tomlinson, A.P. Schwarzenberger, W.W. Stobbs, and J.E. Evetts, Nature 326, 857 (1987).

In situ electrical resistance measurements were made on some films during oxygen anneals using platinum probes contacted to the film surface with silver paste.

Post-deposition film structure was studied using XRD, SEM, and EDAX analyses. Four-point probe electrical resistance measurements were performed on the annealed films from room temperature down to liquid helium temperatures. Electrical contacts were made by indium soldering gold wires onto sputter deposited gold dots.

3.0 Results

When dc sputtering was performed in the "sputter-up" configuration onto large area substrates such as glass plate, it was observed that in the area directly above the target the films were appreciably thinner than in areas off to the side of the target. In some cases, no film at all was deposited in the area directly above the target. This "resputtering" effect has been observed by others,[4] and has been attributed to the presence of sputtered negative oxygen ions which are accelerated away from the negatively biased target toward the growing film. These energetic ions can affect film growth and composition by resputtering the film away as it is being deposited.

RBS measurements were performed on deposited films as a function of position on the substrate for a target-substrate distance of eight inches. The measured Ba/Y and Cu/Y ratios of the films are shown in Figure 1 as a function of the distance away from the point on the substrate intersected by a line which is perpendicular to the target surface at its center. In the region directly above the 2.25-inch diameter target, the Ba and Cu atoms have been preferentially resputtered away. The dependence of film thickness on substrate position is also shown in Figure 1, indicating that the film is thinner than expected in the area directly above the target.

The simplest route was taken to circumvent this resputtering effect, namely to place the substrate outside the resputtering area.[5] The target-substrate geometry chosen for film growth is depicted in Figure 2. A typical RBS measurement for a film

4. S.I. Shah and P.F. Garcia, Appl. Phys. Lett. 51, 2146 (1987).

5. R.L. Sandstrom, W.J. Gallagher, T.R. Dinger, R.H. Koch, R.B. Laibowitz, A.W. Kleinsasser, R.J. Gambino, B. Bumble, and M.J. Chisholm, Appl. Phys. Lett. 53, 444 (1988).

deposited on a substrate at this location is shown in Figure 3, which gave a film composition of $Y_{1.1}Ba_2Cu_{3.8}O_x$. Although the films were copper-rich, results of other workers [6-8] have indicated that copper-rich material can produce good quality superconductors. In fact, excess copper acts as a fluxing agent and promotes grain growth in these materials.[6]

The as-deposited films were generally brownish in color, semitransparent, and insulating. High temperature annealing in an oxygen atmosphere is normally done to form the proper crystallinity and oxygen content necessary for $YBa_2Cu_3O_x$ superconductors. The initial furnace anneals were performed completely in one atmosphere of oxygen, with four-point probe resistance measurements performed in situ during some of these anneals. Resistance versus temperature curves measured during annealing for two of the films are shown in Figures 4(a) and 4(b) and are similar to results reported by other workers.[9-11] Both films exhibit a decrease in resistance upon slow heating in oxygen from room temperature up to about 650°C, after which the curves show distinctly different characteristics.

Above 675°C, film 29-4 resistance increases with temperature and reaches a maximum at about 750°C before decreasing sharply again as it approaches the maximum anneal temperature of 870°C. Upon cooling slowly from this temperature, the resistance decreases in a metal-like manner. For film 29-3, however, as the temperature is increased above 675°C its resistance continues to decrease until 700°C, at which point it drops precipitously by

6. A.H. Hamdi, J.V. Mantese, A.L. Micheli, R.A. Waldo, Y.L. Chen, C.A. Wong, M.M. Karmarkar, and K.R. Padmanabhan, J. Mater, Res. 3, 1311 (1988).

7. N. Yang, J.H. Kung, and P.T. Wu, J. Crystal Growth 91, 439 (1988).

8. A.F.J. Levi, J.M. Vandenberg, C.E. Rice, A.P. Ramirez, K.W. Baldwin, M. Anglowar, A.E. White, and K. Short, J. Crystal Growth 91, 386 (1988).

9. A. Davidson, A. Palevski, M.J. Brady, R.B. Laibowitz, R. Koch, M. Scheuermann, and C.C. Chi, Appl. Phys. Lett. 52, 157 (1988).

10. S.I. Shah, Appl. Phys. Lett. 53, 612 (1988).

11. P. Alnot, R. Cabanel, J.Chazelas, G. Creuzet, D. Dieumegard, J.P. Ganne, G. Garry, R. Korman, J.C. Mage, J. Olivier, I. Zaguire, Solid State Commun. 67, 275 (1988).

more than an order of magnitude. Further temperature increase results in a slight increase in film resistance up until about 800°C where contact was lost to the film. Of all the films for which in situ resistance measurements were made during annealing in oxygen, about half of them had resistance versus temperature curves similar to that of figure 4(a) and the other half were similar to figure 4(b).

The resistance versus temperature curve of Figure 4(a) is similar to that reported by Davidson, et al,[9] who measured a local maximum in the curve at around 700°C, followed by a sharp drop at 750°C which they attributed to the creation of $YBa_2Cu_3O_x$. It is reasonable to assume that the extremely sharp drop in resistance at 700°C shown in Figure 4(b) could also be due to the formation of this structure. On the other hand, x-ray diffraction measurements performed by Shah[10] on similarly annealed films have shown that the first formation of crystalline peaks occurs around 500°C. The small indentation in the Figure 4(b) curve in the temperature range 500-550°C could correspond to this early crystalline formation.

Four-point probe electrical resistance measurements were made on films 29-3 and 29-4 as they were cooled from room temperature to liquid helium temperatures. The results of these measurements are shown in Figure 5. Upon cooling from room temperature both films displayed semiconductor-like properties with resistance increasing as temperature is lowered. Although the resistance for both films eventually dropped upon cooling below 75K, zero resistance was not achieved for either film at the lowest temperatures reached. These results are typical for films which were completely annealed in oxygen. Of all films annealed this way, the best one achieved zero resistance at 30K after exhibiting a semiconductor-like characteristic at higher temperatures.

In an attempt to improve the quality of these films, a different annealing technique[9] was applied which consisted in a rapid heat-up of the films in the presence of He followed by slow cooling in oxygen. Figure 6 shows four-point probe resistance versus temperature curves measured on two films annealed in this manner. It is evident that this method of annealing has a very beneficial effect on film superconducting characteristics. These films were rapidly heated to 900°C in flowing He, kept at this temperature for 1-3 minutes, and then cooled down to room temperature in flowing oxygen over a period of 2-3 hours. The curves in Figure 6 show a linear metal-like decrease in resistance when cooled from room temperature with a superconducting onset temperature around 90K. The transition to zero resistance was rather broad, zero resistance being achieved in the temperature range 70-72K. Broad transitions such as these

are usually attributed to material inhomogeneities, and could possibly be related to the presence of excess copper for the films reported here.

RBS measurements performed on a film deposited on a carbon substrate indicated that oxygen was present in a quantity (O_{10}) which was in excess of that required to form the orthorhombic phase (O_7) of the material. Heating these films in the presence of He is known to remove oxygen from the films.[9] Therefore, the improved results achieved by heating the films in He could be due to the removal of excess oxygen, which is possibly inhibiting the formation of the proper material structure.

The x-ray diffractometer curve of Figure 7 for a He annealed film exhibits traces which indicate an orthorhombic structure for the film. The microstructure of a similarly annealed film shown in Figure 8 indicates a surface roughness associated with boulder-like structures interspersed with needle-like structure regions. Energy dispersive x-ray analysis revealed regions having Ba and Cu compositional inhomogeneities.

In summary, triode magnetron dc sputtering from a $YBa_2Cu_3O_x$ target produced a "resputtering" effect which was very pronounced in the area directly above the target. Films deposited onto unheated MgO substrates placed outside this area were Cu-rich. Poor results were obtained when the films were post-deposition annealed in oxygen only. Rapid heat-up of the films in He to $900^{o}C$ followed by slow cooling in oxygen greatly improved film superconducting characteristics.

The authors thank Donald Eckart for SEM and EDAX measurements on the films.

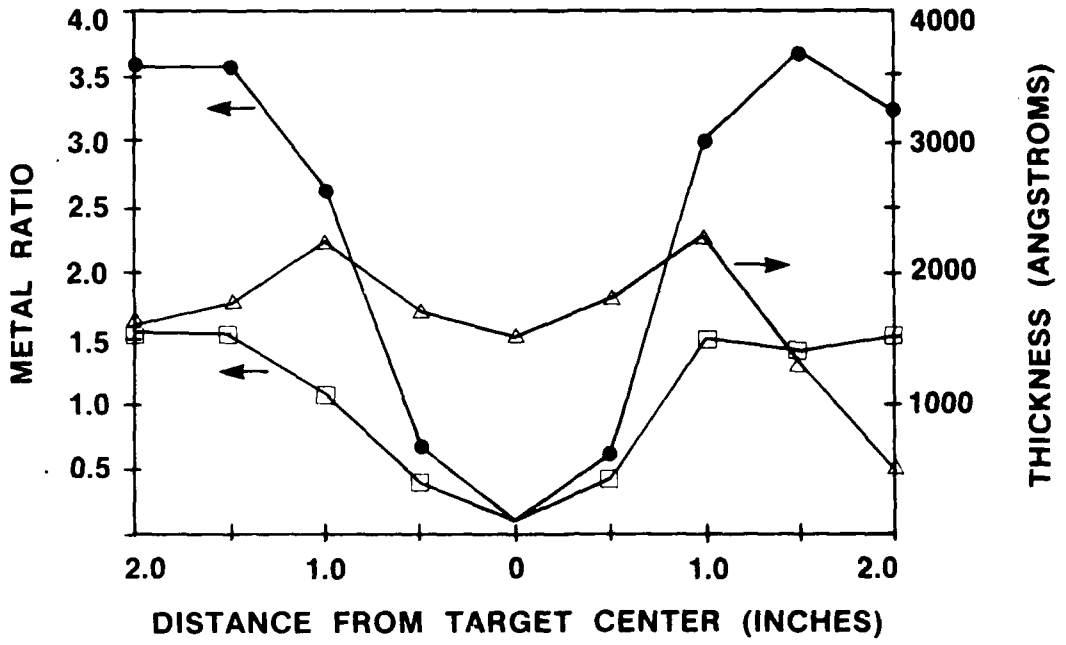

Figure 1. Ba/Y (□) and Cu/Y (●) ratios for deposited films as a function of distance from point directly above the target. Also shown is film thickness (▲) as a function of distance from point directly above the target.

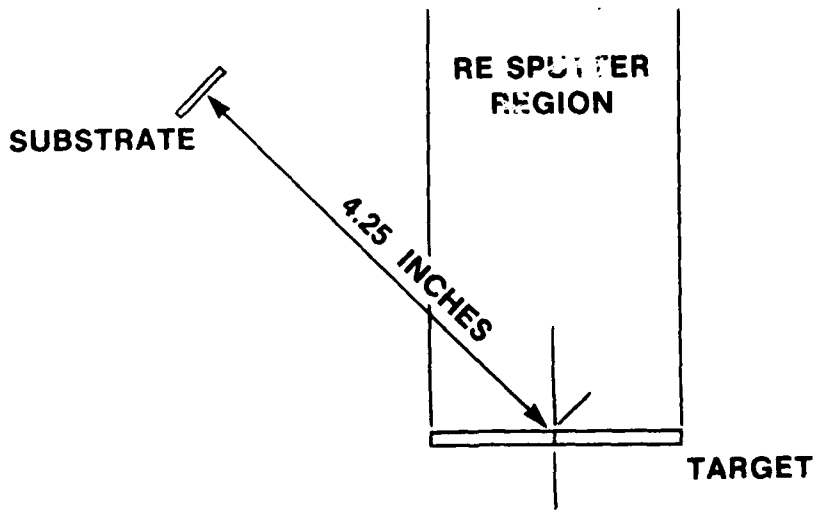

Figure 2. Target-substrate orientation used for thin film deposition.

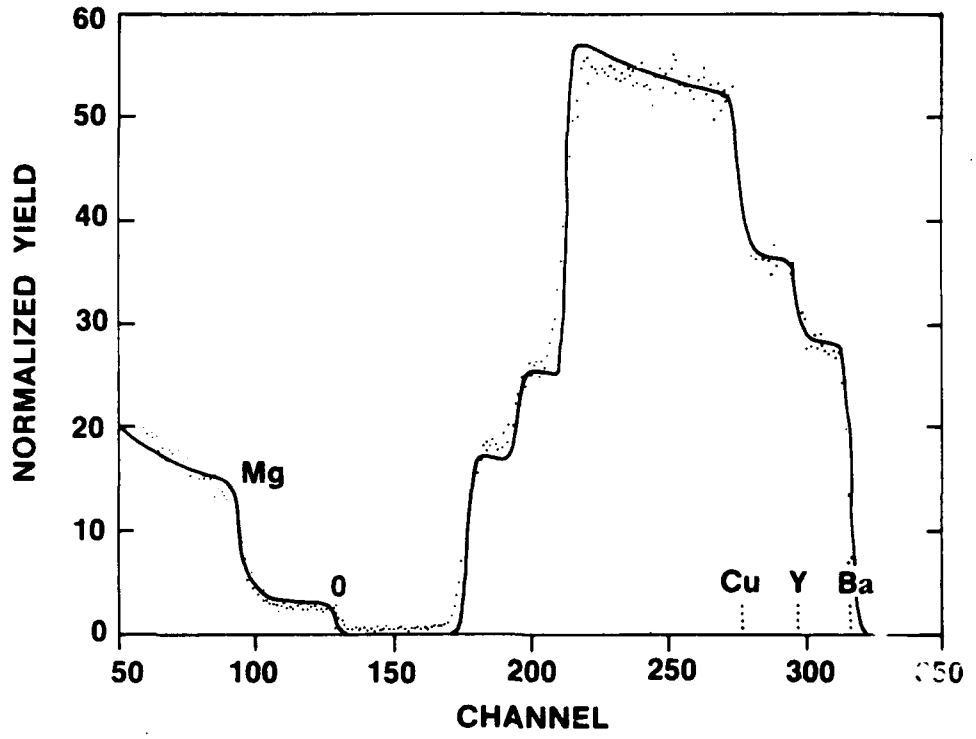

Figure 3. Rutherford backscattering spectrometry data and simulation curve for typical as-deposited film. The simulation curve (solid line) yielded a composition of $Y_{1.1}Ba_2Cu_{3.8}O_x$

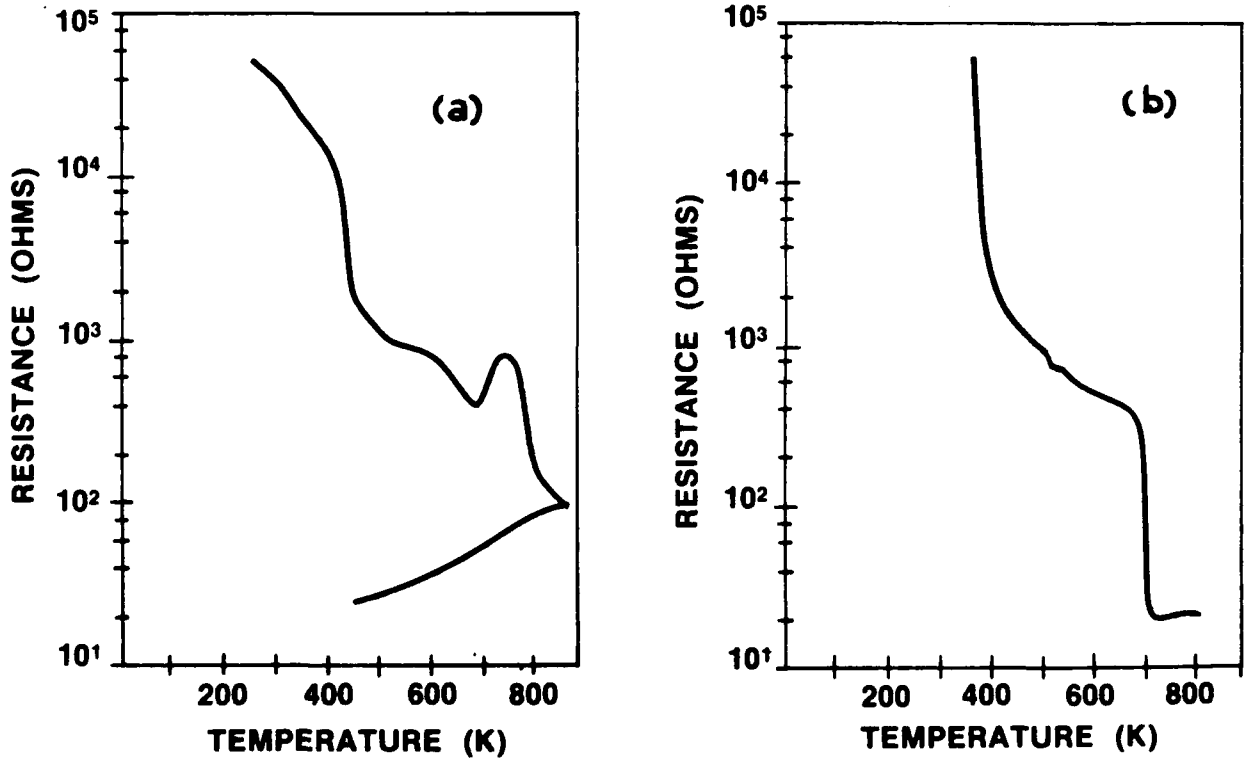

Figure 4. Electrical resistance vs. temperature measured during oxygen anneal for film 29-4 (curve a) and film 29-3 (curve b).

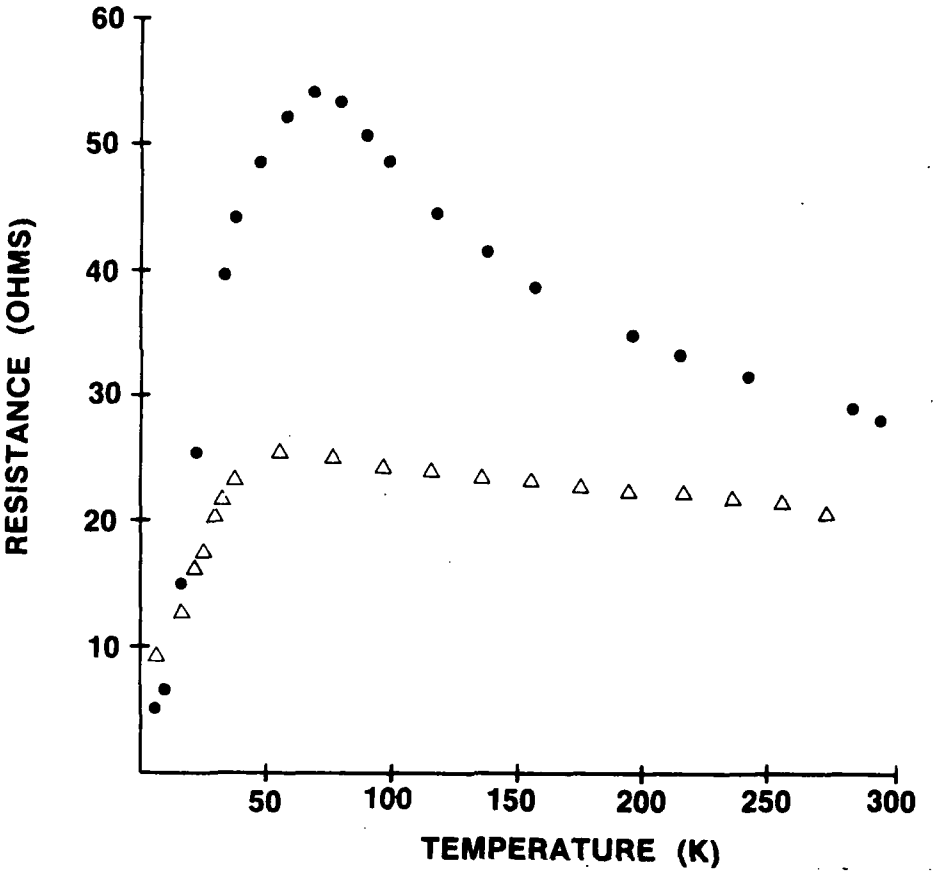

Figure 5. Electrical resistance vs. temperature measurements for film 29-3 (▲) and film 29-4 (●) measured between room temperature and liquid helium temperature.

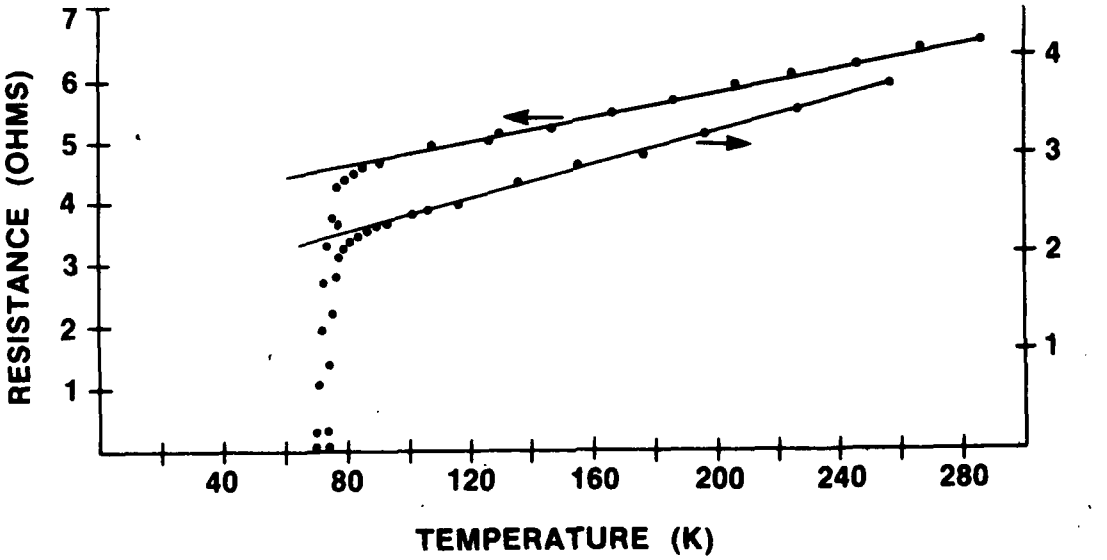

Figure 6. Electrical resistance vs. temperature measurements for two films annealed by rapidly heating to 900°C in He followed by cooling in oxygen. The zero resistance temperatures were measured as 70K and 72K.

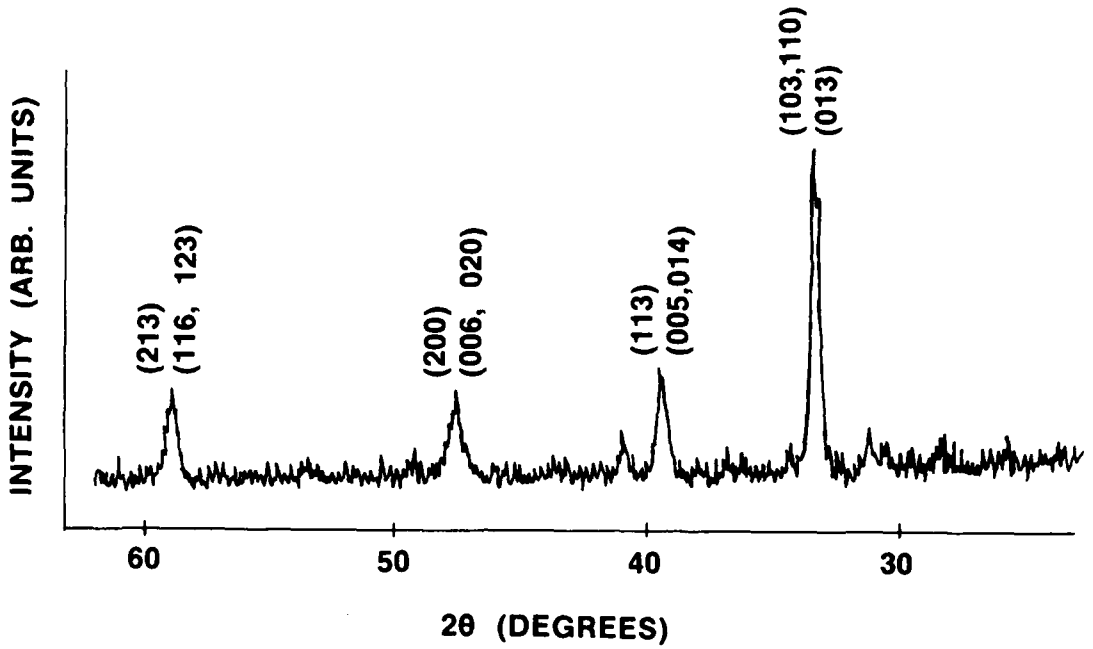

Figure 7. X-ray diffraction measurements for a film annealed by rapidly heating in He followed by cooling in oxygen.

Figure 8. Scanning electron micrograph of a film annealed by rapidly heating in He followed by cooling in oxygen.

Presented at the Workshop on High Temperature Superconductivity
23-25 May 1989 GACIAC PR-89-02

Light Detection using Superconducting Films.

U. Strom, J.C. Culbertson, and S.A. Wolf
Naval Research Laboratory
Washington, D.C., 20375

ABSTRACT

Light detection by superconducting films is reviewed. Possible detection mechanisms discussed include that expected for arrays of boundary Josephson junctions or weak links, as well as excitations specific to two-dimensional superconducting films. The role of such detection mechanisms in the optical response of high temperature superconductors is discussed. Evidence is presented for the observation of a nonequilibrium response in high T_c films. This type of response may have potential detector applications in addition to the ubiquitous bolometric response.

1. INTRODUCTION

Superconductors have been considered for use as sensitive radiation detectors as early as 1938 when Andrews[1] and Goetz[2] proposed the development of a bolometer for operation in the infrared spectral region. Such a device, based on a thin tantalum wire, was first demonstrated in 1942 by Andrews et al[3]. Subsequent efforts[4] culminated in the development of a very sensitive bolometer with a noise equivalent power NEP $\approx 1.7 \times 10^{-15}$ W/Hz$^{1/2}$ at 1 K. These bolometers were inherently slow devices, because optimizing the responsivity involves coupling the photon absorber weakly to a heat bath.

After the discovery of the Josephson effect in 1962 it became evident that sufficiently resistive films and compressed powders could be viewed as three-dimensional arrays of Josephson junctions. A single Josephson point contact tunnel junction had been shown[5,6] to be a sensitive detector of microwave radiation. Arrays of such detectors occur naturally in resistive films or powders; the synchronization of series arrays of microjunctions or bridges, which has been experimentally observed [7-10], means powders and films can be sensitive detectors of microwave and far infrared radiation. The increased detector noise in such structures, compared to a single junction device, has limited their usefulness. The most sensitive microwave detector yet developed is the superconductor/insulator/superconductor (SIS) tunnel junction, in which quasi-particle tunneling (rather than pair tunneling) occurs with the assistance of a microwave or far infrared photon. The reader is referred to the recent review by Tucker and Feldman[11] on the properties of these devices. The SIS quasi-particle tunnel junction is potentially sensitive to photons with energies several times larger than the superconducting energy gap. For a proposed gap of around 50 μm for $Y_1Ba_2Cu_3O_7$ (YBCO) this could imply quantum noise limited photon detection at wavelengths as short as 25 μm. In the absence of such a device we are limited to the use of superconducting films as radiation detectors. The purpose of this paper is to review briefly the previous use of superconducting films as radiation detectors, and then to present recent data on the photoresponse of YBCO which illustrates some of the potential of this high T_c material as a radiation detector.

2. 3-D Films - Arrays of Josephson Junctions

(a) Compressed powders

The electrical and optical properties of compressed powders of superconducting grains have been investigated by several groups. For example, Kovalenko and Leshchenko[12] investigated fine Nb powders which were compressed into thin glass tubes. After sufficient compression a dc current could be passed through the composite. They then investigated the change in resistance R when the sample was illuminated by the long wavelength portion of the black body radiation which had passed through a far infrared cutoff filter. They observed no significant response when "clean" Nb particles were used (i.e. for which the oxide coating had been chemically etched), but observed a distinct response near the resistive onset of the composite when the sample was purposefully oxidized. This observation was interpreted in terms of the direct coupling of the infrared radiation to the Josephson junction. Unfortunately, no attempt was made to determine the relative response to photons with energies above and below the Nb superconducting energy gap. These materials have several significant deficiencies as detectors, including irreproduceability, large electrical noise, as well as hysteresis effects. Nevertheless, these composites are very instructive for demonstrating the principle of the enhanced microwave and infrared detection of an array of Josephson junction.

(b) Films

Rose and coworkers[13,14] have made detailed investigations of the microwave and infrared response of Sn films as a function of the film sheet resistance. They also carried out noise measurements[15] on these samples which proved to be sensitive microwave detectors. Finally, they investigated the sensitivity of their films to variations in microwave power, temperature T, and current I. Details can be found in the review article by Rose, Bertin, and Katz[16]. The results of Rose and coworkers are very pertinent for the interpretation of optical response measurements carried out recently by others on high temperature superconducting films.

In Fig.3 of Ref.13 Bertin and Rose display the optical response of two Sn films with sheet resistances of 185 and 1600 Ω/square, respectively. They used both 9.84 GHz and 1 μm photons. Each film exhibited a bolometric response which is proportional to I dR/dT, where I is the dc current passing through the film and R is the film resistance at temperature T. There is also a second component at lower temperatures which is peaked near the R = 0 onset of the resistance. The lower temperature component is referred to by Bertin and Rose as the "direct" mechanism. The direct component is greatly enhanced over the bolometric peak for the film with the larger sheet resistance. The direct response is <u>not</u> observed for 1 μm incident light; only the bolometric peak near the dR/dT maximum is observed. Rose and coworkers interpreted these results in terms of the direct modulation of the intergrain Josephson current by microwave radiation. This mechanism will be effective for microwave energies which are comparable to or less than the gap energy of the appropriate superconductor. At higher energies, pair breaking processes will compete. In the Sn films such pair breaking processes did not lead to a detector response near R = 0, but only to the bolometric response near the dR/dT maximum. There may be various reasons for the latter observation: the penetration depth of infrared light may have been much shorter than the film thickness; the film may have been metallic in the normal state (in spite of the high sheet resistance); or the approach to R = 0 does not involve a 2-D

topological phase transition. As will be shown in the next section, the 2-D NbN/BN and YBCO films considered here generally exhibit a distinct response near R=0 to above gap light.

Suzuki, Enomoto, Murakami and J. Noda[17-20] have investigated the optical response of $Ba_1Pb_{0.7}Bi_{0.3}O_3$ (BPB) films. For $T << T_c$ these films exhibit the characteristics of boundary Josephson junctions, whereas at higher temperatures they change over to weak link I-V curves observed for shunted junctions. Suzuki et al investigated the optical response primarily in the less noisy weak link limit. They observed an optical response which is fast (GHz) and increases with increasing wavelength of the incident radiation. The latter observation may suggest that a photon rather than bolometric mechanism is responsible for the PR in BPB. This observation is also consistent with the decrease in response with increasing frequency expected for a shunted Josephson detector. The grain sizes reported for the BPB films were about 0.2 μm, comparable to the thickness of the films. Although a two-dimensional (2-D) behavior of these films is possible, no evidence for this was provided. Nevertheless, it is clear that the BPB films are competitive with semiconductor detectors in the far infrared spectral range, especially when both high speed and high sensitivity are required. The competitiveness of the films as sensitive detectors for shorter wavelength radiation[20] (< 10 μm) is less certain.

3. 2-D Films

It is known that sufficiently thin superconducting films undergo a topological phase transition near a temperature T_c where the film resistance R approaches zero. This phase transition has been modeled as a Kosterlitz-Thouless (KT) transition[21] involving vortex-antivortex pair excitations. For $T < T_c$ the vortex-antivortex pairs are bound. Generally, $T_c < T_{co}$, where T_{co} is the mean-field Ginzburg-Landau transition temperature. The KT theory applies to a superconductor because for sufficiently thin granular superconductors there is a logarithmic interaction between vortices, provided the vortex separation is much less than the magnetic screening length and is much greater than the vortex core size.[22] These conditions are often realized in thin superconductors with high resistivity in the normal state.[23] The KT transition has been observed in many 2-D "low" T_c materials, including amorphous indium/indium oxide[24] and granular films of Al[25], NbN[26], as well as NbN/BN cermet[27].

Anodized NbN films, with effective thickness less than 10 nm, have been shown to be sensitive and fast detectors of photons and phonons[28]. The photoresponse for granular NbN/BN has been measured and the material was shown to be a sensitive detector of far infrared[29] as well as near infrared[30] light. The PR has a peak at a temperature near the resistive onset, i.e. near the KT transition temperature. Furthermore, the dependence of the PR on bias current is consistent with predictions of 2-D behavior. A preliminary measurement of the detector sensitivity has yielded a $D^* \approx 10^{-8}$ W/Hz$^{1/2}$. The important difference between the measurements for NbN/BN and those of Rose and coworkers for Sn is the response to above gap radiation. Rose and coworkers observed a response to near infrared light which was consistent with a bolometric mechanism near the dR/dT maximum. Their "direct" response near R = 0 was only observed for subgap radiation, i.e. in the microwave range. In contrast, the 2-D NbN/BN has a definite PR near the R = 0, which is observed for above gap as well as below gap radiation.

As will be shown in the next section, caution is advisable when interpreting temperature dependences of the PR. An upturn in the low T region does not in itself imply evidence for a nonbolometric mechanism, but may in fact be consistent with

a thermal model. There is evidence from the PR of NbN/BN to pulsed visible light that the PR for $T > T_c$ (the R = 0 onset) increasingly involves a thermal response mechanism. The PR for $T < T_c$ is considerably larger than can be interpreted in terms of the ratio of dR/dT and temperature dependent thermal factors. This conclusion is not inconsistent with the proposed physical mechanism that is envisioned for the PR of the 2-D materials, that is the light induced dissociation of vortex-antivortex pairs. Vortex pairs are likely to be pinned, whereas single vortices with a biasing current applied can be mobile and lead to dissipation in a manner as discussed by Bardeen and Stephen.[31]

4. High Temperature Superconductors

There has been much interest in the investigation of the new superconductors as high temperature radiation detectors. Many of the investigations have been concerned with the detection of microwave radiation. For example, Blazey et al[32] have investigated the superconducting glass like properties of various copper oxides. In this case the microwave absorption in the presence of a weak magnetic field is related to flux slippage. Jeffries at al[33] have observed a nonlinear response of bulk YBCO samples in the radio frequency region which they interpreted in terms of flux-quantized supercurrent loops containing Josephson junctions.

A very clear demonstration of the direct microwave coupling to Josephson junctions has been made by Afanasyev et al[34] who investigated the microwave (70 GHz) response of YBCO films as a function of temperature, current, and film sheet resistance. For example, a 1 μm thick polycrystalline YBCO film with a resistivity of 3×10^{-4} Ωcm at 300 K and critical current density $J_c = 100$ A/cm^2 at 77 K, exhibited the direct response near R = 0 around 85 K, as well as the bolometric response near the dR/dT maximum at 89 K. A more granular film with a factor of 10 higher resistivity was dominated by the direct response which was observed for temperatures as high as 65 K. These results clearly demonstrate that two distinct types of detection modes for microwave radiation are possible for YBCO, very similar to the observation of Rose and coworkers for low T_c materials. Our remaining discussion will focus on the possibility of observing these two detection mechanisms in high T_c films for above gap light with wavelength greater than 50 μm.

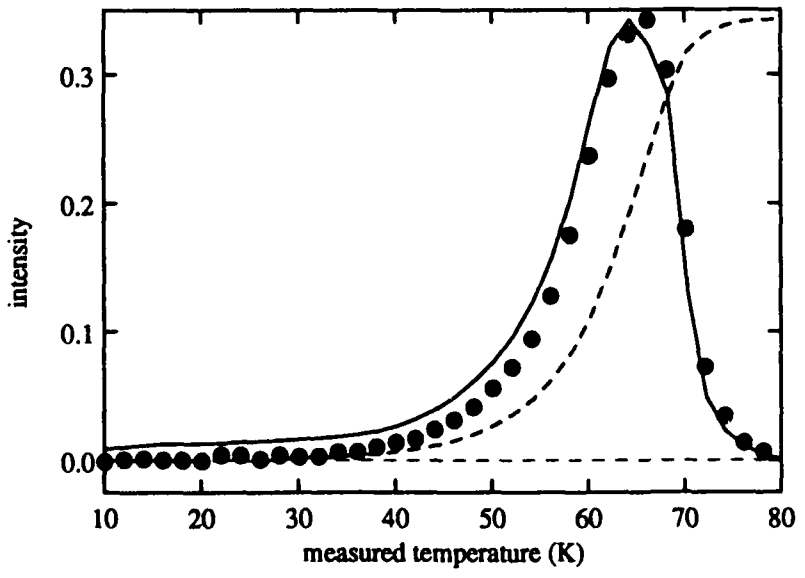

Figure 1. Photoresponse (solid lines) of a 0.6 μm thick $Y_{0.65}Ba_{1.44}Cu_{3.0}O_{7-x}$ film on MgO to a 1 mW HeNe laser light chopped at 100 Hz. Dashed curve - resistance R vs temperature measured under same exciting light conditions. Dots - dR/dT. Bias current = 1 mA.

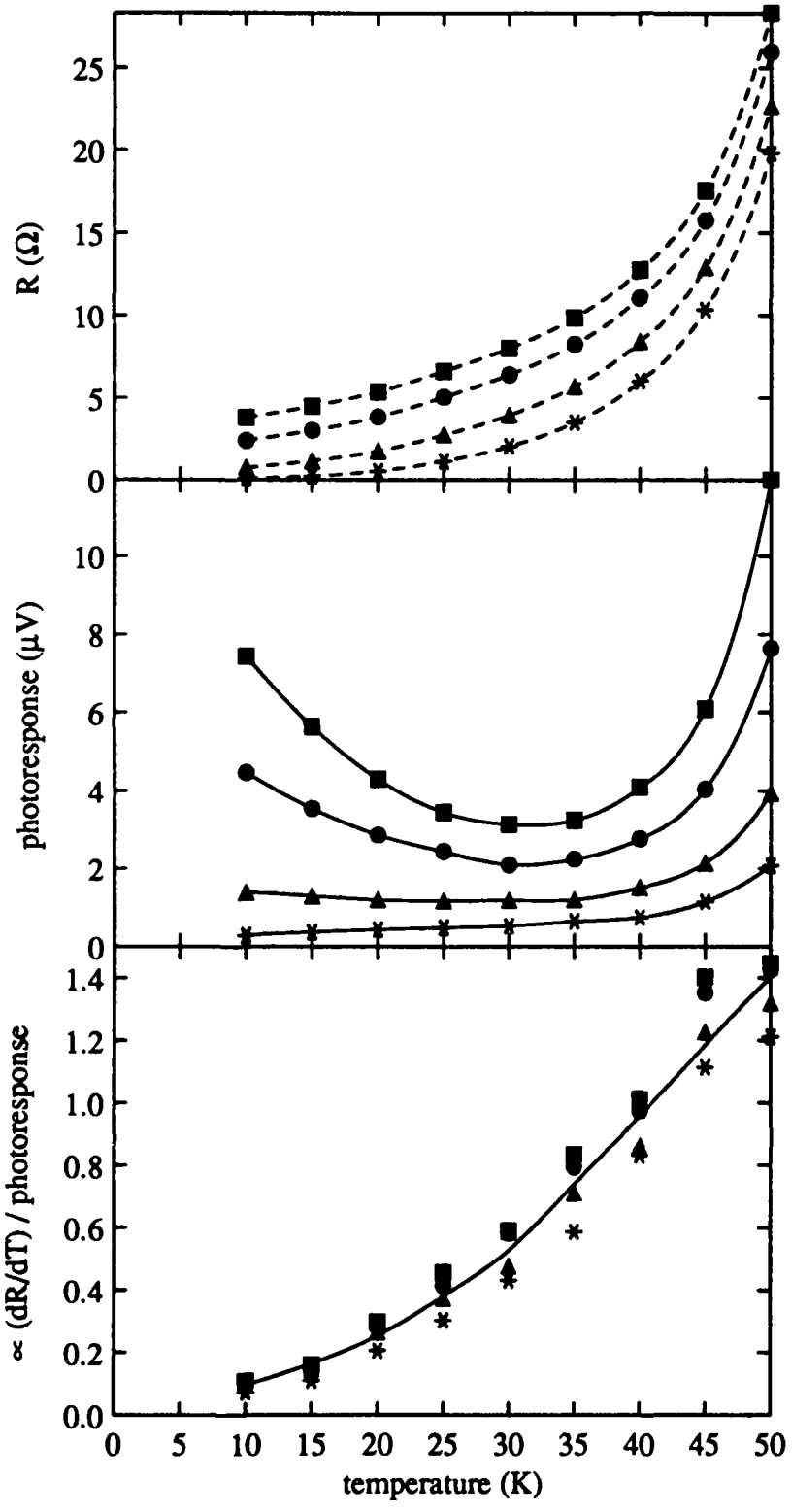

Figure 2. Temperature dependence of resistance (4-probe) for same film as in Fig. 2 for different bias currents (crosses - 1 mA, triangles - 2 mA, dots - 4 mA, squares - 6 mA).

Figure 3. Photoresponse vs temperature for same film as in Figs. 1 and 2 (crosses - 1 mA, triangles - 2 mA, dots - 4 mA, squares - 6 mA).

Figure 4. Plot of function (I dR/dT)/PR vs temperature for same film as in Figs. 1-3. (crosses - 1 mA, triangles - 2 mA, dots - 4 mA, squares - 6 mA).

The first report of a photoresponse to visible and far infrared radiation using YBCO by Leung et al[35] demonstrated the potential usefulness of high T_c films as radiation detectors. Subsequent reports by other research groups focussed on the question whether the PR of the high T_c films could be described by equilibrium mechanism, or if there was any evidence for a nonequilibrium response as suggested earlier by Testardi[36] for low T_c materials.

Various groups reported the observation of a high T_c infrared photoresponse which could be explained satisfactorily in terms of an equilibrium bolometric mechanism alone. Noteworthy here is the work of Forrester et al[37], as well as Brockelsby et al[38]. In fact, we have also observed that for certain YBCO films the PR is predominantly bolometric. A typical example of an YBCO film on MgO is shown in Fig. 1. The dashed curve represents R(T), the solid curve is the PR to a 1 mW HeNe laser, and the solid dots represent dR/dT, measured at the same 1 mA bias current under the same incident light conditions. It is seen that the PR is essentially bolometric. The small deviations between the PR and dR/dT can be accounted for by the temperature dependence of an effective thermal conductivity. Fig. 2 shows the film resistance in the low T region for bias currents of 1, 2, 4, and 6 mA, respectively. The increase in resistance with increasing bias current is directly reflected in an increase in the PR, as shown in Fig. 3. This increase in PR as the temperature approaches zero should not be confused with the PR near the finite temperature where the resistance R approaches zero, as observed for the microwave PR measurements by Afanasyev et al[34]. The film is driven into a resistive state, with dR/dT increasing with increasing bias current. The bolometer response is proportional to the product of dR/dT and $1/K_{eff}$, where K_{eff} is an effective thermal factor, which takes into account the film and the substrate. If the above statement is correct then a plot of dR/dT divided by the PR should yield a single curve, independent of bias current. This is approximately confirmed in Fig. 4.

The results shown in Figs. 1-4 do <u>not</u> prove the lack of a nonbolometric contribution to the PR. They only show that the PR is dominated by a bolometric response. However, it has recently been shown[37] that a nonbolometric component of the PR can be observed in high quality epitaxial films under conditions where the bolometric component is sufficiently reduced or suppressed. Specifically, Zeldov et al[39,40] have reported an enhanced PR near 85 K in an epitaxial film of YBCO which was deposited onto a substrate with a high thermal conductivity. The PR, which is orders of magnitude greater than would have been predicted by a thermal model alone, was interpreted[39,40] as due to photoenhanced flux creep. The nonbolometric PR was not as evident for a film grown on a substrate having a lower thermal conductivity; this substrate yielded a larger temperature rise in the film and a correspondingly larger bolometric response.

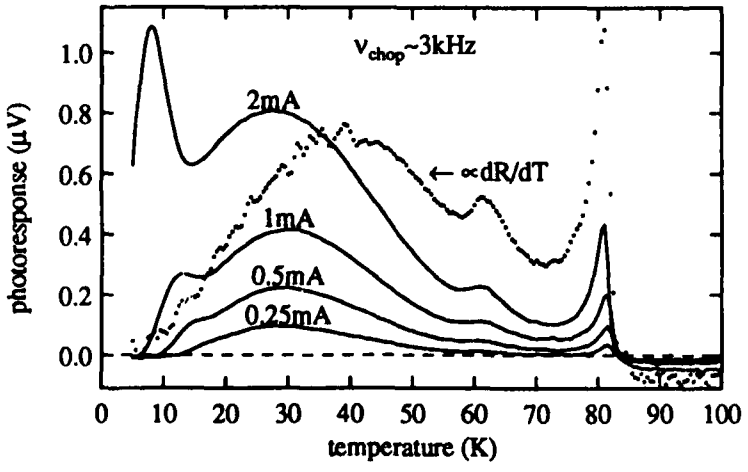

Figure 5. Photoresponse (solid lines) of 0.25 μm thick film of $Y_1Ba_{2.1}Cu_{3.4}O_{7-x}$ to a 1 mW HeNe laser (chopped at 3 kHz) for various bias currents. Dotted line - dR/dT measured concomitantly with photoresponse measurement using 2 mA bias current.

The 2-D type of PR which was observed for NbN/BN[32] near the KT phase transition temperature[27] has also been recently observed[41] for YBCO. This observation is perhaps to be expected since the KT transition was observed in epitaxial $Y_1Ba_2Cu_3O_7$ films[42] and even in crystals of $Bi_2Sr_2CaCu_2O_8$[43], as well as a single crystal of YBCO[44]. These observations have been interpreted in terms of the intrinsic 2-D character of the CuO planes. The PR then can be interpreted as due to the photoinduced dissociation of vortex-antivortex pairs, for $T \leq T_c$ where T_c is defined as the KT temperature. The results for a film of YBCO which has an onset of superconductivity near 80 K, but which does not reach a zero resistance state until 11 K, are shown in Fig. 5. The light source is a HeNe laser chopped at 3 kHz. The PR is dominated by a bolometric mechanism for $T > T_c$. The shift between the dR/dT curve, which was measured for a 2 mA current, and the PR for T between 15 K and 60 K is well accounted for by the temperature dependence of an effective thermal conductivity. The bolometric signal is seen to be linearly dependent on the bias current. The PR peak near 10 K is approximately quadratically dependent on bias current, as is expected on the basis of the observed I-V curves which are indicative of the KT transition. Figure 6 shows the PR for a chopping frequency of 15 kHz. It is evident that the PR is dominated by the peak near 11 K with only a weak bolometric response at higher temperatures. The data at 3 kHz and 15 kHz below 15 K can not be interpreted in terms of a bolometric response of the form $(1/K_{eff})(dR/dT)$ for any feasible T dependence of K_{eff}. A dependence $K_{eff} \propto T^3$ is the strongest T dependence expected. If the PR is entirely due to a bolometric mechanism with such a thermal conductivity ($\propto T^3$), then a plot of $(dR/dT)/(T^3$ PR) versus temperature should yield a straight line. The dash-dot curve in Fig. 6 is such a plot. The bolometric response between 25 K and 50 K approximates a straight line, suggesting an approximate T^3 dependence for K_{eff}, which is consistent with the expected temperature dependence of the thermal conductivity of MgO or the thermal boundary resistance between the YBCO film and the MgO substrate. The peak in the dashed curve near 18 K indicates that the temperature dependence of K_{eff} is weaker than T^3. At these lower temperatures, the thermal link (principally copper) between the MgO and the heater comes into play, and the "effective" thermal factor can depend on the specific heats and thermal conductivities of the various materials. We have performed measurements of the frequency dependence of the PR as a function of temperature to sort out the various thermal time constant regimes. These will be reported in detail elsewhere. The important point we wish to make with regard to Fig. 6 is that the ratio $(dR/dT)/(T^3$ PR) falls abruptly below 15 K and is effectively zero for $T < 10$ K. This observation is consistent with a model where the vortex pair excitations are unpaired by nonequilibrium processes for $T < T_c$. For $T > T_c$ bolometric depairing processes become increasingly important.

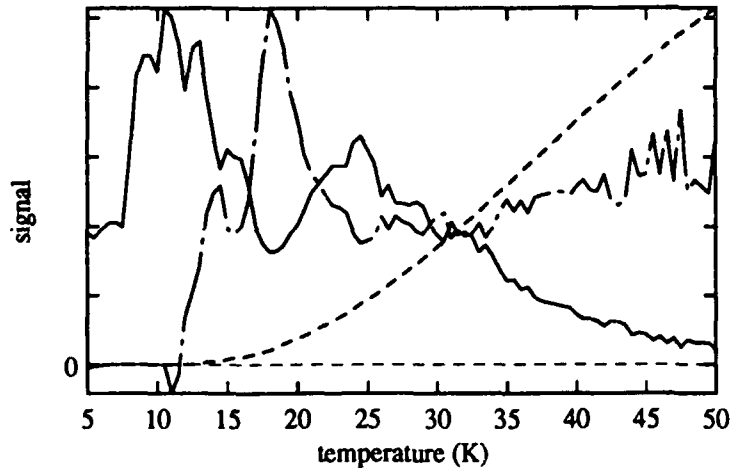

Figure 6. Photoresponse for same sample as in Fig. 5 for a 15 kHz chopping frequency.
Dashed curve $\propto R(T)$.
Dash-dot curve $\propto (dR/dT)/(T^3 PR)$.

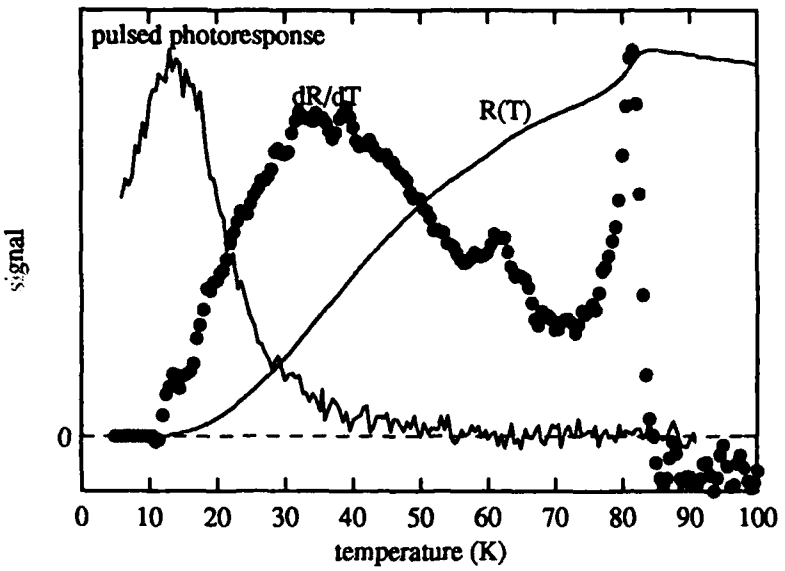

Figure 7. Pulsed photoresponse and film resistance measured as a function of temperature.

Figure 7 shows the response of the 0.25 μm thick YBCO film to pulsed visible light. The laser wavelength was 5838 Å and the pulse duration was 8 ns. The photoresponse of the film is characterized by a fast risetime (≈ 2 ns) comparable to that of the laser pulse and a slow decay (≈ 50 ns to decay to half the peak height). The photoresponse in Fig. 7 represents the integrated response in a 50 ns time window. The film resistance was measured was measured under the same conditions as the photoresponse measurements. The PR is seen to be dominated by a peak at temperatures near where R = 0. The width of this peak is a factor of two larger than that observed for chopped, lower power, HeNe laser light. We conclude that heating effects make significant contributions to the PR particularly for $T > T_c \approx 11$ K. These fast bolometric components are not evident for T > 50 K. For T < 10 K the shape of the PR vs temperature curve can not be interpreted in terms of thermal constants and dR/dT. A fast "nonthermal" response has also been reported by Frenkel et al[45] as well as Kwok et al[46] on oriented YBCO films. The interpretation of this fast optical response and its relationship to the PR observed for 2-D films needs to be established.

5. Conclusion

The focus in this brief review was to outline various detection mechanisms which may be of interest for potential infrared detector applications. We believe that there is sufficient evidence for mechanisms which are distinct from an equilibrium heating of the superconducting film, and which may provide attractive alternatives to a slow resistance edge bolometer. For consideration as devices however, noise and detectivity measurements have yet to be carried out. In addition, the 2-D KT PR must be scaled to significantly higher temperatures than the 11 K reported here. This should certainly be feasible, based on the PR measurement of 2-D NbN/BN films and the microwave PR measurements of Asanasyev et al[34] for YBCO films.

6. References

1. D.H. Andrews, American Philosophical Society Yearbook (1938), p. 132.
2. A. Goetz, Phys. Rev.**55**, 1270 (1939).
3. D.H. Andrews, W.F. Brucksch, W.T. Ziegler, and E.R. Blanchard, Rev. Sci. Instr.**13**, 281 (1942).
4. J. Clarke, G.I. Hoffer, P.L. Richards, and N.H. Yeh, J. Appl. Phys. **48**, 4865 (1977).
5. S. Shapiro, Phys. Rev. Lett. **11**, 80 (1963).
6. C.C. Grimes, P.L. Richards, and S. Shapiro, J. Appl. Phys. **39**, 3905 (1968).
7. T.D. Clark, Phys. Rev. Lett.**27A**, 585 1968); also, Phys. Rev. **B8**, 137 (1973).
8. D.R. Tilley, Phys. Rev. Lett. **33**, 205 (1970).
9. D.W. Jillie, J. Lukens, and Y.H. Kao, IEEE Trans. Mag-**11**, 671 (1975).
10. W.J. Ayer,Jr. and K. Rose, IEEE Trans. Mag-**11**, 6878 (1975).
11. J.R. Tucker, M.J. Feldman, Rev. Mod. Phys. **57**, 1055 (1985).
12. A.S. Kovalenko and G.F. Leshenko, IEEE Trans. Mag-**11**, 81 (1975).
13. C.L. Bertin and K. Rose, J. Appl. Phys. **39**, 2561 (1968).
14. C.L. Bertin and K. Rose, J. Appl. Phys. **42**, 13 (1971), and **42**, 631 (1971).
15. R.M. Katz and K. Rose, Proc. IEEE **61**, 55 (1973).
16. K. Rose, C.L. Bertin, and R.M. Katz, "Radiation Detectors", in *Applied Superconductivity*, vol. 1, ed. by K.L. Newhouse, Academic Press, N.Y. 1975, pp. 268-308.
17. M. Suzuki, Y. Enomoto, and T. Murakami, J. Appl. Phys. **56**, 2083, 1984.
18. Y. Enomoto, M. Suzuki, and T. Murakami, Jap. J. Appl. Phys. **23**, L333 (1984).
19. Y. Enomoto and J. Noda, Jap. J. Appl. Phys. **26** Suppl. 26-3, 1145 (1987).
20. Y. Enomoto, T. Murakami, and M. Suzuki, Physica **C153-155**, 1592 (1988).
21. J.M. Kosterlitz and D.J. Thouless, J. Phys.C **6**, 1181 (1973). 22. B.I. Halperin and D.R. Nelson, J. Low Temp. Phys. **36**, 599 (1979).
23. M.R. Beasley, J.E. Mooij, and T.P. Orlando, Phys. Rev. Lett. **42**, 1165 (1979).
24. A.F. Hebard and A.T. Fiory, Phys. Rev. Lett. **50**, 1603 (1983).
25. P.A, Bancel and K.E. Gray, Phys. Rev. Lett. **46**, 148 (1981).
26. S.A. Wolf, D.U. Gubser, W.W. Fuller, J.C. Garland, and R.S. Newrock, Phys. Rev. Lett. **47**, 1071 (1981).
27. D.U. Gubser, S.A. Wolf, W.W. Fuller, D. VanVechten, and R.W. Simon, Physica **135B**, 131 (1985).
28. K Weiser, U. Strom, S.A. Wolf, and D.U. Gubser, Appl. Phys. Lett. **52**, 4888 (1981).
29. M.Leung, U. Strom, J.C. Culbertson, J.H. Claasen, S.A. Wolf, and R.W. Siimon, Appl. Phys. Lett. **50**, 1691 (1987).
30. U. Strom, E.S. Snow, M. Leung, P.R. Broussard, J.H. Classen, and S.A. Wolf, SPIE **948**, 10 (1988).
31. J. Bardeen and M.J. Stephen, Phys. Rev. **140**, A1197 (1965).
32. K.W. Blazey, K.A. Mueller, J.G. Bednorz, W. Berlinger, G. Amoretti, E. Buhggiu, A. Vera, and F.C. Matacotta, Phys. Rev. B**36**, 7241 (1987).
33. C.D. Jeffries, Q.H. Lam, Y. Kim, L.C. Bourne, and A. Zettl, Phys. Rev. B**37**, 9840 (1988).
34. A.S. Afanasyev, A.F. Volkov, V.N. Gubankov, Yu. Ya. Divin, and P.M. Shadrin, IEEE Transac. Magnetics **25**, 2571 (1989).
35. M. Leung, P.R. Broussard, J.H. Claassen, M. Osofsky, S.A. Wolf, and U. Strom, Appl. Phys. Lett. **51**, 2046 (1987).
36. L.R. Testardi, Phys. Rev. B**4**, 2189 (1971).
37. M.G. Forrester, M. Gottlieb, J.R. Gavalev, and A. T. Braginski, Appl. Phys. Lett. **53**, 1332 (1988); IEEE Trans. Magnetics **25**, 1327 (1989).
38. W.S. Brocklesby, D. Monroe, A.F.J. Levi, M. Hong, S.H. Liou, J. Kwo, C.E. Rice, P.M. Mankiewich, and R.E. Howard, Appl. Phys. Lett. **54**, 1175 (1989).
39. Zeldov, N.M. Amer, G. Koren, and A. Gupta, Phys. Rev. B**39**, 9712 (1989).
40. Zeldov, N.M. Amer, G. Koren, A. Gupta, R.J. Gambino, and M.W. McElfresh, Phys. Rev. Lett. **62**, 3093 (1989).
41. J.C. Culbertson, U. Strom, S.A. Wolf, P. Skeath, E.J. West, and W.K. Burns, Phys. Rev. B**39**, 12359 (1989).
42. A.T. Fiory, Phys. Rev. Lett. **61**, 1419 (1988).
43. S. Martin, A.T. Fiory, R.M. Fleming, G.P. Espinosa, and A.S. cooper, Phys. Rev. Lett. **62**, 677 (1989).
44. N.C. Yeh and C.C. Tsuei, Phys. Rev. B**39**, 9708 (1989).
45. A. Frenkel, M.A. Saifi, T. Venkatesan, Chinlon Lin, X.D. Wu, and A. Inam, Appl. Phys. Lett **54**, 1594 (1989).
46. H.S. Kwok, J.P. Zheng, Q.Y. Ying, and R. Rao, Appl. Phys. Lett **54**, 2473 (1989).

THIS PAGE IS INTENTIONALLY BLANK

Presented at the Workshop on High Temperature Superconductivity
23-25 May 1989 GACIAC PR-89-02

HIGH TEMPERATURE SUPERCONDUCTING DETECTOR RESPONSE MODEL

24 May 1989

J. N. Farrell

Science Applications International Corporation
6725 Odyssey Drive
Huntsville, Alabama 35806

ABSTRACT

The purpose of the computational model developed in this work is to characterize the light-induced electrical response of a thin detector element made of high temperature superconducting material as a function of bias current, critical current, and transition temperature. This phenomenological model simulates results reported in several recent publications, including both bolometric and non-bolometric responses. This kind of model should be useful also for distinguishing various effects observed and for detector design optimization studies.

1. BACKGROUND

The photoresponse of high temperature superconductors (HTS) is being investigated as a basis for constructing highly sensitive, broadband, and producible detectors in the visible and infrared spectral regions. Several experimental studies have been published[1-8] investigating the potential usefulness of HTS for such an application, though many questions remain about how and when such detectors might be feasible. The purpose of the work described here is to develop a computational tool useful for both understanding the phenomena observed and for providing detector design guidance.

The phenomena observed in the HTS photoresponse experiments published thus far are diverse. A key issue is whether the response observed is due to a bolometric effect[3,4,6] (a simple temperature increase) or some other more exotic means. Such mechanisms as photoinduced pair breaking,[5] phase slippage,[7] and fluxon motion[2,8] have been suggested as explanations of

possible "non-bolometric" effects. The model presented here yields differing responses for the bolometric and non-bolometric modes; this model and its future elaborations should help to distinguish the phenomena observed.

Also, the design of superconducting detectors will require a careful consideration of response, noise, and power dissipation properties. This kind of model can facilitate design trade studies and optimization to be carried out due to its simplicity and qualitative accuracy.

2. MODEL

The photoresponse model used in this work is based on the standard results pertaining to BCS superconductors, the Josephson effect, and thermal fluctuations. Though the nature of high temperature superconductivity is still unclear, the theoretical ingredients used here nonetheless provide a useful description of macroscopic superconducting properties.

The kind of device being described here is a HTS sample with a fixed current bias and temperature, and a thin enough geometry such that the material is uniformly illuminated. Only steady-state (or slowly chopped) situations are considered here. A fixed value for the superconducting transition temperature T_c is assumed, the broadening of the resistance transition being due to current fluctuations.

The current-voltage characteristic and resistance are described with the Resistively Shunted Junction model, and using the thermal-fluctuation-averaged solution of Ambegaokar and Halperin.[9] A low-capacitance, weak-link structure is assumed, implying inherent Josephson effect properties. The solution represents the average voltage across a junction, and can be written in the form[9]

$$\langle V \rangle = 2 \frac{i_c R_o}{\gamma \pi} \frac{\sinh \frac{\beta\pi}{2}}{\left| I_{j\beta}\left(\frac{\gamma}{2}\right)\right|^2} \qquad (1)$$

$$\gamma = \frac{h i_c}{2\pi e k T}, \qquad \beta = \frac{h i}{2\pi e k T},$$

where i_c is the superconducting critical current, i is the bias current, R_o is the normal resistance, T is the temperature, and e, k, and h are the usual fundamental constants. $I_{jy}(x)$ is a modified Bessel function with imaginary index.

The critical current i_c used here has the form

$$i_c(T) = i_c(0)\left(1 - \frac{T}{T_c}\right)^{\frac{3}{2}} \qquad (2)$$

which gives an approximate representation for long, weak-link junctions. T_c here is the superconducting critical temperature. Of course, real devices will have other functional forms for the critical current; nonetheless this expression provides a simple, useful, starting point.

Due to fluctuations, the resistance of a device in this model is nonzero below the nominal T_c. In a sense, the net voltage

(and resistance) is a average of zero-voltage and finite-voltage states,[9] resulting in a low-temperature tail in the resistance transition. As will be shown below, it is on this tail that some interesting photoresponse effects are observed in the model.

A steady-state bolometric effect[10] may be derived from Equation 1,

$$\frac{\partial \langle V \rangle}{\partial P}(\text{Bolo}) = \frac{\partial \langle V \rangle}{\partial T}\frac{\partial T}{\partial P} = \frac{1}{K(T)} i \frac{\partial R}{\partial T} \qquad (3)$$

where K(T) is a thermal conductivity factor for the detector and substrate system, R is the resistance, and P is the incident light power absorbed. An analytical form of this derivative may be derived, but it is simpler to take a numerical difference of values of <V> for a temperature increment. As shown below, the bolometric effect thus calculated sits near the position of the maximum change in the resistance, but is shifted due to K.

The more interesting non-bolometric mode is considered from the point of view that electron pair breaking causes an increase in the quasiparticle density, resulting in a decrease in the superconducting energy gap Δ.[11] Other non-bolometric effects, such as phase slippage, might be accommodated within this scheme, but are not considered here. A change in Δ then results in a change in i_c, a parameter in Equation 1:

$$\frac{\partial \langle V \rangle}{\partial P}(\text{Non-bolo}) = \frac{\partial \langle V \rangle}{\partial i_c}\frac{\partial i_c}{\partial \Delta}\frac{\partial \Delta}{\partial P} \qquad (4)$$

An expression for $\partial\Delta/\partial P$ has been derived by Parker,[12] for $T < T_c/2$, and steady state, as

$$\frac{\partial \Delta}{\partial P} \propto \left[A + \Delta kT\, e^{\frac{-2\Delta}{kT}}\right]^{\frac{-1}{2}} \qquad (5)$$

where A depends, among other factors, on i. Equation 5 was derived by considering steady-state electron pair breaking and recombination.[12] For low temperatures $\partial i_c/\partial\Delta$ should vary little with respect to current and temperature.

From Equation 1 we find

$$\frac{\partial \langle V \rangle}{\partial i_c} = \frac{-2R_o}{\pi}\,\frac{\sinh\frac{\beta\pi}{2}}{\left|I_{j\beta}(\frac{\gamma}{2})\right|^4}\,\mathrm{Re}\left[I^*_{j\beta}(\tfrac{\gamma}{2})\, I_{j\beta+1}(\tfrac{\gamma}{2})\right] \qquad (6)$$

For the range of parameters studied, $\partial\langle V\rangle/\partial i_c$ has a form and temperature dependence similar to $\partial\langle V\rangle/\partial T$. $\partial\Delta/\partial P$ on the other hand is very strongly peaked towards low temperatures, enhancing the non-bolometric effect at low temperatures. However, in the temperature range around $T_c/2$, the bolometric and nonbolometric effects tend to overlap in this model. As shown in the next section, it is the lower temperature region where the two modes should be most easily distinguished.

3. EXAMPLES

We now apply the above formulas to the simulation of resistance and response properties such as have been seen in recent experimental work.

Figure 1 shows a comparison of the resistance transition, the bolometric response, and the nonbolometric response

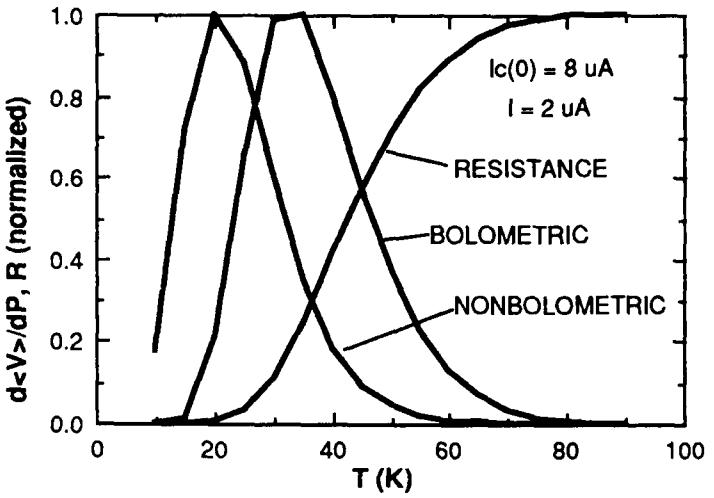

FIGURE 1. Comparison of resistance transition, bolometric response, and non-bolometric response, all normalized to unity peak height. The bolometric peak lies near the maximum change in the resistance transition, while the non-bolometric peak is near the part of the resistance transition approaching zero.

calculated from the equations above. A critical temperature of 90 K was used. The model gives, for the choice of critical current and bias current used, a broad resistance transition similar to those shown in recent publications.[1,3] No separate definition for a $T_{c\text{-}zero}$ is required. The value of R_o used only scales the final results.

The critical current and bias currents used in this simulation, 8 and 2 μA respectively, are considerably less than the mA current levels which characterize most of the experiments published to date.[1-6,8] This is reasonable, given that the device described might be thought of as an aggregate of junctions, whether due to twin boundaries, grain boundaries, or fluxon structures. A choice of a much higher $i_c(0)$ would tend to give a sharp transition near T_c, and corresponds, as one would expect, to a higher-quality sample. The effect of increasing i, on the other hand, would be to broaden the transition.

Figures 1 and 2 show a bolometric effect as would be expected for a device whose thermal conductivity is dominated by a substrate with an idealized T^3 dependence. The peak of that effect occurs near the steepest part of the resistance transition, but is shifted downward by the thermal conductivity factor. Figure 2 further shows how the peak value both shifts downward and increases with increasing bias current. The peak value more than doubles for a doubling of i. Qualitatively similar results have been reported recently.[3]

The nonbolometric peak shown in Figures 1 and 3 has a more striking increase in intensity and a marked downshift in peak position. Similar results were found in Reference 2. In calculating the results in Figure 3, the same value for $i_c(0)$ as before was used. The parameter A in Equation 5, which relates to pair recombination effects, was taken to be zero here. (Using instead $A = 10^{-6}$, a value like that measured by Parker [for Sn samples of a particular geometry], quite similar results are calculated in this temperature range. A larger value of A will reduce the size of the peak, and make its position nearer to the bolometric peak.)

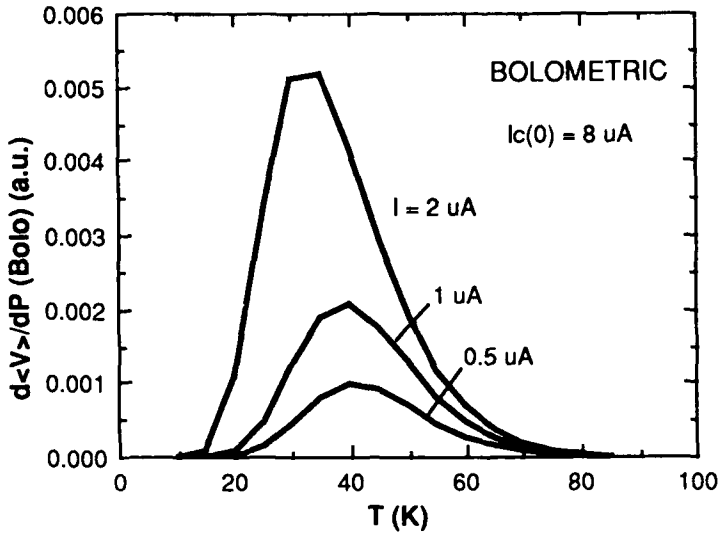

FIGURE 2. Variation of bolometric response with increasing bias current. A doubling of bias current increases the peak height nearly linearly, while shifting the peak position downwards in temperature.

The value for Δ used, 15 meV, is near the zero temperature BCS value for T_c = 90 K. The many measurements of this value to date have not yielded a definitive result. The sharp increase in the peak value with current in Figure 3 is due largely to the factor for $\partial\Delta/\partial P$ (Equation 5), an expression valid only for $T < T_c/2$. That factor is of order unity at higher temperatures, increases

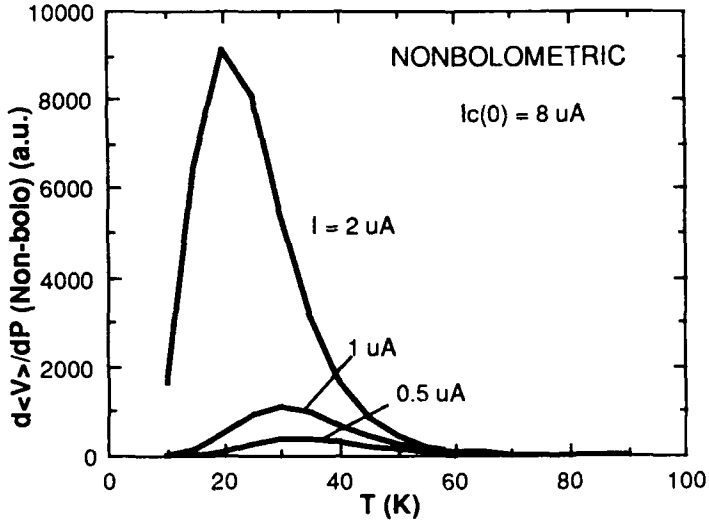

FIGURE 3. Variation of non-bolometric response with increasing bias current. In this case, the peak height increases very nonlinearly with bias current, and the peak position decreases strongly

exponentially at low temperatures, but tends towards a constant at very low temperatures and finite A.

The comparison of the nonbolometric and bolometric peaks given in Figure 1 shows how the nonbolometric peak might be expected to occur at lower temperatures, similar to results reported recently.[5,7] However, the factor $\partial i_c/\partial\Delta$, ignored in these calculations, might be of considerable consequence in the temperature range near T_c used in those studies.

These calculations also suggest that in some situations the bolometric peak might be shifted somewhat from the maximum value of dR/dT. Perhaps time-dependent measurements can provide a more definitive way to distinguish the two kinds of peaks.

4. SUMMARY

The model presented here is a first step in developing a computational model of the diverse phenomena observed in HTS photoresponse studies. The results presented are intended to elucidate the nature of those phenomena, as well as to show how to enhance the response. The model successfully simulates the trends of the photoresponse with respect to bias current and temperature, while indicating that photoresponse peaks seen at low temperatures might be due to a non-bolometric mechanism.

Future elaborations of this work will need to take into account device geometry, reactance, and noise.

ACKNOWLEDGEMENTS

This author wishes to acknowledge helpful discussions with F. Madarasz and U. Strom. This work was carried out with the support of the Science Applications International Corporation IR&D program.

REFERENCES

[1] Leung, M., et al., Appl. Phys. Lett. 51, 2046 (1987).
[2] Strom, U., et al., Proc. SPIE 948, 10 (1988).
[3] Forrester, M. G., M. Gottlieb, J. R. Gavalier, and A. I. Braginski, Appl. Phys. Lett. 53, 1332 (1988).
[4] Richards, P. L., et al., Appl. Phys. Lett. 54, 283 (1989).
[5] Frenkel, A., et al., Appl. Phys. Lett. 54, 1594 (1989).
[6] Brocklesby, W. S., et al., Appl. Phys. Lett. 54, 1175 (1989).
[7] Zeldov, E., N. M. Amer, G. Koren, and A. Gupta, to be published in Phys. Rev. B.
[8] Culbertson, J. C., et al., to be published in Phys. Rev. B.
[9] Likharev, K. H., *Physics of Josephson Junctions and Circuits.* New York: Gordon and Breach, 1986.
[10] K. Rose, C. L. Bertin, and R. M. Katz, in *Applied Superconductivity* (V. L. Newhouse, ed.). New York: Academic Press, 1975, p. 272.
[11] Enomoto, Y. and T. Murakami, J. Appl. Phys. 59, 3807 (1986).
[12] Parker, W. H., Solid State Commun. 15, 1003 (1974).

Presented at the Workshop on High Temperature Superconductivity
23-25 May 1989 GACIAC PR-89-02

Y-Ba-Cu-O THIN FILMS AS HIGH SPEED INFRARED DETECTORS

H.S. Kwok, J.P. Zheng and Q.Y. Ying
Institute on Superconductivity
State University of New York at Buffalo
Bonner Hall, Amherst, NY 14260

ABSTRACT

Y-Ba-Cu-O thin films and a high speed gold-doped germanium detector were compared for CO_2 laser detection. Operation of the Y-Ba-Cu-O detector in both the bolometric and nonbolometric modes were studied. It was found that the responsivity of the superconducting detector was considerably better than conventional detectors. The speed of both detectors were comparable within the instrument resolution of 10 ns. With further optimization, high temperature superconductors should become very attractive for IR detection. The superconducting film quality is critical to the performance of these detectors.

1. INTRODUCTION

One of the major potential applications of high temperature superconducting (HTS) materials is in detection of infrared radiation. In the far infrared region, sensitive and wideband bolometers have been demonstrated with conventional superconductors such as NbN[1]. These detectors are more sensitive than semiconductor based materials, but very low operating temperatures are required.

For HTS materials, infrared (IR) detection has been studied recently by many groups[2-10]. Sensitivities in the 0.01 - 10^3 V/W regime, and response times from 0.1 ms to <1 ns at $\lambda = 1$ μm have been reported. However, it is expected that the major application of HTS is at wavelengths of 5 μm and beyond, since very sensitive and high speed detectors are available at shorter wavelengths. In this letter, we report a study of HTS thin film detectors at the CO_2 laser wavelength of 10.6 μm. Both the speed and responsivity were measured and compared to conventional detectors at this wavelength. It will be shown that HTS detectors are superior to commercial high speed gold-doped germanium (Ge:Au) detectors.

The Ge:Au detector was chosen as a reference because of its high speed (2 ns). Similar speed HgCdTe detectors, on the other hand, are not commonly available. Anyway, since the performance of different semiconductor IR detectors have been well characterized and compared, the results reported here can be used to place the new HTS material amongst these conventional detectors.

2. SAMPLE PREPARATION

The HTS film preparation and patterning procedures have been described previously[11,12]. Basically, we employed an all-dry processing scheme with no high-temperature post annealing, in both the deposition and patterning steps. Superconducting microstrips that were 70 μm wide and 5 mm long were fabricated by direct laser writing of in situ laser deposited films. The materials used here were Y-Ba-Cu-O on $SrTiO_3$. The critical temperature T_c and critical current J_c of these films have been measured to be 90 K and 4×10^6 A/cm^2 (20 K) respectively[12]. However for the detector study reported here, the film thicknesses were $\sim$100 nm, and T_c and J_c were reduced to 53 K (1 μA bias current) and 0.7×10^6 A/cm^2 (10 K) respectively. The critical current was $\sim$45 mA through the strip. Detection by a 4-probe method was employed, with a digital oscilloscope/computer combination for data acquisition[2].

3. EXPERIMENTAL RESULTS

We have demonstrated previously that at low temperatures, the HTS detector operates in the fast nonbolometric (NB) mode[2], while at $T \sim T_c$, the detector is in the bolometric mode of operation. Fig. 1 illustrates some of the results for the NB mode at 10 K. The upper trace shows the signal when a TEA (transverse electric atmospheric) CO_2 laser was irradiated onto the HTS film. The laser spot size was 5 mm in diameter and the bias current was 5 mA. The lower trace shows the laser pulse detected with a commercial high speed Ge:Au detector (Santa Barbara Research Center). The laser fluence in both cases were $\sim$ 0.5 mJ/cm^2. It can be seen that the temporal profiles are the same. Mode-beating of the laser is not visible in these traces because of the slow speed of the oscilloscope (10 ns), but can be resolved in

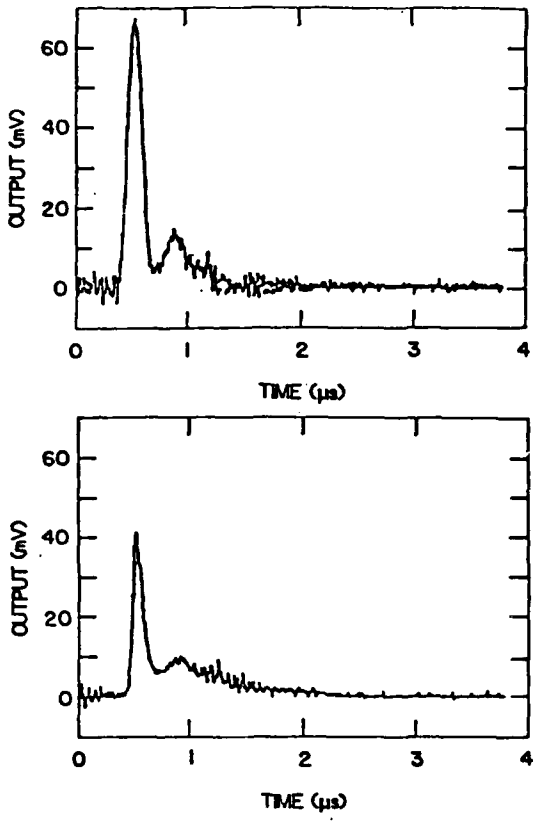

Fig. 1 Oscilloscope traces for the voltage output. Upper trace: HTS film at 10 K, lower trace: Ge:Au detector at 77 K.

both cases with a faster oscilloscope. Therefore, within our instrument resolution, the speed of the two detectors are essentially the same.

The laser fluence dependence of the HTS detector signal at 10 K is shown in Fig. 2. It can be seen that the response is linear, but exhibits a minimum threshold of ~0.2 mJ/cm^2. This is a common phenomenon for superconducting detectors operating in the NB mode at temperatures much below T_c. Basically, a sufficient number of quasiparticles have to be created in order to switch the superconductor into the resistive state[6]. This threshold is determined by both the bias current and the temperature dependent critical current.

From Fig. 1, it can be seen that the HTS detector is about 80 times more sensitive than the Ge:Au detector. It is because the detector element in the case of HTS is 55 times smaller in area than the 5 mm diameter Ge:Au element and

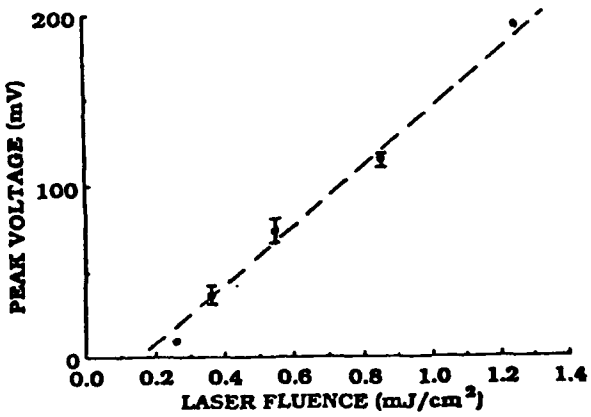

Fig. 2 HTS detector signal as a function of laser fluence at 10 K, well within the nonbolometric mode of operation.

the signal is 50% stronger. It should be noted that the current bias into the Ge:Au detector was optimized in terms of the detector dark resistance and shot noise. On the other hand the HTS detector bias current had not been optimized carefully yet. Therefore the factor of 80 in higher responsivity for the case of the HTS detector can in principal be increased further.

From Fig. 2, the unoptimized voltage responsivity of the HTS detector in the fast NB mode is ~0.007 V/W at 5 mA bias. This number was obtained by using the instantaneous intensity of the laser pulse, and hence is valid for an operating speed of at least 10 ns. Thus the detector bandwidth is at least 100 MHz. It is speculated that the HTS material can operate at a much faster speed[2,3,14], which implies an even larger bandwidth. The question of speed and bandwidth is important for heterodyning or microwave signal processing applications[1], and is currently being investigated.

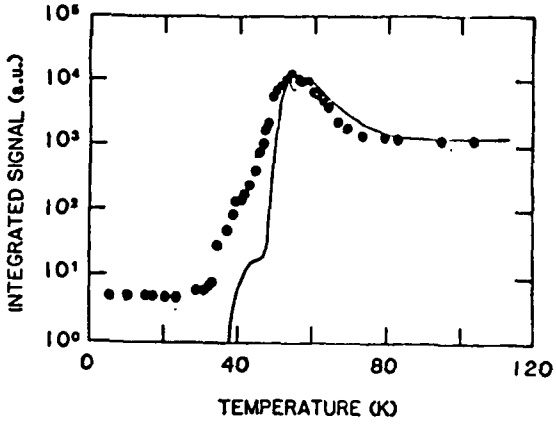

Fig. 3 Integrated signal from the HTS detector as a function of temperture. Solid curve is the calculated dR/dT value from the R versus T measurement. The mode of operation depends solely on the operating temperature at $I_{bias} < I_c$.

At higher temperatures, the HTS detector operates in the bolometric mode. Fig. 3 shows the temperature dependence of the HTS signal at 1 mA bias. The solid curve is a plot of dR/dT from the measured resistivity curve. For a bolometric type response, the data should follow the solid curve. This is indeed the case for T > 50 K. However, at low temperature, there is a constant optical response even though dR/dT is zero. This curve confirms our previous result with a 1.06 μm Nd:YAG laser that at $T < T_c$ the signal is nonbolometric in nature, and is possibly due to quantum effects such as quasiparticle generation[14], photoinduced flux creep[7] and phase slip[9], or photo-enhanced Josephson tunneling[15].

In the bolometric mode, the speed of the HTS detector is considerably slower than the laser pulse duration. In this case, the signal is defined by integrating the voltage output over time. It is interesting to note that the integrated signal of the HTS film at T_c is ~ $3x10^3$ times higher than at low T. The increased signal is due mostly to a much longer output duration. Fig. 4 shows the HTS detector response at 48.2 K. The temporal decay of the signal is dominated by the rapid thermal diffusion time (~ 15 μs) in the HTS film. It demonstrates that the increased responsivity comes at the expense of reduced speed. In this mode of operation, the operating bandwidth is reduced to ~ 70 kHz and the responsivity is ~ 20 V/W (at 1 mA bias). This responsivity can be increased to ~ 10^3 V/W by operating near the critical current. This latter value is consistent with some of the reported bolometric results[5].

4. DISCUSSIONS

It is interesting to note that the HTS detector signal is almost constant between 80 K and room temperature. This signal is due to the constant dR/dT of a metal in the normal state. The signal is slow, but rather large, and is only a factor of 10 below the maximum bolometric response at T_c. This small difference is due to the broad superconducting transition in the film. For sharper transitions, dR/dT should be much larger at T_c.[3]

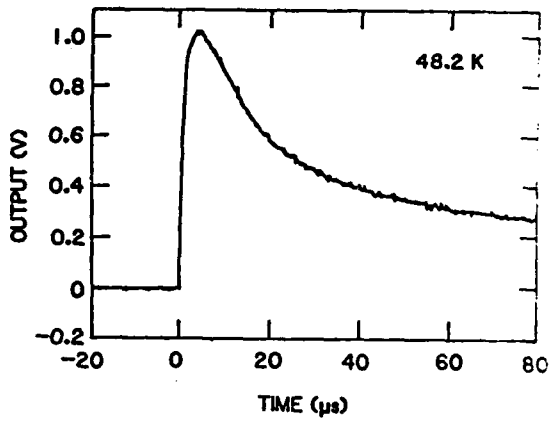

Fig. 4 Voltage trace for the HTS detector at 48.2 K. The initial fall is due to heat diffusion and the final fall is simply the electronic RC decay.

The detectivity D^* is a better measure of the quality of the detector. Unfortunately, it cannot be calculated because the detector noise is not measurable with our present set-up, even with the laser turned-off. (The noise in Fig. 1 is due to electromagnetic interference from the TEA laser and is not real detector noise). In the NB mode of operation, the detector resistance is zero, making all common noise generation mechanisms such as thermal noise and shot noise inappropriate. In this case, the noise arises mainly from quantum fluctuations across the superconducting weak links and 1/f noise[1,16] and should be very small. In the bolometric mode, the noise is considerably higher, implying that the higher responsivity is not necessarily desirable for IR detection. To a large extent, granularity of the films also affect the noise performance[4]. The optimization of D^* involves a careful measurement of both the responsivity and the detector noise. This can be done by varying the bias current, temperature of operation, and the quality of the HTS film. As a reference, high speed HgCdTe and Ge:Au detectors have D^* values of $\sim 3\times10^9$ cmHz$^{1/2}$/W at 10 μm.

In summary, we have compared a HTS detector with a high speed Ge:Au detector at 10.6 μm. The HTS detector is about 80 times more sensitive. It is believed that the sensitivity and D^* can be improved even further by optimizing the film thickness, area, film quality and the operating conditions. With a high T_c film, high speed-high sensitivity detection can operate at liquid nitrogen temperature, which should make the HTS IR detector extremely attractive for CO_2 laser detection. Such wideband detectors should find applications as mixers for microwave signal processing as well. However the major potential drawback is that there is a threshold intensity effect (Fig. 2) in the NB mode of operation. The threshold can in principle be reduced by operating near the critical current, at the risk of compromising the noise and speed performance.

This work was supported by NSF and New York State Institute on Superconductivity. HSK is a NSF Presidential Young Investigator.

References

1. K. Rose, C.L. Bertin and R.M. Katz, p. 267 in **Applied Superconductivity**, ed. by V.L. Newhouse, Academic Press, New York 1975.
2. J.P. Zheng, Q.Y. Ying, H.S. Kwok and R. Rao, Appl. Phys. Lett., 54, 2473 (1989).
3. A. Frenkel, M.A. Saifi, T. Venkatesan, C.L. Lin, Y.D. Wu and A. Inam, Appl. Phys. Lett., 54, 1594 (1989).
4. M. Leung, P.R. Broussard, J.H. Claassen, M. Osofsky, S.A. Wolf and U. Strom, Appl. Phys. Lett., 51, 2046 (1987).
5. M.G. Forrester, M. Gottlieb, J.R. Gavaler and A.I. Braginski, Appl. Phys. Lett. 54, 1332 (1988).
6. Y. Enomoto, T. Murakami and M. Suzuki, Physica C 153-155, 1592 (1988).
7. E. Zeldov, N.M. Amer, G. Koren and A. Gupta, Phys. Rev. B39, 9712, 1989.
8. W.S. Brocklesby, D. Monroe, A.F.J. Levi, M. Hong, S.H. Liou, J. Kwo and C.E. Rice, Appl. Phys. Lett. 54, 1175 (1989).
9. J.C. Culbertson, U. Strom, S.A. Wolf, P. Skeath, E.J. West and W.K. Burns, Phys. Rev. B39, 12359, 1989.
10. W.R. Donaldson, A.M. Kadin, P.H. Ballantine and R.Sobelowski, Appl. Phys. Lett. 54, 2470 (1989).
11. S. Witanachchi, S. Patel, H.S. Kwok and D.T. Shaw, Appl. Phys. Lett., 54, 578 (1989).
12. J.P. Zheng, Q.Y. Ying, H.S. Kim, P. Bush, R. Barone, D.T. Shaw, H.S. Kwok and R. Rao, submitted to Appl. Phys. Lett.
13. H.S. Kwok and E. Yablonovitch, Appl. Phys. Lett., 27, 583 (1975).
14. Y. Enomoto and T. Murakami, J. Appl. Phys. 59, 3808 (1986).
15. D.R. Dykaar, R. Sobelowski, T.Y. Hsiang and G.A. Mourou, IEEE Trans. Mag. MAG-23, 767 (1987).
16. R.H. Koch, W.J. Gallagher, B. Bumble and W.Y. Lee, Appl. Phys. Lett., 54, 951 (1989).

THIS PAGE IS INTENTIONALLY BLANK

Presented at the Workshop on High Temperature Superconductivity
23-25 May 1989 GACIAC PR-89-02

ELECTRICAL RESPONSE OF HIGH-T_c SUPERCONDUCTING FILMS TO LASER RADIATION*

M. G. Forrester, J. Talvacchio, and A. I. Braginski
Westinghouse Research and Development Center
Pittsburgh, PA 15235

ABSTRACT

We have measured the voltage response of current-biased films of $YBa_2Cu_3O_{7-\delta}$ to chopped laser radiation in the visible and infrared. Although such films might be expected to exhibit a response due to a light-induced nonequilibrium population of quasiparticles, we observe only a bolometric, or heating response. Superficial differences between the temperature dependences of the response of granular versus epitaxial films appear to be consistent with the temperature dependence of the thermal properties of the superconducting film and its interface with the substrate, which become significant for films with broad resistive transitions.

INTRODUCTION

There has recently been a considerable amount of interest in the application of high-temperature superconductors (HTS) to infrared detection. Work to date can be loosely divided into two categories; (1) The practically-oriented application of HTS films (or thinned bulk materials) as temperature-sensitive elements in bolometers, where the use of HTS brings the potential for operation at temperatures above 77 K; (2) The investigation of novel detection mechanisms based on a light-induced nonequilibrium population of quasiparticles.

In the first category, analysis of noise considerations generic to a bolometer operating at high-temperature, and measurements of low-frequency noise in high-quality epitaxial $YBa_2Cu_3O_{7-\delta}$ (YBCO) films, have shown that such a bolometer could exhibit noise equivalent powers (NEP) in the range $(1\text{-}20) \times 10^{-12}$ W/Hz$^{-1/2}$, comparing favorably with other detectors operating at or above liquid nitrogen temperatures for wavelengths greater than 20 μm.[1] Experimental realizations of a composite bolometer (with independent radiation absorber) have yet to attain such performance.[2]

More attention has been focussed on the second category, the nonequilibrium detector, both from the practical viewpoint of developing a *quantum* detector able to operate at long wavelengths at easily accessible temperatures, and for the investigation of basic physics issues such as quasiparticle recombination times in HTS. Several studies of quasiparticle dynamics under the influence of above-gap radiation were performed in low-temperature superconductors (LTS) during the hey-

* Work supported by SDIO Contract No. 84-88-C-0042.

1 P. L. Richards, J. Clarke, R. Leoni, Ph. Lerch, S. Verghese, M. R. Beasley, T. H. Geballe, R. H. Hammond, P. Rosenthal, and S. R. Spielman, "Feasibility of the High T_c Superconducting Bolometer," Appl. Phys. Lett. 54, 283 (1989).

2 J. C. Brasunas, S. H. Moseley, B. Lakew, R. H. Ono, D. G. McDonald, J. A. Beall, and J. E. Sauvageau, "Construction and Performance of a Thin-Film, Transition-Edge, High-Temperature-Superconductor Composite Bolometer," manuscript submitted to Applied Physics Letters.

day of nonequilibrium superconductivity.[3] However, excitement over the potential of HTS as nonequilibrium-type photon detectors stems from more recent work on granular films of the low-T_c oxide superconductor $BaPb_{1-x}Bi_xO_3$ (BPB), which claimed responsivities as large as 10^4 V/W and specific detectivities greater than 10^{10} cm$\sqrt{\text{Hz}}$/W.[4] The response was attributed to a reduction in the critical currents of intergrain "boundary Josephson junctions" due to the creation of a nonequilibrium excess of quasiparticles.

The existence of a nonequilibrium detection mechanism in HTS has not yet been conclusively demonstrated. Early reports on granular YBCO films suggested a non-thermal response in which the maximum optically-induced voltage shift, ΔV, occurred at a temperature somewhat below $T_c(R=0)$.[5] The authors now interpret these results in terms of the effect of nonequilibrium quasiparticles on vortex dynamics, possibly including the modification of a vortex-unbinding (Kosterlitz-Thouless) transition or perhaps simply vortex depinning by photons.[6] In contrast, our results on both epitaxial and granular YBCO films showed only a bolometric response, with the maximum in $\Delta V(T,I)$ occurring at the same temperature as that in $dV(I)/dT$, the temperature derivative of the dc voltage at the same bias current.[7] Subsequent reports by other authors supported this conclusion for epitaxial films, under both continuous-wave and pulsed laser excitation.[8,9]

Our intent here, rather than to review the results of the numerous publications and preprints on the optical response of HTS, is to briefly present some of our more recent data on both granular and epitaxial YBCO films, which lend support to our initial conclusion that the observed response is predominantly bolometric, with any nonequilibrium component significantly smaller than the equilibrium response.

EXPERIMENTAL DETAILS

Fabrication details for our YBCO films have been reported elsewhere.[10] Briefly, films were produced by sequential magnetron sputtering from elemental targets, at substrate temperatures from 400 to 650 °C, onto $SrTiO_3$, sapphire and MgO substrates. Epitaxial films on $SrTiO_3$ were predominantly *a*-axis oriented, with transport critical current densities, J_c, typically 2×10^5 A/cm^2. In contrast, the granular films on sapphire and MgO typically had $J_c \approx 100$ A/cm^2.

---

3 For a review see, for example, D. N. Langenberg, "Nonequilibrium Phenomena in Superconductivity," in Low Temperature Physics – LT14, edited by M. Krusius and M. Vuorio (American Elsevier, New York, 1975), Vol. V, p. 223.

4 Y. Enomoto and T. Murakami, "Optical Detector Using Superconducting $BaPb_{0.7}Bi_{0.3}O_3$ Thin Films", J. Appl. Phys. **59**, 3807 (1986).

5 M. Leung, P. R. Broussard, J. H. Claassen, M. Osofsky, S. A. Wolf, and U. Strom, "Optical Detection in Thin Granular Films of Y-Ba-Cu-O at Temperatures Between 4.2 and 100 K," Appl. Phys. Lett. **51**, 2046 (1987).

6 J. C. Culbertson, U. Strom, S. A. Wolf, and P. Skeath, "Nonlinear Optical Response of Granular Y-Ba-Cu-O Films," to appear in Phys. Rev. B, June 1989.

7 M. G. Forrester, M. Gottlieb, J. R. Gavaler, and A. I. Braginski, "Optical Response of Epitaxial Films of $YBa_2Cu_3O_{7-\delta}$," Appl. Phys. Lett. **53**, 1332 (1988). M. G. Forrester, M. Gottlieb, J. R. Gavaler, and A. I. Braginski, "Optical Response of Epitaxial and Granular Films of $YBa_2Cu_3O_{7-\delta}$ at Temperatures from 25 K to 100 K," IEEE Trans. Magn. **MAG-25**, 1327 (1989).

8 Y. Enomoto, T. Murakami, and M. Suzuki, "Infrared Optical Detector Using Superconducting Oxide Thin Film," Physica **C153-155**, 1592 (1988).

9 W. S. Brocklesby, D. Monroe, A. F. J. Levi, M. Hong, S. H. Liou, J. Kwo, C. E. Rice, P. M. Mankiewich, and R. E. Howard, "Electrical Response of Superconducting $YBa_2Cu_3O_{7-\delta}$ to Light," Appl. Phys. Lett. **54**, 1175 (1989).

10 J. R. Gavaler, A. I. Braginski, J. Talvacchio, M. A. Janocko, M. G. Forrester, and J. Greggi, "Fabrication of High-Tc Superconducting $YBa_2Cu_3O_7$ Films," in High Temperature Superconductors II, edited by D. W. Capone II, W. H. Butler, B. Batlogg, and C. W. Chu, Materials Research Society, Pittsburgh, 1988.

Optical response measurements presented here are for two films — a 200 μm × 200 μm × 1000 Å granular film on MgO, with $T_c(R=0) \approx 10$ K, and a 100 μm × 50 μm × 1000 Å *a*-axis epitaxial film on $SrTiO_3$, with $T_c(R=0) = 65$ K. Both were patterned by photolithography and ion-milling.

Four-probe electrical connections were made through pressed contacts to either gold or indium contact pads, and the samples were mounted on the copper cold-finger of a variable-temperature continuous-flow He cryostat. The samples were illuminated by several visible and infrared lasers, mechanically chopped at frequencies up to 4 kHz. The optically-induced voltage shift measured by a lock-in amplifier and the dc voltage measured by a microvoltmeter were recorded simultaneously. The results reported here are principally for wavelengths of 0.63 and 1.15 μm.

EXPERIMENTAL RESULTS

Epitaxial Film

Figure 1 shows the optically-induced resistance change as a function of temperature, $\Delta R(T)=\Delta V(T)/I$, for the epitaxial film at I = 100 μA. The radiation wavelength is 0.63 μm, chopped at 1 kHz, with an intensity of about 0.4 W/cm^2. Also shown is the temperature derivative of the dc resistance, dR/dT, at the same bias current, measured simultaneously. As reported previously [7] the maximum response coincides with the maximum in dR/dT, and in fact ΔR and dR/dT are here seen to be proportional over the entire measurement temperature range, with the constant of proportionality, ΔT, corresponding to a temperature rise of about 10 mK for the film:

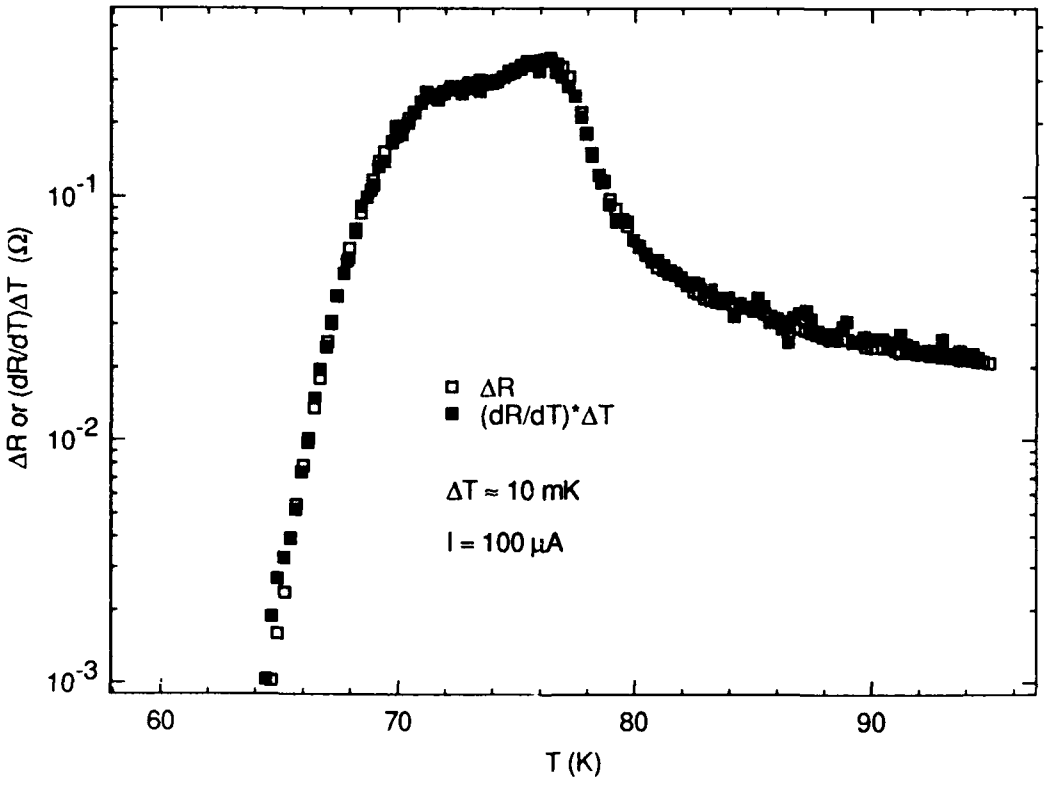

Figure 1. Comparison between ΔR, the optically-induced resistance change, and dR/dT, both measured at a bias current of 100 μA, for a 1000 Å epitaxial YBCO film. The sample was illuminated by a 0.63 μm laser beam, chopped at 1 kHz. The close correspondence between the two quantities indicates a bolometric response, with a temperature rise of approximately 10 mK.

$$\Delta R(T,I) \approx \frac{dR(I)}{dT}\Delta T. \qquad (1)$$

Data taken with I =10 μA and 1 mA show the same agreement between ΔR and dR/dT. Results for 1.15 μm radiation were virtually identical .

We thus conclude that this thin epitaxial film shows only a bolometric response over the temperature range covered by these measurements (T > 56 K). Specifically, we see no evidence for a systematic shift in the peak positions of ΔR and dR/dT recently reported in high-quality *c*-axis YBCO films.[11] We can not, however, preclude the existence of a non-bolometric response at appreciably lower temperatures since the currents required to bias the sample into the voltage state at lower temperatures are large enough that ohmic dissipation in the contacts becomes significant. Limited measurements at I = 10 mA (for which the sample was in the voltage state down to T ≈ 14 K) showed no evidence for novel behavior.

Granular Film

The optical response of the low-quality granular film, again to 0.63 μm radiation chopped at 1 kHz, is shown in Fig. 2(a), for four values of bias current. Compared to results for the epitaxial film shown in Fig. 1 ΔR(T) shows a great deal of structure, including peaks at T ≈ 80 and 63 K, and, for sufficiently high bias, a rise at low temperature. Figure 2(b) compares ΔR(T) and dR/dT for I = 1 mA and shows that the peaks in the photoresponse at 63 and 80 K are due to local maxima in dR/dT. However the low-temperature rise in ΔR(T) observed at 300 μA and 1 mA clearly does not correlate with dR/dT.

It is tempting to associate the low-temperature rise in ΔR with nonequilibrium effects. As the temperature decreases the effective quasiparticle lifetime, τ_{eff}, should increase as $\exp(\Delta/k_BT)$, leading to an exponential temperature dependence for the time-average excess quasiparticle density $n_q \propto \tau_{eff}$, for the change in the gap $\delta\Delta$, and ultimately for the measured voltage shift, ΔV. In fact the low-temperature data for I = 300 μA and 1 mA *do not* fit such an exponential temperature dependence, but rather appear to be approximately linear in temperature for this particular sample.

Our interpretation of the low-temperature rise in ΔR(T) is simply that the thermal properties of the film, and its interface with the substrate, are temperature dependent, so that the temperature rise ΔT in eqn. 1 depends on the sample temperature T. To account for this in a simple way we may compare ΔT [instead of ΔR(T))] for various bias currents:

$$\Delta T \approx \frac{\Delta R(T,I)}{\left[\frac{dR(T,I)}{dT}\right]} \propto \frac{1}{G(T)} \qquad (2)$$

If the thermal model is correct then G(T) represents either a thermal conductance linking the film and the cold-stage, or a combination of a thermal conductance and the heat-capacity of the film/substrate combination, depending on whether or not the film reaches a steady state during the time that the laser beam is "on." In either case G(T) should be approximately independent of current,† so that the superficially different ΔR(T) data of Fig. 2(a) should reduce to one curve when plotted as ΔT, or G(T) ∝ 1/ΔT, vs. T.

---

[11] E. Zeldov, N. M. Amer, G. Koren, and A. Gupta, "Non-thermal Optical Response of $YBa_2Cu_3O_{7-\delta}$ Epitaxial Films," submitted to Phys. Rev. B.

† We say approximately since the ohmic power dissipation due to the bias current leads to a positive thermal feedback which effectively reduces the thermal conductance with increasing current. Such an effect would be important in a film with a very sharp transition.

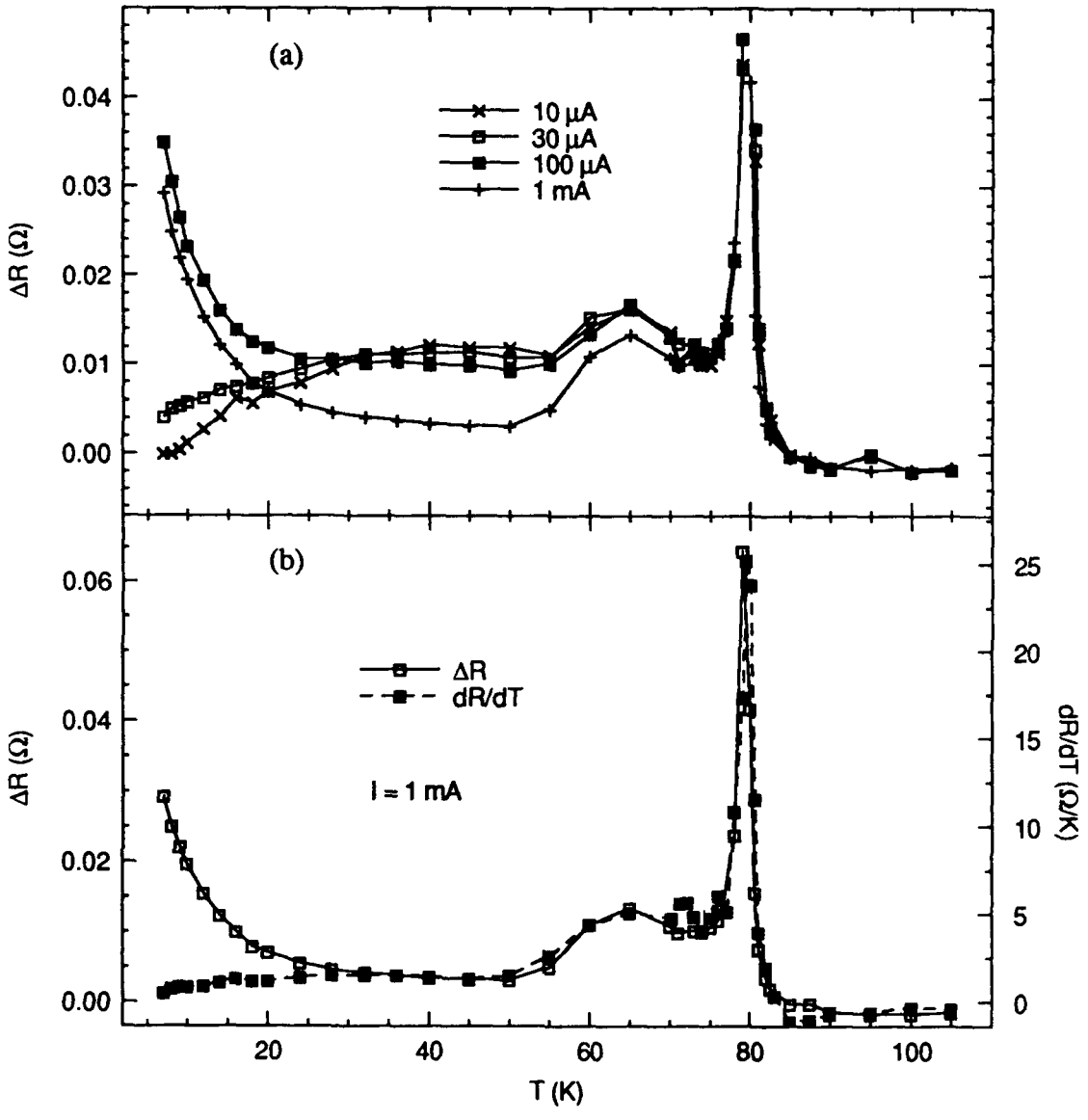

Figure 2. (a) The optically-induced resistance change, ΔR, at various levels of bias current, for a poor quality 1000 Å granular YBCO film, illuminated by a 0.63 μm laser beam, chopped at 1 kHz. (b) Comparison between ΔR and dR/dT at a bias of 1 mA. The disparity between the two quantities at low temperatures can be explained by the temperature dependence of the film's thermal conductance.

Figure 3 shows a plot of $1/\Delta T$ derived in this manner. One sees that the data for various currents fall approximately on one curve, despite the superficial differences in the ΔR(T) data. The data are qualitatively similar to published data on the thermal conductance of YBCO,[12] shown in Fig. 3 as the solid curve, including a low-temperature T^3 dependence, and some suggestion of a broad maximum near T = 50 K. The discrepancy between our data and the thermal-conductivity data is probably due to the presence of another thermal impedance in series with that of the film,

[12] J. Heremans, D. T. Morelli, G. W. Smith, and S. C. Strite III, "Thermal and Electronic Properties of Rare-Earth $Ba_2Cu_3O_x$ Superconductors," Phys. Rev. B37, 1604 (1988).

presumably that of the film/substrate boundary, and possibly a layer of degraded superconductor adjacent to the substrate. Quantitatively, the approximate expected temperature rise for our 1000 Å film at T = 60 K, given a laser power density of 0.4 W/cm^2 and a thermal conductivity of 4×10^{-3} W/cm·K, would be $\Delta T \approx 1$ mK, compared to the measured 2.3 mK. Again, the presence of an additional thermal impedance in series could explain the discrepancy.

As mentioned earlier, the identification of $1/\Delta T$ with simply a thermal conductance, rather than a combination of thermal conductance and heat capacity, assumes that the sample reaches a steady-state temperature during the time that the laser is on. In fact the data support this conclusion over essentially the entire temperature range considered in the analysis above ($T \lesssim 70$ K). We have reported previously [7] that the response of our films at $\lambda = 0.63$ μm exhibits two components, a "fast" response which we have subsequently learned is limited by the rate at which the beam is occluded by the chopper, and a slow component. We believe that the fast component is related to the thermal response of the film itself, into which the heat is predominantly delivered by the laser, and the slow component to the thermal response of the substrate. Regardless of the exact explanation of the two components, the data presented above were obtained with a sufficiently fast chopping rate that only the fast component contributed appreciably for $T < 70$ K, so that the detector exhibited a square-wave like response when viewed on an oscilloscope, with the finite slope of the response rise being due to the finite rate at which the beam was occluded by the chopper.

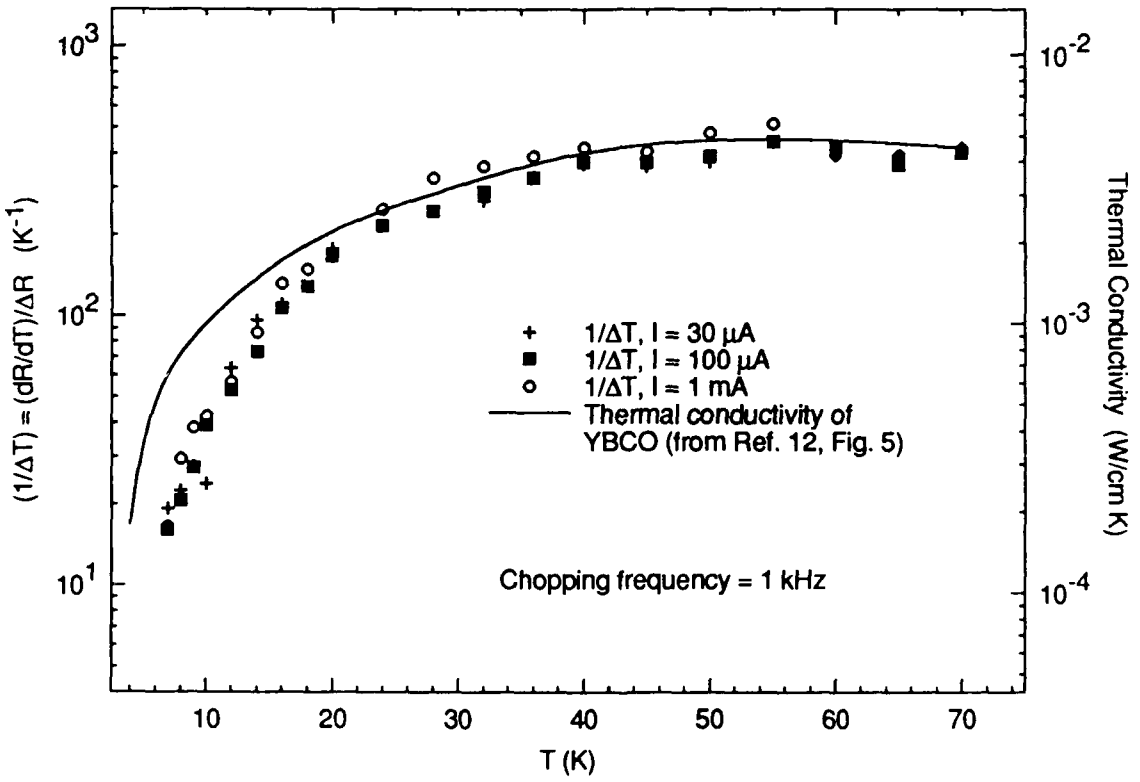

Figure 3. Temperature dependence of ΔT, the temperature increase due to optical illumination, derived from the data of Fig. 2. The data fall approximately on a single curve, independent of current, reflecting the thermal conductance of the YBCO film and its interface with the substrate. The solid curve is the measured thermal conductance of YBCO, from Ref. 12.

This point is further illustrated by Fig. 4, which shows the dependence of the optical signal on chopping-frequency, f, at three temperatures. The fall-off in ΔR for $f \lesssim 100$ Hz at T = 7 K and

40 K is due to the slow response. For $f \gtrsim 100$ Hz only the fast response remains at these low temperatures. It is worth noting that, had a lower chopping frequency been used to obtain the data of Fig. 2, the peak at $T \approx 79$ K would have appeared much larger than the signal at $T \approx 7$ K. This changing in the relative magnitudes of the response at high and low temperatures as a function of chopping frequency has been reported by other workers and used to support the notion that different detection mechanisms are present in these two regimes.[6] However we believe that the temperature dependence of thermal properties probably provides the explanation.

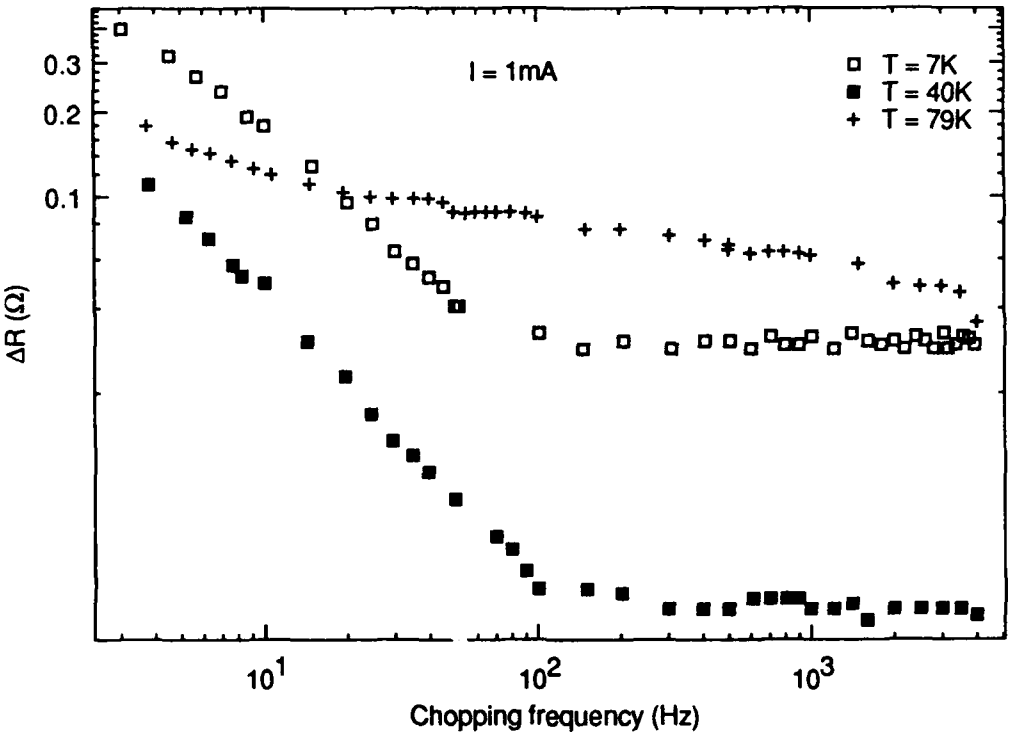

Figure 4. Chopping-frequency dependence of ΔR for the sample of Figs. 2 and 3. At T = 7 K and 40 K the fall-off in ΔR for $f \lesssim 100$ Hz is due to the "slow" response dominated by the thermal properties of the substrate, while for $f \gtrsim 100$ Hz only the fast response (dominated by the thermal properties of the film) remains. For $T \gtrsim 70$ K the slow response is significant over the entire frequency range.

SUMMARY AND CONCLUSIONS

We have presented some of our recent results on the optical response of 1000 Å epitaxial and granular YBCO films. Consistent with our previous results on 3500 Å films, epitaxial samples exhibit close agreement between the optically-induced resistance change, ΔR, and the slope of the resistive transition, dR/dT, measured at the same bias current. The results indicate that the response is predominantly bolometric, with the radiation simply raising the film temperature by $\Delta T \approx 10$ mK.

Results for granular films with broad resistive transitions exhibit a low-temperature response which increases with decreasing temperature. We have demonstrated that this effect is due not to nonequilibrium quasiparticles, but simply to the temperature dependence of the thermal properties of the film. The "fast" response which we have reported previously has been found to be limited

by the rate at which the laser beam is turned off by the chopper. The data are consistent with this response being determined by the thermal conductance of the YBCO film itself, at least for $T \lesssim 70$ K. Values for the thermal conductance derived from our data are in reasonable agreement with published data for YBCO, if we allow for an additional thermal impedance (such as the film/substrate interface) in series with that of the film. On the other hand, the "slow" response is thought to be determined by both the thermal conductance and heat capacity of the film and substrate.

We are presently attempting to place a more stringent upper bound on the response time of the fast response. Pulsed laser experiments have the advantage that the bolometric response is smaller, so that subtle nonequilibrium effects may be more evident. There is however a potential pitfall in using too-intense a laser pulse, in that the film, whose thermal response can be very rapid, may be heated well into the normal state, making subtle nonequilibrium effects difficult to unfold.

It may be that nonequilibrium effects will always be difficult to detect in HTS, because the quasiparticle recombination times are too short. For example, using the known quasiparticle recombination times near T_c for LTS, τ_0, and the approximate relation, $\tau_0 \propto T_c^{-3}$,[13] we infer a value of $\tau_0 \sim 10^{-13}$ sec for YBCO. Although this "intrinsic" lifetime will be lengthened by the pair-breaking effect of recombination phonons, leading to a longer effective lifetime for a nonequilibrium quasiparticle population,[14] the lifetime might still be short enough that laser pulses only picoseconds wide will be needed to directly resolve it. If the lifetime is indeed so short then the time-average excess quasiparticle density in response to a continuous-wave laser, which is proportional to the lifetime and to the pair-breaking rate, may be too small to be observable. Of course the lifetime is expected to diverge exponentially at low temperatures so that nonequilibrium effects may become more obvious there. However, trapping of optically-excited quasiparticles by impurities and defects in the film may mean that this exponential behavior exists only over a very narrow temperature range, with the lifetime saturating at still too low a value to be useful.

Clearly the potential usefulness of HTS films as quantum detectors is far from established. Even if a quantum response with high responsivity is observed, the usefulness of such a device may be limited because of the excess "1/f" noise typically observed in HTS films.[7] Novel detector concepts may be required to circumvent these problems.

We are pleased to acknowledge the assistance of M. Gottlieb with the optical apparatus, and H. Buhay for sample patterning.

---

[13] S. B. Kaplan, C. C. Chi, D. N. Langenberg, J. J. Chang, S. Jafarey, and D. J. Scalapino, "Quasiparticle and Phonon Lifetimes in Superconductors", Phys. Rev. B14, 4854 (1976).

[14] A. Rothwarf and B. N. Taylor, "Measurement of Recombination Lifetimes in Superconductors," Phys. Rev. Lett. 19, 27 (1967).

Abstract of Paper Presented at the
Workshop on High Temperature Superconductivity
23-25 May 1989 GACIAC PR 89-02

Electronic Device Research at Los Alamos In High T_c Superconducting Thin Films

Ross A. Lemons
Los Alamos National Laboratories
MS D429
Los Alamos, NM 87545

ABSTRACT

At Los Alamos National Laboratory we have a broad interest in the electronic device applications of high T_c superconductors. The applications of interest include LWIR detectors, microwave components, SQUIDs, and Josephson devices. Our team includes materials scientists, characterization specialists, device engineers, and theorists.

We have concentrated our efforts on $YBa_2Cu_3O_7$. After exploring several techniques for depositing thin films of this material, including laser evaporation and deposition from solution, we focused on coevaporation. We use a vacuum system with independent electron beams to evaporate the Y and Cu and a thermal boat to evaporate BaF_2. The rates of deposition from each source are controlled by independent thickness monitors calibrated with a fourth thickness monitor mounted at the sample position. The resulting films are annealed in wet oxygen to remove the fluorine and to convert the film into the superconducting phase. Our best films have been prepared on $SrTiO_3$ single-crystal substrates. The crystallographic orientation of the superconducting film can be controlled by the film thickness and annealing conditions. Pre-dominant c-axis normal orientation is achieved in thin (~2500Å) films annealed above 850°C. These films have T_c in the range of 85 K to 93 K and critical currents of 10^5 A/cm^2 at 77 K. We pattern these films by sputter etching through a photoresist mask and apply gold contacts with a photoresist liftoff technique.

To date, our device research has focused on LWIR detector applications. Our test devices are current constriction patterns in which slots etched into 2.0-mm square pads of superconducting film force the current through a narrow constriction in the center, or serpentine patterns with aspect ratios of 20 to 200.

THIS PAGE IS INTENTIONALLY BLANK

Presented at the Workshop on High Temperature Superconductivity
23-25 May 1989 GACIAC PR-89-02

Infrared Study of (Bi,Pb) - Sr - Ca - Cu - Oxide High-T_c Superconductors

May 23-25, 1989

H. L. Luo
Department of Electrical and Computer Engineering, R-007
University of California, San Diego
La Jolla, CA 92093-0407

and

B. H. Loo
Department of Chemistry
University of alabama
Huntsville, Alabama 35899

ABSTRACT

Infrared spectroscopic study has been conducted on the high-T_c (Bi,Pb) - Sr - Ca - Cu - oxide system, using the conventional transmittance and the diffuse reflectance techniques in the range of 200-4000 wavenumbers (2.5-50 μm). Preliminary date indicated that the absorption spectrum can be divided into two groups:

(1) Absorption peaks in the 200-400 wavenumber region which is quite typical for most oxide materials.

(2) Strong absorption is indicated throughout the entire 400-4000 wavenumber range except for a few possible windows which may be useful in simple detecting devices application.

A more systematic study, careful analysis and calibration are needed to gain a more fundamental understanding of the IR behavior of this material and to evaluate the true application potential.

Introduction

Ever since the discovery of superconducting oxides with critical temperature (T_c) above liquid nitrogen[1-3], their infrared (IR) behaviors have become a fascinating research topic. On the one hand, the IR spectrum, if accurately recorded and correctly analyzed, can provide information concerning the fundamental mechanism of the high-T_c superconductivity such as the superconducting gap, phonon interaction, various vibrational modes etc. On the other hand, potential applications also exist in the IR range. Several research groups have already attempted studies on the IR spectra of $YBa_2Cu_3O_{7-\delta}$ [4-11]. The work on the Bi-Sr-Ca-Cu-oxide system is just beginning[12]. Reported here is the preliminary results of our experiments.

Experimental Procedures, Results and Discussion

All IR experiments were conducted with specimens held at room temperature. For the purpose of comparison all IR specimens were prepared from the same master piece which was a single-phase ceramic material with the composition $Bi_{1.7}Pb_{0.3}Sr_2Ca_2Cu_3O_y$. The general preparation procedures through solid state reaction is reported separately in this proceeding[13]. The critical temperature of the master sample is ~ 115 k with zero resistance at 96 K, as shown in Figure 1.

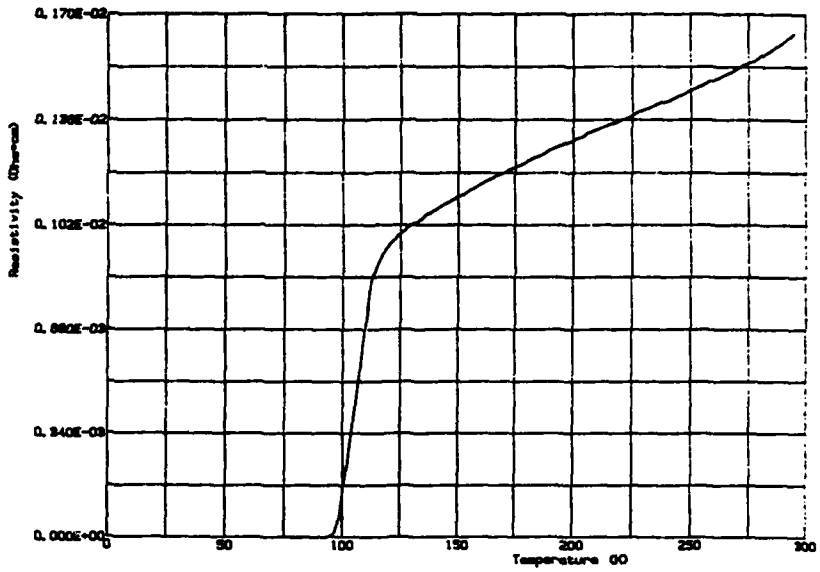

Figure 1. Resistive transition of the $Bi_{1.7}Pb_{0.3}Sr_2Ca_2Cu_3O_x$ sample.

Three independent IR measurements were conducted using different instruments:

(I) A small piece of the master sample was powdered and mixed with KBr powders in the ratio of 1 : 75 ~ 80. The mixture was then pressed into a disk (1 cm in diameter, ~ 1 mm thick) using a stainless steel die. The IR transmittance measurements were performed in the range of 400 ~ 4000 cm^{-1} using a Nicolet 7199 FTIR spectrometer with a liquid-nitrogen cooled (Hg, Cd)Te detector. As shown in Figure 2, the material is highly absorbent above 1000 cm^{-1} and the only discernable structure is at ~ 600 cm^{-1}.

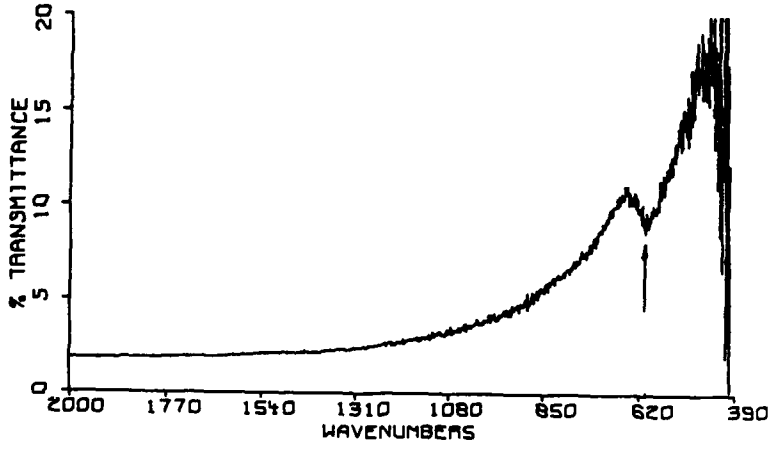

Figure 2. Room temperature IR transmittance of $Bi_{1.7}Pb_{0.3}Sr_2Ca_2Cu_3O_x$. Sample powders were mixed in KBr.

(II) Because of the cutoff of KBr at 400 cm^{-1}, a second set of transmittance experiments was carried out on a Perkin-Elmer 1330 IR Spectrometer in the range of 200 ~ 1000 cm^{-1}. The IR specimens were prepared in the same manner as in Experiment I except CsI was used as the diluent. As shown in Figure 3, there are definite activities between 200 and 400 cm^{-1}. The transmittance minimum at 605 cm^{-1} is also confirmed.

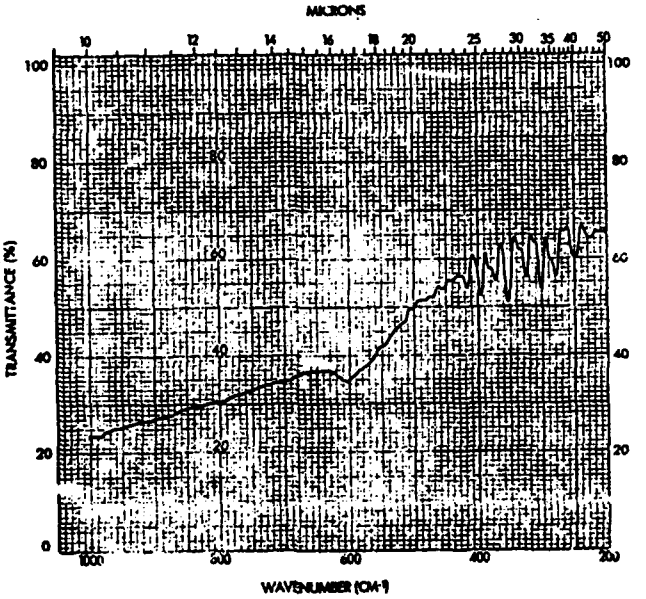

Figure 3. Room temperature IR transmittance of $Bi_{1.7}Pb_{0.3}Sr_2Ca_2Cu_3O_x$. Sample powders were mixed in CsI.

(III) Due to the strongly absorbent nature of the material, an additional series of diffuse reflectance experiments were conducted on a Nicolet 740 FTIR Spectroscopy System in the range of 400 - 1300 cm^{-1}. The specimen was a solid piece and the reflecting surface was mechanically flat. For easy comparison, the experimental results were converted to absorbance (shown in Figure 4) through programmed data processing which included subtraction of background and exorbitant expansion of intensity scale.

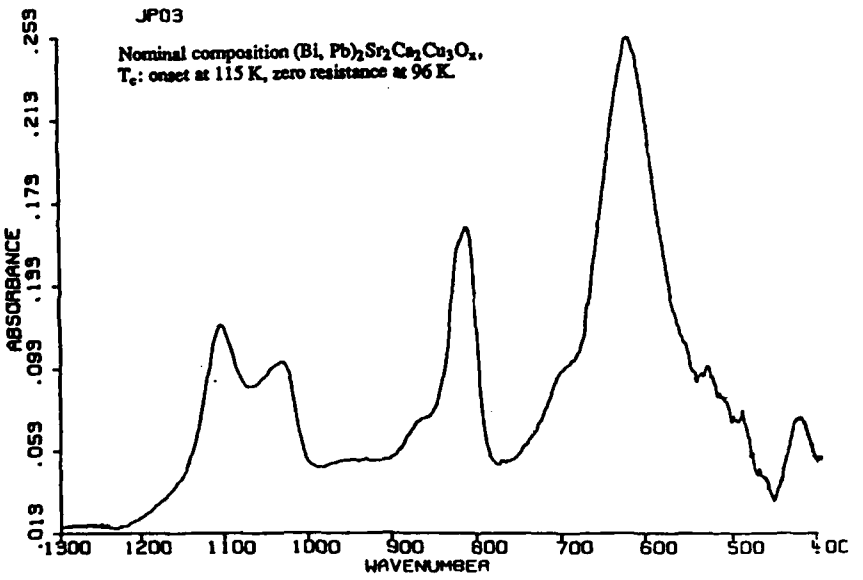

Figure 4. Diffused reflectance infrared Fourier-transformed spectrum of $Bi_{1.7}Pb_{0.3}Sr_2Ca_2Cu_3O_x$ at room temperature.

The three sets of data are summarized in Table I for comparison. Although they cover different ranges of frequencies the agreement is very good in the limited overlapped region (400 ~ 600 cm^{-1}). It must be emphasized that the data presented here are preliminary. Before any application can be realized, more systematical and more detailed work is required to assign definitive meaning of the experimental results.

Following the conventional approach, the absorbance peaks below 700 cm^{-1} can be assigned to the various vibrational modes associated with the planar CuO_4 configuration[4]. Peaks at higher frequencies would have to belong to smaller atom groups, such as an out-of-plane oxygen ion.

Table I. Summary of IR data from three independent measurements on the same $Bi_{1.7}Pb_{0.3}Sr_2Ca_2Cu_3O_x$ ceramic material

Transmittance Minima (cm^{-1})		Absorbance Maxima (cm^{-1})
Experiment I	Experiment II	Experiment III
----	227	----
----	250	----
----	280	----
----	303	----
----	326	----
----	353	----
----	373	----
----	396	----
----	418	423
600	605	620
----	----	810
----	----	1030
----	----	1105

Acknowledgement

Part of this work was supported by a short term grant from Science Applications International Corp. to UCSD arranged by Dr. J. C. Solinsky. The authors are indebted to Dr. M. Smith of Nicolet Instruments Corp. for the diffuse reflectance measurements.

References

(1) M. K. Wu, J. R. Ashburn, C. J. Torng, P. H. Hor, R. L. Meng, L. Gao. Z. J. Huang, Y. Q. Wang and C. W. Chu, *Phys. Rev. Lett.* 58, 908 (1987).

(2) H. Maeda, Y. Tanaka, M. Fukutomi and T. Asano, *Jpn. J. Appl. Phys.* 27, L209 (1988).

(3) Z. Z. Sheng and A. M. Hermann, Nature 332, 138 (1988).

(4) G. Burns, F. H. Dacol, P. Freitas. T. S. Plaskett and W. König, *Solid State Commun.* 64, 471 (1987).

(5) D. A. Bonn, J. E. Greedan, C. V. Stager, T. Timusk, M. G. Doss, S. L. Herr, K. Kamaras and D. B. Tanner, *Phys. Rev. Lett.* 58, 2249 (1987).

(6) L. Genzel, A. Wittlin, J. Kuhl, H. Mattausch, W. Bauhofer and A. Simon, *Solid State Commun.* 63, 843 (1987).

(7) M. Stavala, D. M. Krol, W. Weber, S. A. Sunshine, A. Jayaraman, G. A. Kourouklis, R. J. Cava and E. A. Rietman, *Phys. Rev.* B36, 850 (1987).

(8) G. A. Thomas, H. K. Ng, A. J. Millis, R. N. Bhatt, R. J. Cava, E. A. Rietman, D. W. Johnson, G. P. Espinosa and J. M. Vandenberg, *Phys. Rev.* B36, 846 (1987).

(9) I. Bozovic, D. Mitzi, M. Beasley, A. Kapatulnik, T. Geballe, S. Perkowitz, G. L. Carr, B. Lou, R. Sudharsanan and S. S. Yom, *Phys, Rev.* B36, 4000 (1987).

(10) Z. Schlesinger, R. T. Collins, D. L. Kaiser and F. Holtzberg, *Phys. Rev. Lett.* 59, 1958 (1987).

(11) H. J. Ye, W. Lu, Z. Y. Yu, X. C. Shen, B. C. Miao, Y. M. Cai and Y. J. Qian, *Phys. Rev.* B36, 8802 (1987).

(12) M. Reedyk, D. A. Bonn, J. D. Garrett, J. E. Greedan, C. V. Stager, T. Timusk, K. Kamaras and D. B. Tanner, *Phys. Rev* B38, 11981 (1988).

(13) H. L. Luo, S. M. Green, Yu Mei and A. E. Manzi, Proc. Workshop High Temp. Superconductivity, Huntsville, AL (1988).

Presented at the Workshop on High Temperature Superconductivity
23-25 May 1989 GACIAC PR-89-02

IN-SITU DIAGNOSTICS OF LASER ABLATED FILMS OF YBaCuO

P.W. Morrison, Jr., D.G. Hamblen, and P.R. Solomon
Advanced Fuel Research, Inc.
87 Church Street, East Hartford, CT 06108 (203) 528-9806

L. Lynds, B. R. Weinberger, and T.W. Grudkowski
United Technologies Research Center
Silver Lane, East Hartford, CT 06118 (203) 727-7364

ABSTRACT

Developing an in-situ diagnostic for the deposition of thin films of YBaCuO could play an important role in improving the material's properties and eliminating the separate annealing step. If one has an in-situ probe of the temperature, thickness, and structure of the deposited films, designing and testing improvements to the deposition reactor and its operating conditions becomes more efficient, the search for new materials and stoichiometries is greatly facilitated, and process control becomes a realistic possibility. The in-situ diagnostic described here is Fourier Transform Infrared (FT-IR) spectroscopy between 6500 cm^{-1} and 220 cm^{-1}. Emission FT-IR yields substrate temperature while reflection or transmission FT-IR provides information on film thickness, morphology, and crystalline phase (tetragonal vs orthorhombic). The deposition process uses a YAG laser to ablate material from a superconducting pellet of YBaCuO. The substrate is $SrTiO_3$, and the deposition times last up to 10 minutes (about 5 micrometer films). Films are subsequently annealed to produce superconductivity. Emission measurements from $SrTiO_3$ show that emission bands at 870 cm^{-1} and 482 cm^{-1} produce a

very accurate measure of substrate temperature. The reflectance spectra of as-deposited films have well defined features below 2000 cm^{-1}. These features contain both morphological and compositional information and are a function of film thickness. After annealing, these well defined features disappear, and the reflectance increases smoothly at low wavenumbers.

This work has been perform for SDI under contract number DASG60-88-C-0083.

INTRODUCTION

The rate of development of thin film deposition of high temperature superconductor could be increased if investigators did not have to remove samples from the deposition reactor for analysis. An in-situ diagnostic of the film's stoichiometry, temperature, thickness, and structure would significantly aid the thin film technology. The in-situ diagnostic reported here is Fourier Transform Infrared (FT-IR) spectroscopy. A combination of emission, reflection, and transmission FT-IR yields substrate temperature, phase changes, film thickness, and water contamination. Inferring oxygen content, grain size, and ambient gas concentration and temperature is also possible. We have applied the FT-IR diagnostic during laser ablation of YBaCuO (YBCO) films.

EXPERIMENTAL

FT-IR Spectroscopy - The FT-IR spectroscopy is divided into three broad classes of experiments: transmission, reflection, and emission. Figure 1 shows schematically the optics for these experiments. Transmission measurements use the FT-IR in its standard configuration as shown in Fig. 1a. The reflectance apparatus is a small modification of the transmission setup (Fig. 1b). For both of these configurations, radiation from the source travels along the interferometer's optics and reaches the sample. A mask allows only radiation from the sample to reach the detector. Emission spectroscopy utilizes the apparatus in Fig. 1c. Radiation from the sample follows the same path of the transmission beam except that the sample radiation leaves the spectrometer via a side port and enters the emission detector. A mask still acts as an aperture, but it is held above the sample surface and kept cooled.

The FT-IR spectrometer used in this research is the Bomem Michelson 102. It is specially equipped with CsI windows and CsI beam splitter to permit measurements down to ~200 cm^{-1} (50 μm). The Michelson 102 uses a pyroelectric bolometer, deuterated triglycine sulfate (DTGS), as a detector. It also has a flexible optical path that converts easily from transmission (or reflection) to emission. Future designs will be capable of simultaneous emission and transmission measurements.

Laser Ablation - The deposition reactor is a cylindrical vacuum chamber with twelve windows equally spaced in 30 degree increments (Fig. 2). Ablation and diagnostic measurements are arranged in a horizontal, co-planar configuration. Pulsed Nd:YAG (1064 nm) radiation is focused onto the target surface at an angle of 30 degrees to the target normal. The flash lamp excited laser has a stable resonator and generates a multi-mode pulse train consisting of 100 ns peaks with a persistence of about 150 μs per flash. In the far field, the spatial intensity distribution is rather flat with an approximate diameter of 0.04 cm in the focal plane of a 25 cm focal length quartz lens. To avoid pitting the target, the target holder is continuously rotated and translated to scan the laser across the target.

The bulk samples used for laser ablation are synthesized at United Technologies Research Center (UTRC) by the following standard procedure. Appropriate quantities of the metal oxide precursors (Y_2O_3, $BaCO_3$, CuO) are dissolved in HNO_3, dried at 200°C, and then sintered in air in two steps: 800°C and 930°C each for 24 hr with an intervening grinding. The powder is subsequently cold pressed at 25,000 psi into disks (1.3 cm diameter and 0.2 cm thick). Complete transformation to the superconducting phase occurs after annealing in O_2 at 920°C for 24 hours and then at 700°C for another 24 hours.

The substrate for the YBCO film is $SrTiO_3$. During deposition, the substrate temperature is 350-450°C. The laser fluence (determined by calorimetry of the pulse train persisting for about 100 μs) is 180 J/cm^2. The repetition rate is 8 pulses per second. The target and substrate are 3-5 cm apart during ablation. Typical film thicknesses are approximately 4-5 microns for 10 minutes of ablation. During ablation, there is a background gas of O_2 at 0.5-1 mtorr pressure. Asymmetry in the spatial distribution of stoichiometry necessitates careful positioning of the substrate to minimize undesirable phases (1). It is important to constrain collection angles to within 10 degrees of the target normal despite the temptation to collect in more "specular" regions where the deposition rates are greater.

Films are typically annealed at 900°C in dry O_2 for 2 hours followed by a slow cool to 700°C. After remaining at 700°C for several hours, the films are cooled to room temperature.

Integration of FT-IR Spectrometer with Deposition Apparatus - Temporary modifications to the deposition apparatus are necessary before making in-situ FT-IR measurements. Under normal

(1) Lynds, L., Weinberger, B.R., Potrepka, D.M., Peterson, G.G., and Lindsay, M.P., "High Temperature Superconducting Thin Films: The Physics of Pulsed Laser Ablation", submitted to Physica C (1989).

operating conditions, both the target and substrate are near the center of the chamber. Due to limitations on the focal lengths of readily available mirrors, the sample has been moved closer to the windows. To accomplish this, we moved both the target and substrate off center and have used a mirror to redirect the laser onto the target (Fig. 3). The mirror is on a crank shaft to move the beam across the surface of the target. This arrangement is for demonstration purposes only. It cannot be used under routine conditions because the focused laser radiation destroys the mirror. Future design(s) will use special FT-IR optics to avoid changing the deposition geometry.

There are separate FT-IR configurations for reflection and emission. The reflection configuration (Fig. 3a) uses a flat mirror and an off-axis parabolic mirror to direct radiation from the spectrometer onto the substrate. Reflected IR leaves the chamber through a second window. Both IR windows are CsI. To protect the windows from moisture, heating tape keeps the windows warm. The reflection apparatus does not require an aperture because the substrate itself acts as an aperture. The emission configuration employs the same flat mirror and off-axis mirror to couple radiation from the substrate into the interferometer. This optical arrangement requires a limiting aperture to make the emission results quantitative. The limiting aperture ensures that the size of the focal volume is the same during both the path correction (black-body) and substrate measurements. For simplicity, we employ an aperture on a retractable arm. The aperture covers the sample only during FT-IR measurements, not during deposition. Future designs will have the limiting aperture at another point in the optical path. Filters for the laser radiation are not necessary because the laser is turned off during the acquisition of FT-IR spectra.

RESULTS AND DISCUSSION

This section is divided into discussions of substrate temperature, ex-situ results, in-situ measurements, and annealing studies.

Substrate Temperature - Following the analysis of Chase (2), the radiance of a hot sample at a temperature T is given by

$$S(\nu,T)/R(\nu) = \epsilon(\nu) [H(\nu,T) - H(\nu, 300\ K)]$$

(2) Chase, D.B., Applied Spectroscopy, **35**, 77, (1981).

where ν = wavenumber, $S(\nu,T)$ = output signal of a room temperature detector, $R(\nu)$ = instrument response function (path correction), $\epsilon(\nu)$ = emissivity of the sample, and $H(\nu,T)$ = Planck function for a black body of temperature. A separate calibration determines $R(\nu)$.

Temperature of the sample can be measured if $\epsilon(\nu)$ at any ν is known. In the case of $SrTiO_3$, two such values are available. In general, radiation incident on the $SrTiO_3$ must be reflected, absorbed, or transmitted. A 1 mm thick substrate of $SrTiO_3$ has a transmittance of zero below 1400 cm^{-1} (Fig. 4a).

Furthermore, the reflectance of $SrTiO_3$ drops to zero at 870 and 482 cm^{-1} (Fig. 4b). (The dispersion relation of $SrTiO_3$ shows that the index of refraction is equal to unity at these two points). Thus the$SrTiO_3$ is completely absorbing at those two wavenumbers and has $\epsilon(870\ cm^{-1}) = \epsilon(482\ cm^{-1}) = 1$. Substituting either of these values into Eq. 1 and solving for the unknown T yields the temperature of the substrate.

Figure 4c shows quantitative measurements of $\epsilon(\nu)$ and temperature for a $SrTiO_3$ substrate. The prediction in Fig. 4c ($H(\nu, 542K) - H(\nu, 300\ K)$) has been fit to the $SrTiO_3$ data by using $\epsilon(870\ cm^{-1}) = 1$. As shown, the predicted radiance and the measured radiance also match at 482 cm^{-1} where ϵ also equals unity. The radiance at 870 cm^{-1} is the best point to fit because of the higher signal to noise at that point. The thermocouple measurement on the surface of the substrate is about 12K lower than the temperature determined by the fit. The fit is accurate to ± 5 K. The FT-IR can clearly make accurate surface temperature measurements without contacting the substrate.

Ex-Situ Measurements - Transmission measurements yield valuable information about contamination and grain size. Figure 5 is the spectrum of film (2-3 μm thick) on a KBr single crystal. The sloping baseline indicates scattering from morphological features in the film. From the shape, the size of these features is less than 1 μm. The feature near 3000 cm^{-1} is due to water; this feature grows substantially when the film is exposed to air (Fig. 5b).

Some information can be gained by taking transmission spectra of the YBCO films deposited on $SrTiO_3$. Figure 6 shows the differences between the $SrTiO_3$ substrate (a), the ablated film (b), and the annealed film (d). The sloping baseline in spectrum (b) is again due to scattering from the "grains" of the ablated YBCO. Spectrum c is the ratio of b to a which removes most of the $SrTiO_3$ effects in the spectrum. As the reader can see, spectrum c is substantially the same as Fig. 5a. On the other hand, the transmittance of the annealed film is zero (Fig. 6d). This is consistent with the results of other

authors who find that τ is zero when the film thickness is greater than 0.4 μm (3).

The as-deposited and annealed thin films show dramatic differences in reflection (Fig. 7a-b); the reflectance from $SrTiO_3$ is included for reference (c). The as-deposited films do not display metallic behavior reflectance (increasing reflectance at low wave numbers). After annealing, the ablated film becomes a metal and has a spectrum similar to the annealed bulk. Magnetometry shows that this film is a superconductor (Meissner fraction = 10-15%). Clearly, the FT-IR can distinguish between ablated and annealed films.

In-Situ Measurements - Two kinds of in-situ measurements have been made: reflection and emission. The deposition conditions are similar to those discussed above except that there is no oxidizer present during ablation and the substrate temperature is nominally 300°C.

Reflection - Figure 8 contains in-situ measurements of the reflectance of a growing film at 0, 1, 2, and 3 minutes (corresponding to thicknesses of 0, 0.5, 1.0, and 1.5 μm). The background for these spectra is a gold mirror mounted over the $SrTiO_3$ substrate. The reference mirror must be slightly misaligned, since the reflectance exceeds 100% at some wavenumbers. Note that the reflectance at wavenumbers above 5000 cm^{-1} slowly decreases with thickness. There is also a broad peak that moves as the YBCO thickness increases. The source of this feature is unknown, but it could be scattering from grains in the film.

The reflectance of these films is different from the reflectance of film deposited with oxidizer in the reactor (Fig. 9). Besides the differences in features below 800 cm^{-1}, the specular reflectances at 6500 cm^{-1} are very different. One possible explanation is the graininess of the films. Films deposited in vacuum (Fig. 9b) could be more grainy because there is no buffer gas to slow the ablated material and/or because the low substrate temperature prevents sintering. The resultant graininess would substantially reduce the specular reflectance.

Emission - Figure 10 contains emission spectra taken in-situ during another deposition experiment. The spectra correspond to 0, 2, 4, and 6 minutes (roughly 0, 1, 2, and 3 μm thick). The emission from the bare $SrTiO_3$ is slightly different than the emission spectrum in Fig. 4c. The in-situ spectrum is different because the $SrTiO_3$ is fixed to the heater using an adhesive which has emission bands above 900 cm^{-1}. Please note that the fit to the $SrTiO_3$ emission yields a temperature of 499 K while the nominal substrate temperature is 573 K.

(3) Bozovic, I. Kirillov, D., Kapitulmik, A., Char, K., Hahn, M.R., Beasley, M.R., Geballe, T.H., Kim, T.H., and Heeger, A.J., Phys. Rev. Lett., **59**, 2219, (1987).

The emission spectra of ablated YBCO have characteristic features that are similar to the reflectance features. In particular, there are two high emissivity bands, one between 800 and 500 cm^{-1}, and another between 480 and 460 cm^{-1} (arrows in Fig. 10). Both bands shift to smaller wavenumbers as deposition time increases; the shift for the 480-460 cm^{-1} band is barely noticeable. The locations of the emission bands are the same as the low reflectance bands in the in-situ reflectance spectra (arrows in Fig. 8). Both low reflectance bands also shift to smaller wavenumbers as deposition time increases. There are two possible explanations for this phenomenon. The transmission spectrum of Fig. 5a shows an absorption peak near 600 cm^{-1}. The moving band could be the result of the transition from the 870 cm^{-1} of bare $SrTiO_3$ to the 600 cm^{-1} band of a thick ablated film. The second possibility is that the ablated film is forming an anti-reflectance coating. Figure 5a shows that the film is fairly transparent below 900 cm^{-1}. As stated above, the scattering centers (grains) in the film are less than 1 μm so that destructive interference could develop at wavenumbers below 1000 cm^{-1} (λ = 10 μm). Consequently, as the film becomes thicker, the two anti-reflectance wavelengths would gradually shift to longer wavelengths (smaller wavenumbers).

Annealing Studies - Additional experiments have focused on the changes induced by annealing YBCO films. As mentioned before, annealing a film into a superconductor causes a radical change in the reflectance of the film (Fig. 7). FT-IR reflectance can also detect more subtle effects, however. Figure 11 shows the reflectance spectra of a sample that has been re-annealed at 700°C (de-annealing). De-annealing in air produces a small change near 650 cm^{-1} while de-annealing in flowing helium has a dramatic effect. These changes may be due to either a change of phase or oxygen stoichiometry.

CONCLUSIONS

The above feasibility study demonstrates that FT-IR has great promise as an in-situ monitor for the deposition of superconducting films. Using transmission, emission, and reflection configurations, FT-IR can monitor: substrate temperature ($\pm$5 K), phase changes (ablated/annealed/de-annealed), film thickness (0-2 μm), water contamination, infer oxygen content, and infer grain size. In-situ FT-IR has also been demonstrated on a laser ablation reactor. Coupling the spectrometer to a preexisting deposition chamber is relatively straightforward. In-situ reflection and emission measurements of the film yield valuable processing information in real time. In addition, transmission through the background gas also yields gas composition. Further development of the FT-IR monitor could have a large scientific impact on understanding the relationship between film properties and processing conditions.

ACKNOWLEDGEMENTS

The authors gratefully acknowledge the support of this work by the Innovative Science and Technology Office of the Strategic Defense Initiative. The U.S. Army Strategic Defense Command has managed this research under contract DASG60-88-C-0083.

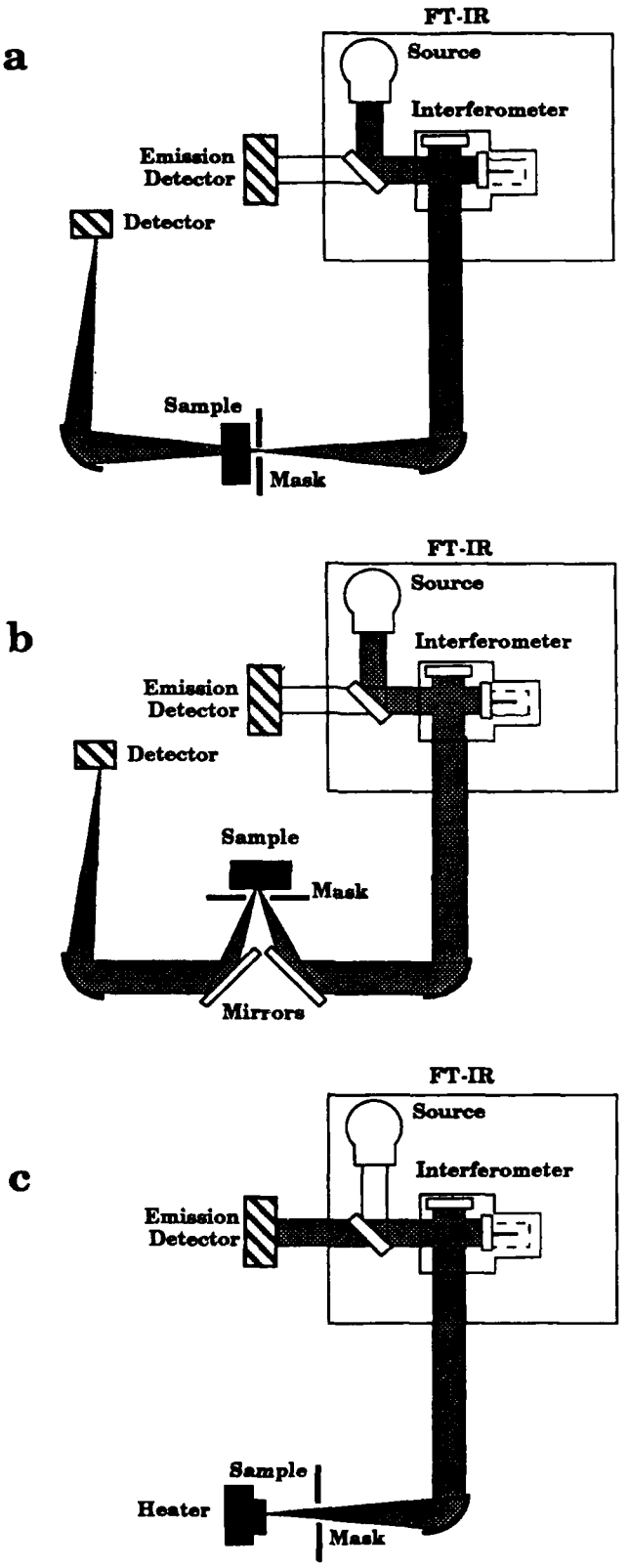

Figure 1. Three Optical Configurations for FT-IR: a)Transmission, b) Reflection, and c) Emission.

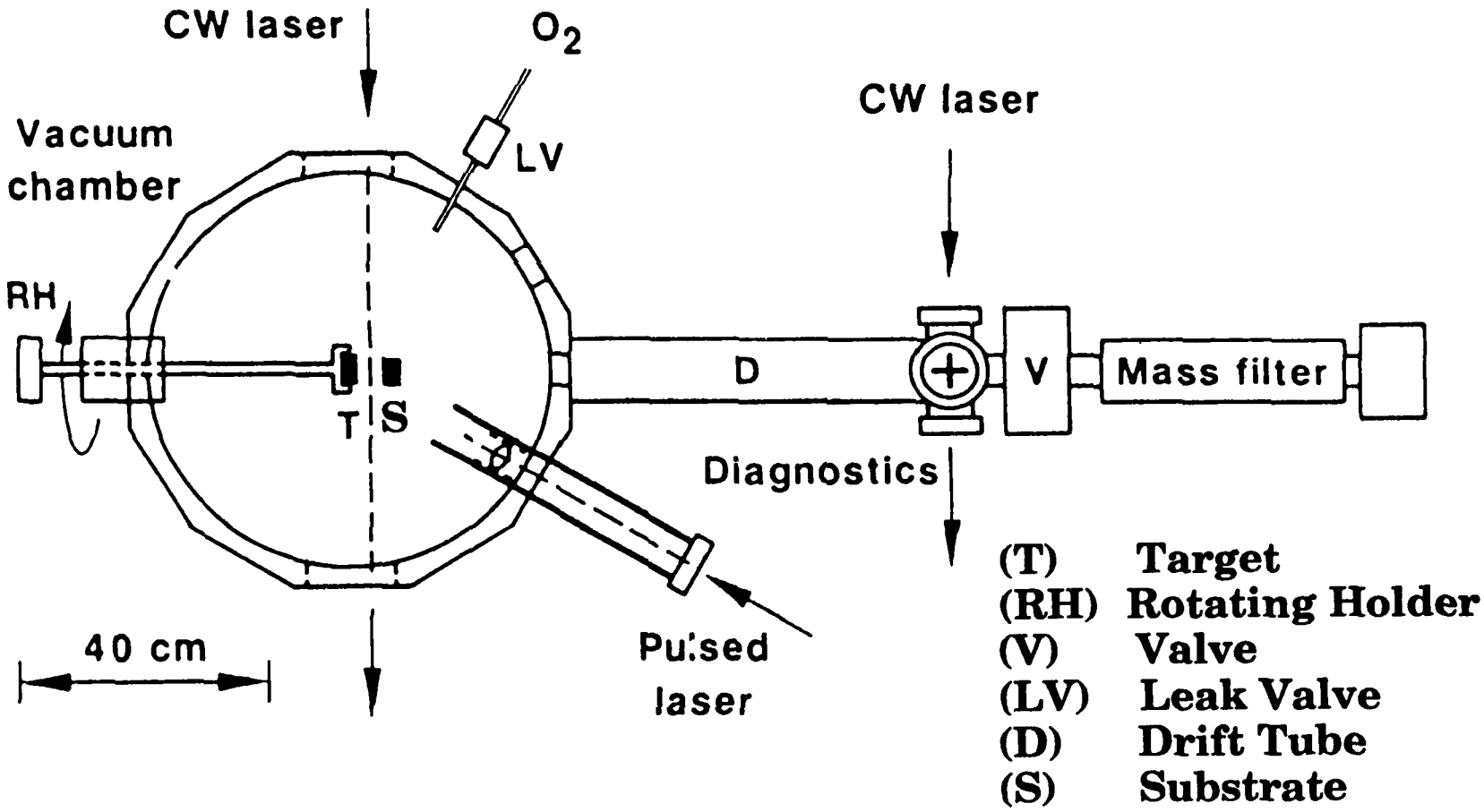

Figure 2. Schematic Diagram of the Laser Ablation System at United *Technologies Research Center.*

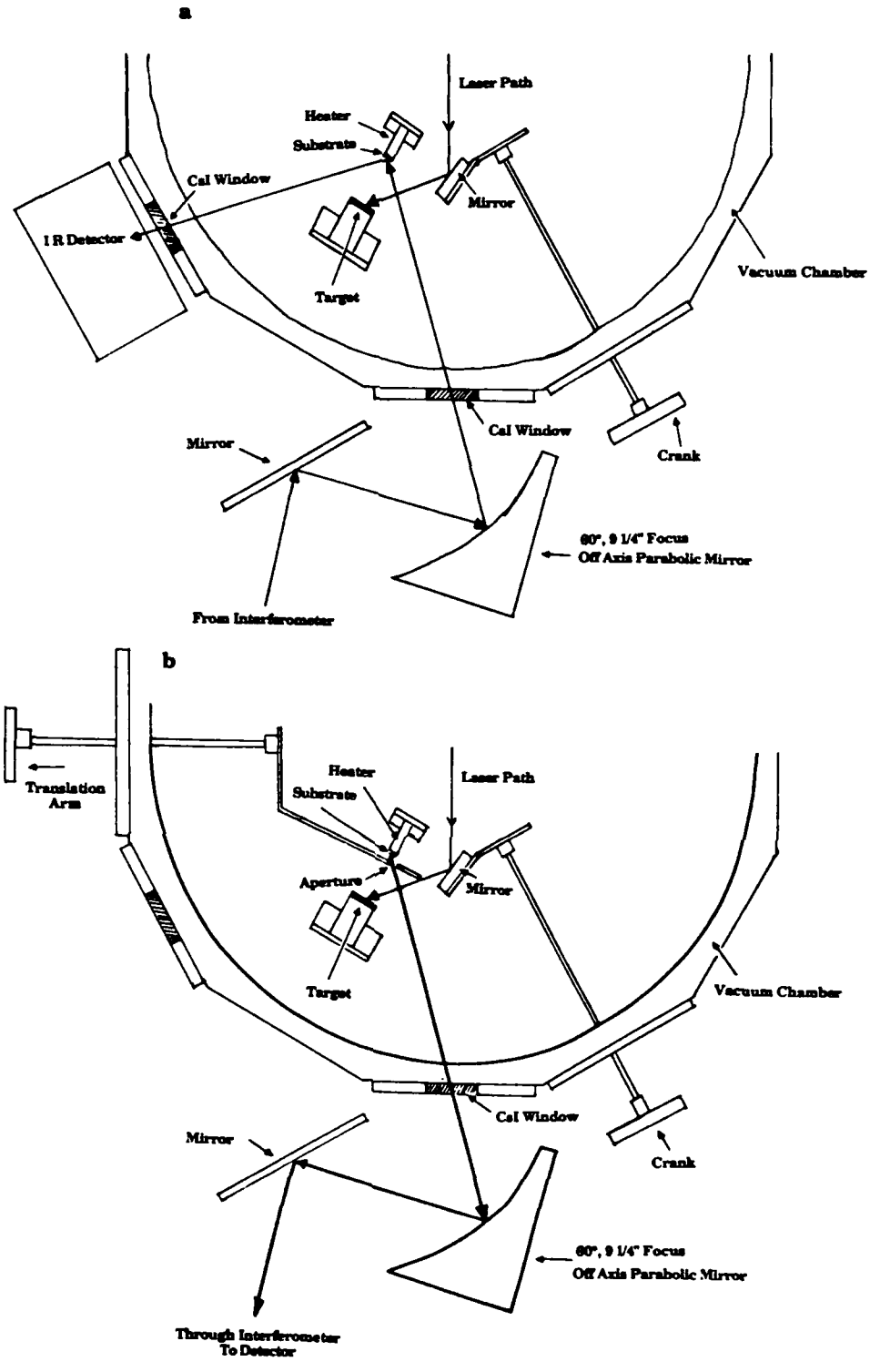

Figure 3. Optical Arrangements for Coupling IR Beams into Deposition Reactor: a) In-Situ Reflection and B) In-Situ Emission.

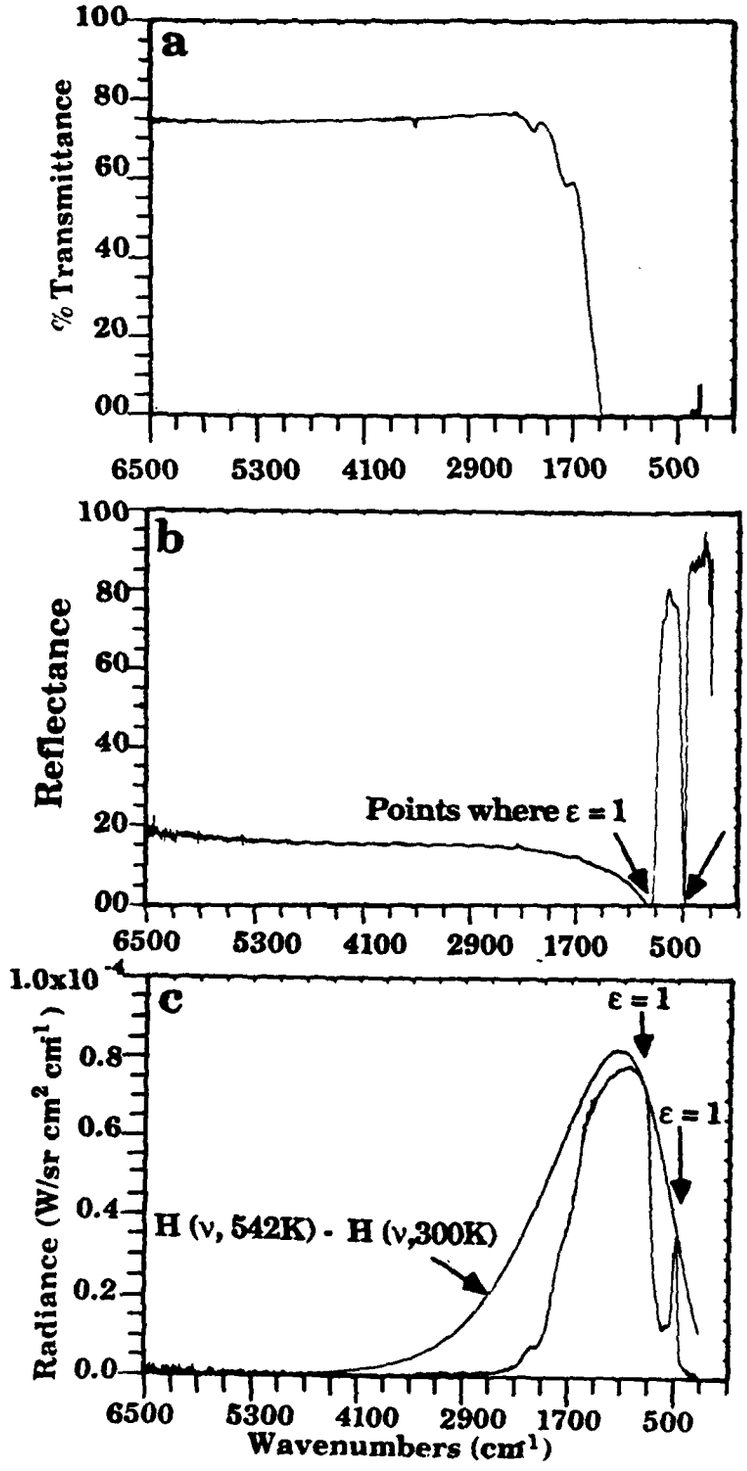

Figure 4. a) Transmittance, b) Reflectance, and c) Radiance of a 1 mm Thick Slab of $SrTiO_3$ Crystal.

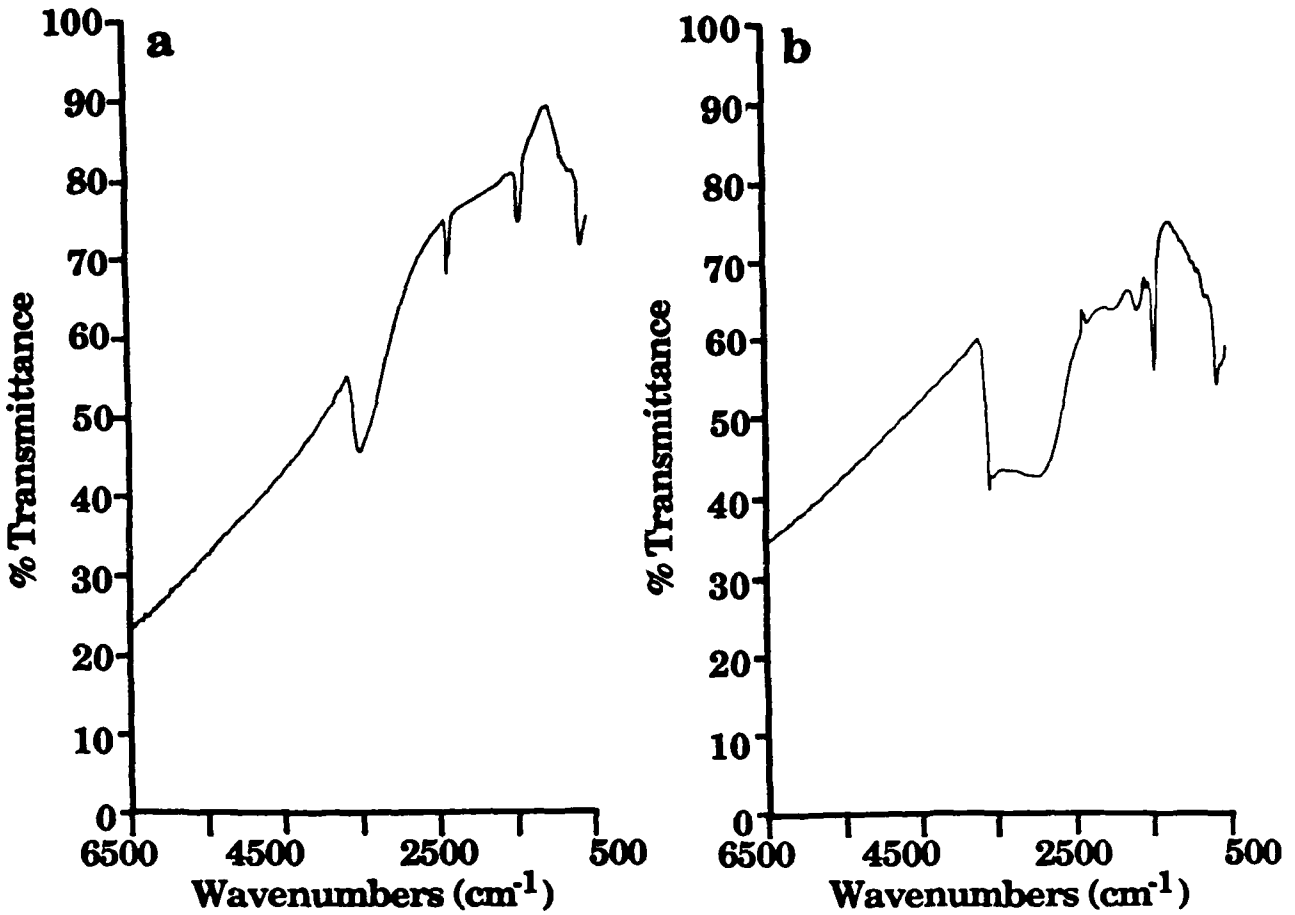

Figure 5. FT-IR Transmittance Spectra of Ablated YBCO Film on a KBr Window. a) Uncontaminated Film, b) Film Exposed to Air.

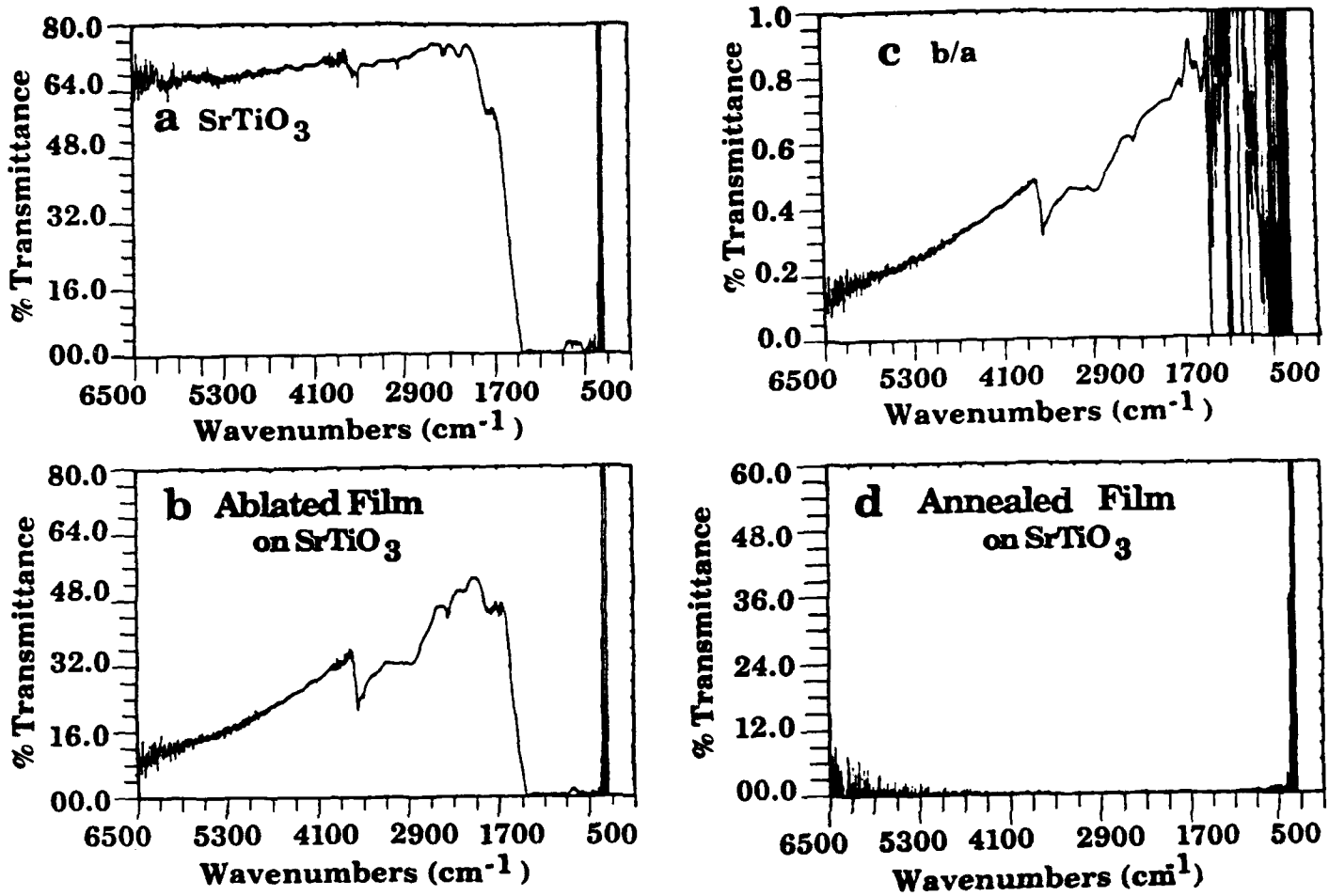

Figure 6. Transmission Spectra of YBCO Thin Films on $SrTiO_3$: a) $SrTiO_3$, b) Ablated Film on $SrTiO_3$, c) b/a and d) Annealed Film on $SrTiO_3$.

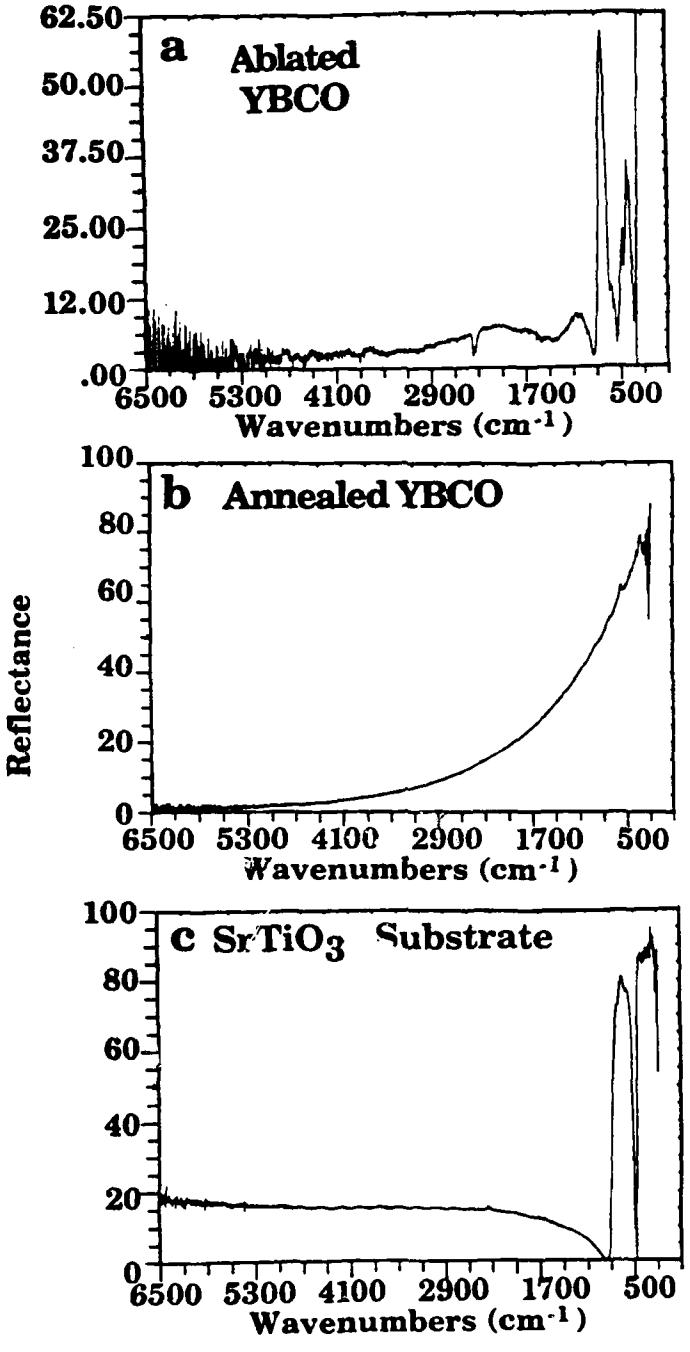

Figure 7. Reflectance From a) Ablated YBCO Film, b) Annealed YBCO Film, and c) $SrTiO_3$ Substrate.

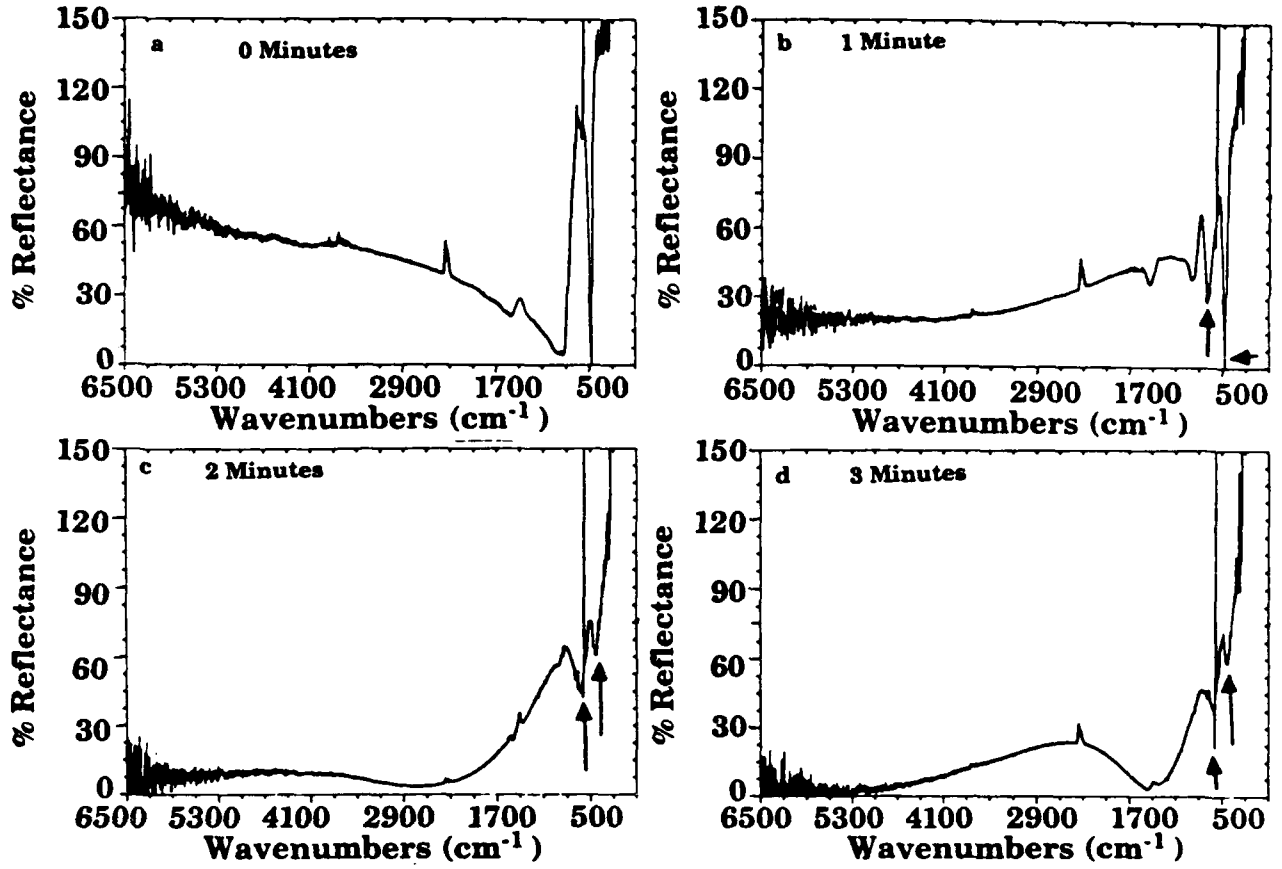

Figure 8. In-Situ Reflectance Measurements During Laser Ablation: a) 0 Minutes, b) 1 Minute, c) 2 Minutes, and d) 3 Minutes.

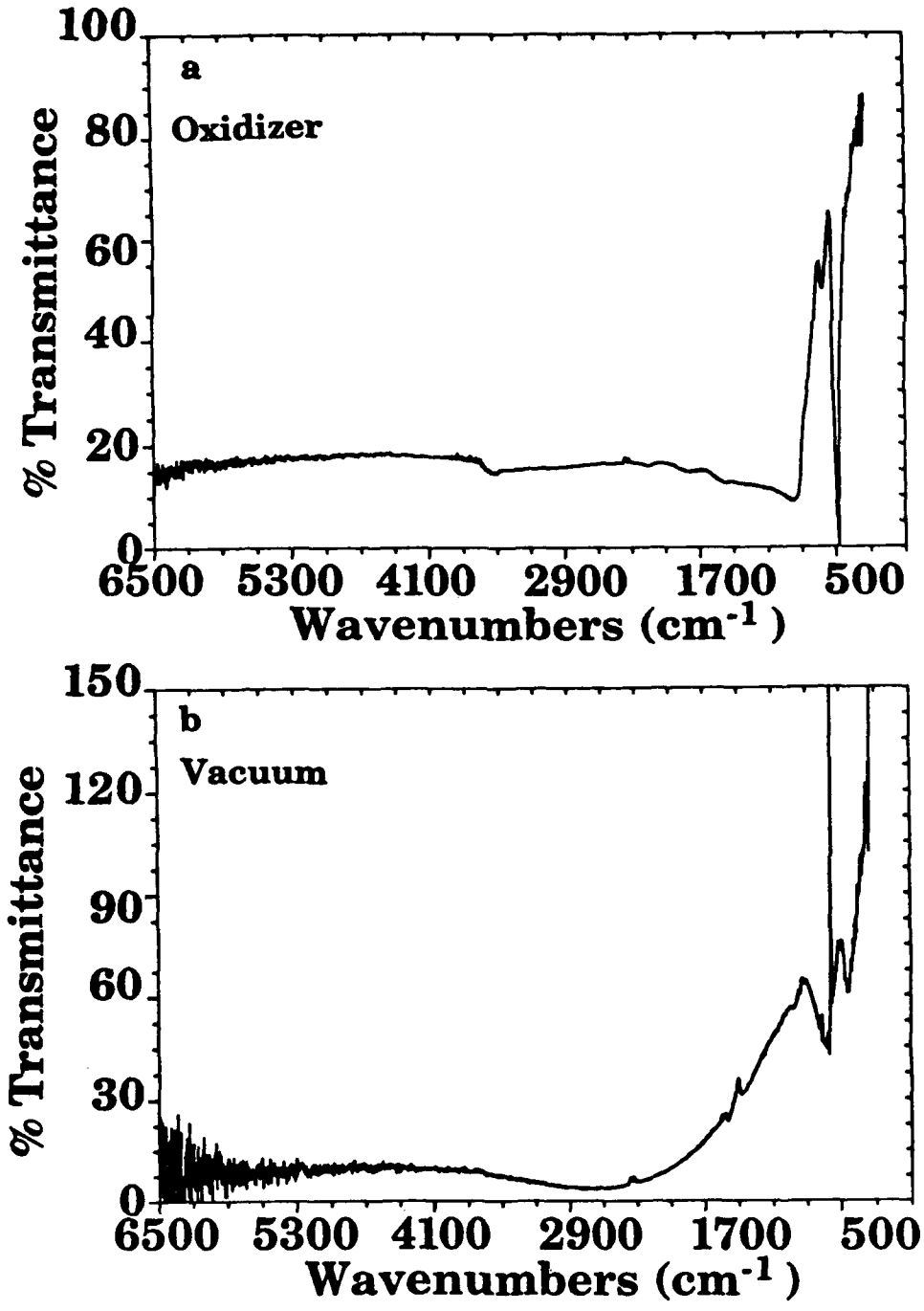

Figure 9. Reflectance From Films Ablated at Two Different Deposition Conditions: a) With Oxidizer and b) in Vacuum.

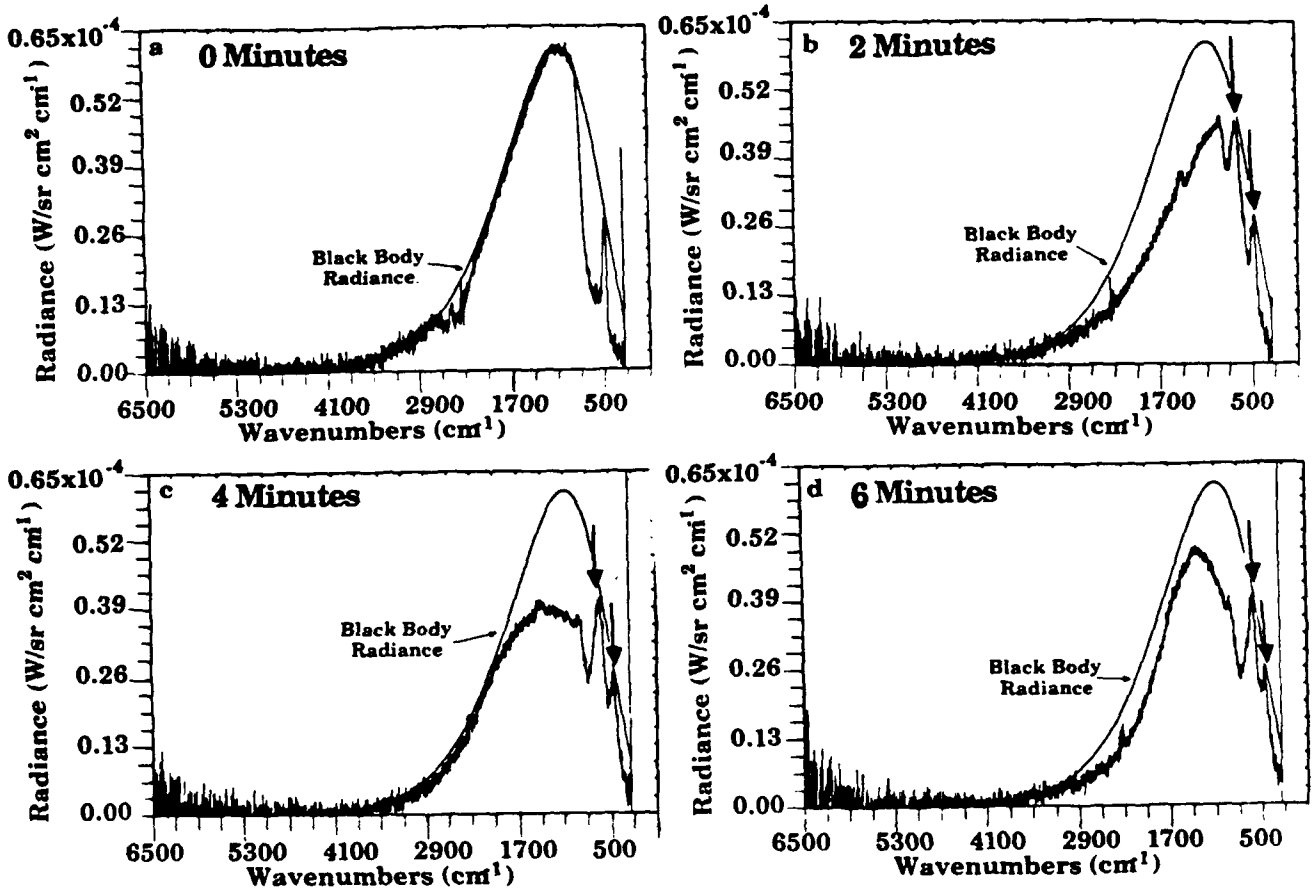

Figure 10. In-Situ Emission Measurements During Laser Ablation: a) 0 Minutes, b) 2 Minutes, c) 4 Minutes and d) 6 Minutes. The Smooth Curve is the Radiance of a 499K Blackbody.

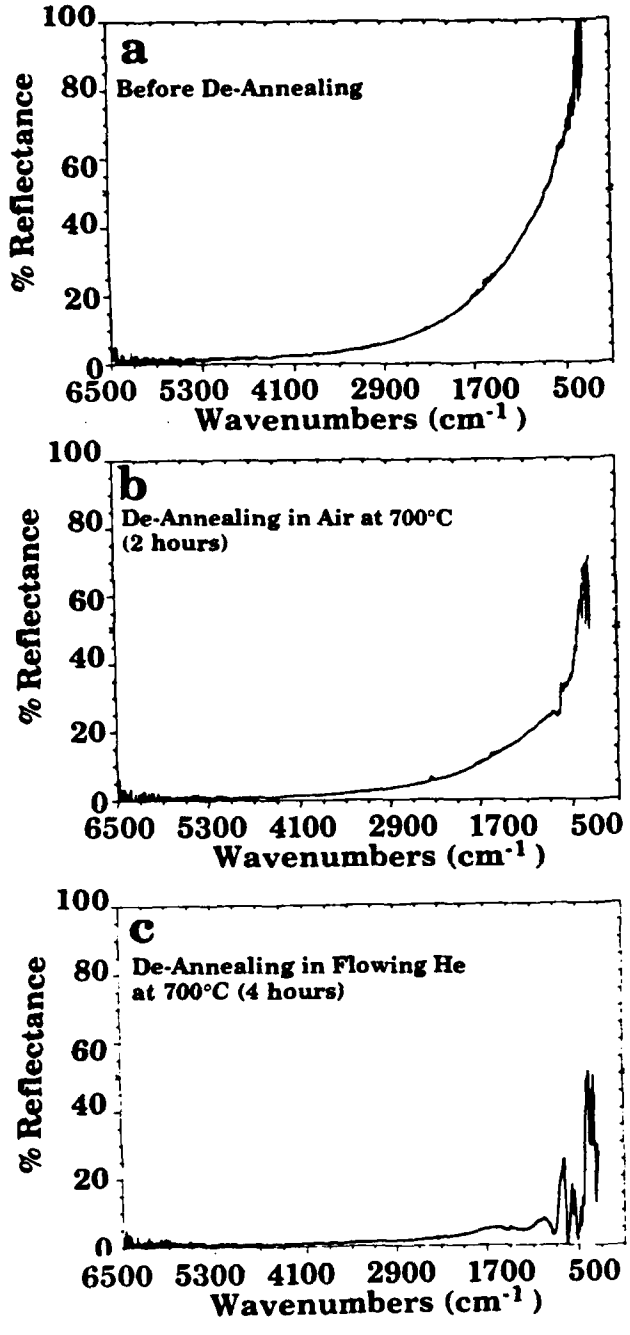

Figure 11. Reflectance of YBCO Films After De-Annealing: a) Before De-Annealing, b) De-Annealing in Air at 700°C (2 hours), and c) De-Annealing in Flowing He at 700°C (4 hours).

THIS PAGE IS INTENTIONALLY BLANK

Presented at the Workshop on High Temperature Superconductivity
23-25 May 1989 GACIAC PR-89-02

FABRICATION AND CHARACTERIZATION OF HIGH TEMPERATURE SUPERCONDUCTING SQUIDS SENSORS

by

I.S. Gergis, J.A. Titus,* P.H. Kobrin and A.B. Harker
Rockwell Science Center, Camino Dos Rios, Thousand Oaks, California 91360
and
*Rockwell Marine Systems Division, Anaheim, California 92803

ABSTRACT

D-C SQUIDs were fabricated from YBaCuO polycrystalline thin films utilizing the intergrain boundary weak links already existing in the films. The films were grown on single crystal MgO substrates using reactive ion beam sputtering from a single ceramic target in a partial pressure of oxygen. The SQUIDs were patterned using nonaqueous lithography and ion beam milling. The SQUID response varied from a well-defined an periodic form in some devices to aperiodic response in other devices. We have operated the SQUIDs in a flux-locked feedback loop and measured the noise output in that mode. The noise was dominated by a 1/f component below 50 Hz and room temperature electronics noise at higher frequencies. At 1 Hz, the SQUID sensitivity was 10^{-3} $\phi_o/\sqrt{Hz}$ and 10^{-4} $\phi_o/\sqrt{Hz}$ at 100 Hz. Hysteretic response was also observed in all devices with varying degrees and is attributed to flux trapping and detrapping in the body of the SQUID, the same mechanism which is responsible for the low frequency 1/f noise.

1.0 INTRODUCTION

One of the unique applications of superconductors has been in sensors based on superconducting quantum interference devices (SQUIDs). SQUIDs fabricated using conventional superconductors have shown exceptionally high sensitivities approaching the quantum limit at very low temperatures.[1] Several laboratories have reported SQUIDs made from thin films of high temperature superconductors with various compositions.[2-5] We reported previously on the first SQUID from thin film BiSrCaCuO.[6] In this paper, we report on the results obtained from thin film YBaCuO dc SQUIDs, including the operation in flux-locked mode and noise measure-

ments in the frequency range 0.1-1000 Hz. We also discuss the limitations on the performance of SQUIDs based on grain boundary junctions.

2.0 DEVICE FABRICATION

The superconducting thin films were grown using reactive ion beam sputtering from a single ceramic target onto single crystal MgO substrates.[7,8] The sputtering is done using a 1 kV Ar ion beam in the presence of a controlled oxygen background. The substrate can be heated, during deposition, up to 750°C. This technique has a very important advantage over plasma discharge sputtering in that it is free from negative ion back sputtering[9] and thus offers much better control of the stoichiometry of the film. Post deposition anneals were made to 900-950°C. YBaCuO films that had been deposited at low substrate temperatures, < 200°C, consisted of partially c-axis oriented grains. With higher substrate temperatures, 600-700°C, the as-grown films were epitaxial or very highly c-axis oriented. Only granular films, with J_C in the range 10^3-10^4 A/cm^2, produced SQUIDs with well-defined periodic response to magnetic fields. The granular films had transitions starting near 90K and zero resistance in the range 50-70 K. Devices were made by delineating the films using a nonaqueous lithographic process and ion beam milling. Au pads were deposited by evaporation and lifting off using a photoresist process. Most YBaCuO film thicknesses were 1.0 μm. The devices contained several SQUID patterns similar to that shown in Figure 1. The length of the weak link constrictions were in the range 5-10 μm and the width were in the range 2-7 μm. The SQUID loop area varied from 25 × 25 to 40 × 40 μm^2 corresponding to loop inductances from 40 to 63 pH. The devices were mounted and wired to ceramic packages which could be tested in magnetically shielded variable temperature cryostats.

3.0 EXPERIMENTAL RESULTS

We have fabricated and tested a large number of devices made on films of different morphologies. Devices made on granular films have shown a response to applied magnetic field but most responses were aperiodic. Devices from several films showed well-defined periodic response with a flux periodicity which corresponds to reasonable values of flux focusing factor. In general, devices showing periodic response were fabricated from films of relatively large grains and relatively low critical current densities (2-5 × 10^3 A/cm^2 at 10K). The SQUID critical currents were from 18 μA to 300 μA corresponding to β ($4eI_cL/h$) of 0.7 to 18 where L is the SQUID loop inductance.

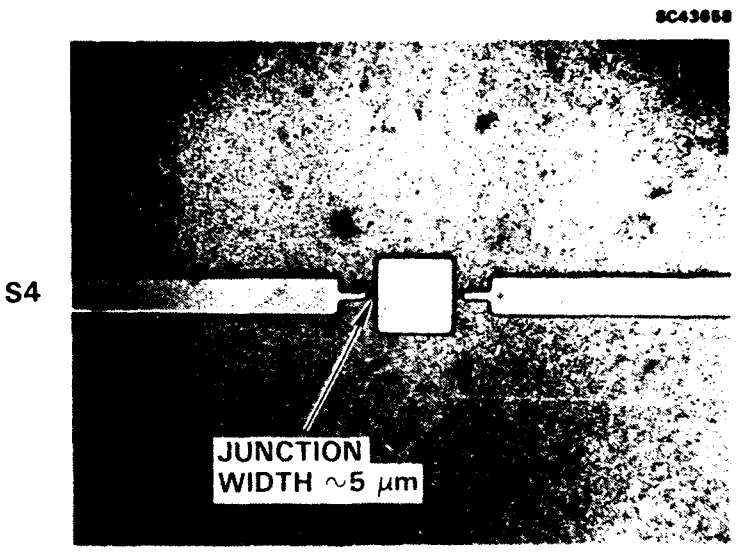

Figure 1. Photomicrograph of a YBaCuO thin film SQUID.

3.1 Measurement of SQUID Characteristics

Preliminary measurements included the I-V characteristics and the differential response to magnetic field. All measurements were made using the 4-point method to reduce the effects of contact resistances. A typical I-V curve is shown in Figure 2 for a SQUID fabricated from YBaCuO thin film. The departure from zero voltage was fairly abrupt with only small rounding unlike devices from films of higher J_c where the departure from zero voltage is very gradual. The I_cR product was from 0.1 to 0.5 mV, where R is the dynamic resistance. There are two possible reasons why some films produced devices with well-defined response and others did not. The first is the occurrence of fewer phase slip centers, most likely grain boundaries, in the narrow constrictions of devices showing well-defined response as compared to other films. In fact, we have found that the range of bias current where a well-defined response occurs was fairly narrow, from slightly above I_c to about 1.2 -1.7 I_c in concurrence with the conjecture[5] that only one or very few grain boundary junctions are biased above their critical currents in the SQUID operating range. The second possibility is that the intergranular junctions are of a different nature in these two types of films. This conjecture is also based on the observation of different temperature dependences of the device critical currents. For films showing SQUID signals, the dependence was as shown in Figure 3a where the curve is mostly convex up to slightly below T_c in contrast to the general behavior seen in films with $J_c > 10^4$ A/cm^2 (except for a few BiSrCaCuO films) where the curve is almost linear with slight concavity as shown in Figure 3b.

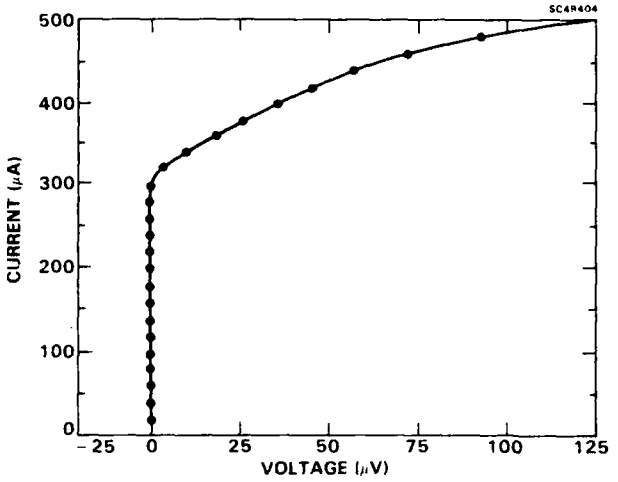

Figure 2. The I-V characteristics of a SQUID made from YBaCuO thin film measure at 8K.

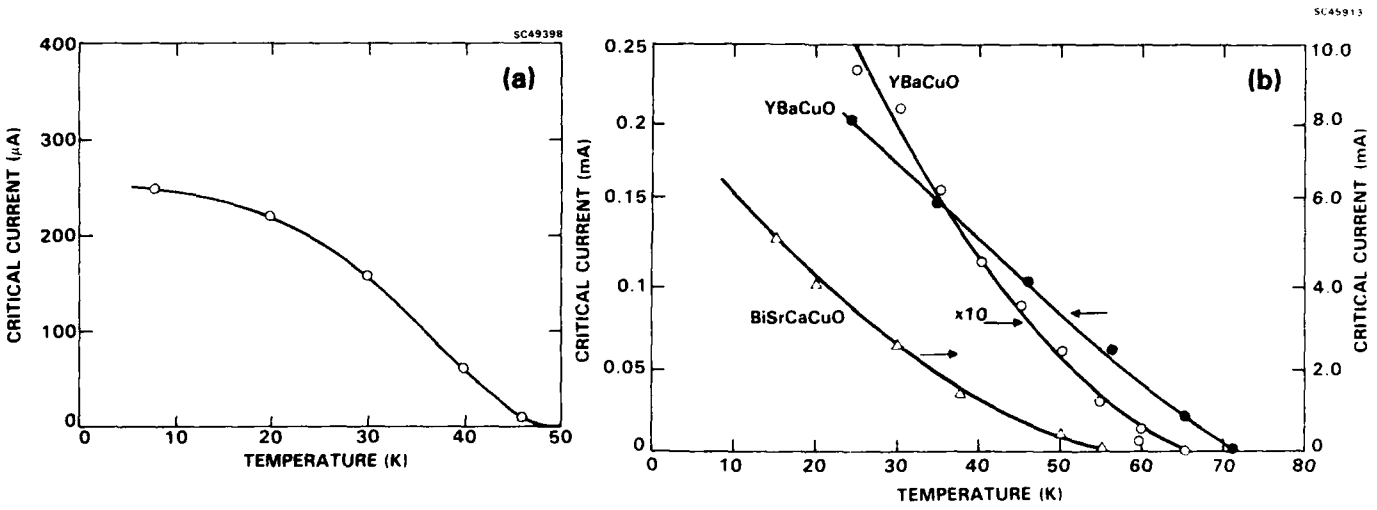

Figure 3. The critical currents of weak link constrictions in high temperature superconducting thin films as functions of temperature, (a) a YBaCuO from which SQUID has been fabricated, (b) typical temperature dependence for films with higher J_c.

The response of the SQUIDs to magnetic field was measured by applying a combination of d-c and a-c currents to a small 5-turn coil that surrounds the device package and generates a field normal to the device plane. The a-c current peak-to-peak amplitude was made to correspond, after taking the focusing factor into consideration, to about one half a flux quantum (h/2e) in the SQUID loop. The output of the SQUID, which is biased by a constant current source, is measured using a lock-in amplifier synchronized to the a-c current source. The

output of the lock-in amplifier is then plotted as a function of the d-c current. Figures 4a-c show the response at three different temperatures of a YBaCuO SQUID plotted on a storage scope by slowly sweeping the dc current. The periodicity of the response varied from 2.25×10^{-3} Gauss at 8K to 3.3×10^{-3} Gauss at 36K. For this device (40×40 μm^2 loop area), this corresponds to one flux quantum if we assume a flux focusing factor that decreased from 5.6 at 8K to 3.8 at 36K. The focusing effect is due to the presence of the large pads which tend to expel the applied field from their interior. Other SQUIDs from the same film and from different films showed focusing factors up to 19 at low temperatures. Other authors have reported focusing factor of similar values.[2] As mentioned above, the SQUID output was very sensitive to the bias current, and the periodic response occurs over a fairly narrow range. In the particular device discussed above, this range was 30 μA to 55 μA at 8K, as shown in Figure 5. Other devices had an even narrower bias range. The output generally decreased with increasing temperature, as shown in Figure 6 most likely due to the rapid decrease of the junction dynamic resistance with temperature. This occurred even in devices where the modulation factor beta was closer to 1 at the higher temperatures due the decrease in I_c.

We also observed that the SQUID response exhibits some hysteresis, with varying degrees, where sweeping the field up and down sometimes did not produce a repeatable response. In some devices, this occurred with sweeping over as low as 0.01 Gauss. In addition, we observed that the phase and amplitude of the SQUID response would often change spontaneously. We believe this is due to fluxon migration through the body of the SQUID essentially through weak links not biased beyond their critical currents. The observation of hysteresis in SQUIDs made from high temperature superconducting thin films has also been made by us[6] in BiSrCaCuO and by Koch et al[5] in both YBaCuO and TlBaCaCuO.

3.2 Operation in the Flux-Locked Mode and Noise Measurements

We operated several devices, from both Y BaCuO and BiSrCaCuO, in a feedback flux-locked loop shown schematically in Figure 7. The testing was made in an rf screened room to minimize interference from outside sources. The output of the SQUID is connected to transformer with a 1:10 turn ratio to provide a voltage gain and improve the impedance mismatch between the SQUID and the high input impedance preamplifier. The integrated output of the lock-in amplifier is fed back as a d-c bias field applied to the SQUID which is added to the ac bias modulation and an adjustable dc source. For a large enough open loop gain, the SQUID operating point can be maintained in very close vicinity to a zero response crossing.

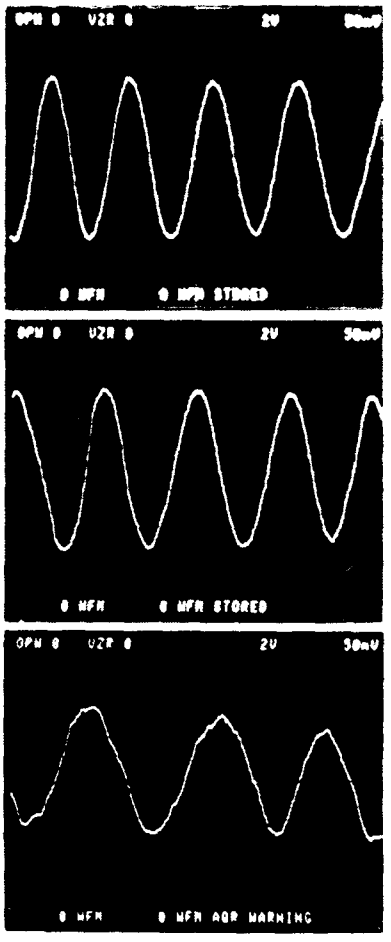

T = 10K
Y = 0.2μv (rms) DIV
X = 1.0×10^{-7} T DIV

T = 20K
Y = 0.2μv (rms) DIV
X = 1.0×10^{-7} T DIV

T = 36K
Y = 0.02μv (rms) DIV
X = 1.0×10^{-7} T DIV

Figure 4. The response of a YBaCuO SQUID at different temperatures, (a) 10K, (b) 20K, and (c) 36K. The bias current was 40 μA, the x-axis calibration is 10^{-7} T/div, the y-axis calibration was 0.2 μV(rms)/div for 10 and 20K and 0.02 μV(rms)/div for 36K.

The lock-in output very nearly compensates for the externally applied field, within an initial whole number of flux quanta, and the SQUID operates as a null detector.

The operation in the flux-locked mode was stable over different lengths of time for SQUIDs from different films, interrupted by the switching of the operating point to another zero crossing associated with a different number of enclosed flux quanta. The switching might be triggered by a large transient noise associated with flux migration as mentioned above. The most stable operation was obtained for SQUIDs made from YBaCuO films where stable operation at 4K for up to 10 min was observed.

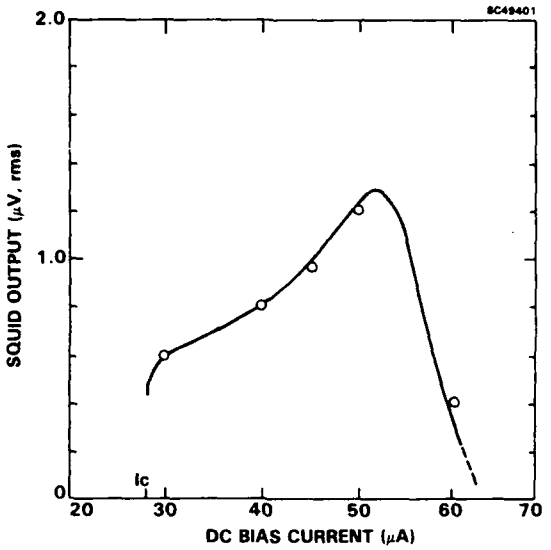

Figure 5. The voltage modulation of the YBaCuO SQUID shown above as a function of bias current at 10K.

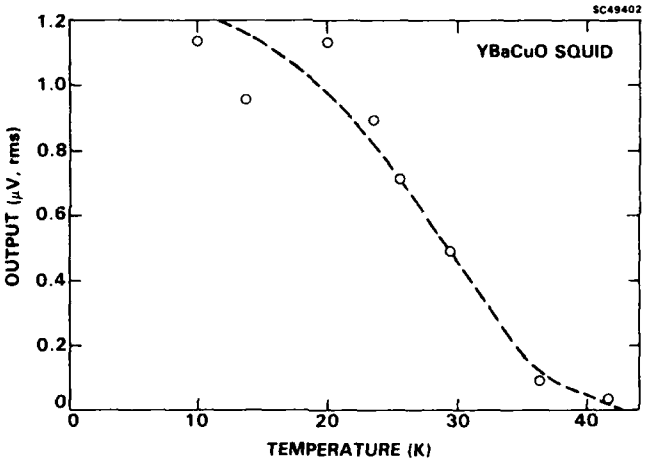

Figure 6 The voltage modulation of the SQUID shown above as a function of temperature at constant bias of 40 μA.

The sensitivity of the SQUIDs was determined from measurements of the responsivity and the noise output in the flux-locked mode. The noise measurements were made using a spectrum analyzer, from 0.1 to 100 Hz. Some of the devices, from YBaCuO, show relatively good sensitivity, as shown in Figure 8, where the noise output in terms of $\phi_0^2/\sqrt{Hz}$ is plotted as a function of frequency. The noise is dominated by 1/f noise below 50 Hz and by room temperature electronics noise at higher frequencies. This corresponds to a slightly lower sensitivity than that of commercial rf SQUIDs for frequencies > 50 Hz, and is about two orders of magnitude lower than commercial dc SQUIDs.[10] The low frequency 1/f noise is most likely

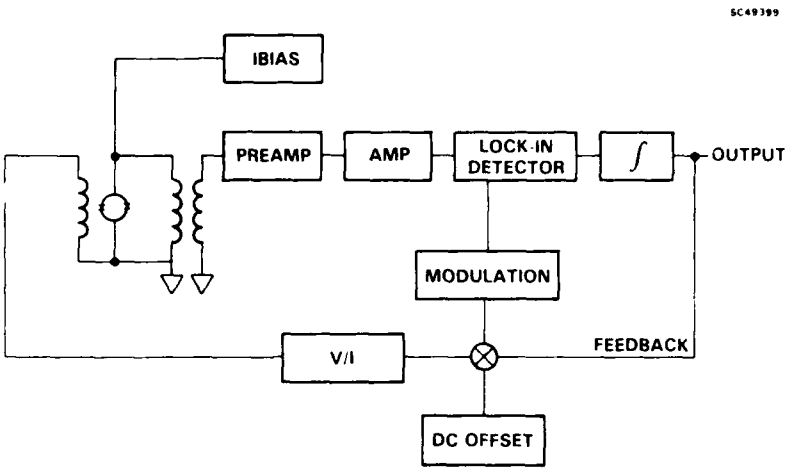

Figure 7. Schematic diagram of the flux-locked feedback loop used to test SQUIDs.

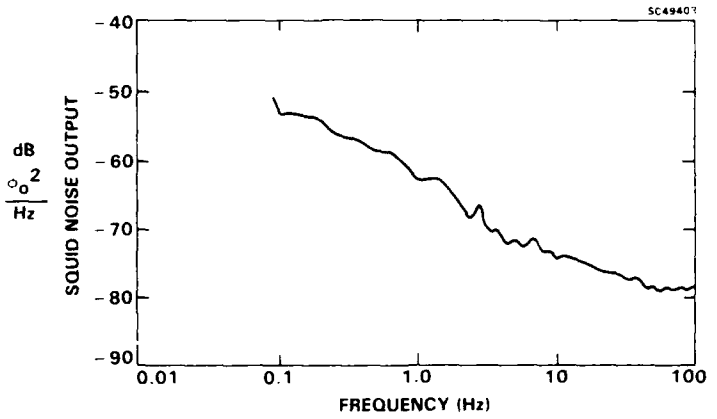

Figure 8. The noise output spectrum of a YBaCuO thin film SQUID in units of flux ($\phi_o^2/\sqrt{Hz}$).

caused by flux migration in the superconducting films making up the SQUID, the same source of the hysteretic response discussed above.

4.0 DISCUSSION

The results described above demonstrate the feasibility of dc SQUIDs using the new high temperature superconductors at temperature much higher than that of liquid He and in ranges accessible to other means of cooling. However, the present state-of-the-art of preparing these devices, namely using the as grown grain boundary junctions to effect the SQUID operation, has serious drawbacks. This stems from the fact that the junctions which also occur everywhere in

the rest of the SQUID are also the origin of the observed hysteretic response and low frequency noise in the SQUID. It has been shown[11] that fluctuation in the flux enclosed by in YBaCuO thin films loops decreases in films with higher critical current densities, indicating that such noise is associated with the intergrain boundary coupling. However, devices fabricated from films with higher J_c did not produce SQUID response most likely because the grain boundary junctions are either absent altogether or they do not exhibit the Josephson effect. The conclusion is that other means of fabricating Josephson junctions in the new high temperature superconductors will have to be developed. This will be necessary, not only for SQUID applications , but also for other types of active superconducting devices.

REFERENCES

1. J.M. Cox M.B. Ketchen, IEEE Trans. Mag. MAG-17, 400, 1981.
2. R.H. Koch, C.P. Umbach, P. Chaudhari, and R.B. Laibowitz, Appl. Phys. Lett. 51, 200, 1987.
3. H. Nakane, Y. Tarutani, T. Nishino, Japn. J. Appl. Phys. 26, 1925, 1987.
4. B. Hauser, M. Diegel, and H. Rogalla, Appl. Phys. Lett. 52, 844, 1988.
5. R.H. Koch, W.J. Gallagher, and B. Bumbles, Appl. Phy. Lett. 54, 951 (1989).
6. I.S. Gergis, J.A. Titus, P.H. Kobrin, and A.B. Harker, Appl. Phys. Lett. 53, 2226 (1988).
7. P.H. Kobrin, J.F. DeNatale, R.M. Housley, J.F. Flintoff, and A. B. Harker, Adv. Ceram. Mater. 2, 430 (1988).
8. A.B. Harker, P.H. Kobrin, P.E.D. Morgan, J.F. DeNatale, J.J. Ratto, I.S. Gergis, and D. G. Howitt, Appl. Phys. Lett. 52, 2186 (1988).
9. S.I. Shah and P.F. Garcia, Appl. Phys. Lett 51, 2146 (1987).
10. J. Clarke and R.H. Koch, Science 242, 217 (1988).
11. M.J. Ferrari, M. Johnson, F.C. Wellstood, J. Clarke, P.A. Rosenthal, R.H. Hammond, and M.R. Beasley, Appl. Phys. Lett. 53, 695 (1988).

THIS PAGE IS INTENTIONALLY BLANK

Presented at the Workshop on High Temperature Superconductivity
23-25 May 1989 GACIAC PR-89-02

MAGNETIC SHIELDING WITH HIGH T_c SUPERCONDUCTORS

O.G. Symko, W.J. Yeh, D.J. Zheng
Dept. of Physics, University of Utah, Salt Lake City, Utah 84112
S. Kulkarni, Ceramatec, Salt Lake City, Utah 84115

ABSTRACT

A shield of $YBa_2Cu_3O_7$ has been developed for operation at 77 K. This device attenuates external magnetic fields by a factor larger than 10^6 for fields up to 50 gauss making it useful for shielding superconducting electronics.

I. INTRODUCTION

The application of superconductivity to shielding against external electromagnetic interferences has made it possible to develop and use devices which have extremely high sensitivity[1-3]. Such devices are usually based on Josephson junctions and they can be used in magnetometers or as the building blocks in superconducting electronics. In many applications the devices are operated at a temperature of 4.2 K, the shield being also at that temperature in order to be near the device. The ultimate sensitivity and performance of a device depends on how well it is shielded against external noise and interference; hence, shielding plays a very important part in the applications and uses of superconducting devices. Because high T_c materials will be important in many applications and in particular in superconducting electronics, we have developed high T_c shields which operate at 77 K. Results on their performance and behavior are presented here.

The shielding characteristics of a superconductor rely on two properties,

(i) $R = 0$

(ii) $B = 0$

The first property of zero resistance leads to shielding because for a continuous circuit with zero resistance, the total flux through that circuit must be constant. Hence, a superconducting tube, for example, will shield a sample located inside it by having induced currents set-up in its walls when an electromagnetic disturbance is produced; such induced currents will maintain the flux inside the tube constant. The second property, the Meissner effect, maintains the magnetic field B at a zero value inside a bulk sample of superconductor. This also leads to shielding; however, the thickness of the shield must be larger than the London penetration depth, λ_L.

The shielding requirements can be divided into two areas, low magnetic field shielding and high magnetic field shielding. The low field shielding is a necessity with sensors and devices where external disturbances of a few gauss have to be attenuated by many orders of magnitude; this is especially important for devices based on the magnetic flux quantum, ϕ_o. The high field case is more difficult as shielding of devices is required when they are exposed to large magnetic field disturbances such as produced by machines. Since type I superconductors are limited by the upper field H_c they

can shield, it may be convenient to use a type II superconductor and thus be able to shield a very wide range of external magnetic field disturbances. For type II materials, the shielding effectiveness will be reduced above H_{c1} due to flux motion; nevertheless, effective shielding still persists[4] since the resistance remains zero up to the upper critical field, H_{c2}. The geometry of the shield will depend on the particular application. In this work results are presented on superconducting tubes, which is a geometry used extensively in SQUID applications, especially in magnetometers.

2. EXPERIMENTAL DETAILS

Tubes of $YBa_2Cu_3O_7$ were fabricated using conventional techniques. They were pressed into shape and then fired, care being taken to maintain the roundness of the tubes. Their dimensions were: 0.96 cm inner diameter and 1.2 cm outer diameter, the length ranging from 5.5 cm to 10 cm. The shielding characteristics were studied at 77 K with a Hewlett-Packard model 4288R Fluxgate Magnetometer and a Hall probe. After zero-field cooling the sample, the inside magnetic field was measured while an external magnetic field parallel to the tube axis was slowly increased from zero. The shielding factor was then determined for a wide range of external fields; this factor is defined as the ratio of the inside magnetic field at the center, H_{ic}, to the applied field H_e.

3. RESULTS AND DISCUSSION

The shielding characteristics of a typical tube are shown in Fig. 1. Here the measured axial magnetic field inside the tube at its center is plotted as a function of axial external applied field. As seen on the figure, shielding exists up to a critical field H_m. This depends on the critical current density of the tube. Beyond the critical field H_m, flux starts entering the tube and it then approaches rapidly the limit where the inside field is equal to the external field. Although the flux entry region shows some shielding, there is significant noise due to flux flow characterized by special time dependencies[5]. The critical field H_m in our samples varied from a few gauss up to about 50 gauss for our best tubes. Improved tube fabrication processing led to a higher critical current density and hence shielding up to a higher critical field H_m. In the region of external magnetic field, $0 \leq H_{ext} \leq H_m$, excellent shielding characteristics were observed. Within the limits of our magnetic field probe, the shielding factor was better than 10^{-6}.

The axial dependence of the shielding factor has also been investigated. Calculations have shown[3] that the axial magnetic field inside the tube decreases as

$$H = H_o \exp(-3.4z/a) \qquad (1)$$

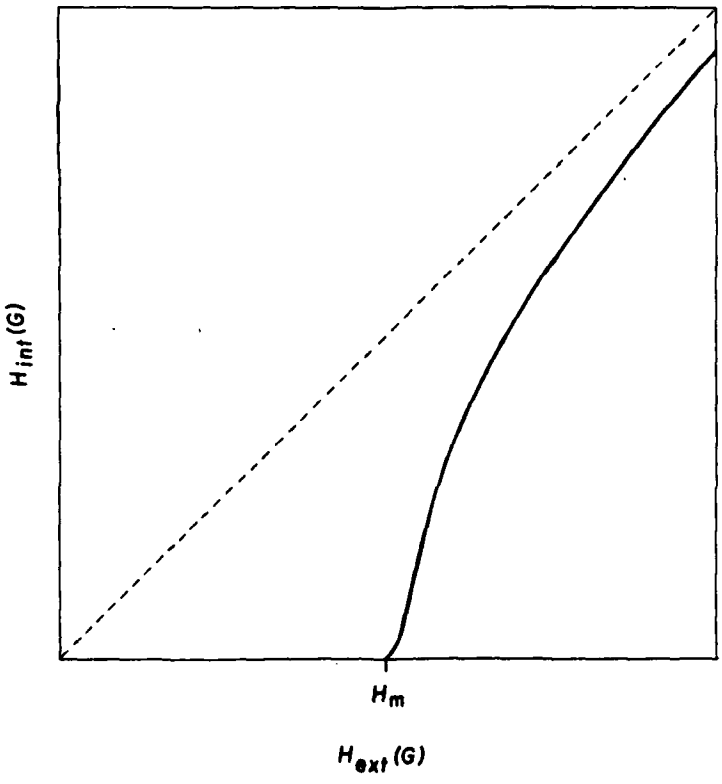

Figure 1. Shielding characteristics of superconducting tube showing inside field when an external field is applied. Dotted lines show no shielding.

while the transverse field falls off as

$$H = H_o \exp(-1.8z/a) \qquad (2)$$

where a is the inner radius of the tube and z is the axial position along the tube. Our results for the axial component yield a prefactor of 3.0 in equation 1; the discrepancy from the calculated value could be due to inhomogeneity of the current distribution in the tubes or just simply misalignment of the probe insides the tube. The application of equation 1, with the prefactor of 3 to our tubes leads to an attenuation factor of about nine orders of magnitude at

the center of the tube.

We have used such a high T_c shield with a r.f. biased SQUID operating at 77 K. The SQUID was made out of $YBa_2Cu_3O_7$ and it was the fractured type of device[6]. The high T_c superconducting shielding was effective in reducing external interferences so that the SQUID could be used in a flux-locked mode.

Although our values of H_m are low, due to the small critical current density of the tubes, shielding of fields much larger than H_m can be reached by improving material processing. Actually, shielding above H_{c1} can be achieved. The difference in magnetic field between the interior and external values, $H_{ext} - H_i$, is produced by the shielding current in the tube wall. When this current is saturated everywhere in the wall, the tube reaches its critical state[7]. Further increase in external magnetic field leads to flux entry as observed in Fig. 1. Better shielding characteristics could be achieved by using thicker tubes for a given material. The results presented here are limited to low field shielding; the maximum field which can be shielded, H_m, is comparable to what has been achieved by other groups[8,9]. The limiting H_m is high enough for applications to a large variety of superconducting devices and electronics. In some applications, the tube geometry may not be adequate as it takes up space (according to equation 1 the highest shielding is achieved well inside the tube) and it can be bulky. A flat plate geometry[10] should then be considered.

We have shown that high T_c magnetic shields can be effective in reducing small field disturbances, thus allowing a SQUID to be operated at 77 K. For high field shielding, larger transport critical current densities have to be achieved[11] and this may be possible in bulk ceramic samples with improved processing techniques[12].

REFERENCES

1. W.O. Hamilton, Rev. Phys. Appl. 5 (1970) 41.
2. W.O. Hamilton, Methods of Experimental Physics, Solid State Physics, Ed. by Marton, Academic Press, vol. 11, p. 609, 1974.
3. B.S. Deaver and W.S. Goree, Rev. Sci. Instr. 38 (1967) 311.
4. D.U. Gubsen, S.A. Wolf, T.L. Francavilla, J.H. Claassen, and B.N. Das, IEEE Trans. on Magn., MAG-21 (1985) 320.
5. O.G. Symko, W.J. Yeh, D.J. Zheng, and S. Kulkarni, J. Appl. Phys. 65 (1989) 2142.
6. C.H. Harmston, O.G. Symko, W.J. Yeh, and D.J. Zheng, IEEE Trans. on Magn. MAG-25 (1989) 878.
7. Y.B. Kim and M.J. Stephen, Superconductivity, ed. by R.D. Parks 1969, p. 1107.
8. J.W. Purpure and T.R. Chen, IEEE Trans. on Magn. MAG-25 (1989) 2506.
9. E. Tjukanov, R.W. Cline, R. Krahn, M. Hayden, M.W. Reynolds, W.N. Hardy, J.F. Carolan, and R.C. Thompson, Phys. Rev. B 36 (1987) 7244.
10. A. Yahara and H. Matsuba, IEEE Trans. on Magn. MAG-25 (1989) 2498.
11. T. Okada, K. Takahata, S. Nishijima, S. Yoshida, and T. Hanasaka, IEEE Trans. on Magn. MAG-25 (1989) 2270.
12. K. Salama, V. Selvamanickam, L. Gao, and K. Sun, Appl. Phys. Lett. 54 (1989) 2352.

THIS PAGE IS INTENTIONALLY BLANK

Presented at the Workshop on High Temperature Superconductivity
23-25 May 1989 GACIAC PR-89-02

THE ELECTRIC FIELD INDUCED BY A GRAVITATIONAL WAVE IN A SUPERCONDUCTOR: A PRINCIPLE FOR A NEW GRAVITATIONAL WAVE ANTENNA

26th May 1989

Huei Peng
Physics Department, The University of Alabama in Huntsville,
Huntsville, AL 35899, USA

ABSTRACT

In this paper we investigate an application of superconductivity which is based on a new effect of gravitational wave (GW) on a superconductor. The new effect, the presences of induced electric current J, density ρ and field E in the interior of the superconductor, results from that GWs will penetrate a superconductor. There is an ion-supercurrent which is also responsible for the Meissner effect. We argue that the induced E field might provide a significantly more sensitive means of detecting gravitational waves. It appears likely that existing resonant-mass superconducting antennas with $L \simeq 3$, $Q \simeq 10^7$ could be readily modified to detect E fields induced by GWs of dimensionless amplitude, $h \simeq 10^{-23}$.

1. INTRODUCTION

This work was stimulated by the discovery of 95^0K superconductor[1] in the way that we started to think how superconductivity would affect gravitational experiments, e.g., detection of gravitomagnetic fields[2] and gravitational waves (GW). In this paper we study the effects of an incoming GW on a superconductor. In doing so, one must take into account two properties of a superconductor, zero resistance and perfect diamagnetism.

First, the effect of a GW on Cooper pair in a superconductor was studied[3]. Based on this effect, a non-resonant superconducting GW antenna has been proposed. Then we studied the effects of a GW on both ions

and Cooper pairs in a superconductor. We[4] found that (1) under the influence of a GW, there will be an electric current and an electric field in the interior of a superconductor. This effect results from that a GW will penetrate a superconductor, and differs from the behaviour of a superconductor under the influence of electromagnetic fields[5]; (2) The ions are also resposible for expelling time-dependent magnetic fields from the interior, the Meissner effect. The estimate of the induced electric fields in the interior have been obtained for both a practical GW superconducting cylindrical antenna[6] and a damped harmonic oscillator model of a GW superconducting antenna[7], respectively.

The induced electric field by a GW with dimensionless amplitude $h \simeq 10^{-23}$ is sufficient large to be detected. We suggest to detect GWs by measuring the induced electric field in the interior[6,7].

2. NET CURRENT AND CHARGE DENSITY INDUCED BY A GW

According to the two fluid model[5], a superconducting antenna (S-antenna) consists of positive ions, Cooper pairs and normal electrons. If small vibrations of ions do not destroy superconductivity of a S-antenna, then, a GW of frequancy ω drives the ions, superelectrons and normal electrons to vibrate independently along the axis x of the antenna.

First, we consider the effect of a GW on normal electrons. Ohm's law, $J_n = \sigma E$, needs to be generalized to include the effects of GWs. Ohm's law implies that a normal current proportional to the force (F) acting on normal electrons, $J_n = \sigma F/e$. Therefore in the presence of forces due to a GW and an induced E field, the normal current is given by

$$J_n = \sigma(m_e a_{GW} + eE)/e, \qquad (1)$$

where m_e is the mass of an electron, a_{GW} is the acceleration that results from projecting the tidal gravitational force due to a GW onto the antenna.

Now consider the effects of a GW on ions and superelectrons. A S-antenna is equivalent to a number of oscillators, provided certain conditions are satisfied[6]. In this section, we choose a damping time τ_i and natural frequency ω_i to model the fundamental eigenmode of a bulk ions in the S-antenna. Taking into account the effect of

the induced electric field on ions, the equation of motion can be written as

$$\frac{d^2x_i}{dt^2} + \frac{dx_i}{\tau_i dt} + \omega_i{}^2 x_i = a_{GW} + \frac{e}{m_i} E, \qquad (2)$$

where x_i corresponds to the displacement with respect to the center of mass of the S-antenna, e and m_i are the charge and mass of an ion, respectively.

Since superelectrons can move freely in a S-antenna, the equation of motion of Cooper pairs is

$$\frac{d^2x_e}{dt^2} = a_{GW} - \frac{e}{m_e} E. \qquad (3)$$

Eqs.(2,3) become algebraic equations by assuming all time-dependent quantities vary with time as $\exp(-i\omega t)$. Then the displacements of ions and superelectrons are respectively

$$x_i = G(\omega) \left[- a_{GW} - e/m_i \; E \right], \qquad (4)$$

$$x_e = 1/\omega^2 \left[- a_{GW} + e/m_e \; E \right], \qquad (5)$$

where

$$G(\omega) = (\omega^2 - \omega_i{}^2 + i\omega\omega_i/Q_i)^{-1}, \qquad (6)$$

$$Q_i = \omega_i \tau_i, \qquad (7)$$

$G(\omega)$ is the harmonic oscillator response function. Obviously, if we ignore the effect of the induced E field on ions, the displacement given by Eq.(4) reduces to that of a normal GW antenna (N-antenna).

The independent motions of ions and superelectrons produce respectively the ion-current and electron-current

$$J_i = 2ne \; dx_i/dt = i2ne\omega G(\omega) a_{GW} + J_{is}(x,t), \qquad (8)$$

$$J_e = - 2ne \; dx_e/dt = - i2ne/\omega \; a_{GW} + J_{es}(x,t), \qquad (9)$$

where n is the concentration of Cooper pairs,

$$J_{is} = \frac{i2ne^2}{m_e} \frac{m_e \omega G(\omega)}{m_i} E(x,t), \qquad (10)$$

$$J_{es} = \frac{i2ne^2}{m_e \omega} E(x,t). \qquad (11)$$

We refer to J_{is} and J_{es} as the ion- and electron-supercurrents,

respectively. The J_{is} and J_{es} are in the same direction. Eqs.(10,11) imply that the induced time-dependent E field creates not only the electron-supercurrent which includes the London supercurrent, $J_{Ls} = -2ne^2A/m_e$, but also an ion-supercurrent.

The ratio of J_{is} to J_{es} is

$$\frac{J_{is}}{J_{es}} = \frac{\omega^2 d}{\omega^2 - \omega_i^2 + i\omega\omega_i/Q_i}. \qquad (12)$$

Corresponding to different values of ω and Q_i, we may have $|J_{is}| > |J_{es}|$, $|J_{is}| < |J_{es}|$, or $|J_{is}| = |J_{es}|$. At $\omega = \omega_i$, we have

$$|J_{is}/J_{es}| = m_e Q_i/m_i. \qquad (12)'$$

The net current induced by the incoming GW is

$$J = J_n + J_e + J_i.$$

Therefore there is indeed a GW induced net current and a charge density ρ.

3. GENERAL EQUATIONS

The behaviors of a S-antenna under and without the influence of a GW are different. For instance, according to the London theory of superconductivity, there is no net current, charge density and electric field in the interior of a superconductor in the presence of external electromagnetic fields. However, there is indeed a net current, charge density and induced E field in the interior in the presence of a GW, because the GW will penetrate the S-antenna and thus drive the ions, superelectrons and normal electrons not only on the surface but also in the interior to vibrate. We need to derive a set of equations to study the electromagnetic properties of a S-antenna under the influence of a GW. Following the method of London[5], the relationships between the net current J and electromagnetic fields are obtained

$$-\nabla \times J = \frac{B}{\Lambda} + \sigma \frac{\partial B}{\partial t}, \qquad (13)$$

$$\frac{\partial J}{\partial t} = \frac{E}{\Lambda} + \sigma \frac{\partial E}{\partial t} + \left(2ne[\,\omega^2 G(\omega) - 1\,] - \frac{im_e\omega\sigma}{e}\right)a_{GW}, \quad (14)$$

where

$$\Lambda \equiv m_e/\{2ne^2[\,\omega^2 G(\omega)d + 1\,]\}, \quad (15)$$

$$d \equiv m_e/m_i. \quad (16)$$

If we ignore the effects of a GW, i.e., a_{GW} and ω terms, Eqs.(13,14,15) become the London equations[5].

The equations which can be used to estimate the current J, charge density ρ and induced E field in the interior are obtained by substituting the net current into the Maxwell equations,

$$\frac{\partial^2\rho}{\partial t^2} + \frac{\sigma}{\epsilon_0}\frac{\partial\rho}{\partial t} + \frac{\rho}{\Lambda\epsilon_0} + \left(2ne[\,\omega^2 G(\omega) - 1\,] - \frac{im_e\omega\sigma}{e}\right)\nabla\cdot a_{GW} = 0. \quad (17)$$

$$\nabla^2 J = \frac{J}{(\lambda')^2} + \left(i\omega 2ne[\,\omega^2 G(\omega) - 1\,] \quad \frac{m_e\omega^2\sigma}{e}\right)a_{GW}, \quad (18)$$

$$\nabla^2 E = \frac{E}{(\lambda')^2} + \left(\mu_0 2ne[\,\omega^2 G(\omega) - 1\,] - \frac{im_e\omega\sigma\mu_0}{e}\right)a_{GW}, \quad (19)$$

$$\nabla^2 B = \frac{B}{(\lambda')^2}, \quad (20)$$

where

$$\frac{1}{(\lambda')^2} = \frac{\mu_0}{\Lambda} - i\omega\sigma\mu_0 - \omega^2. \quad (21)$$

The real part of λ' represents the penetration depth.

The $\omega^2 G(\omega)d$ terms in Eq.(15) and thus in Eqs.(17-21) represent the contributions of ion-supercurrent. If we ignore the a_{GW} and ω terms Eqs.(17-21) reduce to the London equations[5].

4. ELECTRODYNAMICS OF S-ANTENNA AND MEISSNER EFFECT

In this section we study the electromagnetic properties of a S-antenna in the presence of a GW by use of Eqs.(17-21).

First we consider the GW induced charge density which includes a damping part and a vibrational part, from Eq.(17),

$$\rho = \rho_d e^{-\gamma t} + \rho_0 e^{-i\omega t}, \tag{22}$$

where ρ_d is an integration constant, and

$$\rho_0 = \frac{\{2ne[\omega^2 G(\omega) - 1] - im_e\omega\sigma/e\}\epsilon_0\nabla\cdot a_{GW}}{\omega^2\epsilon_0 - 1/\Lambda + i\omega\sigma}. \tag{23}$$

The relaxation time τ is defined by

$$\tau = 1/\gamma \simeq \Lambda\sigma \leq 10^{-12} \text{ sec.}$$

Therefore the damping part of the charge density which might occur in the S-antenna would disappear within this extremely short time as pointed out by London[5]. Then we have

$$\rho \simeq \rho_0 e^{-i\omega t}. \tag{24}$$

Unlikely, in the London theory, there is no ρ_0 term, thus there is no charge density in the interior after a short time.

The vibrational charge density will create a E field,

$$E_{int} = \frac{2ne(\omega^2 G - 1) - im_e\omega\sigma/e}{\omega^2\epsilon_0 - 1/\Lambda + i\omega\sigma}. \tag{25}$$

This induced E field will decrease the speeds of ions' vibrations and increase that of superelectrons'.

The induced net current consists of two parts, from Eq.(18),

$$J = J_s + J_{int}, \tag{26}$$

where J_s is the screen current which only exists in a very thin layer of surface, J_{int} is the current remaining in the interior

$$J_{int} = -\{i2ne\omega[\omega^2 G(\omega) - 1] + m_e\omega^2\sigma/e\}a_{GW}(\lambda')^2. \tag{27}$$

Now we show that the magnetic field B induced by the J_{int} in the interior will be canceled out by that created by the variation of the E_{int} field. Substituting Eqs.(25,27) into one of Maxwell equations, we obtain

$$\nabla x B_{int} = \mu_0 J_{int} + \partial E_{int}/\partial t = 0. \tag{28}$$

which implies that there is no magnetic field in the interior, the Meissner effect. Actually, Eq.(20) directly describes the Meissner effect.

We conclude that (1) Eqs.(17-20) are self-consistent; (2) There is a net current J_{int}, charge density ρ, electric field E_{int} and vector

potential A_{int} in the interior of a S-antenna. But the effects of J_{int} and E_{int} are canceled out such that $B_{int} = 0$, i.e., the vibrations of the magnetic field B die away within the penetration depth Re(λ') (the Meissner Effect). It is very interesting to compare this with the Aharonov-Bohm effect[8] in which particles pass a $B = 0$ and $A \neq 0$ region and are affected; (3) The ions are also responsible for expelling the time-dependent magnetic field, especially on resonance. The mechanism of that the net current including both ion-supercurrent and London supercurrent expels the magnetic field may be explaned as the following. The vibrations of ions, superelectrons and normal electrons driven by a GW will be adjusted by the induced E field such that there will be no maqnetic B field in the interior; (4) Part of energy of a GW will transfer to the electromagnetic energy.

5. THE PRINCIPLE OF A NEW ANTENNA

As we have shown above, an incoming GW will induce an electric field in the interior. Based on this new effect we propose that one may detect the GW induced electric field E_{int} which is, from Eq.(25)

$$E_{int} \simeq - a_{GW} \frac{m_e}{e} \frac{(\omega_1^2 - i\omega/\tau_1)}{[\omega^2 - \omega_1^2 + \omega^2 d + i\omega/\tau_1]}, \qquad (29)$$

where we have ignored small terms. The E_{int} is a narrow-band resonant function centered at $\omega_1/\sqrt{(1+d)}$ with a full width at half maximum of ω_1/Q_1. One might expect that a more significant bandwidth restriction comes from the readout system.

For a polarized wave, the Fourier transform of the gravitational acceleration is[9]

$$a_{GW}(\omega) = - \frac{1}{2} l\omega^2 h(\omega) \sin^2\theta \cos 2\phi, \qquad (30)$$

where $h(\omega)$ is the Fourier transform of the dimensionless amplitude $h(t)$, θ and ϕ are the polar angles of the S-antenna relative to the wave-determined x,y,z-axes.

All the equations derived above are for the oscillator model of a S-

antenna. In order to estimate a representative value for E_{int}, we need to find the equivalence relations between a S-antenna and its oscillator model. The bulk modulus of elasticity, ϵ, is slightly different in the superconducting and normal states[10], but the effects are extremely small. Thus the speed of sound, v_s, in both states can be considered to be approximately the same. It has been shown[6] that when one takes into account the effects of the GW induced E_{int} field, a S-antenna with the length 2L, quality factor Q_s, and resonant frequency ω_{sK} is identical to a damped oscillator with the length 2l, quality factor Q_i, and resonant frequancy ω_i, provided

$$l \simeq \frac{4L}{\pi^2\sqrt{(1+d)}}, \tag{31}$$

$$Q_i = Q_s,$$

$$\omega = \omega_{sK} = \omega_i/\sqrt{(1+d)}, \tag{32}$$

where

$$\omega_{sK} = (K + 1/2)\pi v_s L^{-1},$$

$$Q_s = \epsilon(\omega_{sK}D)^{-1},$$

K is an integer number, for $K = 0$, $\omega_{s0} = \pi v_s/(2L)$, and D represents all the effects of the dissipative processes. Eqs.(31,32) are slightly different from that for a N-antenna. The d terms represent the effects of the induced E field.

Averaged over all possible directions of an incoming unpolarized GW, an optimum representative magnitude of the E_{int} field at the end of the S-antenna is then given by

$$E_{int} \simeq \frac{4}{\pi^2\sqrt{15}} \frac{m_e}{e} Q\omega_{sK}^2 Lh, \tag{33}$$

where Eqs.(29-30) have been used and small terms have been neglected. Integrating (33), the voltage drop V between the central point at the end face and the center of mass is obtained. Then the sensitivity of a S-antenna detecting the GW induced E field is found to be:

$$h = \frac{\sqrt{15}\ \pi^2 eV}{2Q_s m_e \omega_{sK}{}^2 L^2}. \qquad (34)$$

If it proves to be technically feasible to measure a voltage drop of 10^{-22} V[11], say by using a superconducting quantum interference device (SQUID) magnetometer, the sensitivity of a S-antenna with $Q \simeq 10^7$, $\omega_{s0} \simeq 10^3$, and $2L = 3m$, is of the order

$$h \simeq 10^{-23}. \qquad (35)$$

Comparing this sensitivity with that of the third generation antennas[12] for which $h \simeq 10^{-20}$, it appears to be worthwhile to investigate this new concept for the detection of GWs further. We suggest that one might measure the displacement at one end and the GW induced E field at the other end of S-antennas.

ACKNOWLEDGEMENTS

I would like to thank Dr. D. G. Torr for useful discussions. This work was supported by NASA/MSFC grant #NAG8-067 and by incentive funding from the Physics Department at the University of Alabama in Huntsville.

REFERENCES

[1] M. K. Wu, et al, Phys. Rev. Lett., 58 908, 1987.

[2] H. Peng, A New Approach to Study Local Gravitomagnetic effects on a Superconductor, Gen. Rel. Grav., in press, 1989

[3] H. Peng, Bull. Amer. Phys. Soc. 33 2213, 1988.

[4] H. Peng, On a Superconducting Antenna and Its Sensitivity, in press, 1989.

[5] F. London, Superfluids, Dover Publications, Inc. New York, 1961.

[6] H. Peng and B. Peng, Interaction of Gravitational Waves with a Superconducting Cylindrical Antenna, in press, 1989.

[7] H. Peng and D. Torr, The Electric Field Induced by a Gravitational Wave in a Superconductor: a Principle for a New Gravitational Wave Antenna, First award in 1989 Gravity Research Foundation Essays Contest, in press.

[8] Y. Aharonov and D. Bohm, Phys. Rev. 115 485-487, 1959.

[9] C. W. Misner, K. S. Thorne, and J. A. Wheeler, Gravitation, W. H. Freeman & Co., San Francisco, 1973.

[10] E. Lynton, Superconductivity, Methuen & Co. Ltd., 1969.

[11] A. Jain, J. Lukens, and J. Tsai, Phys. Rev. Lett., 58, 1165, 1987.

[12] J. Price, Phys. Rev., D36, 3555-3570, 1987.

Abstract of Paper Presented at the
Workshop on High Temperature Superconductivity
23-25 May 1989 GACIAC PR 89-02

Theory of Superconductivity Theories

A.J. Fennelly
Teledyne Brown Engineering
MS-50
Cummings Research Park
Huntsville, AL 35807-3801

and

J.A. Fennelly
University of Alabama in Huntsville
Research Institute Room C-5
Huntsville, AL 35899

ABSTRACT

We review the large numbers and varieties of theories of superconductivity which have been proposed to explain the mechanism of superconductivity in the lately discovered ceramic, metal-oxide, "high-temperature," superconducting (HTS) materials. The gross majority of the "new" theories are really a collection of theories, published between five and fifteen years ago, and now re-exhibited by their authors, who justify those theories as descriptive of the mechanisms in the HTS materials. In each case the claim has been that the proposed mechanism is the mechanism for those HTS materials, to the exclusion of its "opponents." However, there is nothing really wrong with the physics contained in most of those proposed theories (as well as the truly new ones). The obvious resolution is that all those mechanisms are correct to differing degrees, and that all of them are present in differing amounts in any given superconducting material. We therefore propose a superconductivity theory (a "theory of superconductivity theories") which incorporates the different mechanisms with the results of experiment in a standard physical approach: (1) Determine the thermodynamic and statistical conditions under which the distributions of pairing excitations, proposed for each mechanisms, can exist (simultaneoulsy or mutually exclusively) to provide an attractive potential to combine fermions into boson pairs. (2) Determine the percentage of pairing that is contributed by each mechanism at finite temperature. (3) Determine which mechanisms are mutually exclusive and which ones cannot exist in the candidate material. (4) Then go to determine the critical temperatures, current densities, and magnetic fields; and penetration depth and coherence length for the candidate material. Note that we are proposing that

mechanisms can appear, disappera, and reappear as pairing excitations are allowed or forbidden by the thermodynamic and chemical state of the material and its environment. A key role is played by the lattice instability of the material, as its exists at a transition point between two or more recognized states of matter (i.e., metal, insulator, antiferromagnet, semimetal, etc.) and quantum fluctuations allow available conduction-band electrons to experience those states almost simultaneously. The allowed paring interactions must exist for the material in each of those states. Other pairing interactions will be mutually exclusive for given states. It is zero-temperature Schrodinger theory and zero-temperature quantum theory which has been responsible for the general lack of insight into this resolution of competing proposed mechanisms (a dialogue of "crossed monologues"). It must be replaced by finite-temperature theory in all problems of this type in physics, condensed-matter or otherwise. It may be that only polarons (electron-induced phonons) are available for pairing in aluminum at 1.75 K, but a HTS material at 77 K, poised between metallic, insulating, and antiferromagnetic states, is likely to be a jungle of pairing excitations, all vying for dominance.

**Abstract of Paper Presented at the
Workshop on High Temperature Superconductivity
23-25 May 1989 GACIAC PR 89-02**

Superconducting Stripline Resonator Performance

B.R. McAvoy, G.R. Wagner,
J.D. Adam, and J. Talvacchio
Westinghouse Research and Development Center
1310 Beulah Road
Pittsburgh, PA 15235

and

M. Driscoll
Westinghouse Electronics System Group
Baltimore, MD 21203

ABSTRACT

Reliable techniques for evaluating the microwave properties of superconductors are essential in providing calibrated data for exchange between laboratories and for developing practical device designs. We are examining the techniques which utilize microwave stripline resonators. These resonators provide for the rapid measurement of microwave parameters in a repeatable fashion with minimal constraints on processing. Sandwiched microstrip line resonators are used to compare the performance at 4.2 K of OFHC copper and superconducting films of Pb, Nb, and $YBa_2Cu_3O_7$ (YBCO) at C-band and X-band. Typical results for the Nb resonators show a loaded Q_L of about 8×10^4 with a transmission insertion loss of 5 dB at 3 GHz. Initial results on a YBCO a-axis film used as a ground plane in the Nb resonator yield a surface resistance value of about 10^{-3} Ω at 2.8 GHz. Preliminary results on the phase noise performance of a Nb resonator at 2.9 GHz are presented.

THIS PAGE IS INTENTIONALLY BLANK

Presented at the Workshop on High Temperature Superconductivity
23-25 May 1989 GACIAC PR-89-02

PRODUCTION OF WIRES AND COILS FROM HIGH-TEMPERATURE SUPERCONDUCTING MATERIALS*

M.T. Lanagan, U. Balachandran, M.T. Cao, S.E. Dorris, J.T. Dusek, K.C. Goretta, R.B. Poeppel, J.P. Singh, and C.A. Youngdahl

Materials and Components Technology Division
Argonne National Laboratory
Argonne, IL 60439

ABSTRACT

Coils of high-T_c superconductors, which are essential for the development of highly efficient motors and generators, have been fabricated by plastic extrusion. Wires have been extruded in long continuous lengths, wrapped into coils, and subsequently sintered. Coils, 2 cm in diameter and comprising up to 30 turns, have been made with critical current densities of about 200 A/cm^2 at 77 K. Critical current density has been found to be dependent on both sintered density and wire geometry.

Large-scale implementation of high-T_c superconductors will depend greatly on our ability to process these ceramic materials into useful shapes, and to achieve high critical current density (J_c) in large magnetic fields. Monolithic and composite superconductors in the form of wires and tapes are candidates for a wide array of potential applications: conducting rings for magnetic energy storage, windings for power generation, and long continuous wire for power transmission lines.

Several processes for the fabrication of superconducting filaments, wires, and coils have been studied. Fabrication methods include extrusion, tape casting, powder-in-tube processing, melt texturing, and oxidation of metallic precursors.[1,2] Plastic extrusion is a viable technique for manufacturing high-T_c ceramic wires and is presented in detail.

The extrusion process originated with a well-characterized $YBa_2Cu_3O_{7-x}$ (YBCO) powder. The powder was made by calcining oxide and carbonate precursors (Y_2O_3, $BaCO_3$, and CuO). The decomposition of $BaCO_3$ is essential for a complete reaction, and is influenced by CO_2 partial pressure. Thermodynamic studies show that the formation of YBCO is favored when less than 2% CO_2 is present in O_2.[3] The kinetics of CO_2 removal become important for large-size batches owing to the large volume of CO_2 produced during the decomposition reaction.

The degree of phase purity was compared for two calcination methods. In the first method, constituent powders were compacted into pellets and calcined in air. The pellets were subsequently crushed and ground into powder. The interior of the calcined pellets was often green and contained significant amounts of Y_2BaCuO_5 phase. Compacting the powder into pellets may have hindered CO_2 evolution. The calcination procedure was repeated four times to achieve phase purity, as judged by x-ray diffraction.

---

*Work supported by the U. S. Department of Energy, BES–Materials Sciences, under Contract W–31–109–ENG–38.

[1]Poeppel, R. B., Dorris, S. E., Youngdahl, C. A., Singh, J. P., Lanagan, M. T., Balachandran, U., Dusek, J. T., and Goretta, K. C., "Shape–Forming High–T_c Superconductors," J. Met. Vol X, 11–13 (1989).

[2]Gruen, D. M., Calaway, W. F., Maroni, V. A., Tani, B. S., and Krauss, A. R., "Formation of Perovskite Surface Layers by Oxidation of Cu–La–Sr Alloys," J. Electrochem. Soc., Vol. 134, 1588–1589 (1989).

[3]McCallum, R. W., unpublished information.

Another method was developed to facilitate the CO_2 removal. A calcination furnace was modified to remove gas at 4 liters per minute, and was adequate for CO_2 removal from a 300 g batch. The constituent powders were loosely packed on a zirconia setter and calcined at 890°C for 24 h, a significant improvement was observed in large-size batches . Two calcinations were sufficient to produce a phase pure powder by this method.

Wires were formed by plastic extrusion. In the plastic forming process, the YBCO powder is combined with a set of organics and mixed by a sigma blade blender for optimal homogeneity. A solvent provides the basic vehicle into which the oxide powder and other organics are placed. Care must be taken in selecting a solvent that is compatible with the YBCO powder and the other organic constituents. Typical organic solvents include methyl ethyl ketone, methanol, and xylene. Dispersants are used to deflocculate the inorganic particles in the solvent and to assist in obtaining higher green densities. Binders impart strength to the green body, and plasticizers promote flexibility.

The extrusion process consists of placing a large pressure (approximately 20 MPa) on the plastic mass and forcing it through a small aperture. Wires with radii between 0.1 and 1.5 mm have been manufactured in lengths of well over 200 cm. The wire has great flexibility in the unfired state, and 3 cm diameter coils of 1 to 40 turns have been fabricated. Some degree of particle alignment can occur as a result of the high shear stresses induced during the process. Texturing may enhance the J_c owing to the anisotropic transport properties observed in YBCO.

The extruded wire must be heated to consolidate the powder. The heat treatment schedule for fabricated shapes is divided into three parts: removal of organics, sintering, and annealing. Initially, a slow increase in temperature is required to remove organics from the green body. If the organics are removed rapidly, the final product will have large voids and a bloated appearance. Sintering will generally induce formation of a liquid phase at a temperature between 920 and 950°C. The temperature that marks the onset of melting depends upon the partial pressure of oxygen and the phase purity of the powder. The liquid phase is utilized extensively to achieve dense samples. Annealing was carried out at 450°C for 10 h to transform the tetragonal phase to the superconducting orthorhombic phase.

Characterization of the microstructure by means of a polarized light microscope is useful because of the large anisotropy exhibited by the YBCO crystal structure. Figure 1 depicts the change in grain size as a function of sintering temperature. The initial median particle size was 2.7 μm, and there was very little grain growth in the YBCO specimen sintered at 930°C. At 950°C, YBCO exhibits a large amount of grain growth, with some of the grains over 30 μm long. The grains exhibit a platelike morphology, and large aspect ratios are observed. A small increase in the sintering temperature results in a significant amount of grain growth, and is indicative of liquid phase sintering. The onset of minor-phase melting between 930 and 950°C has been confirmed by differential thermal analysis.

Density and J_c are also dependent upon sintering temperature (see Fig. 2). A small degree of uncontrolled variation in the macroscopic properties of the YBCO can be seen from the separate firings at 930°C. A correlation between density and theoretical density is also seen in Figure 2. The increase in J_c with density is attributed to the decrease in porosity, which reduces the effective cross-sectional area of the wire. Porosity can be observed in the micrographs of Fig. 1.

In Fig. 2, the data are shown for 0.7 mm diameter wires with the exception of one data point that was for a 0.2 mm wire. The relationship between wire diameter and J_c was studied statistically because the J_c data was inherently uncertain. Random defects such as porosity and microcracking may cause a large variation in the J_c values. In this study, 10 wire samples each of 0.7 and 0.2 mm diameter were processed identically. The sintering temperature was 950°C. The 0.7 mm wire had a mean J_c of 272.5, with a standard deviation of 24.5 A/cm^2. The 0.2 mm wire had a mean J_c of 544.9, with a standard deviation of 103.8 A/cm^2. It is concluded with a 99% confidence level that the 0.2 mm wire had a significantly higher J_c values than the 0.7 mm wire.

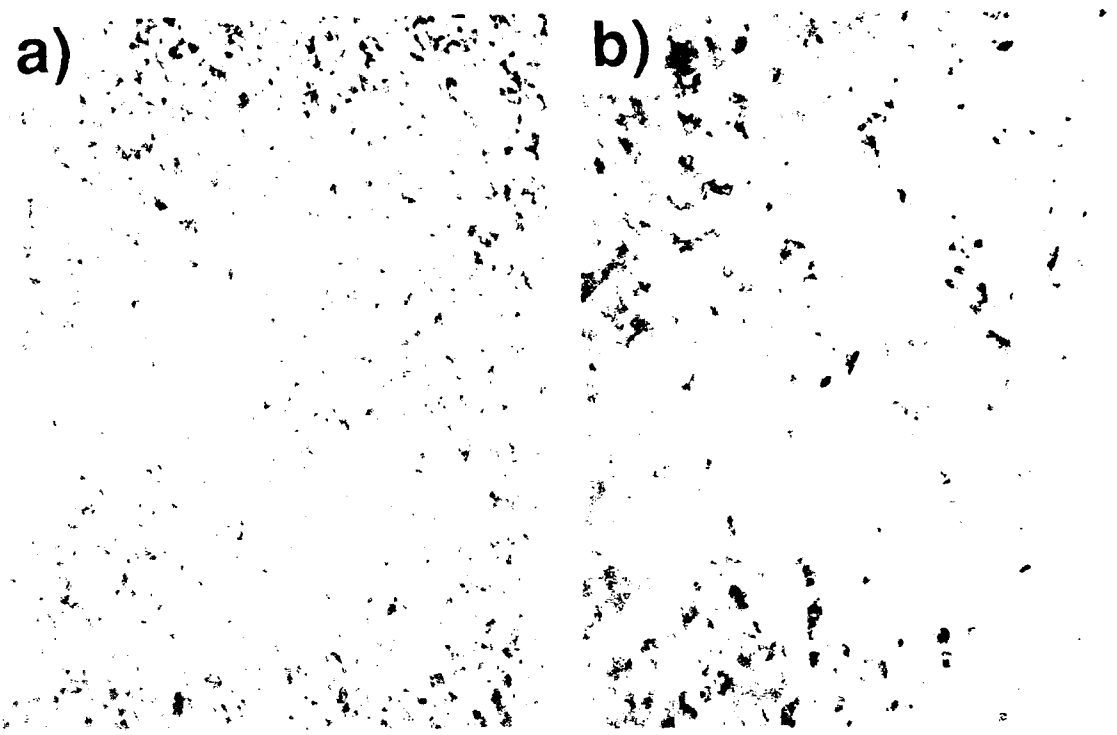

Fig. 1. Microstructures of YBCO wire specimens as observed under a polarized light microscope (Mag. 500X); (a) sintered at 930°C and (b) sintered at 950°C.

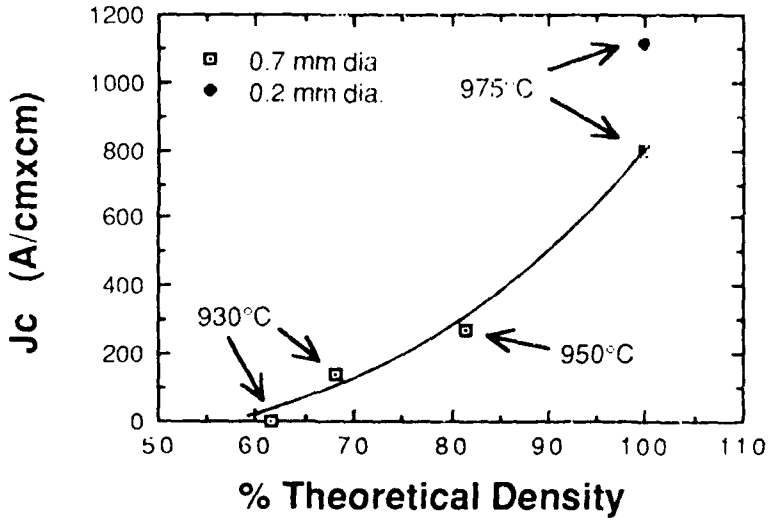

Fig. 2. The effect of sintering temperature on the density and J_c of YBCO.

The effect of specimen geometry on J_c has been observed by other workers,[4] and was attributed to weak coupling between superconducting grains. Microcracking, spurious phases, and distortion in the crystal lattice at the grain boundaries contribute to reduced J_c. The magnetic field generated by the measuring current will cause the links to become resistive, and thereby limit the current-carrying capacity of the entire specimen. Smaller wires generate a lower magnetic field for an equivalent current density; thus, they will have a larger J_c.

The magnetic flux density, calculated from Ampere's circuital law and the critical current in the wire, is on the order of 10 Gauss. This value is consistent with the effect of an externally applied magnetic field on J_c. Large reductions in J_c, on the order of 50%, have been observed in YBCO wire specimens measured in fields of 10 Gauss. Preliminary data show that the size dependence is not observed in a small applied magnetic field.

Coils are fabricated by wrapping the wire around a mandrel in the unfired state. These coils are subsequently sintered, annealed, and tested. The criterion for measuring J_c is a 1 mV drop over the entire coil length. A J_c of 190 A/cm^2 has been measured in a 30-turn coil (total wire length = 240 cm). The highest J_c value for a sample about 1 cm long was 1300 A/cm^2. Data were taken at 77 K in a 0 magnetic field. The fact that J_c values for coils are generally lower than those for 1 cm long wire samples demonstrates the statistical nature of the J_c measurement. The probability of encountering a current limiting defect in a 240-cm long coil is far greater than in a sample 1 cm in length.

In conclusion, increased density has been found to enhance the J_c of extruded YBCO wire. However, the primary deficiency in bulk ceramic materials continues to be the current-carrying properties. Weak link arguments are supported by the observed effects of sample geometry on the J_c. Processing effects on microstructure constitute a subject of continuing research with the aim of improving electrical and mechanical properties.

[4]Stephens, R. B., "Critical Current Limitations in Ceramic Oxide Superconductors," Cryogenics, Vol. 29, 399–404 (1989).

Presented at the Workshop on High Temperature Superconductivity
23-25 May 1989 GACIAC PR-89-02

PROCESSING OF HIGH TEMPERATURE SUPERCONDUCTORS VIA HOT ISOSTATIC PRESSING

15 April 1989

K.T. Richards and R.H. Benfer
Ceramics Research Branch
US Army Materials Technology Laboratory
Watertown, MA 02172-0001

ABSTRACT

Hot isostatic pressing (HIP) was studied as a method for processing bulk superconductors. Superconducting powder was derived from calcination of nitrated Y_2O_3, CuO, $BaCO_3$ powders. The powder was HIPed using pressures of 70, 140, and 210 MPa with temperatures of 820 and 950°C. HIPed samples showed improved density over conventional sintered bodies. Superconducting transition temperatures > 80 K were observed in samples without requiring any post-HIP annealing.

INTRODUCTION

Much work has been devoted to high temperature superconductors since their recent discovery [1,2]. Most advances have come in the area of thin films [3], where prototype applications have been developed and tested. Progress in the processing of bulk shapes (e.g., bars, rods, rings) for use as components in larger systems (motors, magnetic levitation, rail gun) has developed much more slowly.

Hot isostatic pressing (HIP) is a method of fabricating bulk ceramic shapes through the application of high pressures and temperatures. The HIP process may readily consolidate complex ceramic objects at lower temperatures than conventional sintering. Hot isostatic pressing has been used to fabricate new high temperature superconductors [4,5,6]. $YBa_2Cu_3O_{7-x}$ has been HIPed to nearly full density (99.3%) [4]. Loss of oxygen has been noted as a problem [5,6]; however, annealing in air may restore superconducting properties [6].

For this study, superconducting $YBa_2Cu_3O_{7-x}$ powder was HIPed under a range of temperatures and pressures. The bulk density for both sintered and HIPed materials was determined. A.C. magnetization measurements were made to evaluate the effect of HIP processing on critical transition temperatures.

EXPERIMENTAL

Quantities of Y_2O_3, $BaCO_3$, and CuO powders were weighed out according to stoichiometric ratio, mixed, and nitrated with nitric acid. Nitrated powders were reacted at 700°C for 8 hours, then ground using mortar and pestle. Reacted powders were calcined twice, with intermediate grinding, at 940°C for 6 hours. Powders were annealed from 500 to 200°C for 6 hours in order to maximize the oxygen content of the compound. The resulting powders were examined by x-ray diffraction using Cu K-α radiation. Powder samples (4 g) were then cold isostatically pressed in flexible molds at 160 MPa. The sample size was approximately 1.3 cm long x 0.9 cm diameter.

Sintered samples were fired at 960°C for 6 hours, followed by a slow cool in air from 500 to 200°C for 6 hours. Samples to be HIPed were vacuum sealed in Pyrex capsules.

HIPing was performed in an Autoclave Engineers 30M hot isostatic press using N_2 gas and a graphite furnace. HIP runs on 6 sets of samples (T=820, 950°C; P=70,140 and 210 MPa) were performed. A hold time of 60 minutes, followed by furnace cooling, was used. Figure 1 illustrates typical pressure/temperature profiles for both 820 and 950°C runs.

Specimens for measurement were sliced from HIPed and sintered bodies with a diamond saw. Bulk density was determined. Samples of approximately 1.5x1.5x4.5 mm were used for a.c. magnetization tests. Measurements were made by placing the sample within concentric coils driven by a 20 kHz, 1 volt r.m.s. source [HP 651B Test Oscillator]. A lock-in amplifier [EG&G Modell 128A] was used to filter and amplify the pick-up signal (Figure 2). Critical temperatures were determined by noting the abrupt change in the output voltage, which corresponds to a change in the magnetization of the sample. Measurements were made as the sample was warmed through the transition temperature.

RESULTS AND CONCLUSIONS

X-ray diffraction patterns of the calcined powder reveal a single phase $YBa_2Cu_3O_{7-x}$ material with orthorhombic crystal structure in accordance with existing literature [7]. Superconductivity was demonstrated through a.c. magnetization tests. Figure 3 shows the results of bulk density measurements. The samples HIPed at 820°C show a trend of increasing density with increasing applied pressure.

The a.c. magnetization trace for a sintered sample is shown in Figure 4. The transition temperature is 92 K. The transition

temperatures for both sintered and HIPed samples are shown in Figure 5. Transition temperatures greater than 80 K were noted for the HIPed samples, which received no post-HIP annealing.

Hot isostatic pressing has been shown to increase bulk density of $YBa_2Cu_3O_{7-x}$ superconducting materials. Transition temperatures above liquid nitrogen temperature (77K) were achieved without any post-HIP oxygen annealing. An important aspect of further study is to obtain increased transition temperatures via processing modifications. Additional work in progress includes measurements of Knoop hardness and Young's modulus, further electrical testing, and optical/electron microscopy of the microstructure.

REFERENCES

[1] J.G. Bednorz and K.A. Muller, Z. Phys. B., 64, 189 (1986).
[2] Wu et al, Phys Rev Lett, 58, 908 (1987).
[3] P. Chaudhari et al, Phys Rev Lett, 58, 2684 (1987).
[4] J.K. Tien, B.C. Hendrix, J.C. Borofka, T. Abe, T. Coulfield, S.H. Reichman, "Hot Isostatic Pressing of Oxide Superconductors", Materials Research Society Spring Meeting 1988.
[5] K. Sadanada, A.K. Singh, M.A. Iman, M. Osofsky, V. Le Toureau, L.E. Richards, Adv Ceram Mats, 3, 524-26 (1988).
[6] A.M. Campbill, M.F. Ashby, J.E. Evetss, A. D. Hibbs, R. Jones, P.P. Edwards, B. Glowock, M. Stubbs, "Critical Currents and Hot Pressing of High T. Superconductors", Materials Research Society Fall Meeting 1987.
[7] Powder Diffraction, 2, 192 (1987).

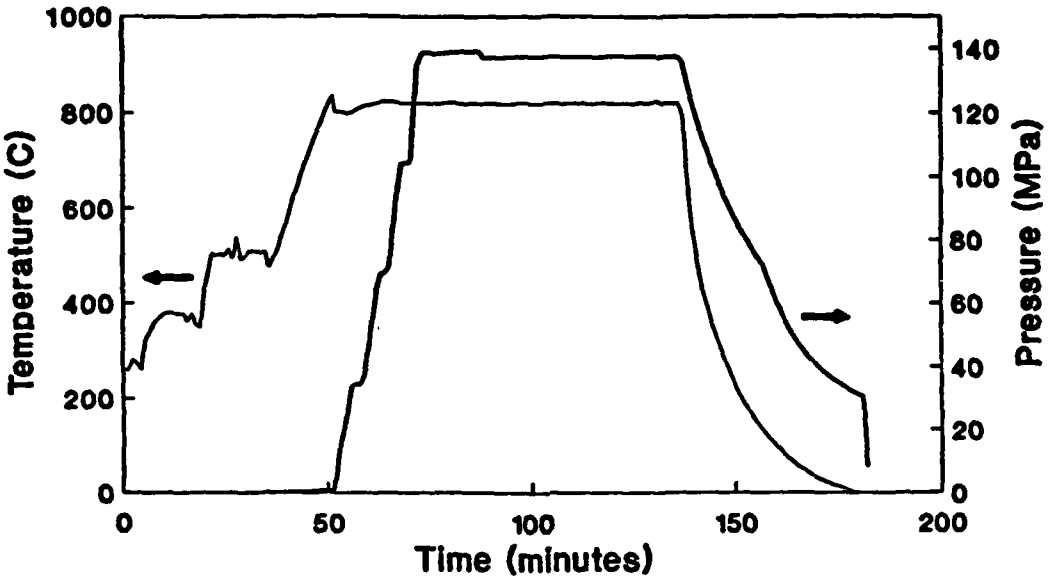

Figure 1a. Pressure/temperature profile for a HIP run at 820°C and 140 MPa.

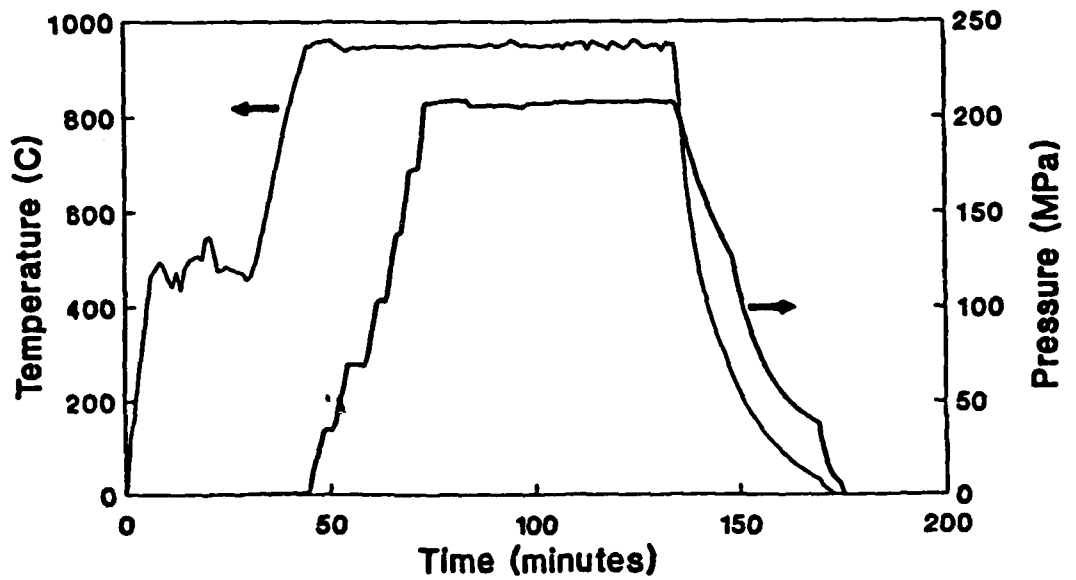

Figure 1b. Pressure/temperature profile for a HIP run at 950°C and 210 MPa.

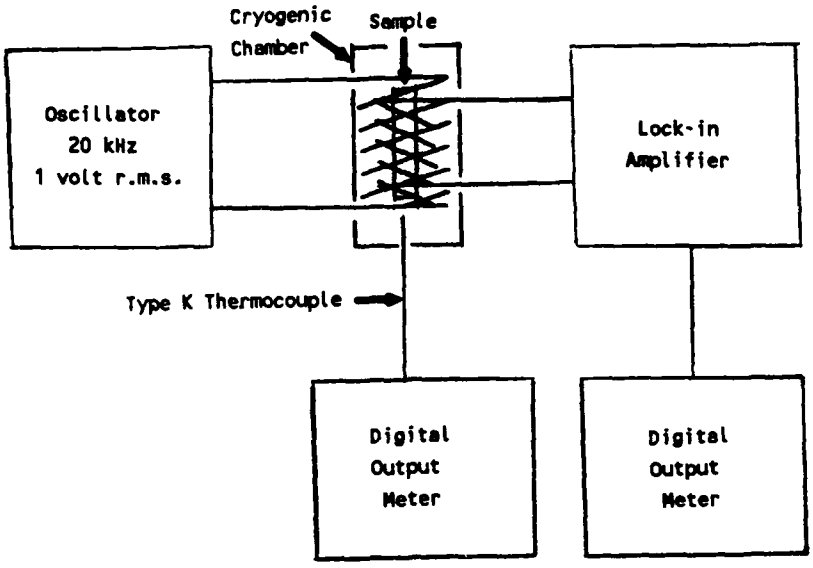

Figure 2. Block diagram of a.c. magnetization test equipment.

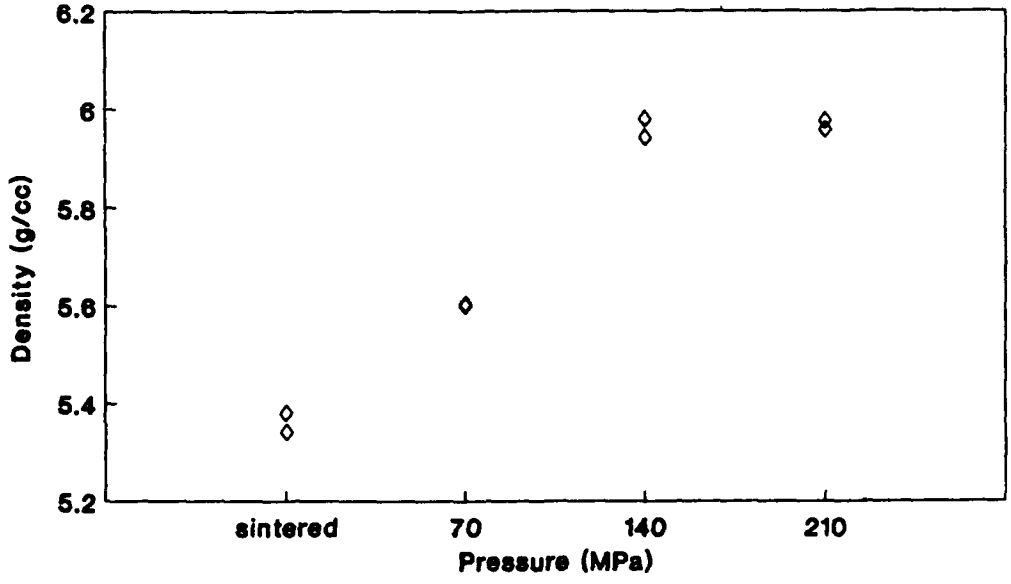

Figure 3. Sample density vs. processing pressure for samples HIPed at 820°C.

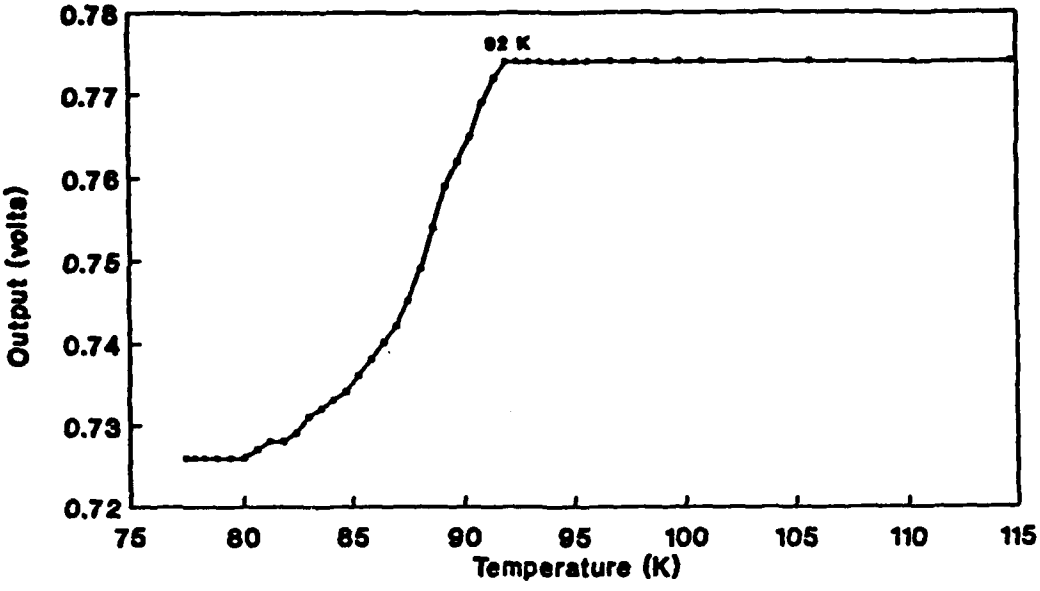

Figure 4. A.C. magnetization trace for a sintered sample. Transition temperature of 92 K determined by the abrupt change in the output voltage.

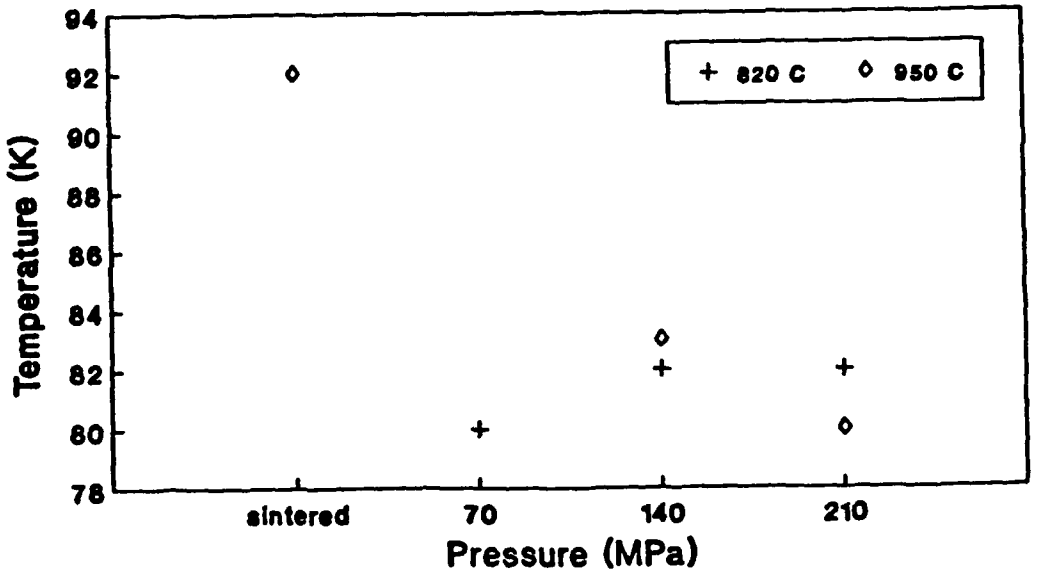

Figure 5. Superconducting transition temperature vs. processing pressure for both sintered and HIPed samples.

THIS PAGE IS INTENTIONALLY BLANK

Presented at the Workshop on High Temperature Superconductivity
23-25 May 1989 GACIAC PR 89-02

SUPERCONDUCTING ANTENNAS

R. C. Hansen
Consulting Engineer
PO Box 215
Tarzana, CA 91356

ABSTRACT

The applicability of superconductors to antennas is examined, with emphasis on the roles of external and internal fields.

1.0 INTRODUCTION

The advent of high T_c superconducting materials has prompted a re-examination of the opportunities for improving antenna performance. Areas where superconductors have been or should be considered include superdirective arrays, millimeter wavelength arrays, electrically small antennas, and inductive matching of large transmitting antennas. Each of these is discussed in a section of this paper. Although a SQUID could be used directly as an antenna, these devices are not discussed here. It is believed that no areas of superconductor applicability to antennas have been omitted. Since the distinction between external and internal fields is crucial, this topic is addressed first.

2.0 EXTERNAL AND INTERNAL FIELDS

The effect of using a superconductor in constructing an antenna can be easily understood by a careful consideration of the roles of external and internal fields. Take a cylindrical dipole antenna as an example. The radiated field and its associated radiation resistance, and the stored energy in the near-field and its associated reactance, are produced by the currents on the surface of the dipole; these

are external fields. Fields internal to the dipole cylinder are important only in relating to the conduction loss, which is usually small. Use of a superconductor will produce a negligible change in the external fields, hence in impedance, pattern, and directivity, since the dipole cylinder diameter is typically small in wavelengths. Only the internal fields experience major change, leading of course to a zero or low conduction loss. Similar conclusions apply to almost all antennas: all antenna properties except efficiency depend upon external fields, and these are essentially unchanged by superconductors. One might construct an exception to this rule, where an antenna with a volume of solid conductor has a pattern due to current throughout the conductor that is different from that due to surface currents. But almost all antennas use relatively thin conductors.

Miniaturization of antennas can also be understood via external fields. The size of most antennas is controlled by the need for certain dimensions in free space wavelengths, e.g. circumference of a two-arm spiral antenna should be a wavelength at the lowest frequency of operation. And antennas such as log-periodics and Yagi-Udas need dipole arms of certain lengths. All of these requirements relate to the external fields, thus use of superconductors will not allow miniaturization of these types of antennas.

3.0 SUPERDIRECTIVE ARRAYS

Superdirectivity, formerly called supergain, exists with an antenna when its directivity is greater than normal; for an array normal directivity could be taken as that when the elements are spaced half-wavelength apart. Superdirective arrays possess a fundamental limitation (Hansen, 1981A & B)*, as the Q tends to increase rapidly as the directivity increases. Thus utility of superdirective arrays is limited by very narrow bandwidth (bandwidth $\approx 2/Q$). Limitations also exist because the input resistance of the elements decreases, thereby making impedance matching difficult, and because the allowable tolerances on the excitation of the elements also decreases. Along with low radiation resistance may go low efficiency, if the conduction loss resistance is comparable to the radiation resistance.

Since superconductors offer the possibility that the conduction loss can be eliminated, or at least reduced significantly, it is appropriate to examine superdirective arrays quantitatively to determine changes in performance that might be realized. A convenient vehicle for doing this is a linear endfire array. Superdirective broadside arrays have lower directivity and higher Q than comparable

---

* Hansen, R. C., "Fundamental limitations in antennas", Proc. IEEE, Vol. 69, Feb 1981A, pp. 170-182

Hansen, R. C., "Some new calculations on antenna superdirectivity", Proc. IEEE, Vol. 69, Oct 1981B, pp. 1365-1366

endfire arrays; for fixed number of elements and fixed element spacing, maximum directivity occurs at endfire. The directivity expression for a linear endfire array of dipoles in terms of mutual resistances is used (Hansen, 1983)*:

$$G = \frac{120 \left| \sum A_n V_n^* \right|^2 \tan^2 \pi \ell/\lambda}{\sum_n \sum_m A_n A_m R_{nm}}$$

The tangent factor is used only when the dipole length ℓ is less than half-wavelength. Excitation coefficients are A_n, and are complex; V_n is the excitation vector, with components $\exp(-jkd(n - 1))$, where $k = 2\pi/\lambda$; R_{nm} is the mutual resistance between the n and m elements. Normally the latter would, for thin wire dipoles, be computed by the efficient algorithm using Sine and Cosine Integrals developed by Hansen (1972)**. But superdirectivity typically involves subtracting large numbers, especially for Q, which is given by:

$$Q = \frac{120 \sum A_n A_n^*}{\sum_n \sum_m A_n A_m^* R_{nm}}$$

It is necessary to employ double precision in the calculation of the mutual resistances, and hence in the Sine and Cosine Integrals. Since such a subroutine could not be found, a Chebyshev economized series expansion is used to construct a double precision Sine and Cosine Integral subroutine. The maximum directivity excitation vector is simply found from the mutual resistance matrix inverse: $[A_n] = [V_m][R]^{-1}$.

Calculations have been made of directivity, Q, and input resistance (of each element) for endfire linear arrays of parallel thin wire dipoles, where for each array the excitation coefficients are calculated to produce maximum directivity. The results differ from the results previously calculated for arrays of isotropic elements in two ways. First, for certain arrays, the mutual resistance matrix is sufficiently ill conditioned that a maximum directivity solution is not found. Second, much larger deviations from the straight line behavior of log Q versus *G* are observed. This is commensurate with the behavior versus frequency or scan angle of impedance of elements in small arrays of dipoles. All of the many cases calculated show the same trends.

---

* Hansen, R. C., "Linear arrays", in "The Handbook of Antenna Design, Volume 2", A. W. Rudge et al eds., IEE/ Peregrinus, 1983

** Hansen, R. C., "Formulation of echelon dipole mutual impedance for computer", Trans. IEEE, Vol. AP-20, Nov 1972, pp. 780-781

Endfire linear arrays of $\ell = .1\lambda$ dipoles have been optimized; Fig. 1 gives log Q versus directivity for arrays of length 1, 2, and 5λ. Note that the slope of the log Q curve decreases as the array length increases. Although the calculated points in Fig. 1 fit straight lines reasonably well, as the element spacing decreases the mutual effects overwhelm the superdirective effects, and the points begin to scatter. Most of the endfire arrays in Fig. 1 have element spacings larger than $\lambda/4$, thus the patterns will exhibit significant backlobes.

Fig. 2 shows Q versus radiation resistance of the center element for a variety of maximum directivity arrays, ranging from 3 to 10 elements, with spacings from $.1\lambda$ to $.45\lambda$. Arrays with odd and with even number of elements seem to fit slightly different envelopes. The significance of these data is that for $Q \simeq 1000$ the radiation resistances are greater than .2 ohm, and that for radiation resistance of roughly .1 ohm, the Q's are greater than 3000. Antennas with such high Q are generally unuseable due to detuning from environmental changes. The question then is, what is a typical loss resistance. For a dipole with sinusoidal current, the feed point equivalent resistance is: $R_\ell \simeq (R_s \ell/\pi a)(1 - \text{sinc } K\ell)$, where R_s is the surface resistance, and a is the wire radius. For copper wires, the surface resistance is: $R_s = .000261 \sqrt{f_{Mhz}}$. Over the range 10 to 1000 Mhz, R_s varies from .000825 to .00825; for these frequencies then the range of R_s is roughly .001 to .01 ohms/$\square$. At even lower frequencies, the surface resistance will be lower than .001 ohms/$\square$.

Thus for all the endfire arrays with useable Q, the radiation resistance is much larger then the loss resistance, so superconductors offer no significant improvement. For broadside arrays, the radiation resistance for a given Q is larger than values in Fig. 3, so the same conclusion applies on the lack of benefit from superconductors.

Arrays of loops have also been considered (Walker et al, 1977; Hansen, 1978)*. For loops whose perimeter is small in wavelengths, radiation resistance varies with diameter/wavelength to the fourth power. Thus small loops have very small radiation resistances, and similarly even smaller input resistances when closely spaced in an array. Superconductors here can increase efficiency close to unity, but this increases antenna Q, as total resistance has been decreased. Because of the very high Q's of superdirective loop arrays, superconductors again will not offer an advantage.

Although superconductors are not useful in practical superdirective arrays,

---

* Walker, G. B. et al, "Superconducting superdirectional antenna arrays", Trans. IEEE, Vol. AP-25, Nov 1977, pp. 885-887

Hansen, R. C., "Comments on 'superconducting superdirectional antenna arrays'", Trans. IEEE, Vol. AP-25, Nov 1978, p. 891

they may be very important in allowing a high efficiency matching/feeding network to be constructed. Matching a radiation resistance of an ohm or less to 50 ohms normally incurs significant loss, while matching a reactance of thousands of ohms also involves major loss. Here the superconductors can be used to provide very high Q (low loss) matching circuits. We can expect to see applications of super-directive arrays of modest directivity increase, constructed with normal conductors, but with matching/feeding circuits utilizing superconductors.

4.0 MILLIMETER WAVELENGTH ARRAYS

Most reflector and array antennas have low dissipative losses; losses are primarily due to impedance mismatches. However at millimeter wavelengths, transmission line loss, whether waveguide, stripline, or microstrip, is important in determining the feasibility of an array. To illustrate this point, examples have been calculated for both waveguide and microstrip planar arrays; only the waveguide case will be discussed in detail.

A planar array of waveguide slots (Flat Plane Array) is typically constructed of side-by-side waveguide linear slot arrays (sticks), with these fed by another waveguide at right angles, utilizing cross-guide couplers. Often the array is divided into quadrants for monopulse operation. Resonant stick array design produces a fixed, broadside beam. For a square array of width L, the feed path length is 2L. And for small to moderate loss, the array efficiency due to waveguide loss, is just: effic = $1 - 4\alpha L$ where α is the attenuation coefficient. Formulas for α are widely available, and are not repeated here. For an example, the lower portion of a waveguide band is used: $\beta/k = .5$, and $a = 2b$, using common waveguide notation. Assuming the conductivity of copper, array efficiency due to guide loss is calculated for arrays of directivity 40, 50 and 60 db; see Fig. 3. Gain then is the directivity minus the efficiency (in db). Although the curves show that modest gain (40 db) may be realizable at 100 GhZ, the higher frequencies often require large gains to offset increased path loss. In practice, for all arrays, the actual loss will be greater, due to surface roughness, metal imperfections, etc. Thus waveguide loss has been a major factor against construction and utilization of high gain arrays in the 40 to 100 GhZ range.

Calculations for a planar array of microstrip patches have produced results similar to those of Fig. 3, but with lower efficiencies (Hansen, 1989)*.

Use of superconducting waveguides would in principle allow the efficiency to approach 0 db, and thus high T_c materials may allow a significant extension of array techniques, both waveguide and microstrip.

---

* Hansen, R. C., "Superconducting Antennas", submitted for publication, 1989

5.0 ELECTRICALLY SMALL ANTENNAS

Antennas small in wavelengths are usually dipoles (monopoles) or loops; both are considered.

5.1 ELECTRICALLY SHORT DIPOLES

Consider a short cylindrical dipole, matched by an inductive reactance. Fig. 4 shows antenna efficiency versus dipole half length h/λ, for $h/a = 100$ and several matching coil Q's. Unless the dipole is very short and the matching Q very high, the dipole loss resistance can be omitted. These curves show dipole efficiency as a result of matching coil Q; using a superconducting matching coil would increase the efficiency to roughly 100% for any length h/λ. Since the conductive loss is negligible, there would be no advantage in using superconducting wire for the dipole itself. An unfortunate concommittant of the higher efficiency is the higher Q; Fig. 5 gives Q versus length for a loss free matching coil; now the Q is controlled by radiation resistance alone. With a lossy tuning coil, the overall Q is never larger than the coil Q; for the loss free coil case, $Q \simeq 700$ for $h/\lambda = .05$, for example. There is, therefore, in the use of a superconducting tuning coil for a short dipole (or monopole), a tradeoff between efficiency and Q (or bandwidth). The problem of matching to the low radiation resistance is eased by use of a superconducting shorted stub (Khamas, 1988)*, which provides both the inductive reactance for resonance, and a 50 ohm point for a feed line.

5.2 ELECTRICALLY SMALL LOOPS

In several respects the small loop is the obverse of the short dipole. It is tuned typically with a capacitor, and these can have very high Qs. Thus there is little point in attempting to improve the efficiency due to matching. However the radiation resistance is typically smaller than the conductive loss; for a small circular loop the radiation resistance varies as diameter/wavelength to the fourth power. Q of superconducting loops can be very high; Fig. 6 gives Q for a loop of diameter/wire radius of 100.

6.0 INDUCTIVE MATCHING OF LARGE TRANSMIT ANTENNAS

Monopoles with top loading, all supported by tall towers, are used for VLF submarine communications, Omega and Loran navigation, etc. Since these towers are usually well below resonant length, a tuning coil is used at the antenna base to produce a resonant input impedance. These large coils are candidates for

---

* Khamas, S.K. et al, "A superconducting short dipole antenna", Electronics Ltrs., Vol. 24, Apr 1988, pp. 460-461

superconducting cables, just as for other electrically small antennas. For details, see Hansen (1989)*.

7.0 CONCLUSIONS

Only two areas appear to offer performance advantages. Arrays above 5 GhZ will certainly benefit from low conduction loss. Inductive matching of electrically short antennnas, both small and large (low frequency), will allow significant efficiency improvement. Most important, size reduction of antennas will generally not be aided by superconductors.

---

* Hansen, R. C., "Superconducting Antennas", submitted for publication, 1989

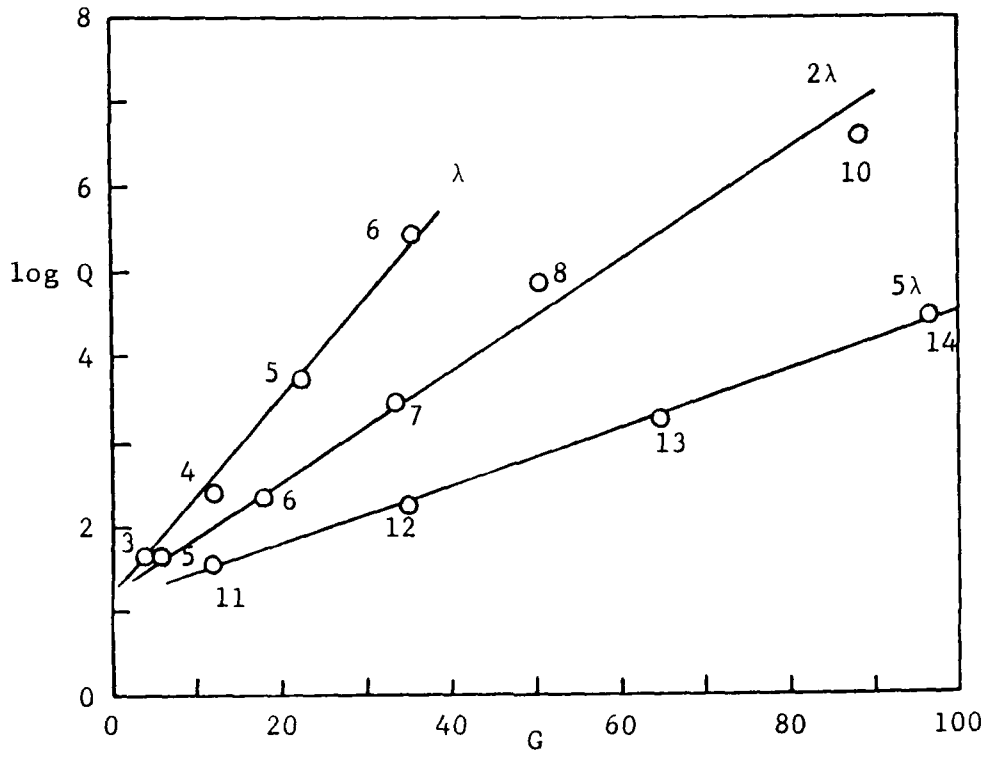

Fig. 1

Q of Endfire Arrays of Parallel Dipoles

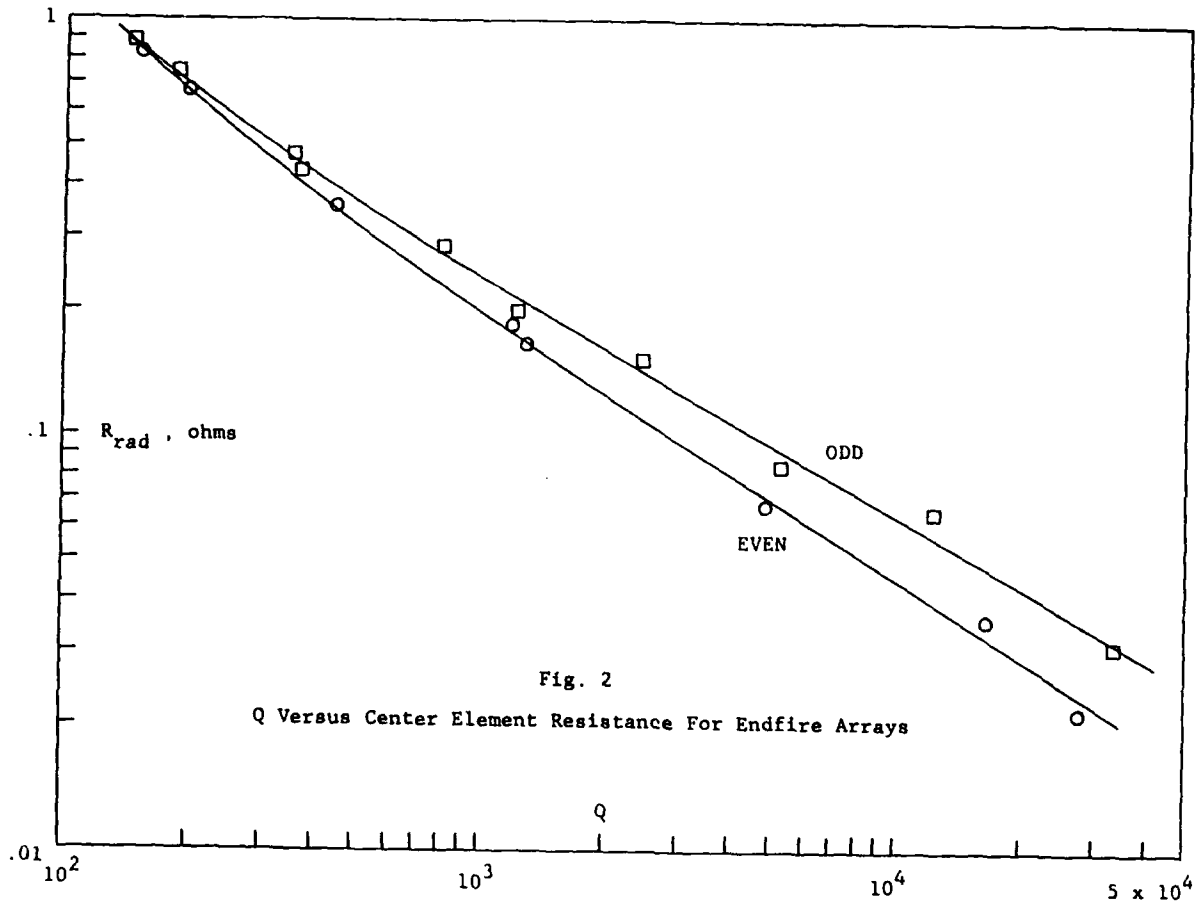

Fig. 2

Q Versus Center Element Resistance For Endfire Arrays

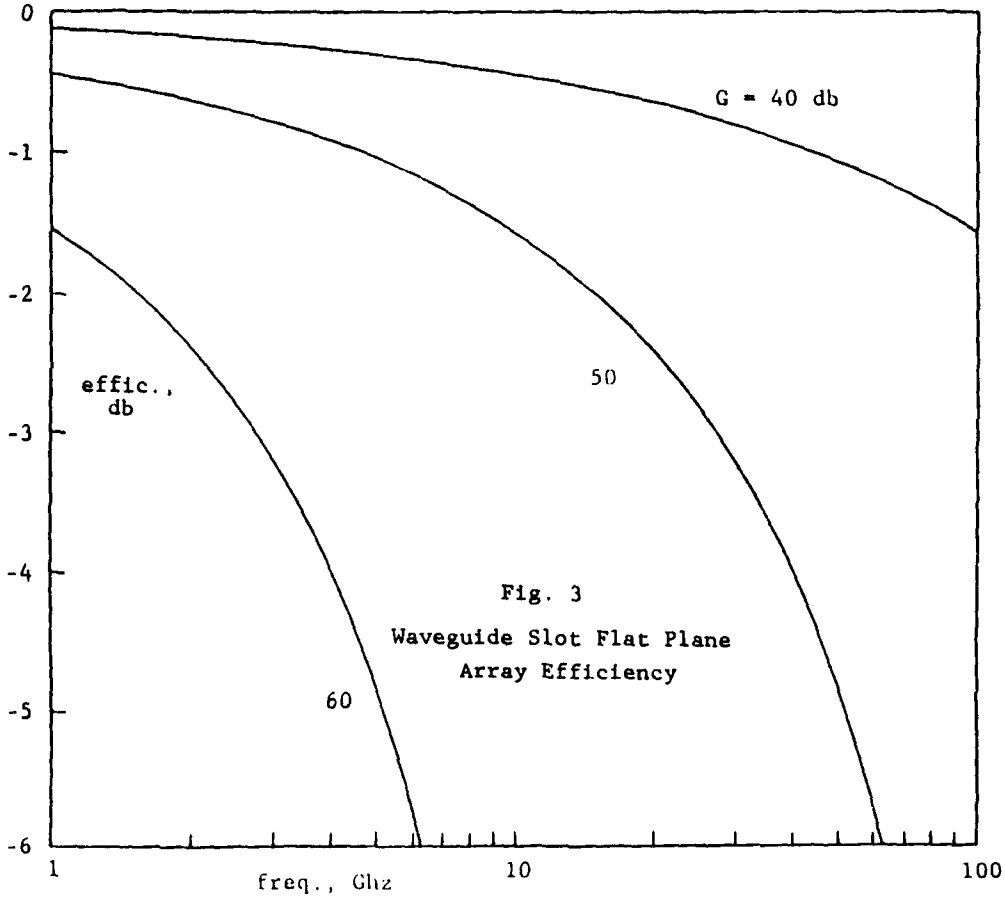

Fig. 3

Waveguide Slot Flat Plane Array Efficiency

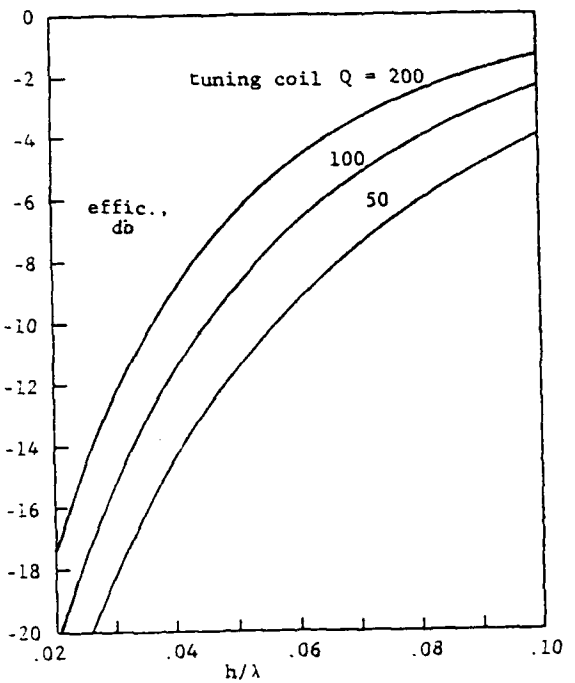

Fig. 4

Efficiency of Dipole With Tuning Coil

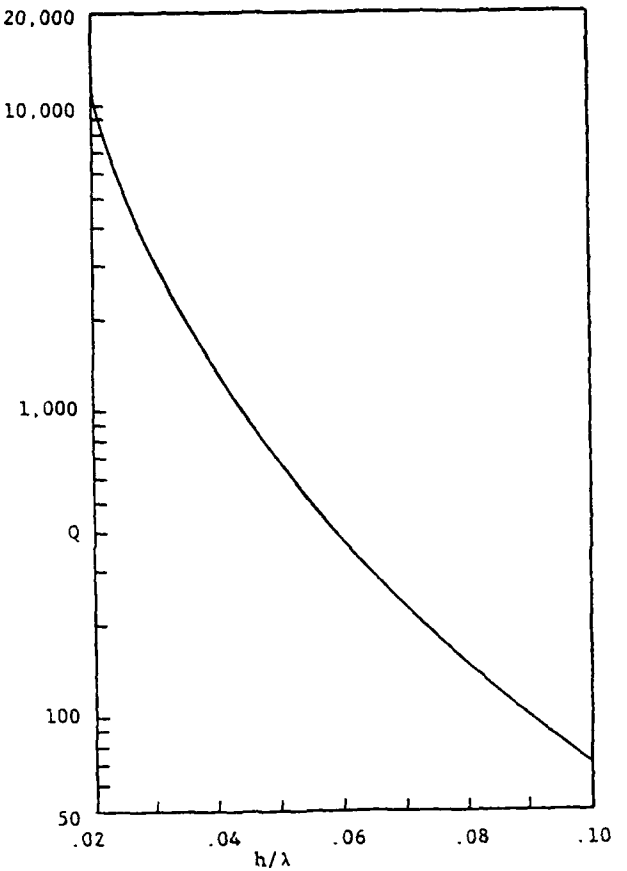

Fig. 5

Q of Dipole With Lossless Tuning Coil

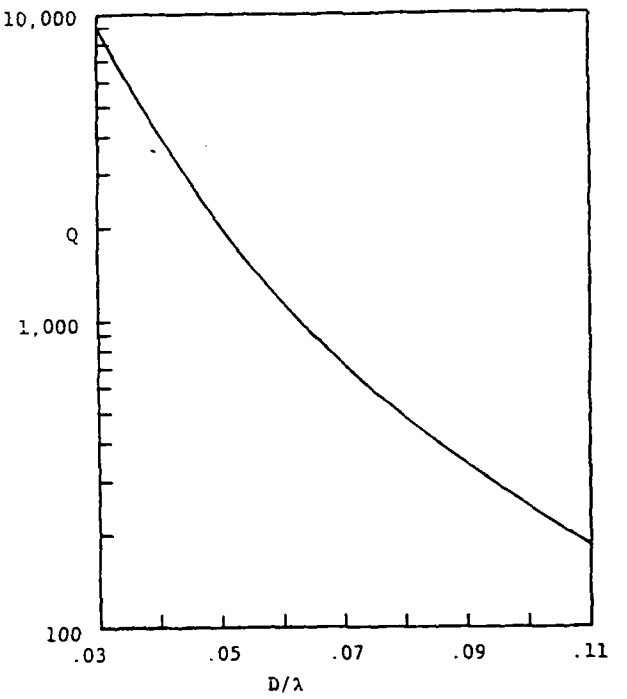

Fig. 6

Q of Loop Without Loss

THIS PAGE IS INTENTIONALLY BLANK

Microwave generator Using Phase Locking Of Josephson Junction Arrays In High Temperature Superconductors

Ali E. Khalil*

GE Astro Space Division, Princeton NJ, 08543

Abstract:

A conceptual design for a microwave generator utilizing coherent oscillations (phase locking) in series arrays of Josephson junctions and weak link junctions which can be formed between the grain boundaries in the newly discovered high temperature superconductors is presented. It is shown that when a purely external resistive impedance shunts the circuit a local domain of stable and coherent oscillation (local stability) between series of linear arrays may exist. The analysis is based upon the resistivity shunted junction (RSJ) model in which a relationship between the junctions spacing, optimum number of junctions, and external load parameters was derived to ensure maximum power output and synchronization conditions.

* To appear in the proceedings of Workshop On High Temperature Superconductivity 23-25 May 1989, Huntsville, Alabama.

Introduction

The discovery of high temperature superconducting materials has triggered intensive efforts to exploit their properties in the design of a new generation of devices (sensors, emitters, interconnects, etc). The unusual properties of these materials can be utilized for new and, in most cases, unconventional designs of components or hybrid systems. The Josephson tunnel junction (JTJ) is one of the early devices that has contributed to our basic understanding of the quantum mechanical behavior of the superconducting phenomena. The construction of Josephson junctions from the new high temperature superconductors can be a difficult task since the small value of the coherence length, which is smaller than the barrier width, will inhibit the tunneling process. Fortunately, it appears that inherent in a polycrystalline film of the high temperature superconductor material are many Josephson junctions[1] formed naturally between each grain boundary.

This property was exploited in designing infrared (IR) detectors fabricated using the low-temperature (13K) superconducting oxide $Ba(Pb,Bi)O_3$, which has many similarities to the High-Tc YBaCuO material (known as 123 compound). In Early efforts to understand the nonequilibrium response of the device, the uniformity of the current-voltage (IV) characteristics of the "intrinsic" series arrays of JTJ formed between the grain boundaries have been successfully demonstrated[2]. Stable coherent oscillations of large numbers of Josephson junctions coupled in arrays have proven to be a possible source of microwave generation[3]. The superior properties of Josephson arrays to conventional technology and certainly to single junctions as generators of microwave and far-infrared radiation have been realized[4]. Only recently has an understanding of the dynamics of systems consisting of several similar (or nearly similar) Josephson junctions begun to emerge[5].

An array of JTJ is mutually phase-locked when Josephson phases ϕ_k of all the junctions are equal. This produces a coherent state of the array which can be maintained even in the presence of random variations or fluctuations of the junction parameters. Initial evidence of phase coherence was seen in the coupling of weak short-range quasi-particle interaction resulting in weak-locking at low frequencies. However, coherence disappears[6] at microwave and higher frequencies where arrays have most potential for practical applications. It is now fully understood that this short range coupling is inherently unstable against long-range phase deviations. Further investigations have revealed that the high frequency electromagnetic interaction is the only mechanism which is strong enough to produce stable phase locking in real arrays where the junction parameter spreads and

time-dependent fluctuations tend to destroy the coherent state.

Coherent microwave oscillations of arrays consisting of up to 100 Josephson junctions (thin-film microbridges) have been obtained and relatively large values of radiated power (up to 5 nW) were observed[1]. It is possible to injection-lock all of the junctions to a small external rf current passing in series through the array. The Josephson oscillations of each junction are then phase-locked to the external rf current which provides a common reference phase to all of the junctions. Practical coherent arrays can be designed which will offer significant improvement over the present technology for a number of applications in microwave engineering. For higher power, more complex traveling-wave arrays should be employed.

Theoretical Analysis and Stability Criteria

A) Phase Coherence in Linear Arrays

An array of Josephson junctions biased by an external circuit can, in principle, be analyzed for phase coherence and stability. When an external biasing circuit is applied to an array, the Josephson oscillations of a given junction induce currents of the same frequency in other junctions. The junction nonlinearity gives rise to the possibility of synchronization of the junction oscillations through these external currents only if an array has a special coupling circuit that permits the oscillation currents induced by one junction to flow through the others. Two separate equations for each junction in the array have to be solved simultaneously. One is an intrinsic equation which describes the dynamics of the phase ϕ which relates the quasi-particle wave functions on both sides of the barrier due to a current I(t) flowing through the junction. The phase equation determines the stability conditions and the requirements under which the array may or may not form a coherent state. The second equation is an electrodynamic equation which determines the current $I_c(t)$ in the external circuit due to a voltage across the junction.[2] In general, this voltage is given by,

$$V(t)=(1/2\pi)d/dt(\phi\phi_o) \qquad (1)$$

where ϕ_o is the flux quantum constant.

The intrinsic equation of an array can be difficult to obtain in an exact form. However, a simple representation can more easily be obtained by employing the model of a resistivity shunted junction (RSJ). In this model, the total current contribution in each junction is due to the sum of the supercurrent which is proportional to sin ϕ, the quasi-particle current which is determined by the voltage across the junction and its normal resistance, the displacement current due to the intrinsic capacitance of the junction, and finally, the fluctuation current $I_f(t)$ which describes the intrinsic noise current. In the following model the contribution of this current component will be ignored. The phase equation of a single junction can be written as (see Fig.1a),

$$\alpha \ddot{\phi} + \dot{\phi} + \sin \phi = I \qquad (2)$$

α is a dimensionless measure of the capacitance of the junction. In natural units ($\hbar = 1$) this constant is given by $2eI_c R^2 C/\hbar$ where C is the capacitance of the junction, R is the external load resistance, and I is the normalized current (relative to the critical current I_c). An array of junctions biased with a purely resistive load is shown in Fig. 1b. The phase equation in reduced units is given by,

$$\alpha \ddot{\phi}_j + \dot{\phi}_j + \sin \phi_j + 1/R \Sigma_j \dot{\phi}_j = I_t \qquad (3)$$

$$j = 1,2,\ldots,N$$

N is the number of junctions in the array and I_t is the normalized bias current (relative to the critical current I_c). The condition of phase coherence implies that all the junctions in the array oscillate together with the same phase $\phi_j = \phi$ and the N equations of the array (3) reduce to the following single equation,

$$\alpha \ddot{\phi} + (1+N/R)\dot{\phi} + \sin \phi = I_t \qquad (4)$$

Equation (4) is a nonlinear differential equation in the phase ϕ. An approximate semi-periodic solution exists in terms of incomplete elliptic integrals of the first kind. In the special case when N=R the solution will converge slowly for a value of $I_t = 2$ and $\sin(\phi_m/2)$ is equal to 0.54, where ϕ_m is the minimum phase angle for which coherence is allowed. A solution ϕ_s of equation (4) is locally stable when its perturbation in the form $\phi(t) = \phi_s(t) + \Theta(t)$, the small perturbation parameter is damped out

with time. $\Theta(t)$ is a parameter representing small deviations from the stable solution ϕ_s. This linearization procedure will yield an equation in the form,

$$\alpha \ddot{\Theta} + 2\dot{\Theta} + \Theta \cos\phi = 0 \qquad (5)$$

A general solution of equation (5) can be written in the form

$$\Theta(t) = L(t) \Sigma_{i=1,2} \exp(a_i t) \qquad (6)$$

$L(t)$ is a periodic function having the same period as ϕ. The values of the constants a_i are determined from the two independent solutions of equation (5). when the real parts of these constants (Liapunov exponents) are negative the solution is locally stable. It is easy to rigorously show that,

$$\Sigma_i \delta_i = -1/\alpha \qquad (7)$$

and $$\delta_i = \text{Real part}(a_i)$$

The imaginary part of a_i determines the oscillatory nature of the system response to small perturbations. Numerical solutions to equation (5) exist. These solutions will converge only for those values of ϕ which satisfy the relationship $\cos\phi \geq 1/4\alpha$. This condition implies that a small perturbation around the stable coherent state will exponentially damp out very rapidly after the initial disturbance occurs. In the special case where $\delta_1 = \delta_2 = \delta$ the value of the exponent is equal to $-2\cos\phi$. Including this result in the domain solution of equation (4), a coherent stable state of an array of Josephson junctions with a purely resistive load can be formed where α is equal to 0.6 and $\delta = -0.83$. These results are in full agreement with the recent findings of reference (8). Numerical solutions to the set of differential equations can be used in the design of series arrays. A knowledge of the constant α will determine the number of junctions required and the value of the external load resistor, R, for phase coherence.

B) Linear Arrays In High Temperature Superconducting YBaCuO Compound

A series array of JTJ can phase lock and form a coherent state with a purely resistive load. These conditions can equally apply to weak links. The design of series arrays for phase coherence on a wafer of high temperature superconductor will require careful attention during manufacturing. The size and

uniformity of the grains will be affected as a result of the deposition conditions and the post-deposition treatment. Of more importance is the exact nature of the grain boundaries and the critical current density per junction. A granular film of high temperature superconductor YBaCuO provides a more obvious realization of an array of weak links. It is also possible that epitaxial films could contain an intrinsic weak link structure due to weakly coupled Cu-O planar defects, such as, stacking faults or boundaries between single crystal domains of different orientations.

The idea of phase coherence was recently exploited in designing very sensitive infrared (IR) detectors[9]. The detector was manufactured from a thin film of superconducting oxide $Ba(Pb,Bi)O_3$ using RF sputtering method on sapphire substrate. This material is very similar in structure to the ceramic high temperature superconductor material, YBaCuO. The grain size was found to be 0.2 μm in diameter. Potential barriers were formed at the grain boundaries and all the barriers became Josephson junctions. Due to the small value of the maximum power available from a single junction P_o, series arrays will have the advantages of increasing the power output due to the large number of junctions. Within the RSJ model, the maximum power radiated by a junction to a matched wideband transmission line and for frequencies below the critical frequency is given by,

$$P_o = 0.4\ I_c V \qquad f<f_c \qquad (8)$$

where I_c is the amplitude of the supercurrent with an average value of 3 mA and V is the average voltage per junction. In the long-wave millimeter band (f=40 GHz) V is about 80 μV and $P_o \sim 100$ nW which is too small for any practical application. The actual microwave power given by a single junction is much smaller than this amount due to the small value of the microwave impedance Z of the Josephson junction which is of the order 100 mΩ . A microwave source with such a small impedance is seriously mismatched with a typical microwave transmission line. However, a series array of Josephson junctions offers a simple solution. When the power is maximized by optimizing the transformed load impedance R the essential constraint on the array will be the critical current I_c. The impedance match is achieved by optimizing the number of junctions according to,

$$N_o = R/Z = I_c R/\sqrt{3}V \qquad (9)$$

and the optimized power in this case is given by $N_o P_o$.

Another consideration in the design of an array is the minimum spacing,S, between junctions that is allowed by heat dissipation without driving the superconductor into the normal state. For an array of length d the spacing S is given by,

$$S=d/N_o=dV\sqrt{3}/I_cR \qquad (10)$$

Where d is the length of the array. In practical applications, if the length of the array is limited to quarter wavelength $d=\delta/4$ and the frequency bandwidth to an octave or less, a junction spacing less than 1 μm is required. In lumped arrays it may be necessary to decrease S below 1 μm to make full use of critical currents greater than few milliamps which is very difficult to achieve using presently available techniques.

The higher power requirements are easily met using series arrays of JTJ's naturally formed between the grain boundaries in YBaCuO compound. In a thin film of YBaCuO with 1 mm^2 surface area, the grain size is approximately 0.2 μm in diameter and the number of series-connected junctions are estimated to be 10^4. For a microwave source with similar dimensions, the maximum power generated (for in-phase coherence) by the array (see Fig.2) is 1 mW compared to 100 nW for a single junction. In practice when the amount of thermal energy generated is large compared to the cooling capacity of the dissipative environment, an upset of the superconducting state may occur and heating can be the limiting factor which may affect the performance of large series arrays. In addition, partial phase coherence between different sets in the series array can minimize the amount of power generated.

The implementation of the HiTc superconductors as very efficient microwave generators is unparalleled. It was shown that a purly resistive shunt impedance can, in principle, produce the phase coherence which is necessary for microwave emission in JTJ's series arrays. On the other hand, in the field of microwave detection, coherent arrays can be integrated in a number of receiving devices based on the Josephson effect, such as, self-pumped mixers and self-selective quadratic detectors. These devices make the most complete use of the unique electrodynamic properties of the JTJ and do not require an external pumping source (local oscillator) for their operation. In addition, utilization of coherent arrays can avoid the limitation imposed by the small value of the Josephson junction resistance thus enabling the design of very simple receivers. Estimates show that such receiving devices can have noise temperature and noise equivalent power as low as 10 K and E-19 $W/\sqrt{Hz}$, respectively throughout the millimeter band[6].

References:

1) M.G. Forrester et al,"Proc. 1988 Applied Superconductivity Conference", IEEE Trans.Magn. MAG-25,1989.
2) Y. Enomoto et al, J.Appl.Phys.59, 3807(1986).
3) A.K. Jain et al, SQUID 80, 939(1980).
4) T.D. Clark et al, Appl.Phys.Lett.29, 751(1976).
5) T.D. Clark, Phys.Lett.27A, 585(1968).
6) A.K. Jain et al, Phys.Rep.109, 309(1984).
7) P.E. Lindelof et al, J.Low.Temp.Phys.29, 369(1977).
8) P. Hadely et al, Appl.Phys.Lett.52, 1619(1988).
9) Y. Enomoto et al, Physica C153, 1592(1988).

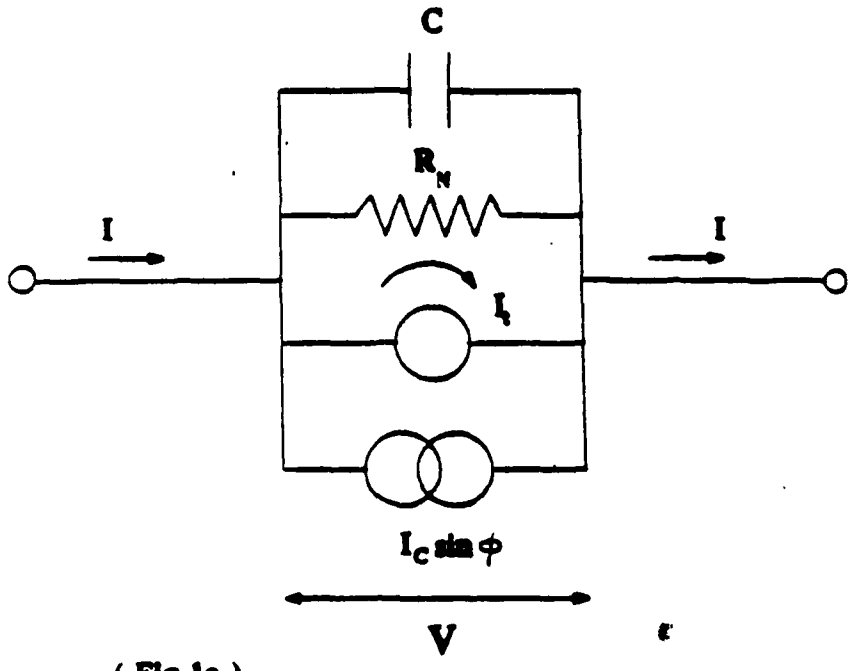

(Fig 1a)

Figure (1a): Equivalent circuit diagram of Josephson Tunnel Junction in the (RSJ) model.

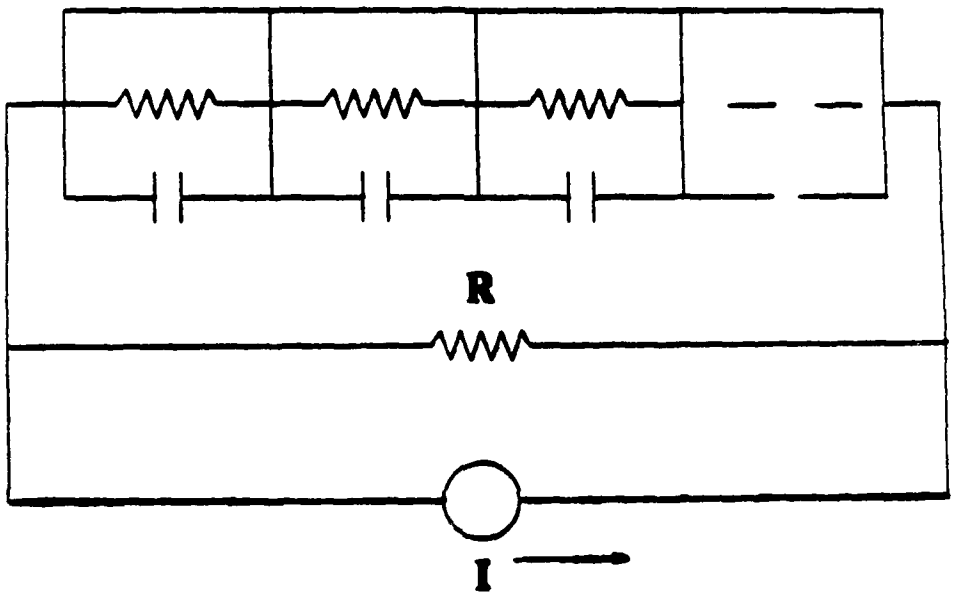

(Fig 1b)

Figure (1b): Josephson Tunnel Junction array representation.

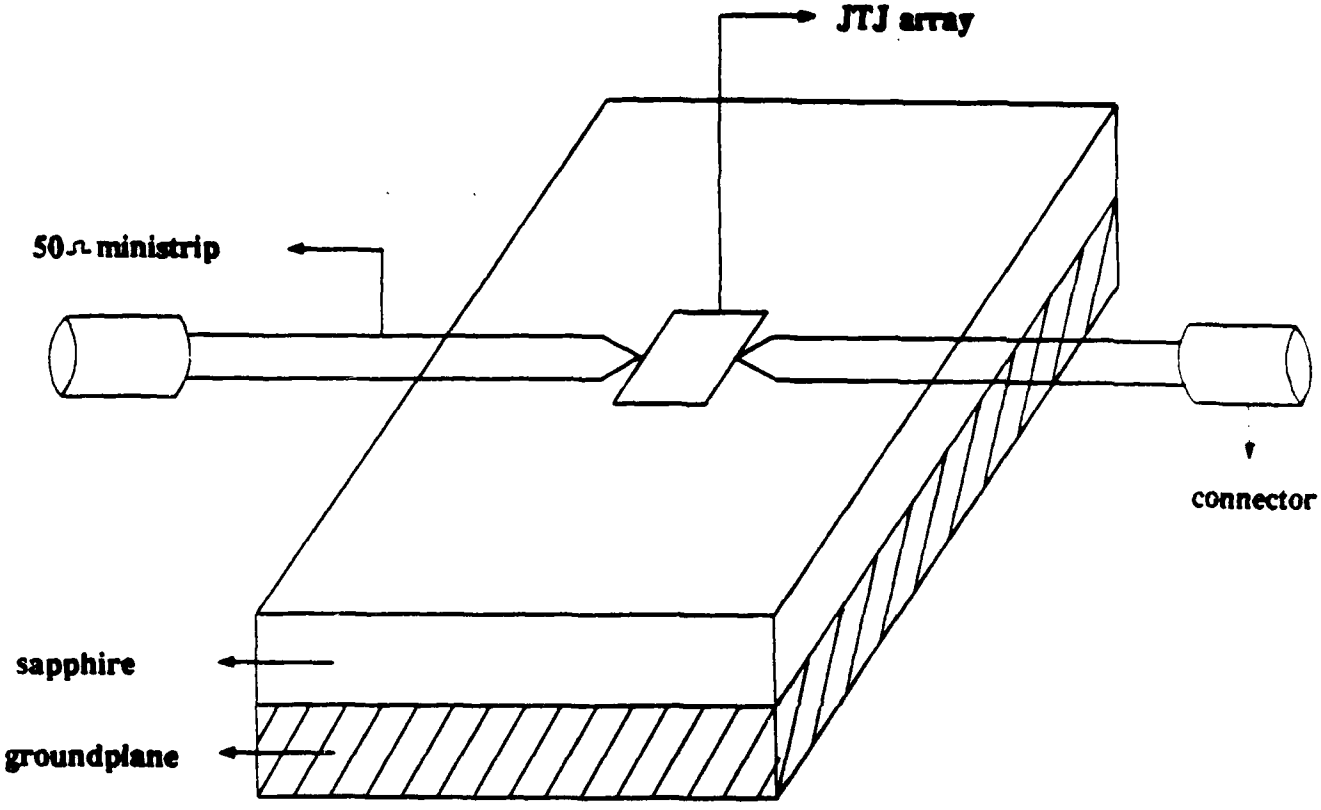

Fig (2)

Figure (2): Array design of Josephson Tunnel Junction.

THIS PAGE IS INTENTIONALLY BLANK

WORKSHOP ON HIGH TEMPERATURE SUPERCONDUCTIVITY

MAY 23-25, 1989

LIST OF ATTENDEES

Achar, B.N.
Memphis State University
328 Manning Hall
Memphis, TN 38152

Adams, Gary
Strategic Defense Command
USASDC, PO Box 1500
ATTN: CSSD-H-DP
Huntsville, AL 35807

Alexovich, Robert
Analex Corporation
21775 Brookpark Road
Fairview Park, OH 44126

Anderson, Elmer
UAH, Physics Dept
Huntsville, AL 35899

Ashburn, James R.
UAH, Physics Dept
Room 102 Science Bldg
Huntsville AL 35899

Baginski, Mike
Auburn University
EE Department
200 Broun Hall
Auburn, AL 36849

Baity, S.W.
Oak Ridge Nat'l Labs
PO Box 2009
Oak Ridge, TN 37831-8071

Belohoubek, Erwin
David Sarnoff Research Center
DSRC, CN 5300
Princeton, NJ 03543

Beiser, Mitchell A.
Auburn University
200 Broun Hall
Auburn, AL 36849

Benfer, 1LT Richard H.
US Army Laboratory Command
Ceramic Research Brance
Watertwon, MA 02172-0001

Bennett, J.S.
MICOM Research Dir
AMSMI-RD-RE
Redstone Arsenal, AL 35898-5248

Besser, Paul J.
Rockwell International
3370 Miraloma Avenue
Anaheim, CA 92803

Bijvoet, Jan A.
University of Alabama
Mailbox 209
Huntsville, AL 35899

Burkey, Martin
Huntsville Times
2317 Memorial Parkway SW
Huntsville, AL 35801

Caldwell, Colin
Babcock & Wilcox
Box 785
Lynchburg, VA 24505

Carreiro, Louis
Armky Mtls Tech Lab
ATTN: SLCMT-EMS
Arsenal Street
Watertown, MA 02172

Catrett, Shawna
NASA
ET-43, Bldg 4708
MSFC, AL 35812

Chen, Quark Y.
Honeywell, Inc.
MS-MN65-2600
3660 Technology Drive
Minnesota, MN 55418

Chen, YI
Auburn University
311 W. Toenn, Apt #19
Auburn, AL 36830

Cheng, Hai-Yuin
University of Alabama
Dept. of Physics
Huntsville, AL 35899

Conrad, R.W.
Commander, MICOM
ATTN: AMSMI-RD-DE-UB
Redstone Arsenal, AL 35898

Cooke, D. Wayne
Los Alamos Nat'l Lab
PO Box 1663
MP-14, MS H847
Los Alamos, NM 87545

Corvan, Peter
Eastman Kodak Company
Federal Systems Div
Rochester, NY 14650-2156

Cothran, Bradley R.
Boeing Aerospace
Mail Stop JX-23
PO Box 1470
Huntsville, AL 35807

Courtland, L. Bohn
Argonne National Laboratory
Argonne, IL 60439

Cunniff, John
Hypres, Inc.
500 Executive Blvd
Elmsford, NY 10523

Curtis, John
Ford Aerospace
3939 Fabian Way
MS/G-18
Palo Alto, CA 94303

Cutshaw, Calvin
Auburn EE Dept.
200 Broun Hall
Auburn, AL 36849

Debsikdar, Jagadish C.
EG&G Idaho, Inc.
PO Box 1625
MS 2218
Idaho Falls, ID 83415

Deaver, Bascom
University of Virginia
Physics Dept
McCormick Road
Charlottesville, VA 22901

Decher, Rudolf
NASA-MSFC
Space Science Lab
MSFC, AL 35812

Delayen, J.
Argonne National Laboratory
9700 S. Cass Avenue
EP-207
Argonne, IL 60439

Delong, Lance
Nat'l Science Foundation
DMR/Room 408
1800 G Street NW
Washington, DC 20550

Denhoff, M.W.
NRC of Canada
Div of Physics
Montreal Rd - Bldg M-36
Ottawa, Canda K1A0R6

Dingus, Mike
Alabama Cryogenic Eng
PO Box 2470
Huntsville, AL 35804

Eisenberg, Sally
American Furnace Co. Inc.
408 Cedar Bluff Road
Suite 374
Knoxville, TN 37923

Eisenman, W.L.
University of Alabama
Huntsville, AL 35899

Ellis, John
Alabam Cryogenic Engineering
PO Box 2470
Huntsville, AL 35804

Ennis, Doug
USASDC
PO Box 1500
Huntsville, AL 35806

Ethridge, Edwin
NASA - MSFC
Space Science Lab ES-74
Huntsville, AL 35801

Farrell, J.N.
SAIC
6725 Odyssey Drive
Huntsville, AL 35806

Fennelly, A.J.
Teledyne Brown Engineering
300 Sparkman Drive NW
Huntsville, AL 35807

Forrester, Martin G.
Westinghouse R&D Center
1310 Beulah Road
Pittsburgh, PA 15235

Fry, Leolau H.
US Naval Coastal Systems Ctr
Code 2130
Panama City, FL 32405

Garland, Michael
Memphis State University
Dept of Physics
Memphis, TN 38152

Gerdt, David
Sperry Marine
1070 Seminole Trail
Charlottesville, VA 22906

Gergis, Isoris S.
Rockwell International Corp
1049 Camino Dos Rios
PO Box 1085
Thousand Oak, CA 91360

Golben, John
NASA-MSFC
Space Science Lab - ES74
MSFC, AL 35812

Goldman, Joel
Commander, ARDEC
ATTN: SMCAR-CCJ
Picatinny Arsenal, NJ 07806

Grant, Peter
NRC of Canada
Dept of Physics, Bldg M-36
Montreal Road
Ottowa, CA K1A0R6

Grodzka, Philomena
Lockheed Corporation
PO Box 1103
Huntsville, AL 35807

Grundkowski, Tom
United Technologies Research Ctr
Silver Lane, MS 31
East Hartford, CT 06108

Hall, William
Luz Construction Mgt
PO Box 488
Boron, CA 93816

Hammond, Robert B.
Superconductor Technologies Inc.
460 Ward Drive, Suite F
Santa Barbara, CA 93111

Hampton, Ann
Georgia Tech Research Institute
EML/MWTD
Atlanta, GA 30332

Hardt, Hugo
NRC
4040 S. Memorial Parkway
Huntsville, AL 35802

Harper, Jim
Physicon, Inc.
3325 Triana, Ste A
Huntsville, AL 35805

Hartman, Richard
BAL
1103 Deborah Drive
Huntsville, AL 35801

Hayes, Herb
SDC
PO Box 1500
ATTN: CSSD-CA
Huntsville, AL 35807

Hayes, Paul
Auburn University
Department EE, 200 Broun Hall
Auburn, AL 36849

Heaston, Robert
IIT Research Institute
Dept GACIAC
10 W. 35th Street
Chicago, IL 60616

Heremans, Jospeh
GM Research Labs
Physics Department
30500 Mound Road
Warren, MI 48090-9005

Hemenger, Pat
US Air Force
ATTN: WRDC/MLPO
WPAFB, OH 45433-6533

Hilal, Mohamed A.
University of Wisconsin
919 Eng. Res. Bldg (ERB)
1500 Johnson Drive
Madison, WIS 53706

Iafrate, Gerald
U.S. Army Labcom
ATTN: SLCET-E
Ft. Monmouth, NM 07703-5000

Imai, Kumiko
The Furukawa Electric Co.
Yokohama R&D Labs
2-4-3 Okano
Nishi-Ku Yokohama 220
Japan

Inguva, Ramarao
Commander, USA MICOM
ATTN: AMSMI-RD-RE-OP
Redstone Arsenal, AL 35898-5248

Isenman, W.L.
UAH
2416 Lorenzo Road
Del Mar, CA 92014

Izatt, Jerald
University of Alabama
Dept of Physics & Astronomy
Tuscaloosa, AL 35487-0324

Jackson, Byron
Jet Propulsion Labs
4800 Oak Grove Drive
MS 301-285
Pasadena, CA 91109

Jahan, M. Shah
Memphis State University
Dept of Physics
Memphis, TN 38152

Jennings, Walter B.
Commander, USA MICOM
Directed Energy Dir, RD&EC
ATTN: AMSMI-RD-DE
Redstone Arsenal, AL 35898-5245

Jirmanus, Munir
Janis Research
2 Jewel Drive
Wilmington, MA 01887

Johnson, Milo
Texas Instruments
PO Box 655936, MS 145
Dallas, TX 75265

Johnson, Robert A.
US Army Missile Command
ATTN: AMSMI-RD-RE-OP
Redstone Arsenal, AL 35898-5248

Kang, S.
Creare, Inc.
PO Box 71
Etna Road
Hanover, NH 03755

Kingsland, Richard
Jaycor
11011 Torreyana Road
San Diego, CA 92121

Knox, Nancy
University of Alabama
164 Oldwood Road
Huntsville, AL 35811

Kogan, V.G.
Ames Lab
Physics Division
Ames, IA 50011

Kawano, Kenneth
United Internat'l Engineering
1500 Perimeter Parkway
Suite 123
Huntsville, AL 35806

Khalil, Ali
General Electric
Astrospace Division
PO Box 800 - MS 410-2-C19
Princeton, NJ 08543-0800

Kirlin, Peter
Advanced Technology Materials
520-B Danbury Road
New Milford, CT 06776-4318

Kollie, Thomas G.
Oak Ridge National Lab
PO Box 2008, MS-6092
Building 4508
Oak Ridge, TN 37831-6092

Kung, Pang-Jen
Auburn University
Dpt of Electrical Engineering
200 Broun Hall
Auburn University, AL 36849-5201

Kwok, Hoi S.
University of NY at Buffalo
Institute on supe conductivity
Bonner Hall
Amherst, NY 14260

Lanagan, Michael
Argonne National Laboratory
9700 S. Cass Avenue

Lansford, Jim
GTRI
225 North Avenue
Atlanta, GA 30332

Lemons, Ross A.
Los Alamos National Laboratory
MEE-11-88-0194L
D 429
Los Alamos, NM 87545

Lesyne, Larry
Grumann Aerospace
MS A01-26
Bethpage, NY 11714

Li, Ming
University of Alabama
Chemistry Department
Science Building Room 208
Huntsville, AL 35899

Loh, Roland R.
HITc Superconco, Inc
PO Box 487
New Hope, PA 18938

Luthra, Jagdish
US Army MICOM
ATTN: AMSMI-RD-RE-OP
Redstone Arsenal, AL 35898

Luo, H.L.
University of California
Dpt of Electrical & Computer
Engineering, Room 007
U of C, San Diego
LaJolla, CA 92093

Madarasz, Frank
UAH Center for Applied Optics
Huntsville, AL 35899

Martin, William
USASDC
ATTN: CSSD-H-VP
Huntsville, AL 35807

Matsuba, Hironori
The Furukwawa Electric Co, Ltd
Yokohama R&D Labs
2-4-3 Okano
Nishi-Ku Yokohama 220
Japan

May, Douglas
Commander
US Army Missile Command
ATTN: AMSMI-RD-PR
Redstone Arsenal, AL 35898

McAvoy, Bruce R.
Westinghouse R&D
1310 Beulah Road
Pittsburgh, PA 15235

McDonald, Joseph K.
US Army Missile Command
ATTN: AMSMI-RD-RE-OP
Redstone Arsenal, AL 35898-5248

McDowell, Brenda
ARI
PO Box 11220
Huntsville, AL 35814-1220

McHenry, M.E.
Los Alamos National Lab
MST-6 MS K765
Los Alamos, NM 87545

McLane, George F.
US Army ETDL
ATTN: SLCET-ED
Ft. Monmouth, NJ 07703-5000

Miller, John
University of North Carolina
CB #3255, Phillips hall
Chapel Hill, NC 27599-3255

Montgomery, Albert G.
The MITRE Corporation
MS R250, Burlington Road
Bedford, MA 01730

Morrison, Philip
Advanced Fuel Research, Inc.
87 Church Street
PO Box 18343
East Hartford, CT 06118

Morton, J.R.
National Research Counsil
of Canada
Division of Chemistry
Bldg M-12, Montreal Road
Ottawa, Ontario, Canada K1A OR6

Mosko, Joseph
Naval Weapons Center
Code 35203
China Lake, CA 93555

Muhaluk, Jonathan
US Army Liaison Office
PO Box 1401
Huntsville, AL 35807

Neifeld, Rick
US Army ETDL
ATTN: SLCET-ED
Ft. Monmouth, NJ 07703

Nellis, Mike
Ala Cryogenic Engineering
PO Box 2470
Huntsville, AL 35804

Nelson, Richard D.
Ford Aerospace
12122 Red Hill Avenue
Santa Ana, CA 92705

Nicolas, David P.
NASA-MSFC
EE Parts Branch, EB13
MSFC, AL 35812

Oates, Daniel E.
MIT
Lincoln Laboratory
Lexington, MA 02173-0073

Ogden, Greg
Kaman Sciences Corporation
2560 Huntington Avenue
Suite 500
Alexandria, VA 22303-1490

Olander, Bill
Teledyne Brown Engineering
300 Sparkman Drive NW MS-50
Huntsville, AL 35807-7007

Ortabasi, Ugur
SCI-TECH Int.
5673 W. Las Positas Blvd
Suite 205
Pleasanton, CA 94566

Patton, Elizabeth
Santa Barbara Research Ctr
75 Coromar Drive
B-2/MS 8
Goleta, CA 93117

Peng, Huei
UAH Huntsville
CSPAR, UAH
Huntsville, AL 35899

Peters, Palmer N.
NASA-MSFC
Space Science Lab, ES63

Phillips, Richard
Auburn University
1404 E. University Drive
Auburn, AL 36830

Pittman, William C.
US Army Missile Command
ATTN: AMSMI-RD-AS-PM
Redstone Arsenal, AL 35898-5253

Polakos, Paul A.
AT&T Bell Laboratories
600 Mountain Avenue, 1E-234
Murray Hill, NJ 07974

Postan, Aaron
Commander, MICOM
ATTN: AMSMI-RD-RE-OP
Huntsville, AL 35898

Potenziani, Ernest
US Army ET&D Laboratory
SLCET-ED, Hexagon Building
Ft Monmouth, NJ 07703-5000

Ranellone, R.F.
Newport News
Ship Building
4101 Washington Avenue
Newport News, VA 23607

Rao, Dantam
Mech Tech, Inc.
968 Albany Shaker Road
Latham, NY 12110

Rausch, E. Otto
GTRI, Rall/RAD
7220 Richardson Road
Smyrna, GA 30080

Reynolds, Joseph
Louisiana State University
Department of Physics
Baton Rouge, LA 70803

Richardson, Alex
ITT Avionics
3900 Washington Avenue
Nutley, NJ 07110

Rodgers, Richard
USASDC
ATTN: CSSD-H-YP
PO Box 1500
Huntsville, AL 35807-3801

Rogovin, Daniel
Rockwell Science Center
PO Box 1085
Thousand Oaks, CA 91360

Ross, Brian
National Research Council
2101 Constitution Avenue NW
BOSTID Room HA-476
Washington, DC 20418

Roy, Eddie
Deputy Commander
USASDC
ATTN: CSSD-H-V
PO Box 1500
Huntsville, AL 35807

Ryan, Paul A.
AFWAL/AAWW-1
WPAFB, OH 45433-6523

Rybick, Dale
ARI
5025 Bradford
PO Box 11220
Huntsville, AL 35814

Santandria, Robert
Babcock & Wilcox
Box 785
Lynchburg, VA 24505

Schaffhauser, A.C.
ORNL HTSc Pilot Center
PO Box 2008
Bldg 4500S, MS-6140
Oak Ridge, TN 37831-6140

Shaeffer, D. Lynn
Amador Research Corporation
4737 Ross Gate Court
Pleasanton, CA 94566

Schmidt, F.J.
AMETEK, Inc
352 Godshall Drive
Harleysville, PA 19438

Sisk, Charles
NASA-MSFC
Space Science Lab, ES63
MSFC, AL 35812

Smith, James L.
Los Alamos National Lab
Los Alamos, NM 87545

Sova, Ray
Johns Hopkins University
Applied Physics Lab
Johns Hopkins Road
Laurel, MD 20707

Stanley, Ann E.
US Army Missile Command
ATTN: AMSMI-RD-RE-OP
Redstone Arsenal, AL 35898

Stauffer, Sam
AMTEC Corporation
4811 Bradford Boulevard
Huntsville, AL 35805-1948

Stetson, ED
Corporation for Studies
& Analysis
11222 La Cienega Blvd
Inglewood, CA 90304

Strom, Ulrich
Naval Research Lab
Code 6873
Washington, DC 20375

Suchow, Lawrence
New Jersey Inst of Technology
Chemistry Division
Newark, NJ 07102

Swift, Wesley R.
University of Alabama
RIC-10
Huntsville, AL 35899

Symko, Orest G.
University of Utah
Depart of Physics
201 James Fletcher Bldg
Salt Lake City, UT 84112

Tanger, Charles
217 Payne Street
Auburn, AL 36830

Tanton, George
US Army Missile Command
ATTN: AMSMI-RD-RE-OP
Redstone Arsenal, AL 35898-5248

Tauber, Arthur
US Army ETDL
ATTN: SLCET-ED
Ft. Monmouth, NJ 07703-5000

Teller, Edward
Lawrence Livermore Nat'l Lab
PO Box 808, L-0
Livermore, CA 94550

Tin, Chin C.
Auburn University
Department of Physics
206 Allison Lab
Auburn University, AL 36849

Tucker, John R.
University of Illinois
Dept of Elec & Computer Eng
1406 W. Green Steet
Urbana, IL 61801

Tzeng, Yonhua
Auburn University
Dept of Elec Eng
200 Broun Hall
Auburn, AL 36849

Urban, Eugene W.
NASA-MSFC
Space Science Lab, ES63
MSFC, AL 35812

Valco, George J.
The Ohio State University
Dept of Electrical Eng
205 Dreese Laboratory
2015 Neil Avenue
Columbus, OH 43210-1272

Vlasse, Marcus
NASA-MSFC
Space Science Laboratory, ES74
MSFC, AL 35812

Vought, Carl D.
Amtec Corporation
4811 Bradford Blvd
Huntsville, Al 35805

Walch, Ahmad
Applied Science Consultants Inc
621-B River Oaks Parkway
San Jose, CA 95134

Weaver, Sam C.
American Matrix Inc.
118 Sherlake Lane
Knoxville, TN 37922

Weaver, Tom C.
Sigma Services
7909 Tea Garden Road
Huntsville, AL 35802

Weinberger, B.R.
United Technologies Research Ctr
Silver Lane, MS 31
East Hartford, CT 06108

Wilber, William
US Army, ET & DL
ATTN: SLCET-ED
Ft. Monmouth, NJ 07703-5000

Willing, Harry
SDC
PO Box 1500
ATTN: CSSD-H-YA
Huntsville, AL 35807

Wilson, B.A.
JPL Electronics
Jet Propulsion Lab
4800 Oak Grove Drive
MS 302-205
Pasadena, CA 91109

Wingefeld, Gerd
Hoechst Celanese Corporation
Robert L. Mitchell Tech Center
86 Morris Avenue
Summit, NJ 07901

Witteles, Eleonora M.
Aerojet ElectroSystems
1100 W. Hollyvale Street
MS 59-1433
Azusa, CA 91702

Wu, M.K.
Columbia University
Dpt of Materials Science
The Mudd Building
New York, NY 10027

Yee, Tin Boo
Commander, USA MICOM
ATTN: AMSMI-RD-ST-CM
Redstone Arsenal, AL 35898

York, Gerry
US Army Liaison Office
PO Box 1401
Huntsville, AL 35807

Zmuidzinas, Jonas
University of Illinois
Department of Astronomy
1011 W. Springfield Avenue
Urbana, IL 61801

THIS PAGE IS INTENTIONALLY BLANK

THE TACTICAL WEAPON GUIDANCE AND CONTROL INFORMATION ANALYSIS CENTER (GACIAC)

GACIAC is a DoD Information Analysis Center operated by IIT Research Institute under the technical sponsorship of the Joint Service Guidance and Control Committee with members for OUSDRE, Army, Navy, Air Force, and DARPA. The U.S. Army Missile Command provides the Contracting Officer's Technical Representative. Its mission is to assist the tactical weapon guidance and control community by encouraging and facilitating the exchange and dissemination of technical data and information for the purpose of effecting coordination of research, exploratory development, and advanced technology demonstrations. To accomplish this, GACIAC's functions are to:

1. Develop a machine-readable bibliographic data base -- currently containing over 36,000 entries;

2. Collect, review, and store pertinent documents in its field of interest -- the library contains over 11,000 reports;

3. Analyze, appraise and summarize information and data on selected subjects;

4. Disseminate information through the GACIAC Bulletin, bibliographies, state-of-art summaries, technology assessments, handbooks, special reports, and conferences;

5. Respond to technical inquiries related to tactical weapon guidance and control; and

6. Provide technical and administrative support to the Joint Service Guidance and Control Committee (JSGCC).

The products and services of GACIAC are available to qualified industrial users through a subscription plan or individual sales. Government personnel are eligible for products and services under block funding provided by the Army, Navy, Air Force and DARPA. A written request on government stationery is required to receive all the products as a government subscriber.

Further information regarding GACIAC services, products, participation plan, or additional copies of these Proceedings may be obtained by writing or calling: GACIAC, IIT Research Institute, 10 West 35th Street, Chicago, Illinois 60616-3799, Area Code 312, 567-4519 or 567-4526.

JSGCC

JOINT SERVICE GUIDANCE AND CONTROL COMMITTEE